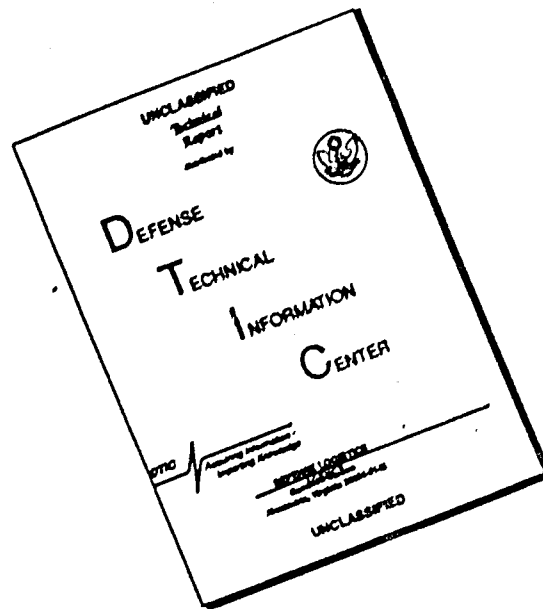


DISCLAIMER NOTICE



THIS DOCUMENT IS BEST QUALITY AVAILABLE. THE COPY FURNISHED TO DTIC CONTAINED A SIGNIFICANT NUMBER OF PAGES WHICH DO NOT REPRODUCE LEGIBLY.

AD 461 200

Bulletin 34
Part 5
(of 5 Parts)

CATALOGED BY: [illegible]
AS AD NO.

THE SHOCK AND VIBRATION BULLETIN

FEBRUARY 1965

A Publication of
THE SHOCK AND VIBRATION
INFORMATION CENTER
U.S. Naval Research Laboratory, Washington, D.C.



Office of
The Director of Defense
Research and Engineering

DDC
APR 26 1965
TISA B

461200

Qualified requestors may obtain copies of this
Bulletin from the Defense Documentation Center.

Foreign announcement and dissemination of this
Bulletin by the Defense Documentation Center is
not authorized.

Bulletin 34
Part 5
(of 5 Parts)

THE SHOCK AND VIBRATION BULLETIN

FEBRUARY 1965

A Publication of
THE SHOCK AND VIBRATION
INFORMATION CENTER
U.S. Naval Research Laboratory, Washington, D.C.

The 34th Symposium on Shock, Vibration and Associated Environments was held in Pacific Grove, California on 13-15 October 1964. The Army was host.

Office of
The Director of Defense
Research and Engineering

CONTENTS

PART 5

Vibration Testing

PITFALLS IN RANDOM SIMULATION.	1
W. C. Beecher, Lear Siegler Inc.	
VIBRATION MEASUREMENTS	15
R. W. Mustain, Douglas Space Systems Center	
FORCE-CONTROLLED VIBRATION TESTS: A STEP TOWARD PRACTICAL APPLICATION OF MECHANICAL IMPEDANCE	45
J. V. Otts, Sandia Corp.	
SELECTION OF VIBRATION TEST LEVELS USING FATIGUE CRITERIA	55
L. W. Root, Collins Radio Company	
ANALOG EXPERIMENTS COMPARE IMPROVED SWEEP RANDOM TEST WITH WIDE BAND RANDOM AND SWEEP SINE TESTS	67
G. Booth, MB Electronics and J. T. Broch, Bruel and Kjaer	
SIMULATING MISSILE-FIRING ACOUSTICAL ENVIRONMENT BY EQUIVALENT MECHANICAL VIBRATION	83
J. H. Putukian, Raytheon Company	
TEST CONTROL DEVICES—SNAP 10A VIBRATION TEST PROGRAM	93
E. L. Gardner and R. M. Oliva, Atomics International	
TRANSMISSION OF VIBRATION TEST FORCES BY MEANS OF VISCOELASTIC LAYERS.	99
A. J. Yorgiadis and S. Barrett, North American Aviation	
FREE-FREE BENDING VIBRATION MEASUREMENTS OF THE OAO BOOST VEHICLE UTILIZING AIR-BEARING SUPPORT	115
R. L. Turney, J. D. Jones, and K. F. Koehl, General Dynamics/Astronautics	
THE RESPONSE OF THE OGO SPACECRAFT STRUCTURE TO HIGH-INTENSITY ACOUSTIC LOADING	125
P. J. Alfonsi, Goddard Space Flight Center	
A LOW-LEVEL VIBRATION TEST SYSTEM	141
R. C. Klinger and M. A. Kollodge, Honeywell Inc.	
SYSTEM RESONANCE, A FUNCTION OF VIBRATION TEST PARAMETERS.	145
A. M. Samborsky and C. J. Van Vliet, U.S. Navy Electronics Laboratory	
A TEMPERATURE CONTROLLER FOR COMBINED TEMPERATURE-VIBRATION TESTS	149
R. E. Seely, U.S. Naval Research Laboratory	

Damping

VIBRATION RESPONSE CHARACTERISTICS OF VISCOELASTIC-DAMPED STRUCTURES	155
J. E. Ruzicka, Barry Controls	
MATERIAL DAMPING OF ALUMINUM BY RESONANT-DWELL TECHNIQUE	177
N. Granick and J. E. Stern, Goddard Space Flight Center	

EFFECT OF PRESSURE ENVIRONMENT ON DAMPING OF VIBRATING STRUCTURES.	197
D. G. Stephens and M. A. Scavullo, Langley Research Center	
DEVELOPMENT OF A HIGHLY DAMPED SUBMARINE MACHINERY FOUNDATION	205
E. V. Thomas, U.S. Navy Marine Engineering Laboratory	
DESIGNING STRUCTURES FOR ACOUSTICAL AND VIBRATION ENVIRONMENTS	211
R. P. Thorn and G. E. Warnaka, Lord Manufacturing Company	

Fixture Design

EQUALIZATION AND FIXTURE DESIGN	221
R. M. Mains, General Electric Co.	
DEVELOPMENT OF A LAMINATED VIBRATION FIXTURE MATERIAL	227
R. L. Bergey, Burroughs Corporation	
A REPORT ON THE DESIGN OF INTEGRATED HORIZONTAL AXIS VIBRATION FIXTURES.	231
F. C. Tolleth, Autonetics	
DESIGN OF LARGE VIBRATION FIXTURES FOR SATURN S-IV STAGE DESIGN DEVELOPMENT AND QUALIFICATION PROGRAM	244
L. G. Smith, Douglas Aircraft Company	
SHAKER ATTACHMENTS FOR AEROSPACE GROUND EQUIPMENT IN PORTABLE CASES FOR VIBRATION TESTS.	255
K. A. Jenicek, McDonnell Aircraft Corporation	
DESIGN CRITERIA FOR VIBRATION FIXTURES.	260
L. E. Lutz, Honeywell, Inc.	
DESIGN AND UTILIZATION OF ENVIRONMENTAL TEST FIXTURES	267
W. S. Gorrell, Martin Company	
DESIGNING TIGHT BOLTED JOINTS FOR VIBRATION ENVIRONMENT	273
O. J. Zamparo, MB Electronics	
FIXTURE DESIGN - PANEL SESSION	279
DISTRIBUTION	289

PAPERS APPEARING IN PART 1

Part 1 - Confidential
(Titles Unclassified)

PROGRESS IN THE NAVY'S WAR ON SHOCK H. L. Rich, David Taylor Model Basin
FACTORS AFFECTING THE DEFINITION OF DESIGN AND TESTING CRITERIA FOR NAVAL SHOCK RESISTANT EQUIPMENT P. B. Wishart, Naval Construction Research Establishment
ANALYTICAL METHODS FOR PREDICTION OF MECHANICAL SHOCK ENVIRONMENT FOR SHIPBOARD EQUIPMENT OF SUBMARINES SUBJECTED TO UNDERWATER EXPLOSIONS M. Pakstys, Jr., General Dynamics/Electric Boat
GROWTH IN SHOCK AND VIBRATION ANALYSIS AND CORRESPONDING DESIGN IMPROVEMENTS E. G. Fischer, C. R. Brown, and A. A. Parr, Westinghouse Electric Corporation
A GENERAL-PURPOSE NAVAL MOUNT R. Hall, Naval Construction Research Establishment

EFFECT OF PRESSURE ENVIRONMENT ON DAMPING OF VIBRATING STRUCTURES.	197
D. G. Stephens and M. A. Scavullo, Langley Research Center	
DEVELOPMENT OF A HIGHLY DAMPED SUBMARINE MACHINERY FOUNDATION	205
E. V. Thomas, U.S. Navy Marine Engineering Laboratory	
DESIGNING STRUCTURES FOR ACOUSTICAL AND VIBRATION ENVIRONMENTS	211
R. P. Thorn and G. E. Warnaka, Lord Manufacturing Company	

Fixture Design

EQUALIZATION AND FIXTURE DESIGN	221
R. M. Mains, General Electric Co.	
DEVELOPMENT OF A LAMINATED VIBRATION FIXTURE MATERIAL.	227
R. L. Bergey, Burroughs Corporation	
A REPORT ON THE DESIGN OF INTEGRATED HORIZONTAL AXIS VIBRATION FIXTURES.	231
F. C. Tolleth, Autonetics	
DESIGN OF LARGE VIBRATION FIXTURES FOR SATURN S-IV STAGE DESIGN DEVELOPMENT AND QUALIFICATION PROGRAM	243
L. G. Smith, Douglas Aircraft Company	
SHAKER ATTACHMENTS FOR AEROSPACE GROUND EQUIPMENT IN PORTABLE CASES FOR VIBRATION TESTS.	255
K. A. Jenicek, McDonnell Aircraft Corporation	
DESIGN CRITERIA FOR VIBRATION FIXTURES.	259
L. E. Lutz, Honeywell, Inc.	
DESIGN AND UTILIZATION OF ENVIRONMENTAL TEST FIXTURES	267
W. S. Gorrell, Martin Company	
DESIGNING TIGHT BOLTED JOINTS FOR VIBRATION ENVIRONMENT	273
O. J. Zamparo, MB Electronics	
FIXTURE DESIGN - PANEL SESSION	279
DISTRIBUTION	289

PAPERS APPEARING IN PART 1

Part 1 - Confidential
(Titles Unclassified)

PROGRESS IN THE NAVY'S WAR ON SHOCK H. L. Rich, David Taylor Model Basin
FACTORS AFFECTING THE DEFINITION OF DESIGN AND TESTING CRITERIA FOR NAVAL SHOCK RESISTANT EQUIPMENT P. B. Wishart, Naval Construction Research Establishment
ANALYTICAL METHODS FOR PREDICTION OF MECHANICAL SHOCK ENVIRONMENT FOR SHIPBOARD EQUIPMENT OF SUBMARINES SUBJECTED TO UNDERWATER EXPLOSIONS M. Pakstys, Jr., General Dynamics/Electric Boat
GROWTH IN SHOCK AND VIBRATION ANALYSIS AND CORRESPONDING DESIGN IMPROVEMENTS E. G. Fischer, C. R. Brown, and A. A. Parr, Westinghouse Electric Corporation
A GENERAL-PURPOSE NAVAL MOUNT R. Hall, Naval Construction Research Establishment

AN APPROACH TO THE DESIGN OF A SHOCK/ANTI-VIBRATION MOUNT

T. A. Tugwood, Admiralty Surface Weapons Establishment

A MECHANICAL SHOCK DESIGN METHOD FOR SUBMARINE PRESSURE HULL
ATTACHMENTS UNDER EXPLOSION ATTACK

E. W. Palmer, Underwater Explosions Research Division, DTMB

EVALUATION OF A MACHINERY INSTALLATION BY MECHANICAL IMPEDANCE METHODS

J. E. Smith, Portsmouth Naval Shipyard

A VIBRATION MONITORING SYSTEM USEFUL IN SUBMARINE SILENCING AND
MAINTENANCE OF LOW NOISE EQUIPMENT

W. H. Ezell, General Dynamics/Electric Boat

THE DYNAMIC ENVIRONMENTS OF THE SHERIDAN/SHILLELAGH MISSILE SUBSYSTEM

H. M. Marshall, N. L. Haight, and D. W. Parsens, Aeronutronic Division, Philco Corporation

IDENTIFICATION OF BATTLEFIELD VEHICLES BY SOUND AND VIBRATION TECHNIQUES

D. W. Rees, U.S. Army Tank-Automotive Center

REPETITIVE STRONG SHOCK GENERATION AND PROPOSED FLEXIBLE
SHOCK-ABSORBER SYSTEM

C. V. David and E. A. Day, General Dynamics/General Atomic Division

THE DESIGN OF ELECTRONIC EQUIPMENT FOR DYNAMIC ENVIRONMENTS

R. H. Craig, General Electric Company Ltd.

ANALYSIS OF MISSILE RESPONSE TO HARD-TARGET IMPACT

M. B. Tate, Applied Physics Laboratory, JHU

THE TOW MISSILE LAUNCH ENVIRONMENT MEASUREMENT PROGRAM

A. D. MacLellan, Hughes Aircraft Company

HARD BASE EQUIPMENT-INSTALLATION DESIGN

B. R. Cooke, Martin Company

FIXTURES AND METHODS FOR OBTAINING THE FREE-FREE BREATHING AND
BENDING MODES OF SOLID PROPELLANT ROCKET MOTORS

L. R. West, Hercules Powder Company

PAPERS APPEARING IN PART 2

Mathematical Analysis

PREDICTION OF LAUNCH VEHICLE TRANSONIC BUFFETING FROM WIND TUNNEL DATA

R. E. Bieber, Lockheed Missiles and Space Company

SPACECRAFT ADAPTER RESPONSE TO FLUCTUATING PRESSURE

G. A. Watts, Manned Spacecraft Center

SUBHARMONIC BEHAVIOR OF THIN-WALLED ELASTIC BEAM

W. K. Tso, Northrop Corporation

PREDICTION AND MEASUREMENT OF VIBRATION RESPONSE OF THE PEGASUS
MICROMETEOROID MEASURING SATELLITE

C. E. Lifer and R. G. Mills, Marshall Space Flight Center

SPECTRA OF NONSTATIONARY RANDOM PROCESSES

G. P. Thrall, Measurement Analysis Corporation

RESPONSE OF MULTI-DEGREE-OF-FREEDOM SYSTEM TO RANDOM EXCITATION

R. C. Binder, University of Southern California

STRUCTURAL RESPONSE TO A VELOCITY-DEPENDENT STOCHASTIC EXCITATION

W. J. Stronge and G. K. Fisher, U.S. Naval Ordnance Test Station

VIBRATIONS OF A CANTILEVER BEAM CONSIDERING A NON-RIGID WALL SUPPORT
H. F. Cooper, Jr., Bell Telephone Laboratories, Inc.

Computers in Design

DIGITAL COMPUTER APPLICATION TO NONLINEAR VIBRATIONS
F. H. Collopy and R. Serbagi, AVCO Corporation

INTEGRATION OF A COMPUTER INTO THE DESIGN PROCESS
A. L. Head, Jr., and G. Harris, LTV Vought Aeronautics Division

DYNAMIC RESPONSE ANALYSIS OF COMPLEX MECHANICAL SYSTEMS
S. F. Mercurio and F. E. Niechniedowicz, Sperry Gyroscope Company

CONSIDERATIONS OF CAPTIVE FIRING VIBRATION ON NONOPERATING
PROPULSION SYSTEM COMPONENTS
G. Sardella, Martin Company

A PRACTICAL APPLICATION OF A DIGITAL COMPUTER PROGRAM DURING
THE DESIGN PHASE OF AN AEROSPACE STRUCTURE
B. T. Bata, Martin Company

STATIC AND DYNAMIC ANALYSIS BY A MATRIX FORCE METHOD
S. Kaufman and D. B. Hall, Martin Company

Design Techniques

SONIC AND ULTRASONIC VIBRATION SENSITIVITY OF X-BAND MICROWAVE COMPONENTS
R. Strike and G. G. Sundberg, General Dynamics/Pomona

DESIGNING ELECTRONIC EQUIPMENT FOR THE COMBINED RANDOM AND
SINUSOIDAL VIBRATION ENVIRONMENT
A. W. Sinkinson, RCA

DESIGNING MECHANISMS FOR NONLINEAR DYNAMIC EFFECTS
H. F. Hunter, Lockheed-Georgia Company

PACKAGING ELECTRONICS FOR 250,000 G APPLICATIONS
D. W. Finger, Harry Diamond Laboratories

COMBINED ANALYTICAL AND EXPERIMENTAL APPROACH FOR DESIGNING AND
EVALUATING STRUCTURAL SYSTEMS FOR VIBRATION ENVIRONMENTS
J. C. McClymonds and J. K. Gandung, Douglas Aircraft Company, Inc.

THOR 20-CYCLE LONGITUDINAL OSCILLATION STUDY
W. F. Davis, T. F. Lynch, and T. R. Murray, Douglas Aircraft Company, Inc.

LOW FREQUENCY STRUCTURAL DYNAMICS OF THE SATURN VEHICLES
D. C. Christian, G. C. Marshall Space Flight Center

DESIGN AND TEST OF AN AIRJET ACOUSTIC NOISE GENERATOR TO
REPRODUCE A MISSILE FLIGHT ENVIRONMENT
D. Richards, Applied Physics Laboratory

GRAPHICAL METHOD OF CALCULATING RMS VALUES FOR SHAPED
RANDOM VIBRATION SPECTRA
H. Himmelblau, North American Aviation, Inc.

DESIGN EVALUATION THROUGH VIBRATION TEST PROGRAM
D. A. Hausrath and J. R. Read, Autonetics, Division of North American Aviation, Inc.

DESIGNING FOR THE DYNAMIC ENVIRONMENT OF THE GEMINI INERTIAL PLATFORM
G. R. Grabow and J. E. Cottle, Honeywell Inc., Aeronautical Division

GUN FIRING ENVIRONMENT AND ITS RELATION TO STRUCTURAL AND EQUIPMENT
INTEGRITY
J. E. Gross and R. Pittman, McDonnell Aircraft Corporation

REDUCTION OF NOISE AND VIBRATION IN MILITARY VEHICLES

J. W. Cameron, U.S. Army Tank-Automotive Center

DESIGNING FOR THE DYNAMIC ENVIRONMENT PRACTICAL DESIGN TECHNIQUES

J. G. Perri, Burns and Roe, Inc.

PAPERS APPEARING IN PART 3

Mechanical Impedance

NOTES ON THE DEVELOPMENT OF MECHANICAL IMPEDANCE

C. T. Molloy, Space Technology Laboratories

RECENT ADVANCES IN MECHANICAL IMPEDANCE INSTRUMENTATION
AND APPLICATIONS

F. Schloss, David Taylor Model Basin

MECHANICAL IMPEDANCE OF SPACECRAFT STRUCTURES

C. C. Osgood, RCA-Astro Electronics Division

PRELIMINARY STUDY OF AN EXPERIMENTAL METHOD IN MULTIDIMENSIONAL
MECHANICAL IMPEDANCE DETERMINATION

F. J. On, Goddard Space Flight Center

EFFECTS OF TECHNIQUE ON RELIABILITY OF MECHANICAL IMPEDANCE MEASUREMENT

G. M. Remmers and R. O. Belsheim, U.S. Naval Research Laboratory

RESONANCE FREQUENCY OF LARGE SOLID PROPELLANT ROCKET MOTOR
DETERMINED BY MECHANICAL IMPEDANCE

L. G. Flippin, L. W. Gammell, and G. S. Stibor, Thiokol Chemical Corporation

USE OF MECHANICAL IMPEDANCE IN DYNAMIC MEASUREMENT OF
SOLID ROCKET MOTORS

R. E. Coleman, Rocketdyne

PREDICTING MAXIMUM RESPONSE OF A VIBRATION-EXCITED ELASTIC SUBSTRUCTURE

L. J. Pulgrano, Grumman Aircraft Engineering Corporation

DETERMINATION OF SYSTEM FIXED BASE NATURAL FREQUENCIES BY SHAKE TESTS

R. E. Kaplan and L. P. Petak, U.S. Naval Research Laboratory

EXPERIMENTAL PROGRAM TO DETERMINE DYNAMIC ENVIRONMENT OF
LAUNCH VEHICLES

I. P. Vatz, Brown Engineering Company

SMALL DISPLACEMENT KINEMATIC ANALYSIS OF BAR LINKAGES

C. S. O'Hearne, Martin Company

A PRACTICAL METHOD FOR PREDICTING ACOUSTIC RADIATION OR SHOCK EXCURSIONS
OF NAVY MACHINERY

R. A. Darby, U.S. Navy Marine Engineering Laboratory

A STEADY STATE RESPONSE ANALYSIS OF COMPLEX STRUCTURES USING
IMPEDANCE COUPLING TECHNIQUES

M. J. Baruch and S. Telles, Republic Aviation Corporation

Shock and Vibration Isolation

INVESTIGATION OF A RATIONAL APPROACH TO SHOCK ISOLATOR DESIGN

R. A. Eubanks, IIT Research Institute

VIBRATION ISOLATION SYSTEMS FOR ELECTRONIC EQUIPMENT IN THE B-52
AIRPLANE LOW-LEVEL ENVIRONMENT

R. W. Spring, The Boeing Company

DESIGN AND DEVELOPMENT OF LOW-FREQUENCY VIBRATION ISOLATORS WHICH
EXHIBIT LOW SHOCK AMPLIFICATION CHARACTERISTICS

S. Balan and L. J. Pulgrano, Grumman Aircraft Engineering Corporation

PROTECTING THE "EYES" OF THE OAO SATELLITE

J. T. Gwinn, Jr., Lord Manufacturing Company

DESIGN OF FOCALIZED SUSPENSION SYSTEMS

L. S. Pechter and H. Kamei, Autonetics Division of North American Aviation, Inc.

Shock

ELEMENTARY CONSIDERATIONS OF SHOCK SPECTRA

I. Vigness, U.S. Naval Research Laboratory

SPECTRAL CHARACTERISTICS OF SOME PRACTICAL VARIATIONS IN THE HALF-SINE AND SAW-TOOTH PULSES

E. H. Schell, Air Force Flight Dynamics Laboratory

USE OF SHOCK FOR LOW FREQUENCY VIBRATION TESTING

A. J. Villasenor and T. G. Butler, Goddard Space Flight Center

SPACECRAFT SHOCKS INDUCED BY ELECTRO-EXPLOSIVE DEVICES

D. A. Heydon and W. W. Aichroth, TRW Space Technology Laboratories

SIMULATION OF THE PYROTECHNIC SHOCK ENVIRONMENT

A. L. Ikola, Lockheed Missiles and Space Company

TEST TECHNIQUES FOR INCREASING THE ACCELERATION AND VELOCITY CAPABILITIES OF AN 18-INCH PNEUMATIC ACTUATOR

F. H. Mathews, Sandia Corporation

FIVE-MILLION POUND SHOCK TESTING FACILITY

R. M. Phelan, Cornell University and Lawrence Radiation Laboratory

SHOCK TESTING WITH EXPLOSIVE GASES

W. M. Sigmon, Jr., Sandia Corporation

HAND-HELD SHOCK TESTER WOX-6A

V. F. De Vost, J. E. Messner, and G. Stathopoulos, U.S. Naval Ordnance Laboratory

DESIGN AND DEVELOPMENT OF A HYDRAULIC SHOCK TEST MACHINE PROGRAMMER

J. R. Russell, American Machine and Foundry Company

SHAPING SHOCK ACCELERATION WAVEFORMS FOR OPTIMUM ELECTRODYNAMIC SHAKER PERFORMANCE

W. R. Miller, LTV Ling Electronics Division

SHOCK TESTING WITH VIBRATION SYSTEMS

F. W. Young, Radiation, Inc.

HYGE SHOCK FACILITY IMPROVEMENTS

R. M. Stuart, Hughes Aircraft Co.

PAPERS APPEARING IN PART 4

Instrumentation

MEASUREMENT AND ANALYSIS OF ENVIRONMENTAL VIBRATION ON A SHIP DURING ANY OPERATION AND AT ANY SEA CONDITION

E. Buchmann, David Taylor Model Basin

SYSTEM TO CALIBRATE VIBRATION TRANSDUCERS AT LOW DISPLACEMENTS

J. R. Reed, Naval Boiler and Turbine Laboratory

USE OF RECIPROCITY CALIBRATED ACCELEROMETER STANDARDS FOR PERFORMING ROUTINE LABORATORY COMPARISON CALIBRATIONS

R. R. Bouche and L. C. Ensom, Endevco Corporation

NEW INSTRUMENT FOR ACCELEROMETER CALIBRATION

D. R. Workman, Lockheed Missiles and Space Company

DEVELOPMENT OF AN OMNIDIRECTIONAL ACCELEROMETER

L. E. Dunbar, Grumman Aircraft Engineering Corporation

USE OF MINIATURE FORCE TRANSDUCERS IN THE MEASUREMENT OF SHOCK AND VIBRATION ENVIRONMENTS

G. W. Painter, Lockheed-California Company

ACQUISITION, REDUCTION, AND ANALYSES OF TRANSIENT DATA

E. H. Copeland, T. E. Smart, and J. Arnold, Sandia Corporation

A TELEMETRY STANDARD FOR VIBRATION AND ACOUSTIC MEASUREMENTS

E. J. Kirchman and F. J. Holley, Goddard Space Flight Center

MEASURING LAUNCH-ABORT ENVIRONMENT

C. N. Golub, Pan American World Airways, Inc.

DYNAMIC RESPONSE OF A DIGITAL MAGNETIC FORCE-REBALANCE PENDULOUS ACCELEROMETER TO A VIBRATIONAL ENVIRONMENT

L. R. Beuder and R. C. Rountree, Northrop Division of Northrop Corporation

MEASUREMENT OF RELATIVE DEFLECTIONS OF A GROUND MAPPING RADAR ANTENNA IN A VIBRATION ENVIRONMENT

E. F. Dyer, Westinghouse Electric Corp.

EXPERIMENTAL RESULTS OF THE APPLICATION OF SAMPLING TECHNIQUES TO VARIOUS TYPES OF FLIGHT DATA

J. Sudey, Jr., Martin Marietta Corp.

Environmental Data and Specifications

THE SHIPBOARD DYNAMIC ENVIRONMENT

H. B. Avery and W. L. Goodwin, Raytheon Company

SUMMARY OF MODEL AND FULL-SCALE ACOUSTIC DATA FOR PREDICTION OF MISSILE LIFT-OFF NOISE ENVIRONMENTS

D. A. Bond, Northrop Space Laboratories

PROBLEMS IN ADDING REALISM TO STANDARD SPECIFICATIONS

A. J. Silver, Litton Industries, Inc.

UTILIZING IN-FLIGHT VIBRATION DATA TO SPECIFY DESIGN AND TEST CRITERIA FOR EQUIPMENT MOUNTED IN JET AIRCRAFT

H. Katz and G. R. Waymon, McDonnell Aircraft Corp.

SOME RELIABILITY CONSIDERATIONS IN THE SPECIFICATION OF VIBRATION TEST REQUIREMENTS FOR NONRECOVERABLE COMPONENTS

C. V. Stahle, Martin Company

THE SPECIFICATION PROBLEM - PANEL SESSION

ROLLING CONTACT BEARING VIBRATION—THE STATE OF THE ART

J. I. Schwartz and R. E. Gustafson, U.S. Navy Marine Engineering Laboratory

HUMAN RESPONSE TO RANDOM VIBRATIONS

F. Pradko, U.S. Army Tank-Automotive Center

MEASUREMENT, ANALYSIS AND INTERPRETATION OF F-5A 20MM GUNFIRE DYNAMIC ENVIRONMENT

R. F. Carmichael and D. Pelke, Norair Division, Northrop

Transportation Environments

ACQUISITION AND ANALYSIS OF ACCELERATION DATA FROM THE S. S. WOLVERINE STATE AND LONG-TERM PREDICTION OF SEAWAY INDUCED LOADS ON CARGO

F. C. Bailey and D. J. Fritch, Lessells and Associates

DEPARTMENT OF THE ARMY POSITION ON TRANSPORTATION ENVIRONMENT CRITERIA

R. Kennedy, U.S. Army Transportation Engineering Agency

PROBLEMS ENCOUNTERED IN THE USE OF INSTRUMENTS FOR MEASURING
DYNAMIC ENVIRONMENTS

L. J. Pursifull, U.S. Army Transportation Engineering Agency

TRANSPORTATION ENVIRONMENTS

W. F. McCann, Lyon Aircraft Services

DYNAMIC TESTING OF MILITARY CONTAINERS VERSUS RELIABILITY

W. H. Myers and T. B. Gudis, Aeronautical Systems Division, USAF

IMPACT CONSIDERATIONS OF A NEW AIR DELIVERY SYSTEM

D. L. Griffin, Yuma Proving Ground

DESIGN OF A LIGHTWEIGHT PACKAGING SYSTEM TO SURVIVE DYNAMIC AND
STATIC LOADS

K. D. Robertson, U.S. Army Materials Research Agency

Section 1

VIBRATION TESTING

PITFALLS IN RANDOM SIMULATION

Warren C. Beecher
Instrument Division
Lear Siegler, Inc.
Grand Rapids, Michigan

This paper outlines certain problems in producing proper simulation of field environments and specification requirements for random vibration at the mounting points of the test specimen. These problems fall into two general categories: the equalization process and testing practices. Under the first heading, two general types of equalizers (series-connected and parallel bandpass) are discussed and four methods of equalization by matching transfer plots are compared: constant input-voltage swept-sine G plots, constant-output inverse-input swept-sine plots, constant input-voltage scanning-random g plots and constant-input wide band random g plots. The last method shows consistently good results and is the basis for automatic equalization equipment. A new method is developed for the successful application of wide band noise equalization to the series-connected peak/notch type equalizer.

Under the second heading, the effects of holding fixture design and accelerometer mounting practices are discussed, and the significance of notches in the fixture response curve is explored. The construction of dummy loads is outlined, and their application is explained. Laboratory experiments show the unsuitability of narrow band sweep testing techniques for multi-degree-of-freedom test items. Some tentative boundary selections for wide band segmented random noise tests are recommended.

INTRODUCTION

Ever since the advent of jet and rocket propulsion, an increasing proportion of measured environments have departed from sinusoidal-type vibration and adhered more or less closely to wide band random noise. There has been some controversy in the past about the desirability of duplicating these environments, but the practicing engineer faced with a requirement from a military specification has no doubt about the necessity. It has often been assumed that after the acquisition of random noise vibration test equipment, faithful adherence to the manufacturer's recommendations for its use should result in adequate simulation of the required environment. However, it is impossible for the manufacturer to treat the subject with this much detail in the average

instruction manual; in addition, the nature of certain problems and their solutions are just now becoming evident.

Continuing experiments at this laboratory have resulted in improved practices in the twin fields of random equalization and testing which should prove of interest to others engaged in these fields — either through corroboration of their findings, or by the stimulation of further investigation.

EQUALIZERS

The first equalizers to reach the market consisted of several peak/notch-type filters supplemented by general curve-shaping devices including bandpass filters, low pass filters and

"graphic" equalizers. All filters in use are connected in series or cascade, and only as many filters are used as are required. Although newer devices are considerably more efficient, they also require a considerable capital outlay, and many series-type equalizers are still in use. In the discussion of equalization methods, a new method is proposed which increases the speed and accuracy of equalization with the series equalizer.

The parallel bandpass-type equalizer consists of multiple bandpass filters parallel connected so as to divide the spectrum into small bits, each adjustable in amplitude. If a second set of parallel-connected bandpass filters is furnished, a parallel bandpass filter analyzer can be constructed to monitor the parallel bandpass filter equalizer. When the equalizer is servoed to the analyzer, the automatic equalizer results. It is obvious that the servoed equalization is extracted from a comparison with wide band random noise by inherent design necessity.

STANDARD EQUALIZATION TECHNIQUES

Two standard equalization techniques for peak/notch equalizers are frequently mentioned in the manufacturer's literature, each using a sweeping sine oscillator to scan the test item over the specification range. In the first method the oscillator voltage is established at a fixed point and held constant over the frequency range. The resultant variations in output g levels corresponding to the test item response are plotted. The apparent disadvantage of this method lies in the fact that rather high g levels may be reached at the test item monitoring point if high Q resonances are present. If the actual test item (or in some cases a facsimile thereof) is present, damage may occur. For this reason, a rather low input level is usually chosen.

This difficulty is eliminated by the second method, which frequently utilizes the same reference point as the first, but holds the g level constant instead of the voltage. To see the shape of the test item response, the inverse of the amplifier input voltage is plotted. Where a log converter is employed, it is usually possible to plot in inverse by reversing the polarity of the output cable plug.

The connection diagram used for plotting output g response curves at constant input voltage (Method 1) is shown as Fig. 1. The connection diagram used for plotting inverse input

voltage response at constant g level (Method 2) is shown as Fig. 2.

The third equalization technique utilized involves substitution of a narrow band scanning random generator for the sweeping sine oscillator [1]. With the exception of this substitution, the connection diagram remains unchanged. Two types of narrow band scanning random generators may be employed — constant bandwidth or constant Q types. If a constant Q generator is employed, a 3 db/octave power spectral density rolloff filter must be used to correct the amplitude level for increasing bandwidth as the frequency is increased. This is the method that was employed at Lear Siegler, Inc.

The fourth equalization technique that was employed involves submitting the test item to vibration created by a wide band white random noise generator band limited according to the test specification. The true root-mean-square (TRMS) output g level was adjusted to equal the level called out in the test specification for the final equalized value. The connection diagram is shown as the alternate connection of Fig. 1.

SELECTION OF TEST ITEMS

If an equalization technique is to be accounted satisfactory, it must encompass some of the more difficult test conditions, as well as selected simplified cases. For this reason, a horizontal table driving an intermediate fixture was used. The test item consisted of a rectangular plate fastened at the four corners and suspended across a slot in the end of the main fixture. The dimensions of the plate were made unequal to insure that at least two degrees of freedom would have to be equalized. Two of these plates were used. Evidence collected over a period of time seemed to indicate that equalizing a resonance higher in frequency than that of the driving resonance of the shaker-horizontal table combination presented additional problems. For this reason, Sample A was chosen so that the resonances associated with the lateral and longitudinal modes fell lower in frequency than the shaker-horizontal table driving resonance (hereafter referred to as prime resonance (PR)). Sample B was chosen so that the corresponding frequencies lay above PR.

Figure 3 is a general view of the shaker as it is coupled to the test item. Figure 4 shows

NOTE: References appear on page 14.

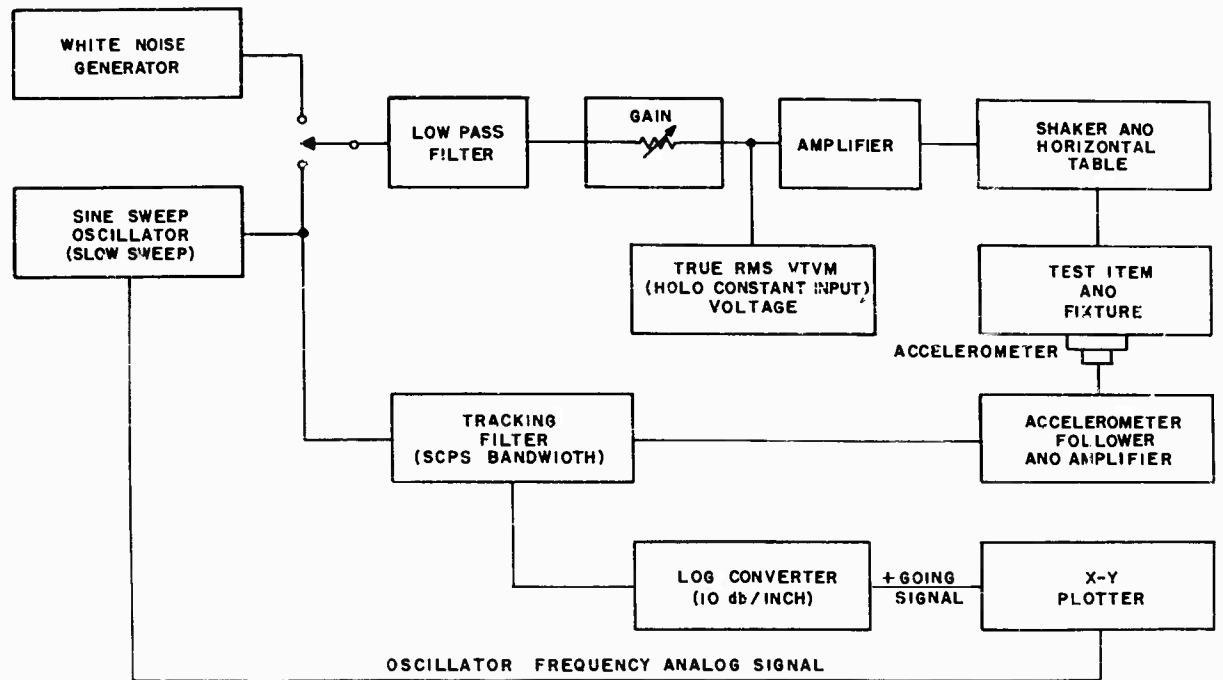


Fig. 1 - Connection diagram for plotting output g response curves at constant input voltage

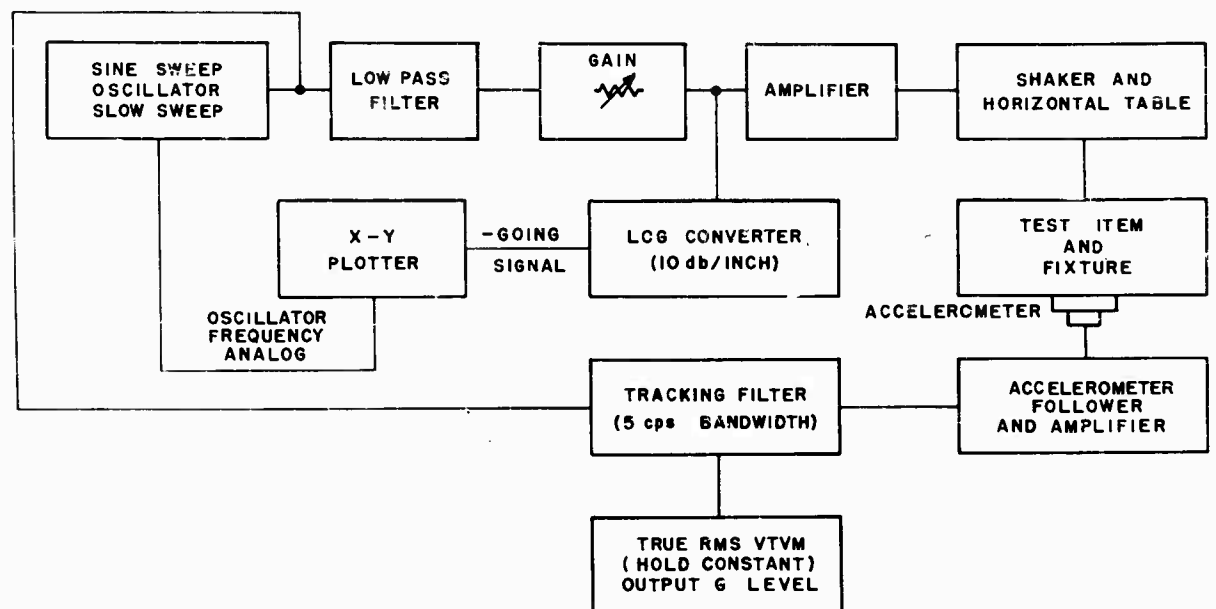


Fig. 2 - Connection diagram for inverse input voltage plots at constant output g

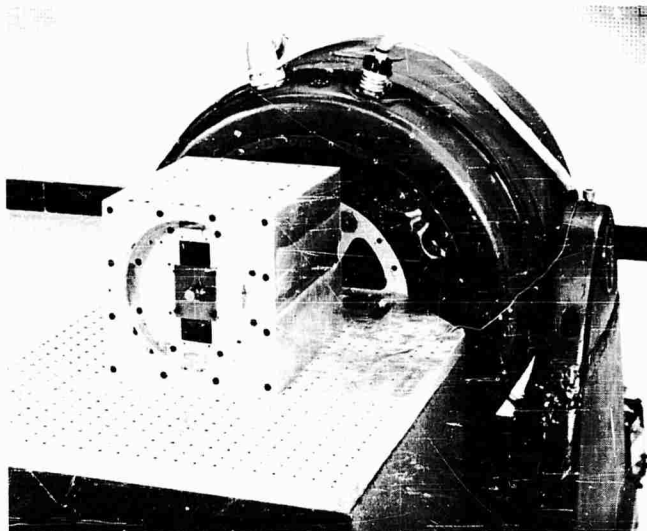


Fig. 3 - General view of shaker and test sample with intermediate fixturing

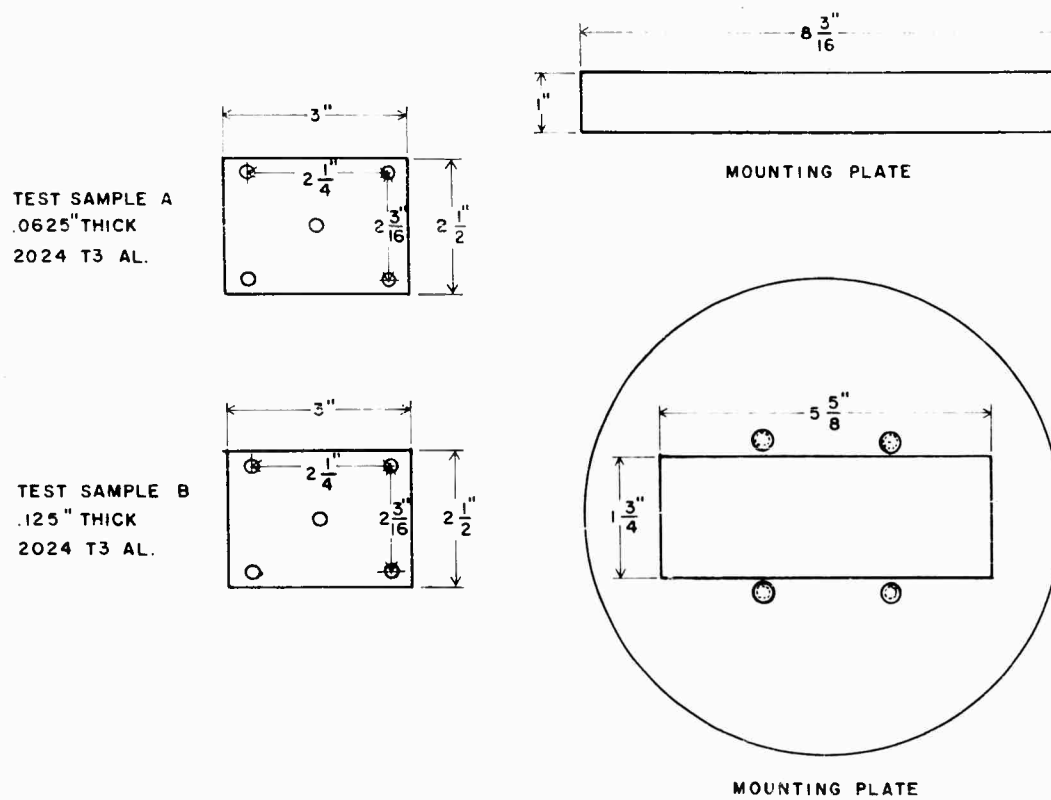


Fig. 4 - Sketch of details of test sample and mounting plate

the details of the two test samples and their mounting provisions. It should be noted that the test item mass was kept very low compared to the fixture mass, so that there could be no backdriving of the fixture by the test item resonances.

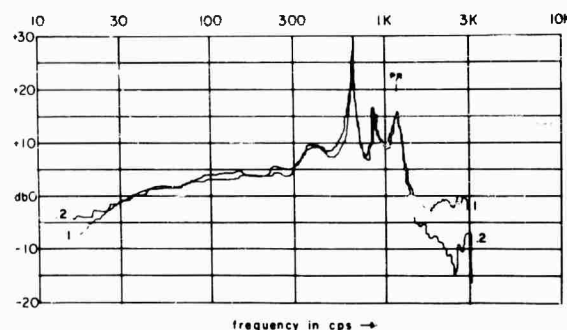
RESULTS OF TESTING PROGRAM

Figure 5 shows actual response plots for Samples A and B using the first three equalization techniques. The results demonstrate differences in both frequencies and amplitudes between the three methods. Furthermore, changing the input reference levels in the case of the sine sweeps caused noticeable changes in the shapes of the response curves, again affecting both frequencies and amplitudes. Although equipment availability at the time the scanning random test was conducted limited the results to only one curve with these test samples, previous testing showed that scanning

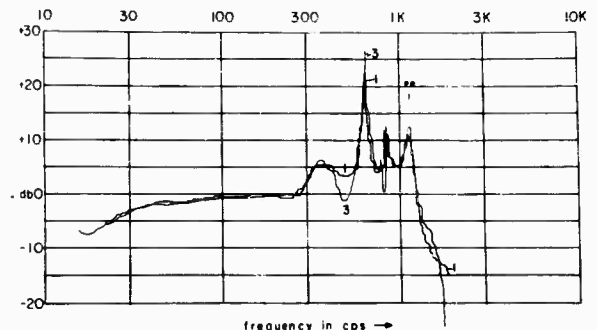
narrow band random testing behaved quite similarly to sweeping sine, and differences nearly vanished as the bandwidth was progressively narrowed. For the curve in Fig. 5d, the bandwidth = $0.15 f_0$ where f_0 is the operating frequency for any point on the curve.

Later it will be seen that if the fourth method of wide band random noise input is used for the basis of an equalization procedure, correct equalization will result. There is a corollary to this proposition; i.e., if some other equalization method is as good as wide band random input, it cannot show significant deviations from the same response curve that wide band random input will produce. For this reason the various response curves produced by the first three equalization techniques are compared with those produced from wide band white noise input for Sample A in Fig. 6 and for Sample B in Fig. 7.

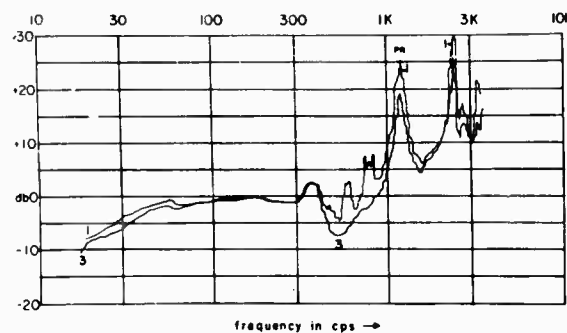
These curves show that constant output g sweeping sine (inverse input voltage) plots



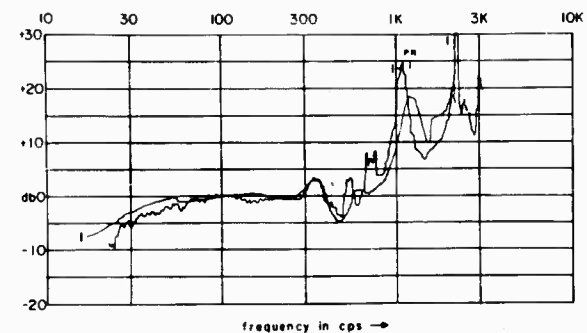
(a)



(b)



(c)



(d)

Fig. 5 - Comparison of sweeping sine response curves with each other and with narrow band scanning random response curve: (a) Sample A with constant input voltage at 1 and 0.2 g rms at 150 cps; (b) inverse input voltage plot of Sample A to 5 and 1 g rms constant output g sine sweep; (c) inverse input voltage plot of Sample B to 3 and 1 g rms constant output g sine sweep; and (d) Sample B - constant input voltage scanning random noise (ref. 1 g rms at 200 cps) vs 1 g rms constant output sweeping sine

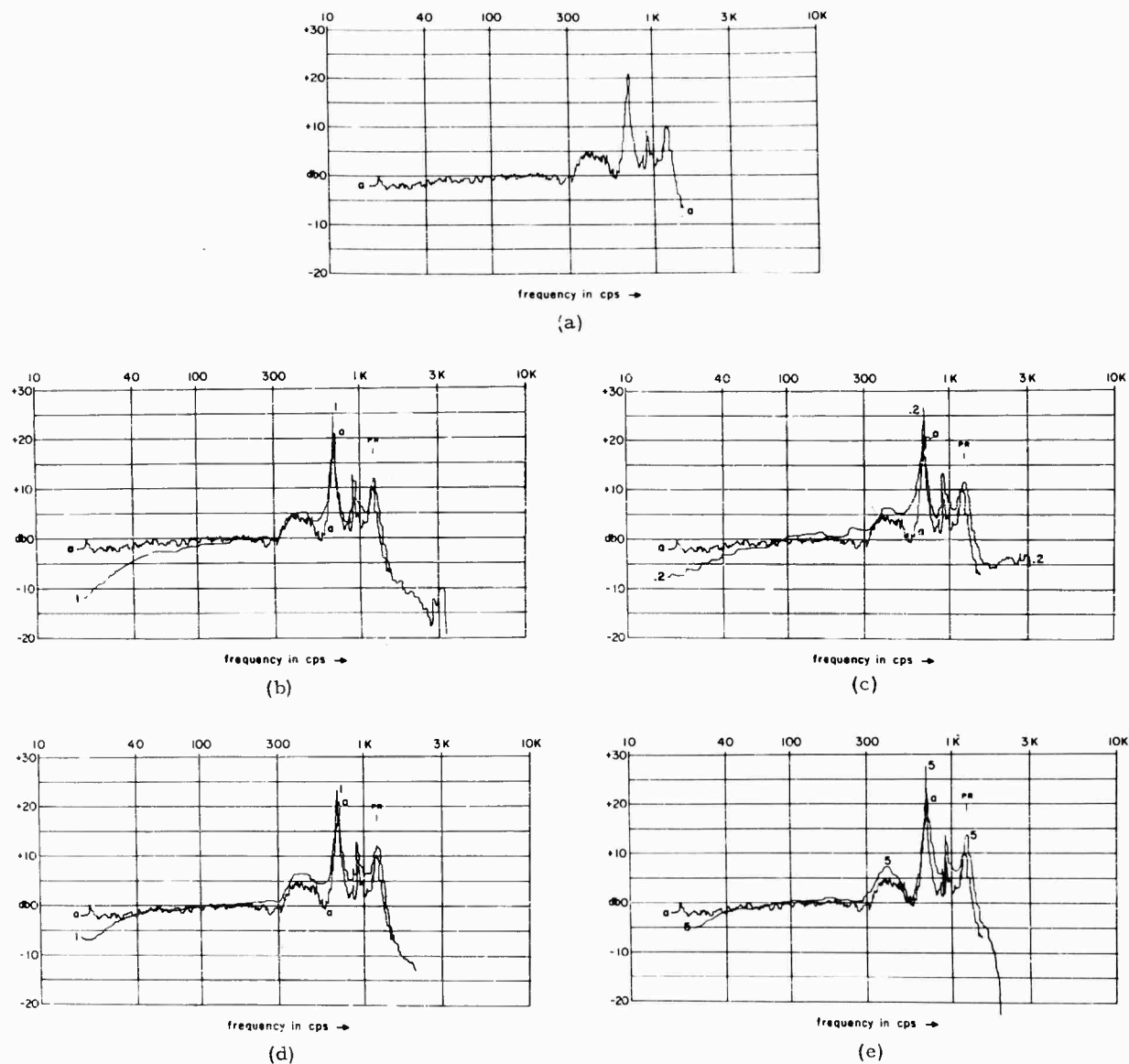


Fig. 6 - Sine vs random response curves for Sample A: (a) response at 10 g rms random vibration; (b) constant voltage (ref. 1 g rms at 150 cps); (c) constant voltage (ref. 0.2 g rms at 150 cps); (d) constant g level (inverse plot of input voltage at 1 g rms); and (e) constant g level (inverse plot of input voltage at 5 g rms). The basic curve for Fig. 6 comparisons is the G/\sqrt{V} cps response of Sample A to an input of wide band white random vibration with a measured output level of 10 g rms, 20-2000 cps.

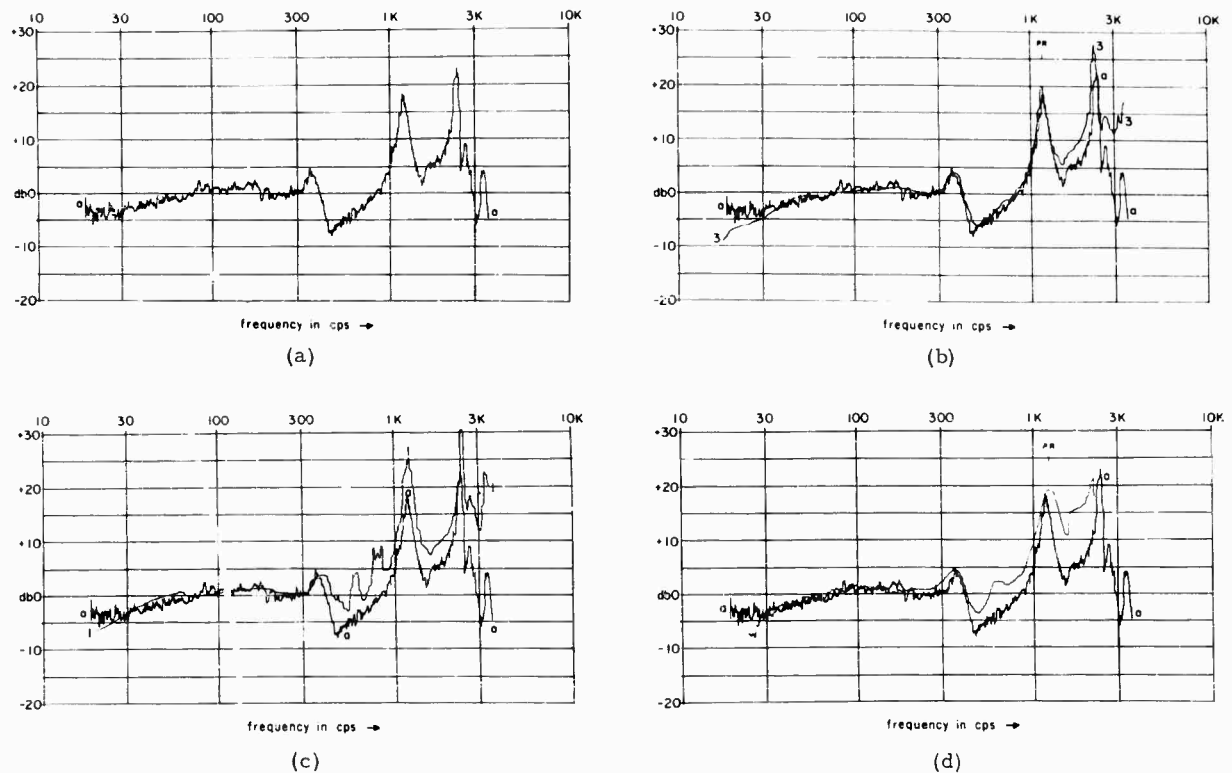


Fig. 7 - Sine vs. random response curves for Sample B: (a) response at 10 g rms random vibration; (b) constant voltage (ref. 3 g rms at 200 cps); (c) constant g level (inverse plot of input voltage at 1 g rms); and (d) constant level uniform power spectral density scanning random noise vs wide band noise. The basic curve for Fig. 7 comparisons is the $G\sqrt{V}$ cps response of Sample B to an input of wide band random vibration with an output level measured at 10 g rms, 20-2000 cps.

produce slightly closer results than constant input sweeping sine when compared to response curves plotted from wide band white noise constant input. Moreover, these curves show much closer correspondence for Sample A (sample resonances below PR) than for Sample B (sample resonances above PR). Since constant output g sine sweeps are less apt to produce damage and tend to correlate better with wide band random, only these are shown for Sample B.

In the case of Sample A (Fig. 6), the largest deviations of the comparison were at the low ends of the spectrum where the sine tended to roll off more rapidly than did the random response curves, especially for the constant input voltage response curves. The amplitude of response at PR was larger for sine than for random. The excessive low-end rolloff could be partially corrected at constant g output by increasing the output level, but this did not necessarily guarantee a match in resonant amplitudes and frequencies. For this reason, and

for the reason that broadband white random input was just as convenient and could produce more accurate results, the best constant g level for sweeping sine has not been determined. It is probable that a best value does exist, however.

In the case of Sample B (Fig. 7), the largest deviations of the comparison took place as a high-end rollup of the sine curve especially in the frequency region above PR. This was accompanied by a tendency for too much sine response rolloff at the extreme low end. Heavier level constant output g shakes tend to match wide band white random response curves, but the chance of finding a sine level which will match all portions of the curves for both frequency and amplitude appears to be quite remote in the case of Sample B, where resonant peaks occur beyond PR.

All of the above is of little importance unless it can indeed be proved that equalization to the wide band white noise response curve will produce a valid equalized response.

Figure 8 shows the steps in a procedure which yields experimental proof of this proposition. In Fig. 8a the unequalized response curve of the test item is obtained with constant input voltage wide band white noise in accordance with the connection diagram of Fig. 1. The input noise level is adjusted for a voltage that will produce the specification output level (10.0 rms g in this instance) when the input noise bandwidth is the same as the specification bandwidth. To equalize to this curve, the equalization filters are connected to the white random noise generator as in the connection diagram of Fig. 9. The bandpass filter is employed to band limit the noise to specification values before feeding it to the equalization filters. Figure 8c shows the inverse response of the filters as matched to the unequalized response of Fig. 8a. The closeness of match attained here was limited by the number of peak/notch filters employed and by the amount of time available for adjusting them. Some discrepancies do exist, so that the resultant equalization will show some small errors. This is

borne out by Fig. 8d which represents a close approach to perfect equalization but with some errors as large as ± 5 or ± 6 db. These were the result of employing too few peak/notch filters to get perfect match in Fig. 8c, rather than of any failure of the method.

TESTING METHODS

Sweeping Sine Tests

Random noise simulation is expensive in both equipment and in man-hours required. For this reason, it has been only reasonable for industry to examine the possibility of substituting sweeping sine tests for wide band random tests. Since we have shown that in almost every instance the measured response of the typical test item is going to be different when subjected to sweeping sine than when subjected to wide band random noise, it is fairly obvious that equivalence of results can be expected only in a few special cases.

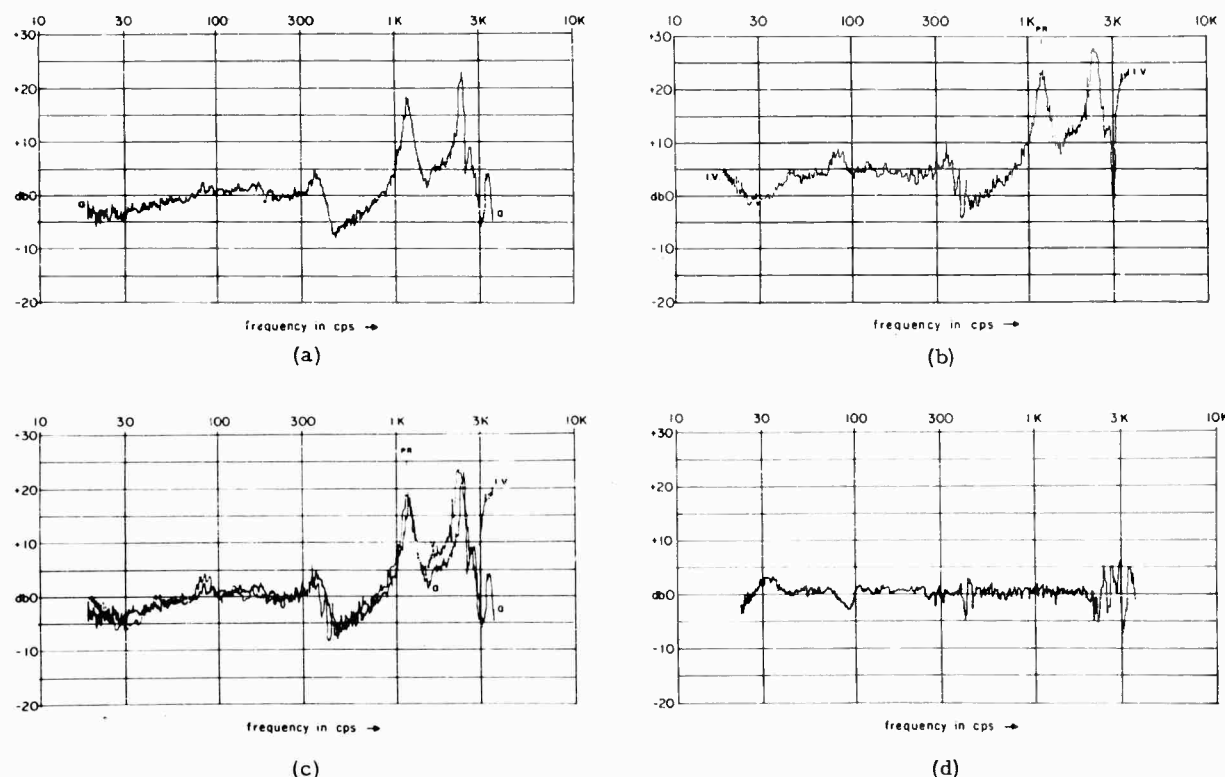


Fig. 8 - Equalizing Sample B to wide band noise response curve: (a) response at 10 g rms random vibration; (b) inverse voltage (IV) plot of console output as modified by equalizers to match (a); (c) comparison of (a) and IV curves showing where filters failed to give perfect match; and (d) resultant response of Sample B as equalized by equalizer adjustment to IV curve. The basic curve for Fig. 8 comparisons is the $G\sqrt{V}$ cps response of Sample B to an input of wide band random vibration with an output level measured at 10 g rms, 20-3000 cps.

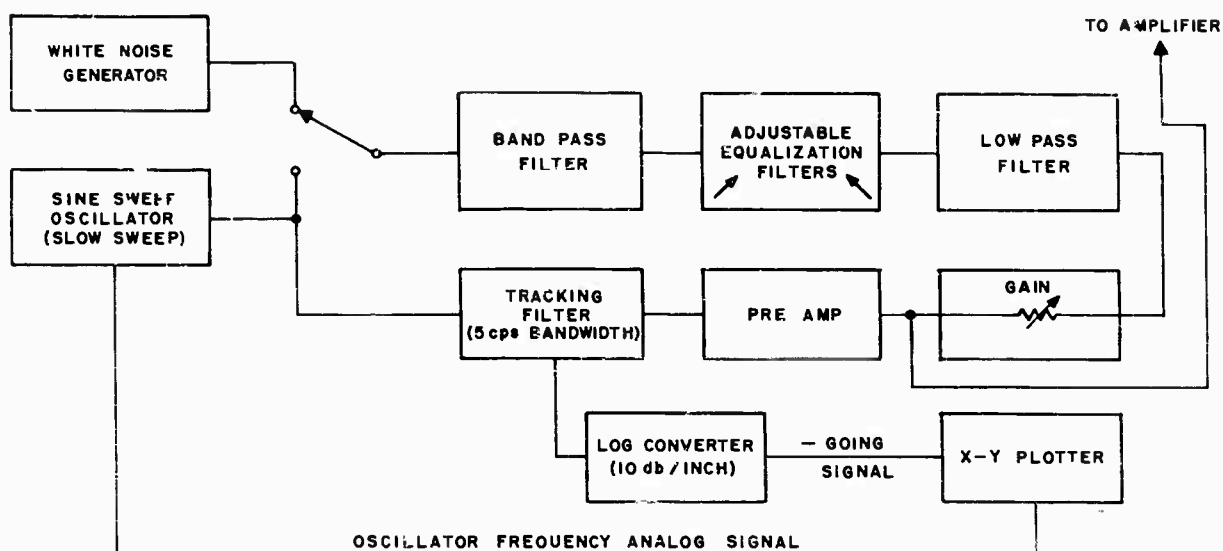


Fig. 9 - Connection diagram for achieving equalization to wide band random response curves

Partitioned Random Tests

Many environmental laboratories have equipment suitable for random noise simulation, but are faced with the problem that modern test specifications frequently involve higher specification power spectral densities than were prevalent in the past. Often the situation is further complicated by heavier test items. As an alternative to purchasing equipment with more force capability, environmental laboratories are considering the practicability of substituting scanning random tests or segmented random tests for a broadband random test covering the required spectrum in one step.

A series of experiments was devised to examine the effects of segmenting random noise spectra into two or more parts covering the total frequency range, and to attempt to arrive at suitable dividing boundaries for the partitioning process. Figure 10a shows the test item response to the unsegmented random noise from 20 to 3000 cps. Figure 10b shows the test item response when the high end is partitioned at 2000 cps, a frequency above PR (at 1200 cps). The shape of the response curve below the partitioning boundary remains unchanged. Figure 10c shows the test item response when the high-end boundary is lowered to 1000 cps, a frequency below PR. In this case, failure to include the PR peak within the segment has altered the frequency response within the segment, producing an excessive low-frequency rolloff. Since it now appears that the

low-frequency segment should include PR within its boundaries, it is necessary to know if the same requirement applies to the high-frequency segment. This was determined as follows:

Figure 10d shows the test item response when the low-end boundary is set at 600 cps to include the PR peak within the segment. The portion of the response well above 600 cps is seen to match the broadband response. Figure 10e shows the test item response when the low-end boundary is set at 1500 cps, so as to be above PR. Again, the portion of the response well above 1500 cps is seen to match the broadband response. In this instance, it is not necessary to include PR within the boundaries of the segment.

In the case of substitution of scanning random tests for wide band random noise tests, one is forced to raise the question of what is likely to be gained over sweeping sine tests. It would appear from the evidence accumulated at this laboratory that very little is to be gained unless the scanning random is broadband, indeed. Originally it was thought that if the scanning random bandwidth would include the first two even and first two odd overtones of the fundamental (a bandwidth of approximately $2 \frac{1}{3}$ octaves), reasonably good equalization would probably result. A glance at the results of segmenting random noise, as demonstrated above, raises serious doubt as to the validity of any test segment below PR which does not include PR.

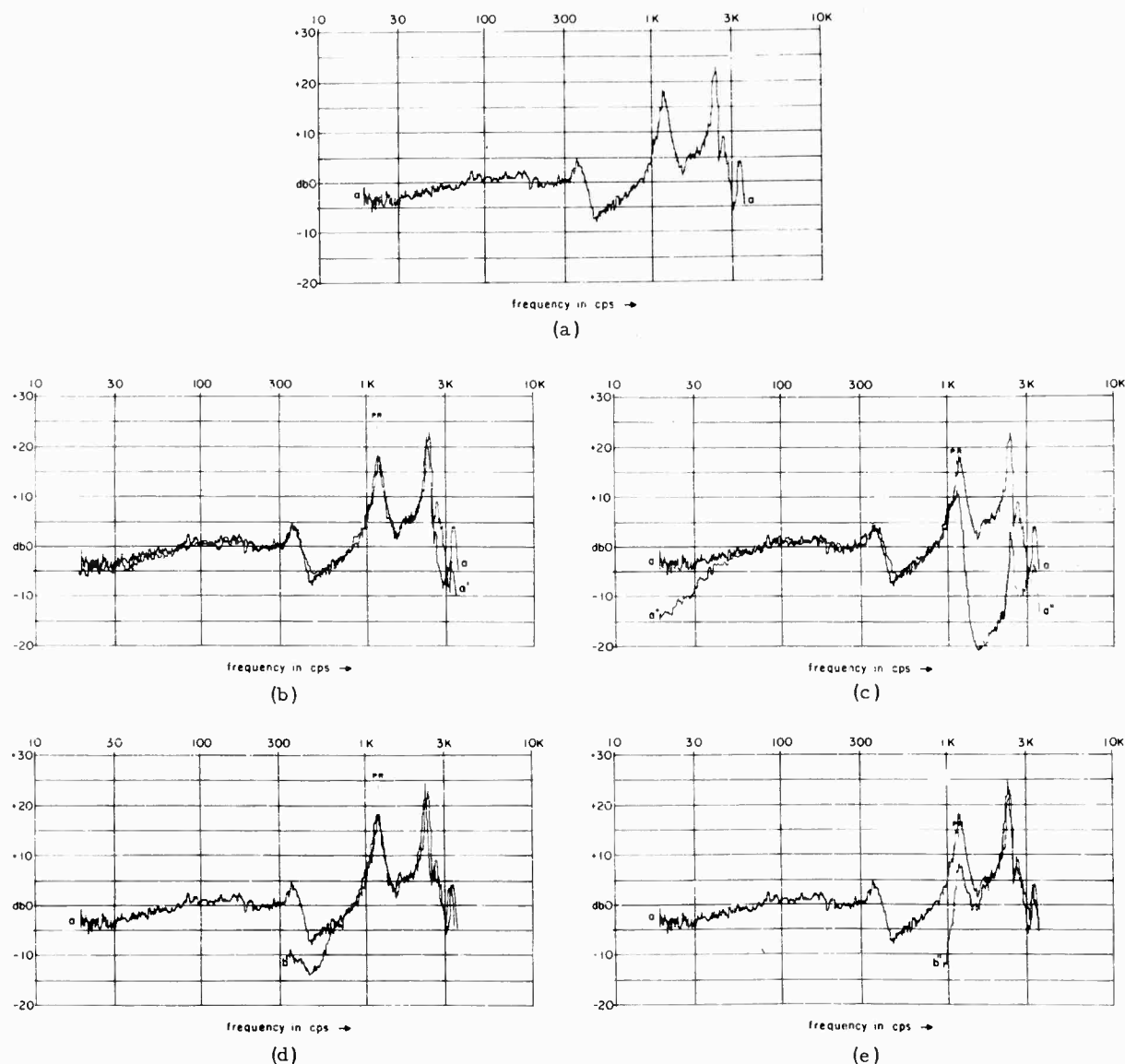


Fig. 10 - Effects of segmenting random noise, Sample B: (a) response a at 10 g rms random vibration; (b) response a' compared with a, if high-end cutoff is reduced from 3000 to 200 cps; (c) response a'' compared with a, if high-end cutoff is reduced from 3000 to 1000 cps; (d) response b' compared with a, if low-end cutoff is raised from 20 to 600 cps; and (e) response b'' compared with a, if low-end cutoff is raised from 20 to 1500 cps. The basic curve for Fig. 10 comparisons is the $G\sqrt{V}$ cps response of Sample B to an input of wide band white random vibration with a measured output level of 10 g rms, 20-3000 cps.

Testing With Parallel Bandpass Filter Systems

Automatic equalizers (and some manual equalizers with parallel bandpass filters) employ parallel bandpass-type analyzers with matching bandwidths. It is possible for a mechanical resonance to have a bandwidth much narrower than that of the filters. In this case, it is likely that the resonance will not be properly equalized, but that the matching analyzer will not indicate any error. For this reason, it is wise to check new fixtures with a second analyzer of narrower bandwidth on the first equalization attempt. Ideally, the bandwidth should be very narrow (of the order of 1- or 2-cps bandwidth) but such bandwidths involve extremely long analysis times. Usually, it is sufficient to check with an analyzer bandwidth that is substantially smaller than that of the parallel bandpass filter analyzer that is being checked. Bandwidths of the order of 5 to 10 cps are normal for this purpose. If no apparent difference in results is recorded, the original equalization should be adequate.

Systems with bandwidths of 25 cps or narrower are not nearly as prone to the type of error under discussion as are some of the wider bandwidth types. It should be realized, however, that narrower bandwidths are required for equalizing low-frequency resonances than for equalizing resonances at the opposite end of the spectrum. This situation arises from the fact that natural mechanical resonances tend to cluster around constant Q , rather than constant bandwidth limits, and this leads to very narrow bandwidths at the low end of the spectrum even if the test item resonance is of only average Q . The majority of resonances fall within the Q range of 3 to 30. Very few show Q 's in excess of 50.

Whether or not the user buys very narrow bandwidth filters at the low-frequency end will depend on his estimate of whether he will need to equalize any large test items with low-frequency resonances. Filters with somewhat wider bandwidths may be employed where the only function is general shaping. Conversely, the user may still find it necessary to buy quite narrow bandwidth filters at the high-frequency end, if he anticipates test items with high Q resonances in this frequency region. Items with high Q resonances also require additional dynamic range from the equalizer. Ranges of 50 db or more may be required with some test items, especially in the case of stepped spectral specifications.

Fixturing and Monitoring

The art of designing and using fixtures is too involved to more than scratch the surface in the space devoted to it here, but a few comments may not be out of order.

The test item is usually mounted to some basic fixture plates at three or more attachment points. When these attachment points are distributed in such a way as to make it feasible to use a single plate, this arrangement is desirable. Even when a single plate is possible, it may be difficult to assure equal inputs at all mounting points. One way to improve the chances for this desirable situation is to place the attachment points as symmetrically as possible on a mounting plate that is in itself symmetrical in a plane transverse to that of the forcing vibration function. Plates that are circular, square, or in the form of the other regular polygons are suitable. If, by careful fixture design, equal inputs at all attachment points are achieved, any location immediately adjacent to these points may be used for the monitoring accelerometer for equalization or for monitoring sine vibration. If this equality is not achieved, worst-point monitoring may be used, or the technique of averaging outputs of accelerometers adjacent to each attachment point to form one electrical signal may be a desirable substitute [2,3].

It is desirable to place all fixture resonant frequencies substantially higher than the top frequency limit of the specification, but when this is impossible, a satisfactory equalization can usually be achieved if there are no pronounced notches in the response curve within the frequency limits of the specification. If these notches occur, they do not necessarily mean a failure on the part of the fixture to absorb energy from the shaker at the notch frequencies. This condition usually indicates that the fixture is absorbing energy in such a way as to produce "oil-canning" or vibration in a direction transverse to the desired direction. Another cause of notches may be the absorption of energy in exciting harmonic or subharmonic modes rather than fundamental modes. The presence of major notches in the response curve of the fixture is a cause for real concern until the extent and nature of the energy absorption is understood and verified to be below acceptable limits for any undesirable modes that may have been excited. A cross-mode vibration greater than 100 percent of the in-line mode is usually considered to be excessive.

When equalization is first attempted on a new fixture, it may be desirable to use a three-axis accelerometer and to analyze the cross-mode response. This practice is particularly recommended when automatic equalization is employed, as the servo will attempt to cancel the notch if this is at all possible. If the notch is caused by cross-moding, the test item may be overtested or even destructively tested along an axis other than the test axis. The only recourse the test engineer can follow upon discovering such a situation is to place the affected channel in the manual mode and reduce the drive to acceptable limits. If this results in excessive notching, he may obtain a deviation by showing the cause of the notch, or he may alter the fixture to remove the problem. Although this problem may be more dangerous with an automatic equalizer because it is more easily overlooked, its solution must be accomplished with any type of equalizer employed.

Since a parallel bandpass filter equalizer with appropriate bandwidths and sufficient dynamic range will "equalize" almost any fixture, there is a natural tendency to slough off the nastier problems of good fixture design on the basis that equalization will take place even if the fixture is not very good. We have just seen that what this attitude really means is that we can excite undesirable modes in the fixture to almost any extent and thereby invalidate the test.

It has been pointed out that a failure to fill a notch may be caused when the energy is being absorbed in harmonic or subharmonic modes. When this occurs, the energy appears as mysterious "unequalizable" peaks at the harmonic or subharmonic frequencies. These peaks cannot be notched out unless the energy is subtracted at the fundamental rather than at the peak frequency.

An even more exotic response has been noticed in a few cases. A fixture may act as a highly nonlinear device. In this case, two prominent signals of different frequencies may mix to form sum and difference peak frequencies, also "unequalizable." In certain cases, the sum frequency peak may lie higher in frequency than the frequency of any energy being supplied to the system. Peaks of this sort will disappear when either of the causative frequency components is removed. An investigation will usually show that the causative components are high level inputs being used in canceling notches.

It is obvious that the existence of drastic response notches usually points to equalization troubles and to fixture design inadequacies.

Dummy Loads

If the test item mass is a substantial fraction of, or is greater than, the holding fixture mass, the holding fixture resonances may shift appreciably in frequency after the test item is mounted in place. If the test item has a stiffening effect on the fixture, other aspects of the fixture response curve may change as well. For this reason, empty-fixture equalizations should be rechecked with the test item in place. The best solution to problems in this area is better holding fixture design with fixture-mass to test-item-mass ratios of 5/1 preferred, or 3/1 if at all possible. However, this ideal solution is not always possible. In some instances, it is known in advance that empty-fixture equalizations will be invalidated when loaded with the test item. In this case, equalization may require that the test item be mounted on the fixture. To preserve the test item from damage during equalization, three alternatives may be pursued:

1. The test item and fixture may be exposed to a short burst of a few seconds of white random noise input band limited to the specification limits and regulated to give an accelerometer output level equal to the specification output level. This short burst is tape recorded and formed into a loop for analysis. This analysis yields the plot for the unequalized response, and the inverse of the equalizer filter output voltages may then be matched to this plot as previously described. This protects the test item by limiting the time of exposure to possibly damaging vibration.

2. The level of the white random noise input may be reduced well below that of the test specification to obtain the unequalized response directly or from a short-burst tape recording, as described above. The results of equalization to a reduced level should always be checked at the full level, as some discrepancies may occur when the level is shifted.

3. The real test item may be replaced with an inert dummy test item which has the same mass, center of gravity, and moments of inertia as the real item. By specifying an inert test item, the intent is to construct a dummy load in which all major resonances within the frequency range of the specification have either been eliminated or damped to very low levels. It is quite difficult to construct dummy loads with these requirements by machining and assembling solid pieces. Where the real unit has an outside case, very satisfactory dummy loads have been constructed by filling a spare case with sand mixed with other granular materials

to provide the proper mass. Partitioning or the addition of local masses may be required to locate the center of gravity properly or to provide proper moments of inertia. The inert dummy is often better than the real test item for testing fixture loading because it eliminates the possibility of test item resonances feeding back into the fixture.

In all fairness to automatic equalization, it should be mentioned that some types of automatic equalizers permit a gradual increase in gain with continual servo action to correct response shifts as the test level is gradually raised to the specification requirement. Pre-calibration of the specification requirements under a no-shake condition is especially desirable in this connection. With these types of automatic equalizers, the precautions used to protect the test item from unequalized shakes as outlined above are no longer required, provided always that the fixture does not have cross-modes, harmonic or subharmonic modes, or intermodulation modes.

CONCLUSIONS

Equalization to wide band white noise inputs is the applicable method for series-type peak/notch equalizers, as well as for parallel bandpass-type manual and automatic equalizers. A satisfactory method of performing this task for series-type peak/notch equalizers has been devised.

The converse of the above proposition is equally true — narrow band sweeping sine or scanning random inputs are not generally applicable to all equalizations. They are satisfactory in some special, and usually simplified, cases. In reviewing the curves in this paper, it may appear that the region of discrepancies is small because of the logarithmic frequency scale employed, but close examination reveals that these regions occupy 30 to 60 percent of the total spectrum.

We cannot equalize satisfactorily to narrow band input methods and cannot get correlation between their response curves and those generated by wide band random noise; therefore, they do not seem to be justifiable as substitute tests for wide band random noise tests.

The only method of reducing the bandwidth of wide band random noise tests that seems to hold much promise is the segmented noise test. However, the segment boundaries cannot be chosen arbitrarily. The lowest segment must have an upper limit above PR. The higher

segments do not require the inclusion of PR on the basis of present evidence and, if more than one segment is used, it appears that the next boundary can be chosen on an arbitrary basis. This approach should be viewed as highly tentative at the present time, and should be investigated in considerably more detail. It is possible, for example, that successive members of a test item would act as a series of consecutive PR's and would have to be treated accordingly. This would explain why a test item such as a relay mounted on a partition, which is part of a black box mounted to a fixture on a shaker, gives such radically different results when subjected to random rather than sine vibration [4,5]. It is hoped that mobility methods may eventually yield exact mathematical models of the observed phenomena.

Parallel bandpass-type equalizers offer tremendous advantages in speed and efficiency of equalization. It is necessary for the buyer to specify bandwidths and dynamic ranges compatible with the characteristics of anticipated test items. Some types of automatic equalizers protect the test item during the equalization process, provided the fixture does not have cross-modes, harmonic or subharmonic modes or intermodulation modes.

Fixture design must be conscientiously perfected for good testing. The presence of deep notches in a fixture response curve usually indicates the presence of undesirable modes caused by inadequate fixture design. These modes can result in severe overtesting or even in destructive testing.

Although automatic equalizers offer many advantages, some precautions are necessary in their use. They tend to conceal the presence of notches in the fixture response, so some check on spurious modes should be made to avoid the dangers just mentioned. They tend to show perfect equalization of high Q resonances much narrower than the bandwidth of the system filters, whether or not the equalization is correct. Some checks with a narrow band analyzer should be made under these conditions.

ACKNOWLEDGMENTS

The encouragement and advice of Otto Altman, Head of the Environmental Test Laboratory at Lear Siegler, Inc., is gratefully acknowledged. Cornelius Van Zoest performed some of the early experiments that led to our investigation of proper equalization techniques, and originated several suggestions which were of much help in its completion. Philip Sweeney

helped with some of the last experiments performed. Thomas Friederich and various other persons in the Environmental Test Laboratory

and in other Departments helped with the illustrations and reproduction of this paper. Their help is greatly appreciated.

REFERENCES

1. Galt B. Booth, "Sweep Random Vibration," Proc. IES (1960).
2. K. Putkovich and Henry W. Holsopple, "Use of Averages in Control of Vibration Testing," Proc. 2nd Envir. Symposium (Ordinance) (1962).
3. Roland E. Seely, "A Vibration Control Accessory For Use With Tracking Filters," Proc. IES (1963).
4. Collins Radio, "Random-Sinusoidal Vibration Correlation Study," WADD Tech. Note 61-23 (DDC No. AD 267 509).
5. Hughes Aircraft Co., "An Investigation of Functional Failure Due to Random and Sinusoidal Vibration," WADD Tech. Note 61-24.

* * *

VIBRATION MEASUREMENTS

R. W. Mustain
Douglas Missiles and Space Systems Division
Huntington Beach, California

A general discussion of desirable methods and systems for the collection of vibration information is presented, including a brief review of previously used and presently available methods of transducing, transmitting, and calibrating dynamic excitations. Vibration instrumentation techniques applicable to flight tests and to laboratory vibration tests are studied. Calibration methods and circuits are reported, with special attention given to end-to-end calibrations of complete systems. The usage of parallel end-to-end calibrations is recommended, and empirical data are presented which show the effects of different attenuators in parallel end-to-end calibrations.

The limitations of telemetry systems are considered. Various telemetry systems are available for the transmission of flight data. Because of the diverse instrumentation requirements of aircraft, missiles, and space vehicles, no single telemetry package, with fixed capabilities, will satisfy even a majority of applications. Several of the telemetering systems are described. Measurement of mechanical impedance is briefly discussed. Impedance measuring techniques are reported, and suggestions are given for obtaining reliable impedance measurements.

INTRODUCTION

The eminence of vibration measurements has increased during the past decades with each advance in aircraft, missiles, space vehicles, and propulsion systems. For instance, the transition from one type of propulsion system to newer and more powerful units has resulted in greater flight velocities, larger payloads, system complexities, and intensification of dynamic environments.

The trend to greater power plants has accompanied the tremendous expansion of the aerospace industry through two world wars, the Korean War, and one major depression. World War I provided the first real encouragement in this rapid development as the airplane began to revolutionize warfare. In the 1920's and 1930's, the advent of in-line and powerful radial engines created noticeable vibration problems and minor acoustic enigmas. With the World War II, the airplane came into its own as a mighty weapon of attack and destruction. The accelerated developments of this second major conflict produced manned aircraft which were complex systems with powerful engines capable of

inducing relatively large vibrations. Furthermore, development of delicate airborne electronics for controls and guidance created components with low fragility levels. A notable transition in aircraft engines occurred near the end of World War II when the first jet-propelled aircraft appeared (the P-59 and the P-80) to present a new dynamic environment encompassing troublesome acoustic excitations. In due time, the dynamic engineers became acquainted with the many pitfalls of the jet engines and their attendant vibrations that caused failures of equipment, systems, and structures.

It was during this period, in the 1940's, that some of the first airborne recordings of vibration data were obtained. It was then that recording oscillographs with string-type galvanometers were first utilized to collect vibration data transduced by potentiometers, strain gages, and variable reluctance pickups. The potentiometer accelerometers provided data at very low frequencies and were used rather unsuccessfully to record aircraft maneuvers, landings, and takeoffs. The most useful and meaningful vibration data were obtained during this period by the utilization of

strain gages. These data consisted of structural loads measured with bonded strain gages and dynamic excitations reproduced rather faithfully by unbonded strain gage accelerometers. Bonded strain gages were used in great quantities on various aircraft for many purposes. For example, loads on longerons, spars, frames, panels, landing gears, landing hooks, and similar items were measured by the application of strain gage elements smaller than postage stamps. Many unique schemes were devised to take advantage of these small devices. Bonded strain gages were cemented to Bourdon tubes, rudder pedal links, control sticks, and special beams to measure pressure, rudder forces, stick forces, and relative position, respectively, in flight test aircraft. The unbonded strain gage accelerometers (considerably larger than the bonded gages) provided electrical signals of semistatic aircraft motions and structural vibrations. The useful frequency range, in general, of these unbonded seismic elements ranged from dc to somewhere around 100 cps. These unbonded strain gage accelerometers became the first real work-horse instruments for the definition of aircraft vibration environments.

Simple calibration techniques were the rule of the day for these early instrumentation systems. For instance, it was accepted procedure during the 1940's to perform only zero g, +1 g, and -1 g static calibrations within the aircraft. These static calibrations were accomplished by turning the accelerometer around physically while it was connected to the balancing circuit and the recording equipment. Also, additional calibration steps were provided by precision calibration resistors connected across the strain gage bridge. However, these calibrations resulted in static or dc values only and, consequently, yielded no information on the frequency response of the system.

The last decade has seen the space age become a reality with its multistage vehicles and its thunderous rocket engines producing thrusts in the millions of pounds. Phasing into the high-thrust rocket systems created severe shock, vibration and acoustic environments. The previous engines had produced some difficulties, but these difficulties were magnified by several degrees in the missile and space programs. These conditions enhanced the value of defining dynamic environments. Since it was apparent that dynamic excitations existed (both in jet aircraft and rocket-propelled vehicles) well above 100 cps, it became highly desirable to develop instrumentation systems with

high-frequency characteristics [1]. This impetus resulted in noticeable advancements in vibration measurements during the 1950's. This rapid advancement led to the popular acceptance of piezoelectric accelerometers with their inherently higher frequency response. Concurrently, advances in electronics and recording media augmented the piezoelectric capabilities to create inestimable improvements in the measurement of dynamic environments. Thus, the 1950's and the early 1960's have seen the profitable use of high-fidelity magnetic tape recordings, with and without telemetry systems, to compile immense amounts of vibration data from aircraft, missiles, and space vehicles.

Because there is a never-ending quest for information and improvements on vibration instrumentation, this report continues with a general discussion on methods and systems for the collection of vibration data. This discussion includes a brief review of previously used and presently available methods of transducing, transmitting, recording, and calibrating dynamic excitations. System parameters and procedures that will prevail within the next few years are described and recommended.

TRANSDUCERS AND CONSIDERATIONS

Many variegated versions of transducer elements have been developed for the purpose of converting mechanical motions into equivalent electrical signals. These elements include strain gage, piezoelectric, variable inductance, variable capacitance, variable resistance, and magnetoelectric instruments. Although most of these elements have been used in various instrumentation systems to measure vibrations, the elements that have provided the most satisfactory vibration measurements are the strain gage bridge and the piezoelectric crystal. In general, the bulk of vibratory measurements in aircraft, missiles, and space vehicles has been compiled by utilization of these two devices. In environmental laboratories, the strain gage and the piezoelectric sensors have been augmented by the self-generating velocity transducer. However, these self-generating (magnetoelectric) transducers are rapidly being replaced in most environmental laboratories by piezoelectric accelerometers with their inherently higher frequency response.

Primarily, the unbonded strain gage element owes its remaining popularity as an accelerometer to its low-frequency response.

NOTE: References appear on page 43.

Of all the practical sensing elements, the unbonded strain gage accelerometer provides the best response in the low-frequency end, for this element is useful down to dc. Thus, the strain gage accelerometer, on occasion, is specified in place of, or in support of, the piezoelectric accelerometer to investigate low-frequency motions. The strain gage is defined as an element, or group of elements, which change resistivity as a function of applied stress. The unbonded strain gage accelerometer consists of four fine wires or filaments arranged so that two wires are stretched (tensioned) and two wires are relaxed (contracted) upon application of the force being measured. The application of tensile force to a filament increases the length, decreases the radius, and increases the resistivity of the filament. These changes are related to Poisson's ratio, $(\Delta r/r)/(\Delta L/L)$, where r is the radius and L is the length of the filament. The utilization of the stressed filament is based on the above effects of strain on the electrical resistance of the filament. The change in resistance ΔR is a function of strain, $(\Delta L)/L$, i.e., increased resistance for tension and decreased resistance for compression. In usage, the strain gage wires or filaments are connected electrically to form a Wheatstone bridge. The active elements are wired so that opposite legs of the Wheatstone bridge increase or decrease their resistance at the same rate for a given mechanical input. The greatest sensitivity of the strain gage Wheatstone bridge is attained when two opposite legs are in compression (decreasing resistance) and when, simultaneously, the other two legs are in tension (increasing resistance) (Fig. 1). Electrically, under these conditions, the results are additive in the Wheatstone bridge, and thus, the four active legs, correctly wired, provide the greatest sensitivity of the

Wheatstone bridge. In this case, the output voltage, E_0 , is a function of the algebraic factor,

$$\frac{\Delta R_1}{R_1} - \frac{\Delta R_4}{R_4} + \frac{\Delta R_2}{R_2} - \frac{\Delta R_3}{R_3}$$

Whereas the unbonded strain gage is used to measure accelerations, the smaller bonded strain gage is admirably suited to establishing fatigue criteria on panels and structural members. Strain-gaged panels have been used to study fatigue failures caused by extreme pressure fluctuations associated with high-intensity acoustic excitations from jet and rocket engines.

In 1880, Pierre and Jacques Curie founded the science of piezoelectricity when they discovered that certain crystals generated an electric charge when compressed in particular directions. The Curie brothers noted that the charges were proportional to the applied pressure and disappeared when the pressure was withdrawn. They observed the piezoelectric effect on zinc blende, sodium chlorate, boracite, tourmaline, quartz, calamine, topaz, tartaric acid, cane sugar, and Rochelle salt. Since that time, over 1,000 piezoelectric crystals have been identified [2]. Some of the materials investigated for their ability to perform as piezoelectric accelerometers are barium titanate, lead titanate—lead zirconate, ammonium dihydrogen phosphate (ADP), potassium dihydrogen phosphate (KDP), quartz, lithium sulfate, lead metaniobate, Rochelle salt, and tourmaline. These materials contain crystal domains oriented in the same direction, either by nature or by polarization during the manufacturing process. When stress is applied to

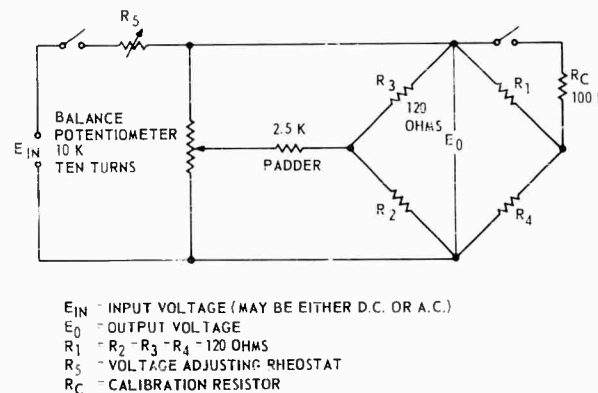


Fig. 1 - Typical strain gage circuitry

these piezoelectric materials, minute motions of the crystal domains generate electrical charges Q proportional to the applied force [3,4]. A strain ϵ causes an electric polarization equal to the strain times an appropriate piezoelectric stress coefficient. Similarly, an electric field causes a piezoelectric stress equal to the electric field times the piezoelectric stress coefficient. Figure 2 [5] shows a simplified test circuit for the measurement of open circuit crystal voltage. The following relationship applies:

$$Q_p = E_M (C_p + C_d + C + C_M) \quad (1)$$

The crystal open circuit voltage $= E = Q_p / C_p$ and the energy $= 1/2 Q_p E_p = 1/2 C_p E_p^2$ expressed in joules.

The importance of obtaining high-frequency vibration measurements has resulted in the general selection of piezoelectric accelerometers for most aircraft, missile, and space vehicle applications. These self-generating crystals have the ability to reproduce faithfully high-frequency excitations. The frequency range of the piezoelectric accelerometer is a function of the type of material, the mechanical design, and the desired sensitivity. Elements have been made with natural frequencies as high as 90 kc [6]; however, most environmental

vibration tests have been limited to 2000 cps, and supporting field data have not greatly exceeded this limit. A partial cause for this limitation has been the lack of telemetry systems with responses greater than 2100 cps. Recent developments in single sideband telemetry have resulted in frequency ranges from 50 cps to approximately 3000 cps. Satisfactory magnetic tape recorders are available with FM electronics for recording from dc to 20,000 cps. Presently, the response range of commercially available piezoelectric accelerometers is indeed adequate for vibration measurements. Piezoelectric elements have been developed as integral impedance heads for the measurement of the "esoteric" parameter of mechanical impedance. The measurement of mechanical impedance is becoming a requirement throughout the aerospace industry.

Any consideration of the application of accelerometers must encompass various characteristics influencing the quality of the data to be obtained. The user and the maker of accelerometers are concerned with fundamental characteristics such as frequency response, linearity, axial sensitivity, transverse effects, response to acoustic excitations, temperature effects, vacuum effects, shock fragility, and vibration fragility. In addition, other factors such as transducer location, impedance matching, recording media, method of transmission, method of installation, service life, storage life, and reliability are of primary interest to the user.

An indication of expected values of pertinent transducer characteristics can be obtained by examining Table 1 which gives data on some of the piezoelectric accelerometers that are available commercially. No one accelerometer is capable of matching the transducer characteristics given in this table. The values listed are the extremes of many different accelerometers taken from commercial literature. From this array of characteristic ranges, the transducer best suited for the task can be selected.

The location of sensing elements is dependent on the particular environmental problem. Pickups may be required to establish panel fatigue criteria, to measure vibration response of primary structure, and to measure the response of equipment in dynamic environments. Panel fatigue criteria are best measured by bonded strain gages. Response can be determined by the use of accelerometers.

Obviously, panel fatigue studies are best obtained with bonded strain gages applied at the point of greatest stress. The exact method of

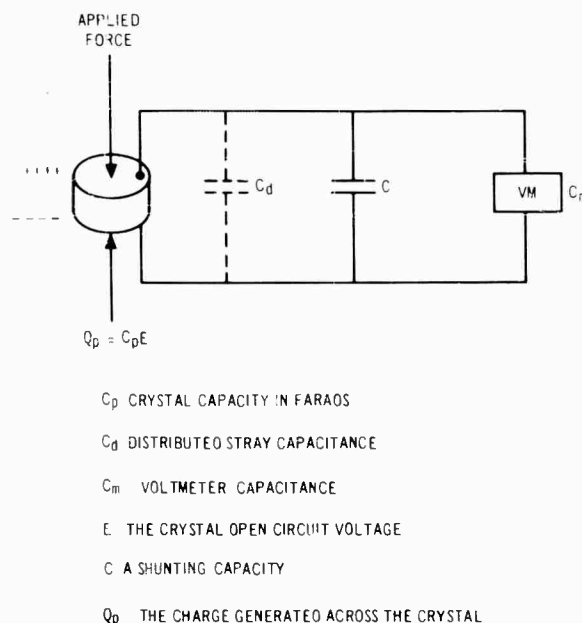


Fig. 2 - Simplified test circuit for measurement of open circuit crystal voltage

TABLE 1
Characteristics of Some Commercially Available
Piezoelectric Accelerometers

Characteristic	Value
Dynamic range (g)	10 ⁻⁵ - 10 ⁵
Frequency response (cps)	0.1 - 32,000
Temperature range (°F)	-452 - +750
Linearity (%)	±0.5, ±1, ±2
Sensitivity (Mv/g)	0.5 - 3500
Lowest resonant frequency (kc)	1.6 - 140
Transverse sensitivity (%)	±0.25, ±.5, ±1, ±3, ±5
Acoustic response at 155 db SPL (g)	0.01 - 0.1

locating the strain gage will vary with each type of panel. Gages should be located adjacent to fasteners, rivets, and boundaries of panels. Most panel failures caused by acoustic excitations will tend to propagate outward from rivet and fastener lines. It is also useful as a method of monitoring panel response to place strain gages in the middle of panels where the greatest deflection occurs and where there are no steep stress gradients. In laboratory tests, this serves as a warning of impending trouble.

The determination of vibration gradients through aircraft, missiles, and space vehicles can be accomplished by placing accelerometers on primary structure. Accelerometers, with a minimum of bracketry, should be mounted on heavy members such as spars, longerons, intercostals, and rigid ring frames. The location of accelerometers on skin panels should be avoided for this will produce data with panel resonances. The primary structure serves as a better reference for future investigations and tests. Figure 3 shows an ideal installation of accelerometers on primary structure. Accelerometer mounting blocks are not used. Whenever possible, environmental simulations in the laboratory should be referred to flight or field measurements obtained on primary structure. The measurement of the vibration environment surrounding individual critical items can be established by installing accelerometers on the critical items' supporting structure. Where equipment is mounted on flimsy structure, measurements should be obtained on both the flimsy structure and on the nearest rigid structure. This recommendation is made so that laboratory tests will correlate with flight and field tests. Laboratory vibration tests are difficult to control when the control accelerometer measures the response of soft structures such as skin panels. It is more desirable to control on rigid primary structure; therefore, the vibration test specimen should, if practicable, include rigid primary structure.

The selection of accelerometer locations for optimum control of shaker equipment deserves additional discussion. Figure 4 displays a vibration test specimen with numerous accelerometers. The test specimen consists of a large fiberglass panel, with electronic equipment, which is mounted on special vibration isolation strips and supporting structure. The supporting structure consists of intercostals, ring frames, and vehicle skin. In turn, the supporting structure is secured to a strong magnesium fixture and an electrodynamic exciter with a force rating of 30,000 pounds. Accelerometers have been located to measure vibration inputs to the isolators, transmission across the isolators, response of the panel, and responses on some of the electronic equipment. If the vibration test criteria apply to the structure side of the isolators, where is the best place to locate the control accelerometer? The optimum test control occurs when all of the supporting structure is vibrating at the same vibration level. This is difficult to achieve, for there is only one shaker input; furthermore, the large specimen will display modes which will create various levels throughout the structure. Any method of control will provide only a compromise for the ideal test control. Improvements in control methods are always in order; new measuring devices, vibration surveys, experience, and good engineering judgment will tend to improve control conditions. With the specimen shown in Fig. 4, the control could be placed at several locations on the structure. As noted earlier, the control accelerometer should not be placed on the skin panel, for the response of the panel will not permit adequate control of the test. Fortunately, this specimen has relatively rigid boundaries: the ring frames and the intercostals. The test was conducted satisfactorily by controlling at the left upper corner (accelerometer No. 1) where the intercostal and the ring frame connect.

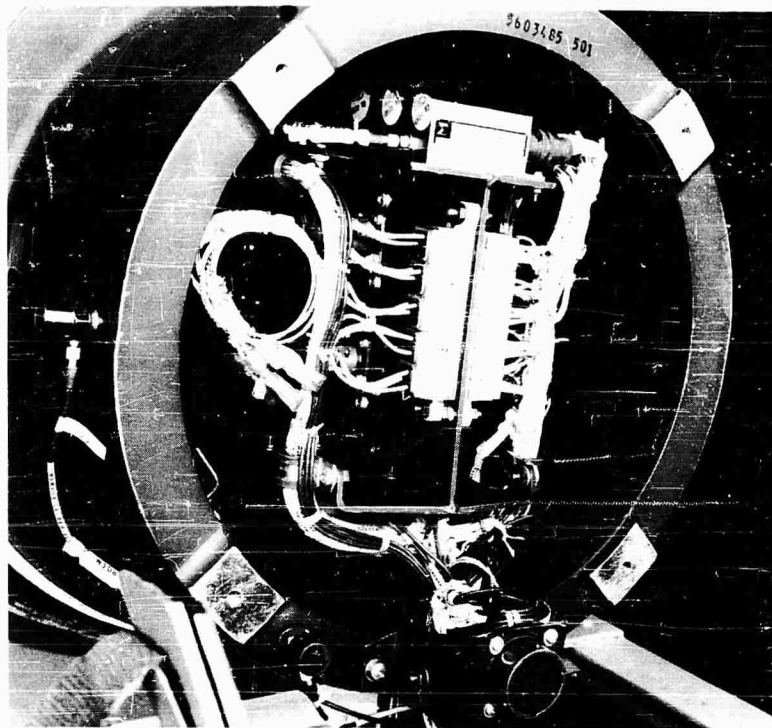


Fig. 3 - Ideal installation of accelerometers
on primary structure

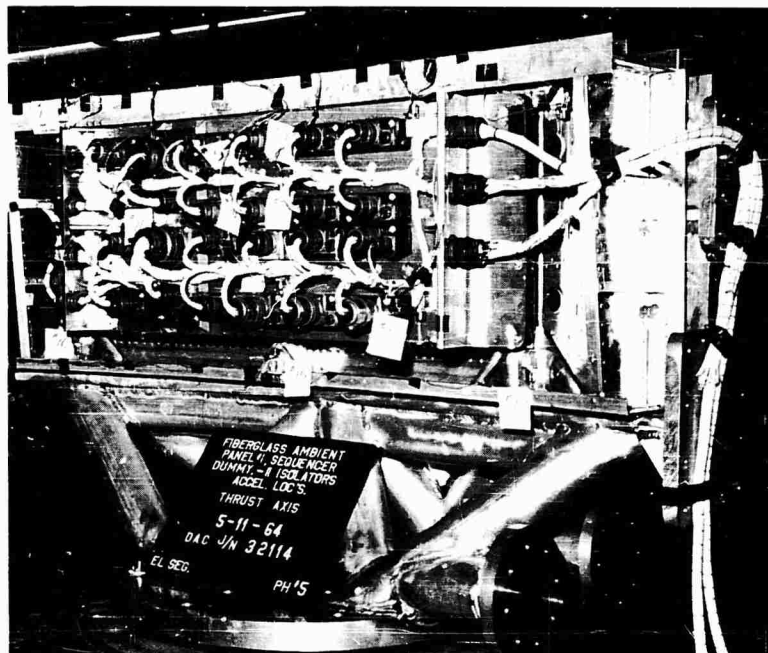


Fig. 4 - Accelerometer locations on typical
complex vibration test

Commercially available maximum amplitude and averaging control circuits were not used during the above vibration test because limitations were found in both of these instrumentation systems during previous tests. The maximum amplitude control circuit selects the largest of several (1 to 5) accelerometer signals for controlling the shaker servo system. The limitation of this particular system is the slow switching time of the electrical components which causes the shaker to generate harmful transients. Similarly, the averaging system causes transients in the shaker system when out-of-phase signals from the accelerometers add to an algebraic sum of zero. This zero signal has occurred with as many as four accelerometer signals being averaged. It is recommended that the maximum amplitude and averaging systems be improved electronically to eliminate their limitations. These improvements are a simple design problem for any competent electronic engineer. Transistor switching circuits are available which can provide the fast switching needed for the maximum amplitude control circuit, and rectification circuitry can be used to provide an absolute value for the averaging circuit. If it is desired to use the present averaging system without modification, odd numbers of accelerometers should be used to avoid the out-of-phase problem and the accelerometers should be placed on the specimens where known in-phase amplitudes occur.

AMPLIFIERS

Signals from dynamic transducers are transmitted to magnetic tape recorders either directly or through telemetry systems. Additional support is provided by amplifiers designed to match transducer impedances. The recording oscillograph, formerly the primary recording medium, has been delegated the role of displaying playbacks of magnetic recordings for examination of signal fidelity and dynamic time histories.

Amplifiers designed for dynamic instrumentation place certain limitations on the transmitted signal. The term "amplifier" includes cathode followers (primarily matching devices) and electronics used to increase the dynamic signals to levels satisfactory for transmission and recording. These units are available in miniaturized and transistorized versions with a range of characteristics. Table 2 shows the range of characteristics found in some of the presently available accelerometer amplifiers.

Since telemetry systems are used to transmit vibration data in most missile and space

TABLE 2
Characteristics of Some Available
Accelerometer Amplifiers

Characteristic	Value
Input impedance (megohms)	0.1 - 1000
Gain	0.90 - 500
Frequency response (cps)	1 - 100,000
Output impedance (ohms)	10 - 10,000
Linearity (%)	± 1 - ± 5
Gain stability (%)	± 0.25 - 5

vehicle applications, it is appropriate to present the specifications of an amplifier which produces the required 5-volt peak-to-peak signal for telemetry. Subminiature "charge" amplifiers suitable for telemetry have been developed by several of the accelerometer/amplifier manufacturers. The specifications for one of these amplifiers are as follows:

Source impedance:	not less than 50 M
Output impedance:	500 ohms
Bias:	$\pm 2.5 \pm 5\%$ vdc with 100 K load
Maximum linear ac output voltage:	± 2.5 v, nominal. Instantaneous out- put limited at 0 v $+ 0.05$ v / -0.00 v and 5.50 v ± 0.15 v.
Load impedance:	100 K or more
Charge gain:	2 to 20 mv output/ picocoulomb input
Frequency response:	$\pm 5\%$, -10% ; 3 to 10 kc $\pm 5\%$; 5 to 10 kc
Linearity:	$\pm 2\%$
Warmup time:	30 sec, maximum
Power:	$28 + 4$, -8 vdc at 20 ma, maximum
Dimensions:	$1 \times 1.115 \times 2.165$ in.
Weight:	95 grams nominal

Phase shift data on accelerometer amplifiers are displayed in Fig. 5 [7]. The upper curves represent the phase shift found in a typical cathode follower under no load and full load conditions. The lower curves are phase shift data for amplifiers with gains of 10 (solid line) and 100 (dashed line). It can be seen that the cathode follower with its impedance matching properties deviated less from ideal zero phase shift conditions. Response spectra of some amplifiers are shown in Figs. 6 and 7 [7]. Figure 6 shows the response for a galvanometer amplifier with an output of 110 ma into 10 ohms. The amplifier is flat from 15 to 1500 cps; however, this amplifier, with proper calibration techniques, can be used to encompass the frequency range from 5 to 10,000 cps. Figure 7

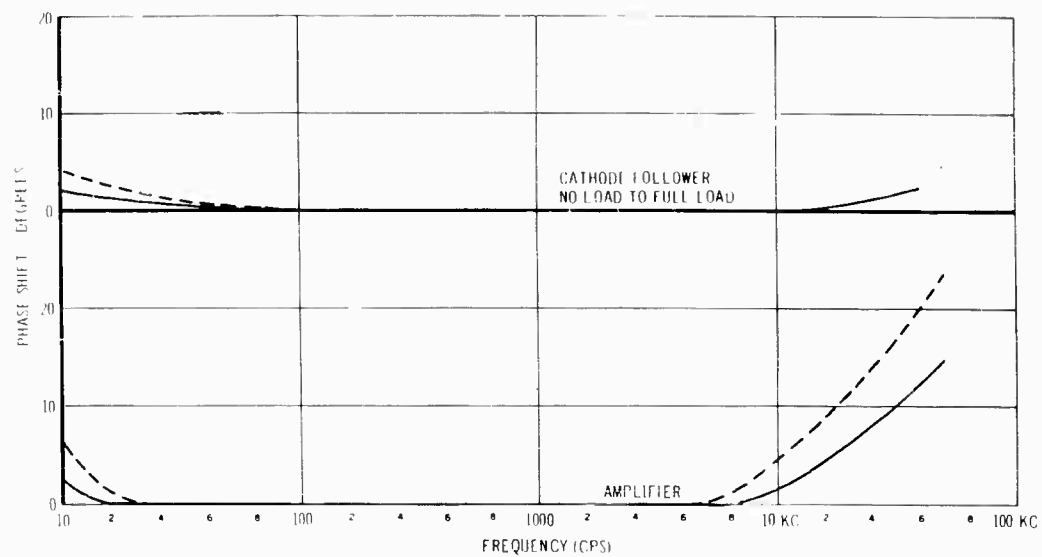


Fig. 5 - Typical phase shift of amplifiers

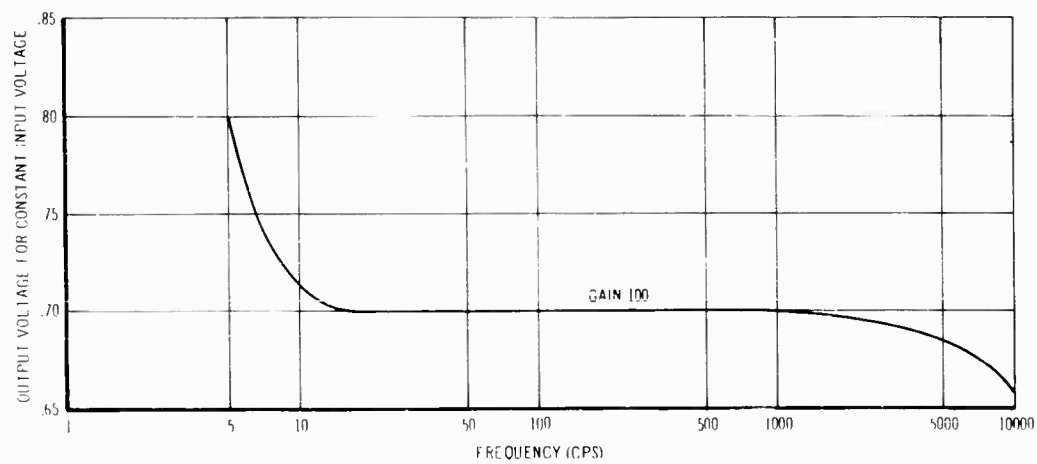


Fig. 6 - Typical frequency response of galvanometer amplifier

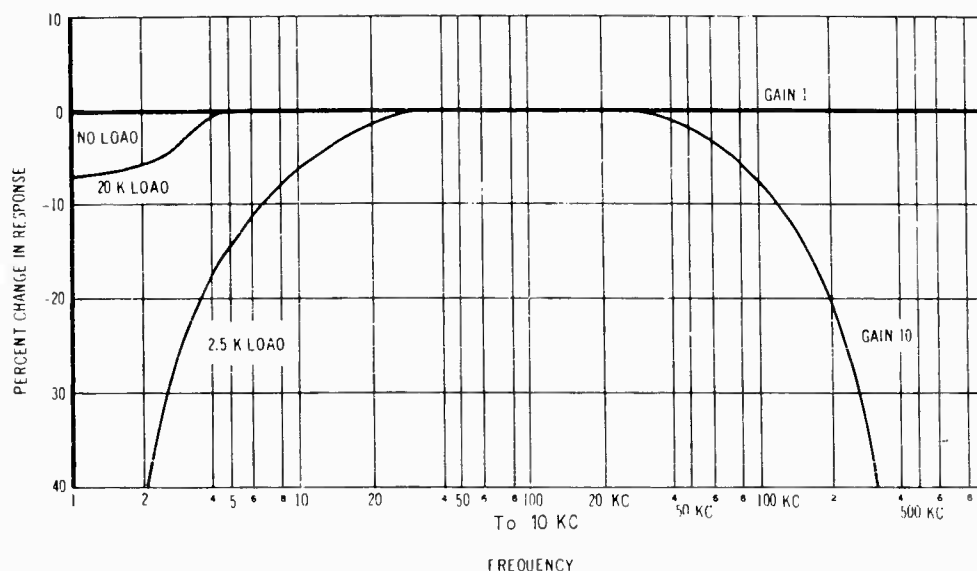


Fig. 7 - Response of laboratory amplifier

depicts the response of a laboratory amplifier used to obtain voltage gains of 1 and 10 with no loads down to 2500 ohms. The left side of the graph shows the effect of load on the low-frequency response of the amplifier. The amplifier's response rolls off with increased load below 30 cps. The right side of the graph shows the effect of gain on the high-frequency response of the amplifier. The amplifier's response rolls off with increased gain at frequencies above 30 kc. The no load/gain of 1 curve is essentially flat from 1 cycle to 500 kc. On the other hand, the 2.5-K load/gain of 10 curve rolls off rapidly from 30 to 2 cycles on the low end and from 30 to 300 kc on the high end. In spite of this, it is felt that usable data can be obtained from 5 to 150,000 cycles under these 2.5 K-load/gain of 10 conditions.

TELEMETRY

Whereas transducers and amplifiers have been discussed briefly, the next logical step is consideration of the advantages and limitations of telemetry systems. Various telemetry systems are available for the transmission of flight data. Because of the diverse instrumentation requirements of aircraft, missiles, and space vehicles, no single telemetering package with fixed capabilities will be satisfactory for all applications; however, the FM-FM system has been used widely to compile dynamic data. Following are some of the telemetering systems that are available:

FM	Frequency modulation
FM-FM	Frequency modulation—frequency modulation
SSB-FM	Single sideband—frequency modulation
DSB-FM	Double sideband—frequency modulation
PCM-FM	Pulse code modulation—frequency modulation
AM	Amplitude modulation
AM-AM	Amplitude modulation—amplitude modulation
FM-AM	Frequency modulation—amplitude modulation
PAM	Pulse amplitude modulation
PAM-FM	Pulse amplitude modulation—frequency modulation
PCM	Pulse code modulation
FSK-PCM	Frequency-shift keying—pulse code modulation
PSK-PCM	Phase-shift keying—pulse code modulation
PACM	Pulse amplitude code modulation
PACM-FM	Pulse amplitude code modulation—frequency modulation
PDM	Pulse duration modulation
PDM-FM	Pulse duration modulation—frequency modulation

The FM-FM system is the workhorse of aircraft, missile, and space vehicle telemetry; however, advancing missile and space vehicle data acquisition and transmission requirements will result in the utilization of other telemetry

systems. Recently, the PAM-FM system was used by one of the missile contractors to provide eight vibration channels of 2-kc response. The PACM combination has frequency response capabilities to 10 kc, according to its backers. The FM-AM system has been used for years by British engineers to supply 10- to 10,000-cps information over six simultaneous channels. A system is presently being used which employs the SSB-FM techniques. A new development is a DSB-FM telemetry system which provides wide band (dc to 3 kc) response. Most of the telemetry equipment used today is analog, but digital systems should play an important role in the future.

The British system, known as the Bristol High Frequency Telemetry System, is a FM-AM system which provides six continuous channels with a response from 10 cps to 10 kc with proper calibration. The calibration is necessary, for there is some falling off in response outside the 50- to 2000-cps band. The Bristol system has an accuracy of ± 5 percent for only the telemetering equipment. Bristol engineers have used barium titanate accelerometers with ± 5 percent accuracy (separate from the telemetry accuracy) and inductance transducers with ± 2 percent accuracy. The frequency of the Bristol system is within one percent. One

drawback of this British system is the limited range of 20 miles. The range can be increased by approximately 50 percent by reducing the usable bandwidth and by using only two channels. The range can be increased by 100 percent with the addition of low-pass filters attenuating above 2000 cps. In this system the subcarrier signal of each channel is FM modulated and the mixed subcarriers are used to amplitude modulate a 465-Mc transmitter [8].

The single sideband technique is being used presently on space vehicles. Basically, the SSB-FM system consists of 15 single sideband subcarriers summed into a composite signal to modulate a FM carrier. The data signals are fed to a balanced (first) modulator with a 455-kc carrier (Fig. 8). The 455-kc carrier is modulated by 0.05- to 3.0-kc data input signals which produce sidebands near the carrier frequency. Following the first modulator is a two-stage amplifier and a bandpass filter which passes only the upper sideband of 455.0 to 458.0 kc and rejects all others. Next, the upper sideband signal is sent to the second modulator with a carrier frequency selected to place the difference signal at the desired location in the 15-channel passband. The outputs of the second modulators provide 15 evenly spaced frequencies: 1.74 to 4.74 kc (Channel 1), 6.48 to

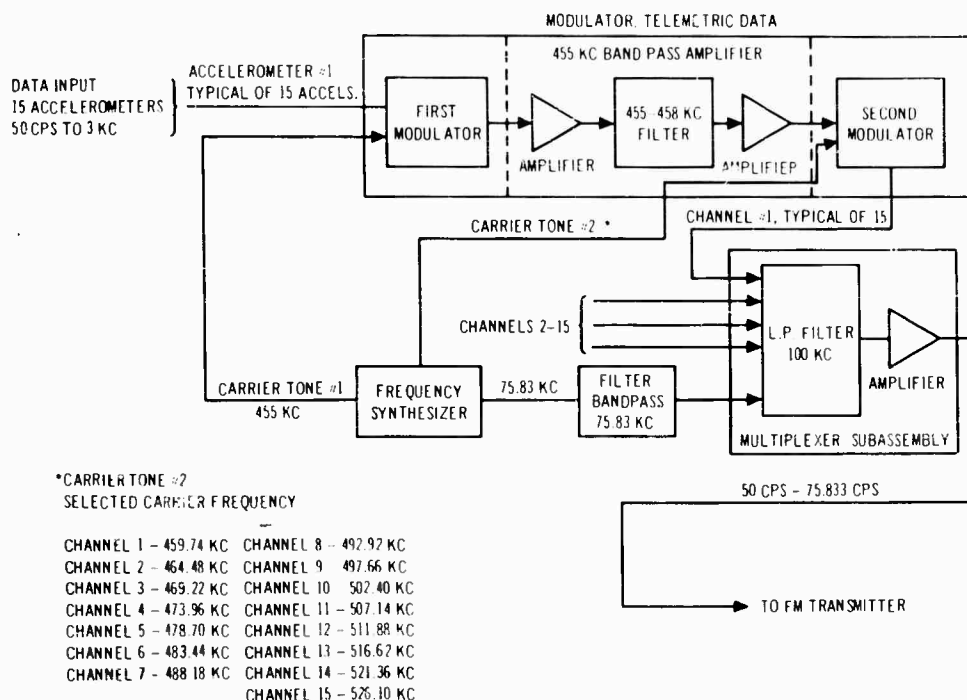


Fig. 8 - Block diagram of single sideband multiplexer

9.48 kc (Channel 2), . . . 68.10 to 71.0 kc (Channel 15). Thus, each of the 15 data channels contain a first modulator (455-kc carrier) and a second modulator with a selected carrier frequency. All 15 signals from the second modulators are combined in a linear mixing network with an amplitude and frequency reference tone (75.83 kc). The composite signal is passed through a 100-kc low-pass filter and amplified prior to modulating the FM signal in the FM telemetry transmitter. The composite signal to the transmitter is 50 to 75,833 cps. Figure 9 is a simplified block diagram of the SSB demultiplexer. The demultiplexer reverses the frequency transposition process of the multiplexer. Input signals to the demultiplexer are provided by a standard telemetry receiver or a suitable instrumentation tape recorder. The multiplexed signal (50 cps to 75.83 kc) passes through a 76-kc low-pass filter which prevents entry of extraneous high-frequency information into the demodulating channel units. Next, the baseband signals are attenuated and isolated by a splitting network for injection to the 15 individual channel units. From the splitting network, the signals enter the first demodulator with the same selected carrier frequency used in the multiplexer. The sidebands produced by the carrier tone and baseband frequencies fall within the ranges of 461.48 to 464.48 kc and 458.0 to 455.0 kc. The first modulator is

followed by a two-stage amplifier with a 455.0- to 458.0-kc bandpass filter. The second step of demodulation uses a phase split demodulator. The 455.0- to 458.0-kc information signal is demodulated into the frequency range from 0.05 to 3.0 kc. Finally, the data signal is passed through a 3.0-kc low-pass filter, amplified, and presented to a data recording device [9]. The 15 channels of the SSB/FM systems have bandwidths from 50 to 3000 cycles. Empirical calibration data recorded over 15 channels of a SSB/FM telemetry system show a 10 db decrease at 50 cps (Fig. 10); therefore, FM-FM channels are required for lower frequency vibration data.

Although various techniques have been utilized to apply modulations, the most reliable and commonly used method is the FM-FM telemetry system. In the FM-FM system, the transducer signal modulates a subcarrier frequency which is mixed with other subcarriers to create a composite signal that, in turn, frequency modulates the main carrier frequency (usually from 215 to 260 Mc). A study of FM-FM telemetering characteristics requires an examination of the main units that comprise the FM-FM systems. Major units include sub-carrier oscillators, radio-frequency transmitters, amplifiers, bandpass filters, radio-frequency receivers, and subcarrier

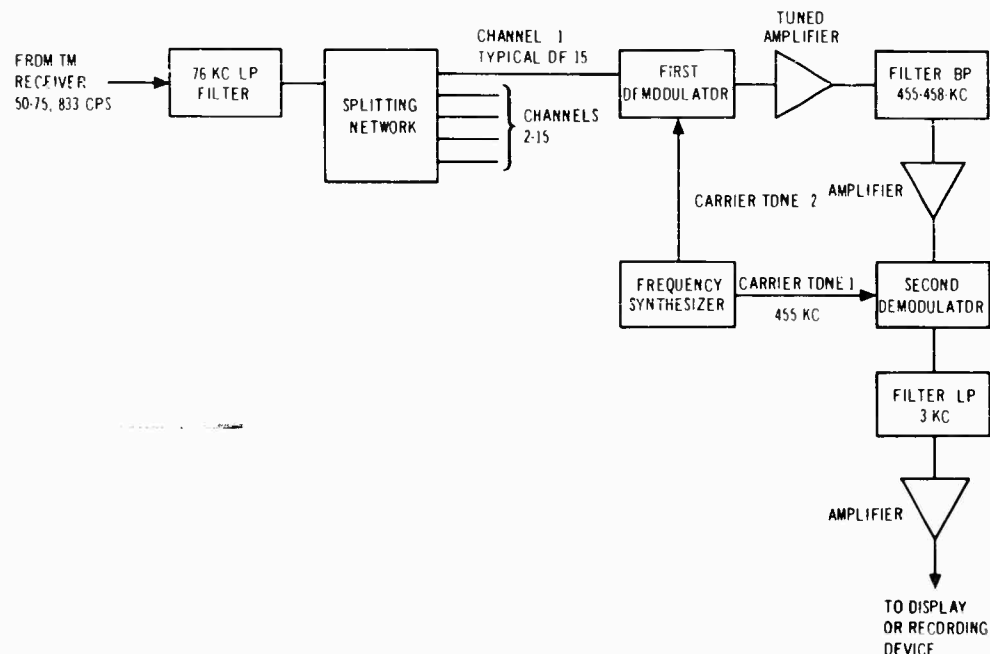


Fig. 9 - Block diagram of single sideband demultiplexer

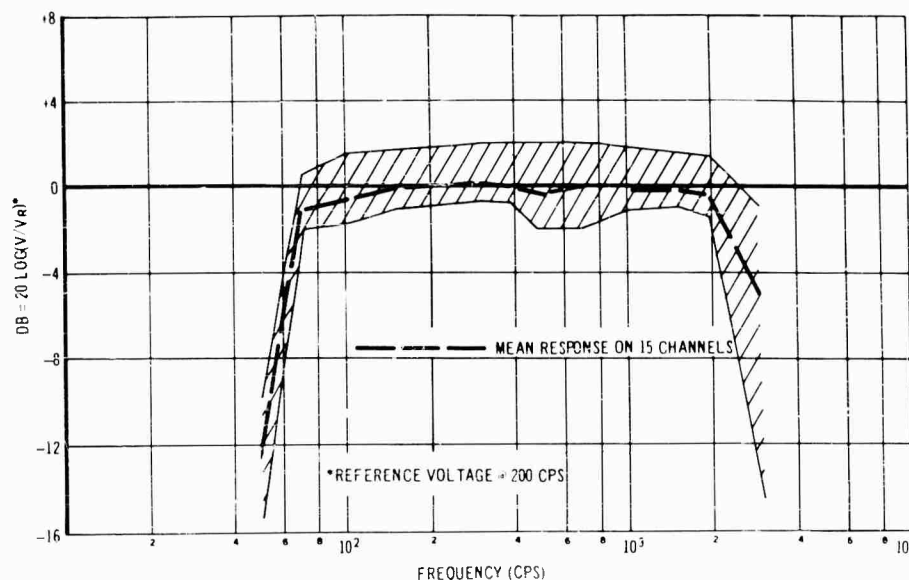


Fig. 10 - Envelope of frequency response curves - 15 channels - SSB/FM telemetry system

discriminators. FM-FM channels are standardized according to Inter Range Instrumentation Group (IRIG) specifications. Eighteen subcarrier frequencies are available for FM modulation. The intelligence frequency which can be transmitted by individual subcarriers is proportional to the subcarrier bandwidth in cycles. Table 3 gives the IRIG subcarrier bands; Table 4 gives a proposed expansion of IRIG specifications.

Sample information on the characteristics of FM-FM telemetry is displayed in Figs. 11 through 15. Figure 11 shows linearity data from a 40-kc (Channel 16) subcarrier oscillator. The curve of Fig. 11 (input signal vs frequency deviation) shows that the subcarrier oscillator has excellent linearity. Subcarrier oscillators are available commercially that maintain this linearity with negligible sensitivity shift over the temperature range from 75 to 150°F. Response curves, based on actual field calibrations, for Channels A (22 kc ± 15 percent deviation) and C (40 kc ± 15 percent deviation) are given in Figs. 12 and 13. These data were obtained from end-to-end calibrations of the telemetry system. The calibration signal was inserted across 100 ohms in series with a piezoelectric accelerometer installed in a missile. The calibration signal passed through a charge amplifier, a low-pass filter, a voltage-controlled oscillator (VCO), a wide band amplifier, a FM transmitter, antennas, a FM receiver, tape recorders, a discriminator, and a Gaussian filter. The calibrations were

performed at the band edge of the voltage controlled oscillators (5 volts peak-to-peak). Figures 12 and 13 show data passed through a 1200- and a 2100-cps low-pass Gaussian filter, respectively. The data in these two figures indicate that the better frequency response is obtained with the 2100-cps low-pass Gaussian filter; however, the S/N ratio is decreased and the noise floor is raised (4 to 10 db) with the higher filter. To assure intelligent transmission in FM systems, interchannel modulation can be kept at a minimum by keeping the output potentials from transducers and amplifiers between 0 and 5 volts dc. This can be accomplished by the addition of limiting circuits that prevent any higher-than-anticipated vibration signals from exceeding the 5-volt range and causing undesirable intermodulation. Various limiting circuits are available; one is described in Ref. 1. The radio frequencies generally used for FM-FM transmission lie in the range from 215 to 260 Mc. Other frequencies (108, 378, and 960 Mc) have been used for space probe telemetering systems with low-frequency subcarrier bands, IRIG Channels 1 to 6. The FM-FM telemetry signals may occupy a bandwidth from 75 to 500 kc. IRIG specifications call for the rf carrier frequency to be stable within ± 0.01 percent of the carrier frequency. The relationship between noise and rms error in a receiver with a bandwidth of 500 kc is exhibited in Fig. 14 [10]. The rms error, an average of 8 subcarrier bands, approaches one percent for signal-to-noise ratios of 12 or greater. The rms error as a

TABLE 3
IRIG Subcarrier Bands

Band	Center Frequency (cps)	Lower Limit (cps)	Upper Limit (cps)	Max. Dev. (%)	Frequency Response (cps)
1	400	370	430	7-1/2	6.0
2	560	518	602	7-1/2	8.4
3	730	675	785	7-1/2	11
4	960	888	1032	7-1/2	14
5	1300	1202	1398	7-1/2	20
6	1700	1572	1828	7-1/2	25
7	2300	2127	2473	7-1/2	35
8	3000	2775	3225	7-1/2	45
9	3900	3607	4193	7-1/2	59
10	5400	4995	5805	7-1/2	81
11	7350	6799	7901	7-1/2	110
12	10500	9712	11288	7-1/2	160
13	14500	13412	15588	7-1/2	220
14	22000	20350	23650	7-1/2	330
15	30000	27750	32250	7-1/2	450
16	40000	37000	43000	7-1/2	600
17	52500	48560	56440	7-1/2	790
18	70000	64750	75250	7-1/2	1050
A*	22000	18700	25300	15	660
B	30000	25500	34500	15	900
C	40000	34000	46000	15	1200
D	52500	44620	60380	15	1600
E	70000	59500	80500	15	2100

Based on maximum deviation and deviation ratio of 5.

*Bands A through E are optional and may be used only by omitting adjacent bands as follows:

<u>Band Used</u>	<u>Omit Bands</u>
A	15 and B
B	14, 16, A and C
C	15, 17, B and D
D	16, 18, C and E
E	17 and D

function of rms carrier deviations for a 300-kc bandwidth is displayed in Fig. 15 [10]. This curve indicates that values of 100-kc deviation or less are desirable; however, most FM-FM systems in use today are set for carrier deviations of 125 kc. Receiver bandwidths from 200 to 500 kc with rms carrier deviations from 60 to 125 kc are considered to be practical systems. Accuracies of 2 to 3 percent rms are considered to be reasonable in FM-FM telemetry systems (aside from transducer and amplifier accuracies).

Proposed uses for space telemetry include the utilization of new spectra: 136 to 137 Mc

(replaces 108 Mc), 400 to 401 Mc (takes overflow from 136 to 137 Mc band), 1427 to 1429 Mc, 1435 to 1535 Mc and 2225 to 2300 Mc. The 2290 to 2300 Mc band will be used for primary telemetry and tracking for deep space. This is considered to be the nearly ideal frequency for present 85-foot antenna dishes; use of this band permits high gain and narrow beamwidth. Concentrating all deep space research into this nearly ideal frequency area will result in economy [11]. Telemetry is supposed to move into the 1435 to 1535 and 2200 to 2300 Mc bands by 1970. The overcrowded 215 to 260 Mc band continues to be used extensively because there has been a lack of components for use in the

TABLE 4
Future Expansion of IRIG Standards

Channel No.	Center Frequency (kc)	Intell. $\beta = 5$	Frequency (cps) $\beta = 1$
(a) 7-1/2% Dev.			
18	70	1,050	5,250
19	92	1,380	6,900
20	120	1,800	9,000
21	160	2,400	12,000
22	210	3,150	15,750
23	280	4,200	21,000
24	370	5,550	27,750
25	490	7,350	36,750
26	650	9,750	48,750
27	860	12,900	64,500
28	1,100	16,500	82,500
(b) 15% Dev.			
F	120		18,000
G	210		31,500
H	370		55,500
J	650		97,500
K	1,100		165,000
(c) 30% Dev.			
N	10.5		3,150
P	20.0		9,000
Q	70.0		21,000
R	160.0		48,000
S	370.0		111,000
T	860.0		258,000
(d) 40% Dev.			
W	14.5		5,800
X	70.0		28,000
Y	220.0		88,000
Z	750.0		300,000
(e) Base Bands			
HH	320		100,000
J	650		97,500
KK	1,100		100,000

UHF bands and because engineers prefer to use familiar workhorse equipment. Some equipment is available commercially to cover the additional telemetry bands. An advanced VHF/UHF receiver accepts frequencies from 55 to 2300 Mc. This receiver has nine tuners: 55 to 260, 135 to 155, 215 to 260, 215 to 315, 370 to 410, 920 to 1000, 1435 to 1535, 1700 to 1850, and 2200 to 2300 Mc. Solid state telemetry transmitters are presently available that cover the

215 to 270, 430 to 500, 1435 to 1535, and 2200 to 2300 Mc bands. Thus, a gradual transfer to the higher telemetry bands can be expected.

Future developments in the transmission of dynamic data encompass the use of digital techniques with high sampling rates (PCM and PACM), satellite relays, on-board reduction and analyses of data, higher frequency FM sub-carriers, and the transmission of vibration

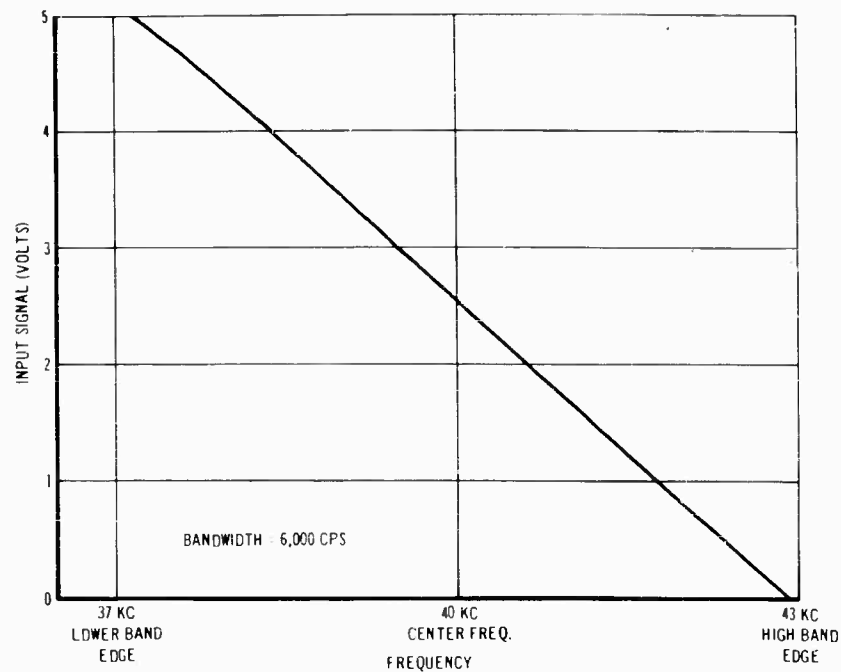


Fig. 11 - Sample curve illustrating Subcarrier oscillator linearity

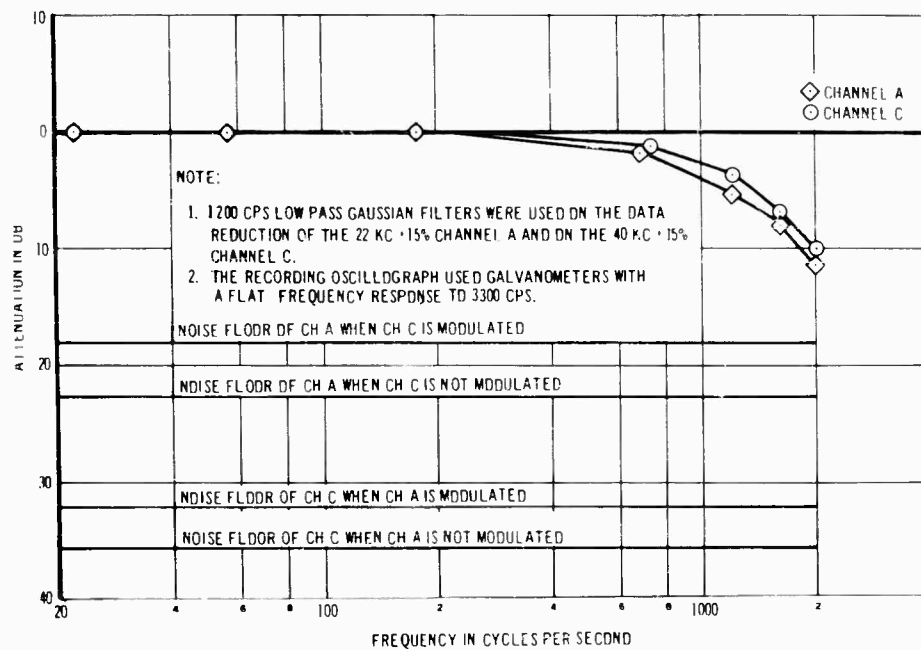


Fig. 12 - Empirical frequency response of IRIG Channels A & C - 2100-cps filter

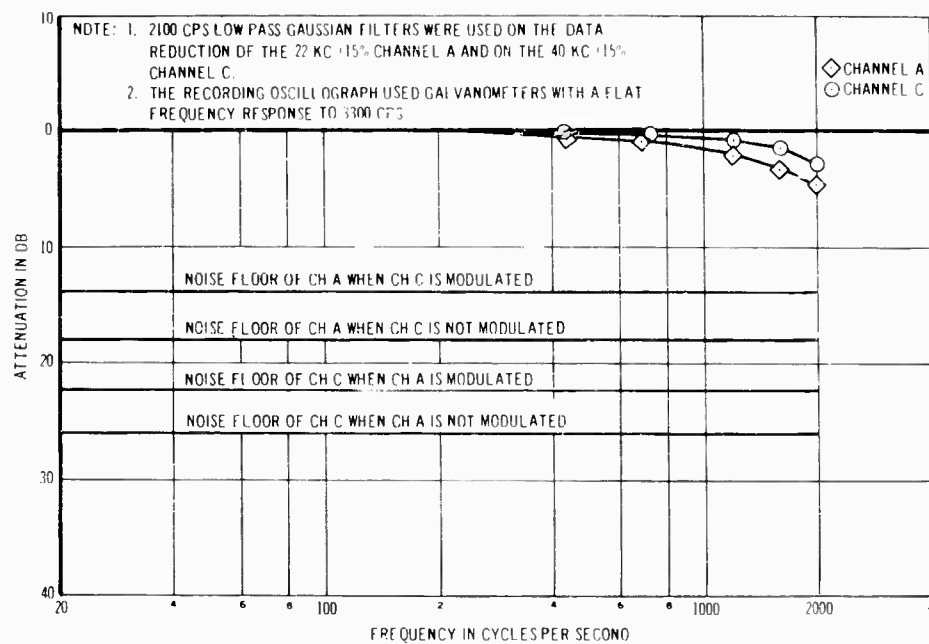


Fig. 13 - Empirical frequency response of IRIG Channels A & C - 2100-cps filter

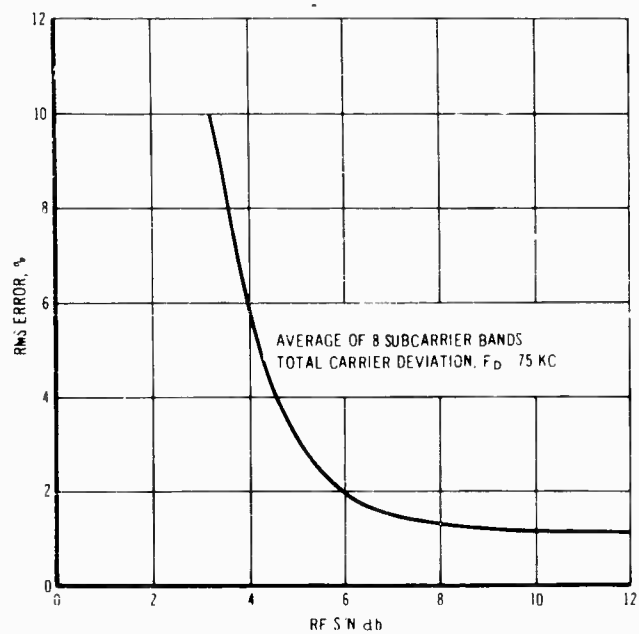


Fig. 14 - FM-FM error vs S/N, receiver bandwidth, $B = 500$ kc

ALL SUBCARRIERS ON, UNMODULATED
40 KC BAND MEASURED
B 300 KC

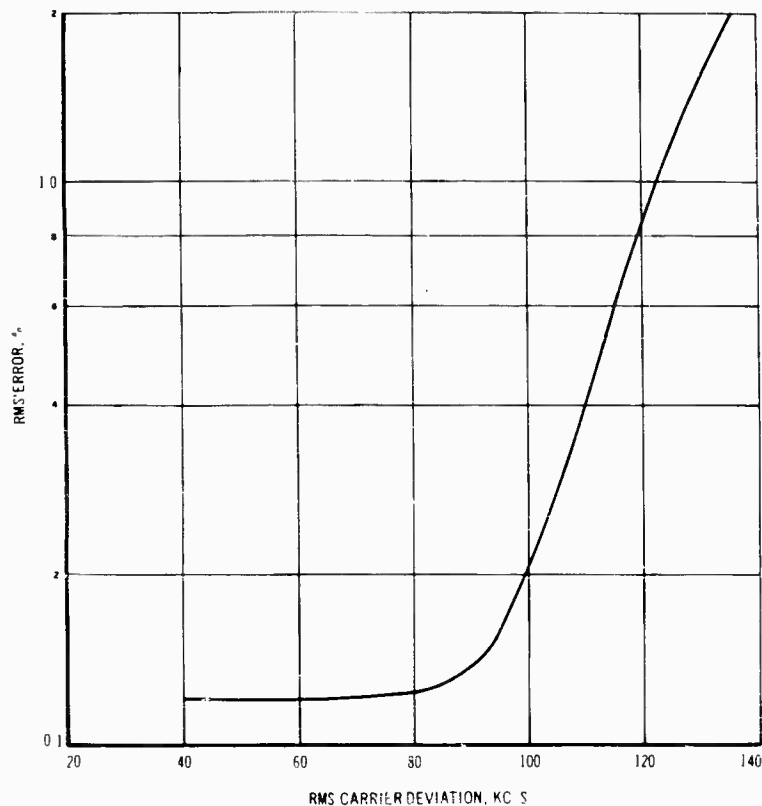


Fig. 15 - FM-FM distortion error versus carrier deviation

analyses (in the form of X-Y plots) by television. In the far distant future are telemetry systems that use ultraviolet waves (photomultiplier sensors) and coherent light (laser amplifiers).

MAGNETIC TAPE RECORDERS

Since magnetic tape recordings provide the optimum storage of dynamic data, a brief discussion on magnetic tape recorders is in order. Basically, magnetic tape recorders fall into three general classes: direct (AM), frequency modulated (FM), and digital recorders. The direct recorders do not have the ability to reproduce low-frequency signals, but have an excellent high-frequency response; consequently, AM recorders are suitable for recording composite and rf telemetry signals. In the direct recording process, the signal to be recorded is amplified, mixed with a high-frequency bias, and presented directly to a recording head as a

varying electric current. No coding or modulation are used in the AM recorders. Variations in the signal level are recorded directly as a magnetic-signal level on the tape. The FM tape recorders are ideal for recording vibration and acoustic signals. The FM recording technique overcomes the two basic limitations of the AM recorders, i.e., the inability to record very low frequencies and the instability caused by tape dropouts. Using FM recording techniques, it is possible to multiply or divide the frequency of an FM carrier without affecting the modulation. An FM tape may be played back slower or faster than it was recorded, changing the time base without changing the absolute or relative amplitude of the data. This time base expansion and contraction permits the frequency components of a given signal to be scaled up or down by large factors. For example, high-frequency data can be analyzed on low-frequency readout devices. Most FM tape units provide frequency responses from dc to 10,000 cps at tape speeds of 60 ips. Several FM recorders are available

presently with responses from dc to 20,000 cps at tape speeds of 60 ips. A modification of the FM recorder is the wide band (multi-megacycle) recorder for radar, video, and high-frequency pulse techniques. In the wide band method, the carrier is frequency modulated by the data, but the modulated carrier is recorded transversely across the entire width of the tape. The recorded signal is similar to the FM carrier signal except that much higher frequencies are accommodated. Wide band recorders are available with frequency ranges from 10 cycles to 4 Mc [12,13]. The digital recorders have fast stop and start features and are utilized to record pulse data where the magnetic tape is either saturated or nonsaturated. Digital recording is accomplished by magnetizing the tape to saturation in either of its two possible directions (+ or -) at discrete points along its length. Thus, there is only one of two states of magnetization at any point on the recorded tape; namely, saturation in one direction (+) or saturation in the opposite direction (-) [12]. Pulse code modulation signals are recorded on the digital tape units. Other recording techniques such as pulse duration modulation are used also for recording pulses. The AM recorders which are used to record composite telemetry signals are, generally, ground-based units. Some airborne AM units are being used to record composite telemetry signals during re-entry blackouts and flame attenuation blackouts of rf signals. Flame attenuation blackouts can be caused by firing of retro and ullage rockets. Antennas are normally designed for optimum coupling into the characteristic impedance of free space, 377 ohms. The engine exhaust products are highly ionized and they alter the dielectric constant of the surrounding medium which may be translated into a change in characteristic impedance. Thus, the total available energy is not radiated. The portion radiated is attenuated by the collision of charged particles, chiefly electrons [14]. Aside from these limited uses of airborne AM recorders, most airborne recordings of dynamic data are made on FM airborne recorders. Also, all hardwire recordings on ground installations utilize FM magnetic tape recorders.

Many commercial versions of airborne and laboratory magnetic tape recorders are presently on the market. Recently, a small recorder was developed for recording during blackouts in space vehicles, and for later playback during favorable transmission periods. This airborne recorder has a record or playback time of 3 minutes at a tape speed of 60 ips. The frequency response of this recorder is ± 3 db or less from 300 cps to 125 kc. Composite telemetry signals can be recorded during the blackout

and played back (on command) into the FM transmitter. The power requirement for this small recorder is less than 40 watts at 28 ± 4 vdc, and the weight is approximately 8 pounds.

A ruggedized FM recorder, suitable for airborne operations, has been developed for high-g sled test operations. This recorder has 14 FM channels and can be operated at tape speeds of 3-3/4, 7-1/2, 15, 30, or 60 ips. The recording time of this recorder is 4 minutes 20 seconds at 60 ips and the power requirements are either 115 volts, 400 cycles, or 24 vdc. The input impedance is 100 K and the sensitivity is 0 to 5 volts or ± 2.5 volts for full-scale deviation. The frequency response is dc to 10 kc at 60 ips. The drift of this sled recorder is ± 1 percent in center frequency and ± 2 percent in bandwidth over the temperature range from -20 to +185° F. Linearity of this recorder is ± 2 percent.

The specifications for one of the popular airborne magnetic tape recorders are as follows:

- Tape speeds: 1-7/8, 3-3/4, 7-1/2, 15, 30 and 60 ips
- Tape specifications: 1/2- or 1-in. tape, 10-1/2-in. reels
- Heads: Interchangeable, plug-in, referenced by precision base-plate
- Track configurations: 7 analog or 8 digital on 1/2-in. tape; 14 analog, 16 or 32 digital or a combination of 7 analog and 16 digital for 1-in. tape
- Recording: Direct, FM-carrier, PDM and NRZ digital
- Frequency response: Direct—100 to 100,000 cps ± 3 db with 34-db signal-to-noise at 30 ips; FM-carrier—dc to 20,000 cps at 60 ips with 0.5-db total
- Weight: 120 pounds
- Volume: 1.9 cubic feet of space
- Power requirements: 200 watts, 28 vdc

The finest magnetic tape recorders are those that have been developed for laboratory operations. Excellent tape units with many desirable ancillary functions have been marketed. These include "Cadillac" systems with 14 channels of recording at tape speeds to 120 ips and frequency response to 1.5 Mc. These precision instrumentation recorders are ideal for predetection recording of telemetry signals which has been developed within the past five years and is steadily growing in popularity. The popularity of this recording method is due to its many advantages over conventional recording methods. Predetection recording consists of heterodyning the intermediate frequency

carrier of a receiver so that a new i-f carrier and its sidebands fall within the passband of a recorder. Then, this new i-f carrier and sidebands can be easily recorded and reproduced on magnetic tape recorders. Predetection equipment consists of a telemetry receiver, a predetection recording converter, and a wide band recorder; all are available commercially. The advanced vhf/uhf receiver described in the section on telemetry can be obtained with a predetection recording converter that has a range of i-f center frequencies. These center frequencies are 112.5, 225, 450, 600, and 900 kc. During predetection data collection, the i-f of the telemetry receiver is heterodyned by the predetection converter to the center frequency. The "Cadillac" tape recorder with a response to 1.5 Mc and a 1.2 Mc bandwidth is suitable for predetection recording. Basically, predetection recording stores information as a spectrum before the information is detected. In this manner, the data signal is stored for detection at a later time. Predetection recording has many advantages:

1. A single predetection system can handle several data formats: FM/FM, SSB/FM, PCM/FM, PAM/FM, and PDM/FM.
2. Predetection recording almost totally eliminates the detrimental effects of dropouts.
3. High-quality third or fourth generation copies of original tapes can be reproduced.
4. Excellent linearity and amplitude stability are attained in predetection systems.
5. There is less signal-to-noise degradation in predetection recordings.
6. Predetection recording methods offer simplified operation, reliability, and reduced maintenance [15,16].

SYSTEM CALIBRATIONS

The optimum vibration instrumentation system will provide accurate data only when competent calibrations are made of the complete system. These calibrations must be supported by satisfactory transducer calibrations. Most laboratory calibrations of vibration transducers are referenced to secondary laboratory standards calibrated by the National Bureau of Standards (NBS). Secondary laboratory standards can be calibrated by NBS from 10 to 20,000 cps. The NBS calibrations from 10 to 2000 cps are performed on electrodynamic vibration standards previously calibrated by the

reciprocity method [17,18,19]. Dynamic calibrations between 2000 and 20,000 cps are performed on piezoelectric vibration exciters at NBS [20]. Satisfactory calibrations of transducers are supplied with each accelerometer by accelerometer vendors. These calibrations are usually supplemented by additional laboratory calibrations conducted by accelerometer users prior to and/or after laboratory vibration tests and field or flight tests. Actual system calibrations for laboratory vibration tests can be accomplished on complete vibration measuring systems by using vibration exciters to provide a mechanical input as the calibration stimulus. The use of vibration shakers in field and flight tests is rarely practical, although it is possible to provide a partial system check by using small shakers in field and flight test vehicles. A small portable device which provides a 60-cps 10-g rms sinusoidal motion to accelerometers is described in Ref. [21].

The strain gage circuit shown in Fig. 1 and modifications of that circuit were used by the author in the 1940's to obtain strain gage data from flight test vehicles. The circuit of Fig. 1 is suitable for both bonded and unbonded strain gages. For an unbonded accelerometer, the unbalance produced by a given calibration may be determined by the formula:

$$R_c = \left[\frac{10^6}{N(4K)} - 0.5 \right] R \quad (2)$$

where

R_c = calibration resistor (ohms),

R = bridge resistance (ohms),

N = g equivalent to bridge unbalance, and

K = sensitivity factor (microvolts open circuit output per volt input per g input).

The strain gage circuit of Fig. 1 provides output signals satisfactory to drive low-current devices such as sensitive galvanometers which operate with microamperes of current; consequently, this circuit requires amplification for transmissions via telemetry. Figure 16 shows a strain gage carrier system developed in the early 1960's to provide signals from 0 to 5 vdc for telemetry. Included in the amplifier are balancing and gain potentiometers. The accelerometer is fed a 10-kc square wave carrier of 5 volts (nominal) peak-to-peak. Capacitor C_b is selected to obtain an optimum signal wave shape across pin F and ground. Calibration

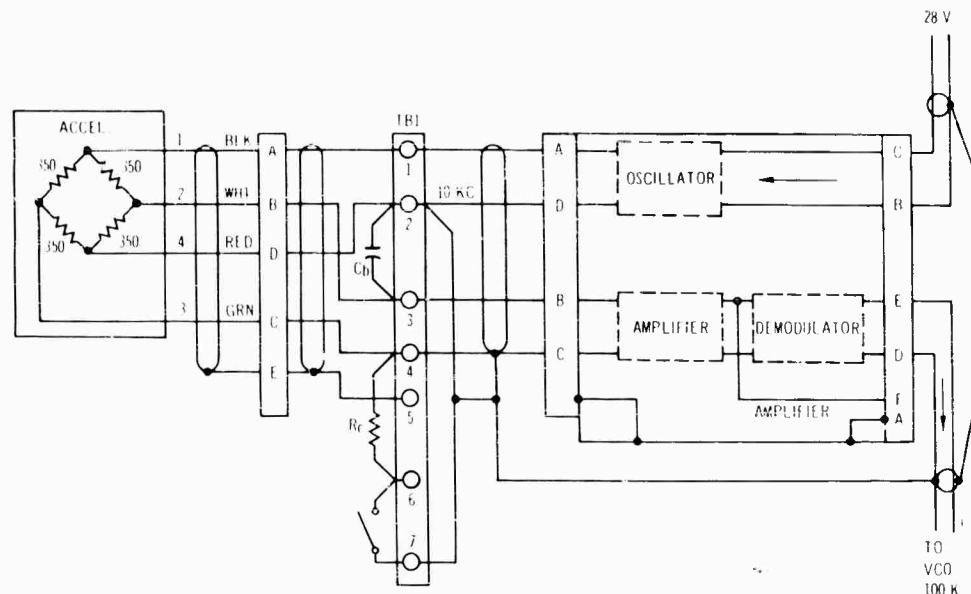


Fig. 16 - Strain gage carrier system

unbalance is provided by R_c . This accelerometer system may be calibrated in the laboratory by turning the accelerometer around physically, by connecting R_c across the strain gage bridge, or by vibrating the accelerometer on a vibration exciter. All three of these methods should be used and correlated for field and flight calibrations. Sample calibrations of a strain gage carrier system are shown in Figs. 17 and 18. A 2-g turnover calibration which utilizes the earth's gravitational field as a calibration standard is plotted in Fig. 17. Plus 1-g, zero-g, and minus 1-g static calibrations are shown with and without the calibration resistor, R_c , in the circuit. The calibration data of Fig. 17 are augmented by the calibration data of Fig. 18 which were obtained on a vibration exciter. The dynamic calibration data of Fig. 18 correlate fairly well with the static calibrations of Fig. 17. It must be noted that the amplifier output of Fig. 17 is given in volts dc, and that the amplifier output in Fig. 18 is given in volts rms. The data from Fig. 18 must be increased by 1.414 for comparison with the data of Fig. 17.

An ideal piezoelectric accelerometer system is displayed in Fig. 19. This system has provisions for end-to-end calibrations of six accelerometers simultaneously by the insertion method. This common insertion reduces calibration time in the field. Each accelerometer circuit contains either a 100-ohm resistor or a 100-ohm resistor plus a 62-picofarad capacitor in series with the piezoelectric crystal. The input calibration voltages are inserted across

the six 100-ohm resistors in parallel. The optional 62-picofarad capacitor is used only when additional attenuation is required in the instrumentation system. System noise is minimized by mounting the calibration resistor and capacitor in shielded containers. Also, the calibrators should be installed near the transducers to lessen cable capacitance, and laboratory shaker calibrations of the accelerometers should include the complete system. Charge amplifiers are used in the system of Fig. 19 to optimize impedance matching. The insertion voltages may be determined from the following relationships [22]:

$$E_{in} = \frac{Q_p}{C_p + C_1} \quad (3)$$

where

E_{in} = calibration voltage sensitivity (peak volts/peak g),

Q_p = transducer charge sensitivity (peak picocoulombs/peak g),

C_p = transducer capacitance (pf), and

C_1 = external capacitance (pf) between accelerometer and point of calibration voltage insertion.

Also

$$E_{in} = E_s \left[\frac{C_p + C_c}{C_p + C_1} \right] \quad (4)$$

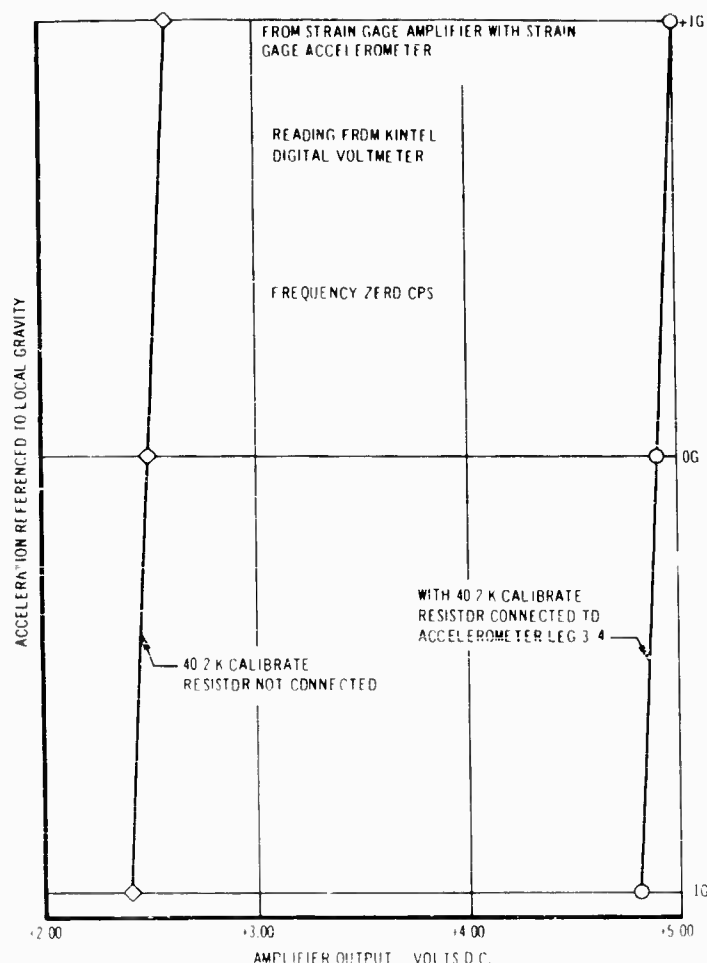


Fig. 17 - Calibration of strain gage system, output to VCO

where

$$F_s = \frac{Q_p}{C_p + C_c}$$

known voltage sensitivity (peak volts/peak g) with an external capacitance, C_c .

An empirical investigation was conducted in the laboratory to study the effects of calibrators on six parallel circuits. Data from typical vibration exciter calibrations of a piezoelectric accelerometer system are exhibited in Figs. 20 and 21. The calibrations were conducted on a system such as that displayed in Fig. 19. The data in Fig. 20 present empirical values of input voltage E_{in} vs frequency for 5-, 10-, and 15-g peak inputs from a vibration exciter. The vibration input was applied to one accelerometer while it was connected electrically to its associated amplifier

and five other systems as shown in Fig. 19. Data are given in Fig. 20 for two different system calibrations: one with six of the 100-ohm calibrators (Type 2944.1) and the other with six of the 100-ohm plus 62-pf calibrators (Type 2945.2) in the circuits. The input calibration voltage E_{in} was measured across the calibrators. Thus, in this calibration, E_{in} was actually an output voltage across the calibrator caused by the mechanical input. These data were in reasonable agreement with calculated values of E_{in} based on Eq. (4). Additional data on the effects of calibrators on accelerometer systems are presented in Fig. 21. This figure displays the output of an accelerometer amplifier vs acceleration (g peak) for different calibrator configurations: no calibrators in the system, six 100-ohm shielded calibrators (Type 2944.1) in the systems, six 100-ohm plus 62-pf shielded calibrators (Type 2945.2) in the systems, six unshielded 100-ohm resistors (denoted

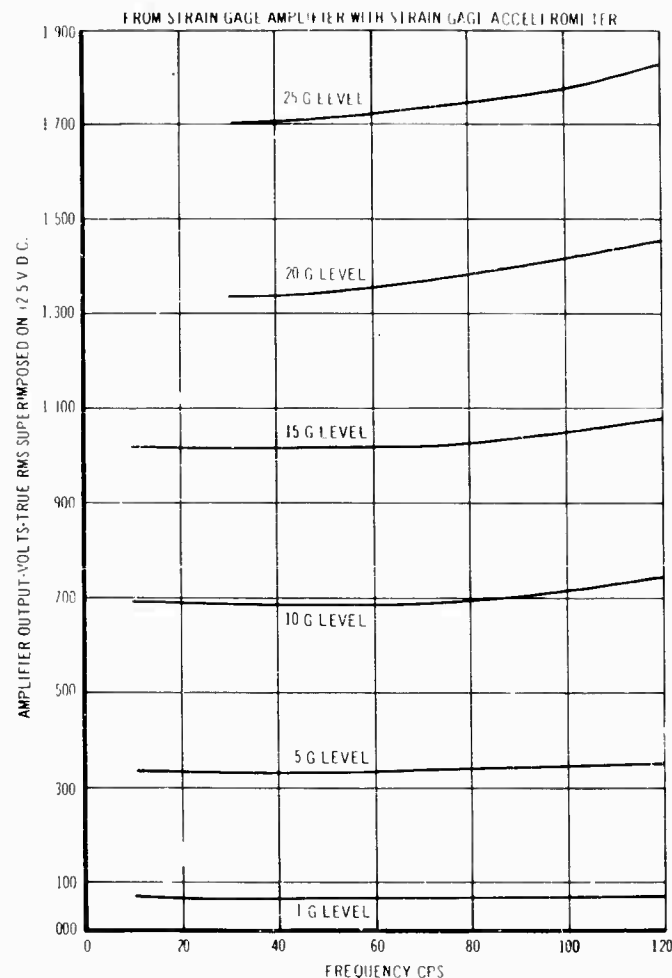


Fig. 18 - Calibration of strain gage carrier system, output to VCO

on the graph as 16.5 ohms) in the systems, and six unshielded 100-ohm resistors in the systems with an unshielded 62-pf capacitor in the circuit of the accelerometer being vibrated. An examination of the data shows that the largest deviations are displayed by the data obtained with unshielded resistors in the systems. This is probably due to electrical noise pickup in the laboratory by the unshielded portions of the circuit. It is concluded that the use of shielded calibrators for end-to-end system calibrations is desirable, practical and most satisfactory.

This section has presented a brief description of some calibration techniques used on strain gage and piezoelectric accelerometer systems. Of these techniques, the end-to-end system calibrations provide the most accurate data acquisition. In the past, many aircraft, missile, and space programs have obtained

vibration data without using end-to-end calibrations. It is recommended that all vibration measurements be obtained with ac end-to-end system calibrations. End-to-end system calibrations include the complete instrumentation system from the transducer through the recording media and the data reduction system.

IMPEDANCE/ADMITTANCE MEASUREMENTS

Within recent years there has been a gradual increase in the number of studies and experiments dealing with mechanical impedance and admittance parameters. The application of impedance/admittance techniques to dynamic problems will result in improved performance and greater reliability of aircraft, missiles, and space vehicles. Admittance measurements of

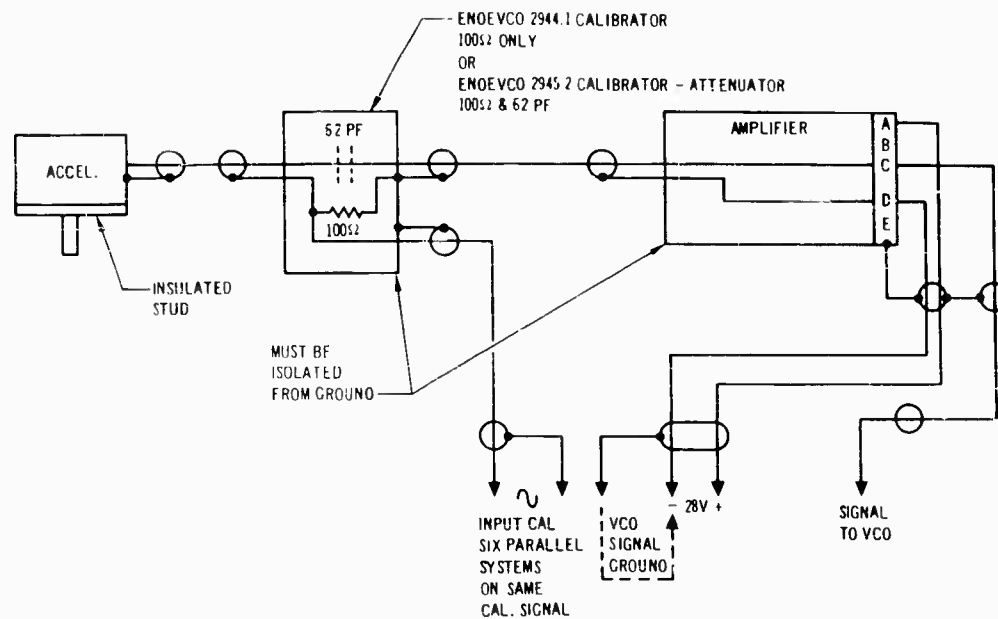


Fig. 19 - Piezoelectric accelerometer system

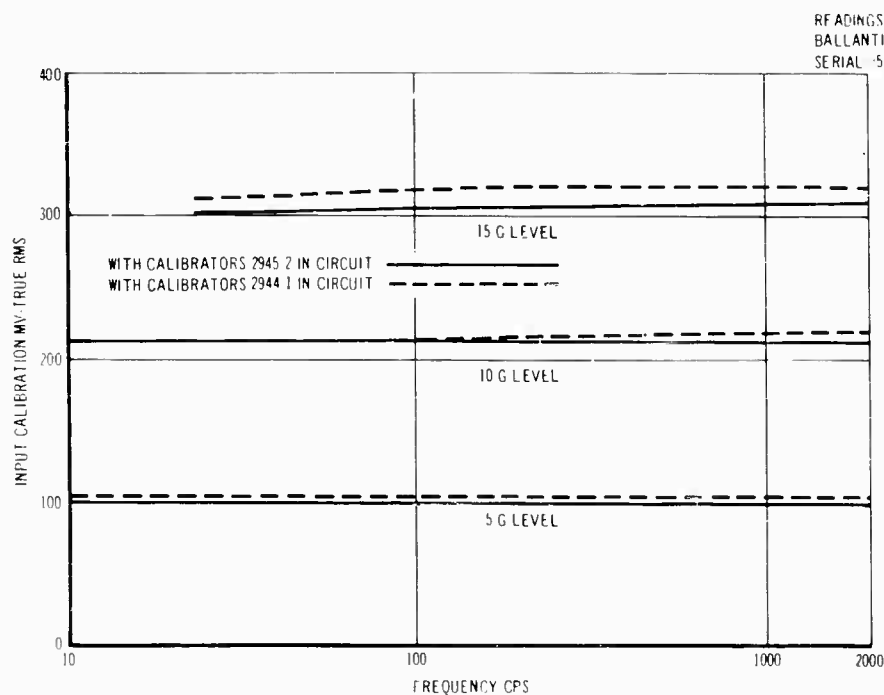


Fig. 20 - Accelerometer calibration (serial no. AG16, amplifier serial no. DA11)

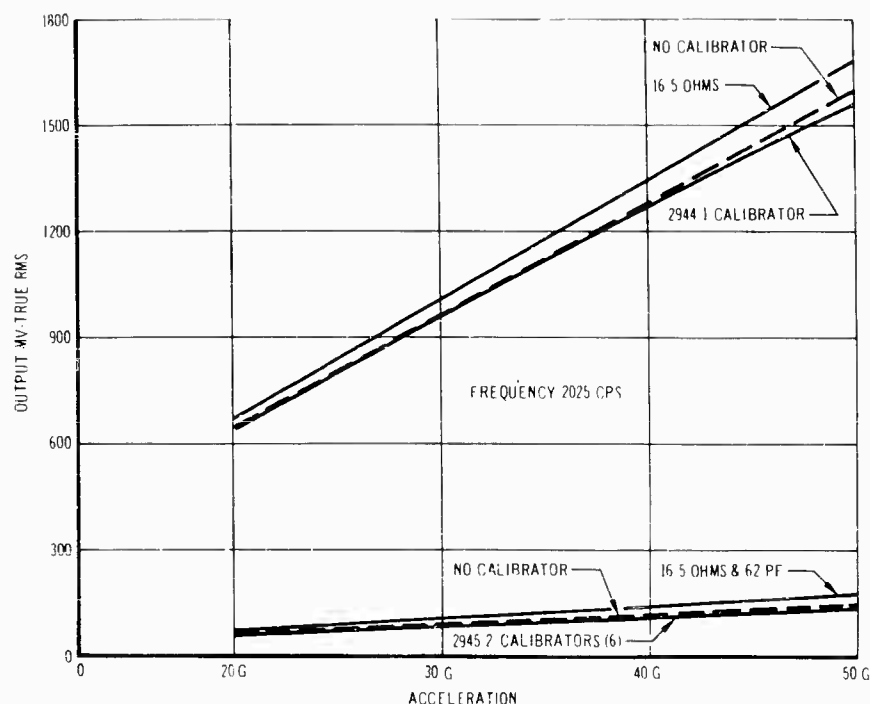


Fig. 21 - Accelerometer calibration, piezoelectric accelerometer with amplifier

sources are essential to the selection of optimum dynamic designs. Proper application of admittance source data can produce designs wherein fragility levels safely exceed the dynamic environment levels. Admittance source data allow the calculation of transmissibilities of equipment mounted directly to the source or installed on isolator/source combinations. A procedure for such a dynamic design has been developed by the SAE G-5 Committee on Aerospace Shock and Vibration [23,24,25,26].

The G-5 procedure requires measurements of source mechanical admittance, the motion of the source, and fragility levels of the equipment. In this case, the source is considered to be the supporting structure and the equipment is considered to be the receiver. The mechanical admittance of the source is the ratio of the complex amplitude of velocity to the complex amplitude of the driving force producing that velocity, both quantities being measured at the structural support of the equipment. The mechanical admittance of the source Y_s is equal to $A_s + jB_s$ where A_s and B_s are the real and imaginary parts of the admittance, respectively. The reciprocal of admittance is the mechanical impedance Z_s which is equal to $R_s + jX_s$ where R_s and X_s are the real and imaginary parts of the mechanical impedance, respectively. At first, the G-5 procedure was based on the

utilization of mechanical impedance; however, it was found advantageous to use the mechanical admittance because the isolator-source combination produces a modified source whose admittance is the sum of the admittance of the source and of the isolator.

It is apparent that the measurement of mechanical admittance (or its reciprocal, impedance) is essential to the accomplishment of suitable dynamic designs and analyses. The coverage of all the problems associated with the measurement of mechanical admittance is beyond the scope of this paper; nevertheless, a few notes on admittance/impedance measurements will be presented (see [23,27,28,29,30,31,32,33] for detailed coverage). The instrumentation engineer is called upon to develop and employ special transducers and supporting circuitry designed to obtain measurements of mechanical admittance (synonymous with "mobility"). The success of future dynamic progress depends on the utilization of mechanical impedance heads and force generators with improved recording media which provide accurate measurements of force, motion, and phase relationships. Transducers for obtaining mechanical impedance or admittance data are available commercially. In the past, numerous measurements were obtained with separate force and motion transducers. Furthermore, most

measurements and resultant analyses were made without measurements of phase angles between force and motion signals. Today, there is an increasing use of integral instruments containing both the force sensing and motion sensing transducers. Several versions of these integral instruments have been developed that are ideal for measurement of driving point admittance. When the velocity and force are referenced to the same point and in the same direction, the resulting quantity is called the "mechanical driving point admittance." When the velocity and force are referenced to different points, the resulting quantity is called the "mechanical transfer admittance." The measurement of impedance or admittance requires an input force to drive both the impedance head and the structure being investigated. Electrodynamic vibration exciters are, generally, used to supply the input driving force necessary for the impedance or admittance measurements. Satisfactory head-driver combinations should provide driving point capability, high-frequency response, high sensitivity, center mounting, minimum relative phase shift between transducers, and a high stiffness for suitable admittance or impedance measurements. Dynamic characteristics of three presently available impedance heads are given in Table 5.

Many instrumentation systems have been devised to measure mechanical impedance and admittance. The trend in impedance measuring instrumentation has been from manual systems to efficient automatic systems. These systems have run the gamut from simple meters requiring tedious manual measurements to complex automatic equipment with graphical and digital outputs. The simplest systems consist of impedance heads, force generators, amplifiers, oscillators, power supplies, voltmeters, and

phase angle meters. In these simple systems, the motion, force, and phase angles are obtained by visual observations and are tabulated by hand. Variable bandpass filters may be added to this array of equipment to eliminate harmonics and noise from the transducer signals. Additional equipment may include oscilloscopes to monitor signal quality and to assist in the determination of phase angle relationships, eput meters to establish signal frequencies, and special electronics such as mass cancellation circuits. The automatic systems may include additional items such as tracking filters, logarithmic voltmeter converters, sweeping oscillators, X-Y, Y¹ recorders, analog to digital converters, and digital printers. One system computes mechanical impedance digitally from tape-recorded analog signals [32]. This system is composed of analog recording equipment, playback equipment which converts analog data to a digital format, a computer program to determine the mechanical impedance digitally, and automatic digital data plotters. The outstanding advantage of using this digital system (or any similar system) is that large volumes of data can be conveniently handled and processed in computational routines to solve a variety of dynamic problems.

It is obvious that the use of taped data and large computers offers the greatest versatility; however, inexperience and technical problems associated with magnetic recorders and computers in the acquisition of impedance data have delayed the wide acceptance of digital computer systems for the measurement of mechanical impedance or admittance. Thus, there is presently an increasing utilization of automatic impedance measuring systems which provide analog plots of motion/force ratios (or their inverse) and phase angle relationships. One of these popular automatic mechanical impedance

TABLE 5
Dynamic Characteristics of Impedance Heads

Characteristic	Value		
	Model #1	Model #2	Model #3
Accelerometer sensitivity (mv/g)	25	200	70
Force gage sensitivity (mv/lb)	400	200	5 ^a
Frequency range (cps)	1-10,000	1-4,000	2-4,000
Mass below force gage (lb)	0.065	0.35	0.3
Stiffness (lb/in.)	6 × 10 ⁶	5 × 10 ⁸	3 × 10 ⁸
Relative phase shift (degrees)	± 1	± 1	± 1
Maximum acceleration (g)	1,000	1,000	2,000
Maximum load in compression (lb)	500	20,000	22,000
Matching force generators (lb)	0.75	1.5	1

^a In mv/g.

measuring systems contains the following equipment: an automatic vibration exciter control, integral impedance heads, force generators, a two-channel tracking filter, a carrier generator, a constant output level adapter, two log voltmeter converters, a precision phase-meter, two high impedance accelerometer amplifiers, a dc power supply, a X-Y, Y^1 recorder, and an 80-watt monophonic power amplifier. The system incorporates also a control panel with artificial integration, mass cancellation, system calibration, and signal monitoring jacks. The automatic vibration exciter control provides a 5- to 5,000-cps signal, in a continuous logarithmic sweep, to the 80-watt power amplifier. The exciter control supplies also a dc voltage proportional to the logarithm of the excitation frequency for driving the X axis of the X-Y, Y^1 recorder, and a dc voltage utilized in the artificial integrator. The 80-watt power amplifier drives the force generator that, in turn, drives the impedance head and the structure being investigated. The signals from the force and motion transducers are conditioned by the accelerometer amplifiers and the tracking filters. The filters track to the excitation frequency and eliminate the noise and distortion from the force and motion signals. The constant output level adapter takes a signal from the vibration exciter control and maintains it at a constant level for input to the carrier generator. Next, the carrier generator drives the tracking filter at the system excitation frequency. The logarithmic converter performs a logarithmic conversion of the linear input signals and provides a visual check, on meters, of the input levels over a 70-db dynamic range. Since each channel has a 70-db dynamic range, the resulting dynamic range of any ratio is 140 db. The precision phasemeter sends a signal to the Y^1 axis of the X-Y, Y^1 recorder which is proportional to the phase angle between the motion and force signals over a range from 0 to 180 degrees. The force and motion signals pass from the logarithmic voltmeter converters to the artificial integrator, are converted to select ratios or functions, and are sent to the Y axis of the X-Y, Y^1 recorder for final plotting.

This system automatically provides X-Y, Y^1 plots of various amplitude ratios and the phase angle that the acceleration leads the force vs frequency. On selection, any of the following ratios can be plotted as a function of frequency:

1. Force/acceleration, effective mass or apparent mass;
2. Force/velocity, mechanical impedance or immobility;

3. Force/displacement, dynamic or apparent stiffness;

4. Acceleration/force, inertness;

5. Velocity/force, mechanical admittance or mobility;

6. Displacement/force, dynamic flexibility or compliance; or

7. Acceleration/acceleration, transmissibility.

In addition, individual curves of displacement, velocity, acceleration, and force can be plotted as a function of frequency by this system. The determination of the real, A_s , and the imaginary, B_s , parts of the admittance can be accomplished by automatically recording $|Y_s|$, the ratio of the velocity amplitude to the force amplitude, and the phase angle that the acceleration leads the force. It then becomes a simple calculation to use the admittance amplitude, $|Y_s|$, and the phase angle, θ , to determine the real, A_s , and imaginary, B_s , parts of the admittance:

$$A_s(f) = |Y_s(f)| \sin \theta, \quad (5)$$

and

$$B_s(f) = |Y_s(f)| \cos \theta. \quad (6)$$

Figures 22, 23, and 24 present some data recorded on the automatic system described above. Figure 22 shows three calibrations of the system obtained by using the weight below the force gage as a calibration weight. This type of calibration does not require any information on the sensitivities of the force and motion transducers. The impedance head used during these sample calibrations had a mass below the force gage of 0.065 pound. Actually, the upper curve represents two different calibrations that were equal and identical. These two identical calibrations were made with the driver-head combination oriented vertically, facing upwards, and vertically, facing downwards. The lower curve on Fig. 22 was obtained by a third calibration with the driver-head combination in a horizontal position. On the basis of these data, it is recommended that admittance/impedance measurements be obtained with the driver-head combination oriented in a vertical direction. Furthermore, this eliminates cantilever torques created by hanging driver-head combinations horizontally on structures. Figure 23 shows the effect of the mass cancellation circuit in the automatic impedance measuring system. One curve shows data

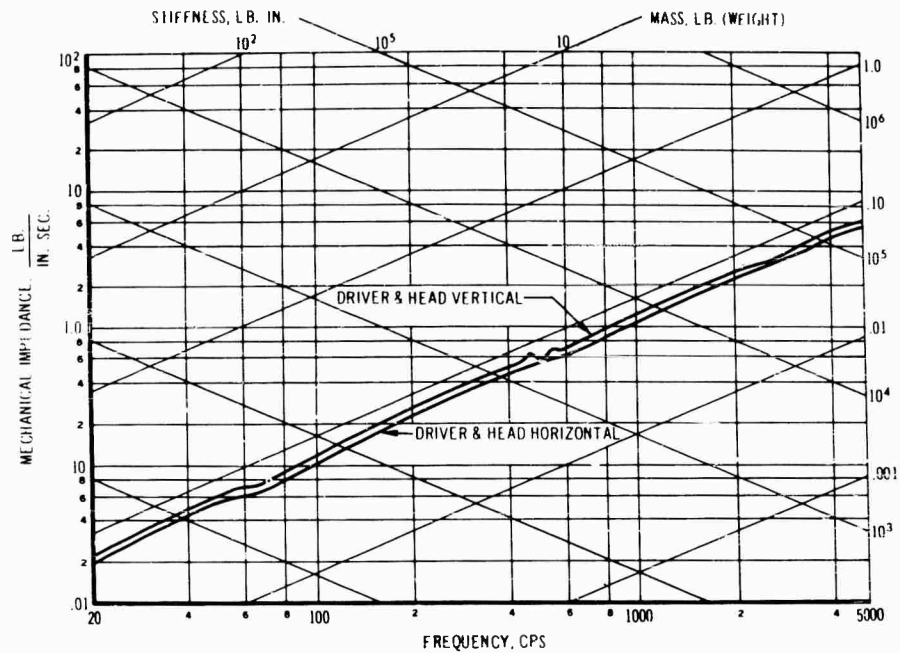


Fig. 22 - Calibration of driver and impedance head

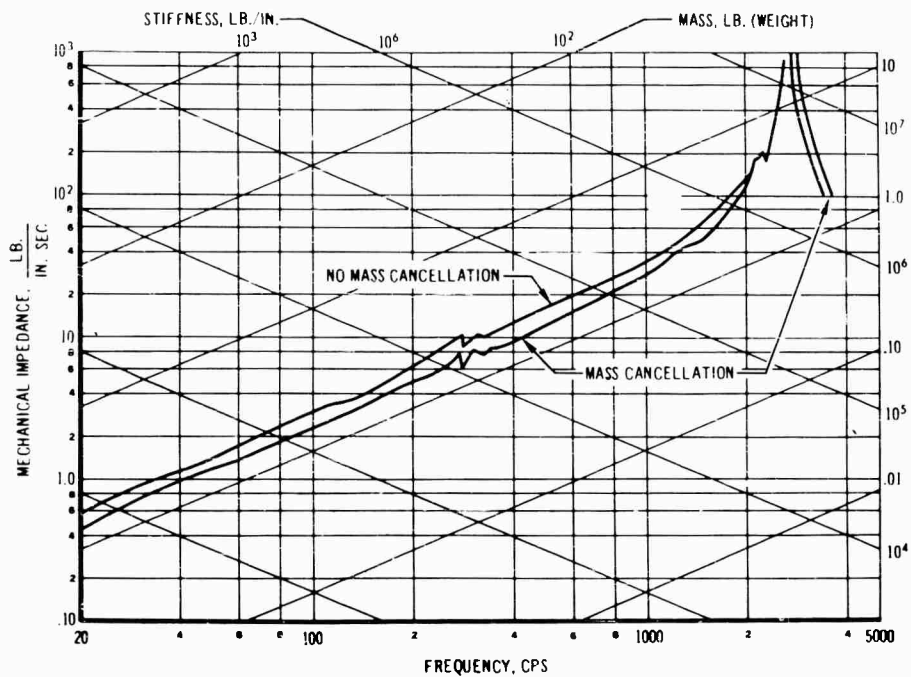


Fig. 23 - Effect of mass cancellation

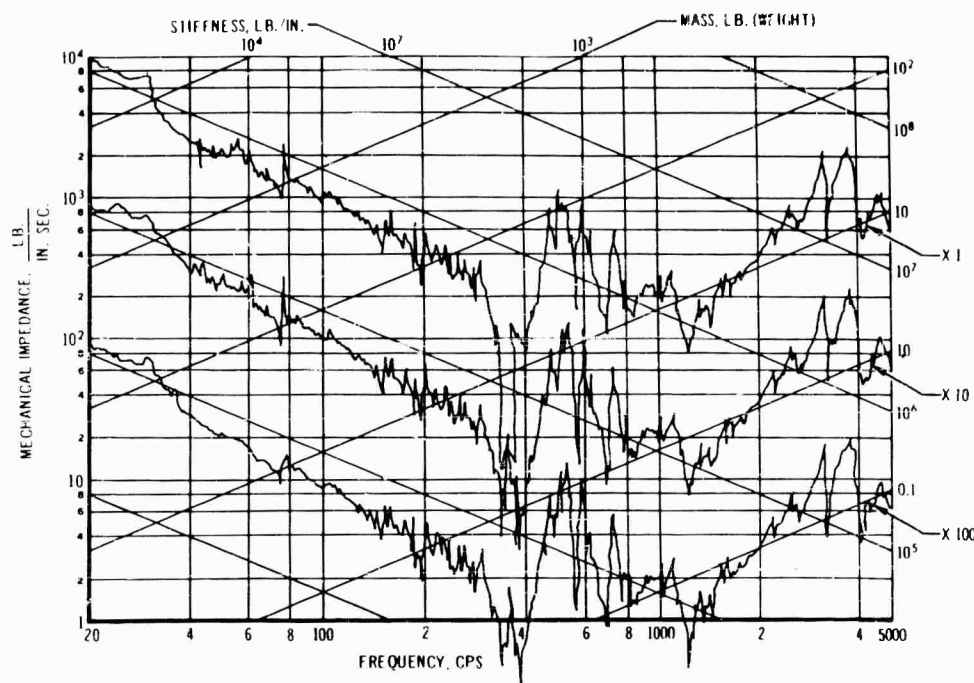


Fig. 24 - Impedance measurements, check of 3 gain settings

obtained without mass cancellation, and another curve shows data obtained with mass cancellation. Mass cancellation is an electronic method of cancelling the effect of the weight below the force gage. In the automatic system, mass cancellation is accomplished by subtracting from the force signal a feedback from the acceleration channel equal to the force signal being developed by the mass below the force gage. This cancellation (Fig. 23) is effective as long as the impedance head and adapter (in this case, 1.625 pound) display mass characteristics. As seen in Fig. 23, the mass cancellation actually increases or adds to the impedance value when the impedance head and adapter exhibit stiffness characteristics. Since structural impedances display many peaks and valleys and corresponding changes from mass to stiffness characteristics, it is recommended that systems be calibrated with weights (as in Fig. 22) and without mass cancellation. This recommendation is supported also by the results presented in Ref. [30]. Figure 24 displays mechanical impedance measurements of a structure recorded with three different system gain settings. These three sets of data agree reasonably well and show stiffness controlled characteristics below the first resonance of 400 cps, antiresonances at 500 and 3,500 cps, and mass-like characteristics above 1,200 cps.

This section has presented a short discussion and explanation of mechanical impedance measurements. It is predicted that practical applications of mechanical impedance and admittance measurements to the solution of dynamic problems will greatly increase during the next decade. In addition, it is recommended that impedance and admittance measurements be obtained on more aircraft, missile, and space programs; and that these data be applied to solve dynamic structural and equipment designs.

CONCLUSION

Information on vibration transducers, amplifiers, telemetry systems, magnetic tape recorders, and impedance measurements has been given herein. The scope of this report has limited the discussion to salient details; thus, each subject has received but minimum coverage. It is felt that many improvements are desirable in vibration instrumentation systems, and that the science of vibration measurements will expand and advance with each new aircraft, missile, and space project. An adequate definition of dynamic environments can be obtained by careful attention to the techniques of transducing, transmitting, recording, and reproducing dynamic signals.

Finally, the compilation of reliable dynamic data requires more than perfunctory calibration techniques. Complete system calibrations are a definite necessity to produce valid dynamic information. This calls for end-to-end system calibrations wherein a full range of frequencies and amplitudes are injected into the transducer end of the instrumentation system, transmitted through each unit in the chain,

and recorded on magnetic tape for final data reduction and analysis.

ACKNOWLEDGMENTS

The author is greatly indebted to A. G. Fritz, Jr., K. E. Elliott, and H. R. Smith of the Douglas Missile and Space Systems Division for their contributions to this paper.

REFERENCES

1. R. W. Mustain, "Dynamic Instrumentation for Establishing Environmental Criteria on the SM-62 Missile," Shock, Vibration and Associated Environments Bull. No. 25, Part II, pp. 117-136 (Dec. 1957).
2. W. G. Cady, Piezoelectricity, Vols. 1 and 2 (Dover Publications, 1964).
3. W. Bradley, Jr., "Performance of Three 500° F Crystal Accelerometers," National Telemetering Conf., El Paso, May 1957.
4. W. D. Hancock, "Primer on Piezoelectric Accelerometers," Environ. Quarterly (Oct. 1959).
5. E. H. Mullins, "Charge and Open Circuit Voltage as a Function of Very Large Compressive Forces," NBS Report 2654, Proc. of Symposium on Barium Titanate Accelerometers, Washington, D. C., May 14-15, 1953.
6. T. A. Perl and C. W. Kissinger, "A Barium-Titanate Accelerometer with Wide Frequency and Acceleration Ranges," NBS Report 2390 (April 1963).
7. W. Bradley, Jr., "Electronic Design Considerations in the Application of Piezoelectric Transducers," Part 9, 1956 IRE Convention Record.
8. T.C.R.S. Fowler, "A Six-Channel High-Frequency Telemetry System," IRE Trans. on Space Electronics & Telemetry, Vol. Set-6 (June 1960).
9. L. Wilson and R. Hess, "Development of an Air to Ground Single Sideband FDM Telemetry System," Phase I, Final Summary Report, Lenkurt Electric Co., Inc. (April 1960).
10. "Telemetry System Study," Aeronutronic Publication U-743, Vols I, II and III (Nov. 1959).
11. "Policy Planning for Space Telecommunications," Staff Report, U. S. Senate Committee on Aeronautical and Space Sciences (Dec. 4, 1960).
12. P. J. Weber, "The Tape Recorder as an Instrumentation Device," Ampex Data Products Co. (1959).
13. Readout, Vol. 3, No. 6, Ampex (Aug.-Sept. 1961).
14. A. H. Bartels, "Telemetry Signal Strength Evaluation of the S-IV-6 Flight," Douglas Aircraft Co. Memorandum (June 1964).
15. G. N. Johnson and W. R. Johnson, "A Pre-detection Recording Telemetry System," Part 5, 1961 IRE International Convention Record.
16. J. D. Williamson, "Advantages of Storing Data Before Detection," Electronic Ind. (Aug. 1964).
17. M. Harrison, A. O. Sykes, and P. G. Marcotte, "The Reciprocity Calibration of Piezoelectric Accelerometers," J. Acous. Soc. Am., 24(4): (July 1952).
18. H. M. Trent, "The Absolute Calibration of Electromechanical Pickups," Ann. Meeting, ASME, Atlantic City, N. J., Dec. 1-5, 1947.
19. S. Levy and R. R. Bouche, "Calibration of Vibration Pickups by the Reciprocity Method," Res. Paper 2714, J. Res. NBS, 57(4):227-243 (Oct. 1956).

20. R. R. Bouche and J. A. Miller, "National Bureau of Standards Calibration Service for Vibration Pickups," Shock, Vibration and Associated Environments Bull. No. 27, Part IV, pp. 127-131 (June 1959).
21. E. Rule, F. J. Suellentrop, and T. A. Perls, "A Pick-up to Read-Out Calibrator for Vibration Channels," Shock, Vibration and Associated Environments, Bull. No. 27, Part III, pp. 215-219 (June 1959).
22. J. E. Rhodes, "Piezoelectric Transducer Calibration Simulation Method Using Series Voltage Insertion," Environ. Quarterly (March 1962).
23. "Design of Vibration Isolation Systems," Advances in Engineering, Vol. 3, SAE Committee G-5 Aerospace Shock and Vibration (1962).
24. "A Rational Procedure for the Design of Vibration Isolation Systems," SAE Paper SP-223, SAE Committee G-5 Aerospace Shock and Vibration (Oct. 1961).
25. R. W. Mustain, "The Role of Mechanical Impedance Measurements in Reducing Vibration Environments," Instrument Soc. of Am., Fall Instruments Automation Conf. and Exhibit, Los Angeles, Calif. Sept. 11-15, 1961.
26. R. W. Mustain, "Application of Mechanical Admittance Data to the Solution of a Practical Problem," Bull. No. 30, Shock, Vibration and Associated Environments, Part II, Jan. 1962.
27. J. W. Young, Jr., and R. O. Belsheim, "Experimental Measurement of Mechanical Impedance," NRL Report 5458.
28. R. Plunkett, "Experimental Measurement of Mechanical Impedance or Mobility," J. Appl. Mech., 21(33):250-256.
29. E. L. Hixson and A. F. Wittenborn, "The Measurement of Mechanical Impedance and Its Applications," SAE National Aeronautic Meeting, Los Angeles, Calif., Sept. 30-Oct. 5, 1957.
30. R. R. Bouche, "Instruments and Methods for Measuring Mechanical Impedance," Bull. No. 30, Shock, Vibration and Associated Environments, Part II, Jan. 1962.
31. J. E. Smith, "Portsmouth Naval Shipyard Automated Mechanical Impedance Measuring Instrumentation System," Test Branch, Design Div., Portsmouth Naval Shipyard (Sept. 1962).
32. F. J. Benedetti and D. Brown, "A Digital System for Mechanical Impedance Measurement," SAE National Aeronautic and Space Eng. and Manuf. Meeting, Los Angeles, Calif., Sept. 23-27, 1963.
33. F. Schloss, "Recent Advances in the Measurement of Structural Impedance," SAE National Aeronautic and Space Eng. and Manuf. Meeting, Los Angeles, Calif., Oct. 9-13, 1961.

* * *

FORCE-CONTROLLED VIBRATION TESTS: A STEP TOWARD PRACTICAL APPLICATION OF MECHANICAL IMPEDANCE

John V. Otts
Sandia Corporation
Albuquerque, New Mexico

The Vibration Division at Sandia Corporation is experimenting with, and in some cases testing under, a test concept whereby the test item is allowed to affect its own environment as it does in the field. This test concept includes controlling the vibratory force input below a test system which consists of the test item and a mass representing that of the foundation. Results from this type of vibration test are presented and compared with the test results where the input to the test item is motion controlled. In addition, the methods used in deriving and controlling the force input levels, and the mass magnitude representing the foundation are discussed.

INTRODUCTION

Vibration tests, as they are presently conducted throughout the country, rarely (if ever) simulate the environmental conditions for which they are intended. Consequently, the true environmental response characteristics of the test item are seldom determined or even approximated. The test results often force designers to concentrate on unrealistic problem areas and/or overlook those that are potential problems.

The two basic reasons for unrealistic vibration tests are constant motion control of the input to the test item, and the methods used in deriving motion-input specifications. The first requires the false assumption that the foundation has infinite mechanical impedance. Consequently, the test item is not allowed to affect its own environment. Unfortunately, test specifications are sometimes arbitrarily selected without reference to any applicable field data. However, it is just as unfortunate that those specifications derived from field data consider only the peak responses of the foundation, neglecting the characteristic valleys. Again, the test item's environmental effects are neglected. When the above practices are combined in a vibration test, overtests as high as 100:1 can result at some frequencies. At other frequencies, the test item may not be tested sufficiently.

A few individuals have insisted for years that we are basically wrong in utilizing the constant-motion/input-control philosophy. At the same time, it has been suggested that the ultimate solution lies in the complete incorporation of the mechanical impedance concept. Unfortunately, there are factors which prevent this concept's immediate practical application. Some of these factors are the lack of field data from which to derive test specifications, the practical inexperience in applying the mechanical impedance concept, and the complexity of the concept.

In the past, we have been somewhat like the man who lost his billfold in a dark alley and hunted for it under a streetlight. Most people involved in vibrations will admit to the fallacies of our present test methods. However, the ease with which accelerometers can be used and the complexities involved in changing over to force transducers create some resistance to the change.

We in the Vibration Division at Sandia Corporation, with support of the Dynamic Stress Group, have begun to utilize a form of the mechanical impedance concept—thus inserting more meaning into test results. The area in which we are now working comprises controlling the mechanical impedance of the foundation at a finite value and controlling the force input below the simulated foundation.

The intentions of this paper are to illustrate the fallacies that exist under the constant-motion/input-control concept, discuss the advantages of force-input control below a simulated foundation, and consider some of the methods used in applying this concept.

DISCUSSION

Vibration tests naturally differ in their objectives and complexity. Thus, to be specific in this presentation is impossible. Although this discussion is limited to considering simple systems and constant sinusoidal inputs, the ideas apply to complex systems and inputs as well.

Mechanical impedance Z is the complex ratio between an applied force (sinusoidal) and the resulting velocity. Effective mass M_e is the complex ratio of an applied sinusoidal force to the resulting acceleration. Thus, the relationship between Z and M_e is expressible as $\omega M_e = Z$, where $\omega = 2\pi f$. There is also a 90-degree phase difference between M_e and Z . Since M_e is directly related to acceleration, this term will be used throughout this discussion rather than the more commonly used term Z .

INFINITE M_e TEST

Constant motion control of the vibration input to a test item is equivalent to assuming that the foundation's motion is independent of the test item. This is physically possible only if the foundation M_e is nearly infinite compared to that of the test item. Thus, this type of test is classified as an infinite M_e test.

The system in Fig. 1 represents a test item m_T mounted on a foundation m_S . The spring and damper are representative of the inherent characteristics of the test item and/or the connection between m_T and m_S . In this discussion, all equipment above the control point is assumed similar to that in the field.

For a constant sinusoidal acceleration input at Point 2, the force required below m_S and the acceleration responses of m_S and m_T are as shown in Figs. 2a, 2b, and 2c, respectively. The following discussion is based on these response characteristics. Although the test concept implies that m_S is infinite, it is finite in any test setup. In this particular illustration, m_S is representative of the shaker armature and test fixture mass located below the interconnector.

Fig. 1 - Vibration system

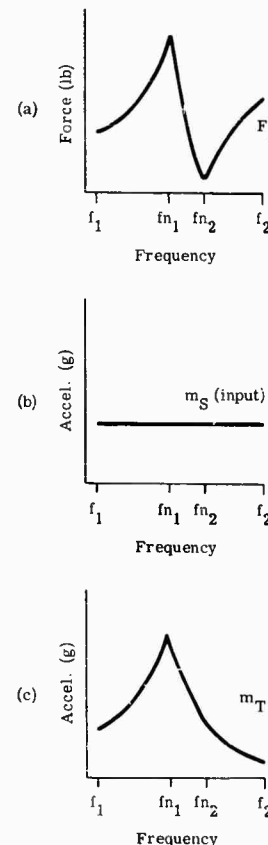
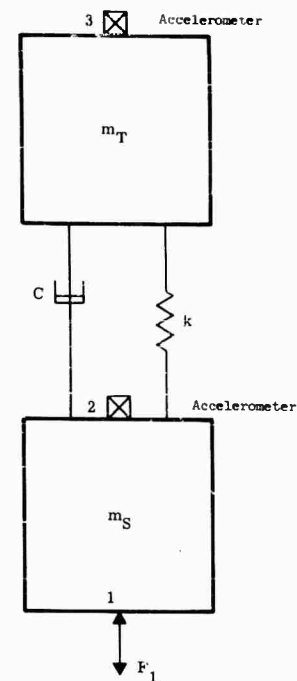


Fig. 2 - Response to infinite M_e test: (a) force below m_S , (b) acceleration of m_S , and (c) acceleration of m_T

The test item, m_T , is not allowed to affect its own environment. This is obvious, since the foundation motion is not variable over the frequency range (Fig. 2b). Thus, the true antiresonant and resonant response amplitudes are not allowed to occur. Antiresonance of the complete system (Fig. 1) is defined as:

$$f_{n1} = \frac{1}{2\pi} \sqrt{\frac{k}{m_T}} \quad (1)$$

Resonance is defined as:

$$f_{n2} = \frac{1}{2\pi} \sqrt{\frac{k(m_T + m_S)}{m_T m_S}} \quad (2)$$

The important results of not allowing m_T to affect its own environment are discussed below.

At f_{n1} , a large amount of force is required to maintain the input motion of m_S at the specified magnitude (Fig. 2a). The resulting response of m_T is thus extremely high, which leads to overtesting.

In the true environment, and where the system is lightly damped, m_T is more susceptible to a high response at f_{n2} than at any other frequency; i.e., applying the same level of sinusoidal force input (F_1) across the frequency test range, the response of m_T is many times greater at f_{n2} than at any other frequency (even f_{n1}). The low response of m_T (at f_{n2}) caused by the severe notching of the force is radically unrealistic compared to the condition that exists in the field. Consequently, the test results are vulnerable to undertesting at this frequency.

Unfortunately, a design engineer controls the frequencies where high force requirements occur during testing by physically changing m_T , k , and c . Also, these extremes will shift in frequency due to test items and/or interconnectors having different properties, even though they are fabricated from the same design.

In summary, infinite M_e testing causes excessive overdesign due to overtesting at f_{n1} , and in all probability results in a low safety factor or undertest at f_{n2} .

TEST SPECIFICATIONS

The faults of the infinite M_e testing, specifically the overtest at f_{n1} , are further magnified by the methods used in deriving test specifications. Input specifications are usually derived from field data obtained under one of the following conditions:

1. The foundation response is monitored while the test item is mounted;
2. The foundation response is monitored without the test item being mounted;
3. The foundation response is monitored with a different test item mounted; and
4. Input specifications are arbitrarily selected without reference to any applicable field data.

The field data are analyzed into an amplitude vs frequency spectrum. Unfortunately, the highest peaks from this spectrum are sometimes encompassed, and this level is called out as the constant motion input.

What is wrong with these practices? Condition 1 disregards the antiresonant frequency (f_{n1}), where the foundation motion has a tendency to be low. The test item's influence on its environment is again ignored. Condition 2 completely ignores the test item's environmental influence. We are often forced to use one of the last two methods due to a lack of field data. As will be discussed later, the new test methods will allow more intelligent test specifications when this problem exists.

ALTERNATE TEST METHODS

The penalty for not allowing the test item to affect its environment as it does in the field is that the amount of overtest and undertest cannot be predicted from the test results. As the demand for higher field performance and reliability increases, with the simultaneous requirement of reduced size and weight of the test item, future vibration tests must be more accurate.

Several alternate test methods have been recommended and/or used in an attempt to insert more meaning into vibration testing. Some of these alternatives are discussed below.

Zero M_e Testing

Controlling the force input to the test item (Point 2, Fig. 1) is classified as zero M_e testing, since the force is maintained independent of the foundation M_e . Assuming the force input to be constant results in the force requirement below m_S and the acceleration responses of m_S and m_T shown in Figs. 3a, 3b, and 3c, respectively. In this illustration, m_S is representative of the shaker armature and test fixture mass located below the interconnector.

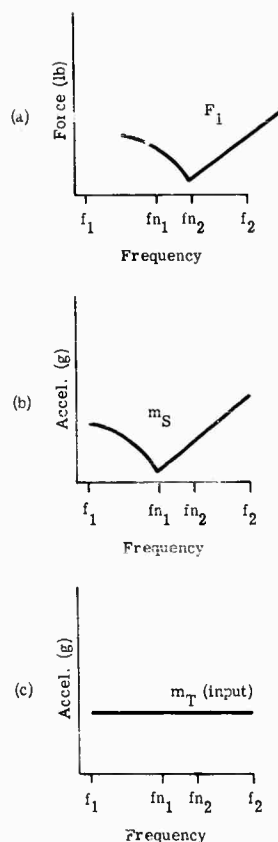


Fig. 3 - Response to zero M_e test: (a) force below m_S , (b) acceleration of m_S , and (c) acceleration of m_T

The test item does affect its environment at f_{n1} , but the responses of m_T at f_{n1} and f_{n2} are both suppressed. Unless the input force is quite high, a low safety factor would result at these two frequencies. If the force were high enough to avoid undertesting at f_{n1} and f_{n2} , an overtest would result at the other frequencies.

Based on the fact that the force below m_S and the response of m_S approach infinity (with increasing frequency) to maintain the input force at the prescribed level (Figs. 3a and 3b), it is apparent that this method is not representative of the conditions in the field.

Simulating Foundation Motion Determined From Field Measurements

Measuring the field response of the foundation (with test item mounted), and reproducing this motion in the laboratory, eliminates the need to be concerned about M_e of the foundation being simulated in the test. As long as the equipment above the control point is the same in the test as it is in the field, the test item responses are closely simulated. With the exception that inaccuracies result because each

test item and foundation do not have the same characteristics, and motion in the field is not repetitive, this method is basically sound.

This practice would undoubtedly be used in our test laboratory if field data were available from which to derive the proper input. However, since this field data is not available, we have adopted another method with which to insert more realism into our vibration tests. This method is discussed below under controlled M_e testing.

Acceleration Limiting

The first method used at Sandia to reduce the ridiculous force requirements at antiresonance was acceleration limiting. Not allowing the acceleration response of a test item or one of its internal components to exceed a predetermined level is classified as acceleration limiting.

During an infinite M_e test, acceleration limiting would allow the test item to have an influence on its environment at frequencies where the specified input level would have resulted in responses above the set limit. This normally means that the high force requirements at f_{n1} will be reduced.

Controlled M_e Testing

Recent efforts at Sandia have been directed toward controlling the sinusoidal force input below the foundation mass m_S , where the effective mass of the foundation is set at some finite value. This method is called constant M_e testing if the foundation M_e is maintained constant across the test range.

For a constant M_e test, and where the sinusoidal force input below the foundation is maintained constant, the response characteristics of the system (Fig. 1) are as depicted in Figs. 4a, 4b, and 4c. The advantages of this method over that of infinite M testing are as follows:

1. There is a definite control of the force input below the foundation (Fig. 4a). Thus, the force will not have sharp peak or notch characteristics across the frequency test range (particularly at f_{n1} and f_{n2}). The magnitude of overtesting and the possibility of undertesting can both be lessened.

2. As can be seen in Fig. 4b, the test item has influenced the response of the foundation.

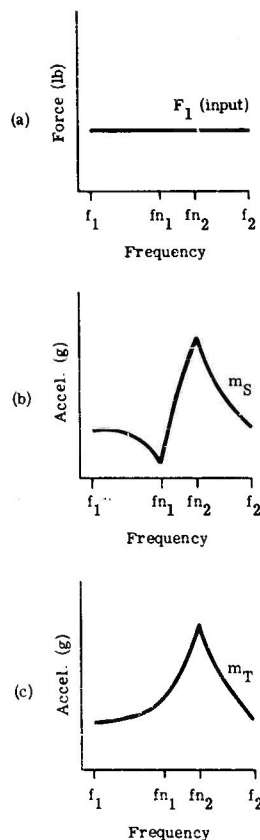


Fig. 4 - Response to controlled M_e test: (a) force below m_S , (b) acceleration of m_S , and (c) acceleration of m_T

As a result, the test item response at f_{n1} is lower than it would be for infinite M_e testing, and the higher response at f_{n2} is allowed to occur.

Another advantage of controlled M_e testing is that the axial fundamental response of the test item is not a function of the test equipment. The test equipment below the force-control point (armature and fixtures) has no fundamental influence on the system above the control point. However, the test equipment's effects on rotation, distortion, etc. are still not eliminated.

The degree of test accuracy resulting from controlled M_e testing obviously depends on the force spectrum used and the M_e used to simulate that of the foundation. At the present time, the selection of these test values is quite arbitrary. However, the basic principle is aimed in the right direction, since the test item is being allowed to affect its environment. As the available field data increase and/or our ability to predict test conditions improves, we will come closer and closer to a truly simulative vibration test.

FORCE LEVEL

Until a better understanding of the environmental forcing function can be obtained through field measurements, a constant sinusoidal force input will be used. Normally, the specified g input level is used as a guide in determining the force input. For example, for a test item of weight W_1 pounds to be tested with a simulated foundation of weight W_2 pounds, if the specified acceleration input was to be 2.0 g from 20 to 2000 cps, the constant force input below the foundation would be set at 2.0 ($W_1 + W_2$) pounds from 20 to 2000 cps. Simulating the foundation weight will be discussed below.

Another method which has been used in the past is the application of 10 percent of the maximum rocket thrust as a constant force input into the payload and simulated rocket motor mass.

REPRESENTING FOUNDATION M_e

As long as a constant force input is used, it is necessary to insert a foundation mass above the control point to allow the test item to affect its environment as it would in the field. Without this mass, a zero M_e test would result.

Currently, the foundation M_e is selected in one of the following ways. In tests where there is no reference available, a constant M_e equal to the mass of the test item is being considered for use. For tests on rocket payloads, an M_e equal to that of the empty rocket motor is held constant across the test range. Motor empty M_e is used rather than that of motor full, since the former results in a higher test item response during testing.

Two methods are used to insert the desired foundation M_e into the test setup. The first is physical addition of a mass. In this case, it is desirable to design a mass that remains rigid across the frequency test range, if at all possible. As long as the mass is rigid, M_e is controlled at a constant known value. The second method, which is being used almost exclusively, is electronic simulation of the desired M_e value. This concept utilizes an analog computer circuit which determines what the force input to the test item would be if the desired M_e were actually inserted in the test setup. A complete description of this procedure will be presented in a detailed paper on this subject at a later date.

Two advantages of electronic representation over physical representation are the economics

and the ability to vary M_c electronically during a test. For example, it is known that a foundation's M_c is not constant. When the variable function is determined from field measurements, it will be possible to reproduce this function in the laboratory.

As mentioned previously, it is quite probable that field data will eventually eliminate the constant force input and the insertion of a simulated foundation M_c . If the input motion at the base of the test item or the force input to the test item is determined from field measurements and reproduced in the laboratory, there is no need for either constant force input or duplication of M_c .

CONSTANT FORCE INPUT AND CONTROLLED M_c TEST ON RFD II RE-ENTRY VEHICLE

The first constant force input and controlled M_c test run at Sandia Corporation was on the



Fig. 5 - RFD II re-entry vehicle mounted on vibration machine

RFD II re-entry vehicle (RV). The RV was designed to furnish re-entry for a SNAP 10A nuclear reactor. The RV and reactor are shown mounted on a vibration fixture in Fig. 5.

At the time of the test request, the 450-pound system was to be powered by a four-stage NASA Scout rocket, which is connected to the RV by the interconnector shown in Fig. 6.

With the exception of momentary pulses at ignition of each stage, field data indicated that the only significant vibration caused by the Scout motors occurred during the fourth stage burning. Thus, only this vibration was requested to be simulated.

Prior to testing, decisions had to be made concerning the input force level, the motor M_c representation, and the type of force transducer to be used. Vibration energy during flight was mainly attributed to burning of the rocket. Since there was no reference from which to determine the proper forcing function, the value of 500 pounds, constant force (recommended by NASA) was used over the frequency range of 20 to 2000 cps.

The test and field setups were identical for the system above the motor. Thus, the only decision remaining was the value of M_c to be used in representing that of the motor. Since field data indicated that the maximum vibration response (30 g) occurred just before fourth stage burnout, when the motor weight was 60 pounds, it was decided to represent the motor empty condition. Another strong factor in the decision to represent the motor empty M_c were the results obtained in an electrical analog study, where the response of the RV was investigated for both motor empty and motor full conditions. For the same force input below the motor, it was determined that the empty condition resulted in RV responses about seven times higher at f_{n2} than for the motor full condition. Thus, a 60-pound cylinder was used to represent the motor (Fig. 6). The attachment between the cylinder and interconnector simulated the actual connection between the fourth stage motor and interconnector.

The force transducer used in the first series of tests is shown in Fig. 6. Forty strain gages were mounted around the periphery, with every fourth gage connected in series to form the four legs of the bridge. Two of these legs were used for temperature compensation. Due to low sensitivity (<0.1 microvolts per pound), the signal-to-noise ratio was low enough to cause accuracy problems during input control. The final test series utilized ten commercial

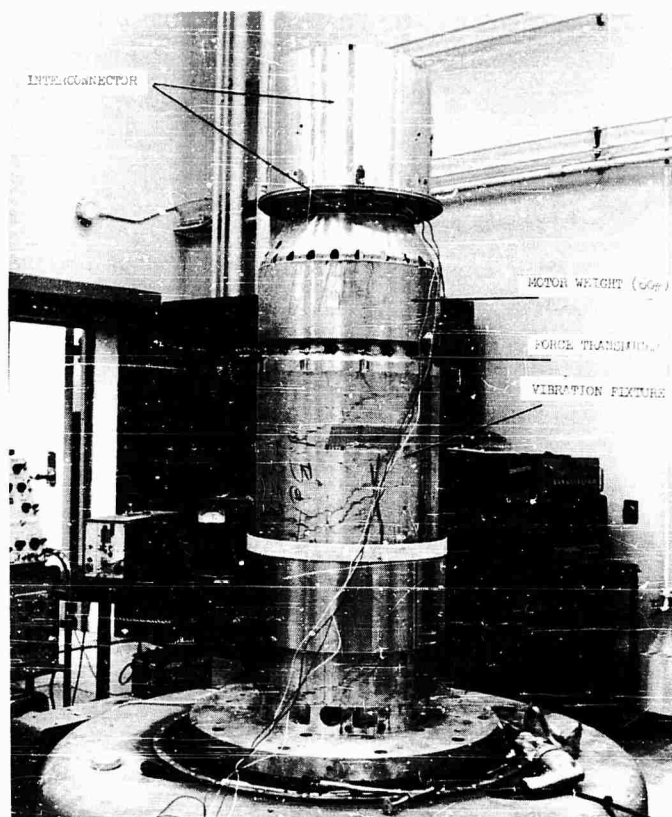


Fig. 6 - RFD II test setup (internal)

transducers mounted under the 60-pound cylinder. The transducer outputs were instantaneously summed. The resulting force sensitivity was about one thousand times that of the first transducer.

Typical response characteristics of the RV and motor are shown in Fig. 7. As predicted, the response characteristics during testing simulated that of the simple system shown in Fig. 8. In this sketch, m_T represents the weight of the RV, the reactor, and all internal components of the RV. The spring k represents the relatively light adaptor's spring characteristics, and m_M represents the 60-pound motor.

As can be seen by the antiresonance (f_{n1}) and resonance (f_{n2}) of the motor, the system above the adaptor was allowed to affect its own environment. As a result, the highest response on the RV occurred at f_{n2} rather than f_{n1} .

Had a constant acceleration of 1.0 g (infinite M_c test) been maintained on the motor,

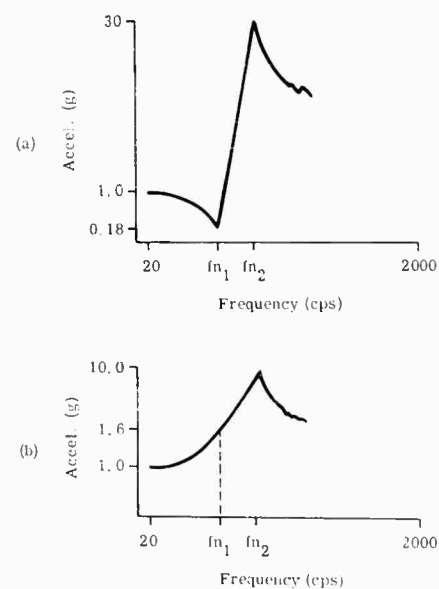


Fig. 7 - Vibration response of RFD II test items: (a) motor, and (b) re-entry vehicle

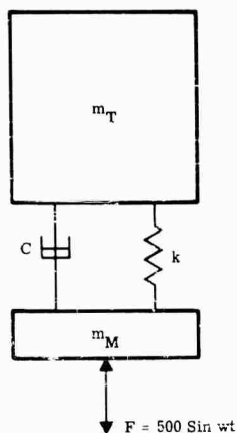


Fig. 8 - Simple representation of RFD II test setup

the force required at f_{n1} would have been about 3000 pounds, six times the force estimate actually used for an input. The resulting RV response at f_{n1} would have been about 10 g rather than 1.6 g. Also, the force required at f_{n2} would have been about 50 pounds, and the resulting RV response approximately 1.0 g.

Belsham and Harris have made apparent weight ($M_e \times 386$) analyses of the full and empty fourth stage motor (X-248) [1]. These plots are reproduced in Fig. 9. The dashed lines superimposed on this figure represent the motor full and motor empty apparent weights that were considered for use in the RFD II tests. The antiresonant frequency (f_{n1}) and resonant frequency (f_{n2}) which were found during vibration tests are also shown on these plots.

Up to about 120 cps, the 60-pound apparent weight used in the test was fairly accurate in its representation of the actual empty motor. There was considerable error involved at the frequency (≈ 130 cps) where there was a peak in the apparent weight (antiresonance). Above 200 cps, 60 pounds was higher than either motor empty or motor full apparent weights, with the exception of two frequencies on the motor empty plot.

NOTE: Reference appears on page 53.

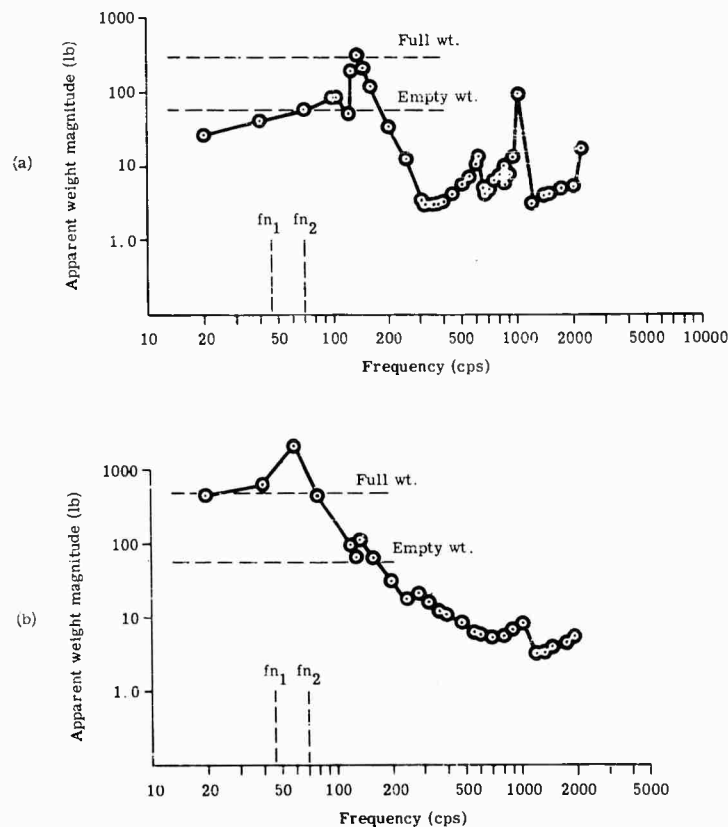


Fig. 9 - Apparent weights of fourth stage motor:
(a) empty, and (b) full

A better representation of the system's response to motor full and motor empty M_e , above 200 cps, would have been obtained if the apparent weight of the motor had been rolled off as some function of frequency after being maintained constant up to 200 cps. However, at the time of this test sequence, we were not aware of the method whereby apparent weight could be electronically varied.

The above discussion applies to random as well as sinusoidal force inputs. Several random tests have been run in which the force spectrum

was equalized, and electronic M_e representation was used. No difficulties or discrepancies in the data were experienced.

In summary, hindsight is a great teacher. We in the vibration test laboratory at Sandia are continually facing up to the fact that our new test philosophy is subject to considerable criticism, mainly from ourselves as we learn more and more each day. In spite of the known limitations in our new test methods and levels, we feel we are advancing in the correct direction, since the test item is allowed to affect its own environment.

REFERENCE

1. R. O. Belsham and J. J. Harris, "Apparent Weight Measurements of Rocket Payload

and Test Structures," NRL Memorandum Report 1099 (1960).

* * *

SELECTION OF VIBRATION TEST LEVELS USING FATIGUE CRITERIA

LaVerne W. Root
Collins Radio Company
Cedar Rapids, Iowa

This paper uses the Palmgren-Miner and the Corten-Dolan hypotheses for fatigue damage accumulation in the development of two sets of equations relating vibration test levels to the use environment. The equations are in terms of excitation levels and are independent of all test specimen properties except the slope of the fatigue curve of the test specimen material. A sample computation is included to clarify the usage of the equivalence equations.

INTRODUCTION

The problem of selecting vibration test levels has received considerable attention at previous shock and vibration symposia. Many techniques have been suggested for a rational selection of the vibration test levels. Historically, these have included the following techniques:

1. Early techniques which appear to be more closely related to limitations of the mechanical vibration table than to the use vibration,
2. Exact reproduction of use vibration following the introduction of the electrodynamic vibration machine, and
3. Recent attempts to simulate failure modes rather than the use environment.

Most of the recent papers [1-13] have been based on fatigue damage. The present paper is also based on fatigue damage, but the results differ in the following three ways from previous papers:

1. Equations relating test levels to use vibration are directly in terms of the environment parameters (that is, acceleration, velocity, or displacement) rather than test specimen stress levels.

2. The derived equations depend on the test specimen material but are independent of the test specimen geometry.

3. The Palmgren-Miner (PM) hypothesis [14,15] for fatigue damage accumulation and the Corten-Dolan (CD) hypothesis [16] are used, respectively, to obtain similar equivalence relationships.

The mathematical model (single degree of freedom, linear oscillator) is comparable to that used in the previous papers so that the limitations of the derived relationships are, in general, identical to previous results. The superiority of the present equations is their independence of the test specimen geometry.

Although the present derivation is based on transforming between like types of vibration (e.g., random-to-random), it is possible to derive analogous equations based on either hypothesis which will relate unlike types of vibration. The equations based on the CD hypothesis have been derived and are to be verified experimentally. Since the experimental verification is just beginning, these equations will not be included in this paper.

NOMENCLATURE

- a Peak amplitudes of random process
- b Stress exponent for fatigue curve equation

NOTE: References appear on page 64.

c	Constant from fatigue curve equation
D(T)	Fatigue damage accumulation at time T
d	Stress exponent from Corten-Dolan modified fatigue curve equation
E[]	Mathematical expectation of quantity in brackets
f	Frequency
K	Constant
N	Number of cycles to failure at constant stress from random or sine fatigue data
N'	Number of cycles to failure at constant stress from Corten-Dolan modified fatigue curve equation
n_i	Number of cycles applied at the i th stress
O()	Order of quantity in brackets
P()	Probability density function
Q	Amplification factor
T	Time
W	Excitation spectral density
X	Excitation amplitude
Y	Relative response amplitude
α_i	Proportion of total cycles at i th stress
β	Dummy variable used in derivations
$\Gamma()$	Gamma function
γ	Dummy variable used in derivations
η	Scaling factor on time or cycles
θ	Dummy variable used in derivations
ν_o	Expected frequency of narrow band process
σ	Peak stress
$\bar{\sigma}$	Root-mean-square stress

Subscripts

l	Associated with highest stress, excitation, etc.
g	Equivalent value
r	Random
s	Sine
t	Test

EQUIVALENCE EQUATIONS BASED ON PALMGREN-MINER HYPOTHESIS

The PM hypothesis is probably the most widely used fatigue damage accumulation hypothesis. For this reason, it will be used to develop a set of equivalence equations. The primary equation of interest from the PM papers is

$$\sum_{i=1}^m \frac{n_i}{N_i} = 1. \quad (1)$$

This can be rewritten in an alternate form (Appendix A) which has some advantages in certain portions of the derivations:

$$\frac{N_g}{N_1} = \frac{1}{\sum_{i=1}^m \alpha_i \left(\frac{\sigma_i}{\sigma_1} \right)^b}. \quad (2)$$

The interpretation of Eq. (2) is the same as in the case of the CD hypothesis which has a similar form (Appendix A). Two slight modifications of Eq. (2) are considered in this paper:

1. In the case of random vibration, the stress will be defined as the root-mean-square stress rather than the peak stress to avoid the possibility of the stress being infinite.

2. In the case of continuously varying stress levels, Eq. (2) can be rewritten as:

$$\frac{N_g}{N_1} = \frac{1}{\int_0^{\sigma_1} P(\sigma) \left(\frac{\sigma}{\sigma_1} \right)^b d\sigma}. \quad (3)$$

The following assumptions are used with Eq. (2) in deriving equivalence equations relating use vibration envelopes to a single equivalent envelope:

1. The test specimen may be represented by several noninteracting linear oscillators.

2. The majority of fatigue damage occurs at the resonant frequencies. This requires smoothly varying use vibration envelopes and/or a high-Q response.

3. The fatigue curve may be represented by a straight line on a log-log plot.

The equivalence equations are given as Eqs. (4) and (5) with the complete derivation being given in Appendix C:

$$X_g = X_1 \left[\sum_{i=1}^m \frac{T_i}{T_s} \left(\frac{X_i}{X_1} \right)^b \right]^{1/b} \quad (4)$$

and

$$W_g = W_1 \left[\sum_{j=1}^{\ell} \frac{T_j}{T_r} \left(\frac{W_j}{W_1} \right)^{b/2} \right]^{2/b} \quad (5)$$

These equations are used to obtain a point-by-point transformation between the use vibration and the equivalent vibration. The equivalence, based on Eqs. (4) and (5) requires times equal to original use vibration times; that is, a dwell test must be performed for a period T_s at each resonance, and a random test of duration T_r must be performed.

In general, it is necessary to shorten the test time since actual use vibration time may be several hours. Once an appropriate test time is selected, it is possible to use the fatigue curves to scale the equivalent levels given by Eqs. (4) and (5). The scaled equivalence equations are obtained using results from Appendix D:

$$X_t = \frac{X_1}{\eta_s^{1/b}} \left[\sum_{i=1}^m \frac{T_i}{T_s} \left(\frac{X_i}{X_1} \right)^b \right]^{1/b} \quad (6)$$

and

$$W_t = \frac{W_1}{\eta_r^{2/b}} \left[\sum_{j=1}^{\ell} \frac{T_j}{T_r} \left(\frac{W_j}{W_1} \right)^{b/2} \right]^{2/b} \quad (7)$$

Equations (6) and (7) are used in the same manner as Eqs. (4) and (5) except that the scaled times T_{st} and T_{rt} are used instead of T_s and T_r .

The following things should be noted about Eqs. (6) and (7):

1. The equations are independent of test specimen geometry with the only limitation being that stresses remain proportional to the excitation.

2. The parameter b is related to the fatigue characteristics of the test specimen material.

3. Any consistent units may be used for the vibration levels; for example, in Eq. (6), the excitation could be acceleration, velocity, or displacement; and in Eq. (7) the excitation could be acceleration spectral density, velocity spectral density, or displacement spectral density.

4. Equations (6) and (7) can be rewritten in terms of continuously varying stress levels:

$$X_t = \frac{X_1}{\eta_s^{1/b}} \left[\int_0^{X_1} P(X) \left(\frac{X}{X_1} \right)^b dX \right]^{1/b} \quad (8)$$

and

$$W_t = \frac{W_1}{\eta_r^{2/b}} \left[\int_0^{W_1} P(W) \left(\frac{W}{W_1} \right)^{b/2} dW \right]^{2/b} \quad (9)$$

DERIVATION BASED ON CORTEN-DOLAN HYPOTHESIS

The CD hypothesis is one of the several modifications of the PM hypothesis which attempt to account more accurately for interaction of varying stress levels. It is shown in Appendix A that it may be considered as a PM summation using a modified fatigue curve which has a different slope on a log-log plot and intersects the sine fatigue curve at the highest stress common to both. The slope of the modified fatigue curve may be obtained by random fatigue tests or from two level programed sine tests as discussed in the CD paper [16].

The primary equation from the CD paper is:

$$\frac{N_g}{N_1} = \frac{1}{\sum_{i=1}^m \alpha_i \left(\frac{\sigma_i}{\sigma_1} \right)^d} \quad (10)$$

It is shown in Appendix A that this may be re-written in an alternate form comparable to the PM equation:

$$\sum_{i=1}^m \frac{n_i}{N'_1} = 1. \quad (11)$$

Two modifications of Eq. (10) are required in this paper. In the case of random vibration, the maximum stress σ_1 will be interpreted as the maximum root-mean-square stress. For continuously varying stress levels

$$\frac{N_g}{N_1} = \frac{1}{\int_0^{\sigma_1} P(\sigma) \left(\frac{\sigma}{\sigma_1}\right)^d d\sigma} \quad (12)$$

The assumptions used in deriving the equivalence equations (Appendix C) are identical to those used in the PM derivation.

The relationships from Appendix D are used to obtain the scaled levels:

$$X_t = \frac{X_1}{\eta_s^{1/b}} \left[\sum_{i=1}^m \frac{T_i}{T_s} \left(\frac{X_i}{X_1}\right)^d \right]^{1/b} \quad (13)$$

and

$$W_t = \frac{W_1}{\eta_r^{2/d}} \left[\sum_{j=1}^p \frac{T_j}{T_r} \left(\frac{W_j}{W_1}\right)^{d/2} \right]^{2/d} \quad (14)$$

These equations are used in the same way as the analogous PM equations. The following things should be noted about Eqs. (13) and (14):

1. The equations are independent of the test specimen geometry.
2. The parameter b is related to the sine fatigue curve and the parameter d is related to the random fatigue curve.
3. Any consistent units may be used for the vibration levels.

4. Equations (13) and (14) may be rewritten in terms of continuously varying stress levels:

$$X_t = \frac{X_1}{\eta_s^{1/b}} \left[\int_0^{X_1} P(X) \left(\frac{X}{X_1}\right)^d dX \right]^{1/b} \quad (15)$$

and

$$W_t = \frac{W_1}{\eta_r^{2/d}} \left[\int_0^{W_1} P(W) \left(\frac{W}{W_1}\right)^{d/2} dW \right]^{2/d} \quad (16)$$

USE OF EQUIVALENCE EQUATIONS

The use of Eqs. (6), (7), (13) and (14) will be demonstrated by performing a set of sample calculations for the test specimen in Fig. 1. Since this test specimen has three natural frequencies, the vibration envelopes are divided into three frequency intervals as indicated by dotted lines in Fig. 2.

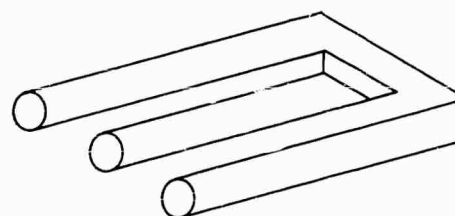


Fig. 1 - Test specimen from Project "Confused"

The test specimen consists of 6061-T6 aluminum. The values of b and d are 6.87 and 6.66, respectively [18].

The final test will consist of a one-hour dwell at each natural frequency followed by a one-hour random vibration test:

$$\eta_s = \frac{T_{st}}{T_s} = \frac{1}{40} = 0.025 \quad (17)$$

$$\eta_r = \frac{T_{rt}}{T_r} = \frac{1}{8} = 0.125 \quad (18)$$

PM Computations

1. Sine

	X_a	X_b	$\frac{T_a}{T_s}$	$\frac{T_b}{T_s}$	$\frac{X_a}{X_1}$	$\frac{X_b}{X_1}$	$\left(\frac{X_a}{X_1}\right)^b$	$\left(\frac{X_b}{X_1}\right)^b$	$\sum \frac{T_i}{T_s} \left(\frac{X_i}{X_1}\right)^b$	X_t
f_1	3	4	0.9	0.1	3/4	4/4	0.138	1.000	0.224	5.44
f_2	5	2	0.9	0.1	5/5	2/5	1.000	0.002	0.900	8.35
f_3	2	1	0.9	0.1	2/2	1/2	1.000	0.009	0.901	3.31

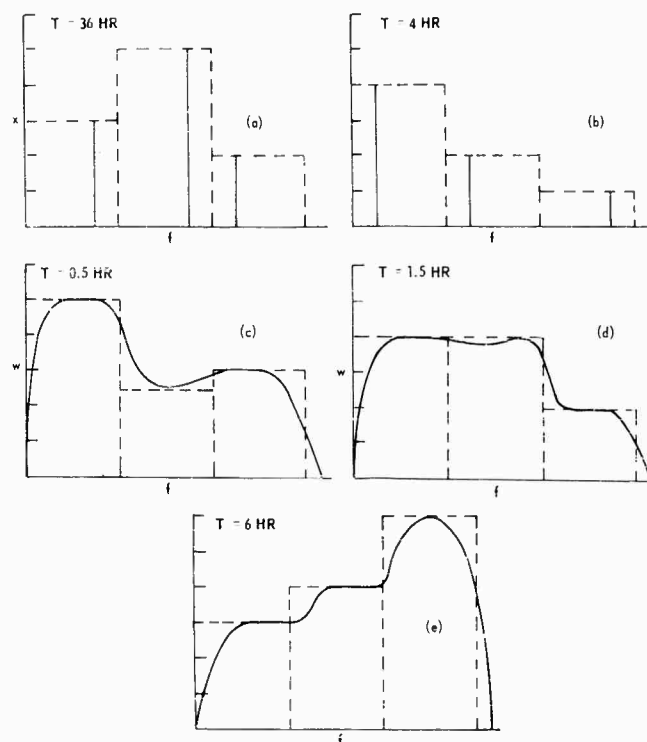


Fig. 2 - Use vibration from Project "Confused": (a) ground transportation by three-legged mule, (b) air transportation by tired pelican, (c) design testing -- substitute for xylophone in local symphonic orchestra, (d) production testing -- paperweight in boiler factory, and (e) end use -- mechanical frequency standard for Project "Befuddled"

2. Random

	W_c	W_d	W_e	$\frac{T_c}{T_r}$	$\frac{T_d}{T_r}$	$\frac{T_e}{T_r}$	$\frac{W_c}{W_1}$
f_1	5	4	3	0.0625	0.1875	0.75	5/5
f_2	2.5	4	4	0.0625	0.1875	0.75	2.5/4
f_3	3	2	6	0.0625	0.1875	0.75	3/6

	$\frac{W_d}{W_1}$	$\frac{W_e}{W_1}$	$\left(\frac{W_c}{W_1}\right)^{b/2}$	$\left(\frac{W_d}{W_1}\right)^{b/2}$
f_1	4/5	3/5	1	0.465
f_2	4/4	4/4	0.200	1
f_3	2/6	6/6	0.092	0.023

	$\left(\frac{W_e}{W_1}\right)^{b/2} \sum \frac{T_i}{T_r} \left(\frac{W_i}{W_1}\right)^{b/2}$	W_t
f_1	0.173	0.2895
f_2	1	0.9500
f_3	1	0.7601

CD Computations

The computational form is similar to the computations of the PM test levels so computations are presented in an abbreviated form.

1. Sine

	X_a	X_b	$\left(\frac{X_a}{X_1}\right)^d$	$\left(\frac{X_b}{X_1}\right)^d$	$\sum \frac{T_i}{T_s} \left(\frac{X_i}{X_1}\right)^d$	X_t
f_1	3	4	0.147	1.000	0.232	5.47
f_2	5	2	1.000	0.002	0.900	8.35
f_3	2	1	1.000	0.010	0.901	3.31

2. Random

	W_c	W_d	W_e	$\left(\frac{W_c}{W_1}\right)^{d/2}$	$\left(\frac{W_d}{W_1}\right)^{d/2}$
f_1	5	4	3	1	0.475
f_2	2.5	4	4	0.208	1
f_3	3	2	6	0.099	0.026

	$\left(\frac{W_c}{W_1}\right)^{d/2} \sum \frac{T_i}{T_r} \left(\frac{W_i}{W_1}\right)^{d/2}$	W_t
f_1	0.182	0.2881
f_2	1	0.9505
f_3	1	0.7611

CONCLUSIONS

Most of the published experimental data indicate that the random fatigue curve has a steeper slope than the sine fatigue curve. The CD hypothesis predicts this difference in slope for $d < b$. This indicates that the CD hypothesis may be a more accurate representation of fatigue damage accumulation than the PM hypothesis.

The CD hypothesis weights the low stresses heavier than the PM hypothesis. Therefore, it is expected that the equivalence equations based on the CD hypothesis will predict equivalent

levels considerably higher than those predicted by the PM hypothesis, if the use environment has a very large percentage of low-level vibration. The sample calculation represents a poor choice of times and levels to demonstrate the two hypotheses, since the differences in test levels were less than five percent.

Both methods are equal in computational ease and intuitive appeal. The CD hypothesis requires the determination of d . This should not preclude its usage if experimental work indicates it is more realistic. It is recommended that a study be undertaken to compare the results in using the two hypotheses for predicting vibration test levels.

Regardless of which hypothesis is used in selecting test levels, the equations as presented in the present paper offer certain advantages over previous formulations. It is possible to go directly from use vibration to the equivalent levels without knowing the specimen stresses or geometry. This should make the present formulation more useful in early design stages when the geometry is still unknown.

ACKNOWLEDGMENTS

The analysis presented in this paper was prepared originally as part of the continuing program at Collins Radio Company to improve the environmental design of its products. Additional analysis and experimental verification are currently being carried out under contract NAS8-11278 with NASA-Huntsville.

Appendix A

ALTERNATE FORMS OF PALMGREN-MINER AND CORTEN-DOLAN EQUATIONS

CASE I: PM EQUATION

The usual form of the PM equation is given as Eq. (1). This equation can be rearranged into a form which is equivalent to the CD equation. It is assumed that the fatigue curve is represented by

$$N \sigma^b = c. \quad (A1)$$

Recognizing that $n_i/N_g = \alpha_i$ and rearranging Eq. (1) after multiplying by N_g/N_g and N_1/N_1 gives

$$\frac{N_g}{N_1} = \frac{1}{\sum_{i=1}^m \alpha_i \frac{N_1}{N_i}}. \quad (A2)$$

Using Eq. (A2) to replace N_1/N_i in terms of a stress ratio gives Eq. (2) which is identical to the CD equation with the exception of the stress ratio exponent.

CASE II: CD EQUATION

The usual form of the CD equation is given as Eq. (10). This equation can be rearranged into a form equivalent to the PM equation.

Rearranging Eq. (10) and recognizing that $a_i = n_i/N_k$ gives

$$\sum_{i=1}^m \frac{n_i}{N_1} \left(\frac{\sigma_i}{\sigma_1} \right)^d = 1. \quad (A3)$$

Defining N'_i as

$$N'_i = N_1 \left(\frac{\sigma_i}{\sigma_1} \right)^d \quad (A4)$$

and substituting this value into Eq. (A3) produces Eq. (11).

Equation (11) is identical in form to the PM equation. Consideration of Eqs. (A4) and (A5) shows that the CD equation can be interpreted as a PM summation on a modified fatigue curve:

$$N'_i \sigma_i^d = N_1 \sigma_1^d = \bar{c} \quad (A5)$$

The equivalence between the PM and the CD hypotheses allows considerable simplification in derivations in Appendixes B and C.

Appendix B

RANDOM FATIGUE EQUATIONS

The fatigue curve may be represented by Eq. (B1), where β and γ may be b and c or d and \bar{c} , respectively, for the PM hypothesis and the CD hypothesis:

$$N\sigma^\beta = \gamma. \quad (B1)$$

The incremental damage due a single stress cycle of amplitude a is given by $1/N(a)$ for the PM hypothesis (or CD hypothesis on the modified fatigue curve). The fractional damage between a and $a + da$ is given by Eq. (B2).

$$\frac{n(a)}{N(a)} = \nu_o \tau \frac{p(a)}{N(a)} da. \quad (B2)$$

The total expected damage is obtained by summing the incremental damage from Eq. (B2). It may be assumed that the stress peaks are represented by a Rayleigh distribution and Eq. (B1) can be used to evaluate $N(a)$:

$$\begin{aligned} E[D(\tau)] &= \frac{\nu_o \tau}{\gamma \bar{\sigma}^2} \int_0^\infty a^{\beta+1} e^{-\frac{a^2}{2\bar{\sigma}^2}} da \\ &= \frac{\nu_o \tau}{\gamma} (\sqrt{2} \bar{\sigma})^\beta \Gamma\left(1 + \frac{\beta}{2}\right). \end{aligned} \quad (B3)$$

At failure, the damage is one and $\nu_o \tau = N$, so Eq. (B3) can be rewritten as follows:

$$N\bar{\sigma}^\beta = \frac{\gamma}{2^{\beta/2} \Gamma\left(1 + \frac{\beta}{2}\right)}. \quad (B4)$$

CASE I

The random fatigue equation for the PM hypothesis is obtained from Eq. (B4) by setting $\beta = b$ and $\gamma = c$:

$$N\bar{\sigma}^b = \frac{c}{2^{b/2} \Gamma\left(1 + \frac{b}{2}\right)}. \quad (B5)$$

This equation indicates that the random fatigue curve should be parallel to the sine fatigue curve when plotted on log-log coordinates.

CASE II

The random fatigue equation for the CD hypothesis is obtained from Eq. (B4) by setting $\beta = d$ and $\gamma = \bar{c}$:

$$N\bar{\sigma}^d = \frac{\bar{c}}{2^{d/2} \Gamma\left(1 + \frac{d}{2}\right)}. \quad (B6)$$

This equation indicates that the random fatigue curve should be parallel to the modified sine fatigue curve when plotted on log-log coordinates.

The preceding derivation follows that given in Ref. [17] in its general form.

EQUIVALENCE EQUATIONS

The test specimen may be represented by a number of noninteracting linear oscillators. In considering any one of the oscillators as depicted in Fig. C1, it is desired to obtain an equivalent excitation, X_g , which will accumulate an identical amount of fatigue damage as the m use vibration envelopes accumulate. The fatigue damage is governed by Eq. (C1) which may represent either the PM hypothesis or the CD hypothesis, depending on the value of θ :

$$\frac{N_g}{N_1} = \frac{1}{\sum_{i=1}^m \alpha_i \left(\frac{\sigma_i}{\sigma_1} \right)^\theta} \quad (C1)$$

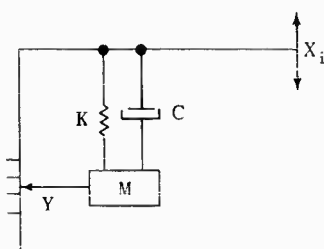


Fig. C1 - Mathematical model representing the i th oscillator

CASE I

The use vibration may consist of m vibration envelopes, each of which may be represented by several fixed frequency components separated by $\Delta f = O(f/Q)$. With each envelope is associated a time T_i . The frequency spacing of the individual components of a given envelope allows the fatigue damage accumulation to be represented by m terms (one from each envelope).

The relative displacement at a given frequency is a linear function of the excitation, and the stress is a linear function of the relative displacement:

$$\sigma_i - K_1 Y_i = K_2 X_i \quad (C2)$$

Equation (C1) can be rewritten in terms of the excitation using Eq. (C2):

$$\frac{N_g}{N_1} = \frac{1}{\sum_{i=1}^m \alpha_i \left(\frac{X_i}{X_1} \right)^\theta} \quad (C3)$$

Since Eq. (C3) is for a given frequency, it is possible to substitute the proportion of the time at the i th level for α_i :

$$\frac{N_g}{N_1} = \frac{1}{\sum_{i=1}^m \frac{T_i}{T_s} \left(\frac{X_i}{X_1} \right)^\theta} \quad (C4)$$

The fatigue curve will be represented as a straight line on log-log coordinates (Fig. C2) leading to Eq. (A1), $N\sigma^b = c$.

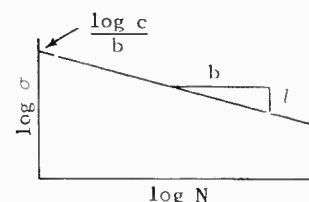


Fig. C2 - Typical straight line representation of fatigue curve on log-log plot

The cycle ratio in Eq. (C4) will be replaced by the stress ratio (excitation ratio) using Eq. (A1):

$$X_g = X_1 \left[\sum_{i=1}^m \frac{T_i}{T_s} \left(\frac{X_i}{X_1} \right)^\theta \right]^{1/\theta} \quad (C5)$$

This equation is applied at each frequency of interest and by correct value of θ will represent either the PM hypothesis ($\theta = b$) as Eq. (4) or the CD hypothesis ($\theta = d$) as

$$X_g = X_1 \left[\sum_{i=1}^m \frac{T_i}{T_s} \left(\frac{X_i}{X_1} \right)^d \right]^{1/d} \quad (C6)$$

CASE II

The use vibration may consist of ℓ vibration envelopes, each of which may be represented

by a smoothly varying spectral density w_j . With each envelope is associated a time T_j .

It is assumed the Q is sufficiently high and the spectral density is sufficiently smooth that a white noise approximation can be used at any given frequency of interest. The root-mean-square relative response at a given frequency is a linear function of the square root of the spectral density, and the root-mean-square stress is a linear function of the response:

$$\bar{\sigma}_j = \bar{K}_3 \bar{y}_j = \bar{K}_4 (w_j)^{1/2}. \quad (C7)$$

Equation (C1) can be rewritten in terms of the excitation using Eq. (C7):

$$\frac{N_g}{N_1} = \frac{1}{\sum_{j=1}^{\ell} \alpha_j \left(\frac{w_j}{w_1} \right)^{\theta/2}}. \quad (C8)$$

As before, α_j will be replaced with the proportion of the total time spent at the j th level.

$$\frac{N_g}{N_1} = \frac{1}{\sum_{j=1}^{\ell} \frac{T_j}{T_r} \left(\frac{w_j}{w_1} \right)^{\theta/2}}. \quad (C9)$$

The random fatigue curve, depending on whether it is obtained using the PM hypothesis

or the CD hypothesis (Appendix B), varies, respectively, as

$$N\bar{\sigma}^b = c_r \quad (C10)$$

or

$$N\bar{\sigma}^d = \bar{c}_r. \quad (C11)$$

These two equations will be represented by a single equation where β can be either b or d and γ_r can be either c_r or \bar{c}_r .

$$N\bar{\sigma}^\beta = \gamma_r. \quad (C12)$$

The cyclic ratio in Eq. (C9) will be replaced by the stress ratio (excitation ratio) using Eq. (C12).

$$w_g = w_1 \left[\sum_{j=1}^{\ell} \frac{T_j}{T_r} \left(\frac{w_j}{w_1} \right)^{\theta/2} \right]^{2/\beta}. \quad (C13)$$

This equation is applied at each frequency of interest; by correct values of θ and β , it represents the PM hypothesis ($\theta = b$, $\beta = b$) as Eq. (5) or the CD hypothesis ($\theta = d$, $\beta = d$) as

$$w_g = w_1 \left[\sum_{j=1}^{\ell} \frac{T_j}{T_r} \left(\frac{w_j}{w_1} \right)^{d/2} \right]^{2/d}. \quad (C14)$$

Appendix D

TIME AND LEVEL SCALING

The use time may be scaled by a factor η to obtain the test time:

$$T_t = \eta T_g. \quad (D1)$$

The cycles to failure at a given frequency is directly proportional to the time:

$$N_t = \eta N_g. \quad (D2)$$

The fatigue curve is represented by Eq. (B1), $N\sigma^\beta = \gamma$.

$$\frac{N_t}{N_g} = \eta = \frac{\sigma_g^\beta}{\sigma_t^\beta} \quad (D3)$$

$$\sigma_t = \frac{\sigma_g}{\eta^{1/\beta}}. \quad (D4)$$

Equation (D4) represents the stress relationship, and the test level scaling equations can be obtained by substituting the relationship for stress and the correct value for β .

CASE I

Sine Levels — PM or CD:

$$X_t = \frac{X_g}{\eta_s^{1/b}}. \quad (D5)$$

CASE II

Random Levels — PM:

$$W_t = \frac{W_g}{\eta_r^{2/b}} \quad (D6)$$

CASE III

Random Levels — CD:

$$W_t = \frac{W_g}{\eta_r^{2/d}} \quad (D7)$$

REFERENCES

1. J. W. Miles, "On Structural Fatigue Under Random Loading," *J. Aeronaut. Sci.*, pp. 753-762 (Nov. 1954).
2. C. E. Crede, "Damage Criterion as a Parameter to Define the Vibration Environment," *Shock, Vibration Bull. No. 24*, pp. 318-323.
3. R. E. Blake and M. W. Oleson, "Substitutes for Random-Vibration Testing," *Shock and Vibration Bull. No. 24*, pp. 338-343.
4. M. W. Oleson, "A Narrow-Band Random-Vibration Test," *Shock and Vibration Bull. No. 25, Part I*, pp. 110-119.
5. C. E. Crede, "Criteria of Damage from Shock and Vibration," *Shock and Vibration Bulletin No. 25, Part II*, pp. 227-235.
6. T. P. Rona, "Equivalent Vibration Program from the Fatigue Viewpoint," *Shock, Vibration, and Associated Environments Bull. No. 27, Part II*, pp. 129-136.
7. R. M. Mains, "Damage Accumulation in Relation to Environmental Testing," *Shock, Vibration, and Associated Environments Bull. No. 27, Part IV*, pp. 95-100.
8. A. J. Curtis, "A Method of Equating Long Duration-Low Intensity and Short Duration-High Intensity Random Vibration," *Shock, Vibration, and Associated Environments Bull. No. 27, Part IV*, pp. 101-105.
9. B. M. Hall and L. T. Waterman, "Correlation of Sinusoidal and Random Vibration," *Shock, Vibration, and Associated Environments Bull. No. 29, Part IV*, pp. 218-225.
10. L. T. Waterman, "Random versus Sinusoidal Vibration Damage Levels," *Shock, Vibration, and Associated Environments Bull. No. 30, Part IV*, pp. 128-139.
11. M. Gertel, "Derivation of Shock and Vibration Tests Based on Measured Environments," *Shock, Vibration, and Associated Environments Bull. No. 31, Part II*, pp. 25-33.
12. K. W. Smith, "A Procedure for Translating Measured Vibration Environment into Laboratory Tests," *Shock, Vibration, and Associated Environments Bull. No. 33, Part II*, pp. 159-177.
13. M. Vet, "Dwell-Sweep Correlation," *Proc. IES*, pp. 433-443 (1963).
14. A. Palmgren, "Die Lebensdauer Von Kugellagern," *Zt. des Ver. Deut. Ing.* (1924).
15. M. A. Miner, "Cumulative Damage in Fatigue," *J. Appl. Mech.*, pp. 159-164 (Sept. 1945).
16. H. T. Corten and T. J. Dolan, "Cumulative Fatigue Damage," *Proc. Internat. Conf. on Fatigue of Metals*, pp. 235-246 (1956).
17. S. H. Crandall and W. D. Mark, *Random Vibration in Mechanical Systems* (Academic Press, New York and London, 1963), pp. 112-117.
18. L. W. Root, "Random-Sine Fatigue Data Correlation," *Shock, Vibration, and Associated Environments Bull. No. 33, Part II*, pp. 279-285.

DISCUSSION

Mr. Phelan (Cornell Univ.): How do you handle the horizontal part of a fatigue endurance limit curve when you get into random vibrations where many of your cycles would be at such low stress that you could have an infinite number without any failure?

Mr. Root: I believe, if you will look into the fatigue data, that even the ferrous alloys

lose this endurance. In other words, they essentially have no endurance limit when you mix stress levels. There are experimental papers to back this point. Probably the representation is better for the nonferrous alloys, but even the ferrous considerably reduces the endurance limit so you probably can use this on either.

* * *

ANALOG EXPERIMENTS COMPARE IMPROVED SWEEP RANDOM TEST WITH WIDE BAND RANDOM AND SWEEP SINE TESTS

Galt Booth
MB Electronics
New Haven, Connecticut

and

Jens Trampe Broch
Bruel & Kjaer
Naerum, Denmark

A major problem with previous sweep random tests has been the relatively long test time required for the same damage-producing capability as a wide band random test. An improved technique is presented which appreciably shortens this test time. A further problem in the application of the sweep random technique to component or subassembly testing has been the difficulty of appraising the degree to which the sweep random process approaches the damage-producing capability of a wide band random excitation. The experimental results presented in this paper should aid in this appraisal.

An experimental study is described in which the electrical analog of a resonant mechanical device on a vibration exciter was subjected to a number of carefully controlled vibration tests. These tests included the common wide band random test, the sweep sine test, and a variety of different sweep random tests with differing system time constants. The responses of this resonant system to the various tests were carefully measured in a standardized manner and plotted in a common form so that the results of the different vibration test techniques may be directly compared.

The measured parameter chosen as having significance for all vibration test techniques is the count of the number of times the analog of the instantaneous acceleration or stress of the resonant mechanical device exceeds a specified reference level during the complete vibration test. To characterize a complete vibration test the distributions of response peaks are formed by making such counts at numerous reference levels. Since the same levels are used for each type of vibration test, the counts for the different vibration test techniques are directly comparable.

Normalized curves are presented which show the counts at each reference level for each of the vibration test techniques. Since these curves show the number of stress or acceleration peaks to be expected above various levels, the curves are useful both to compare the various types of vibration tests and as aids to the mechanical designer concerned with cyclic fatigue in the vibration environment. The plausibility of these experimental curves is enhanced by a comparison with curves predicted by theory.

The results of the experiments are used to develop accelerated sweep random tests. A new sweep random test technique is proposed which better takes into consideration the time available for testing.

HISTORY

Although the wide band random test is generally accepted, it is costly and a less costly substitute has been sought ever since its first introduction. Various "equivalent" sweep sine tests have been proposed but since the sweep sine test cannot produce the same distribution of acceleration and stress amplitudes within the test specimen, no general equivalence between the two types of test is ever likely to be found. In 1957, M. W. Olesen of the Naval Research Laboratory proposed a sweeping narrow band random vibration test which actually constitutes a compromise between a wide band random vibration test and a sweep sine test. It operates on the principle of replacing the low acceleration density wide band random excitation with an intense, narrow band random excitation sweeping slowly over the frequency range of the test. In 1960, G. B. Booth showed how to calculate the acceleration level and the test time needed to make a sweep random test correspond to a wide band test. It was shown that the sweep random test can produce the same number of important stresses and accelerations, at each level, as the wide band test. For a long time the equipment necessary to perform this kind of testing was not commercially available, and very little progress was made in the use of the method. Recently, the complete control equipment required for sweep random vibration testing has been developed in the form of two units: a sine-random generator and a vibration meter. Also, considerable efforts have been and are being made to evaluate and extend the test. The more theoretical parts of the work are being confirmed by tests on electromechanical models, while a number of comparative damage studies are currently in the planning and preliminary test stages.

OBJECTIVES

The program reported in this paper has four objectives:

1. To confirm experimentally the theoretical calculations (appendix) of the distribution of response accelerations to a sweep random test,
2. To determine experimentally other response acceleration distributions obtainable with the control equipment,
3. To develop time-level exchange curves useful in the shortening of sweep-random test times, and
4. To propose an improved sweep random test procedure.

TECHNIQUE

The block diagram (Fig. 1) shows the equipment used to perform the sweep random test. The narrow band random acceleration excitation to the test specimen is monitored by an accelerometer, read on a meter, and applied to a compressor circuit which controls the gain of a variable gain stage. The level of a narrow band random voltage of sweeping center frequency is controlled by this variable gain stage. The power amplifier then amplifies this sweeping narrow band random voltage to a level adequate to drive the vibration exciter and specimen.

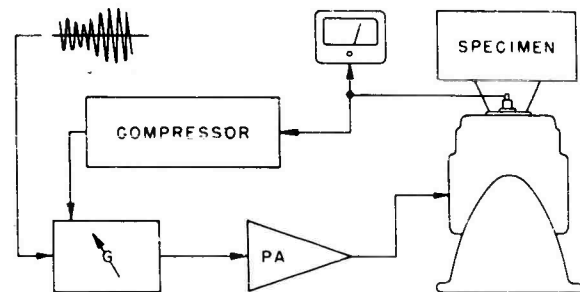


Fig. 1 - Block diagram showing operation of equipment to perform the sweep random test

To study the distribution of response acceleration peaks, an electrical analog of a mechanical specimen was built. Figure 2(a) shows the mechanical block diagram of any normal vibration mode of the test specimen. a_t is the acceleration of the vibration table and a_s is the response acceleration of the mass. The ratio, a_t/a_s of the response acceleration to the table acceleration is shown by the curve to the right.

The electrical analog shown in Fig. 2(b) was chosen for experimental convenience. The input current i is made proportional to the vibrator table acceleration a_t . The integral of the voltage across the capacitor is then proportional to the mass acceleration a_s . The diagram to the right shows that the ratio of the integrated capacitor voltage to the input current has the same form as the response of the mechanical system.

Figures 3 and 4 show the control equipment, the analog, and the measuring instrumentation. The circuit was fed from the sine-random generator set to produce a constant acceleration gradient (Eqs. (A18) and (A19)) by

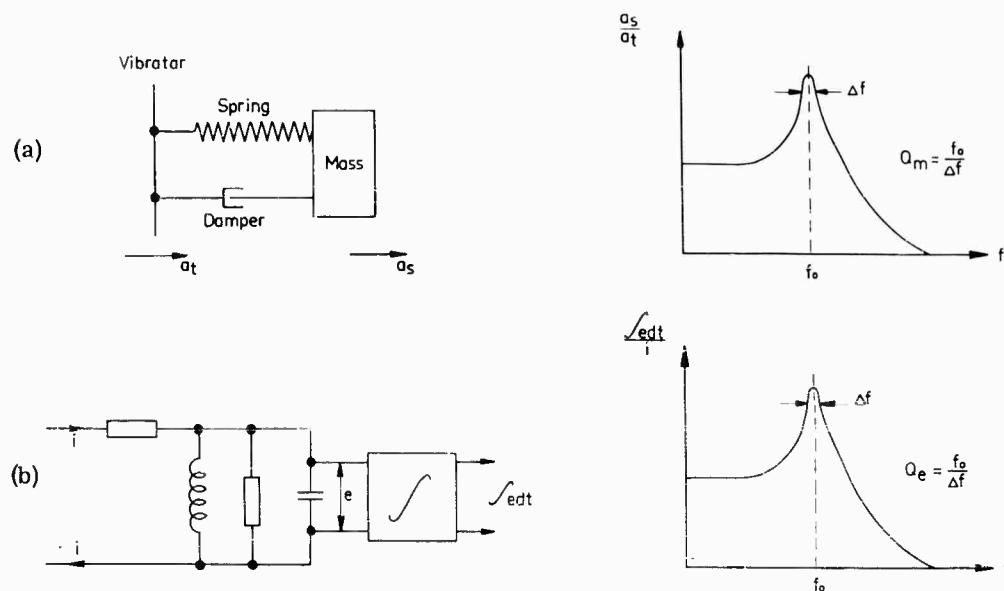


Fig. 2 - Analog of mechanical normal vibration mode: (a) mechanical schematic and ratio of response to input accelerations, and (b) electrical analog and ratio of integrated capacitor voltage to input current

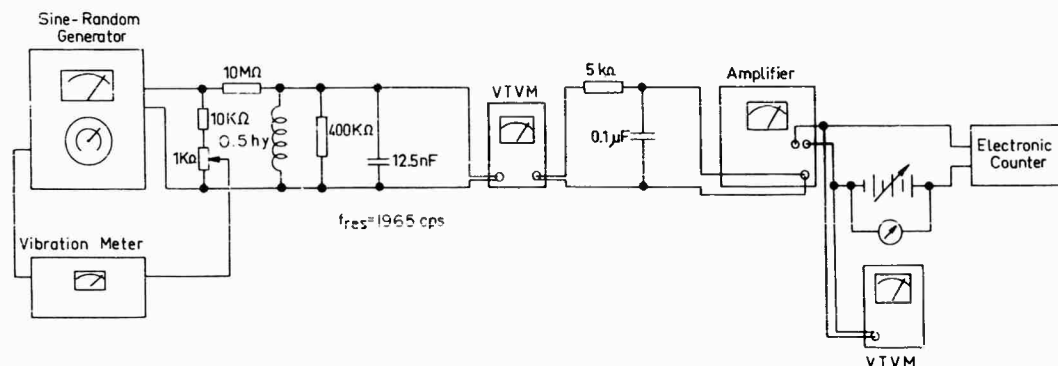


Fig. 3 - Schematic showing control equipment, analog, and measuring instrumentation

the feed-back through the vibration meter. To keep the current independent of the impedance of the test circuit, a 10-megohm isolation resistor was used. The circuit was tuned to 1965 cps and adjusted to a Q of 20.2 by a damping resistor. To measure an output proportional to the acceleration of the mass, the output voltage from the circuit was isolated from the test circuit by an amplifier having a high input impedance (10 megohms). Finally, the output of a second isolation amplifier was fed to a counting arrangement. A special random noise voltmeter, having a wide selection of integration time constants and an rms rectifier, was used to measure the rms value of the output signal.

A counting arrangement was used to count the number of times the signal crossed a reference level b with positive slope (Fig. 5). The level was set by the battery and was adjusted to the following multiples of the rms response level: 0.5, 1.0, 1.5, 2.0, 2.5, 3.0, 3.5. The rms value was arbitrarily chosen to be 8 volts, making the variation in the counter firing level, about 0.2 volts, negligible. A further inaccuracy is due to the difficulty in setting the dc voltage exactly to the correct multiple of the rms value. This is most critical at high multiples of the rms value because of the steepness of the slope of the measured curve. It was found that this error was about ± 0.1 volt. Furthermore,

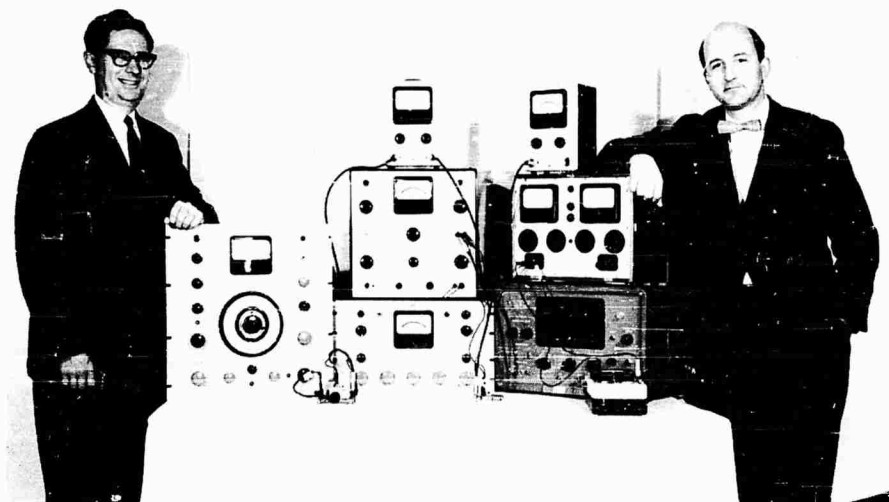


Fig. 4 - Authors, analog shown in front of control equipment (left) and measuring instrumentation (right)

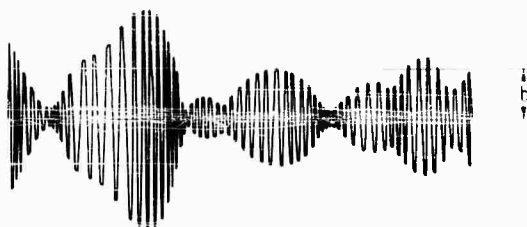


Fig. 5 - Narrow band random acceleration signal and reference acceleration level b (counts made of number of peaks exceeding b)

the resulting counts are subject to the usual statistical errors related to the sample sizes; however, these statistical errors are small except at 3.5 times the rms response level where the counts come in clumps.

MEASUREMENTS

A number of tests were made, keeping the level b in Fig. 5 fixed, and sweeping the narrow band of noise back and forth through the resonance of the analog, counting the number of level crossings.

By changing the level b and repeating the experiments for various settings of the sweeping bandwidth and compressor speed, the set of curves shown in Fig. 6 were plotted. The various curves are marked with β , defined as the

ratio between the compressor speed and the test noise bandwidth. The ratio β is significant because only the interaction between the fluctuations of the noise envelope and the regulation speed changes significantly the distribution of vibration excitation peaks.

The ordinate of the curves is the ratio of the number N_b of peaks exceeding the level b to the total number of peaks occurring in a sweep over the -3 db bandwidth of the analog circuit. Although during the experiments the frequency was varied between the -10 db points of the circuit resonance curve, most of the vibrational energy imported to the specimen during test is between the -3 db frequencies.

It can be seen from the curves that no change in the peak distribution occurs for β lower than 33, which means that for these values of β no interaction takes place between the fluctuations of the noise envelope and the automatic level regulation. The results obtained for these low β values can also be verified theoretically (Fig. 7; appendix).

Finally, for the sake of comparison, the peak distribution obtained by sweeping a sine wave through the resonance is also shown in Fig. 6. A certain upper limit, 1.42, in peak level exists and the shape of the distribution is considerably different from those obtained with a fluctuating signal. Also, when sweeping with a sine wave, the peak buildup repeats itself each sweep, which is significantly

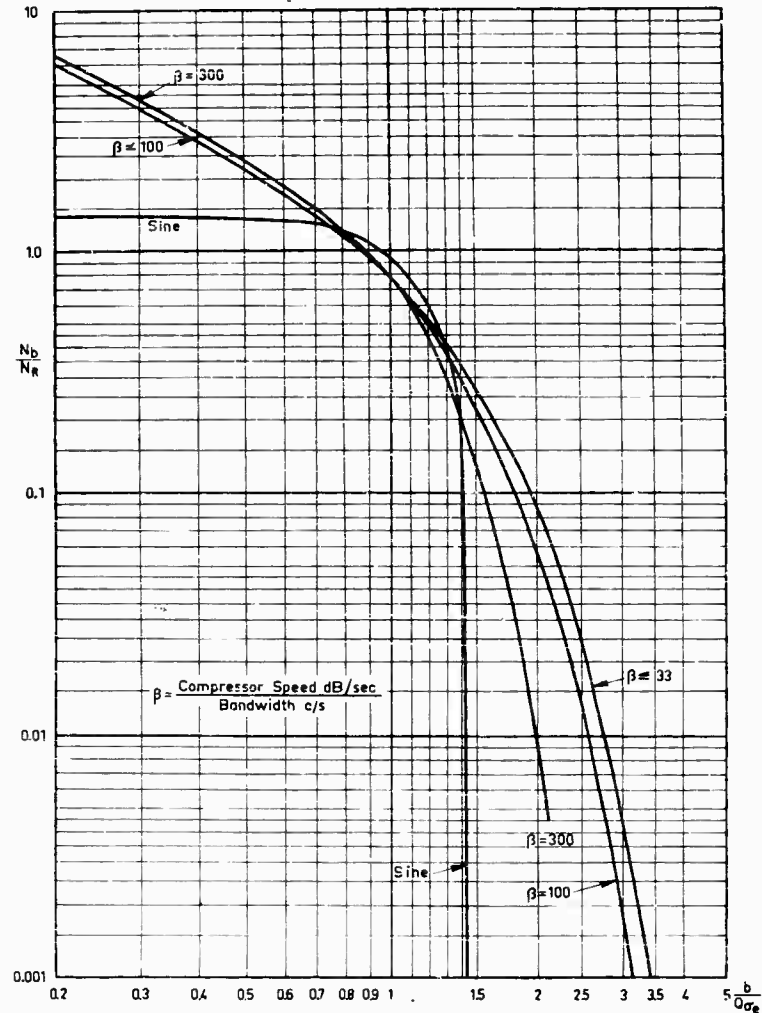


Fig. 6 - Ratio of number of peaks exceeding level b to total number of cycles in resonance bandwidth for sweep random tests with various compressor speeds and for sweep sine test

different when fatigue damage accumulation is considered.

PEAK DISTRIBUTION MATCHING

To obtain an equivalence between a wide band and a sweep random test, the distribution of acceleration response peaks at the higher response levels must be similar. It is well known that the distribution of response peaks of a lightly damped single-degree-of-freedom system follows the Rayleigh distribution when the system is excited by wide band Gaussian noise. Since the integral of the Rayleigh distribution, shown in Fig. 8, is known, it was used to confirm the operation of the instrumentation.

To match a sweep random test to a wide band test, the distribution curves shown in Fig. 6 must be matched to the integrated Rayleigh curve. Figure 9 shows an example of the matching technique. As all curves shown are plotted to logarithmic scales, a "sliding" of the axis by the amounts q and s actually means a multiplication of the quantities involved, as with a slide rule. Thus, looking at the x -axis (abscissas), the rms level of the sweep random test is multiplied by the factor q to provide the best possible peak matching.

The test level of the sweep random equivalence is

$$\gamma = q \sqrt{\frac{G}{80}} \quad (1)$$

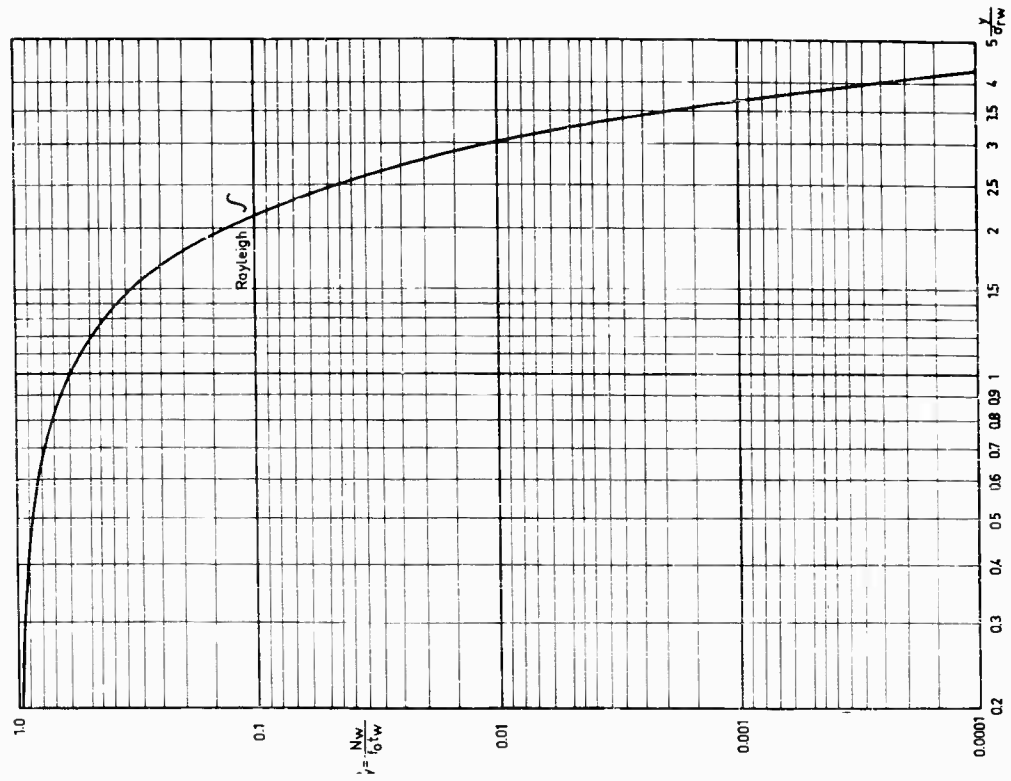


Fig. 8 - Integral of Rayleigh amplitude distribution, showing ratio of number of acceleration peaks exceeding level y to total number of response acceleration peaks for wide band random test

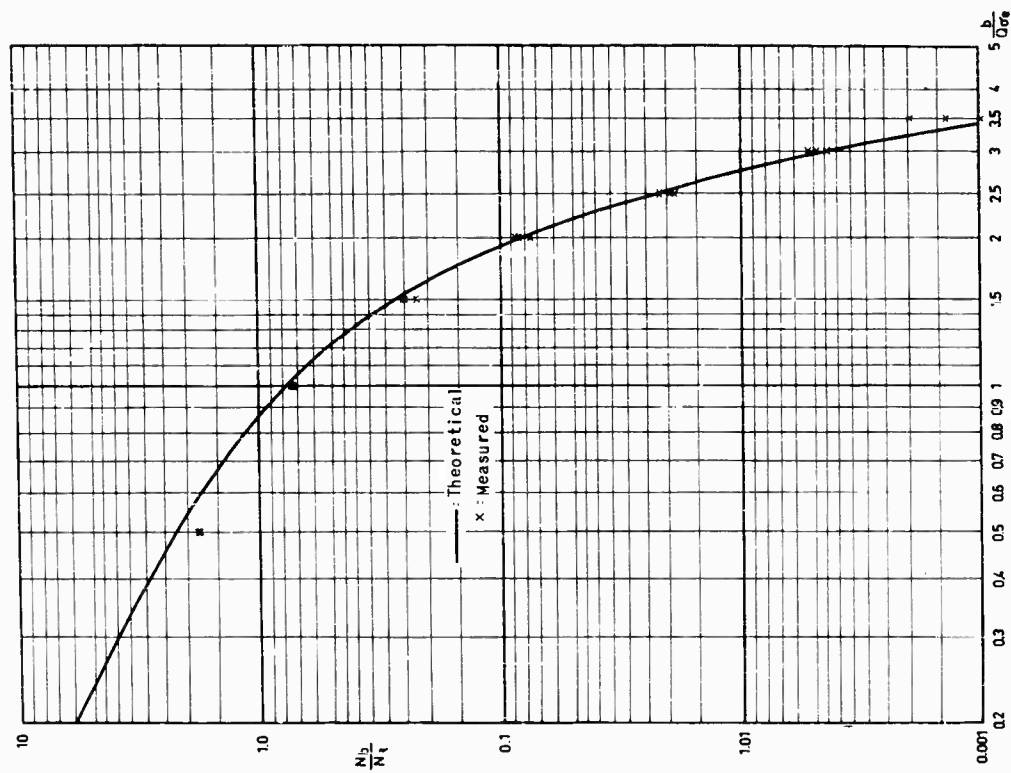


Fig. 7 - Comparison of theoretical and experimental distributions of acceleration peaks for slow sweep random test

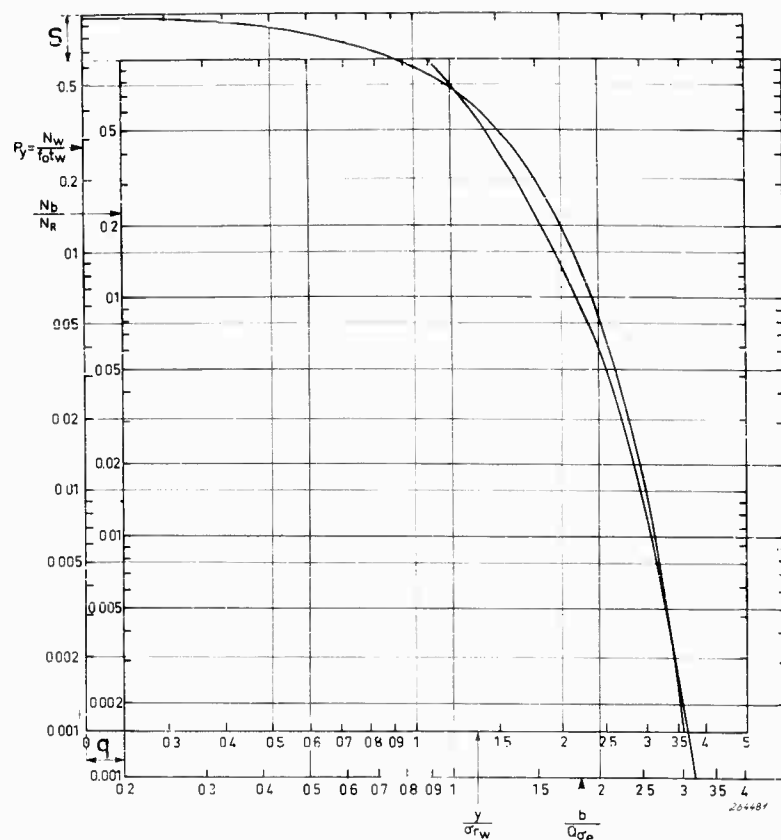


Fig. 9 - Matching of sweep random response acceleration peak distribution to wide band random response acceleration peak distribution showing test time factor, s , and level factor, q

Similarly, the test time for the sweep represented by the ordinates in Fig. 9 must be multiplied by the factor s :

$$t_n = s \cdot 20 t_w \ln \frac{f_H}{f_L} \quad (2)$$

In Eqs. (1) and (2), which are derived in the Appendix, γ is acceleration gradient ($g/\sqrt{\text{sec}}$), G is acceleration spectral density (g^2/cps), t_n is test time for the sweep random test (min), t_w is test time for the wide band test (min), f_H is upper limit of the frequency sweep, and f_L is lower limit of the frequency sweep.

To set up a sweep random test which complies with the wide band specifications, $G = 0.2 g^2/\text{cps}$ from 20 to 2000 cps, and $t_w = 2$ minutes; if the matching shown in Fig. 9 were used, the acceleration gradient would be $\gamma = 0.058 g/\sqrt{\text{sec}}$ and $t_n = 156$ minutes. This test time may be considered too long. It is possible to reduce

this time, while retaining a good distribution of acceleration response peaks, by the technique described in the next section.

ACCELERATED TESTING

As an objective, accelerated testing should reduce the duration of the sweep random test, while keeping the number of response acceleration peaks at each level the same as the wide band test.

Since the curves of Fig. 6 have differing shapes for the various β values, it is possible to match the curves to the integrated Rayleigh curve of Fig. 8 in many ways. Figure 10 illustrates three of the more useful matching situations. In each case the sweep random curve was placed to give approximately the same number of acceleration response peaks during the sweep random test as occurs during the wide band random test throughout the critical region

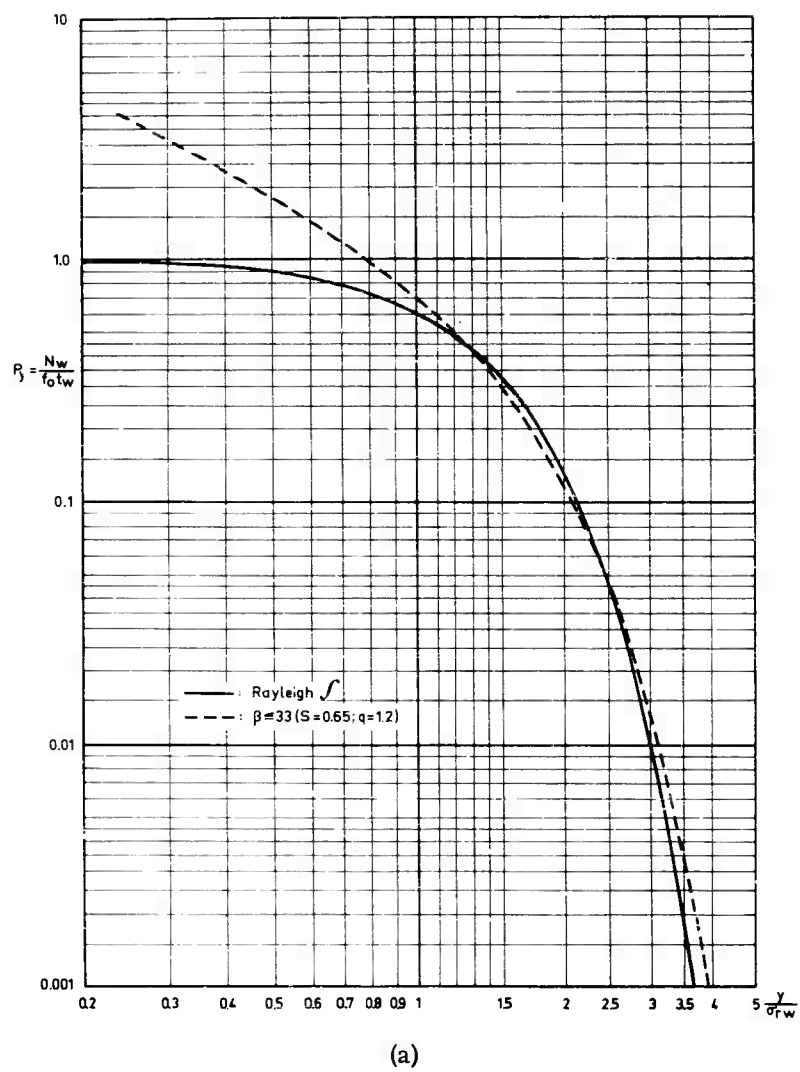
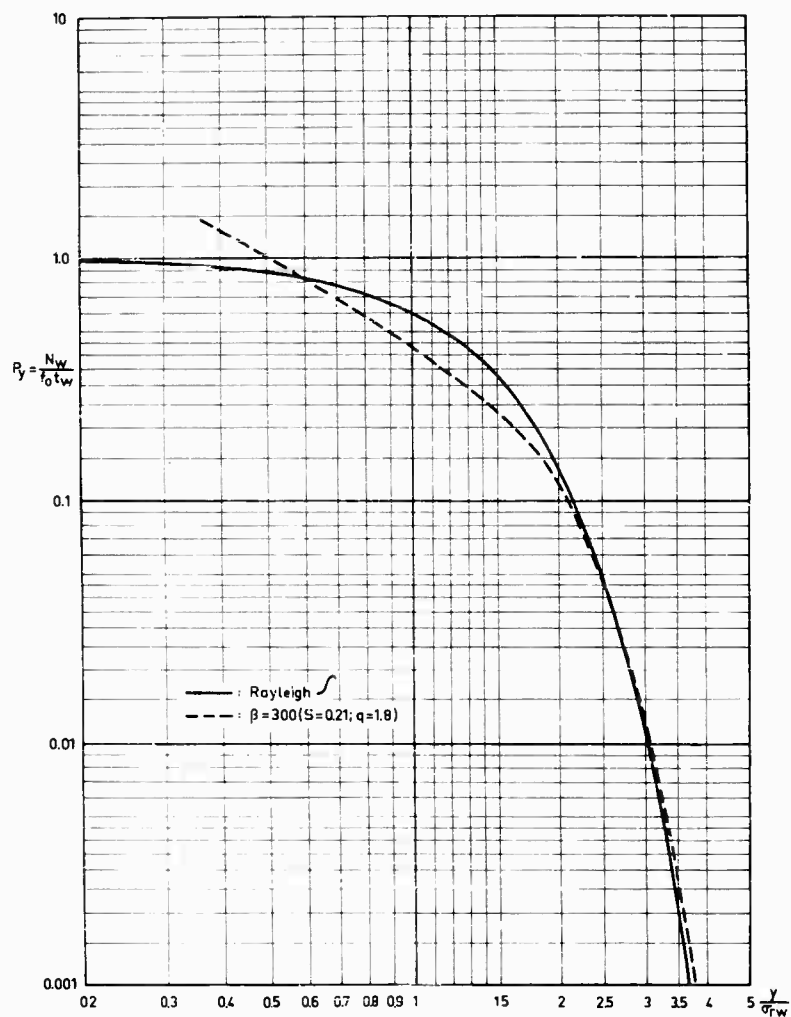


Fig. 10(a) - Distribution matching for slow sweep random test



(b)

Fig. 10(b) - Distribution matching for moderately accelerated sweep random test

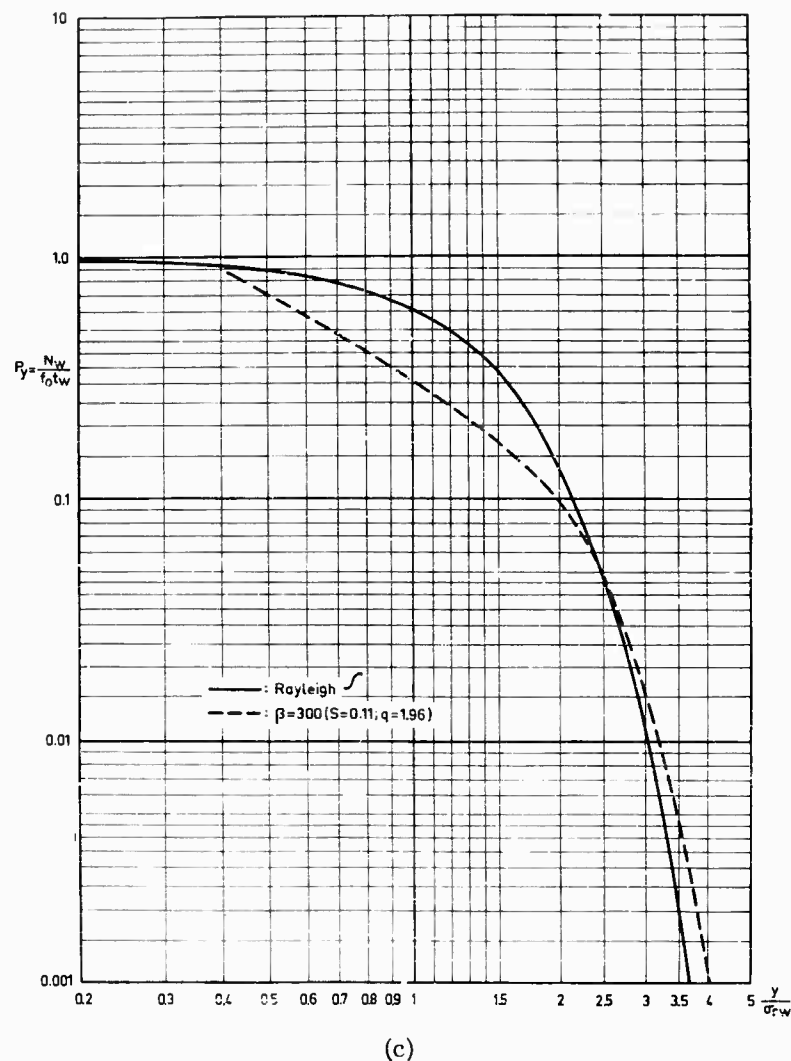


Fig. 10(c) - Distribution matching for sweep random test with six-fold reduction in test time

from two to three times the wide band rms response acceleration.

The result of such matching is to reduce the test time factor s by a relatively large amount and increase the level factor q by a small amount, while maintaining the number of response acceleration peaks at the critical levels essentially unchanged by an adjustment of the compressor speed of the control equipment.

Figure 10(a) shows the matching for the slow sweep random test. A match with the slow compressor speeds, $\beta \leq 33$, provides the desired distribution of acceleration peaks over a very large amplitude range. The test time factor s is 0.65, and the level factor q is 1.2.

Figure 10(b) shows a match which reduces the sweep random test duration to about one third of the time for the slow sweep random test. The number of acceleration peaks is matched within ± 1 db from two to three times the rms response acceleration to the wide band test. Or, in the colloquial language of the test floor, it is matched within 13 percent from 2 to 3 "sigma." Although the test time factor s is reduced to 0.21, it is not without disadvantage, since the level factor q must be increased from 1.2 to 1.8, which requires more force from the vibration exciter system.

Figure 10(c) shows a match which further reduces the test time. The accuracy of the distribution of acceleration peaks is not quite

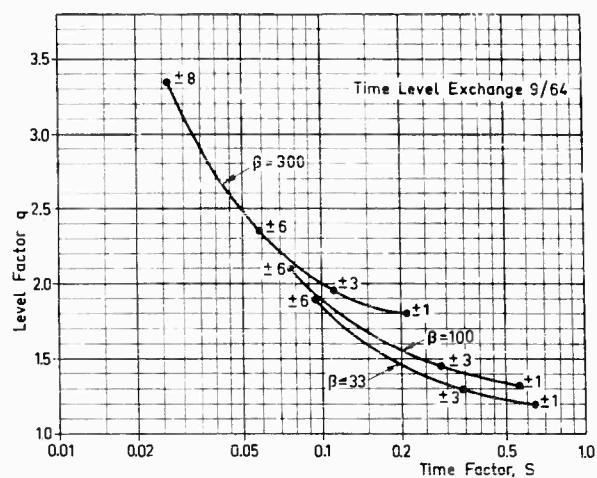


Fig. 11 - Time level exchange curves for selection of level factors, q , and time factors s

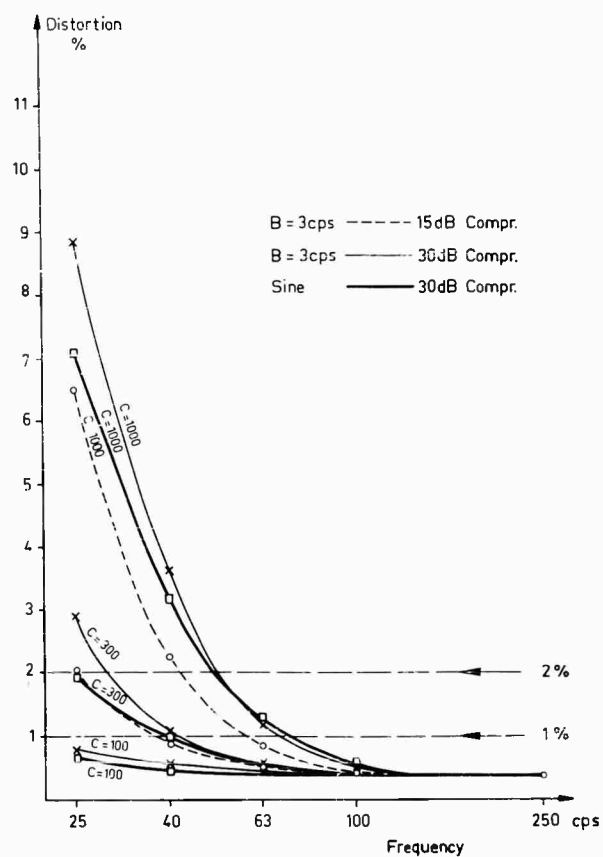


Fig. 12 - Distortion of control equipment signal with high compressor speeds

so good, however, becoming ± 3 db in the critical 2- to 3-"sigma" region. The test time has been reduced by about another factor of two, to $s = 0.11$, with only a small additional increase in drive level, to $q = 1.96$. Visual observation of the response acceleration signal on the screen of an oscilloscope shows that the typical fluctuating narrow band character of the response of a resonating circuit to a random excitation is maintained.

The curves of Fig. 11, providing sets of values for q and s , summarize the results of many such matches. Three curves are shown: one for slow compressor speeds, $\beta \leq 33$; one for an intermediate compressor speed-bandwidth relationship, $\beta = 100$; and one for the highest recommended compressor speed-bandwidth relationship, $\beta = 300$. The accuracy of the match, in decibels, in the 2- to 3-"sigma" region, is shown by notations beside the dots on the curves.

Although it was possible to obtain a compressor speed-bandwidth relationship β equal

to 1000, this is not recommended since the amplitude distribution is unsatisfactory. High compressor speeds also cause distortion at the lower frequencies, since they tend to distort the waveform of the oscillator output. Figure 12 shows the distortion caused by compressor speeds of 1000, 300, and 100 db/sec on both sine and 3-cps bandwidth random signals at both moderate and high compression levels.

NEW TEST APPROACH

A new test approach is proposed. Due to the possibilities shown for accelerated testing it is reasonable to first determine what time is available for testing. With this information, the most suitable β -value and test accuracy are determined and the corresponding q and s values are found from the curves given in Fig. 11.

The control equipment is then adjusted to produce an acceleration gradient given by Eq. (1) and the test continues for a time given by Eq. (2).

Appendix

DERIVATION OF EQUIVALENT SWEEP RANDOM TEST

This derivation is applicable to the normal Rayleigh distribution of acceleration peaks of narrow band random signals. This Rayleigh distribution is produced when the control equipment is adjusted so that the quotient of the compressor speed in decibels per second and the bandwidth in cycles per second is equal to or less than 33.

OBJECTIVE

The sweep random test shall cause the same number of stress reversals at each stress level as does the wide band random test. Since for each resonance, the stresses are proportional to the response accelerations, the number and amplitude distribution of the larger response accelerations for the sweep random test are adjusted until they agree with the number and amplitude distribution of the larger response accelerations for the wide band random test.

WIDE BAND RANDOM EXCITATION

The response of a single-degree-of-freedom system or of a lightly damped mode of a complex

structure to a wide band random vibration excitation is

$$\sigma_{r\omega} = \sqrt{\frac{\pi G f_o Q}{2}} \quad (A1)$$

where

$\sigma_{r\omega}$ = rms accelerations response, wide band (g);

G = acceleration density (g^2/cps);

f_o = frequency of responding resonance (cps); and

Q = magnification factor of resonance.

If a wide band random vibration is filtered to narrow bandwidth, either electrically or mechanically by a resonance, the response is a random vibration of nearly constant frequency but varying amplitude.

The peaks of any narrow band random acceleration response are distributed according to the Rayleigh distribution

$$P_y = \frac{y}{\sigma_r^2} e^{-\frac{y^2}{2\sigma_r^2}} \quad (A2)$$

where P_y is the probability density of an acceleration peak of magnitude y and σ_r is the rms acceleration response. The probability that an acceleration peak will have a magnitude greater than y is given by the integral of P_y from y to ∞ :

$$P_y = \frac{1}{\sigma_r^2} \int_y^\infty y e^{-\frac{y^2}{2\sigma_r^2}} dy \quad (A3)$$

which is

$$P_y = e^{-\frac{y^2}{2\sigma_r^2}} \quad (A4)$$

shown in Fig. 9.

If the wide band excitation continues for a time t_w , the maximum number of acceleration response peaks is $f_o t_w$. The expected number of peaks which exceed the magnitude y is then

$$N_y = f_o t_w P_y \quad (A5)$$

SWEEP RANDOM EXCITATION

If the same structure is excited by a random vibration with bandwidth much narrower than the bandwidth f_o/Q of the resonance, the response is

$$\sigma_{rn} = H \sigma_e \quad (A6)$$

where σ_{rn} is the rms acceleration response, narrow; σ_e is the rms acceleration excitation, narrow; and the transmissibility of the structure, H , is given by

$$H = \left| \frac{1}{1 - \left(\frac{f}{f_o}\right)^2 + \frac{j f}{Q f_o}} \right| \quad (A7)$$

As the center frequency of the sweep random excitation approaches f_o , the response increases until it reaches a maximum rms magnitude $Q\sigma_e$.

If the center frequency of the narrow band random excitation changes so slowly that the resonance can build up to full response, and also if the time constant of the compressor in the control loop is so slow that the amplitude

distribution is unaffected by compressor action, the probability that an individual acceleration peak will exceed the level b is given by

$$P_b = e^{-\frac{b^2}{2H^2\sigma_e^2}} \quad (A8)$$

A logarithmic frequency sweep rate is defined by

$$\frac{df}{dt} = r f \quad (A9)$$

In the time period dt , the number of acceleration peaks exceeding the level b is

$$dN = P_b \cdot f dt = P_b \frac{df}{r} \quad (A10)$$

The total number of peaks exceeding the level b becomes

$$N_b = \frac{1}{r} \int_0^\infty df \cdot e^{-\frac{b^2}{2H^2\sigma_e^2}} \quad (A11)$$

With substitution of $e^x = f/f_o$, expansion of the exponent, and discard of small terms, Eq. (A11) becomes

$$\begin{aligned} N_b &= \frac{1}{r} \int_0^\infty df e^{-\frac{b^2}{2\sigma_e^2} \left[4x^2 + \frac{1}{Q^2} \right]} \\ &= \frac{f_o}{r} \int_{-\infty}^\infty dx e^{-\frac{b^2}{2\sigma_e^2} \left[4x^2 + \frac{1}{Q^2} \right]} \quad (A12) \end{aligned}$$

With the further substitution $y = x - (\sigma_e/2b)^2$, Eq. (A12) becomes

$$N_b = \frac{f_o}{r} \int_{-\infty}^\infty dy \cdot e^{-\frac{2b^2 y^2}{\sigma_e^2}} \cdot e^{-\frac{2b^2}{\sigma_e^2} \left[\frac{1}{4Q^2} - \frac{\sigma_e^4}{16b^4} \right]} \quad (A13)$$

which integrates to

$$N_b = \sqrt{\frac{\pi}{2}} \cdot \frac{\sigma_e}{b} \cdot \frac{f_o}{r} \cdot e^{-\frac{2b^2}{\sigma_e^2} \left[\frac{1}{4Q^2} - \frac{\sigma_e^4}{16b^4} \right]} \quad (A14)$$

Equation (A14) expresses the number of response peaks exceeding the level b when a resonance is excited with a narrow band random

excitation, with bandwidth much narrower than f_o/Q and rms value σ_e , which is swept past the resonance frequency f_o at a sweep rate $df/dt = rf$, when the control compressor time constant is long.

It is convenient to normalize Eq. (A14) by dividing by the total number N_r of acceleration cycles occurring during the sweep through the bandwidth of the resonance

$$f_o \left(1 - \frac{1}{2Q}\right) \text{ to } f_o \left(1 + \frac{1}{2Q}\right):$$

$$N_r = \int f dt = \int_{f_o(1-\frac{1}{2Q})}^{f_o(1+\frac{1}{2Q})} \frac{df}{r} = \frac{f_o}{rQ} \quad (\text{A15})$$

After normalization, Eq. (A14) becomes

$$\frac{N_b}{N_r} = \sqrt{\frac{\pi}{2}} \cdot \frac{Q\sigma_e}{b} \cdot e^{-\frac{1}{2}\left(\frac{b}{Q\sigma_e}\right)^2} \left[1 - \frac{1}{4Q^2} \left(\frac{Q\sigma_e}{b}\right)^4\right] \quad (\text{A16})$$

which is plotted in Fig. 7.

The curve of Fig. 7 may be superimposed on the integrated Rayleigh curve of Fig. 9 to give Fig. 8. The two curves are close in the critical region between $b/\sigma_{r\omega} = 2$ and $b/\sigma_{r\omega} = 3$, and deviate little from $b/\sigma_{r\omega} = 1$ to $b/\sigma_{r\omega} = 4$.

The fact that these curves can be made nearly to coincide is important because it permits the sweep random test to reproduce closely all damage-producing response acceleration peaks over the entire amplitude range.

The sweep random sweep rate and excitation level are determined from the relative position of the graphs when the curves coincide.

The excitation for the sweep random test is found by equating the horizontal axes of Fig. 8:

$$\frac{y}{\sigma_{r\omega}} = q \frac{b}{Q\sigma_e} \quad (\text{A17})$$

The ratio q of the positions of the horizontal axes is 1.2 for the case of slow compressor speed. Since for a wide band excitation, the rms response $\sigma_{r\omega}$ is given by Eq. (A1), the sweep random acceleration excitation becomes

$$\sigma_e = q \sqrt{\frac{\pi G f}{2Q}} \quad (\text{A18})$$

Since this acceleration excitation varies as $f^{1/2}$, it is convenient to introduce a new

parameter, the acceleration gradient γ which is independent of frequency and is maintained constant by action of the compressor during the sweep random test:

$$\gamma = \frac{\sigma_e}{\sqrt{2\pi} f} \quad (\text{A19})$$

The excitation level for the sweep random test may then be expressed as an acceleration gradient

$$\gamma = q \sqrt{\frac{G}{4Q}} \quad (\text{A20})$$

Since the magnification factors Q of the many resonances in a specimen are unknown, a median value must be arbitrarily chosen which is approximately right for all resonances. A value of 20 is recommended for Q , which keeps the response within ± 3 db for the normal Q range of 10 to 40 and within ± 7 db for the extreme range 4 to 100. The test is conservative; the high Q resonances are the ones tested excessively, and the low Q , more resistant resonances, are the ones inadequately tested. Using this recommended value, the acceleration gradient for the sweep random test may now be given by Eq. (1).

The sweep rate is found by matching the vertical axes of Fig. 8:

$$\frac{N_w}{f_o t_w} = s \cdot \frac{N_b}{N_r} = \frac{s r N_b Q}{f_o} \quad (\text{A21})$$

The ratio, s , of the vertical axis positions is 0.65 for the case of slow compressor speed.

Since it is desired that the number of peaks at each level be the same, $N_n = N_w$, the sweep rate becomes

$$r = \frac{1}{s Q t_w} \quad (\text{A22})$$

By using Eq. (A9), the total sweep random test time t_n is

$$t_n = \frac{1}{r} \int_{f_L}^{f_H} \frac{df}{f} = \frac{1}{r} \ln \frac{f_H}{f_L} \quad (\text{A23})$$

where f_L and f_H are the lower and upper limit frequencies, respectively. By using r from Eq. (A22), this becomes

$$t_n = s Q t_w \ln \frac{f_H}{f_L} \quad (\text{A24})$$

When the recommended value of 20 for Q is used, Eq. (2) for the sweep random test time results.

BANDWIDTH

Whenever possible, a narrow test bandwidth, perhaps 3 cps, is chosen. Such a narrow bandwidth requires a relatively slow compressor speed if the high acceleration peaks are not to be compressed undesirably. However, for some tests it may be necessary to sweep rapidly through frequencies where high Q resonances exist. If this is so, then wider bandwidths permit faster compressor speeds and improved correction.

These wide test bandwidths require modification of the test procedure at those low frequencies where the test bandwidth exceeds the bandwidth of the resonant response. A first approximation, exact if the reaction of the resonance on the vibration exciter is negligible, is derived as follows:

If the narrow band excitation is much wider than the resonance, the rms low-frequency response acceleration is like the response to a wide band excitation of Eq. (A1) and becomes

$$\sigma_{rLf} = \sqrt{\frac{\pi G_n f_o Q}{2}} \quad (A25)$$

where

$$G_n = \frac{\sigma_{eLf}^2}{B} \quad (A26)$$

and σ_{eLf} is the low-frequency rms acceleration excitation.

If the rms response acceleration of the prototype wide band test $\sigma_{r\omega}$ is equated to the low-frequency response acceleration of Eq. (A25), the low-frequency acceleration excitation of Eq. (A26) then becomes

$$\sigma_{eLf} = \sqrt{BG} \quad (A27)$$

where G is the acceleration density of the wide band test and B is the bandwidth of the sweep random test.

The low-frequency excitation, Eq. (A27), equals the high-frequency excitation of Eq. (A18) at the frequency

$$f = \frac{2BQ}{q^2\pi} \quad (A28)$$

Below this frequency the excitation acceleration is kept constant at the value of Eq. (A27), and above this frequency the acceleration gradient is kept constant at the value of Eq. (A20).

DISCUSSION

Mr. Gorton (Pratt & Whitney Aircraft): How wide was the narrow band random segment you used? Was it constant bandwidth or percentage bandwidth?

Mr. Booth: Really, it's not too critical as long as the band of random vibration is narrow. We would usually use 10 cps. We'd like to use 3 cps, if possible, but 10 cps turns out to be more convenient. If you use a 3-cycle bandwidth, the instrumentation which has to follow the envelope gets very sluggish and it is awkward for the lab technician. So the compromise is about a 10 cycle bandwidth, but is not critical. It's the energy in the band.

Mr. Stearns (Wyle Labs): What type of electronics do you use to generate this swept, narrow band random?

Mr. Booth: We take a wide band random signal, put it through a filter of the right

bandwidth and heterodyne it down to the audio fringe.

Mr. Beecher (Lear Siegler, Inc.): I noticed in the analog that this was apparently a single-degree-of-freedom system. I wonder if you have attempted anything in more than one degree of freedom.

Mr. Booth: No, we were attempting in the analog to match a single resonant vibration mode — a mode of vibration of a complex structure which would have many vibration modes but which would be separated. So we were trying to simulate a mode, not necessarily just a single-degree-of-freedom system. We didn't perform experiments with multiple-degree-of-freedom systems.

Mr. Beecher: With multiple-degree-of-freedom responses, the responses that I have measured seemed to show that the narrower

the narrow band random was the more it appeared like sweeping sine and the greater discrepancy we had between a wide band

response. I'd like to see some measurements made where there is more than one-degree-of-freedom.

* * *

SIMULATING MISSILE-FIRING ACOUSTICAL ENVIRONMENT BY EQUIVALENT MECHANICAL VIBRATION

John H. Putukian
Raytheon Company
Wayland, Massachusetts

This paper describes the experimental effort undertaken to simulate the acoustical environment of the electronic packages of radar equipment in a rocket motor blast environment. High-frequency shakers replace an expensive high-power (approximately 170-db overall SPL) broadband acoustic test facility. By use of a reverberant acoustic chamber, the vibratory response of the sensitive electronic component is measured and is extrapolated to the high intensity acoustic levels. It is shown, by a theoretical approach, that a "modified" steady state test is suitable even for the transient environment; the total laboratory testing time is limited only by the fatigue properties of the components. The feasibility of simulating the missile-firing environment depends basically on the degree of coupling of the test structure (the closer the coupling between the component mounting and the package panels, the easier the simulation) and on the frequency sensitivity of the mechanical shaker and the shape of the acoustic energy spectrum to be simulated. Operating tests of electronic units in the simulated acoustic environment as high as 171-db overall SPL are described. Some design techniques employed to permit satisfactory performance of sensitive electronic units in the high-level acoustic environment are briefly discussed.

INTRODUCTION

This paper outlines the effort undertaken to simulate, in the environmental testing laboratory, the acoustical environment of the electronic packages of radar equipment in a rocket motor blast environment. The basic idea is the use of high-frequency shakers to replace an expensive high-power (approximately 170-db overall SPL) broadband acoustic test facility. The efficiency of shakers is a few orders of magnitude greater than the efficiency of equivalent sound sources. A shaker is directly attached to the structure being tested. However, in the case of an acoustic test chamber, the prime power has to be converted first into acoustic power with an efficiency of only a few percent. Furthermore, some power is absorbed by the walls of the test room. Thus, the power absorbed by the test object becomes a small fraction of the prime power.

Our effort in this paper consists of:

1. Discussing the conditions which must be satisfied by the structure and its environment

to enable acoustic tests to be replaced by mechanical ones;

2. Presenting a step-by-step procedure of the technique used to simulate the rocket motor blast environment by a vibration shaker;

3. Showing, by a theoretical approach, that a modified steady state test is suitable even for the transient environment; and

4. Describing the application of this simulation method to an operating test and showing some of the design techniques used to prevent malfunction of the sensitive electronic units.

MISSILE-FIRING ENVIRONMENT

Figure 1 shows the energy flow path from the missile-firing noise environment to the sensitive component. The acousto-mechanical path consists of the acoustic excitation of the equipment compartment panel structure, the internal reradiation of the panels, and the

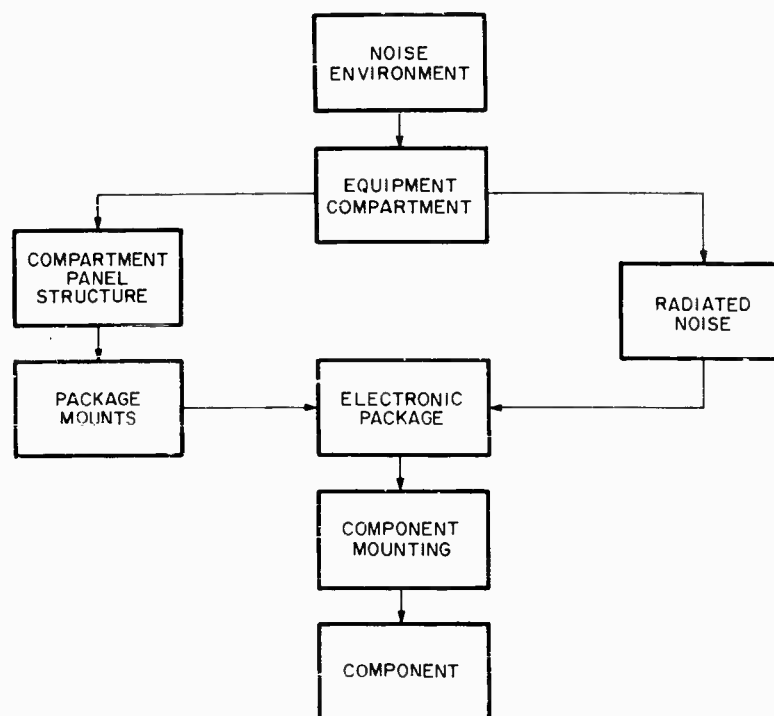


Fig. 1 - Energy flow path from noise environment to component

absorption of acoustical energy by the package. Also, the mechanical path consists of transmission of vibrational energy through the compartment panel structure to the package mounts and into the package which then excites the component mounting and finally the component itself.

ASSUMED SIMULATION CRITERIA

The basic conditions which must be satisfied by the structure and its environment to enable acoustic tests to be replaced by mechanical ones are as follows:

1. The structure must respond linearly, thus permitting scaling of the levels of the monitored points proportionately to the desired level of simulation. We have experimentally verified this assumption to be valid for the various electronic packages tested.

2. The acoustic field to be simulated must be a random noise and a diffuse one with equal probability of incident energy in all directions and random enough in time so that its power spectrum is a fairly smooth function of frequency. The field then is such that it contains most frequency components.

3. The test structure must have many modes within each frequency band and they must be spatially uniformly and randomly distributed throughout the structure. In our simulation we are using one-third octave frequency bands, considered to be sufficiently broad to accept several modes for the statistical model on which the simulation theory is based and yet sufficiently narrow to show significant frequency variations in the response. It can readily be seen that this assumption does not apply at the low frequencies, namely, below the fundamental frequency of the test structure; however, in most equipment, the low-frequency vibrations induced by mechanical vibration inputs exceed those due to acoustic sources, thereby making the response to acoustic excitation relatively unimportant at the low frequencies.

DEFINING MISSILE-FIRING ENVIRONMENT

Figure 2 shows the expected peak reverberant acoustic field around a typical package in each one-third octave frequency band with an overall SPL of 160 db. The spectrum of the assumed peak random vibration input at the mounting points is also given. These levels must be simulated in the laboratory to proof-test the various operating electronic packages.

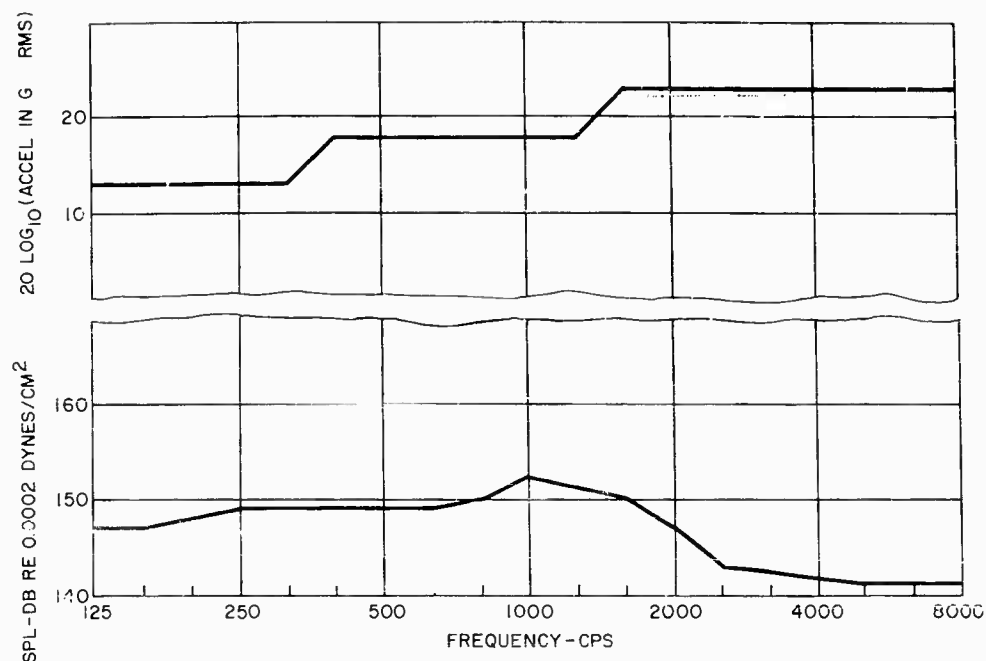


Fig. 2 - Typical package specification random vibration (triaxial) at mounting points and reverberant acoustic field

SIMULATION OF HIGH ACOUSTIC LEVEL BY LOW ACOUSTIC LEVEL SOURCE AND VIBRATION SHAKERS

The idea of using a vibration shaker to simulate the acoustic environment was suggested by Noiseux [1]. This simulation method is applied here using a typical aluminum package having walls 0.09 inches thick and measuring 17 x 5 x 7 inches. Figure 3 shows the three identical circuit boards inside the package used in this investigation. The boards slide tightly down the insides of the package on Birtcher guides. The bottom of the circuit boards is held to a connector chassis, which is in turn fixed to the sides of the package. When the cover of the package is installed, it presses against the tops of the circuit boards. The package and contents weigh about 16 pounds.

The procedure is as follows:

1. The package is suspended in a reverberant acoustic chamber and subjected to a low-level acoustic field in each one-third octave frequency band. The circuit board vibratory response is measured and extrapolated to the specification acoustic level as shown by the solid line in Fig. 4.

NOTE: References appear on page 90.

2. The circuit board vibratory response to random vibration excitation at the mounting points is measured and extrapolated to the specification vibratory levels as shown by the dash-dot line in Fig. 4.

3. The extrapolated circuit board vibratory responses due to the acoustic and vibration excitations are added on an uncorrelated power basis to get the combined response to the total environment (Fig. 4).

4. This combined excitation response is modified to account for the transient condition of the environment (Fig. 4). This phase is discussed in detail later in this paper. This modified combined excitation response should then be the same as the directly measured response of the circuit board during an operational missile firing.

5. An optimum location on the package for attachment of the shaker to produce maximum vibratory response on the circuit board is determined experimentally. The input to the shaker in the one-third octave frequency bands is adjusted to produce the response levels shown by the dotted line in Fig. 4.

6. The overall response level of the circuit board due to a broadband excitation source from 125 cps to 8 kc is then obtained by adding, on a

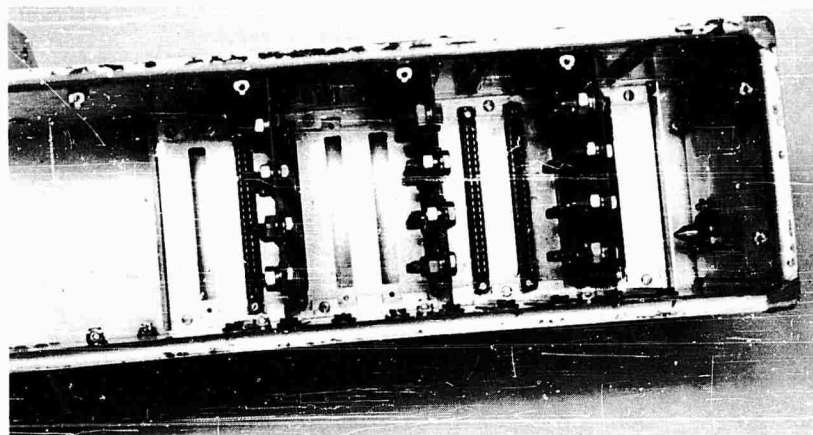


Fig. 3 - Internal view of package

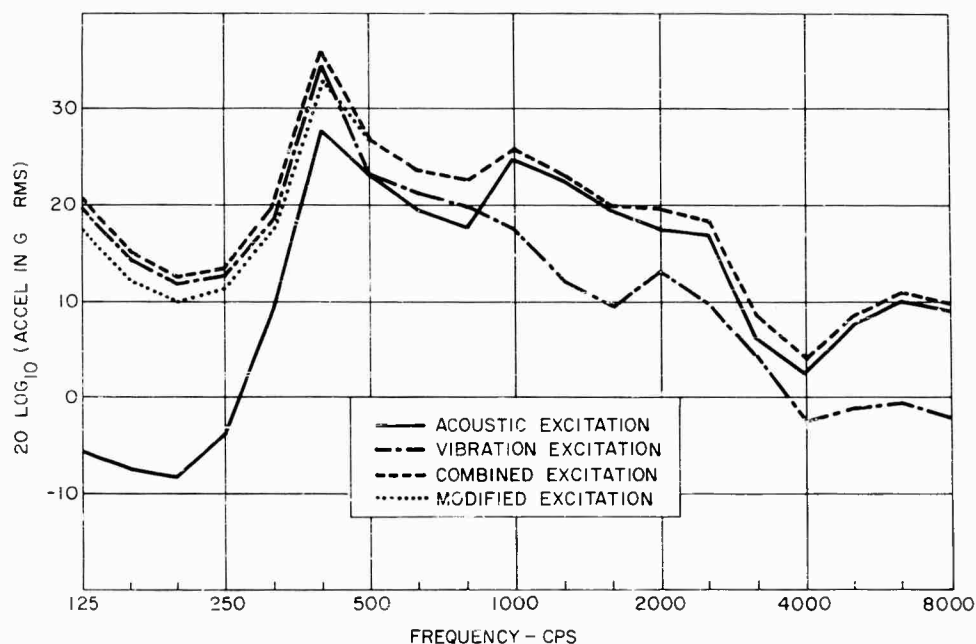


Fig. 4 - Predicted response of circuit board for acoustic and vibration environment

power basis, the response of each one-third octave frequency band. For our problem, this overall level totals 37.2 db (Ref. 1 g rms).

The random mechanical vibration input governs at the lower frequencies and the airborne acoustical input governs at the higher frequencies. Also, the reduction in the acceleration levels to account for the transient condition of the environment is significant only at the low frequencies.

MODIFICATION OF STEADY STATE TESTING TO INCLUDE TRANSIENT EFFECTS

Due to the short duration of the acoustic excitation caused by a missile firing, it becomes necessary to modify the results of the combined excitation response shown in Fig. 4 to account for the transient effect. To substitute a steady state test in the laboratory to replace the short-lived transient environment, the following must be known:

1. Transient effect on energy absorption — an estimate of the portion of the total energy absorbed by the package, which is a function of the duration of the missile excitation and the reverberation time of the package;

2. Dynamic response factor — an estimate of the dynamic response factor, which is a function of the duration of the energy pulse absorbed by the package and the fundamental frequency of the package; and

3. Fatigue characteristics — an estimate of the fatigue life of the sensitive component. The allowable laboratory testing time can be computed if one knows the fatigue life characteristics of the sensitive component by using the cumulative damage concept [2]. This phase is beyond the scope of this paper. For our investigation we have assumed that the sensitive components are designed for a proper stress level which permits us to run our laboratory test for a long time without incurring fatigue damage.

TRANSIENT EFFECT ON ENERGY ABSORPTION

The energy buildup in a structure subjected to a continuous acoustic excitation can be represented by the following relationship:

$$E(t) = E_{\infty}(1 - e^{-\omega\eta t}), \quad (1)$$

where

η = damping loss factor [3] $13.8/\omega T_s$,

ω = center radian frequency of band of random excitation,

T_s = reverberation time — the time it takes for an acceleration to decay to 10^{-3} of original value in a specific frequency band,

t = duration of missile acousto-mechanical excitation, and

E_{∞} = energy at time equal to infinity.

Equation (1) can be written in the following form:

$$10 \log_{10} \frac{E(t)}{E_{\infty}} = 10 \log_{10} (1 - e^{-13.8 t/T_s}). \quad (2)$$

A plot of Eq. (2) as a function of the dimensionless parameter t/T_s is shown by the solid line in Fig. 5.

In the same manner, the energy decay can be represented by the following relationship:

$$E(t') = E_0 e^{-\omega\eta t'} = E_0 e^{-13.8 t'/T_s}, \quad (3)$$

and

$$10 \log_{10} \frac{E(t')}{E_0} = 10 \log_{10} e^{-13.8 t'/T_s}, \quad (4)$$

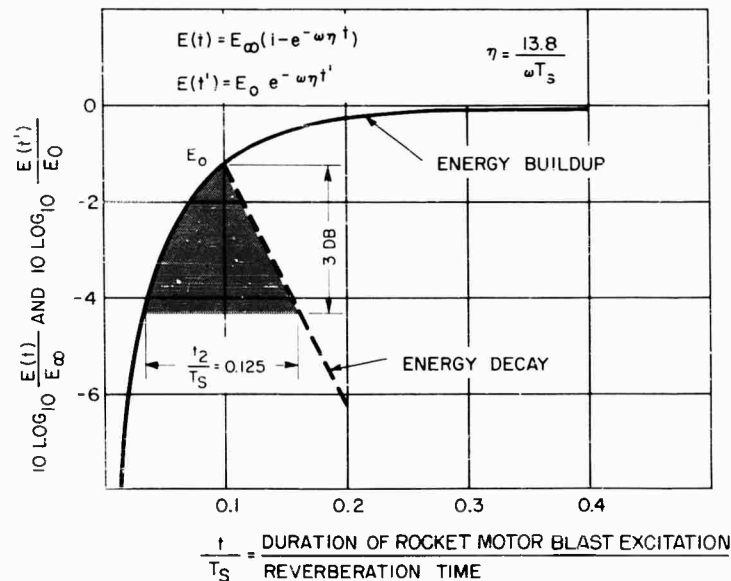


Fig. 5 - Acoustical energy absorbed by package

where E_o = total energy absorbed by the structure. A plot of Eq. (4) is shown by the dashed line in Fig. 5.

As the ratio of duration of rocket motor blast excitation to reverberation time of the structure approaches 0.3, the transient effect can be neglected and the full value of the energy used. For our package, the reverberation time varied from 2.5 seconds at 125 cps, to 0.85 seconds at 630 cps, and 0.2 seconds at 8000 cps. This means that above 630 cps where the ratio t/T_s exceeds 0.3, the package will receive all the generated energy. Therefore, reduction of the steady state energy to account for the transient effect becomes significant only at the low frequencies.

The application of Fig. 5 may be illustrated by considering the one-third octave band having a center frequency of 160 cps for which the ratio t/T_s is equal to 0.1. This gives a value at E_o 1.25 db below the steady state value. Because energy is proportional to the mean square velocity, this implies that the acceleration level for this specific case will be decreased by 2.5 db. From this point the structure will begin to lose energy as shown by the decay curve of Fig. 5. If we go 3 db below E_o , thus assuming that our interest ceases after the energy has decayed to half of the original amplitude, and scale the dimensionless value of $t_2/T_s = 0.125$, then the duration of the exciting pulse, t_2 , using 2.5 seconds as the reverberation time of the package, becomes 0.312 seconds.

DYNAMIC RESPONSE FACTOR

We have thus far shown the portion of the total energy that the typical package would absorb due to the transient missile-firing effect; the second phase of the transient effect is the dynamic response of the package. Figure 6 shows the time history of the energy pulse absorbed by the package. The dashed lines are a straight line approximation of this pulse. For our package, with a natural frequency of 400 cps, the peak dynamic response factor resulting from application of this pulse was calculated, by use of a digital computer, to be 0.992.

This phase of the investigation dealing with the dynamic response factor is negligible because the ratio of the duration of the energy pulse absorbed by the package to the natural period of the package is high, and thus, the peak dynamic response factor approaches 1.0.

$\omega\eta = 5.52$
PACKAGE $f_n = 400$ CPS
REVERB. TIME = 2.5 SEC. DYN. RESPONSE FACTOR = 0.992

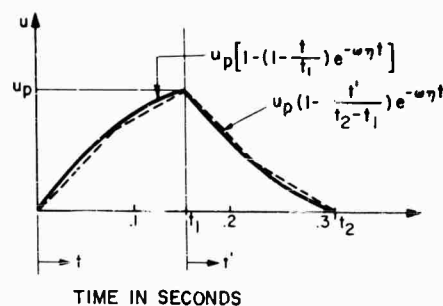


Fig. 6 - Pulse shape of energy absorbed by package

CIRCUIT BOARD ACCELERATION LEVELS TO BE SIMULATED

Making the proper corrections for the energy absorbed and the dynamic response factor gives the acceleration levels in the circuit board to be simulated by using a steady state laboratory test. For our package, these values are shown by the solid line of Fig. 7.

Figure 7 shows the capability of one 20-pound Goodman 390A shaker to simulate the desired acceleration levels. For this package, the capability is below the desired simulation levels by about 6 to 10 db in the 320- to 1250-cps frequency bands and 4 to 6 db in the 4- to 8-kc frequency bands. Thus, it seems that a shaker having the same characteristics as the 20-pound Goodman 390A, but having approximately three times its static force, should be capable of simulating the desired levels. Also by using a rigid vibration fixture and a 1200-pound C-10 M.B. shaker, we were able to simulate easily the desired levels in the 125- to 2500-cps frequency bands, but above 2800 cps the efficiency of the M.B. dropped to levels lower than the Goodman 390A shaker.

SOME OPERATING TESTS

Just as an individual's reaction to noise depends on his daily activities, the malfunction of a component will depend on its operating mode. It will have differing sensitivities to noise, depending on whether it is used in a local oscillator or an amplifier. The proper design of electronic equipment for service in a high-frequency vibration environment thus depends on a knowledge and understanding of the sensitivity to vibration of the individual component.

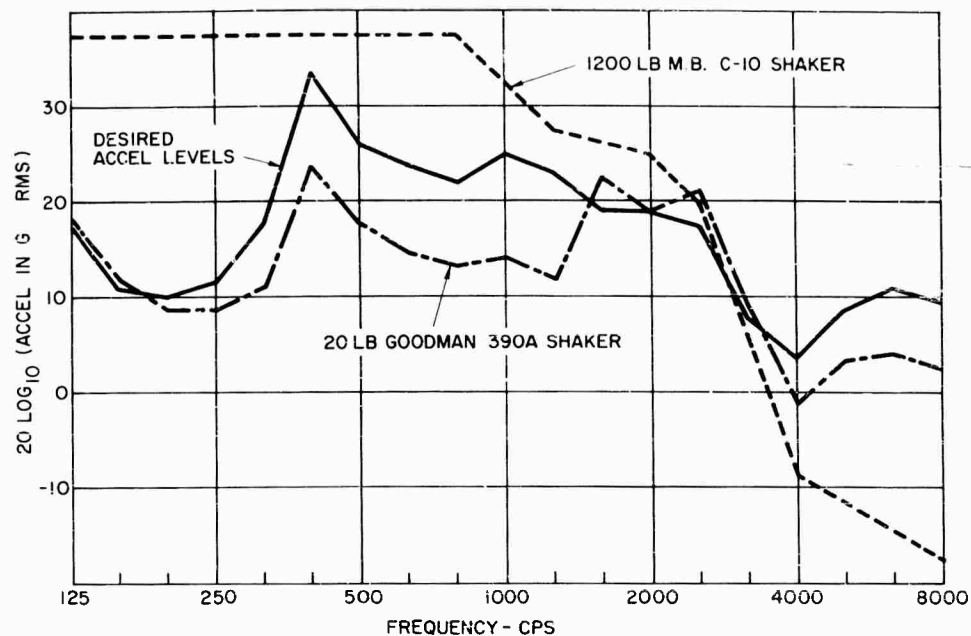


Fig. 7 - Comparison of capability of shakers to produce desired acceleration levels in circuit board

An arc detector device, basically composed of a waveguide and a crystal mount rigidly attached thereto, represents a very closely coupled structure. Figure 8 shows the acoustic spectrum this component has to withstand with an overall sound pressure level of 171 db. Using one 20-pound Goodman 390A shaker and the procedure outlined earlier in this paper, we were able easily to obtain the equivalent mechanical vibration levels and thus proof-test this component in its operating mode.

Mechanical shakers are frequency sensitive. Another spectrum could be drawn with an overall SPL of 171 db which would peak at about 4000 cps instead of at 1000 cps. For this type of spectrum we could not have achieved our simulation in the high frequencies.

Figure 9 shows a schematic view of another sensitive component resting on a plate isolated from the package by vibration isolators. The predicted vibratory levels of the component mounting showed that the component would malfunction under the missile-firing environment. An average acceleration reduction of about 30 db (Ref. 1 g rms) was desired. A successful solution was to use 0.05 inches of lead sheet lining on the inside faces of the package. This increased the composite-structure damping factor and the mass of the package panels. The effect is that the partitioning of the total energy absorbed by the package is mostly in the panels

and a lower value of the energy is thus transmitted to the component mounting [4].

CONCLUSIONS

This investigation revealed the following:

1. It is possible, under certain conditions, to simulate an acoustic environment by use of an equivalent mechanical vibration. The feasibility of this simulation depends basically on the degree of coupling of the test structure (the closer the coupling between the component mounting and the package panels, the easier the simulation) and on the frequency sensitivity of the mechanical shaker and the shape of the acoustic energy spectrum to be simulated.
2. A steady state test is suitable even for the transient environment. The total laboratory testing time is limited only by the fatigue properties of the components.
3. Although the simulated tests now appear capable, in some practical cases, of replacing full-scale acoustic tests, more investigation is needed to provide the detailed knowledge required to make this simulation technique a reliable testing tool.

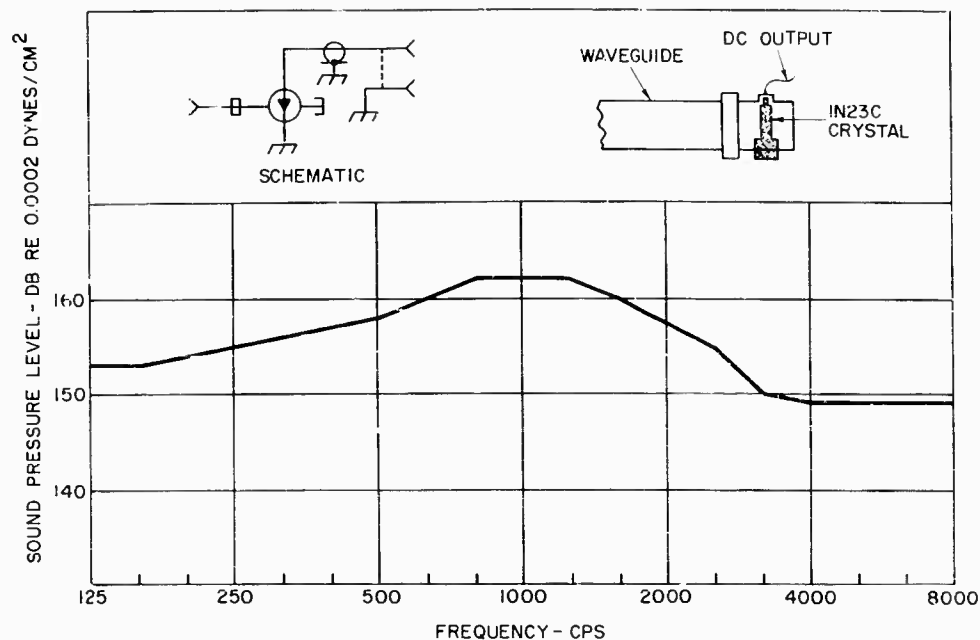


Fig. 8 - Acoustical environment and arc detector configuration

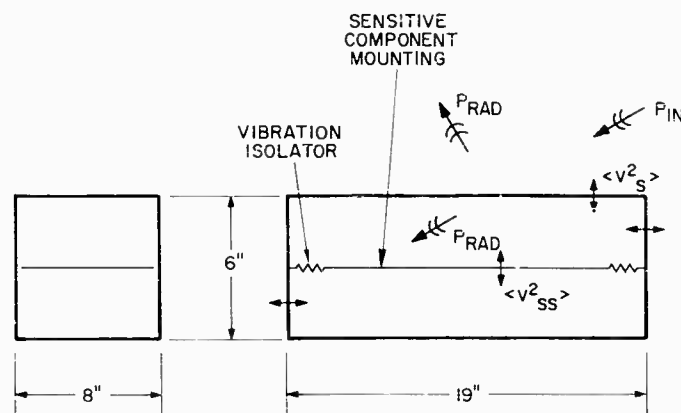


Fig. 9 - Schematic diagram of package

REFERENCES

1. D. U. Noiseux, "Simulation of Reverberant Acoustic Testing by a Vibration Shaker," Shock, Vibration and Associated Environments Bull. No. 33, Part III, pp. 125-136.
2. H. J. Grover, S. A. Gordon, L. R. Jackson, "Fatigue of Metals and Structures," Bureau of Aeronautics, Dept. of the Navy, Doc. NAVAER 00-25-534 (1954).
3. L. L. Beranek, Noise Reduction (McGraw-Hill Book Co., New York, 1960), p. 303.
4. J. H. Putukian, "Predicting Vibratory Response of Circuit Boards Located Inside an Electronic Package Due to a Reverberant Acoustic Field by Energy Methods," Raytheon Report JHP-7 (April 1964), presented in part as paper Z1 at the 67th meeting of Acoust. Soc. Am., New York, May 1964.

DISCUSSION

Mr. Himelblau (North American Aviation): Could you describe how you would handle the problem if you had two sensitive components within the same piece of electronic equipment, each having separate characteristics?

Mr. Putukian: Well, you have either to look at both together or one at the time, whichever can be done. Sometimes you can't do it; sometimes you can.

Mr. Himelblau: For example you had a plot of rms g. I assume that was rms g at a single point. If you have two different components, usually at two different locations, it would be hard for me to visualize how you would handle it for both of them and still have a good test in each case.

Mr. Putukian: Well, that may be true. The only thing I can say is that you may have to put two accelerometers at these two places and then hope for luck. If there is coupling between them, you probably cannot find exactly what each is doing. In this investigation we are looking at one component only. When you have two of them, it's a good question.

Mr. Murray (Wyle Labs.): In your first picture (Fig. 1), you showed the energy paths coming into the package, then combining and going through the component's mount before it gets to the component itself. Assuming that this is the mount on which the board is mounted, the energy can get to the board directly without having to go through its mount even after it gets inside the package. I'm wondering if this really gives you a realistic simulation.

Mr. Putukian: Yes, it does. You will find that it is practically impossible to think of a

case where the airborne acoustical energy around a component has enough amplitude to vibrate that component. Usually it is assumed that the sensitive components would malfunction because of the vibration of the component mounting rather than the acoustical energy around the component itself. Basically, then, you have the problem of malfunction caused by the vibration of the component mounting.

Mr. Nieswiadomy (LTV Military Electronics Div.): I wonder if you would like to comment on Mr. Strike's* paper which he gave yesterday. He was concerned with the energy above 20 kc. You were concerned only to 8 kc, if I recall.

Mr. Putukian: I wasn't here yesterday so I didn't listen to Mr. Strike. In any event, I'm just trying to show a concept which happens to apply only to 8 kc because the reverberant acoustic chamber which we have goes only to 10 kc. There would be no way for us to run a reverberant acoustic test at low levels and then extrapolate. If you had the facility, you could go to 20 kc.

Mr. Nieswiadomy: You still think the equivalence would hold for getting back to mechanical vibration when you carry this out to 20 kc?

Mr. Putukian: Yes.

*R. Strike and G. G. Sundberg, "Sonic and Ultrasonic Vibration Sensitivity of X-Band Microwave Components," Shock and Vibration Bulletin No. 34, Part 2.

* * *

TEST CONTROL DEVICES - SNAP 10A

VIBRATION TEST PROGRAM

Edward L. Gardner and Ralph M. Oliva
Atomics International
Canoga Park, California

The SNAP 10A is a long hollow conical structure approximately ten feet high with a heavy mass (reactor and radiation shield) concentrated at the apex. When attached to the launch vehicle, it becomes the nose cone of the integrated missile assembly. Its dynamic response is not unlike that of an inverted pendulum. The low lateral fundamental resonance, high amplifications, high Q at some frequencies, noise and/or harmonic content on the input or response control instrumentation, etc., combine to present many test control problems to the test engineer. The solutions to various test control problems are recorded in this paper which discusses the input, response, and safety control devices employed during testing on past and current SNAP 10A vehicles. Each device's description, function, and operation are discussed in detail.

Power requirements for space propulsion systems of the future make the use of space-borne nuclear reactors inevitable. By converting reactor heat to electricity, a continuous long-term automatically controlled source of electrical power can be produced for both missile propulsion and missile payload systems. Reactor-conversion systems to satisfy missile propulsion power requirements are destined for the near future. The stepping stones to these systems are the smaller reactor-conversion systems now being developed as power sources for present missile payloads.

In April 1957, an Atomic Energy Commission (AEC) system development contract was awarded to Atomics International for a compact nuclear powerplant capable of converting the heat generated by a nuclear reactor to electrical power. Because this unit was intended for space application, it had the following general design objectives: one-year unattended automatic operation, minimum weight, maximum reliability, operational safety, and launch and orbital environmental capability. Most of these were relatively unimportant in prior land-based nuclear reactor systems where total size, weight, and geometrical configuration were not necessarily critical design parameters and where systems were not called upon to perform in abnormal environments. This vehicle (SNAP 2), which employed a mercury rankine

cycle for power conversion, marked a milestone in nuclear reactor development; a nuclear reactor and compatible conversion system was to be reduced in size and weight so that orbital flight was not only possible but could be attained using existing United States launch vehicles. A subsequent contract was awarded to Atomics International for a nuclear power unit employing a thermoelectric power conversion device. This unit, SNAP 10A, will produce 500 watts in space with no moving parts at a system weight of about 950 pounds. SNAP 10A will be the first nuclear reactor power unit demonstrated in space; the flight testing is scheduled for the spring of 1965.

The structural configuration of the SNAP 10A (Fig. 1) sets it apart from most orbital payloads. Instead of being a small compact package, it is a long hollow conical structure approximately ten feet high with a heavy mass (reactor and radiation shield) concentrated at the apex. When attached to the launch vehicle, the SNAP 10A becomes the nose cone of the integrated missile assembly.

With the reactor-shield mass (in excess of 500 pounds) mounted on the tall thin shell structure, the SNAP 10A system takes the form of an inverted pendulum. Inherent with this configuration is a low first fundamental lateral resonant frequency — in the case of SNAP 10A,

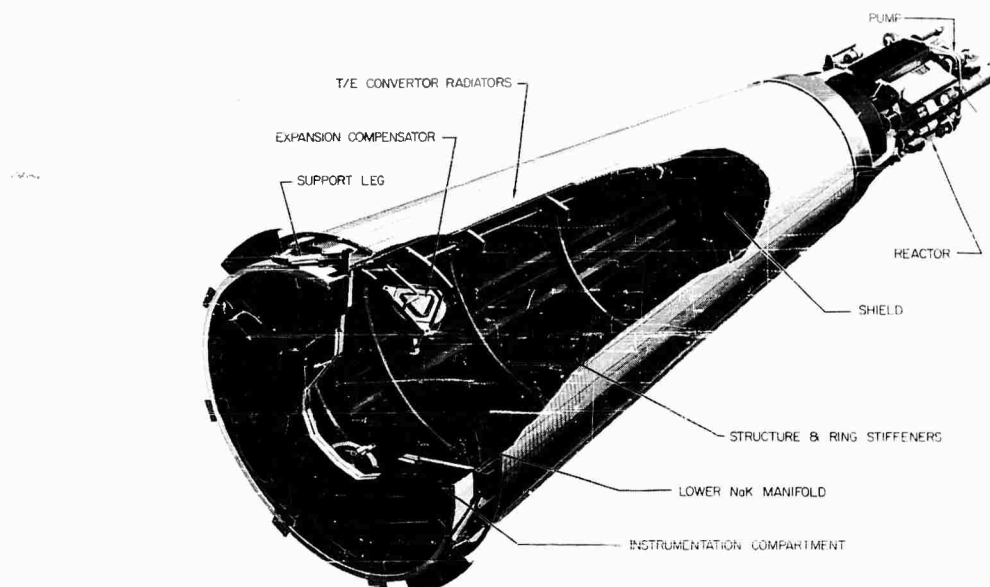


Fig. 1 - SNAP 10A system

between 15 and 20 cps. Amplifications of 20 at this resonant condition make accurate control of vibration test inputs difficult. Vibration and shock test inputs used in the SNAP 10A program are given in Table 1. Because of response limitations which must be necessarily imposed on any large test specimen, the shaker input to the test unit at the first fundamental resonance can at times be so low that the servo systems' output drops into the noise region of the shaker instrumentation. The presence of a high Q at this resonance can complicate control problems because it increases the danger of an accidental overload of the test structure. To further complicate input and response control problems, the test vehicle (like most) never cooperates by responding with a clean sine wave. Signals generated at control points are typically distorted by harmonic and/or noise content.

The methods employed for input and response control on the SNAP 10A program are best described by dividing the instrumentation into the groups noted in Fig. 2. The shaker table input control instrumentation contained in Block A controls and conditions the shaker input. Vehicle response control is maintained by components noted in Block B. Table input control and/or vehicle response control, as the specification dictates, are monitored and maintained by the instrumentation assembled in Block C. A test vehicle safety circuit to preclude the possibility of accidental overload to the specimens is shown in Block D.

TABLE 1
SNAP 10A System Vibration Inputs^a

Test Axis	Frequency Band (cps)	Input Level
(a) Acceptance Test		
Longitudinal	5-9	3/8 in. DA
	9-400	1.5 g
	400-2000	5.0 g
Lateral and normal	5-8	3/8 in. DA
	8-250	1 g
	250-400	3 g
	400-2000	5 g
(b) Qualification Test		
Longitudinal	5-9	1/2 in. DA
	9-400	2.3 g
	400-2000	7.5 g
Lateral and normal	5-8	1/2 in. DA
	8-250	1.7 g
	250-400	4.5 g
	400-2000	7.5 g

^aSweep rate of 1 min/octave.

SHAKER TABLE INPUT CONTROL

No test item can be tested in a shaker incapable of imparting sufficient force to drive

the moving mass to specified test levels over the entire frequency band. An excess of force, then, is generally available at the input point. Without proper control of this force, the danger of exceeding specified inputs (with possible damage to the test item) is always present, especially at vehicle major resonances.

Selection of a point to measure applied input is always a problem, especially on a test package having a large mounting area. One sensor will not do because it cannot give an accurate picture of true specimen input at all frequencies. If the accelerometer happens to lie on a node line, the sensor could be virtually at a standstill while other points of vehicle attachment are greatly exceeding desired input levels. If the sensor happens to fall at a location where excessive localized fixture amplification is taking place, other specimen support points might be grossly undertested. One technique used to solve this problem is to place several accelerometers in strategic locations around the mounting area and average the outputs of the sensors. This average of the

sensors is used as the input signal. Another method uses similarly located sensors which auction from accelerometer to accelerometer depending on which is at the specified test level. This latter technique has been utilized with success on the SNAP 10A test program.

Switching from sensor to sensor is accomplished by a Ling SML-100 multilevel selector which is simply an auctioning device to indicate to the shaker's servo system when one of the input accelerometers (five is maximum) has reached its maximum preset level. If the sensor commanding control reduces for any reason, the multilevel selector automatically commands the servo to increase the input to the shaker until one of the other sensors attains the required table input value. When this occurs, control of the shaker is transferred automatically to the accelerometer reaching its preset value first. Constant auctioning is maintained so that at any instant at least one accelerometer is at the specified test input level.

Filtering of the table input signal becomes an important part of the test because the test

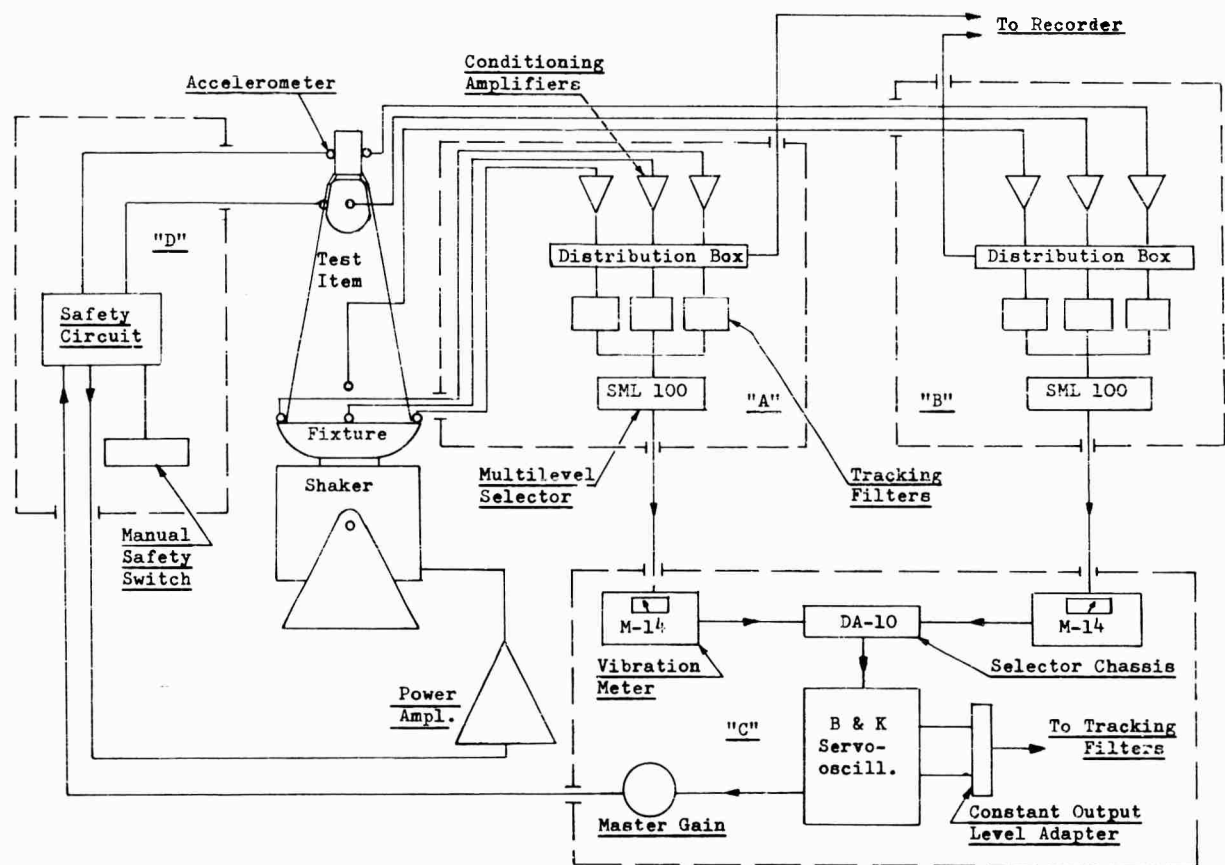


Fig. 2 - Control schematic -- SNAP 10A test program

engineer must know the character of the input waveform. Control on a noise envelope does not result in a realistic sinusoidal input. Only the fundamental waveform can present the most reasonable input condition. To assure that only the fundamental is employed, Spectral Dynamics' tracking filters are placed immediately ahead of the accelerometer auctioning device. The filter is essentially a narrow window that varies with and centers on the oscillator frequency imparted to the shaker. Only those frequencies falling within the window are allowed to pass. Noise and harmonics are virtually eliminated from the fundamental waveform. The placement of these filters is shown in Block A of Fig. 2.

The resultant signal from the shaker table input control circuit emerges as a fairly clean sine wave having peak values in agreement with required input values. In many tests, this signal would be fed directly into the shaker's servo control system to control the shaker. Because the SNAP 10A vehicle had center of gravity response limitations, this signal would lose its prominence whenever vehicle response attained its preset limits. The auctioning between the table input control signal and the vehicle response control is diagramed in Block C of Fig. 2.

VEHICLE RESPONSE CONTROL

The control of test vehicle response is critical in vibration testing. Without exercising proper control, a specimen can be inadvertently and needlessly destroyed when overexcited at its fundamental resonances or when excessive table inputs are accidentally applied. Therefore, every test specification describing a system test

normally defines response limitations which cannot be exceeded during test. These limitations are derived from the dynamic analyses of the integrated flight vehicle and are based on the maximum values that can be attained and/or sustained by the missile system structure during its launch and flight.

On SNAP 10A, three vehicle locations were designated as response control points: reactor, shield, and instrumentation compartment. Acceleration response at these points was not allowed to exceed the values given in Table 2 between 5 and 250 cps. Above 250 cps, response restrictions were not always required.

Response control at the noted points was maintained by the instrumentation noted in Block B of Fig. 2. This instrumentation is identical to that employed for shaker table input control and its function is the same, except that in this case it considers vehicle response rather than table input. Its function is to act as a sensor to warn the servo system whenever a response limitation has been reached at any of its designated vehicle locations. The output from this auctioning circuit is fed into the table input control and/or vehicle response control circuitry (Block C) to effect its contribution to input control.

TABLE INPUT CONTROL AND/OR VEHICLE RESPONSE CONTROL

The function of the table input control and/or vehicle response control circuitry is to consider the signals from the table input control (Block A) and the vehicle response control (Block B) and select the appropriate signal for servo control use. To accomplish this, a third

TABLE 2
SNAP 10A System Response Restrictions

Test Axis	Frequency Band (cps)	Vehicle Response Limits (g)	
		Acceptance Test	Qualification Test
Longitudinal	5-9	3	3
	9-250	3	3.5
	250-400	3	3.5
	400-2000	5	7.5
Lateral and normal	5-8	3	3
	8-250	3	3
	250-400	3	5
	400-2000	5	7.5

auctioning system is used. The preselected table input and vehicle response signals are individually fed into Ling M-14 vibration meters, appropriately calibrated to some predetermined full-scale value. Outputs from the vibration meters are monitored by a single Ling DA10 selector chassis which automatically selects and then controls on whichever channel (table input or vehicle response) has attained its specified value. Table input will normally be the channel in command and will remain at its maximum or peak setting except when control necessarily reverts to the channel covering vehicle response.

A single signal emanates from the DA10 selector. This signal is fed into the shaker servo control system where amplifier output to the shaker is ultimately controlled. This completes the closed-loop circuit controlling shaker operation.

Unfortunately, no system and no one link in the system is infallible. In spite of all precautions, instrumentation malfunction with possible vehicle overload is possible. To safeguard against any such occurrence, a test vehicle safety circuit was developed. The operation of this device is completely independent of the shaker control circuitry.

TEST VEHICLE SAFETY CIRCUIT

The test vehicle safety circuit is a two-channel device that monitors the outputs of two accelerometers and immediately cuts the power to the shaker amplifier in the event that the preset response limitation is exceeded. This instrument has its own power supply and is independent of the driver signal servo system, except for being patched into the signal circuit between the B & K oscillator and the power amplifier.

Since the acceleration signals from the sensors are unfiltered, the safety circuit is equipped with two low-pass filters. Each is manually controlled during test to eliminate high-frequency acceleration inputs to the safety device. The cutoff action of this system occurs in milliseconds; therefore, it is important to look at and sense on essentially a fundamental signal rather than on sporadic high-peak but low-energy spikes.

Calibration of the safety circuit is performed by shaking each control accelerometer to its specified g limit and adjusting a potentiometer in the safety circuit until tripping occurs. Once similar cutoff has taken place during test, reset is required before testing can resume. Resetting cannot take place if the master gain control on the test console has not been reduced to zero. This eliminates the possibility of inadvertently returning the shaker to full power by a reset procedure. Since the shaker drive signal passes through the test vehicle safety circuit's power on-off switch, operation of the shaker is impossible if the safety circuit power is turned off. Three manually operated shutoff switches are incorporated in the system to permit interruption of the test by any of three test observers. These are incidental to the operation of the basic device but are an additional safeguard in the vehicle protection system.

This safety circuit is described in detail in a previous paper [1]. A circuit diagram is shown which will permit any interested laboratory to build an identical overload protection device.

REFERENCE

1. E. L. Gardner, "A Test Vehicle Protection Circuit," Shock, Vibration, and Associated Environments Bull. No. 33, Part III, pp. 79-80.

* * *

TRANSMISSION OF VIBRATION TEST FORCES BY MEANS OF VISCOELASTIC LAYERS

A. J. Yorgiadis and S. Barrett
North American Aviation, Inc.
Downey, California

Environmental vibration testing of large but fragile and relatively light structures, as typified by space vehicles, has introduced many new complex problems. Even to attempt solutions to these problems, some new basic concepts must supplement or replace conventional concepts presently used in vibration testing of smaller, structurally more rigid packages.

The absence of true "hard points" on certain test structures makes it often necessary not only to limit the total vibratory force input at a given location, but also to distribute this force over a significant area to limit its intensity. One practical method of accomplishing this is by using viscoelastic layers to transmit the vibratory forces from the exciter to the test structure. Results are presented of a computer study to determine the behavior of a simple lumped parameter system, driven through a viscoelastic layer. It is shown that actual vibration response of the system can be reasonably well simulated by selecting a viscoelastic layer of suitable properties. Exploratory test data are presented on the vibration transmission properties of a neoprene rubber layer. The results show that adequate vibratory energy can be transmitted through this layer even at frequencies higher than the natural frequency of vibration of the system.

INTRODUCTION

Very significant advances have been made in the field of vibration testing during the past decade. The improvement in the performance of vibration exciters, controls, and instrumentation has been far reaching. Knowledge of dynamic properties of materials has been considerably expanded. Modern computers have simplified the labor involved in obtaining mathematical solutions to multi-degree vibration systems, and hence, have expanded the process of prediction of vibration phenomena. These and many other developments have advanced the state of the art and given better tools to the vibration test engineer. Nevertheless, it would be misleading to state that present-day vibration test programs have all become a matter of routine. It is quite evident that the planning and proper execution of vibration tests is by no means simple, particularly when the test objects are large, flexible, fragile, and mechanically very complex, such as typified by aerospace assemblies and structures.

There are, as is well known, many types of vibration tests, such as environmental tests, modal tests, qualification tests, off-limits tests, and systems tests. Even the nomenclature for the various tests becomes complicated, and not very uniform. There are tests on a given complex assembly in which only one or a few items are of concern. In other tests, many or most of the items in one assembly have to be vibration tested simultaneously with different permissible amplitude limits from one point of the structure to another. Except for small resonance-free components, it is no longer adequate to define a vibration test by the amplitude at one point, either on the exciter table (the input), or at the specimen (the output).

Instead of the actual weight of a test specimen, we now think in terms of its "apparent mass" or mechanical impedance, and these quantities vary with frequency. Not only sinusoidal vibrations, but wide band random vibrations are often required. The path of the vibration test forces through the specimen structure

was previously of no concern because ample strength was available at the attach points with major structural supports to transmit the exciter forces. The fragility of present aerospace structures makes it necessary to analyze carefully the matter of transmission and distribution of vibratory test forces, so as to avoid unnecessary and unrealistic local overloading during the vibration test.

TRANSMISSION OF VIBRATORY FORCES

The principal object of this study is to investigate one aspect of modern vibration testing, namely, the means for transmission of the vibratory forces from the exciter to the test member. While this study is very general and is not limited to one type of exciter, examples and explanations have been written around the electrodynamic vibration exciter, which is most widely used.

Examining the typical vibration test, the overall mechanical system can be considered to have three elements: the item to be vibrated, the moving part of the exciter, and the fixture that mechanically connects the test item to the exciter. The resulting assembly forms a vibration model, with combined dynamic properties that depend on the properties of the individual elements.

There is almost universal acceptance of the philosophy that the best fixture is one that is very rigid, light, and resonance free within the frequencies of the test. True, this requirement could be met when the highest frequency was 500 cps, and when packages were considered large if they exceeded 200 pounds. Current test assemblies can be 10, 20, or 30 feet and larger along one axis and weigh thousands of pounds. Occasionally, the test units contain large volumes of liquids. It has become evident that for such testing, the concept of a rigid resonance-free fixture has no practical significance. These limitations of the vibration system have been overcome or circumvented by techniques such as:

1. Equalization of the vibration excitation spectrum by means of peak and notch filters, and
2. Careful control or monitoring of the vibration responses at one or more sensitive locations on the specimens to protect against local overstressing at a resonant condition.

Another somewhat different approach involves the elimination of the conventional test fixture concept by utilizing many exciters [1], each unit being connected at a different point on the test structure by a thrust rod. This method has considerable merit, in that it eliminates the cost of a fixture. It is particularly applicable to modal testing. Nevertheless, complexities develop in the proper amplitude distribution and phasing of the various exciters, and the force transmission is still concentrated at a few definite points, rather than distributed over larger areas.

In this study, the concept of an unspecified rigid connection is abandoned, and it is assumed that this connection has the properties of a viscoelastic material; namely, it is defined by a finite spring rate and a damping constant. In part, this is the recognition of an existing situation; even a solid metallic connection is technically a spring and a damper, since all materials have elasticity and damping. Of course, the concept of using flexibility as a desirable or acceptable fixture property will be questioned as being contrary to the principles that have been taken for granted for so long.

By using the mathematical models of Fig. 1 and the analytical techniques explained in Appendixes A and B, it will be shown that the use of suitable viscoelastic layers for proper test force transmission has definite possibilities, at least for the lumped parameter models studied. It is realized that such oversimplification of the mechanical system reduces the accuracy of the results, and very wide generalizations should be avoided. Nevertheless, such studies can provide useful pointers towards better solutions.

NOMENCLATURE

M_0	Mass of moving part of vibration jig
M_1	Mass representing outer structure of test specimen
M_2	Mass representing inner structure of test specimen
M_T	Total moving mass, $M_0 + M_1 + M_2$
β	Mass ratio, M_2/M_1
K_1	Stiffness of lower spring
K_2	Stiffness of upper spring

NOTE: References appear on page 114.

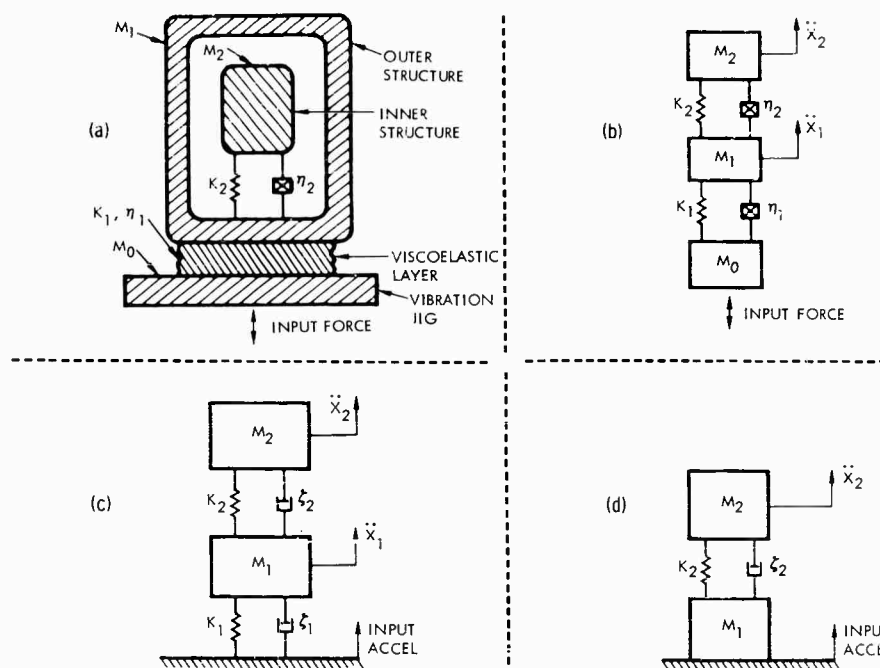


Fig. 1 - Lumped-parameter representations of vibration test systems

ω_1	Uncoupled natural frequency of lower system = $\sqrt{K_1/M_1}$	F	Peak magnitude of sinusoidal excitation force
ω_2	Uncoupled natural frequency of upper system = $\sqrt{K_2/M_2}$	S_o	Acceleration spectral density of random excitation
α	Frequency ratio, ω_2/ω_1	$E[\quad]$	Mean or expected value of stationary random process
Ω	Frequency of sinusoidal excitation	$E[\ddot{X}_o^2]$	Mean square acceleration response of reference system
ζ_1	Viscous damping ratio for lower system	$E[\ddot{X}_1^2]$	Mean square acceleration response of lower mass
ζ_2	Viscous damping ratio for upper system	$E[\ddot{X}_2^2]$	Mean square acceleration response of upper mass
η_1	Hysteretic damping constant for lower system	i	$\sqrt{-1}$
η_2	Hysteretic damping constant for upper system	t	Time
X_o	Deflection of lower mass, M_o		
X_1	Deflection of intermediate mass, M_1		
X_2	Deflection of upper mass, M_2		
\ddot{X}_o	By definition, F/M_T		
\ddot{X}_2	Peak acceleration of upper mass, M_2		

LUMPED PARAMETER MODELS

The models of Figs. 1a and 1b represent the combined three-element mechanical assembly in a vibration test. In Fig. 1a, the test structure is depicted as consisting of two ideal masses M_1 and M_2 connected by linear spring K_2 and with hysteretic damping η_2 as defined

in Appendix B. M_1 corresponds to the primary structure, outer structure, or the member through which vibrations are usually introduced to the test assembly. M_2 corresponds to the inner structure, secondary structure or payload. The approximation of an actual assembly by this mathematical model may sometimes be inaccurate, but the procedure for defining this model simply requires that it have the same total mass as the actual unit, the same major fundamental natural frequency, the same resonance amplification, and the same mass distribution across a line through the first node. The viscoelastic layer is defined by the parameters K_1 and η_1 , the latter also being the same type of damping as in η_2 . This model was used for the study on transmission of sinusoidal vibrations and can be identified as the three-mass two-degree-of-freedom system illustrated conventionally in Fig. 1b.

The model shown in Fig. 1c with motion input was used for the evaluation of the transmission of white noise random vibrations. This model was chosen for the random study because of the existence of analytical solutions, as explained in Appendix A. The model of Fig. 1c has viscous damping, while that of Fig. 1b has hysteretic damping. For purposes of comparing results on the two models, the viscous damping values were represented by the term 2ζ rather than ζ , since in case of systems with medium to low damping

$$\eta \approx 2\zeta \approx \frac{1}{Q}, \quad (1)$$

where Q is the resonance amplification factor.

ANALYSIS OF RESULTS

Before discussing the analytical results, it is appropriate to define the significance of proper vibration force transmission in such tests and to explain the basis for evaluating the various viscoelastic layers. It was previously stated that the test structures under consideration are relatively large and flexible. This means that the models of Fig. 1 have low spring rates K_2 , and therefore, a low natural frequency ω_2 , at least relative to the maximum test frequencies. It was further assumed that the primary object of the vibration test is to simulate or induce certain predetermined vibration acceleration levels \ddot{X}_2 to payload M_2 . These are the rms acceleration levels in the case of random tests, and the peak resonance accelerations for the sinusoidal tests, that would apply if we had absolutely perfect, massless, rigid, but sufficiently powerful vibration exciters and fixtures

to vibrate the structure without changing any dynamic properties of the system. The acceleration value \ddot{X}_2 has an added significance in that it is proportional to the peak dynamic force transmitted through member K_2 , and this represents the peak internal resonance fatigue loading through the test structure. For actual structures in service, these loads are many times the input of external loads because of resonance amplification.

Randomly Excited Model

Translated into mathematical terms, this requires that the rms response $E[\ddot{X}_2]$ of masses M_2 in the models of Figs. 1c and 1d be equal, or nearly equal, for a given motion input. The ratio of these two rms acceleration values was, therefore, plotted as the ordinate of the charts in Figs. 2, 3, and 4. Further explanations of the applicable variables can be found in Appendix A. The plots in Figs. 2a, 3a and 4a are for a specimen damping $2\zeta_2$ of 0.05, while those in Figs. 2b, 3b and 4b are for cases in which the damping is twice as high. The frequency ratio used as the abscissa for these charts was a measure of the spring constant K_1 of the viscoelastic layer, as can be seen in the nomenclature. Four different values of the viscoelastic damping constant were used in each of the figures, as this appeared to be an important parameter. Finally, Figs. 2, 3, and 4 each represent a different mass ratio M_2/M_1 .

As expected, the response ratio approaches the desired value 1.00 when the frequency ratio ω_2/ω_1 is small, since then the system of Fig. 1c approaches that of Fig. 1d. Up to the value $\omega_2/\omega_1 = 1.00$, the response ratio remains within 20 percent of the value 1.00, even though the viscoelastic damping constant varies over a wide range. Furthermore, higher mass ratios M_2/M_1 and higher specimen damping tend to stabilize the value of this response ratio and make it less sensitive to variations in ω_2/ω_1 .

Sinusoidally Excited Model

The plots in Figs. 5 to 13 represent the results of the study on models of Figs. 1a and 1b, as explained in Appendix B. The abscissas of these curves remain ω_2/ω_1 , as in the previous curves. The same variables are again investigated with one addition, namely, the ratio specimen mass to exciter mass, i.e., $(M_1 + M_2)/M_0$.

The ordinate in Figs. 5 to 13 is the ratio \ddot{X}_2/\ddot{X}_0 , defined in Appendix B and representing the actual peak resonance amplification of M_2 ,

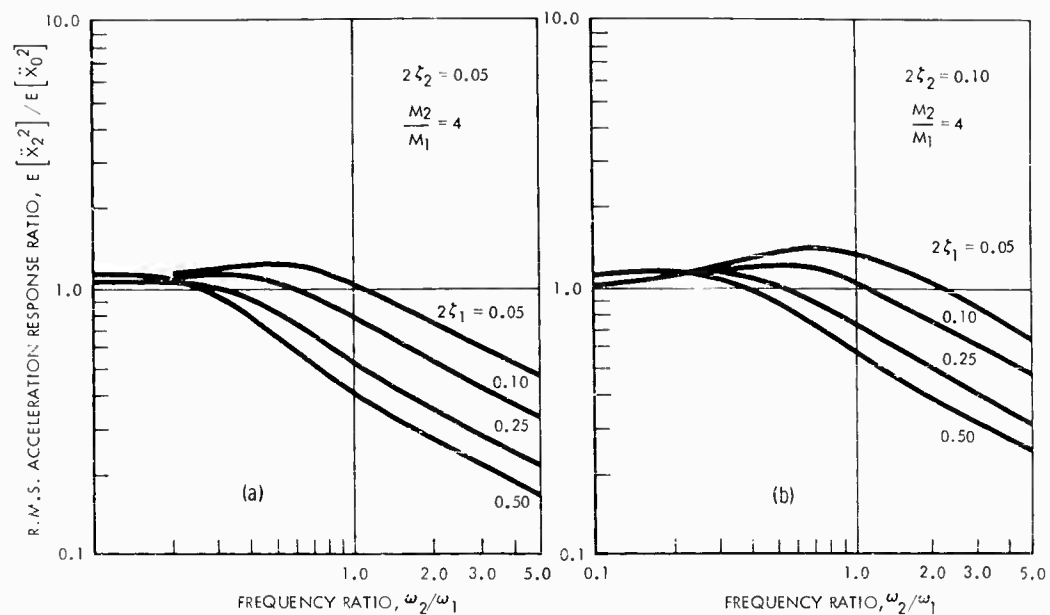


Fig. 2 - Normalized acceleration response to random excitation ($M_2/M_1 = 4$)

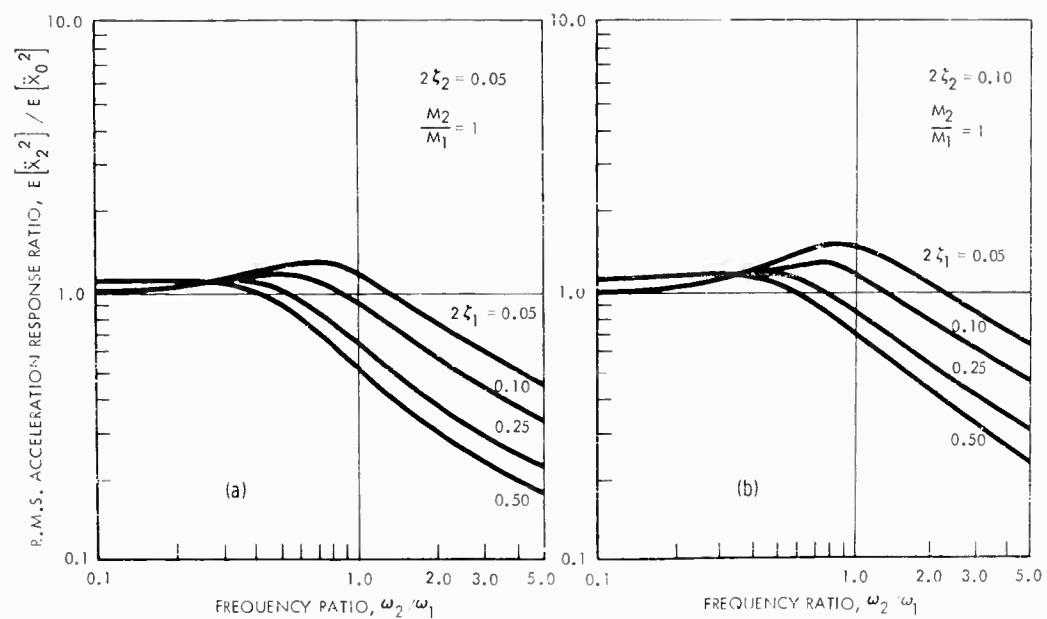


Fig. 3 - Normalized acceleration response to random excitation ($M_2/M_1 = 1$)

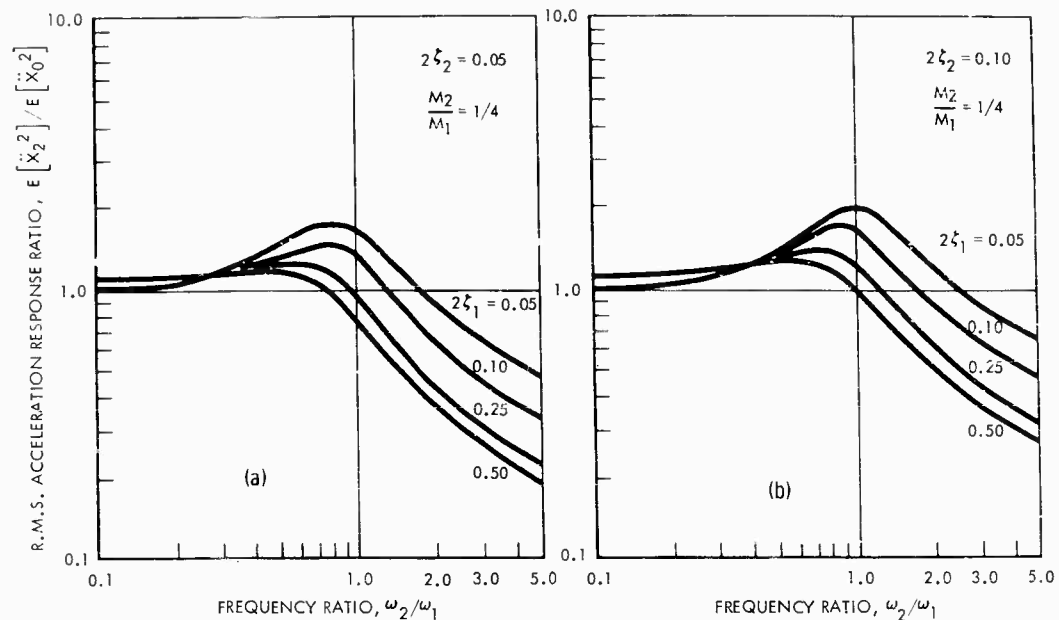


Fig. 4 - Normalized acceleration response to random excitation ($M_2/M_1 = 1/4$)

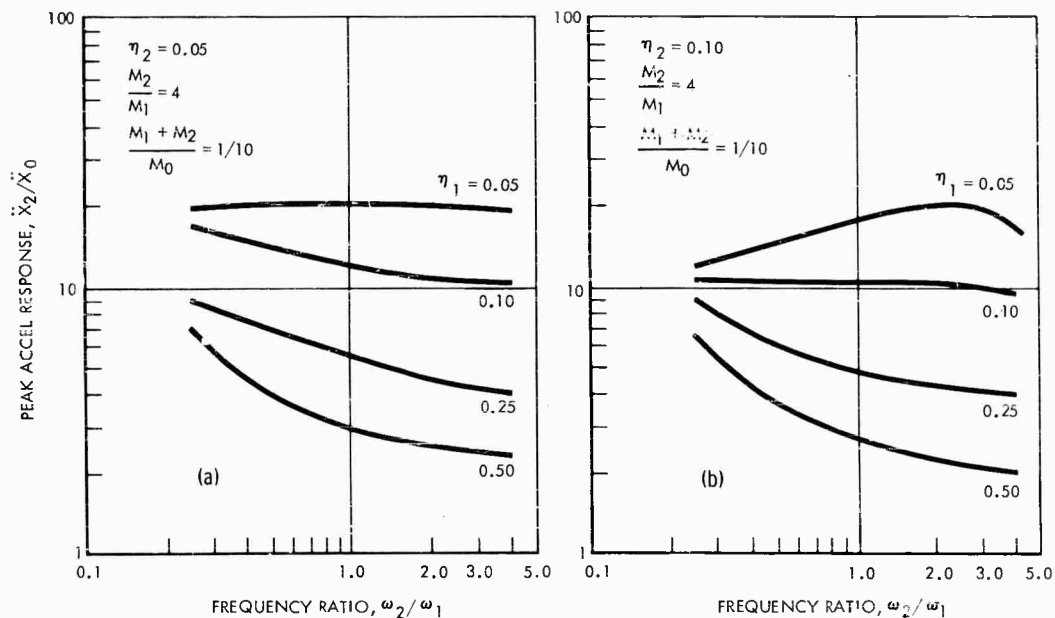


Fig. 5 - Peak acceleration response to sinusoidal excitation

$$\frac{M_2}{M_1} = 4, \quad \frac{M_1 + M_2}{M_0} = \frac{1}{10}$$

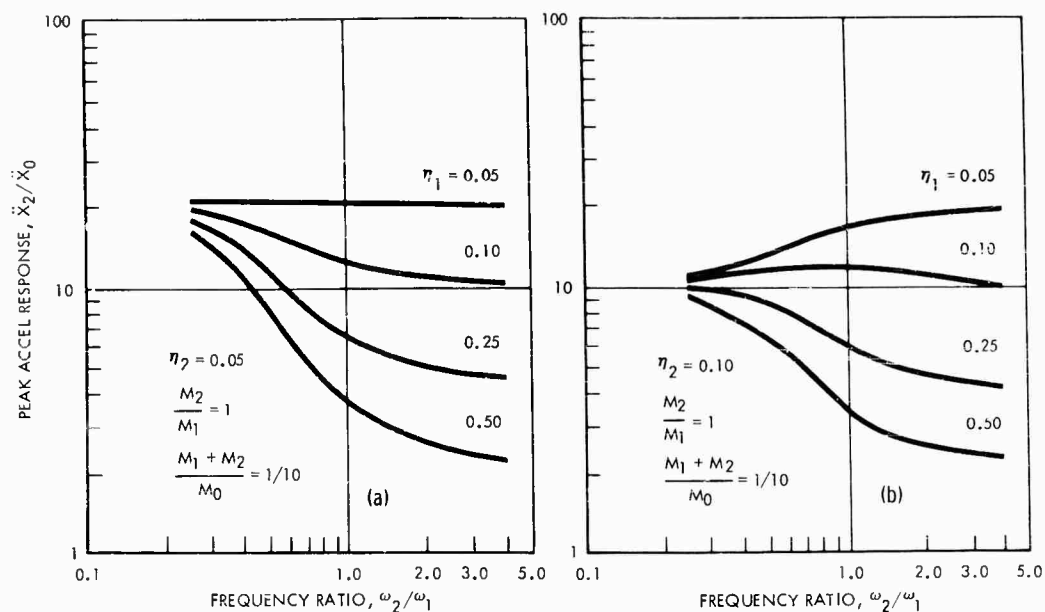


Fig. 6 - Peak acceleration response to sinusoidal excitation

$$\frac{M_2}{M_1} = 1, \quad \frac{M_1 + M_2}{M_0} = \frac{1}{10}$$

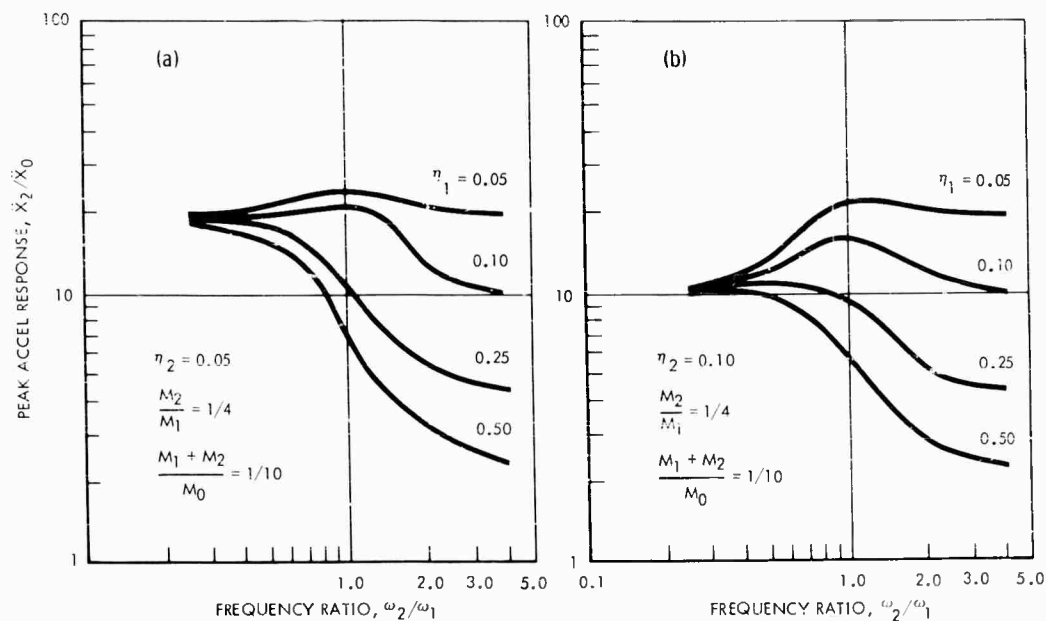


Fig. 7 - Peak acceleration response to sinusoidal excitation

$$\frac{M_2}{M_1} = \frac{1}{4}, \quad \frac{M_1 + M_2}{M_0} = \frac{1}{10}$$

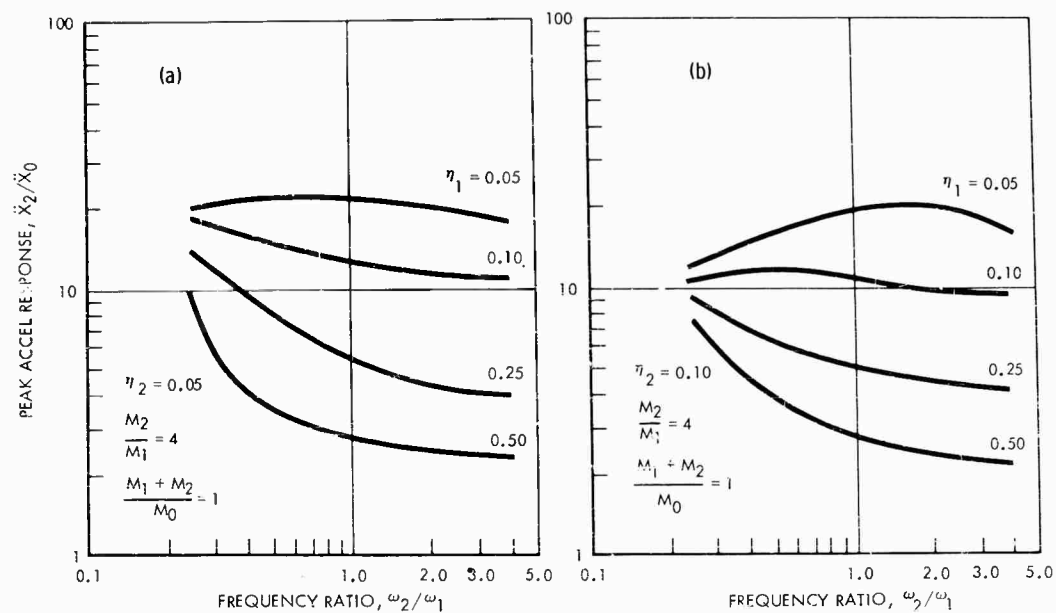


Fig. 8 - Peak acceleration response to sinusoidal excitation

$$\frac{M_2}{M_1} = 4, \frac{M_1 + M_2}{M_0} = 1$$

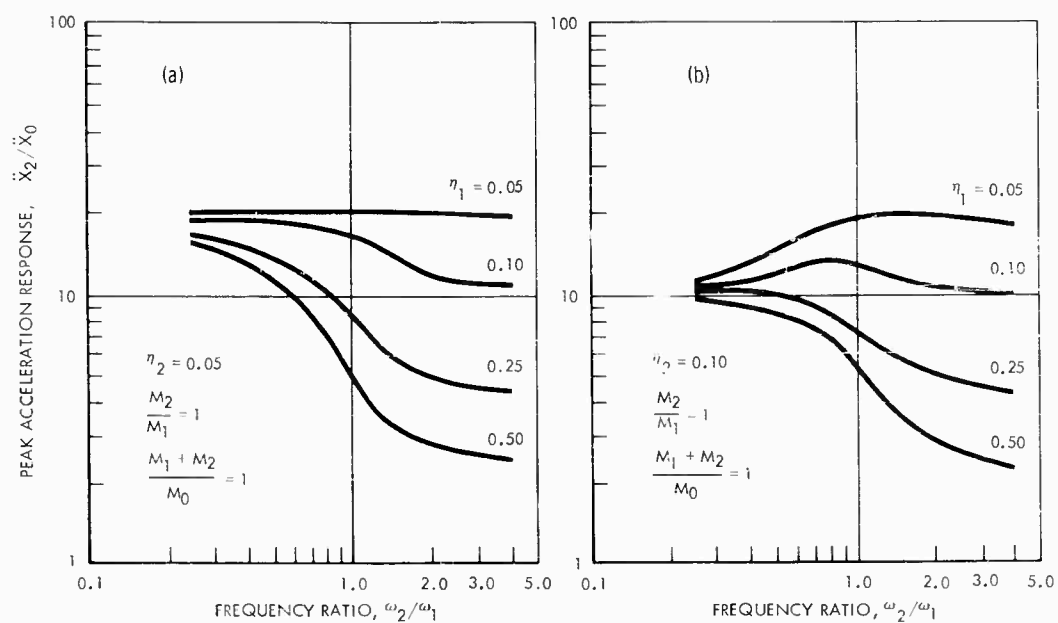


Fig. 9 - Peak acceleration response to sinusoidal excitation

$$\frac{M_2}{M_1} = 1, \frac{M_1 + M_2}{M_0} = 1$$

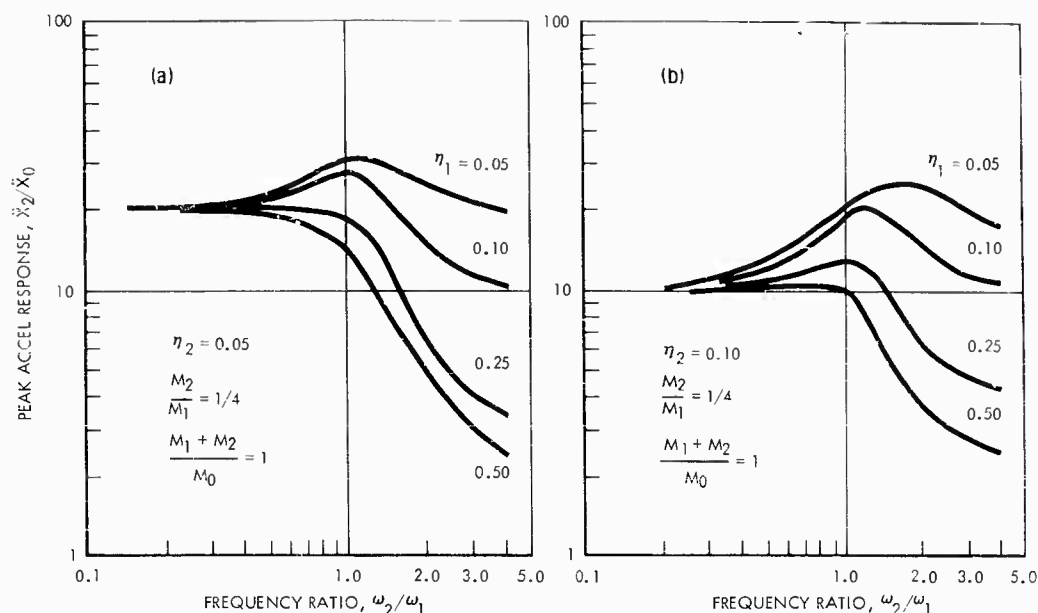


Fig. 10 - Peak acceleration response to sinusoidal excitation

$$\frac{M_2}{M_1} = \frac{1}{4}, \quad \frac{M_1 + M_2}{M_0} = 1$$

as part of a two-degree-of-freedom system. Proper transmission of the vibration test forces requires that this ratio be nearly equal to the resonance amplification of the specimen above which, in turn, is nearly equal to $1/\eta_2$. Thus, to select a viscoelastic layer having proper damping and stiffness, it is necessary to have a peak acceleration response of approximately 20 in cases covered by Figs. 5a through 13a. For Figs. 5b to 13b the corresponding value should be 10.

In this case, the effect of decreasing the mass ratio M_2/M_1 tends to improve the performance of the system by making it less sensitive to the damping of the viscoelastic layer. For example, there is a wider spread in the plots of Fig. 5a than in those of Fig. 7a at values of ω_2/ω_1 less than 1.00. Some curves reach an intermediate maximum value, higher than either of these values, as in Figs. 7b and 10b. The practical significance of this is that peak resonance amplifications can occur which are higher than corresponding amplifications of the two separate individual spring dampers in the systems.

The design and selection of a suitable viscoelastic layer is simplified as the specimen weight increases relative to the exciter weight. This can be seen by comparing the plots in

Figs. 5, 6, and 7, representing small relative specimen weight, with those in Figs. 11, 12, and 13, in which the specimen weight is ten times that of the exciter. In the latter plots, the desired response is achieved over a wide range of values of ω_2/ω_1 . In many of the large test structures, the specimen weight is large relative to the exciter weight.

TEST DATA ON VISCOELASTIC MATERIALS

There is a considerable amount of published data on dynamic properties of viscoelastic materials [2]. However, this information should, in practice, be obtained on the specific material with the same geometric configuration as intended for the test. Exploratory experiments were conducted on neoprene rubber samples, and the results are plotted in Fig. 14. The vibration test setup is shown in Fig. 15. Two washer-shaped samples of Neoprene Rubber AMS 3208, 3/4 inch thick and having a net area of 16 square inches each, were used to hold a 50-pound cylindrical weight on an electrodynamic vibration exciter. The rubber samples were preloaded in compression, and the 50-pound weight was guided by flexures so as to restrict its motion to only one direction (vertical). Using suitable calibrated force, displacement, and acceleration transducers, the

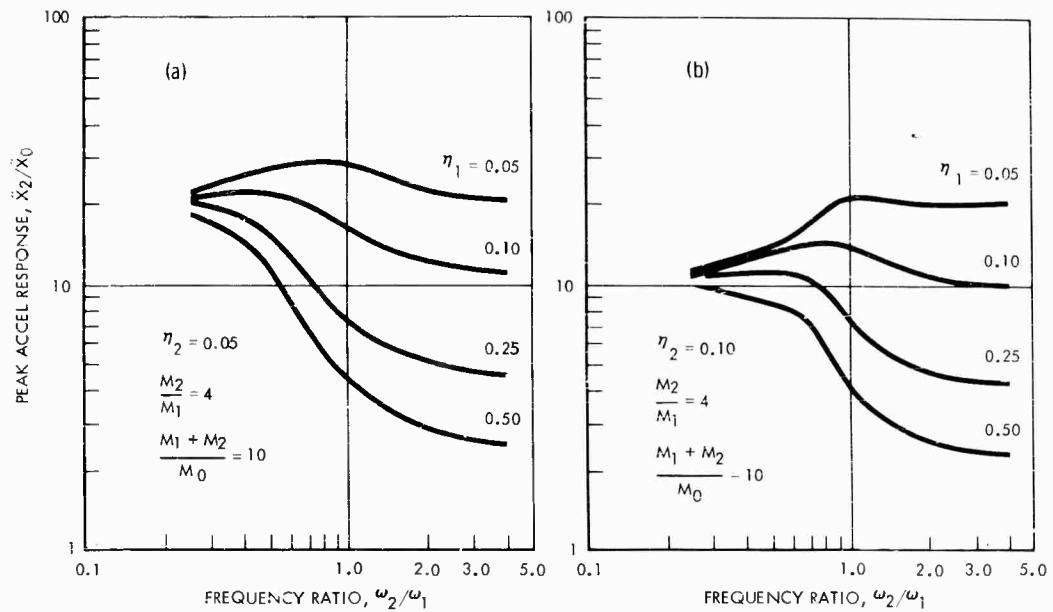


Fig. 11 - Peak acceleration response to sinusoidal excitation

$$\frac{M_2}{M_1} = 4, \quad \frac{M_1 + M_2}{M_0} = 10$$

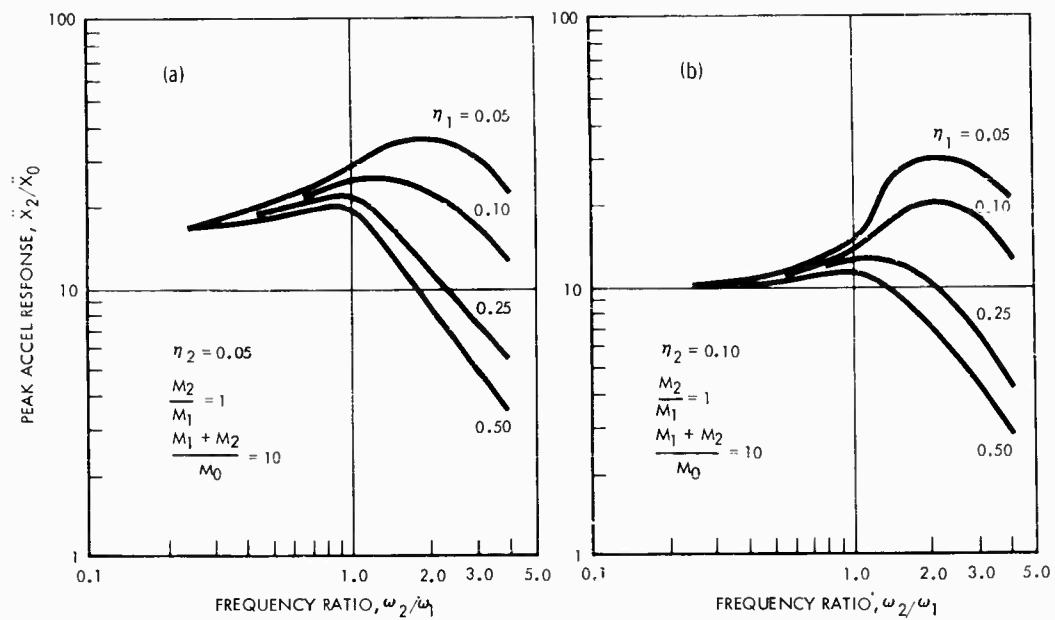


Fig. 12 - Peak acceleration response to sinusoidal excitation

$$\frac{M_2}{M_1} = 1, \quad \frac{M_1 + M_2}{M_0} = 10$$

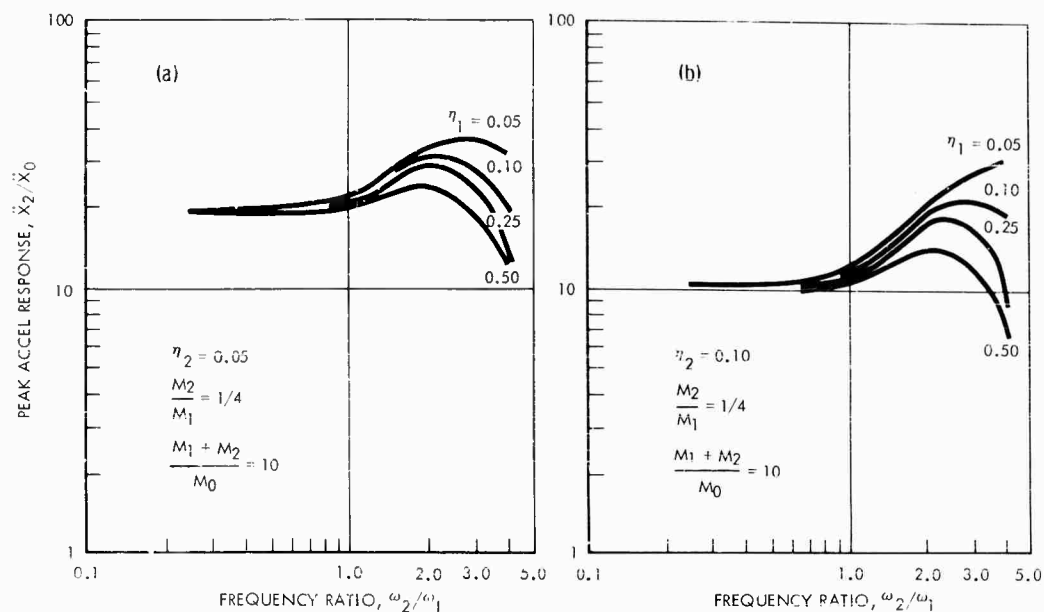


Fig. 13 - Peak acceleration response to sinusoidal excitation

$$\frac{M_2}{M_1} = \frac{1}{4}, \quad \frac{M_1 + M_2}{M_0} = 10$$

following variables were recorded as a function of frequency, during sine sweeps in which the output acceleration \ddot{x}_1 was kept constant:

- \ddot{x}_0 = input acceleration,
- y = deflection amplitude of neoprene layer, and
- ϕ = phase angle between force and deflection amplitudes across neoprene layers.

The plot of Fig. 14a represents the acceleration response ratio of the system at ± 2 g output acceleration (± 100 pounds of transmitted force). The resonance frequency was 185 cps and the peak amplification was 4.5. The variation of the spring constant or stiffness K of the viscoelastic samples is shown in Fig. 14b. This is the ratio of the dynamic force amplitude to deflection amplitude. The measured values of the damping factor, $\eta = \tan \phi$, are plotted in Fig. 14c. The assumptions made in the analytical models, that stiffness and damping are independent of frequency, do not apply for this material. Both of these values tend to increase with frequency in the range of frequencies reported, but the two increases are not comparable. Although these characteristics tend to

complicate such vibration analyses, the actual deviations observed cause desirable effects as regards vibration force transmission. The plot in Fig. 14a also represents the vibration transmission properties of the viscoelastic layer. The transmission efficiency is understandably poor at the higher frequencies since the layer acts as an isolator. At the higher frequencies, vibration transmission depends primarily on the damping of the layer. Thus, damping increase with frequency is a desirable property. The two circled points on the plot of Fig. 14a represent 50 and 20 percent values of transmission efficiency, and they occur at roughly twice and three times the natural frequency of the system, respectively. This efficiency would be reduced had the properties of the viscoelastic remained unchanged with frequency. It was observed that the stiffness and damping of this particular material was not significantly dependent on force amplitude within the range of conditions studied, as shown by the points on Figs. 14b and 14c.

It is well known that such materials are very temperature sensitive, and the temperatures of the samples were observed to be in the range of 82 to 85°F during the period of the experiments. Tests at ± 8 g (± 400 pounds) were also attempted, but the higher damping at this

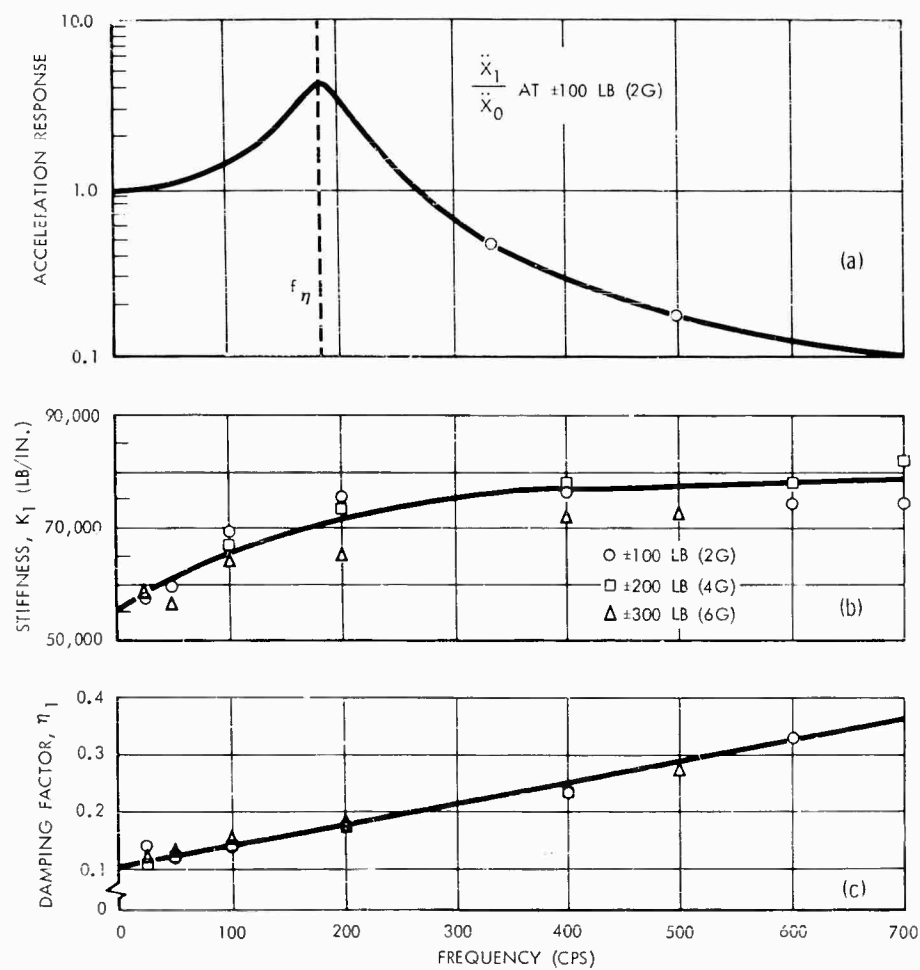
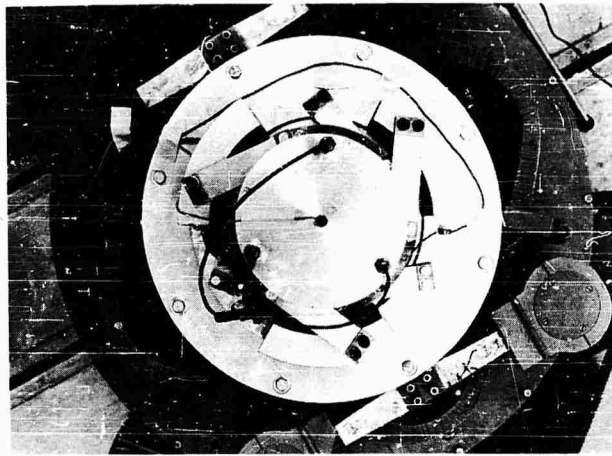
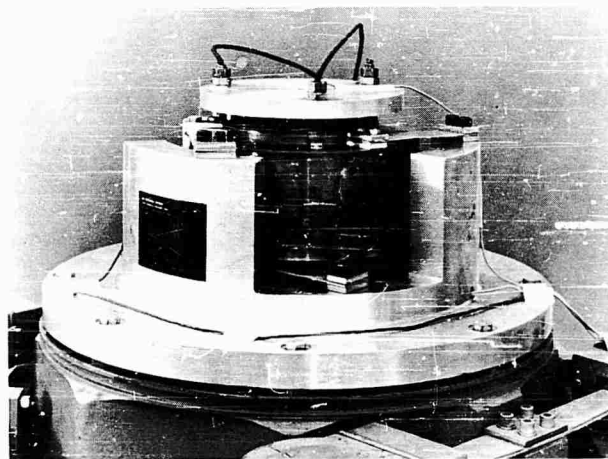


Fig. 14 - Measured dynamic characteristics of viscoelastic material (Neoprene 3208)



(a)



(b)

Fig. 15 - Views of test setup for measuring viscoelastic material characteristics

higher amplitude caused gradual temperature increase beyond the 82 to 85°F range. The stiffness of the rubber kept dropping and the deflection amplitude kept increasing. This indicated that the vibratory force capacity of the material had been exceeded.

To enable proper selection of such a material for a vibration test, it would be essential to conduct such tests on many applicable materials to find the one that has the most desirable properties for the particular application.

CONCLUSIONS

On the basis of the simple analyses presented in this study, it becomes apparent that under certain conditions, transmission of vibration test forces by a so-called "viscoelastic member" is practical, and is possibly the best overall solution to the problem of vibration test design. The advantages of such an analysis are most significant when:

1. The test structure has a low natural frequency.
2. The damping ratio of the structure is relatively high, and a viscoelastic member can be provided with comparable damping.
3. The test structure is heavy relative to the moving parts of the exciter.

ACKNOWLEDGMENTS

The authors would like to acknowledge the assistance provided by L. Tanner of North American Aviation, who developed and programed the solutions to the sinusoidal model study. The properties of neoprene were measured using a Model SD-1002 Spectral Dynamics Impedance Measuring System, by personnel of NAA's Engineering Development Laboratory.

Appendix A

RESPONSE OF TWO-DEGREE-OF-FREEDOM SYSTEM TO RANDOM VIBRATION

The behavior of the randomly excited two-mass system illustrated in Fig. 1c has been studied by several authors [3,4,5]. Morrow [3] assumed that the upper mass did not load the lower, so that the presence of the upper mass did not significantly affect the motion of the lower mass. This assumption is reasonably valid for a system in which the upper mass is very light and flexible compared with the lower mass but would lead to inaccuracies for many practical applications.

The dynamic coupling between the two masses of the system is taken into account by Curtis and Boykin [4], who obtained response in terms of integral functions of the white noise input; these were then evaluated numerically for a range of parameters. Crandall and Mark [5] adopt the same approach but derive closed-form analytical expressions for the mean square responses.

Both of the preceding references restrict their treatment to systems having the upper mass smaller than the lower mass. However, many practical aerospace structures which may be reasonably well represented by the two-mass analogy have upper masses up to ten

times larger than their lower masses, making it desirable to analyze such cases. The response equations of Crandall and Mark [5] were, therefore, coded for the IBM 7090 and a parametric study was performed for an extended range of values of mass ratio, uncoupled frequency ratio and damping coefficients. For coding convenience, and to suit the special requirements of this study, these equations were rearranged into the form summarized below.

The system under consideration consists of two concentrated masses, two linear springs and two viscous dampers. The base of the system is excited by a stationary random process with an ideally white spectrum having zero mean and a uniform acceleration spectral density, for all frequencies from zero to infinity. It follows that the acceleration responses are also stationary random processes with zero mean. It is convenient to normalize the response data by reference to the response of the single-degree-of-freedom system shown in Fig. 1d. This represents the test structure mounted on the vibration machine without an interposed viscoelastic layer, so that the normalized response ratio clearly demonstrates the effects of adding such a layer.

The mean square acceleration response of the single-degree-of-freedom system is

$$E[\ddot{X}_0^2] = \frac{\pi}{2} S_0 \frac{\omega^2}{\zeta_2} (1 + 4\zeta_2^2). \quad (A1)$$

In the two-degree-of-freedom system, the response of the upper mass is

$$E[\ddot{X}_2^2] = 2\pi S_0 \omega_1^2 \omega_2^2 \left(\frac{N}{D} \right), \quad (A2)$$

where

$$N = N_1 \omega_1^3 + N_2 \omega_1^2 \omega_2 + N_3 \omega_1 \omega_2^2 + N_4 \omega_2^3 \quad (A3)$$

and

$$D = D_1 \omega_1^5 \omega_2 + D_2 \omega_1^4 \omega_2^2 + D_3 \omega_1^3 \omega_2^3 + D_4 \omega_1^2 \omega_2^4 + D_5 \omega_1 \omega_2^5. \quad (A4)$$

The coefficients in Eqs. (A3) and (A4) are given by

$$\begin{aligned} N_1 &= \zeta_1 + 4\zeta_1 \zeta_2^2, \\ N_2 &= \beta \zeta_2 + 4\zeta_1^2 \zeta_2 + 4(1 + \beta) \zeta_2^3 + 16\zeta_1^2 \zeta_2^3, \\ N_3 &= \beta \zeta_1 + 4\zeta_2^3 + 4(1 + \beta) \zeta_1 \zeta_2^2 + 16\zeta_1^3 \zeta_2^2, \end{aligned} \quad (A5)$$

and

$$N_4 = (1 + \beta)^2 \zeta_2 + 4(1 + \beta) \zeta_1^2 \zeta_2;$$

and

$$\begin{aligned} D_1 &= 4\zeta_1 \zeta_2, \\ D_2 &= 4\beta \zeta_2^2 + 16\zeta_1^2 \zeta_2^2, \\ D_3 &= -8\zeta_1 \zeta_2 + 16\zeta_1^3 \zeta_2 + 15(1 + \beta) \zeta_1 \zeta_2^3, \\ D_4 &= 4\beta \zeta_1^2 + 16(1 + \beta) \zeta_1^2 \zeta_2^2, \end{aligned} \quad (A6)$$

and

$$D_5 = 4(1 + \beta)^2 \zeta_1 \zeta_2.$$

Dividing Eq. (A2) by Eq. (A1) yields

$$\frac{E[\ddot{X}_2^2]}{E[\ddot{X}_0^2]} = \frac{4\omega_1^2 \omega_2 \zeta_2 \left(\frac{N}{D} \right)}{1 + 4\zeta_2^2}. \quad (A7)$$

This equation gives the normalized mean square response ratio. The root-mean-square response ratio, of course, is given by the square root of this expression.

Appendix B

RESPONSE OF TWO-DEGREE-OF-FREEDOM SYSTEM TO SINUSOIDAL VIBRATION

For this analysis, it was assumed that the test setup could be represented dynamically by the lumped-parameter system illustrated in Figs. 1a and 1b. The system consists of two upper masses and an additional lower mass. These three masses are connected by linear springs and hysteretic dampers. The phenomenon of hysteretic damping (also called structural damping) has been discussed in detail by Bishop [4,5] and Soroka [6]; the expression implies a resisting force which is in phase with velocity but proportional in magnitude to displacement.

The combination of a linear spring and a hysteretic damper produces a resisting force which may be expressed as

$$f = K(1 + i\eta)X, \quad (B1)$$

in which K is the spring rate, η is the damping coefficient, and X is the deflection.

The equations of motion for the system shown in Fig. 1b, when excited by a sinusoidally varying force, are

$$\begin{aligned} M_0 \ddot{X}_0 + K_1(1 + i\eta_1)(X_0 - X_1) &= F \sin \Omega t, \\ M_1 \ddot{X}_1 - K_1(1 + i\eta_1)(X_0 - X_1) &+ K_2(1 + i\eta_2)(X_1 - X_2) = 0, \end{aligned} \quad (B2)$$

and

$$M_2 \ddot{X}_2 - K_2(1 + i\eta_2)(X_1 - X_2) = 0.$$

Steady state conditions are assumed.

By definition

$$\ddot{X}_0 = \frac{F}{M_T}, \quad (B3)$$

and \ddot{X}_2 is the peak acceleration of the upper mass, M_2 . It was required to find the variation of the ratio \ddot{X}_2/\ddot{X}_0 with the ratio of uncoupled natural frequencies, ω_2/ω_1 , for particular values of the mass ratios M_2/M_1 and $(M_1 + M_2)/M_0$.

Using Laplace transforms, Eqs. (B2) were solved and the solution was coded for the IBM 7090. A parametric study was performed, and the results are summarized in Figs. 5 through 13.

REFERENCES

1. "Array-ed for 30,000 Pounds Force," *Environ. Quarterly*, 10 (1):38-41 (1964).
2. J. D. Ferry, Viscoelastic Properties of Polymers (John Wiley and Sons, Inc., New York, 1961).
3. C. T. Morrow, Shock and Vibration Engineering, Vol. I (John Wiley and Sons, Inc., New York, 1963), pp. 190-201.
4. A. J. Curtis and T. R. Boykin, "Response of Two-Degree-of-Freedom Systems to White Noise Base Excitation," *J. Acoust. Soc. Am.*, 33:655-663 (1961).
5. S. H. Crandall and W. D. Mark, Random Vibration in Mechanical Systems (Academic Press, New York, 1963), pp. 80-89.
6. R. E. D. Bishop, "The General Theory of Hysteretic Damping," *Aero. Quarterly*, 7 (P. 1):60-70 (1956).
7. R. E. D. Bishop, "The Treatment of Damping Forces in Vibration Theory," *J. Roy. Aero. Soc.*, 59 (539):738-742 (1955).
8. W. W. Soroka, "A Note on the Relation of Structural and Viscous Damping," *J. Aero. Sci.*, 16:409 (1949).

* * *

FREE-FREE BENDING VIBRATION MEASUREMENTS OF THE OAO BOOST VEHICLE UTILIZING AIR-BEARING SUPPORT

R. L. Turney, J. D. Jones and K. F. Koehl
General Dynamics/Astronautics
San Diego, California

This free-free test program was initiated to verify experimentally the analytically predicted free-free mode shapes and modal frequencies of the Orbiting Astronomical Observatory (OAO) flight vehicle. This verification was desired because the vehicle is of the split-beam variety in that the Agena/OAO combination is an interbeam located within load-carrying fairings. Verification was sought primarily for the first five free-free elastic modes in four different mass conditions. Of the five modes investigated, three were vehicular bending modes and two were engine response modes.

The desired free-free boundary condition was approximated by floating the test specimen vertically on a pair of air bearings attached to the booster engine gimbal points, so as to introduce negligible restraint to motion in the test plane. Stability was provided by horizontal soft springs attached at the nose and at the booster thrust longeron. This technique provided a test configuration that was essentially free in the appropriate plane, accommodated various testing conditions with one test setup, and dissipated negligible energy.

Comparison with analytically predicted modes of the OAO launch vehicle showed good mode shape and frequency agreement in the vehicle bending modes. The booster engine and sustainer engine resonances were somewhat higher than predicted, due to higher spring constants present in the test configuration than those used in the analysis.

INTRODUCTION

The Orbiting Astronomical Observatory (OAO) is to be boosted into orbit by an Atlas/Agena space launch vehicle. This paper presents the results of a bending vibration measurement program conducted on a full-scale article set up to represent the configuration during the boost phase of flight. The program was carried out under NASA Contract NAS3-3807. The actual measurements were made at the General Dynamics/Astronautics Pt. Loma Test Site during March and April 1964.

Verification was sought primarily for the first five free-free elastic modes in four different mass conditions, namely:

1. A fully tanked vehicle representative of a launch condition, herein referred to as full-full condition;

2. A partially tanked Atlas and fully tanked Agena representing 60 seconds of flight time, herein referred to as 60 second — full condition;

3. A dry Atlas and fully tanked Agena representing the Atlas burnout condition, herein referred to as empty-full condition; and

4. A dry vehicle for close comparison with analytical results without liquid effects, herein referred to as empty-empty condition.

The verification was desired because this vehicle is of a split-beam variety in that the Agena/OAO combination is housed within load-carrying fairings, thus requiring a more complex approach to the vibration analysis problem.

The desired free-free boundary condition was approximated by floating the test specimen vertically on a pair of air bearings attached to

the booster engine gimbal points, so as to introduce negligible restraint to motion in the test plane. Stability was provided by soft horizontal springs attached at the nose and at the booster thrust longeron. This technique provided a test configuration that was essentially free in the appropriate plane, accommodated various testing conditions with one test setup, and dissipated negligible energy.

TEST ARTICLE

The vehicle tested consisted of the actual OAO Atlas booster flight tank, with inactive hydraulic and electrical packages, actual flight pneumatic hardware, and the interstage adapter. The Atlas propulsion hardware used was salvaged from a static test vehicle, with the exception of the booster engine nozzles which were cylinders, mass simulated to represent the booster engine nozzles and to provide housing for the lower portion of the air-bearing system. The Agena used was a facility checkout

vehicle representative of the mass and stiffness characteristics of an actual Agena stage. The OAO spacecraft used was a dynamically simulated full-scale model. The external fairings used were actual OAO fairings that were used later for ejection testing. This configuration was in "A" tower at the Pt. Loma Test Site as shown in Fig. 1.

The test article was floated on air bearings located at each booster engine gimbal point and stabilized with soft springs located on the nose cone and the booster thrust longeron.

Figure 2 depicts the general suspension system and a cutaway of the air-bearing installation. The air-bearing plates were made of 4340 steel heattreated to produce austenitic grain structure. These surfaces were nickel-plated for corrosion prevention and the plating was heattreated to increase abrasion resistance. The two surfaces were then handlapped to as fine a smoothness as possible. As evidence of the smoothness and fit of the two

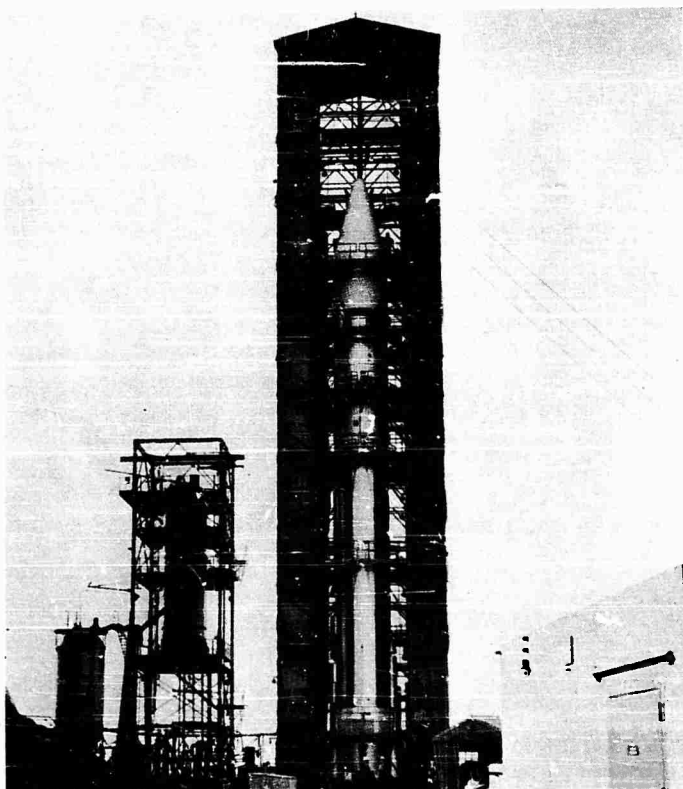


Fig. 1 - Complete OAO test vehicle installed in "A" tower at Pt. Loma; "B" tower (left) containing water storage tank and Building 3 (right) is blockhouse

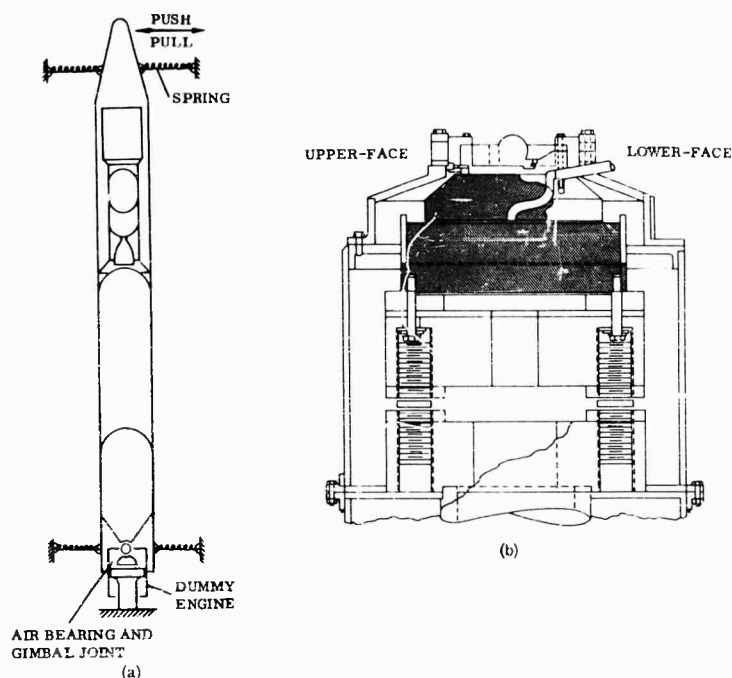


Fig. 2 - Test vehicle: (a) suspension system, and (b) cutaway view of air bearing

surfaces, the bearing would not leak a nitrogen purge until enough gas pressure was applied to separate the surfaces. Dry nitrogen was used as the gas for the air-bearing operation. (A motion picture is available showing the operation and freeness on the suspension system.)

The stabilizing springs were designed to afford very small restraint in the plane of excitation and yet to restrain motion adequately in the plane normal to the plane of excitation. The resultant rigid body frequencies were always $1/6$ or less than the lowest elastic mode frequency to be investigated.

INSTRUMENTATION

Thirty-nine Statham ± 5 g strain gage accelerometers were used to measure the mode shapes and modal frequencies. Several additional accelerometers and linear displacement transducers monitored the total motion of the specimen in all three axes. Standard IRIG multiplexing was used to record all monitor-selected data signals during the test. Later playbacks of the magnetic tape through normalizing networks to the monitoring recorder produced complete data sets for manual analyses. Figure 3 is a block diagram showing the sampling and commutating circuits developed for

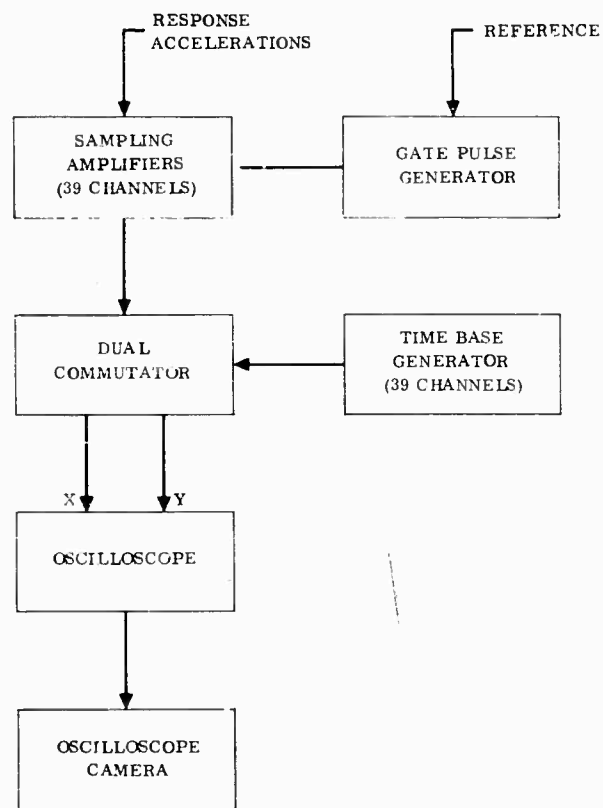


Fig. 3 - Sampling and commutating circuits

this test. Combined with the oscilloscope and camera, this system became a mode shape display and recording instrument for steady state vibration of the specimen. The sampling amplifiers were gated by the pulse generator in phase with the reference signal. Filtering within each amplifier produced dc signal levels proportional to the phase and amplitude of the input signals for steady state conditions; dc signal levels proportional to accelerometer location were provided by the time base generator. Commutating these signals to drive the two axes of an oscilloscope produced mode shape displays similar to that shown in Fig. 4.

Sinusoidal vibration excitation was furnished by three closed-loop servo controlled, linear hydraulic exciters employing displacement feedback. Seismic weights were used to react the exciter forces. The drive points for these exciters were on the nose cone, the top of the OAO and the booster thrust longeron. A mechanical release clamp, hydraulically actuated, was used to uncouple each exciter-seismic system from the specimen for free damping decays (Fig. 5). A mechanical fail-safe unit employing dual shear pins was a part of each system for the protection of the specimen when coupled to an exciter. Load cells were used to monitor excitation forces. All control and monitoring was done remotely from the blockhouse through landline circuits.

TEST PROCEDURE

The Agena and Atlas tanks were filled with distilled water to a level equivalent to the propellant mass condition under investigation.

Flight pressures were used in the launch and 60 seconds of flight conditions. Lower pressures were used in the other two test conditions due to large ullage hazard problems.

After tanking and pressurization, the vehicle was raised on the air bearings a minimum of 0.0003 inch. The various linear motion instruments were monitored to insure that no adverse movement occurred while the vehicle was supported by the cushion of air.

The exciter to be used was then centered and attached to its vehicle drive point. As a general practice, the nose cone exciter was used initially for mode determination. The other exciters were used only when mode definition proved difficult utilizing the nose cone exciter.

A low-level, slow frequency sweep was begun, and exciter force, vehicle displacement, and mode plotter display were noted. The mode plotter and other visual display units would indicate when a natural mode was being approached. Each mode was "tuned" to the frequency of minimum force and/or maximum displacement. The vehicle was then released, vibrations were allowed to decay, and the damped frequency was noted. The vehicle was then "fine tuned" to the indicated damped natural frequency, and the mode shape was recorded. This procedure was repeated for each mode of each tanking condition until the first five modes of all test configurations were determined.

When closely coupled modes were encountered, different exciter units were used to attempt to separate the modes in question. Very

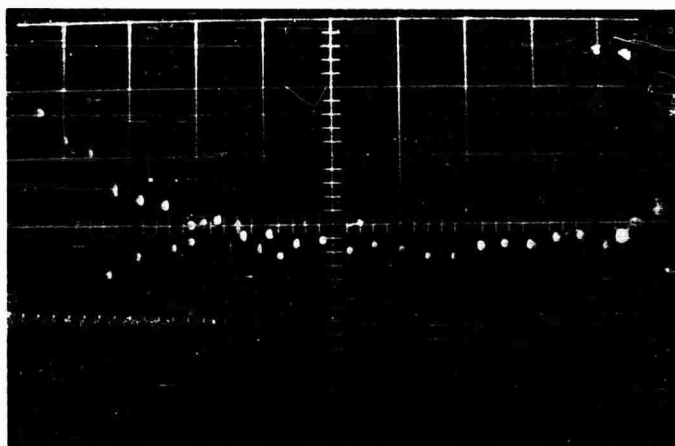


Fig. 4 - Polaroid camera shot of typical mode plotter display

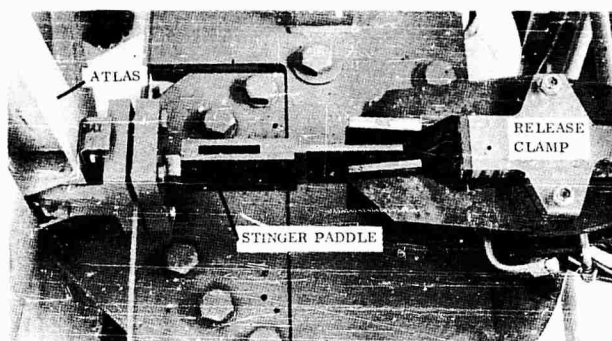


Fig. 5 - Details of release clamp and stinger paddle

fine frequency tuning was used with each exciter along with the mode plotter display until separation of the modes could be accomplished. This proved to be a satisfactory approach in all cases.

TEST RESULTS

Table 1 is a summary of data obtained. Figures 6 through 9 depict the first five mode shapes and frequencies of each test configuration.

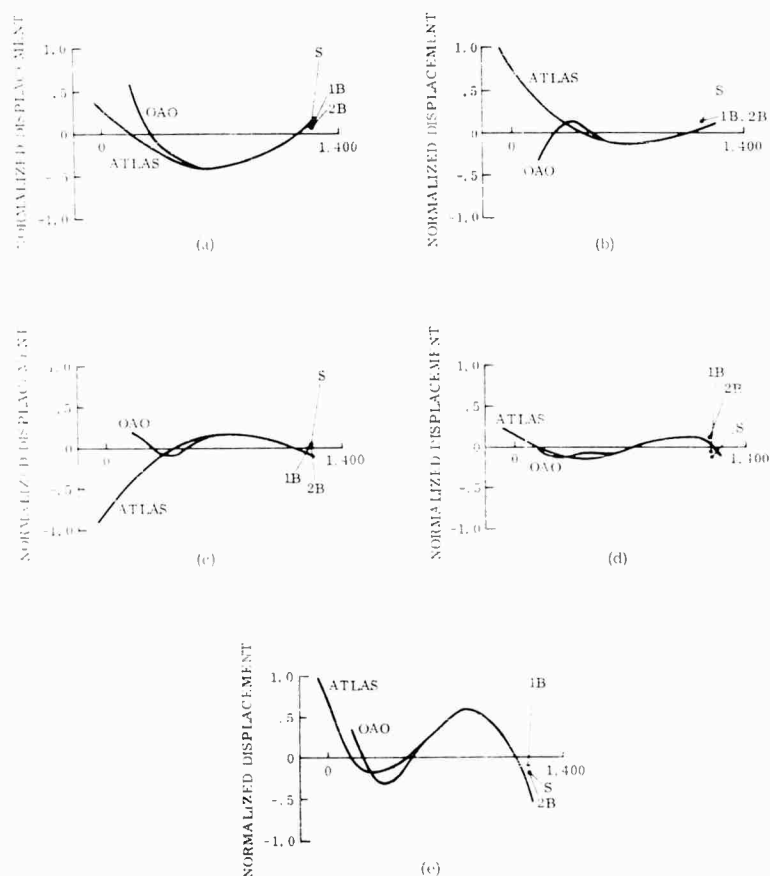


Fig. 6 - Atlas-empty, Agena-empty mass condition: (a) Mode 1, 7.5 cps; (b) Mode 2, 9.3 cps; (c) Mode 3, 9.75 cps; (d) Mode 4, 16.3 cps; and (e) Mode 5, 20.2 cps

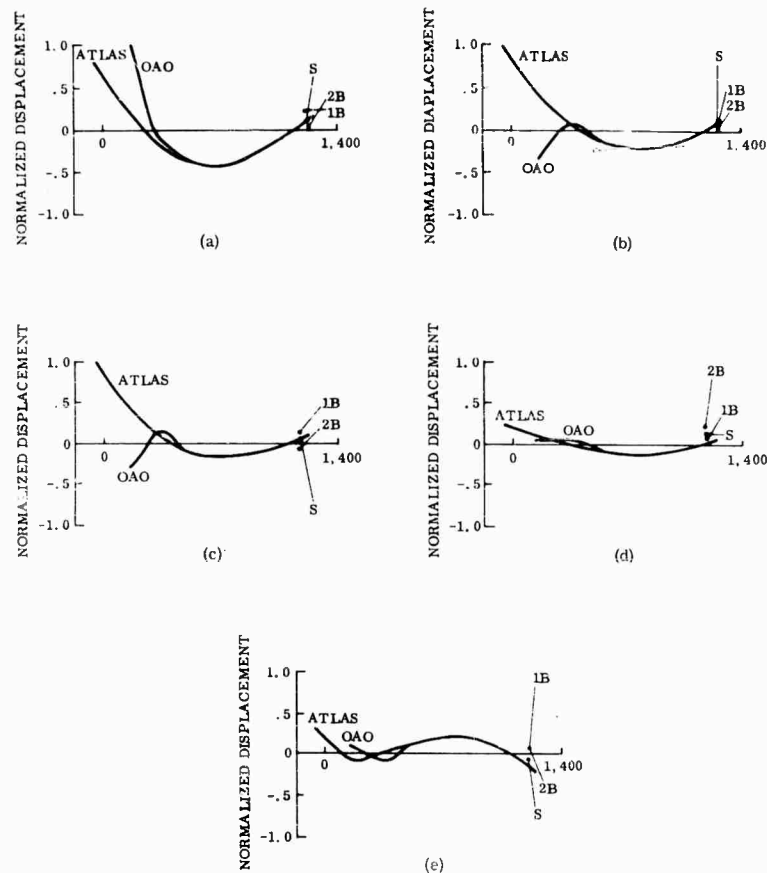


Fig. 7 - Atlas-empty, Agena-full mass condition:
(a) Mode 1, 6.7 cps; (b) Mode 2, 9.4 cps; (c) Mode 3,
9.7 cps; (d) Mode 4, 14.5 cps; and (e) Mode 5, 18.5 cps

Computation of a damping ratio for each mode involved construction of an envelope faired through the harmonic beats and nonlinearities present in the structural acceleration decay of the instrumentation channel possessing maximum response in a given mode. The actual waveshape was then replaced by an equivalent sinusoid of the frequency and following the constructed envelope.

The damping ratio was calculated as

$$\xi(75\% A_i) = \frac{0.11}{N_i} \quad (1)$$

where

ξ = dimensionless damping ratio,

i = cycle number following disconnect,

A_i = wave amplitude at i th cycle, and

N_i = number of cycles to half amplitude after cycle i .

Values of the resulting damping ratios are shown in Table 1.

Inasmuch as the accuracy of this method decreases with increasing i , initial values calculated were weighted heaviest. Repeated runs indicate a 7 percent tolerance on ξ resulting from aggregate variations inherent in these procedures. Figure 10 is a typical record from which the damping ratio was computed.

Reference to Table 1 shows that the values recorded for booster engine resonance are substantially the same for all tanking conditions except the Atlas-empty, Agena-empty case

TABLE 1
Summary of Modal Data

Mode No.	Atlas	Empty	Empty	60 Seconds	Full
	Agena	Empty	Full	Full	Full
1	Frequency (cps) Damping ^a Shaker	7.5 --- #2	6.7 0.0106 #1	3.9 0.0096 #1	3.6 0.0072 #1
(1st Vehicle Bending) →					
2	Frequency (cps) Damping ^a Shaker	9.3 0.0176 #2	9.4 0.0176 #1	8.5 0.0176 #1	7.2 NDA ^b #3
(OAO & Fairing Out of Phase) →					2nd Vehicle Bending
3	Frequency (cps) Damping ^a Shaker	9.75 0.0115 #1	9.7 0.0115 #1	8.7 NDA ^b #1	8.2 0.0157 #1
(Sustainer Resonance) →				2nd Vehicle Bending	OAO & Fairing Out of Phase
4	Frequency (cps) Damping ^a Shaker	16.3 0.0120 #1	14.5 0.0120 #3	9.7 0.0115 #1	9.5 0.0115 #1
(Booster Resonance) →				(Sustainer Resonance)	
5	Frequency Damping ^a Shaker	20.2 0.0170 #1	18.5 0.0202 #3	14.8 0.0120 #3	15.0 0.0120 #3
(2nd Vehicle Bending) →				(Booster Resonance)	
6	Frequency Damping ^c Shaker	26.7 NDT #1	26.2 NDT #1	26.0 NDT #1	25.2 NDT #1
(OAO-Agena 2nd Bending) →					

^aAll damping readings made at 0.1 g acceleration level.

^bNDA = no damping records available due to this mode damping in another mode.

^cNDT = no damping records taken.

which is approximately 2 cps higher than the rest. The Atlas-empty, Agena-empty case was run first before appreciable experience had been attained. During the frequency sweep, a force reduction was noted at approximately 14.5 cps. When released to damp, however, the apparent resonance damped at 16.3 cps. This indication of a strong No. 1 booster response led to the false conclusion that the 16.3-cps

mode was the booster resonance. In the later configurations, it became evident that 14.5 cps was the resonant frequency at which both booster engines were of almost equal amplitude, whereas the 16.3-cps apparent resonance was predominately that of the No. 1 booster engine. Unfortunately, time did not permit the rerunning of this condition to get to 14.5-cps mode.

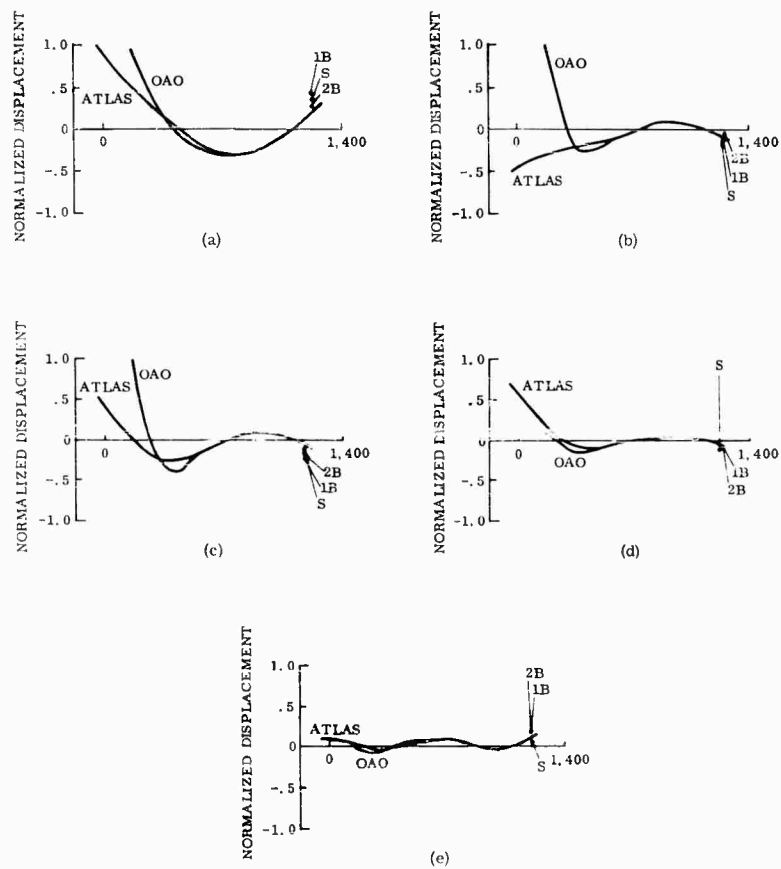


Fig. 8 - Atlas-60 second, Agena-full mass condition:
 (a) Mode 1, 3.9 cps; (b) Mode 2, 8.5 cps; (c) Mode 3,
 8.7 cps; (d) Mode 4, 9.7 cps; and (e) Mode 5, 14.8 cps

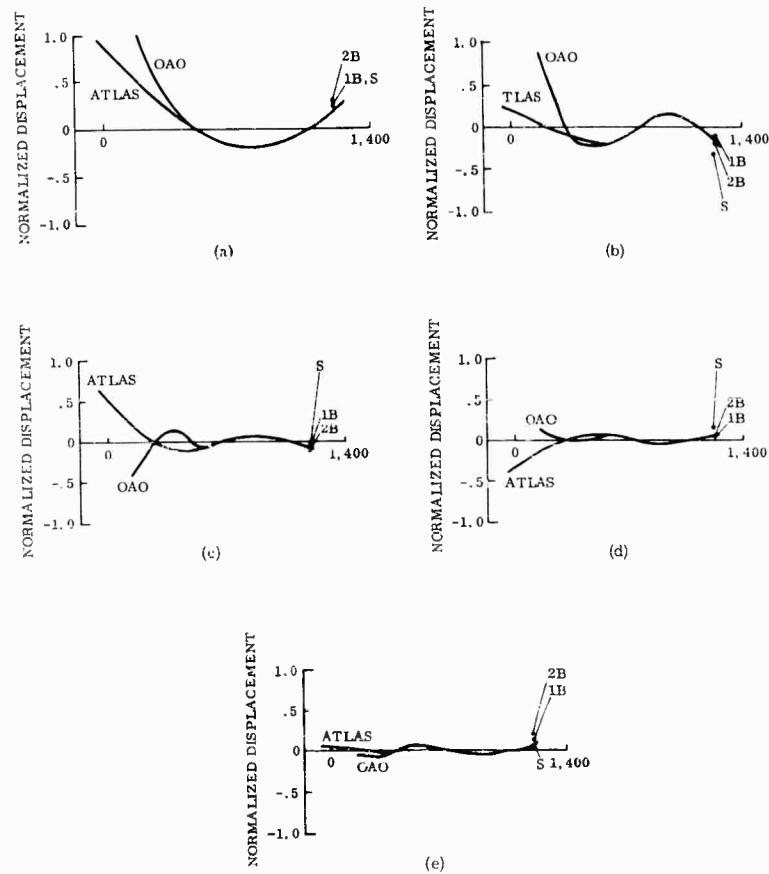


Fig. 9 - Atlas-full, Agena-full mass condition:
 (a) Mode 1, 3.6 cps; (b) Mode 2, 7.2 cps; (c)
 Mode 3, 8.2 cps; (d) Mode 4, 9.5 cps; and (e)
 Mode 5, 15.0 cps

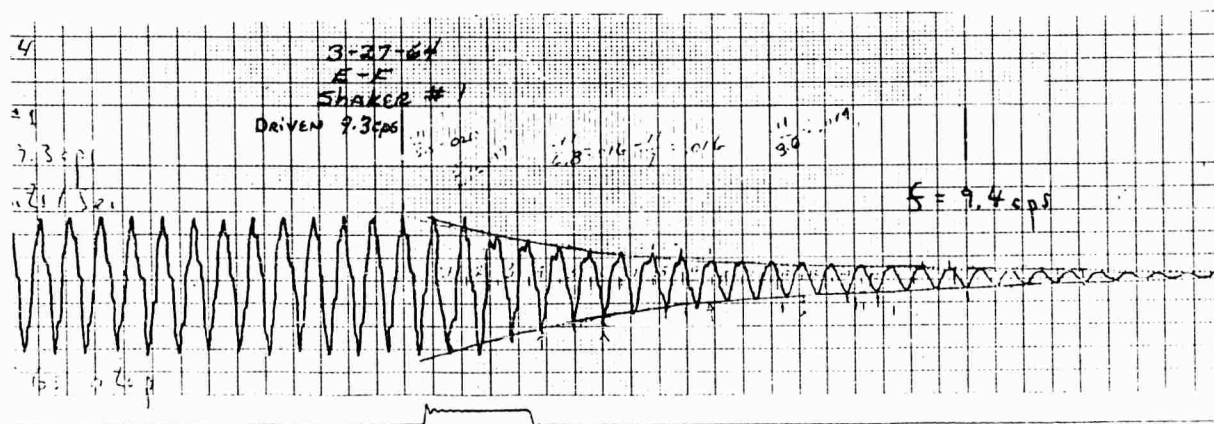


Fig. 10 - Typical record of mode damping

CONCLUSIONS

Comparison with analytically predicted modes of the Atlas/Agena/OAO combination in these test configurations showed good frequency and mode shape agreement in the vehicle bending modes. The major discrepancies existed in the sustainer and booster resonances.

For the analysis, the only spring constants available on the booster engines were those in the pitch plane. Inasmuch as the test vehicle was excited in the yaw plane, which has a higher spring constant, the test results were

approximately 40 percent higher than calculated analytically. The test vehicle sustainer engine was shimmed tight at the gimbal block to take out the normal no-thrust slop that exists on Atlas vehicles. The resulting tight fit may have been tighter than a flight article with an operating sustainer, thus producing an approximate 20 percent increase in the sustainer resonant frequency.

The damping values obtained were higher in all cases than those used in the control systems analysis of the OAO flight vehicle, thus validating the stability analysis of the OAO vehicle.

* * *

THE RESPONSE OF THE OGO SPACECRAFT STRUCTURE TO HIGH-INTENSITY ACOUSTIC LOADING*

P. J. Alfonsi
Goddard Space Flight Center
Greenbelt, Maryland

During the launching phase, a spacecraft is subjected to random vibration with a broad frequency spectrum from about 5 cps to in excess of 10 kc. The lower frequency excitation (up to about 250 cps) is mainly the result of mechanical vibration of the launch vehicle structurally coupled to the spacecraft. The higher frequency spectra are the result of acoustic excitation of the spacecraft and adjacent structure.

To evaluate these effects in the Orbiting Geophysical Observatory (OGO) spacecraft, the full-scale acoustic test program was performed. The specific purpose of this program was to determine experimentally the magnitude and spectra of high-frequency vibration resulting from the OGO spacecraft acoustic environment. Verification of the shroud transmission loss characteristics was a secondary objective.

The test was performed in the sound field generated by the Langley Research Center's 9 by 6 ft thermal structures wind tunnel. The test assemblage was placed in the proximity of the tunnel exhaust, isolated from all but airborne excitation and subjected to a simulated launch environment.

The article was instrumented to provide vibration data pertinent to about 150 positions and acoustic data from about 40 locations. All data were acquired on magnetic tape with the recorders and electronics housed in an instrumentation trailer located approximately 300 ft from the test assemblage.

A preliminary wide band analysis of the vibration data indicated little energy above 3 kc on the spacecraft structure. The initial analysis also showed that the acoustic loading at the reference location on test specimen was uniform within 1 db.

This paper presents a description of the test article, test procedures, acoustic noise environment and results of a detailed analysis of a portion of the acquired data.

BACKGROUND

The Orbiting Geophysical Observatory (OGO) (Fig. 1) was developed as part of a step-by-step program to gain further knowledge of the earth and its environment so that optimum exploration of the universe can be accomplished. The OGO versatility as an observatory-type spacecraft allows it to be launched from several

different boosters and accommodate up to 50 different experiments on each mission.

The main body of the OGO spacecraft is a box-like structure approximately 3 x 3 x 6 feet with projecting panels, gas jets, antennas and experiments. Two sides of the main body are hinged to provide interior access as shown in Fig. 2. Scientific experiments are mounted on

*This paper was not presented at the Symposium.

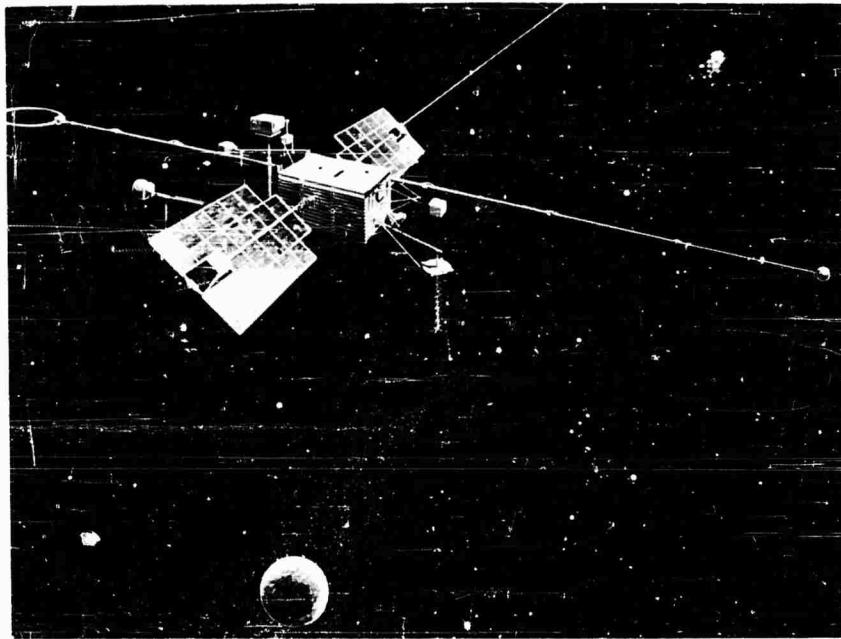


Fig. 1 - Artist's conception of OGO in orbit

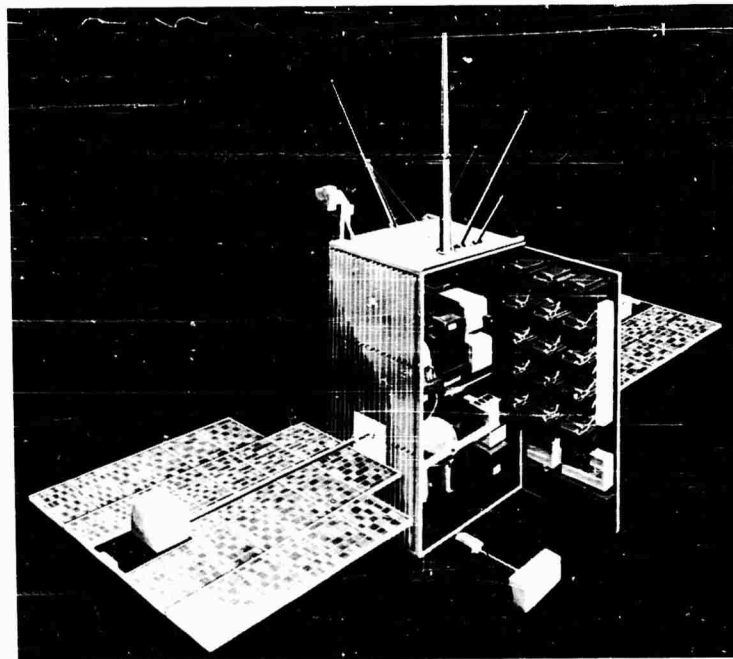


Fig. 2 - OGO with one experiment door open

the inside of these doors and on extendible booms with subsystems mounted on shelves and walls within the structure. Electrical power is supplied by a pair of large solar panels. Coarse orientation is achieved by cold gas jets and fine positioning by a set of reaction wheels. For geophysical missions, the spacecraft carries a number of external experiment packages. Experiments of high sensitivity or special orientation angle requirements are mounted on booms projecting from the spacecraft box. Solar oriented experiments are located on each solar paddle while orbit plane experiments are continuously oriented parallel to the orbital plane. The spacecraft is depicted in the launch configuration in Fig. 3.

INTRODUCTION

During launch and initial stages of boost, a spacecraft is subjected to vibration inputs with a frequency spectrum from 5 cps to more than 10 kc. The lower frequency vibration (up to about 250 cps) is mainly the result of mechanical vibrations of the launch vehicle structurally coupled to the spacecraft. The higher frequency

spectra are primarily due to acoustic energy from the booster engine jet and aerodynamic turbulence during the period of maximum aerodynamic pressure.

Generally speaking, the acoustic environment is most severe at lift-off, with a lesser buildup occurring during maximum dynamic pressure. The main difference between these conditions is that the spectrum peak shifts upward in frequency about two octaves during the latter. The acoustic environment at maximum dynamic pressure is a direct function of the aerodynamic shape of the payload shroud and the induced turbulence.

To evaluate the acoustic environmental effects in the OGO spacecraft, the subject full-scale acoustic test program was performed. The specific purpose of this program was to determine experimentally the magnitude and spectra of high-frequency vibration response in the OGO spacecraft structure due to the associated acoustic environment. The verification of estimated shroud transmission loss characteristics was a secondary objective, related to the first because it governs the degree of acoustic energy impinging on the spacecraft.

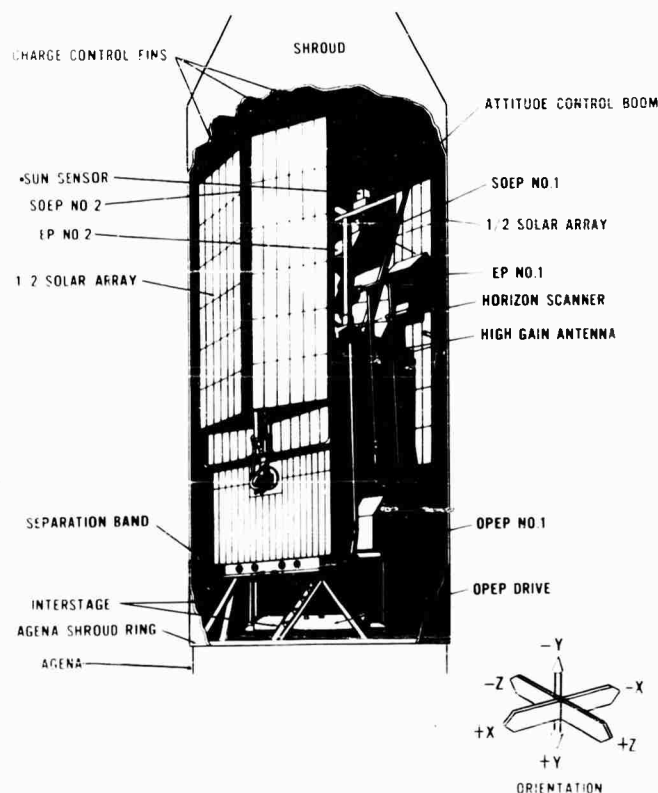


Fig. 3 - OGO in launch (folded) configuration

This paper presents a description of the test program and a summary of the more significant results obtained to date.

DESCRIPTION OF TEST

Test Facility

The OGO acoustic test was conducted at Langley Research Center (LRC) in the sound field generated by the 9- x 6-foot thermal structures wind tunnel (Fig. 4). In this blow-down facility, a large volume of air from high-pressure storage tanks is heated and then released through an aerodynamic test section and exhausted into the atmosphere at supersonic speeds. Since the tunnel utilizes blowdown techniques, the maximum run time is limited to about 40 seconds (providing about 38 seconds of constant noise level), depending on tunnel operating parameters. The force developed by the tunnel discharge is equivalent to a jet with more than 450,000 pounds of thrust and it generates acoustic power on the order of 3 million acoustic watts [1].

its utilization for acoustic testing of large flight payloads.

Specified test conditions are achieved (within limits) by adjusting the tunnel operating parameters and by choice of a suitable location within the sound field. For example, to roll off the high-frequency end of the spectrum, one would choose a location farther from the exhaust exit where this energy originates. The overall level and some spectrum shaping can be accomplished by adjusting the mass flow and heat content of the tunnel exhaust.

Since the facility was utilized for several previous acoustic tests including that on the Mercury capsule [2], sound field data were available pertinent to varied operating parameters.

The tunnel operating parameters and exact sound field location to satisfy the OGO acoustic spectrum requirements could not be specifically met from any of the past data. Past measurements did indicate a general area and the tunnel operating parameters for the test; however, a

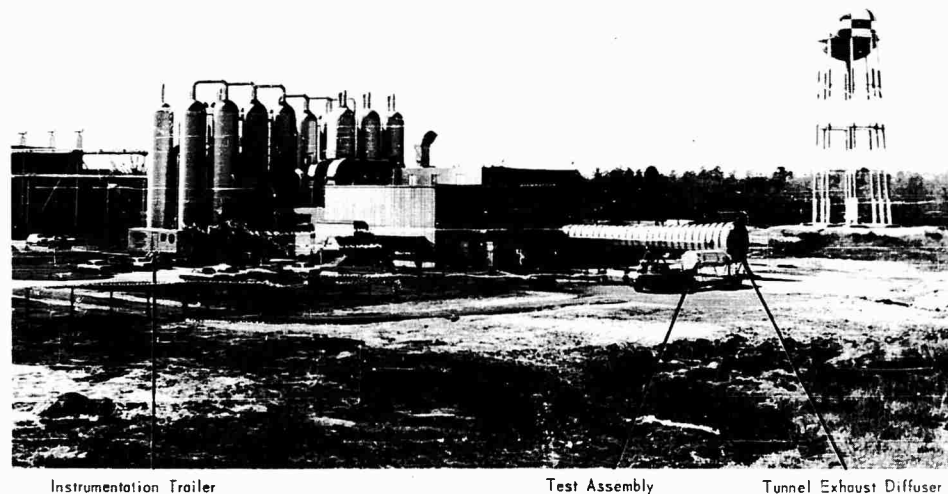


Fig. 4 - Test setup at 9- x 6-foot tunnel

The large amount of acoustic power available makes the sound field generated by the tunnel a very suitable test area for large specimens. Since an actual launch acoustic environment is essentially "free field," the same characteristics of tunnel sound field further enhance

sound survey was necessary to determine an exact location within this area.

After the location was selected, a directional survey was performed to determine the azimuth to the "apparent source" of the energy in the 1000-cps region. The test article was oriented to provide "grazing incidence" of the 1000-cps energy with the Agena skin. Since 1000 cps is the coincidence frequency of the

NOTE: References appear on page 140.

skin, this orientation allows maximum transmission of energy through the skins.

Test Article

The test specimen was an assemblage of the OGO spacecraft structural model, an OGO/Agena forward equipment rack, and the OGO shroud. The assembly is shown in Fig. 5, with half of the shroud in position. As indicated, the OGO structural model was in the launch configuration and presented about the same dynamic characteristics as the flight unit. The OGO/Agena forward equipment rack is the upper portion of the Agena vehicle located adjacent to the spacecraft. This compartment contains a truss network on which the guidance and control systems of the Agena normally are mounted. For this test, dummy masses were utilized to simulate the components normally mounted in this compartment, thereby providing a dynamically similar structure. The forward equipment rack was included in the test assembly to evaluate the magnitude of vibration energy originating in this area and transmitted to the

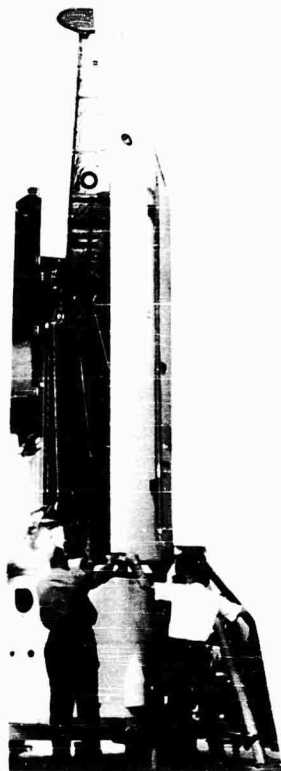


Fig. 5 - Test specimen with one-half shroud installed

spacecraft structure. The aft end of the forward equipment rack was terminated by a sand-filled baffle to simulate the acoustic transmission loss characteristics of the omitted booster structure.

The assembled test specimen was mounted on a flatbed cargo trailer (Fig. 6) where it was supported at four locations. Each support point utilized a vibration isolator to provide an overall suspension system with a natural frequency of less than 15 cps. The purpose of the isolation system was to reject all but airborne energy inputs to the test article. Trailer mounting provided mobility for the specimen and allowed inside storage during periods of nontesting and inclement weather.

Instrumentation

The vibrational responses of pertinent locations on the spacecraft and adjacent structure were sensed by accelerometers oriented in each of the orthogonal axes of the spacecraft. In addition to these, 14 locations were monitored on the interstage fittings and Agena forward equipment rack. A total of 189 measurements were recorded during the test. Of these, 43 were acoustic measurements and 146 were vibration measurements.

Microphones were used to record the acoustic environment within the spacecraft box, between the spacecraft and the shroud, and exterior to the shroud. Acoustic measurements were also taken within the Agena forward equipment rack.

The data were recorded on two 14-channel tape recorders in conjunction with a five-channel constant band multiplex system which allowed a total of 32 recording channels. All instrumentation was located in a trailer located about 300 feet from the test area as shown in Fig. 4.

The requirement to obtain information from some 190 locations with 32 available magnetic tape recording channels necessitated division of the data into seven groups. The first was a group of six "reference" transducers which were recorded during each run. The remainder were divided into six groups which were recorded during one run only.

Test Requirements

The general test specifications listed in Table 1 were derived from predicted and launch data from booster vehicles similar to those

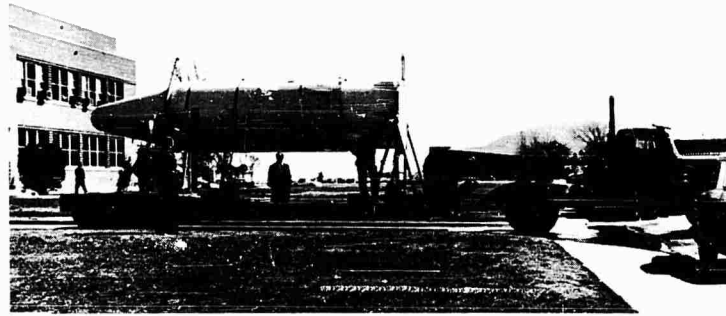


Fig. 6 - Trailer-mounted test assembly

planned for the OGO flight. The test levels are approximately 1.5 times the predicted flight levels to account for combined effects and statistical variations in the actual launch environment. The test specimen also incorporated an increase in the high-frequency end to encompass both the launch and maximum dynamic pressure conditions.

TABLE 1
OGO Acoustic Test Specification Levels^a

Octave Band Frequency (cps)	Level (ab)
20-75	138
75-150	139
150-300	142
300-600	143
600-1200	142
1200-2400	139
2400-4800	135
4800-10,000	129
Overall Level	149

^a Tolerances are ± 3 db on both overall and spectrum levels.

The high-level run provided an increase in the overall level of 3 db, the result of an increase in each of the octave band levels of about 3 db. The purpose of this run was to obtain data on the linearity of the structural response. The high-level run simulated the environment anticipated from a thrust-augmented type booster vehicle.

The initial directional survey led to an erroneous orientation of the test article depicted as Position 1 of Fig. 7. Four 30-second runs were performed in this orientation. On the fifth run, microphones on the +X (downstream) side revealed an asymmetric distribution of the acoustic loading of the shroud. An examination

of the microphone data revealed that the overall level at this location was about 5.5 db too low. A later spectrum analysis (Fig. 8) indicated that the loss was caused by a general decrease of the spectrum. The apparent cause of the discrepancy was shading of this side of the test article from all but the very-low-frequency energy developed several diameters downstream of the exhaust.

A resurvey of the sound field revealed the correct location and orientation to be Position 2 of Fig. 7. The test was performed at this location with symmetrical acoustic loading, as indicated by Fig. 9. The high-level test was conducted with the assembly in Position 3 of Fig. 7.

Test Procedure

During periods of nontesting, the trailer-mounted test assembly was housed in the shop area of the 9- x 6-foot tunnel. The test sequence was initiated with transportation of the trailer to the test site and positioning in the predetermined location and orientation. The transducers monitored during the particular test run were connected and a system calibration was performed. Upon verification of all instrumentation channels, the area was cleared of personnel and the tunnel activated. The period between runs, necessary for recharging the tunnel, was utilized for a quick look at the recorded data and preparation for subsequent test runs.

The initial plan specified six 30-second runs; however, the test time was reduced to six 15-second runs. The factors considered in the reduction of the test time included test time on the shroud during misoriented runs. Since the shroud was a backup flight unit, excessive exposure to the acoustic energy was undesirable. The program was consequently expedited without compromising the number of locations

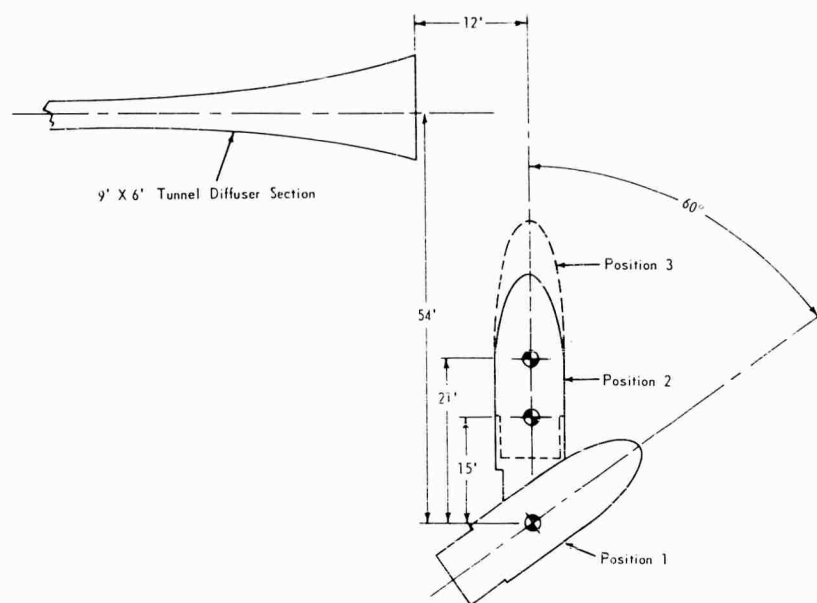


Fig. 7 - Test positions and locations

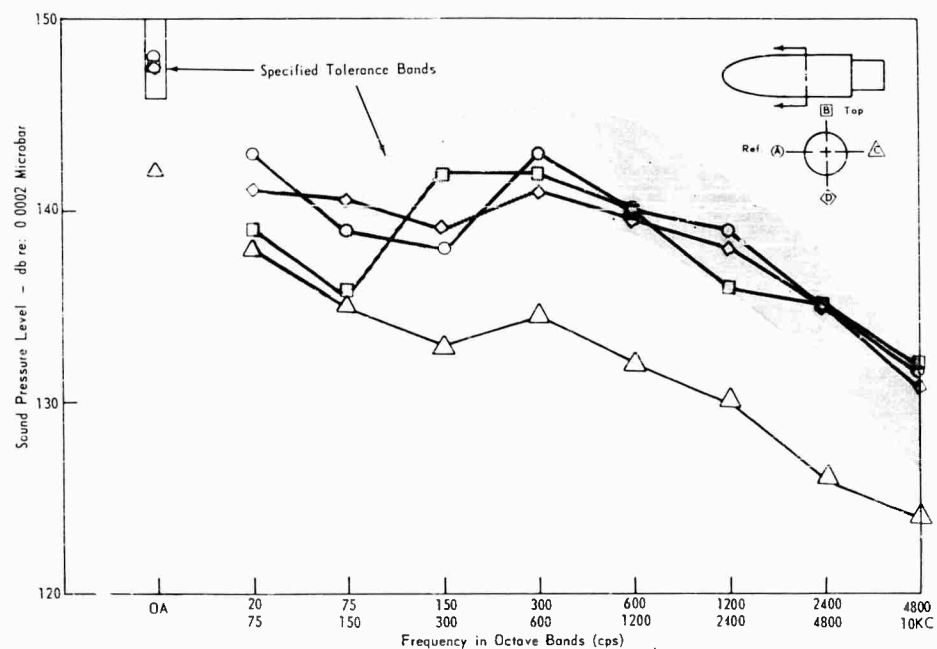


Fig. 8 - Spectrum analysis, misoriented at Position 1

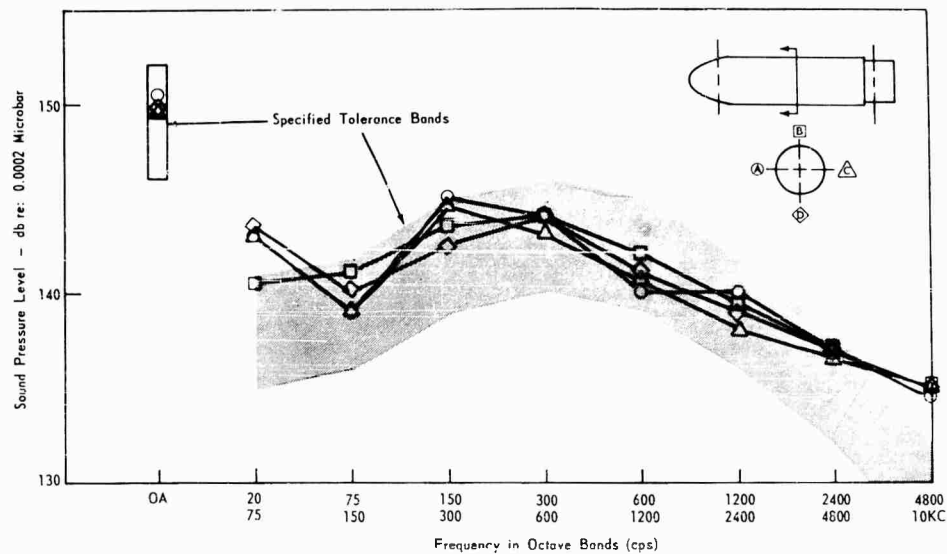


Fig. 9 - Spectrum analysis, correctly oriented at Position 2

monitored by allowing 3 runs per day. The 7th run, an increased-level run with an overall sound pressure level (SPL) of 153 db was a 30-second run, as originally planned, with the specimen located in Position 3 of Fig. 7. The spectrum levels of this run are presented in Fig. 10.

RESULTS

Acoustic Input

There was some concern prior to the test about the repeatability of the sound field generated by the wind tunnel. This was justifiable

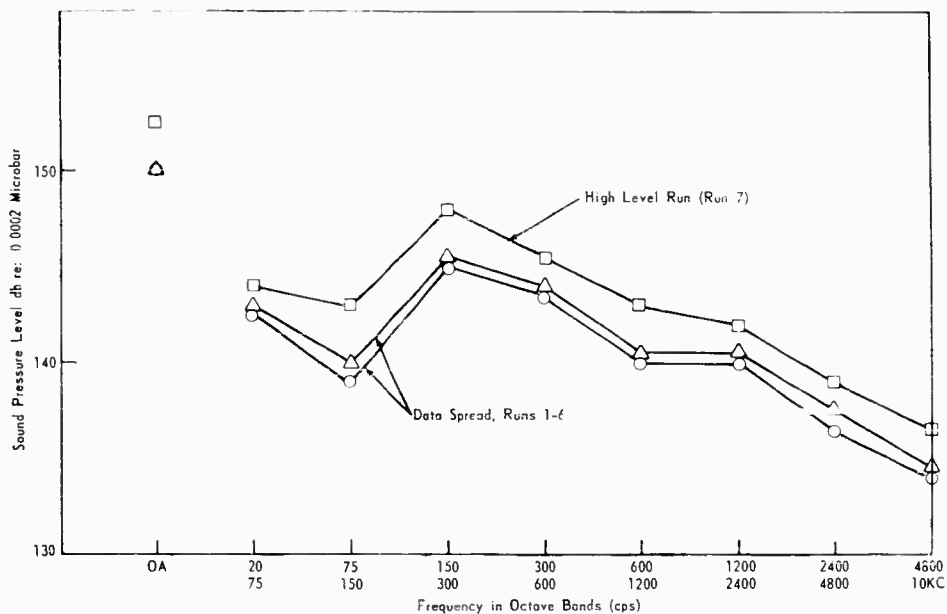


Fig. 10 - High-level run spectrum and data spread at external location 2A

since, because of the large number of data points involved, most data were acquired from one run only. Substantial variation in the excitational forces would have complicated any direct comparison of response data acquired from subsequent runs. The maximum and minimum octave band levels recorded at the reference location during the six low-level runs are presented in Fig. 10. As indicated, the repeatability of the sound field was excellent, with no more than 1-db variation in the data from these runs. The repeatability is further verified by the reference vibration transducers recorded during all runs. Table 2 shows that the overall rms vibration levels at the base of the inter-stage fitting on the Agena ring were virtually the same for each low-level run. It can also be seen from Fig. 9 that the test spectrum was well within the specified tolerance region.

The acoustic loading over the approximately 22-foot length of the test assembly varied somewhat as anticipated, but not severely enough from the specified values to cause concern. The microphone positions are shown in Fig. 11. The specified levels were established in the plane of location II, which is the approximate center of experiment grouping about the spacecraft box. At this location, as shown in Fig. 9, the loading around the shroud was uniform within ± 1 db, with one exception — the upper microphone indicated about 3 db lower than the others at this station, probably the result of a changed ground reflection path.

The distribution of acoustic energy at the forward and aft ends of the shroud are presented in Figs. 12 and 13, respectively. As indicated, the general spectrum shape remained the same fore and aft with the high-frequency

TABLE 2
Vibration: Reference Location rms G^a
(Agena Ring at +27.5Z, -10.125X Sta. 251.5)

Run No.	Rv(Y) (rms)	Rv ₂ (X) (rms)	Rv ₃ (Z) (rms)
1B	3.0	3.6	5.0
2B	3.0	3.5	5.0
3B	3.0	3.5	5.0
4B	3.2	3.8	5.0
5B	3.0	3.5	5.0
6B	3.2	3.8	5.0
7 (high level)	4.0	6.5	4.8

^aRuns 1A through 5A were performed in mis-oriented condition; therefore, B series listed herein.

end raised somewhat at points closer to the tunnel centerline, as might be expected. Even so, the data exhibit uniformity within ± 2 db.

The high level run spectrum is shown in Fig. 10. The overall level was 153 db, about 3 db higher than the low level runs. The increase was attained by a general increase in the overall spectrum of about 3 db per octave, rather than reinforcement in certain frequency bands only.

Shroud sound transmission loss information was obtained from locations I and II and is plotted in Fig. 14 along with estimated values [3]. In general, the values shown are in reasonable agreement.

Vibration Response

To date, only a limited amount of vibration response data has been analyzed. Plots of

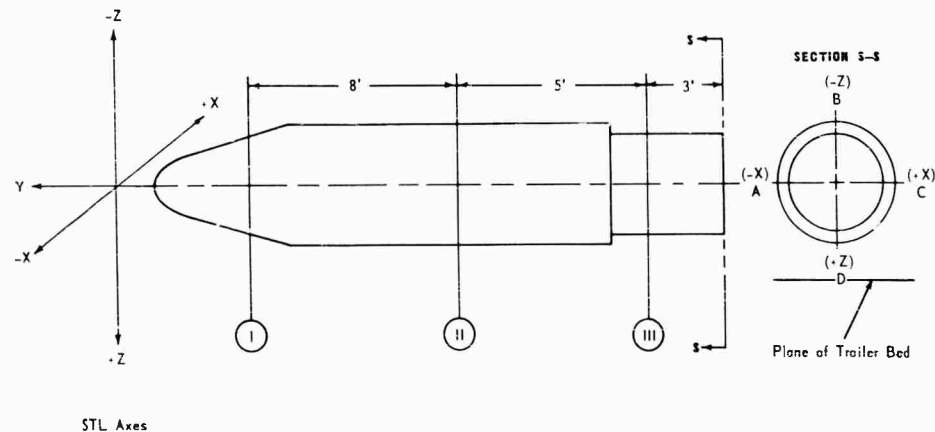


Fig. 11 - Microphone locations

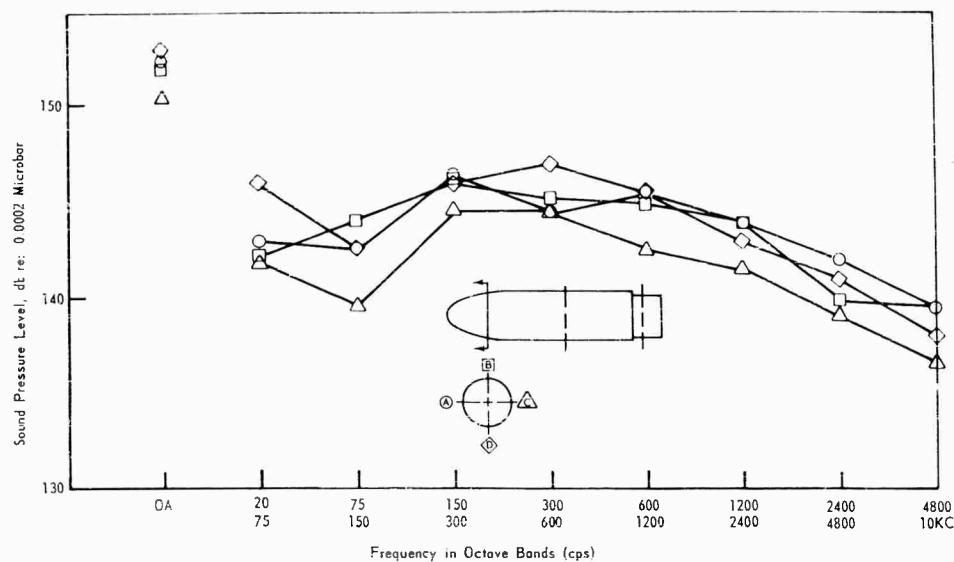


Fig. 12 - Acoustic distribution around shroud (fore)

acceleration spectral density, including overall levels, are presented in Figs. 15 through 18. The analysis was performed on a TPC Model 627 analyzer with the following effective squared filter bandwidths (BW): 20-300 cps with 3-cps BW, 300-1000 cps with 7-cps BW, and 1000-5000 cps with 25-cps BW. These points were selected for the initial analysis since it is felt that they are typical of the vibration response of the base of the interstage, the base of the spacecraft box, the door-mounted experiments

and the boom-mounted experiments. From these plots it can be seen that, although the acoustic input spectrum is continuous up to at least 10,000 cps, the vibration response cuts off sharply at 2500 cps or less. This high-frequency cutoff, plus the fact that the overall levels do not exceed those of the qualification tests, lends some assurance that the environmental vibration qualifications tests, conducted on the spacecraft and experiments, were adequate.

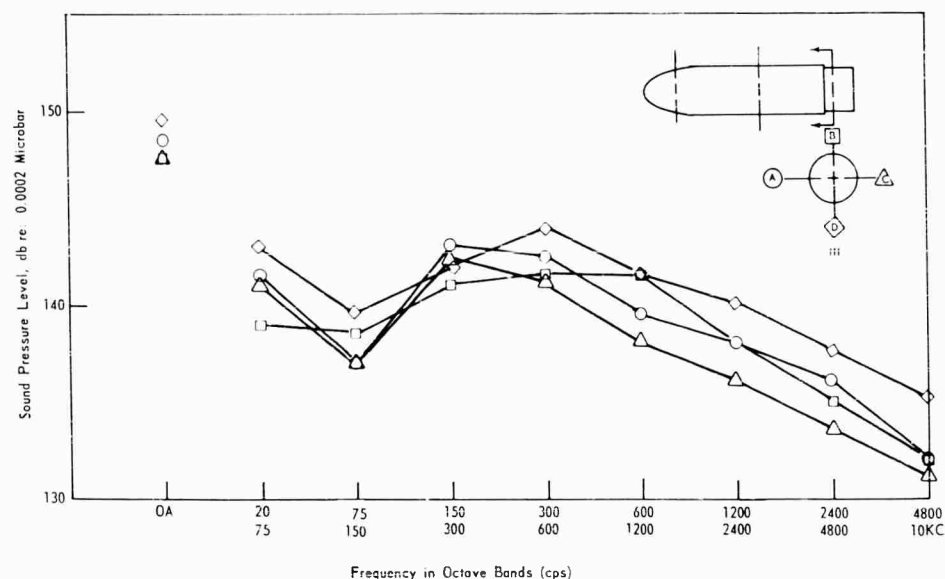


Fig. 13 - Acoustic distribution around shroud (aft)

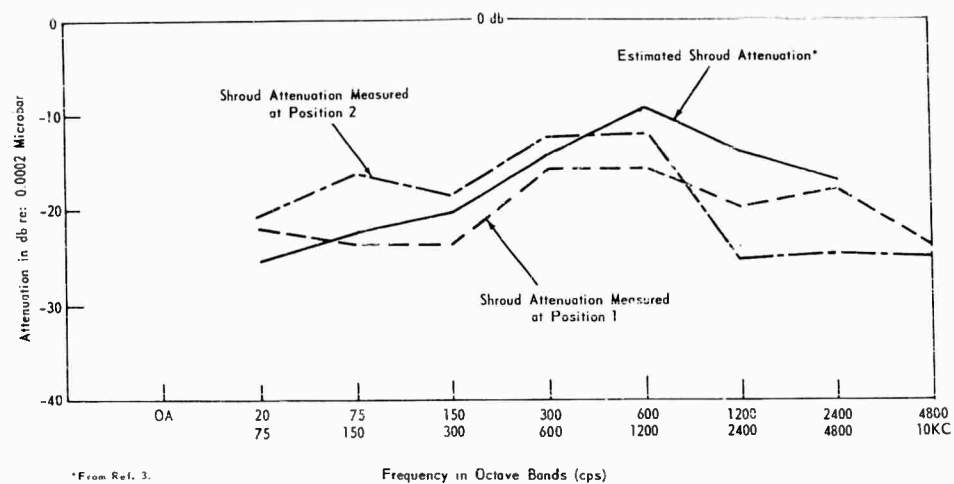


Fig. 14 - Shroud transmission loss characteristics

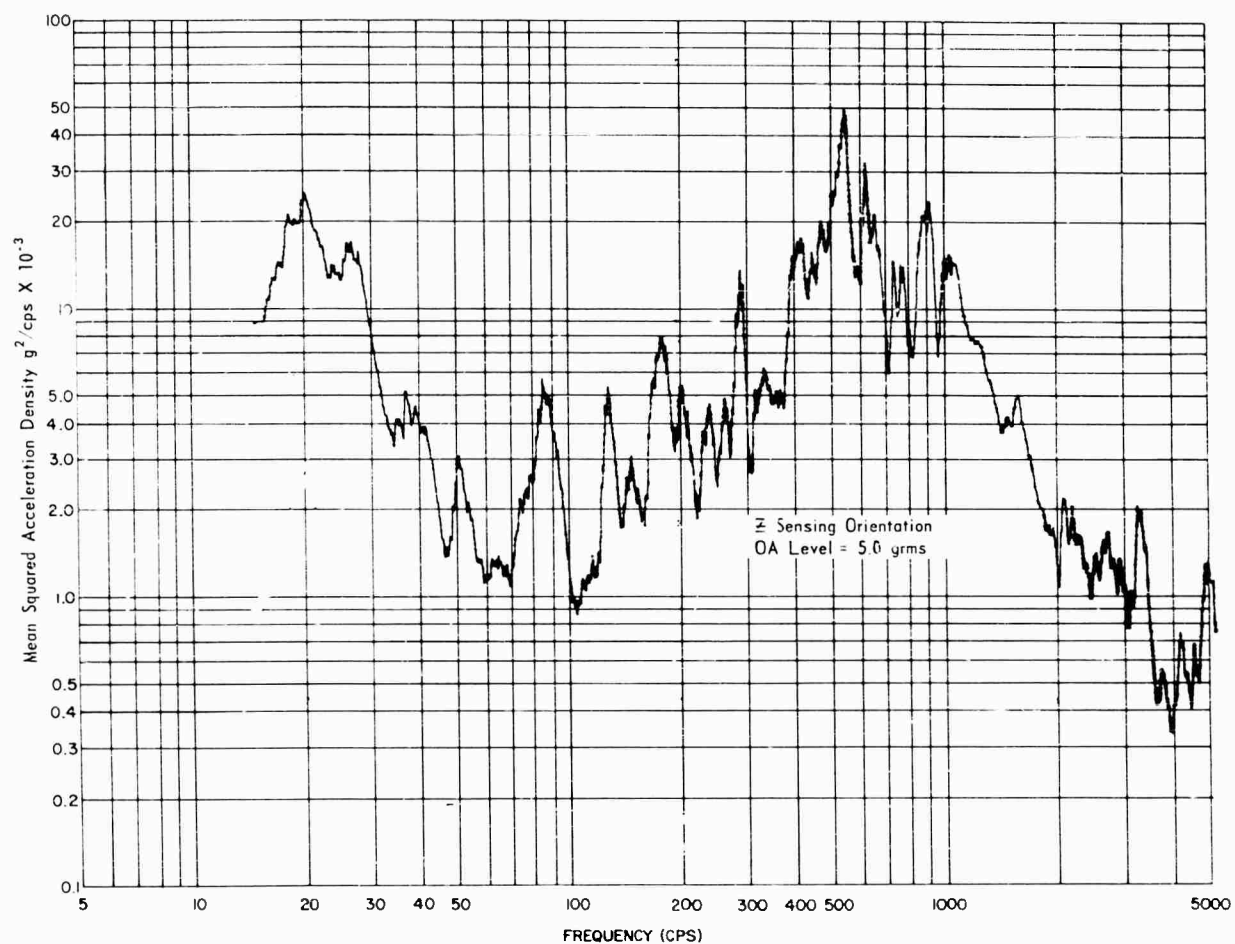


Fig. 15 - Power spectral density plot, base of interstage fitting

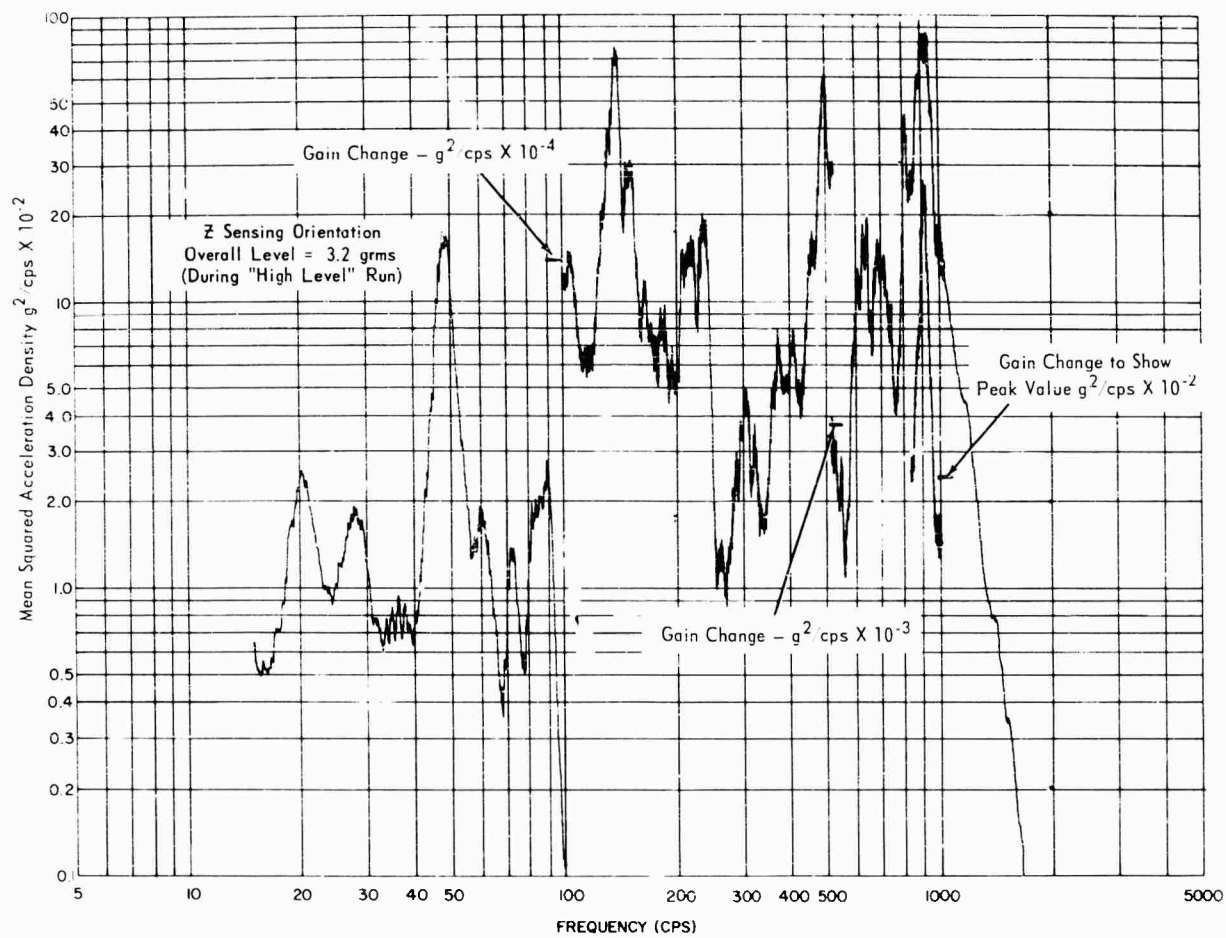


Fig. 16 - Power spectral density plot, +Z experiment door panel

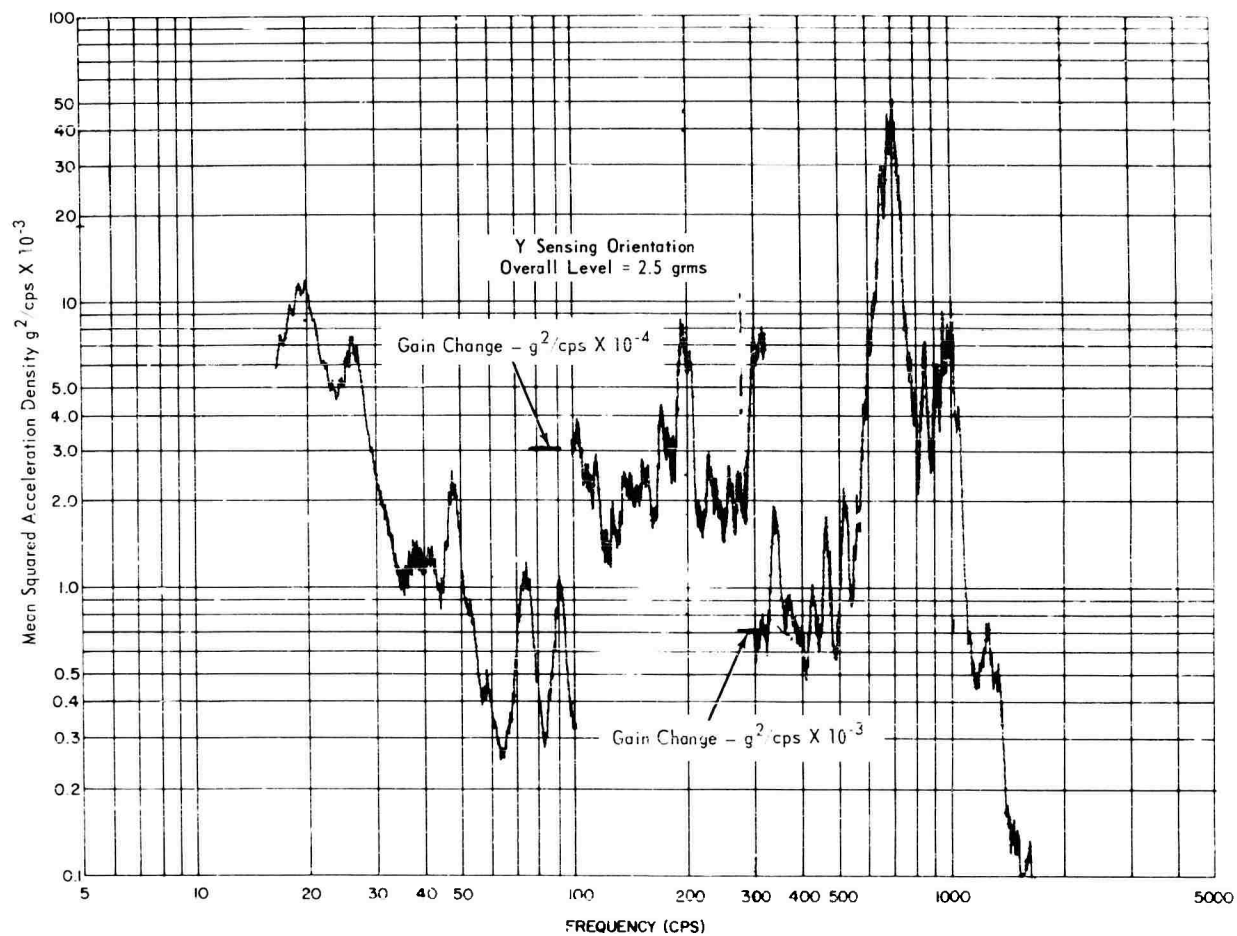


Fig. 17 - Power spectral density plot, top of spacecraft box

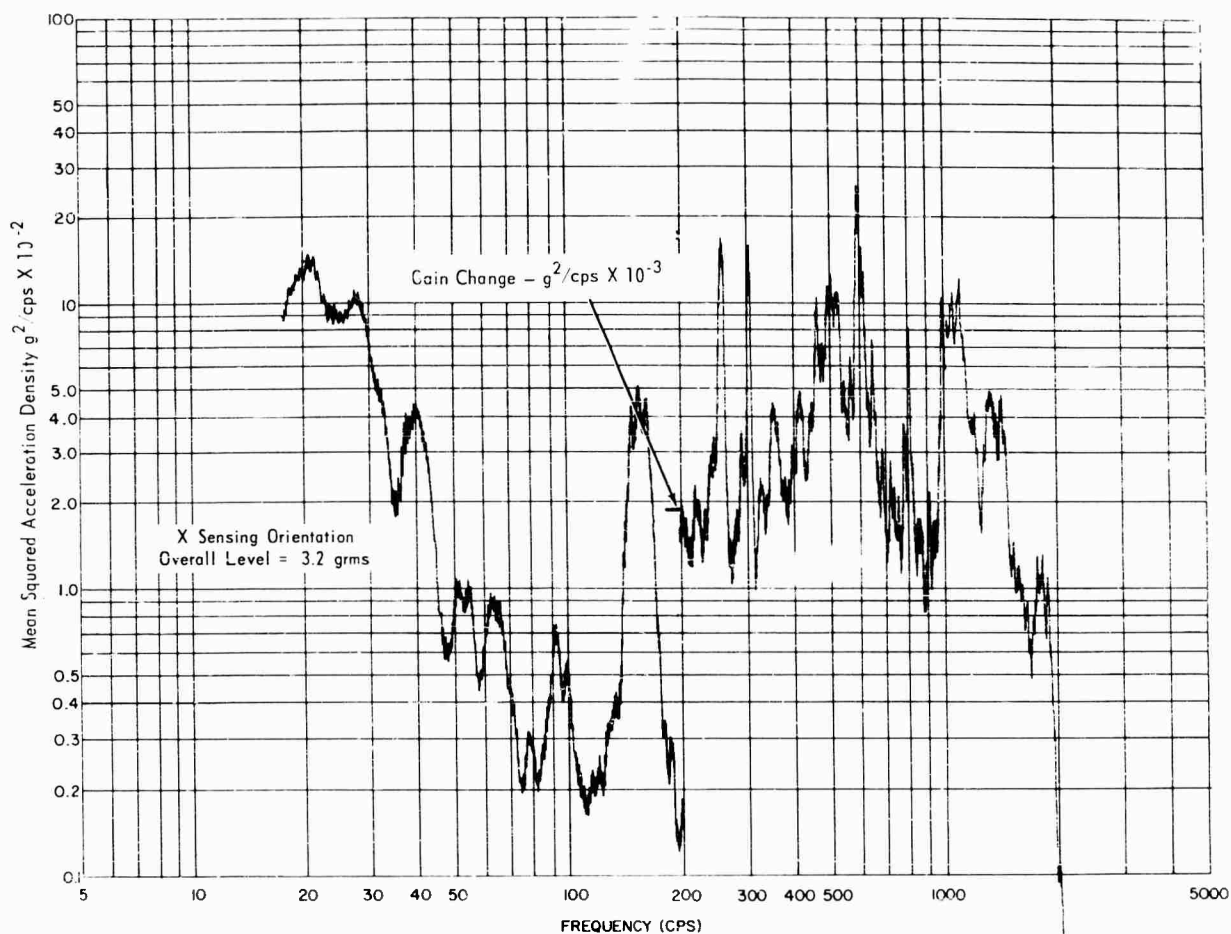


Fig. 18 - Power spectral density plot, base of experiment package

Probability density curves of representative acoustic and vibration data are presented in Figs. 19 through 22. These data were obtained using a Brüel and Kjaer Model 160 Probability Density Analyzer. These curves are very close to a normal distribution and further confirm the qualification test using Gaussian random inputs.

Further Analyses

The plan for the completion of the analysis of the test data includes two separate approaches. The first is to complete the acceleration spectral density analyses of all vibration data. This will provide a large sample of response information covering a wide range of dynamically different structural locations and will enable evaluation of the different empirical and theoretical methods proposed for predicting the response to acoustic inputs.

Secondly, the use of cross-correlation techniques is planned to provide a better understanding of the acoustically induced vibration. The basic question we hope to answer is: "What portion of the vibratory response at a point in a spacecraft structure is due to direct acoustic excitation and what portion is transmitted from the launch vehicle attachment points up through the structure?" The answer to this question will provide information on the relative merits of acoustic vs vibration tests of subassemblies and on the adequacy of random tests of a complete spacecraft.

ACKNOWLEDGMENTS

The author acknowledges the support and cooperation afforded by LRC and, in particular, the Aero-Thermal Facility Branch, without which the program would not have been possible.

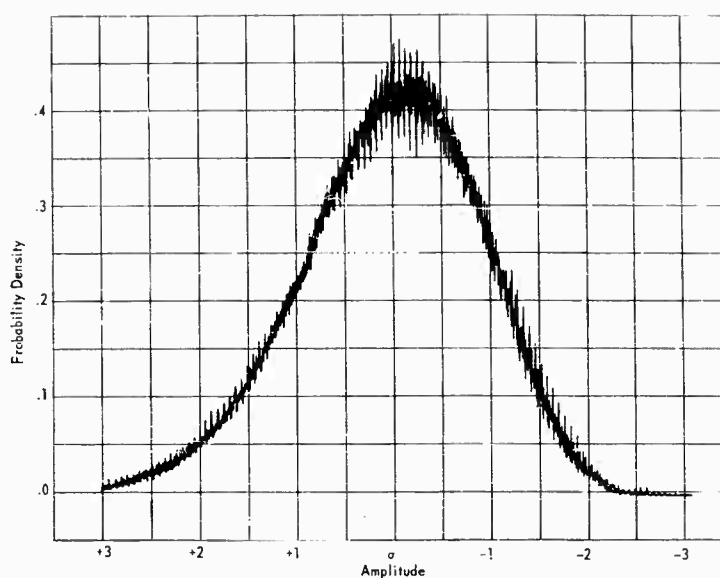


Fig. 19 - Probability density analysis,
acoustic noise exterior to shroud

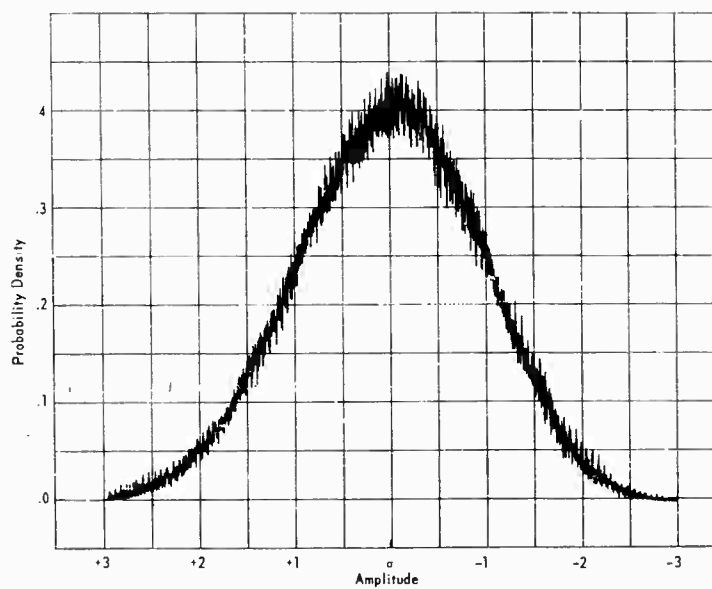


Fig. 20 - Probability density analysis,
acoustic noise within shroud

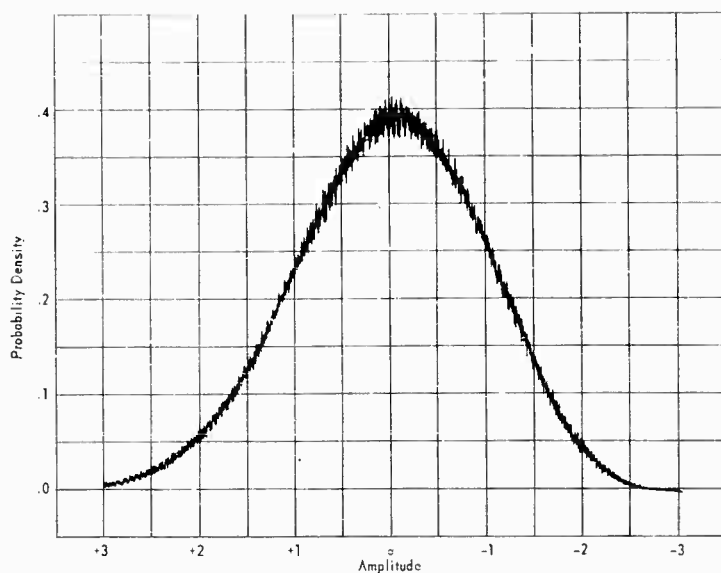
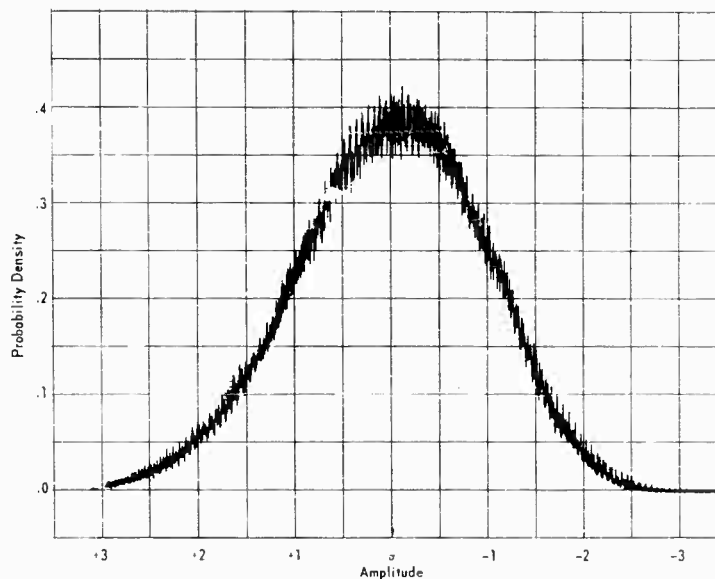


Fig. 21 - Probability density analysis, vibration response at base of interstage

Fig. 22 - Probability density analysis, vibration response at top of spacecraft



REFERENCES

1. W. H. Mayes, P. M. Edge, Jr., and J. S. O'Brien, Jr., "Near-Field and Far-Field Noise Measurements for a Blowdown Wind Tunnel Supersonic Exhaust Jet Having About 475,000 Pounds of Thrust," NASA TN D-517 (1961).
2. S. A. Clevenson, D. A. Hilton, W. T. Lauten, Jr., "Vibration and Noise Environmental Studies for Project Mercury," Proc. Inst. Environ. Sci., p. 541 (1961).
3. G. D. Hinshelwood, "Estimated Shock, Acceleration, and Vibration Environments for Atlas-Agena B and Thor-Agena B Spacecraft," GSFC Report, Agena-Sav-1 (rev. Aug. 1, 1961) (Confidential).

* * *

A LOW-LEVEL VIBRATION TEST SYSTEM*

R. C. Klinger and M. A. Kollodge
Honeywell, Inc.
Minneapolis, Minnesota

A vibration test system used to produce a calibrated low-level vibration environment is described. Salient features of the system are double amplitude of vibration as low as 10 microinches; frequency range of 5 to 300 cps (below 5 cps if sufficient driving power is provided); readout accuracy to better than 1 microinch; isolation from ambient vibration level; high signal-to-noise ratio for table excitation; capability for vibrating test items weighing up to 8 ounces; and selectable vibration waveform.

INTRODUCTION

There are many commercial vibration systems available for test engineering, but a vibration system capable of producing controlled low-level vibrations in the microinch region is unique. In addition, the method used for measuring these low-level vibrations must be tailored to the application. A low-level vibration test system and its associated measuring method are considered here as two separate but related topics. This system is a proven evaluation tool, and it can be fabricated at low cost and tailored to specific applications.

VIBRATION SYSTEM

The low-level vibration test system described meets the following specifications:

1. Double amplitude of vibration as low as 10 microinches and at least as high as 200 microinches;
2. Frequency range of 5 to 300 cps;
3. Ambient vibration levels transmitted to system limited to 10 microinches in a typical environment;
4. Capable of vibrating test items weighing up to 8 ounces; and
5. Selectable vibration waveform.

Figure 1 is a schematic diagram of the vibration test system, and Fig. 2 is an illustration of a typical physical configuration of such a system. The speaker illustrated is a University Model C-15HC 15-inch high-compliance woofer with a free air resonance of 15 cps and a high-frequency response cutoff of 800 cps. A 1/8-inch aluminum plate serves as a mount for the test item, and is attached to the speaker cone by a piece of styrofoam. Styrofoam is light, yet rigid; thus the entire system has a transmissibility of nearly 1 to 1 over the desired frequency range.

Assembly of the aluminum vibration mounting plate to the speaker cone (Fig. 3) was accomplished as follows: styrofoam was poured into a form inserted in the speaker and was allowed to adhere to the speaker cone. After the styrofoam hardened, the form was removed, and epoxy (Epon 934, Shell Chemical Co.) was used to cement the aluminum plate to the styrofoam. This cement was used because it will not chemically attack styrofoam.

The entire system is isolated with nylon cords, selected because of their elasticity without undue springiness. Other isolation means, such as foam rubber cushions, were investigated but proved inadequate. As an example, under typical test conditions, foam rubber will reduce the ambient level transmitted to the system to 70 to 80 microinches as compared to 5 to 10 microinches for the nylon cords.

*This paper was not presented at the Symposium.

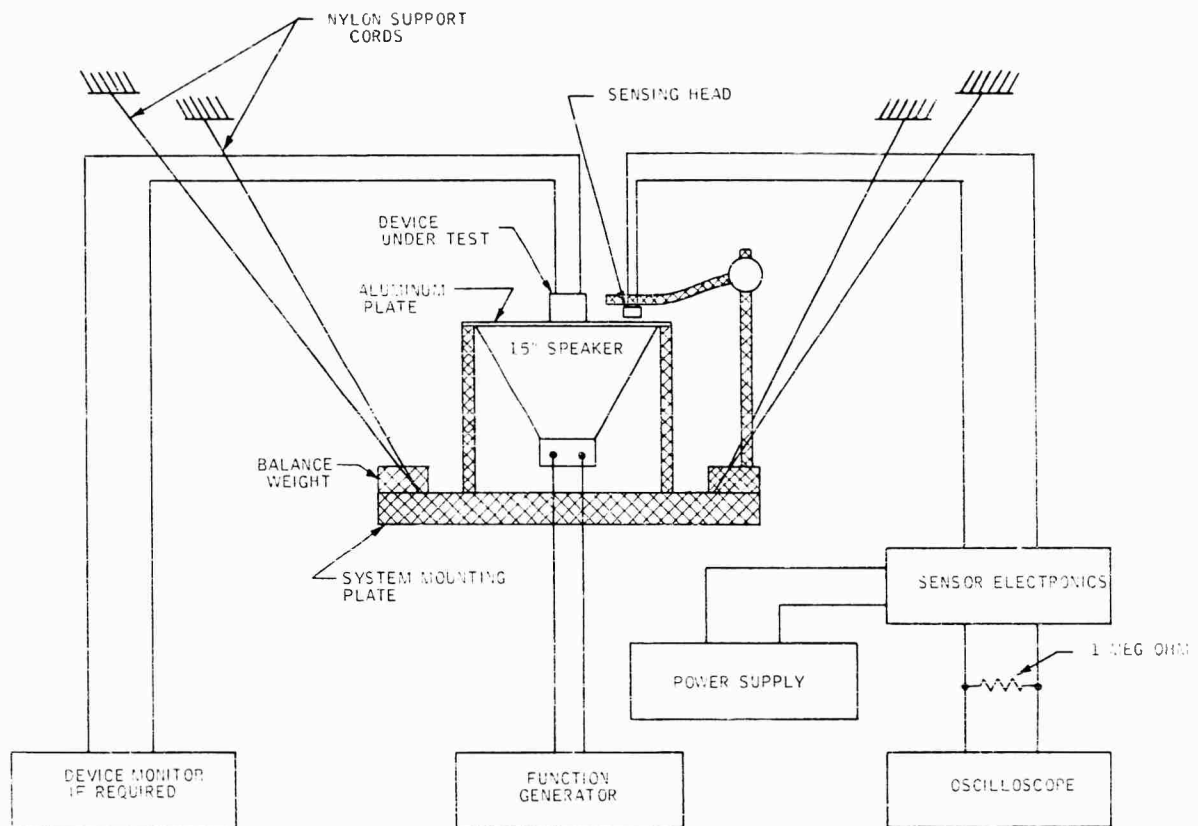


Fig. 1 - Schematic diagram of low-level vibration system with associated instrumentation

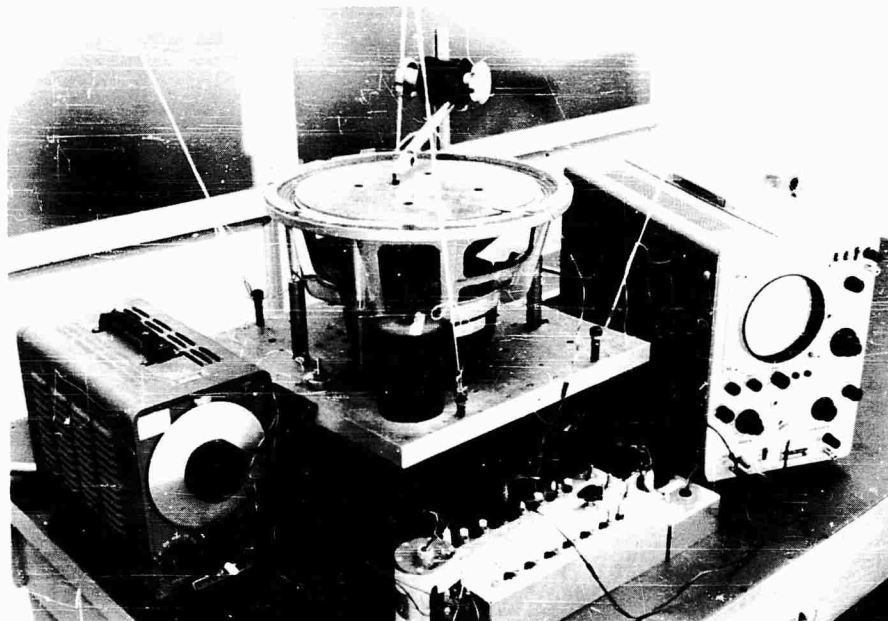


Fig. 2 - Typical configuration of low-level test system

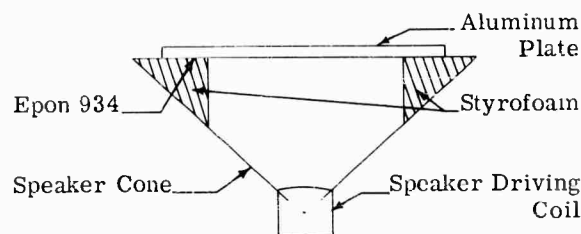


Fig. 3 - Method used to mount aluminum vibration plate to speaker cone

The driving signal to the speaker can be provided by a function generator connected directly to the speaker; however, the particular generator used for the configuration shown is a Hewlett Package Audio Oscillator, Model 400-CD. Such an arrangement provides sufficient power for driving the vibration system over the frequency range of 5 to 300 cps. Frequencies above 300 cps were not a requirement for Honeywell's application, but low-level vibrations at these higher frequencies could be realized with this system by the addition of an amplifier for the driving signal, and by locating the plate closer to the voice coil of the speaker cone so that a smaller plate could be used to reduce the weight to be vibrated.

Use of a speaker as a vibration transducer has two distinct advantages:

1. The transducer is small and light enough so that it can be suspended by elastic cords which provide isolation from ambient vibrations.
2. Because of its light voice coil mass, a speaker does not require a large driving signal at the higher frequencies.

The first advantage is self-evident, but further explanation is presented for the second. Use of a low-mass vibration system permits the use of low-power amplifiers with their inherently better signal-to-noise ratio. In the system described, amplifiers were actually omitted; consequently, noise in the system was mainly limited to that associated with the signal generator. As a result, even at low frequencies where the required driving signal is small, the signal-to-noise ratio remains high.

MEASURING SYSTEM

Specifications for the measuring system used with the vibration system described are as follows:

1. Readout accuracy to better than 1 microinch;
2. No moving mass within the measuring device required for operation; and
3. Readout unaffected by ambient vibrations.

The apparatus used for measuring low-level vibrations consists of a distance detector system (Model D-152, Bently-Nevada Corp.), and a conventional power supply and oscilloscope. The sensing head of the detection system is a precision electromechanical transducer which has the capability of electronically sensing the distance to a conductive surface, which in this application is the aluminum plate used for mounting the test item. Within the sensing head is a pick-off element that consists of a pancake-wound coil which may be electrically loaded by the presence of an externally shorted secondary element (the aluminum plate). The coil loading is proportional to the distance from the coil to the aluminum plate; thus, when the aluminum plate is vibrated, the output voltage of the distance detecting system is proportional to the amplitude of vibration, and the frequency of the output voltage is the same as the frequency of vibration. The signal from the sensing head is detected and amplified, and displayed on an oscilloscope.

Figure 4 is a calibration curve for the distance detection system described. Data for this curve was obtained by making static measurements of the vertical displacement of the aluminum plate for corresponding voltage values of the output of the distance detection system. An output of three volts was selected as a starting point for calibration measurements in order to use the straight line portion of the curve for the distance detection system. The operating point for zero displacement of the aluminum plate during vibration was then chosen at a convenient point (6 volts output) on the straight line portion of the curve. A crystal-pressure device with a meter readout indicator (an Indi-Ac-Jr, Cleveland Instrument Co.), was used to make calibration displacement measurements. This device was in turn calibrated from gage blocks.

As illustrated in Figs. 1 and 2, the sensing head and the vibration system are secured to the same system mounting plate so that ambient vibrations will not affect the measuring system. With the sensing head isolated in this manner, and with the calibration curve of Fig. 4, readout is possible to less than 1 microinch.

No moving mass is required within the selected measuring system, and this feature

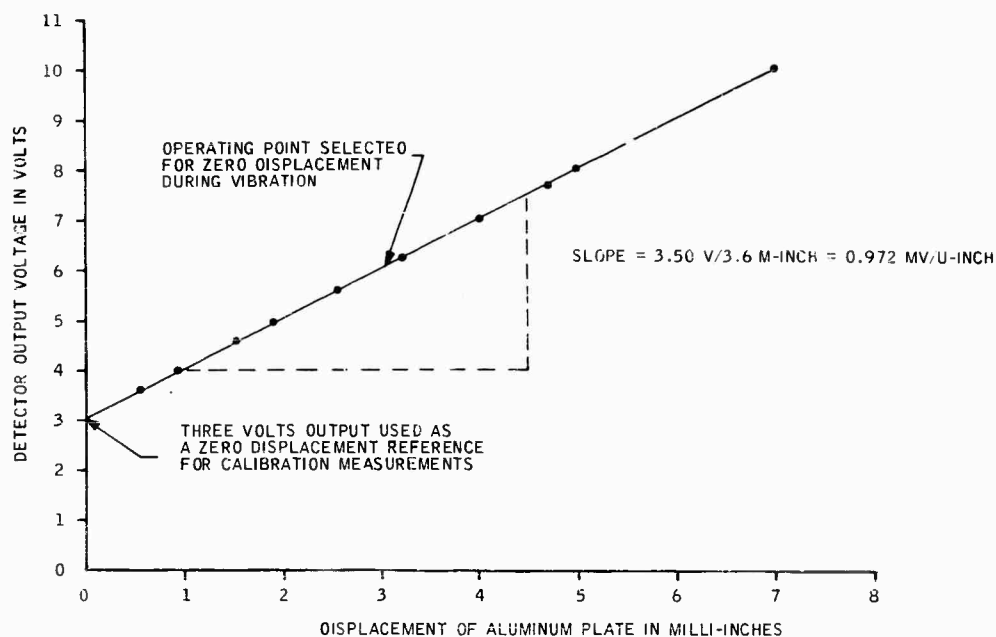


Fig. 4 - Calibration curve for Bently-Nevada distance detector

provides a distinct advantage not offered by conventional measuring devices such as accelerometers. As an example, accelerometers are dependent on a moving mass, and their measuring capabilities are limited to 30 micro-inches of displacement at 10 cps. However, at the higher vibration frequencies, the displacement measuring system described becomes

limited in frequency response because the operating carrier frequency of the sensing device is of such a value that distortion-free modulation of that frequency by the table displacement motion can only be obtained to approximately 300 cps. A piezoelectric accelerometer should be used for displacement measurements at these higher vibration frequencies.

* * *

SYSTEM RESONANCE, A FUNCTION OF VIBRATION TEST PARAMETERS*

A. M. Samborsky and C. J. Van Vliet
U.S. Navy Electronics Laboratory
San Diego, California

Vibration tests have often appeared to reveal complex mechanical design problems and inferior equipments which, in fact, did not exist. These tests were conducted in accordance with Military Standard 167, "Mechanical Vibration of Shipboard Equipment," which requires great care in the proper simulation of vibration frequency and amplitude. However, the vibration tests typically neglect consideration of the fundamental parameters of system damping, mass, and spring constant which appear in the laboratory because of the testing equipment. These fundamental parameters may not be worthy of noting when the test article mass is very small compared to the mass of the vibration test machine; in this case, monitoring of amplitude and frequency is valid and a shipboard condition is simulated with reasonable accuracy. But failure to consider testing system parameters may easily cause vibration test results to be misinterpreted; what appear to be faults in the equipment often are really reflections of conditions related to the testing equipment.

The MIL-STD-167 test is desirable to locate and analyze isolated minor resonances which may result in premature fatigue failures, but if system resonance occurs in the test range of frequencies, more information is needed about the system parameters of mass, damping, and spring constant. A useful test program can provide this information, along with specific recommendations for adaptation of the tested equipment to some unusual shipboard environmental condition. Such a test program is possible only if the test is fully instrumented and the results are completely assayed. It follows, then, that the test must not only be planned to give a time schedule of tests but also designed to direct the tester to make changes in test conditions to take into account the fundamental parameters.

The necessity for such a "designed" test is illustrated by examining what often appears to be a lack of damping. Since the test machine adds little damping but a great deal of mass, the effect on marginal equipment undergoing testing is not only to depress the resonant frequency into the test range but also to cause a phase change to rapidly reach 180 degrees at the resonant frequency. The damping will then appear to have a lower value. If we gage stress level by displacement and use transmissibility as a basic parameter, then the following formula may describe the stress undergone by the test article:

$$\left| \frac{S'}{S} \right| = \left| \frac{A_o + A_i}{A_o - A_i} \right| \quad (1)$$

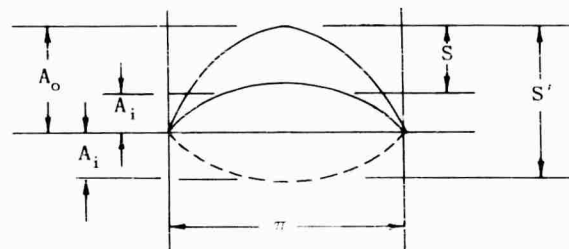
where

S = stress in phase,

S' = stress, 180 degrees out of phase,

A_i = input amplitude, and

A_o = output amplitude.



Under traditional testing, this condition is translated as an equipment damping problem, when it may well be a test system damping problem.

*This paper was not presented at the Symposium.

Recently, at the Navy Electronics Laboratory (NEL), a vibration test was conducted for a large rectangular structure, a planar array radar antenna. Previous tests indicated that resonance had been encountered between 5 and 33 cps. Efforts to raise the resonant frequency by redesign of the structure for increased rigidity seemed to have little effect. The suspicion then arose that system parameters were so oriented as to cause resonance of undetermined severity in the test range of frequencies. It was reasoned that if system parameters caused resonance in the test range of frequencies, then any design modifications made to the equipment would be a function of the particular test system parameters and would be transferable to actual environmental conditions only to the extent that the system parameters of mass, spring constant, frequency, amplitude, and damping simulated the actual environment.

A simple test, based on sound mechanical mathematical concepts, was designed to verify, or refute, the existence of system resonance as being different from article resonance and bring attention to the possibility that such system parameters as mass, spring constant, and damping might be as significant as amplitude and frequency.

The test consisted of loading an additional 7200 pounds of steel plate on an L.A.B.

RVH-96-10,000 vibration machine. It was theorized that this weight change would change the resonant frequency observed if system resonance had occurred. The resonant frequency would not change if only minor article resonance took place. Therefore,

$$\frac{f_{N_1}}{f_{N_2}} = \left(\frac{W_2}{W_1} \right)^{1/2} \quad (2)$$

where f_{N_1} is the system natural frequency for W_1 equal to 27,381 pounds and f_{N_2} is the system natural frequency for W_2 equal to 34,581 pounds [1]. (W_2 equals 27,381 pounds plus the additional 7200 pounds.) f_{N_1} may now be calculated from Eq. (2): $f_{N_1} = f_{N_2} (34,581 \text{ lbs.} / 27,381 \text{ lbs.})^{1/2} = 1.124 f_{N_2}$.

Equation (2) was found to be in good agreement with the test results. Statistical analysis of the test data revealed f_{N_1} and f_{N_2} to be 27.94 and 24.76 cps, respectively, or $f_{N_1} = 1.128 f_{N_2}$, thus proving the existence of two distinct resonant frequencies and verifying system resonance as a basic parameter. This is shown in Fig. 1. For analytical purposes a parabola was used to approximate the two frequencies.

NOTE: References appear on page 148.

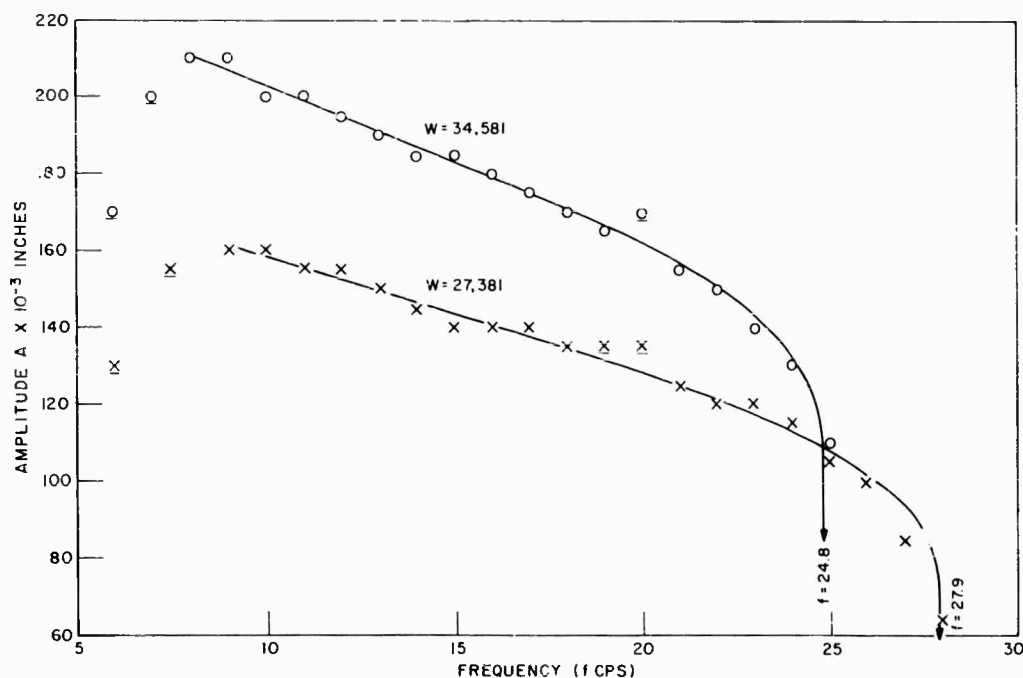


Fig. 1 - Effects of mass as a basic parameter of system resonance

Further study and conservative judgment results in the minimum value for the true natural frequency of the test article, as follows:

where

k_s = combined test article and machine spring constant;

k_m = equivalent machine spring constant; and

k_a = equivalent article spring constant, assuming the minimum value for k_m is k_a ;

according to Timoshenko and Young [2],

$$k_s = \frac{k_a k_m}{k_a + k_m} = \frac{1}{2} k_a \quad (\text{Series}) \quad (3)$$

or

$$k_s = k_a + k_m = 2k_a \quad (\text{Parallel}); \quad (4)$$

therefore, if as according to Thomson [3]

$$f_{N_s} = \frac{1}{2\pi} \sqrt{\frac{k_s}{m_s}}, \quad (5)$$

where

m_s = system mass, and

$$f_{N_a} = \frac{1}{2\pi} \sqrt{\frac{k_a}{m_a}},$$

then

$$\frac{f_{N_a}}{f_{N_s}} = \sqrt{\frac{1}{2} \cdot \frac{w_s}{w_a}} \quad (\text{Series}), \quad (6)$$

or

$$\frac{f_{N_a}}{f_{N_s}} = \sqrt{2 \cdot \frac{w_s}{w_a}} \quad (\text{Parallel}). \quad (7)$$

Consequently, it is apparent that if mass is lowered at a greater rate than the spring constant, or if the spring constant of the system is increased while mass is held constant, system resonance may be avoided or changed.

In the NEL test, system resonance occurred at 24.8 cps. In this case the natural frequency of the test article for a weight of 4400 pounds and system weight of 27,381 pounds is

$$f_{N_a} = 0.707 \left(\frac{w_s}{w_a} \right)^{1/2} \quad f_{N_s} = 0.707 \left(\frac{27,381}{4400} \right)^{1/2} \\ \approx 24.8 \text{ cps} = 43.6 \text{ cps}.$$

This value is well above the test range of frequencies called out in MIL-STD-167, the maximum frequency called out being 33 cps.

Presently, vibration tests of large structures do not, and are not designed to, yield system parameters. Fatigue tests, complying with MIL-STD-167, are performed which are at times unrealistic and destructive.

The mechanical design of vibration tests is necessary since system resonance may occur in the test range of frequencies. If existing procedures are used, minor test article resonance may cause dramatic failure. This will occur since system resonance may result in amplification which appears exceptionally violent. In some cases, this can happen with system resonance barely discernible. The minor assembly then behaves as a dynamic vibration absorber [4] and acts to suppress system motion by absorption of energy. The high energy levels present may even excite assemblies which would normally be sufficiently damped, causing premature fatigue failure and resulting in an unrealistic, destructive test. Equipments which may actually meet the fatigue requirements of MIL-STD-167 are rejected for shipboard use or must be accepted through waiver. Other equipments, which survive system resonance, may be overdesigned. Higher costs, resulting from overdesign, can then restrict acquisition of modern equipment.

REFERENCES

1. F. F. Vane, "The DTMB Midget Vibration Generator and Applications," DTMB Report 936 (Aug. 1955).
2. S. Timoshenko and D. H. Young, "Vibration Problems in Engineering," 3rd Ed. (Jan. 1955).
3. W. T. Thomson, "Vibration," Mechanical Engineers' Handbook, 6th Ed., Ed. by Marks (October 1958), pp. 5-96.
4. J. Ormondroyd and J. P. Den Hartog, "The Theory of the Dynamic Vibration Absorber," Trans. ASME, 50:A9 (1928).

* * *

A TEMPERATURE CONTROLLER FOR COMBINED TEMPERATURE-VIBRATION TESTS*

R. E. Seely
U.S. Naval Research Laboratory†
Washington, D.C.

A compact temperature controller has been designed for use when vibration tests must be performed at extremes of temperature. The control box is inserted into the wall of any enclosure and maintains constant internal temperature over a range of -100 to 300°F. An electric heater is used for the high temperatures while liquid carbon dioxide is used for temperatures below ambient.

INTRODUCTION

It frequently becomes necessary, in most vibration laboratories, to perform tests at extremes of temperature. In those locations where liquid carbon dioxide (LCO_2) is available, the temperature controller described makes the test setup very simple. Control is reasonably accurate and dependable over a range of temperature from -100 to 300°F.

DESCRIPTION

The controller is an assembly of easily available components containing all of the elements necessary to provide either heating or cooling capacity to a temperature chamber and to maintain the temperature automatically to any preset point. In operation it is simply placed in the wall of any chamber, a LCO_2 hose is connected to it by a quick-connect coupling, 110 volt power is provided, and it is ready to function. If temperatures below ambient are desired, a switch indicates this choice and the temperature is adjusted and maintained by the appropriate thermoswitch. A similar procedure is followed for temperatures above ambient, except that a choice of heating rates is provided.

Figure 1 shows the controller installed in the wall of a temperature chamber. Figure 2

shows the front panel with the simple operating controls. Other details are shown on Figs. 3 and 4. Figure 5 is a schematic diagram and identifies many of the components which make up the assembly.

DESIGN FEATURES

The design is the result of experimentation over an extended period of time to find the most suitable combination of features. The most important of these are:

1. LCO_2 is injected into the chamber by a solenoid valve specifically intended for use in this type of service. Nevertheless, it was found that it would operate more reliably if it was modified by using a somewhat stiffer spring. An orifice of 0.032 inches is used.

2. The heating coil is made up of the element from a 660-watt, 220-volt heating unit. By using it with 110 volts, the surface temperature is much reduced and control is much smoother. The power, of course, is reduced to 165 watts but this is sufficient to maintain a constant temperature in all but extremely large chambers. For those cases where a rapid heat increase is desired, a tap is provided so that only half of the element is used. In this position it will dissipate 330 watts.

*This paper was not presented at the Symposium.

†This work was performed while the author was employed at the U.S. Naval Ordnance Laboratory, White Oak, Maryland.

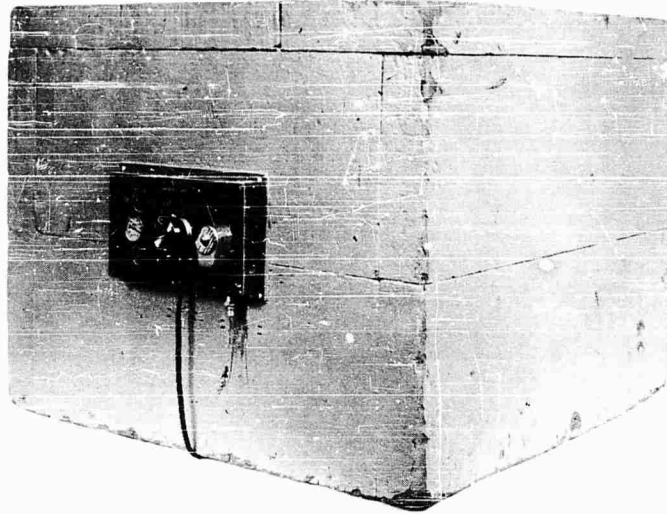


Fig. 1 - Temperature controller mounted
in wall of temperature chamber

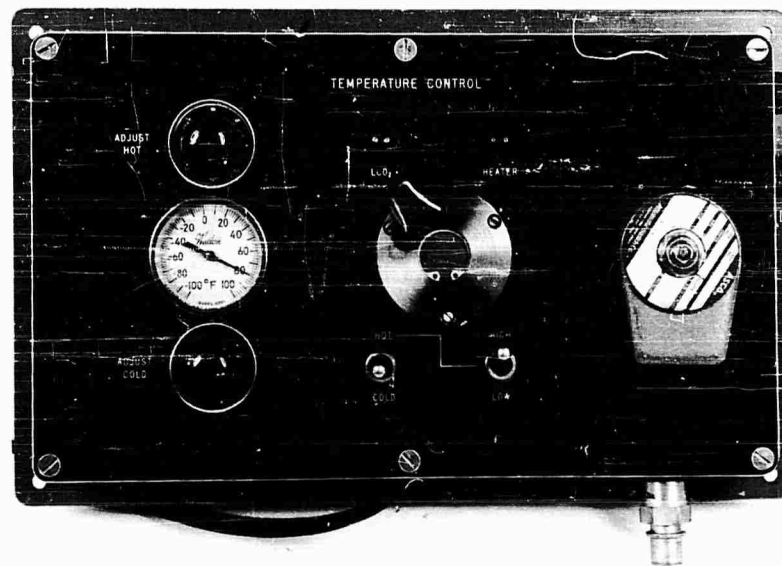


Fig. 2 - Front panel

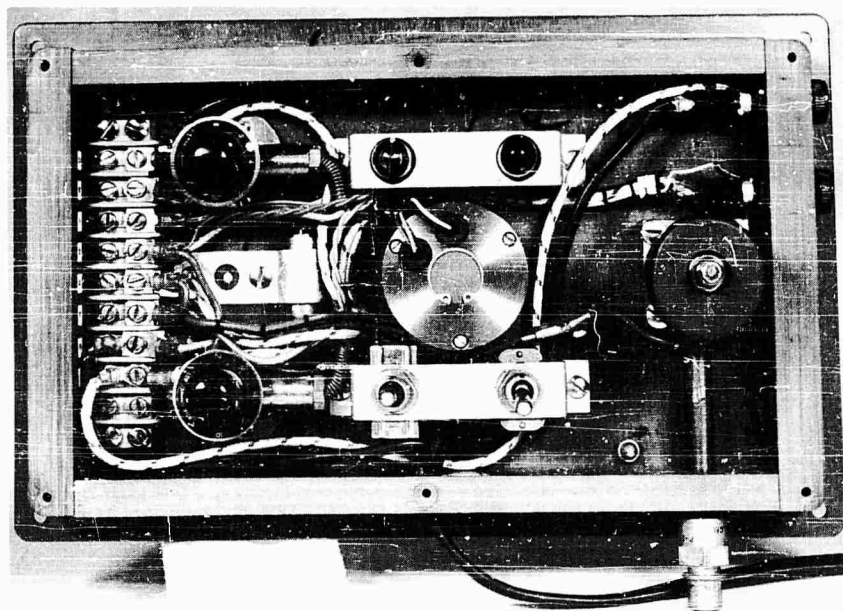


Fig. 3 - Front view with panel removed

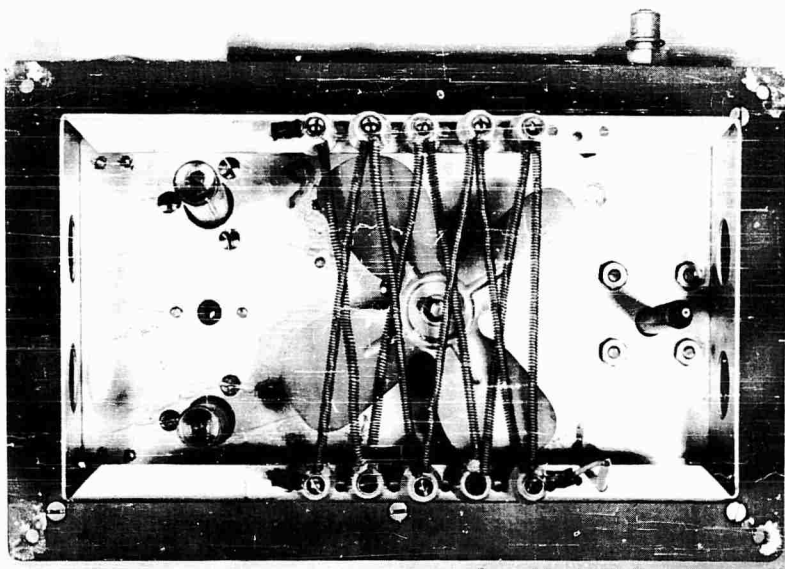


Fig. 4 - Rear view

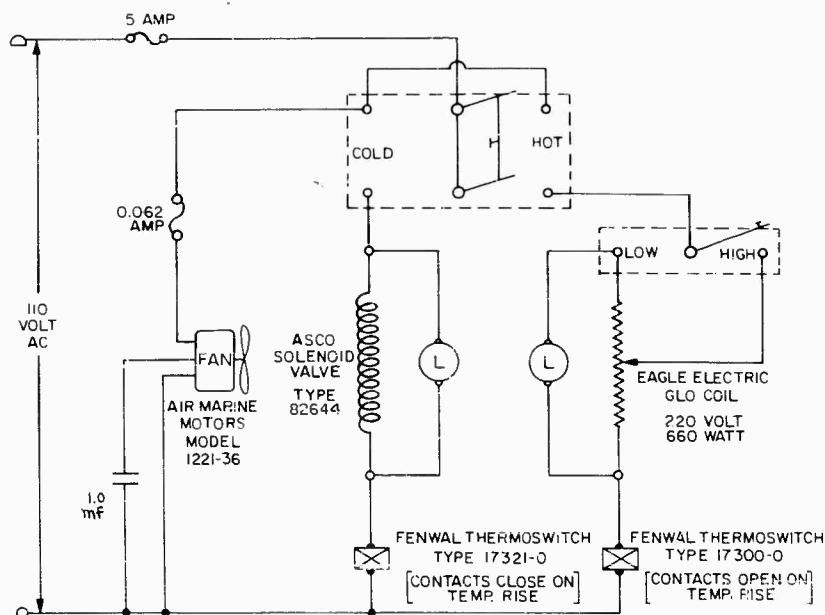


Fig. 5 - Schematic diagram of temperature controller

3. Circulation is provided by a fan mounted in such a way that the shaft and fan blade extend into the chamber while a large part of the body of the motor is on the outside. A major portion is thus exposed to room temperatures. Prior designs had either the entire fan and motor inside the chamber, or the motor entirely on the outside with a fan blade extension shaft supported by separate bearings. Both arrangements proved inferior to the present design. Proper air circulation is provided by beveling one edge of the chamber opening and perforating the aluminum structure.

4. Adjustable thermostatic switches are used which have a 10-amp rating. This eliminates the use of relays. The conservative rating results in long life and dependable service.

5. Simple Weston stem thermometers are used as temperature indicating devices. The sensitive element extends about 8 inches into the chamber and gives a good indication of the temperature of the return air. At least two thermometers must be used to cover the entire useable range of the controller. The accuracy of these thermometers has been found to be surprisingly good. Experiments have shown that they are generally accurate to within 1.0 percent.

6. Pilot lights indicate that the thermostatic switches are adjusting the temperature.

CONTROL ACCURACY

Thermocouple measurements made inside a temperature chamber of moderate size ($2 \times 2 \times 2$ feet, see Fig. 1) have shown that control may be maintained above ambient at any preset point $\pm 2^\circ\text{F}$. Below ambient the injection of the LCO_2 directly into the chamber causes a somewhat wider variation of air temperature. Generally, however, return air temperature may be maintained within $\pm 5^\circ\text{F}$. It should be specifically noted that this accuracy applies to return air temperature; the temperature of a test specimen will vary much less because of the thermal lag. Variation depends on the mass, material, and configuration of the test object but is commonly less than 0.5°F .

Air circulation is such that temperatures measured 6 inches away from the walls of the chamber vary less than $\pm 3^\circ\text{F}$ at any point except for a small area directly at the point of LCO_2 injection.

TEMPERATURE CHAMBER

The controller is a complete instrument which requires only the application of power

and LCO_2 . It will function with any chamber where it may be inserted in the wall. Considerable success has been achieved by using rigid polyurethane foams with a density of about 3 pcf for this purpose. Figure 1 shows one such chamber. They are easily constructed of slab stock with a variety of adhesives; they are very light in weight, quite inexpensive, and have excellent thermal properties. Odd shapes may be built up quickly for special tests.

CONCLUSION

The temperature controller has been in frequent operation for over a year. It has proven to be extremely rugged, simple to use, and quite reliable. It is not intended for extreme precision of temperature control. Nevertheless, it is judged to be entirely satisfactory for the large majority of tests where a combined environment is required.

* * *

Section 2

DAMPING

VIBRATION RESPONSE CHARACTERISTICS OF VISCOELASTIC-DAMPED STRUCTURES

J. E. Ruzicka
Barry Controls
Watertown, Massachusetts

The basic concepts involved in damping structural fabrications using viscoelastic damping materials are reviewed, and a procedure is outlined for designing composite structures consisting of two elastic members with an intervening layer of viscoelastic shear-damping material. Consideration is given to damping, structural stiffness and weight as joint design criteria and the effects of environmental temperature on damping and the structure resonant frequency are discussed. Experimental data are presented indicating the vibration response characteristics of laboratory specimens and practical structural fabrications to establish the degree of vibration control that is available by appropriate application of the damping techniques described.

INTRODUCTION

While the damping characteristics of structural systems have been investigated by scientists and engineers for well over a century, early investigators focused their attention primarily on the internal damping properties of structural materials. More recent investigations have been concerned with the damping properties of composite structures because of the need for a substantial increase in the energy dissipated by structural fabrications undergoing vibration. For flexural vibrations, the most successful approaches developed to incorporate high-energy dissipating mechanisms in structural fabrications involve the use of viscoelastic damping materials [1-9].

This paper presents a review of the basic concepts involved in damping structural fabrications by use of viscoelastic damping materials and outlines various means of designing structural composites incorporating viscoelastic

shear-damping mechanisms. Since practical structural fabrications require consideration of concentrated mass loadings, boundary conditions, fastening devices, strength requirements, and environmental conditions, experimental data are provided for actual in-service damped structures, as well as for idealized laboratory specimens, to aid in determining the degree of vibration control available from viscoelastic-damped structures.

VISCOELASTIC DAMPING CONCEPTS

Structural fabrications may be damped by viscoelastic damping materials employed either as unconstrained layers applied to surfaces of structural members or as constrained layers interposed between the surfaces of members comprising a structural composite. An unconstrained viscoelastic layer experiences primarily cyclic tension-compression strains when applied to a structural member undergoing flexural vibrations, whereas a constrained viscoelastic layer experiences primarily cyclic shear strains when incorporated in a structural

NOTE: References appear on page 175.

composite. Therefore, structures damped by unconstrained layers of viscoelastic material rely predominantly on an extensional-damping mechanism for energy dissipation, and damped structures employing constrained layers of viscoelastic material rely predominantly on a shear-damping mechanism. It generally is necessary to use relatively thick layers of damping material in unconstrained-viscoelastic-damped structural configurations, while relatively thin layers are usually adequate in constrained viscoelastic-damped structural configurations.

Either unconstrained or constrained layers of viscoelastic materials may be employed to damp structural members undergoing flexural vibrations. The unconstrained viscoelastic damping treatment is particularly useful for adding damping to existing structures, whereas the constrained viscoelastic damping treatment has proven to be more suitable for producing integrally damped structural members. Recent

investigations have shown that large structural plates which properly incorporate constrained viscoelastic layers provide more damping with less added weight than plates damped by unconstrained viscoelastic layers [10].

STRUCTURAL COMPOSITE DESIGN CONFIGURATIONS

Special design configurations have been developed which incorporate viscoelastic shear-damping mechanisms in typical structural members such as plates and beams. Satisfactory approaches to damping structural members include designs employing laminated sheets and cell-insert configurations. Cross sections of typical damped structural plates and shapes involving laminated sheets are illustrated in Fig. 1; cross sections of typical cell-insert beams are illustrated in Fig. 2.

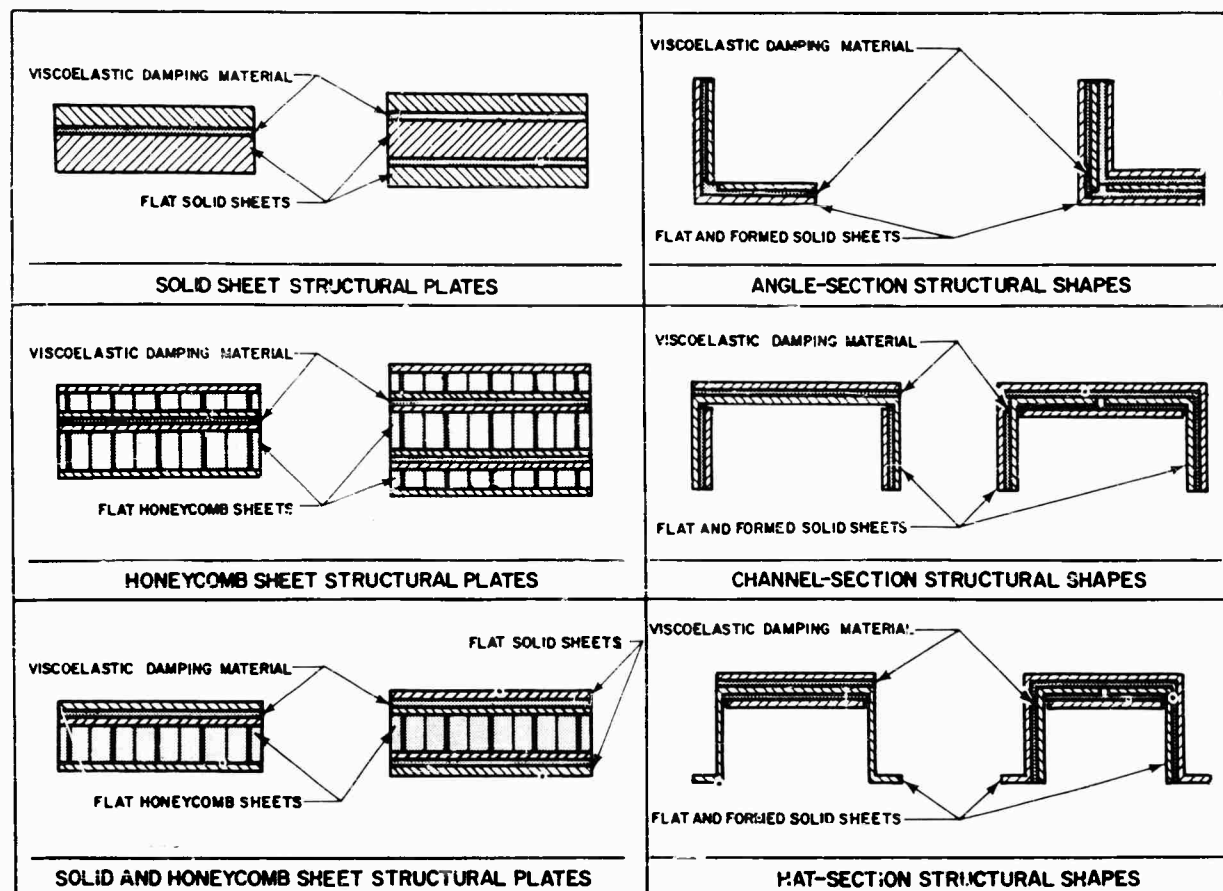


Fig. 1 - Cross sections of typical viscoelastic shear-damped structural plates and shapes

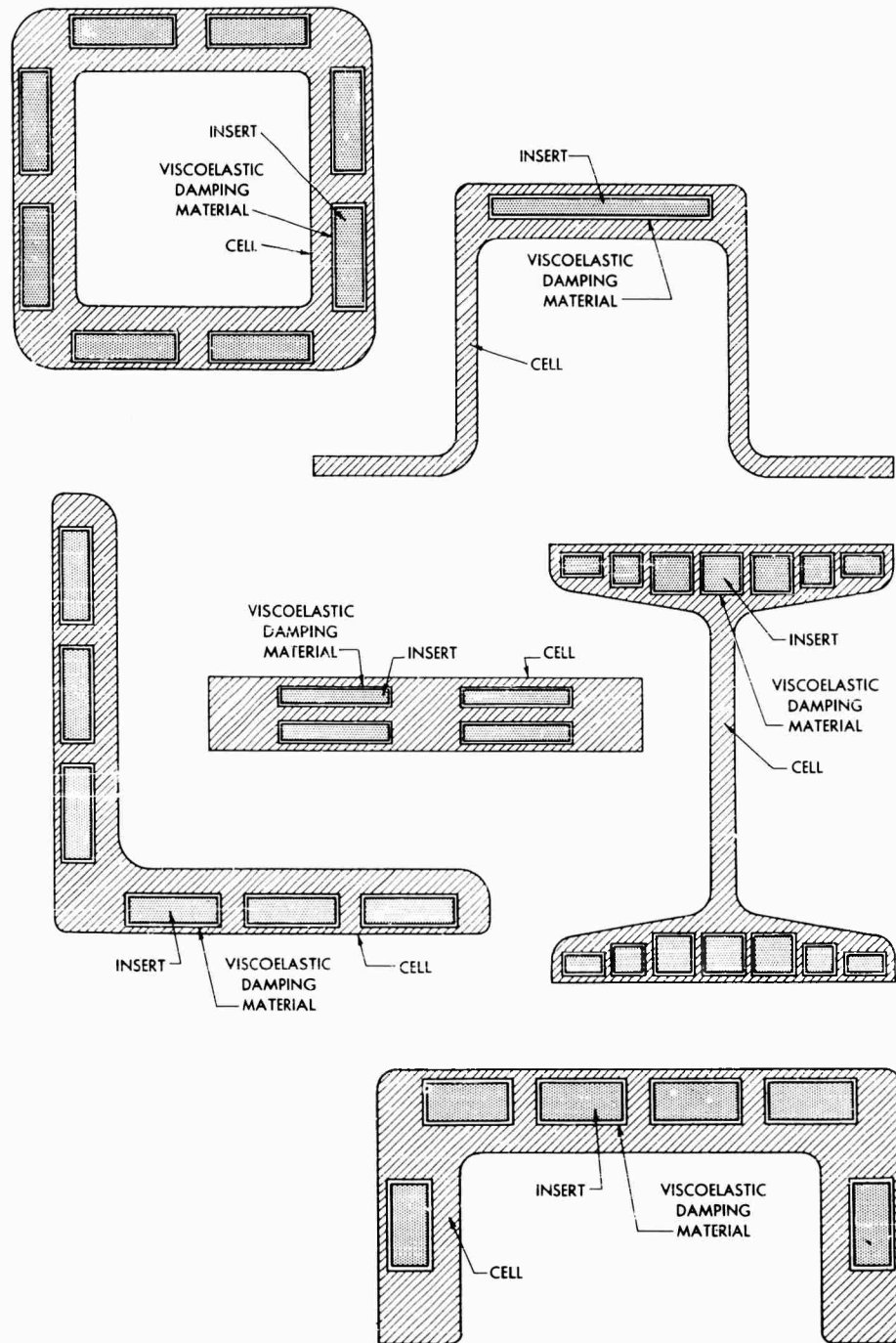


Fig. 2 - Cross sections of typical viscoelastic shear-damped cell-insert beams

The damped laminated structural plates consist of a multiplicity of flat structural sheets which are either solid or honeycomb, whereas the damped laminated structural shapes consist of a multiplicity of flat and formed solid structural sheets; the individual structural sheets in the damped laminated structural members are separated by layers of a viscoelastic shear-damping material. The cell-insert damped beams consist of a longitudinal cellular structural member in which structural insert members are separated from the longitudinal hollow cells by a layer of viscoelastic shear-damping material. When these viscoelastic-damped structural members undergo flexural vibrations, the layers of viscoelastic damping material are subjected to cyclic shear strains, which cause energy of mechanical motion to be converted into thermal energy. As a result of this energy conversion process, viscoelastic-damped structures exhibit extremely high damping properties.

Each individual structural sheet in a damped laminated structural plate or shape and both the cell and insert member of a cell-insert beam are load-carrying members. The number and size of individual sheets, cellular body, and inserts required for specific application is determined by considering weight, stiffness, space, and damping as joint design criteria.

STRUCTURE LOSS FACTOR

Design criteria for most unconstrained viscoelastic-damped structural configurations have been established and are documented in the technical literature; however, the analysis of constrained viscoelastic-damped structural configurations is considerably more difficult to perform and design criteria are available only for relatively simple configurations. Even for simple structural configurations, general equations for the loss factor of the composite structure are extremely complicated and difficult to apply in practical design problems. Design equations may be simplified somewhat for those applications which involve the use of thin layers of viscoelastic damping material that is soft compared to the stiffness of structural materials employed in the structural composite. For these cases, the composite structure loss factor η may be expressed in terms of three parameters, as follows:

$$\eta = \eta(\beta, X, Y), \quad (1)$$

where β is the loss factor of the viscoelastic shear-damping material, X is a shear parameter, and Y is a geometrical parameter. The loss factor β is given by

$$\beta = \frac{G''}{G'}, \quad (2)$$

where G'' and G' are the loss modulus and the storage modulus of the viscoelastic shear-damping material, respectively. The shear parameter X depends in a complicated way on the storage modulus and amount of the viscoelastic damping material used, the weight loading on the structural member, the flexural rigidity and extensional stiffness of the structural member, the geometry of the cross section, and the frequency of vibration.

The geometrical parameter Y is a function only of the geometry of the cross section and may be expressed mathematically as follows [4,6,7]:

$$Y = \frac{(EI)_{\infty}}{(EI)_0} - 1, \quad (3)$$

where $(EI)_0$ and $(EI)_{\infty}$ represent the flexural rigidity of the composite structure for zero and infinite shear modulus of the viscoelastic damping material; that is, $(EI)_0$ is the flexural rigidity of the structural composite when its elastic members are uncoupled and $(EI)_{\infty}$ is the flexural rigidity of the structural composite when its elastic members are completely coupled. Since the natural frequency of a structural beam or plate varies as the square root of its flexural rigidity EI , where E and I represent the modulus of elasticity of the structural material and the cross-sectional moment of inertia, respectively, the geometrical parameter is also given by

$$Y = \left(\frac{f_{\infty}}{f_0} \right)^2 - 1, \quad (4)$$

where f_0 and f_{∞} are the fundamental-mode resonant frequencies of the structural composite for zero and infinite values of the viscoelastic damping material shear modulus.

For the case where the composite structure consists of two elastic members with an intervening viscoelastic damping layer, the structure loss factor η is given by [7,8]

$$\eta = \frac{\beta X Y}{1 + X(Y + 2) + (1 + \beta^2) X^2(Y + 1)} \quad (5)$$

where the geometrical parameter Y is as previously defined and the shear parameter X is given by

$$X = \frac{G' b_v d^2}{\rho^2 h_v Y (EI)_0}$$

In this relation, b_v is the mean length of the viscoelastic damping layer in the cross-section plane, h_v is the constant thickness of the damping layer, d is the distance between the neutral planes of the elastic members, and p is the flexural vibration wave number given by

$$p^2 = \omega \sqrt{\frac{m}{(EI)_d}},$$

where ω is the frequency of vibration, m is the mass per unit length of the structure, and $(EI)_d$ is the effective flexural rigidity of the damped structure. Unfortunately, $(EI)_d$ is difficult to determine since it is a function of the shear parameter χ . The shear parameter is a measure of how well the layers of viscoelastic material couple the flexural motions of the elastic members of the structural composite and the degree of coupling determines the value of the effective flexural rigidity $(EI)_d$. However, it is known that $(EI)_0 < (EI)_d < (EI)_\infty$ and, since the values of $(EI)_0$ and $(EI)_\infty$ are readily calculated, an estimate of $(EI)_d$ is frequently made in lieu of calculating its value through an iteration process.

Optimum Parameters for Maximum Damping

Inspection of the general equation for the structure loss factor η reveals that an optimization of design parameters is required to maximize the degree of structural damping. It is noted that, for values of the shear parameter χ or the loss factor β equal to zero or infinity, η is zero. For intermediate values of χ and β , η is finite and achieves a maximum value when specific relationships exist between χ , β , and Y .

Since a high η is obtained for structural configurations having large values of the geometrical Y , this parameter is generally established prior to determining appropriate values of the shear parameter χ and loss factor β .

Based on the procedure of establishing the geometrical parameter Y and selecting a damping material having specific values of loss factor β and storage modulus G' , the value of the optimum shear parameter χ_{op} for which η is maximized is given by [6]

$$\chi_{op} = \frac{1}{\sqrt{(Y+1)(1+\beta^2)}}, \quad (6)$$

which is shown graphically in Fig. 3. Maximum damping is achieved by incorporating a viscoelastic damping layer having a thickness

$$(h_v)_{op} = \frac{G' b_v d^2}{\omega \chi_{op} Y (EI)_0} \sqrt{\frac{(EI)_d}{m}}.$$

For this condition, the maximum structure loss factor η_{max} is given by [8]

$$\eta_{max} = \frac{\beta Y}{Y + 2 + 2\sqrt{(Y+1)(1+\beta^2)}}. \quad (7)$$

This relation, shown graphically in Fig. 4, indicates the desirability of selecting a damping material having a relatively large loss factor β over the frequency and temperature ranges of interest. The curve for $\beta = \infty$ is an approximate upper-bound curve for the case of pure viscous damping. It must be emphasized that the structure loss factors indicated in Fig. 4 are attainable only when the shear parameter takes on its

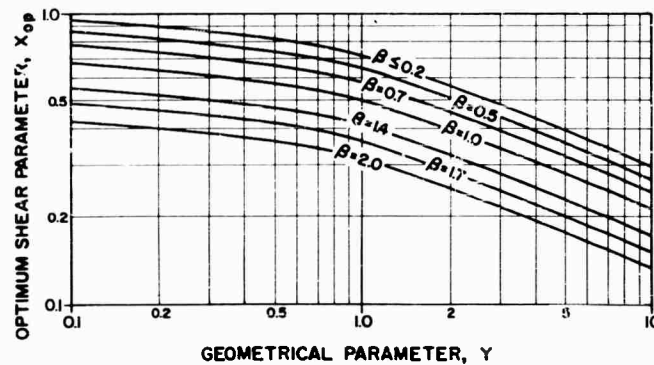


Fig. 3 - Optimum shear parameter χ_{op} for two-element viscoelastic shear-damped member having a geometrical parameter Y and employing a viscoelastic damping material loss factor β [2,8]

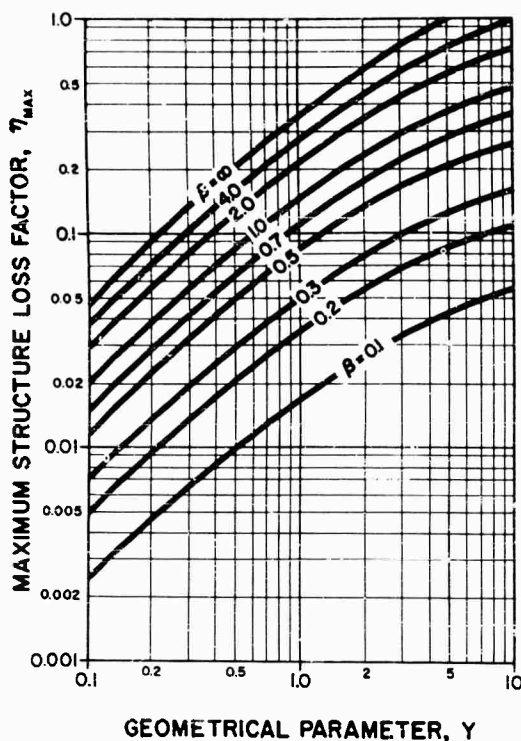


Fig. 4 - Maximum structure loss factor for two-element viscoelastic shear-damped member for which shear parameter has optimum value X_{op}

optimum value X_{op} ; a reduced value of the structure loss factor η will result if the shear parameter X is greater or less than the optimum value.

The approximate reduction in the damping exhibited by a viscoelastic shear-damped composite structure when nonoptimum values of the shear parameter X are employed is indicated in Fig. 5. The variation of η/η_{max} with the shear parameter ratio X/X_{op} is symmetrical about a shear parameter ratio of unity. Curves describing this variation generally fall within the region between the two curves indicated on the graph. The location of a specific curve depends on the values of the damping material loss factor β and the geometrical parameter γ . The lower curve applies for the case of pure viscous damping where β approaches infinity and γ has any value [6]; the upper curve applies for relatively low values of β and values of the geometrical parameter $\gamma < 10$ [2].

Fortunately, a highly damped structure will be obtained by employing a shear parameter having only near-optimum properties. On the

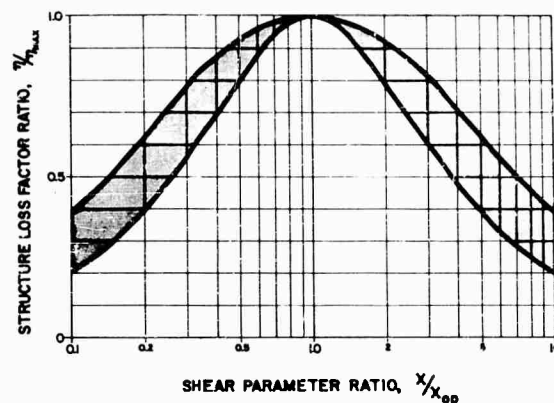


Fig. 5 - Reduction in damping of viscoelastic shear-damped structure for non-optimum values of the shear parameter

average, a structure loss factor that is only 15 percent less than its maximum value is obtained when the shear parameter is one-half or twice its optimum value. In all cases, the structure loss factor is greater than one-half its maximum value when the shear parameter is approximately less than four times and greater than one-fourth its optimum value. The noncritical nature of the shear parameter optimization is of considerable practical significance inasmuch as it provides flexibility in designing structural composites incorporating viscoelastic shear-damping mechanisms.

An alternate procedure for determining optimum parameters for maximum damping involves establishing the geometrical parameter γ , specifying the value of the shear parameter X , and employing a viscoelastic shear-damping material having a loss factor β_{op} which maximizes the structure loss factor η . However, this approach is not as preferred as the one previously outlined because of the practical difficulty in obtaining damping materials having the specific value of the loss factor required.

The preferred method of designing viscoelastic shear-damped composite structures requires evolving a cross-section geometry which will provide a value of the geometrical parameter γ sufficiently high to allow for a high structure loss factor η if near-optimum conditions are met, selecting a viscoelastic damping material that has a high loss factor β over the frequency and temperature ranges of interest, and determining the optimum thickness of the damping material layer $(h_v)_{op}$ which will maximize the structure loss factor. This procedure involves trial-and-error calculations

because of the complex interrelations between the shear parameter χ and the flexural vibration wave member ρ , and because practical considerations from the fabrication point of view may place restrictions on the damping material thickness h_v . It should be noted that the design equations and graphs presented apply only for the case where the composite structure consists of two elastic members with an intervening viscoelastic damping layer; appropriate design relations must be developed for composite structures not satisfying this requirement. However, even for more complex damped structure designs, it is clear that a high value of the geometrical parameter γ is desirable and near-optimum values of the shear parameter χ are required to obtain high degrees of structural damping.

STIFFNESS AND WEIGHT

By applying the viscoelastic damping techniques described, structural fabrications having large loss factors can be produced. However, the stiffness and weight of the structure are design considerations that are frequently as important as the energy dissipation capability of the structure. Therefore, when designing a viscoelastic-damped structure, consideration must be given to the stiffness and weight characteristics of the composite structure, as well as to its loss factor.

Static stiffness and weight characteristics of a viscoelastic shear-damped structure employing a low-modulus viscoelastic damping material are illustrated qualitatively in Fig. 6,

where an increase in the damped structure loss factor η is produced by increasing the geometrical parameter of the structure through variations in the cross-section geometry. When compared on the basis of equal weight, the static stiffness of the damped structure is less than that of the conventional structure, as shown in Fig. 6(a). Consequently, if a conventional structural member having a relatively low loss factor is to be replaced by a viscoelastic-damped member of equal weight, a reduction in static stiffness of the structural member can be expected. However, due to the coupling between the individual elastic members of the structural composite, as determined by the shear parameter χ , the dynamic stiffness of the damped structure will generally be greater than its static stiffness.

When compared on the basis of equal static stiffness, the weight of the damped structure is greater than that of the conventional structure, as shown in Fig. 6(b). Consequently, if a conventional member is to be replaced by a viscoelastic-damped member of equal static stiffness, an increase in the structure weight can be expected. However, due to the dynamic coupling between the individual elastic members of the structural composite, the dynamic stiffness of the damped structure will be greater than that of the conventional structure. Therefore, the resonant frequency of the viscoelastic-damped structure will be greater than that of the conventional structure.

The variation of the static stiffness K_{st} with the value of the geometrical parameter γ of a viscoelastic-damped structure is

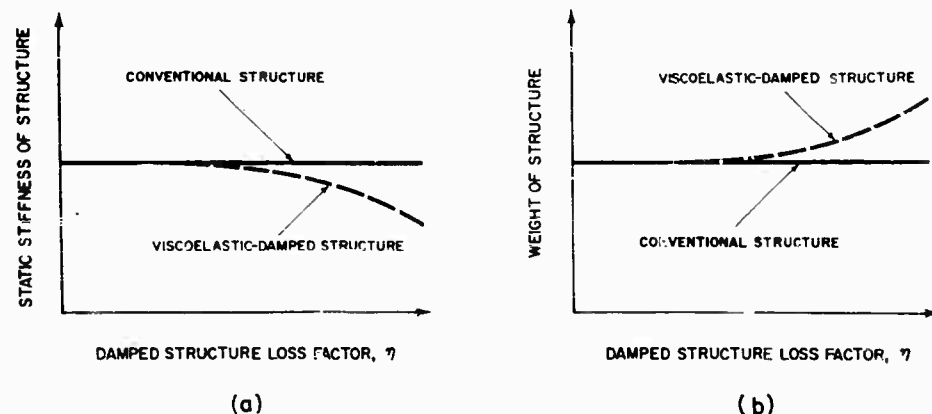


Fig. 6 - Comparison of static stiffness and weight characteristics of solid and viscoelastic-damped structures having (a) equal weight and (b) equal static stiffness, where increase in damped structure loss factor is produced by increasing value of geometrical parameter

shown graphically in Fig. 7 and is given by

$$\frac{K_{st}}{K_{\infty}} = \frac{1}{Y + 1} \quad (8)$$

where K_{∞} is the stiffness of the structure when the individual elastic members of the structural composite are completely coupled. It is assumed that the viscoelastic damping material is soft compared to the stiffness of the structural materials employed in the fabrication and, therefore, the static stiffness of the structure is determined solely by the flexural rigidity $(EI)_0$. Since the stiffness K_{∞} represents the stiffness of the structure prior to adapting its cross section to accommodate a viscoelastic shear-damping mechanism, the curve in Fig. 7 provides a comparison between the static stiffness properties of conventional and viscoelastic-damped structures having the same weight.

A substantial decrease in the static stiffness of the structure results even for relatively low values of the geometrical parameter Y . The static stiffness of the damped structure is one-half that of the equal-weight conventional structure when the geometrical parameter $Y = 1$. For values of the geometrical parameter equal to $Y = 2$ and $Y = 3$, the static stiffness of the structure is reduced by a factor of one-third and one-fourth, respectively. In most cases, the static stiffness will be greater than stated because of the contribution of stiffness by the viscoelastic damping material. Nevertheless, the fact remains that the geometrical parameter Y should have a high value to obtain a large structure loss factor η and a low value to maintain a relatively high static stiffness K_{st} for a specified weight of structure; therefore, selection of the value of the geometrical parameter is made based on the relative importance of damping and static stiffness as design requirements.

FREQUENCY AND TEMPERATURE EFFECTS

The effect that frequency and temperature have on the dynamic elastic properties of viscoelastic shear-damping materials may be used to determine the interrelations between resonant frequency, environmental temperature, and the loss factor of a viscoelastic-damped structure. The effects of environmental temperature and resonant frequency on the loss factor of a viscoelastic-damped structure are illustrated in Fig. 8(a). For very low environmental temperature or high resonant frequency, the viscoelastic damping material operates in its "glassy" region and, since little energy is

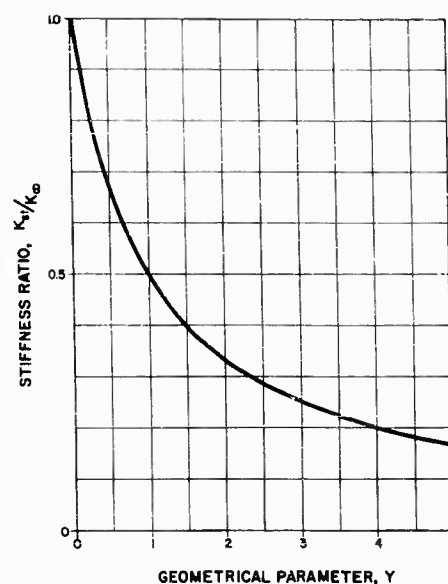


Fig. 7 - Variation of static stiffness of viscoelastic shear-damped structure with geometrical parameter

dissipated (G'' is small), the structure loss factor is small. A similar situation exists for viscoelastic-damped structures that have a very low resonant frequency or are exposed to a very high environmental temperature; the damping material operates in its "rubbery" region and, since little energy is dissipated (G'' is small), the structure loss factor is small. In the "transition" region of the viscoelastic damping material, for intermediate values of environmental temperature and resonant frequency, the viscoelastic-damped structure dissipates a high degree of energy (G'' is large), thereby resulting in a high value of the structure loss factor. Consequently, a specific viscoelastic damping material should be selected for a given application so that its transition region encompasses the frequency range of interest, as well as the expected environmental operating temperature.

The effect of environmental temperature on the fundamental resonant frequency of a viscoelastic-damped structure is illustrated in Fig. 8(b). For very low temperature, the viscoelastic damping material becomes stiff in shear, since it is operating in its glassy region, and the resonant frequency is given approximately by the frequency f_{∞} determined by the stiffness of the structure when its elastic elements are completely coupled. For very high temperature, the viscoelastic damping material becomes soft in shear, since it is operating in its rubbery

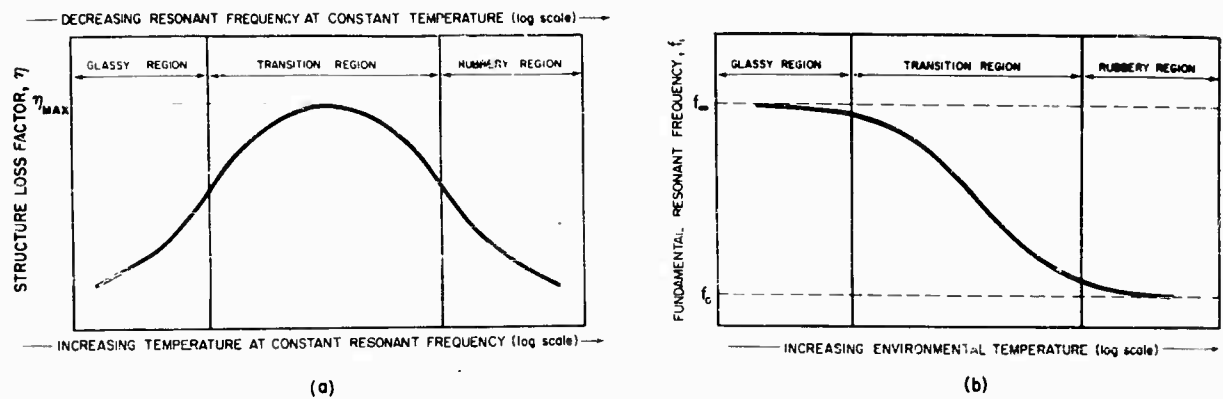


Fig. 8 - Interrelations between environmental temperature, resonant frequency, and structure loss factor of a viscoelastic-damped structure: (a) effects of environmental temperature and resonant frequency on structure loss factor, and (b) effect of environmental temperature on fundamental resonant frequency of structure

region, and the resonant frequency is given approximately by the frequency f_0 determined by the stiffness of the structure when its elastic elements are completely decoupled. The resonant frequency of the structure varies between f_0 and f_∞ for intermediate temperatures at which the viscoelastic damping material operates in its transition region.

EXPERIMENTAL DATA

Experimental dynamic response characteristics have been determined for a series of idealized laboratory specimens, as well as for a number of practical structural fabrications, to demonstrate the effectiveness of viscoelastic shear-damping techniques. Experiments on laboratory beam specimens provide an indication of the effect of varying the geometrical parameter and temperature on the structure loss factor and resonant frequency. Laboratory chassis models are employed to investigate the effectiveness of viscoelastic shear-damping materials incorporated in the chassis structural members; also, the chassis models are used to evaluate viscoelastic junction damping mechanisms. Finally, the response of damped structural fabrications are presented to provide an indication of the degree of vibration control available in practical applications where concentrated mass loadings, boundary conditions, fastening devices, strength requirements, and environmental conditions must be considered. Vibration response and structural damping data are expressed in terms of the transmissibility of the structure and the structure loss factor, respectively, as determined for conditions of harmonic vibration excitation.

Beams

The loss factors of solid and viscoelastic shear-damped clamp-free aluminum beams vibrating in their fundamental mode are presented in Fig. 9 as a function of the vibration amplitude imposed at the clamped boundary. The cross sections of the beams are designed so that the flexural rigidity $(EI)_0$ of the solid and damped beams are equal, thereby giving a comparison of the damping property of solid and damped beams having the same static stiffness.

The loss factor of the damped beam ranges from approximately 0.1 to 0.2, whereas the

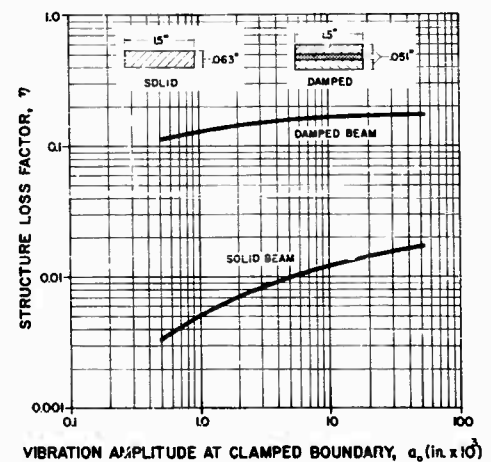


Fig. 9 - Loss factors of solid and viscoelastic shear-damped beams for variations in the amplitude of excitation vibration

solid beam exhibits a loss factor that is less than one-tenth that of the damped beam. The loss factor of the solid beam is strongly affected by the level of vibration excitation because of the nonlinear nature of the hysteretic material damping mechanism, whereas a relatively linear damping characteristic exists for the viscoelastic-damped beam over a wide range of excitation vibration level.

The manner in which the geometrical parameter affects the loss factor of a viscoelastic-damped structure is shown in Fig. 10 for the case where a constant total thickness of a rectangular beam is maintained, but the geometry of the cross section is changed to produce four values of the geometrical parameter γ ranging from 1.3 to 15. For this equal-weight comparison, the loss factors are determined at the fundamental resonant frequencies of the beams, which range from 20 to 300 cps depending on the beam length. The shape of the experimental loss factor curves demonstrates the frequency-dependence of viscoelastic-damped structures. The loss factors of the beams are strongly dependent on frequencies less than approximately 75 cps whereas, for frequencies in the range of 75 to 300 cps, the loss factor is relatively insensitive to changes in frequency.

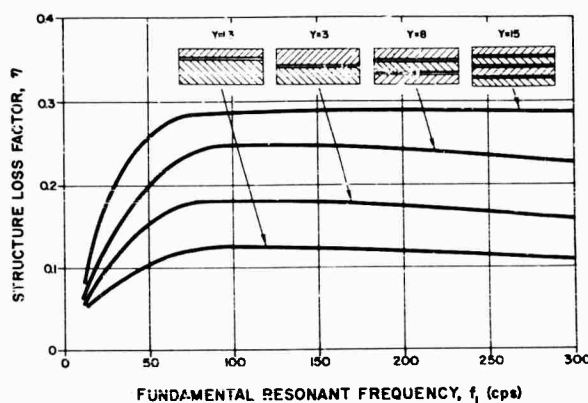


Fig. 10 - Loss factors of viscoelastic-damped rectangular beams as function of the beam resonant frequency

The loss factor η increases from approximately 0.1 to 0.3 by increasing the geometrical parameter γ from 1.3 to 15, thereby demonstrating that damping can be increased by designing structures having large values of the geometrical parameter. However, it should be noted that, beyond a certain point, a substantial increase in the value of the geometrical

parameter is necessary to provide only a slight increase in the structure loss factor. This characteristic is illustrated in Fig. 11 which indicates the approximate variation of the structure loss factor as a function of the geometrical parameter for the four beam configurations; this curve applies for the beams vibrating at frequencies between 75 and 300 cps. A considerable increase in loss factor is provided when the value of the geometrical parameter is increased from 1.3 to 3. By increasing the value of the geometrical parameter from 3 to 8, the loss factor is increased, but not in proportion to the increase in the value of the geometrical parameter. Increasing the value of the geometrical parameter to 15 represents a clear case of diminishing returns inasmuch as the damping has been increased by only a small amount; furthermore, increasing the geometrical parameter to this high value results in a substantial reduction in the static stiffness of the structure which may be undesirable in many applications.

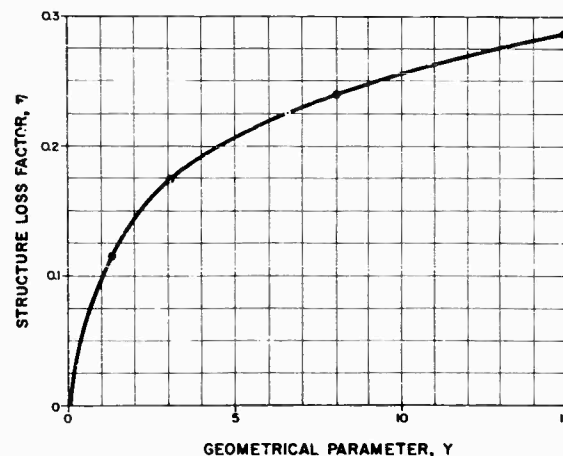


Fig. 11 - Variation of loss factor with geometrical parameter for viscoelastic-damped rectangular beams

The effect that environmental temperature has on the loss factor and fundamental resonant frequency of viscoelastic-damped clamp-free aluminum beams is determined by measuring the damping property and resonant frequency after the beams are subjected to specific temperatures for a period of four hours. The variation of structure loss factor with temperature is shown in Fig. 12 for damped beam specimens employing four different viscoelastic damping materials. Damped beam specimens A and B employ adhesive transfer films as the viscoelastic damping material, whereas specimens

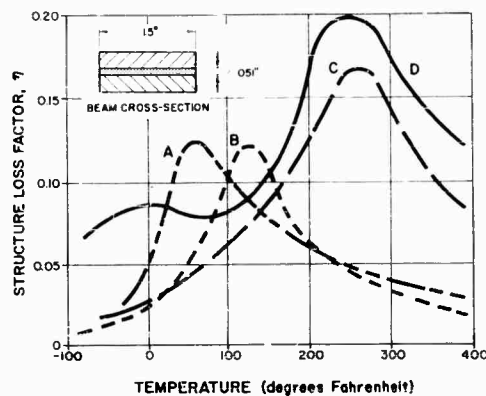


Fig. 12 - Loss factor of viscoelastic-damped rectangular beams as function of environmental temperature for four different viscoelastic shear-damping materials

C and D employ a silicone-based viscoelastic damping material processed through different cure cycles. These curves indicate that the structure loss factor is relatively small at extremely low and high temperatures, as compared with the value of the loss factor at intermediate temperatures. Beam specimens A and B exhibit high damping over a relatively limited temperature range, whereas beam specimens C and D offer high damping over a fairly broad temperature range. The maximum loss factors of beams A and B are approximately equal and occur in the neighborhood of 100°F; beams C and D exhibit their maximum loss factors in the neighborhood of 250°F. Beam D offers the best damping for very low temperatures, beams A and B offer good damping for intermediate temperatures, and beams C and D offer the best damping for higher temperatures. Therefore, viscoelastic damping materials can be selected which provide the maximum amount of damping in the temperature range of interest.

The variation of the fundamental resonant frequency of the beam specimens with environmental temperature is shown in Fig. 13. The curves indicate the resonant frequency of each beam at the specified temperature for which the loss factor is given in Fig. 12. For extremely low and high temperatures, the damped beams exhibit resonant frequencies nearly equal to f_{∞} and f_0 , which are the resonant frequencies resulting for infinite and zero values of the viscoelastic damping material shear modulus. This results from the fact that, for low temperatures, the viscoelastic material operates in its glassy region and becomes rather stiff in shear, whereas for high temperatures the damping material

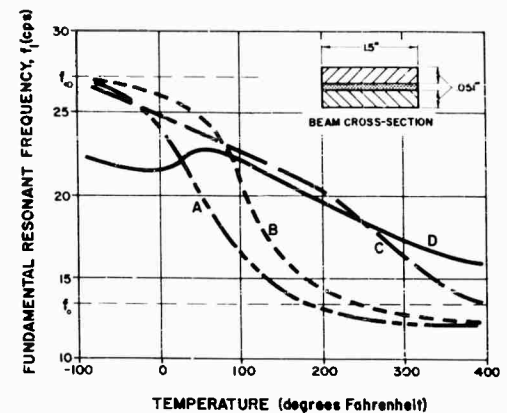


Fig. 13 - Resonant frequency of viscoelastic-damped rectangular beams as function of environmental temperature for four different viscoelastic shear-damping materials

operates in its rubbery region and becomes soft in shear. For intermediate temperatures, the resonant frequencies of the beams have a value between f_{∞} and f_0 as the viscoelastic damping material operates in its transition region.

Chasses

The effect of incorporating viscoelastic shear-damping mechanisms into electronic chasses or box structures is investigated by use of an idealized box chassis having the approximate dimensions 10 x 5 x 1-1/2 inches. Solid and damped chasses are fabricated using solid and viscoelastic-damped structural sheets; the structural sheets are designed so that the weight of the solid and damped box chasses are equal.

Transmissibility and shock response curves are presented in Fig. 14 for both the solid and damped box chasses, where the transmissibility is equal to the ratio of the amplitude of harmonic acceleration at the center of the chassis to the amplitude of the excitation harmonic acceleration. The fundamental resonance of the solid chassis occurs at 170 cps. Due to its laminated configuration, the equal-weight damped chassis has a lower stiffness than that of the solid chassis; the fundamental resonance of the damped chassis occurs at 120 cps. The relatively undamped solid chassis exhibits a resonance-amplification factor of 25, while the viscoelastic-damped chassis exhibits a resonance-amplification factor of 5.5. Thus, the damped chassis exhibits approximately four and one-half times more damping in the

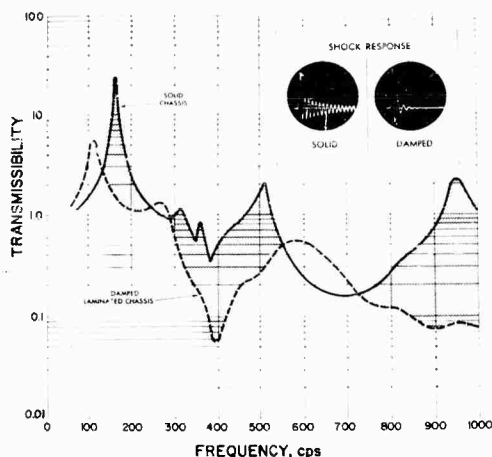
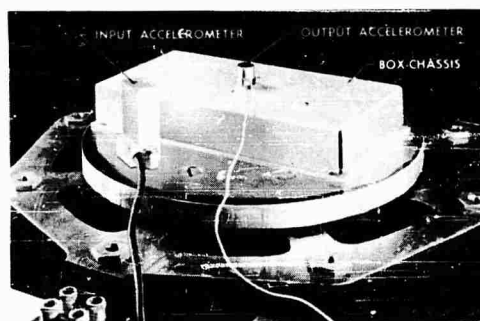


Fig. 14 - Transmissibility curves and shock response time histories for solid and viscoelastic-damped box chassis

fundamental mode of vibration than does the solid chassis. Furthermore, the viscoelastic-damped chassis design provides an appreciable reduction of chassis vibration throughout the broad range of vibration excitation.

The effect of incorporating damping in the corner junctions of aluminum box chassis is indicated in Figs. 15 and 16 which present the vibration and shock response characteristics of box chassis on which are attached a number of concentrated masses to simulate practical loading conditions. The transmissibility curve shown in Fig. 15(a) indicates that the chassis made from solid structural sheet exhibits a resonance-amplification factor of 15 at its fundamental resonant frequency. By replacing the solid structural sheet by a two-laminate viscoelastic-damped sheet, the fundamental-mode resonance-amplification factor is reduced to 5, as shown in Fig. 15(b). By employing viscoelastic-damped structural sheet and incorporating a viscoelastic shear-damping mechanism in the corners of the chassis, the fundamental-mode resonance-amplification

factor is reduced to approximately 2, as shown in Fig. 15(c). The reduction in vibration level at the primary structural resonances of the chassis, as well as the increased attenuation of vibration in the high-frequency region, demonstrate the improvement in structural damping and vibration control that results by employing viscoelastic junction damping mechanisms in addition to damping the structural sheet used to fabricate the chassis. The increased degrees of structural damping provided by application of the viscoelastic shear-damping techniques is also indicated by the transient response time histories presented in Fig. 16

Circuit Boards

It is particularly appropriate to apply viscoelastic damping techniques to electronic circuit boards because of their widespread use in severe dynamic environments. A circuit-board damper can be constructed which consists of a layer of viscoelastic shear-damping material coated on a thin fiberglass constraining sheet. This damper assembly is attached to the bottom side of the circuit board and held in place by virtue of the adhesive property of the viscoelastic damping material. The layer of viscoelastic damping material should be sufficiently thick to allow the circuit-board damper to conform to the surface of the bottom side of the circuit board, which is generally irregular because of wiring and soldering processes.

Transmissibility curves for conventional (solid) and damped circuit boards installed in conventional plastic guide rails attached to a rigid support structure are presented in Fig. 17 for vibration normal to the planes of the circuit boards [11]. As indicated in Fig. 17(a), the fundamental resonant frequency of the conventional circuit-board configuration is 73 cps and the resonance amplification factor is 42; furthermore, resonance amplification factors of approximately 3 are observed at the higher modes of vibration of the circuit board. A substantial reduction in circuit-board vibration is obtained by use of the circuit-board damper without significantly changing the fundamental resonant frequency of the circuit-board configuration. As indicated in Fig. 17(b), the fundamental-mode resonance-amplification factor for the damped circuit-board configuration is 4.5 and the vibration response at the higher modes of vibration is greatly reduced. Therefore, use of the viscoelastic shear-damping techniques increases the damping in the fundamental mode of vibration of the circuit board by a factor of approximately 10 and provides a substantial degree of vibration control

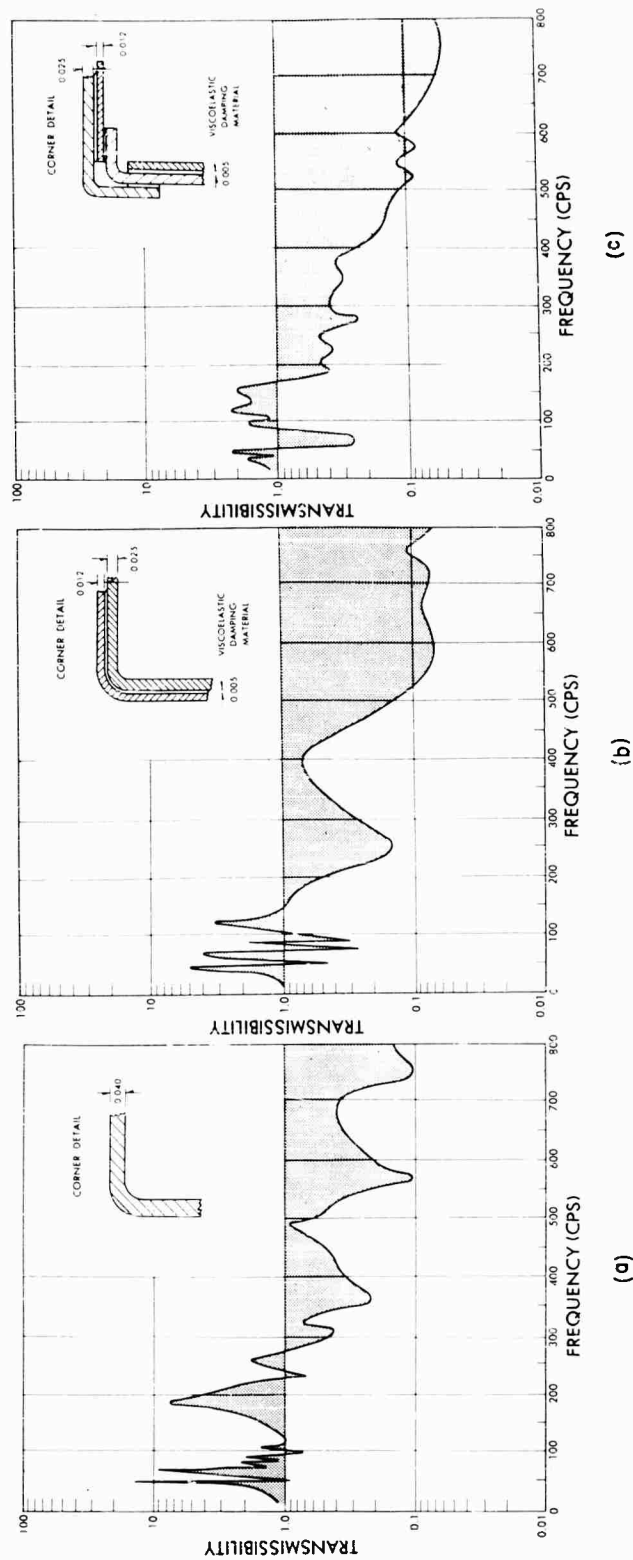


Fig. 15 - Transmissibility curves for solid and viscoelastic-damped box chassis on which are attached a multiplicity of concentrated masses: (a) solid chassis, (b) viscoelastic-damped chassis, and (c) viscoelastic-damped chassis with viscoelastic shear-damping mechanism in its corners

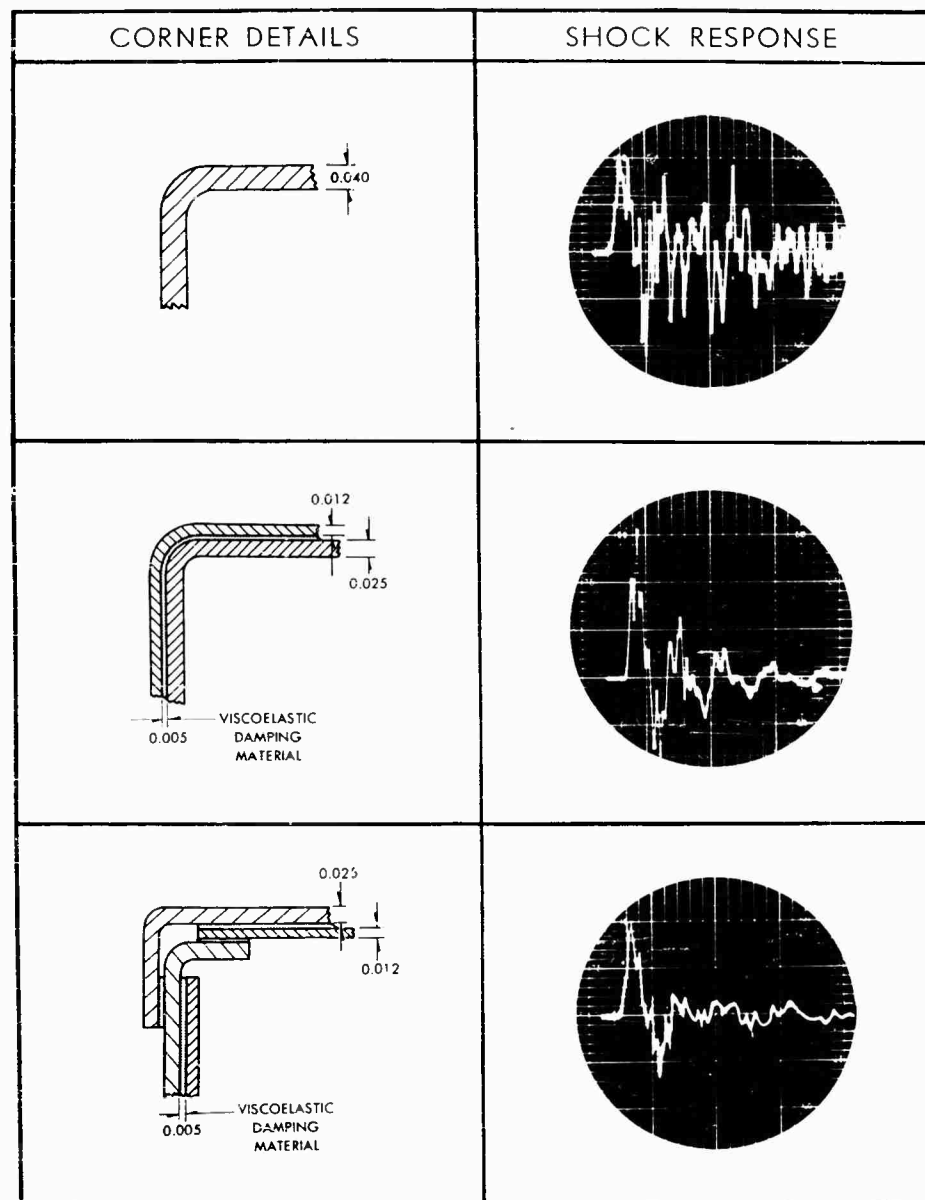


Fig. 16 - Transient response time histories for solid and viscoelastic-damped box chasses employing various corner designs

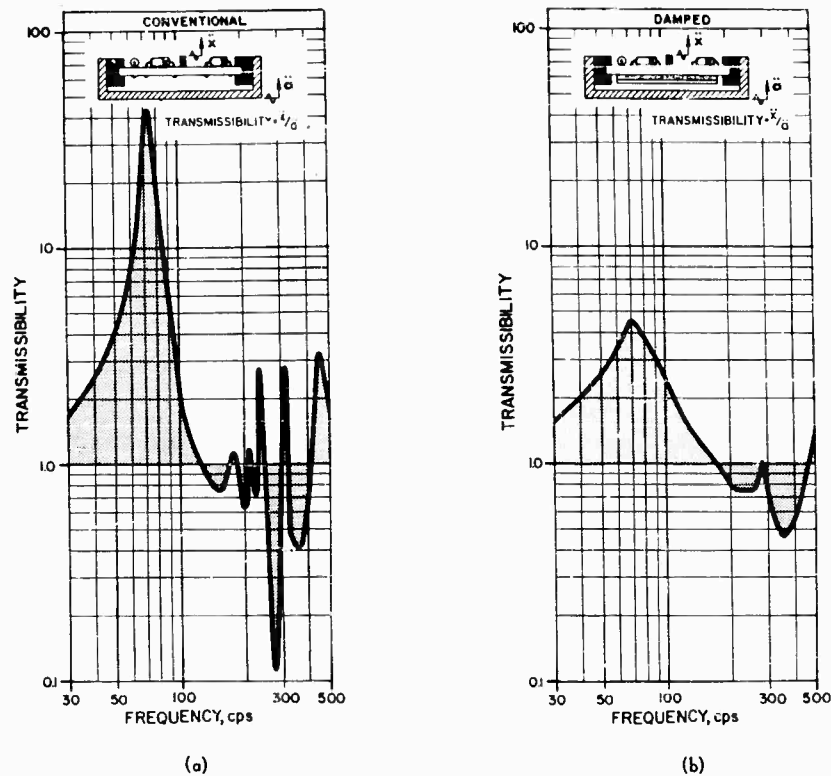


Fig. 17 - Transmissibility curves for (a) conventional and (b) viscoelastic-damped circuit boards installed in plastic guide rails attached to rigid support structure

throughout the frequency range of vibration excitation.

Structural Fabrications

An equipment-rack vibration isolation system used to support four electronic communications units in a jet aircraft is pictured in Fig. 18. The isolation system consists of a viscoelastic-damped aluminum equipment rack, which is approximately 38-1/2 x 15-1/2 x 1-1/4 inches, supported by four elastomeric vibration isolators

positioned near each of the four corners of the equipment rack. The equipment rack supports four electronic units weighing 220 pounds and the total weight of the equipment rack and vibration isolators is 38 pounds. The equipment rack is a box-beam structural fabrication in which the skin members are viscoelastic-damped structural plates consisting of two structural sheets between which is constrained a thin layer of a viscoelastic shear-damping material.

The major difficulty with the rack-mounting concept is the resonant structural vibrations of

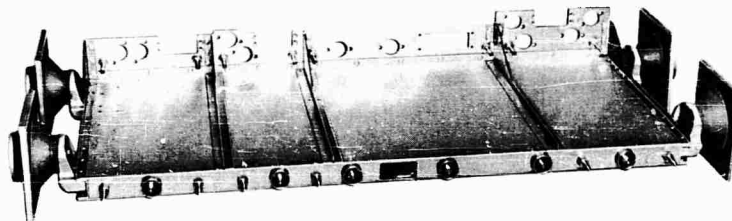


Fig. 18 - Equipment-rack vibration isolation system used to support four communications electronic units in jet aircraft

the rack that are likely to occur at relatively low frequencies because of the heavy weight that the electronic equipment imposes on the long thin equipment rack. This problem is adequately solved by incorporating a viscoelastic shear-damping mechanism in the equipment-rack fabrication, as indicated by the typical transmissibility curve for vibration normal to the plane of the damped equipment rack illustrated in Fig. 19. The fundamental resonant frequency of the equipment rack is approximately 62 cps, and the transmissibility of the isolation system when the equipment rack is vibrating in its fundamental mode of vibration is 0.6. Considerable energy is dissipated by the viscoelastic-damped rack when it vibrates at its various resonant frequencies. Therefore, through the application of viscoelastic shear-damping concepts, the communications electronic equipment is provided with a high degree of vibration control throughout the frequency range of vibration excitation.

An aluminum electronic chassis used to house jet aircraft communications electronic modules is pictured in Fig. 20; the chassis has the approximate dimensions 16 x 10 x 1-1/2

inches with a 6 1/2-inch high rear panel, weighs 6 pounds and supports electronic modules weighing 33 pounds. It was desired to attach the electronic chassis directly to the jet aircraft secondary structure, but excessive resonant structural vibrations of the chassis, when fabricated from solid aluminum sheets, caused fatigue failures to occur, greatly amplified the acceleration experienced by the electronic modules, and caused the closely located modules to collide with each other resulting in equipment malfunction. Clearance was not available for vibration isolators and a high structural stiffness of the chassis was required. Therefore, viscoelastic damped structural stiffeners and gussets were designed and installed in a conventionally fabricated electronic chassis to reduce the vibration experienced by the electronic modules.

Typical transmissibility curves are presented in Fig. 21 for a solid chassis and one with viscoelastic-damped structural stiffeners and gussets installed, for vibration normal to the plane of the chassis [11]. Through the application of viscoelastic shear-damping concepts, the fundamental-mode resonance-amplification factor is reduced from 17 for the

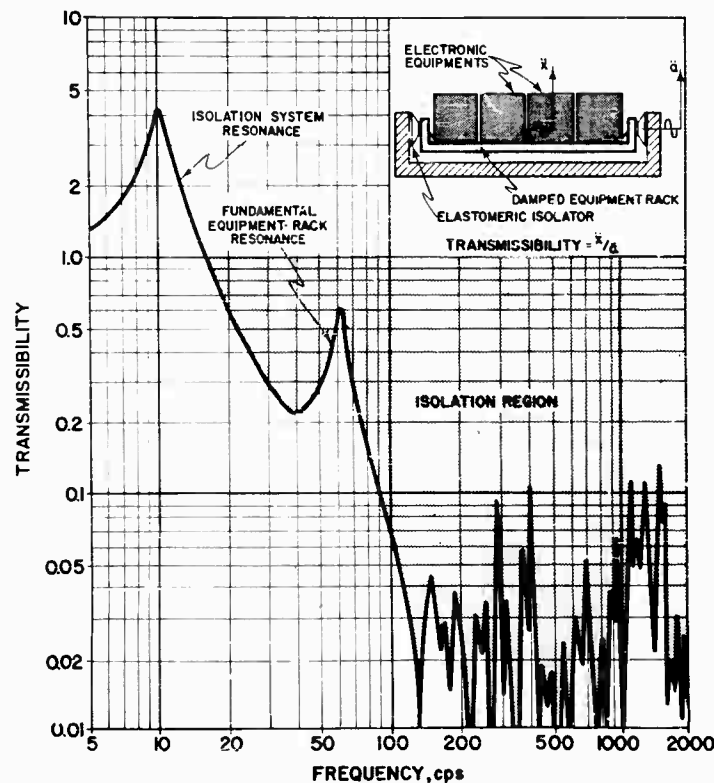


Fig. 19 - Transmissibility curve for damped equipment-rack vibration isolation system

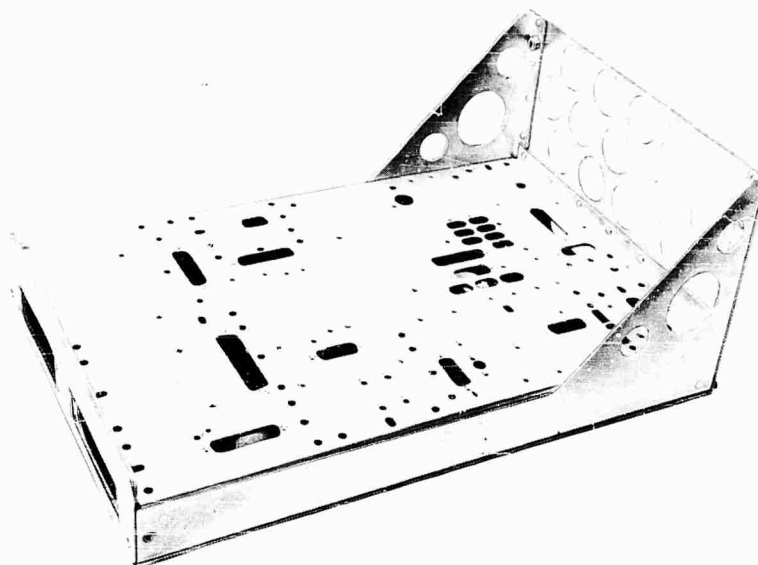


Fig. 20 - Viscoelastic-damped electronic chassis used to support communications electronic modules in jet aircraft

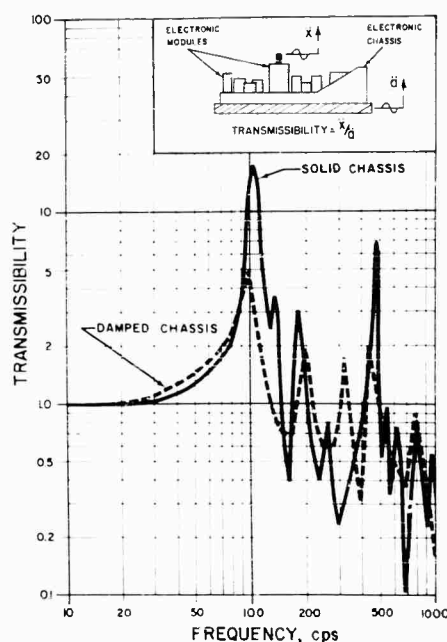


Fig. 21 - Transmissibility curves for a solid electronic chassis and viscoelastic-damped chassis design

solid chassis to 5 for the damped chassis. In addition, the high-frequency vibration response of the chassis is reduced, thereby eliminating the problems of structural fatigue and collisions between electronic modules.

The circular structural plate pictured in Fig. 22 is used to support the arming-and-fuzing electronic components in an ICBM missile. The 1/2-inch thick fiberglass plate structure has a diameter of 20 inches, weighs 8 pounds and supports electronic components weighing 35 pounds. It is bolted at its periphery to the missile structure.

Typical transmissibility curves for vibration normal to the plane of the arming-and-fuzing system plate structure are presented in Fig. 23 [11]. The fundamental resonant frequency of the solid plate structure is 160 cps and the resonance-amplification factor is 38. For excitation frequencies greater than 300 cps, the transmissibility of the solid plate structure ranges between 1 and 2 with no noticeable degree of vibration attenuation at high excitation frequencies.

By fabricating the plate structure out of a viscoelastic-damped plate consisting of three fiberglass sheets between which are constrained thin layers of a viscoelastic shear-damping material, the resonance-amplification factor is significantly reduced and a substantial degree of vibration attenuation is provided at high excitation frequencies. The fundamental resonant frequency of the viscoelastic-damped plate structure is 80 cps, the resonance-amplification factor is 4.6 and vibration attenuation occurs for excitation frequencies greater than 120 cps. Because of the viscoelastic shear-damping mechanism incorporated in the plate structure,

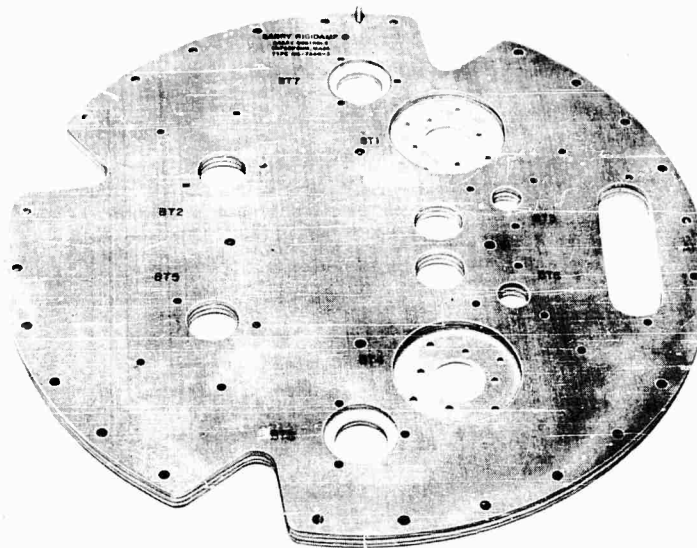


Fig. 22 - Circular structural plate used to support arming-and-fuzing electronic components in ICBM missile

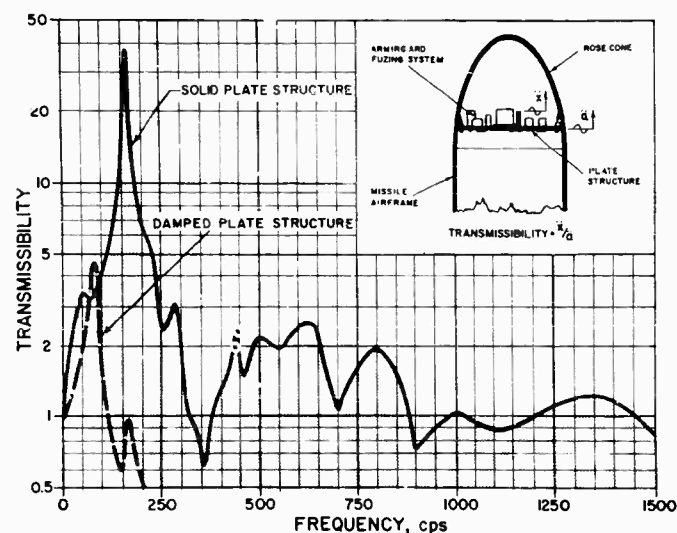


Fig. 23 - Transmissibility curves for solid circular plate structure and viscoelastic-damped design

considerable energy is dissipated by the structure when it vibrates at its various resonant frequencies; for the fundamental mode of vibration, the resonant transmissibility is decreased by a factor of 8 by use of the viscoelastic shear-damping concept. Furthermore, because of the reduction of the fundamental resonant frequency and the damping of the flexural vibration waves, a high degree of vibration attenuation is provided

at high excitation frequencies. Specifically, for excitation frequencies greater than 200 cps, less than one-half the amplitude of excitation vibration is transmitted to the arming-and-fuzing electronic components.

A truncated conical fiberglass structure used to support the arming-and-fuzing electronic components in an ICBM missile is pictured in

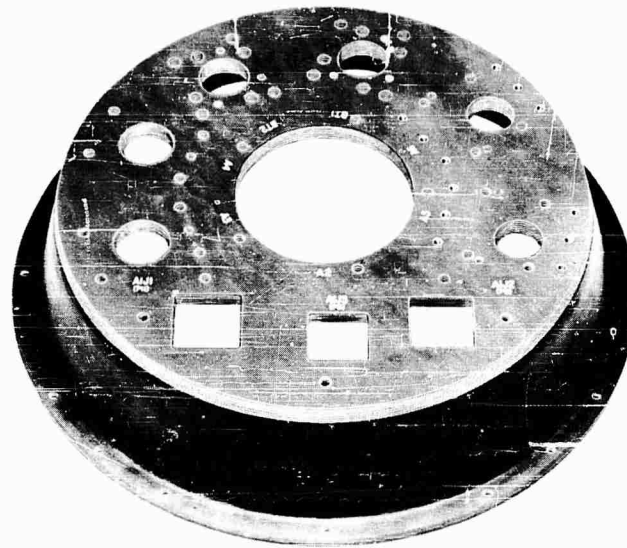


Fig. 24 - Truncated conical structure used to support arming-and-fuzing electronic components in ICBM missile

Fig. 24. The structure weighs 5 pounds and supports 25 pounds of electronic components on its top circular surface, which is 1/2 inch thick and 13 inches in diameter. The conical structure is bolted to the missile at its bottom peripheral ring which is 15-1/2 inches in diameter; the height of the conical structure is 3 inches, which allows sufficient clearance for components to be mounted on either side of the top surface.

Typical transmissibility curves for vibration normal to the truncated plane of the arming-and-fuzing conical structure are presented in Fig. 25 [11]. The fundamental resonant frequency of the conical structure having a solid fiberglass top surface is 320 cps and the resonance-amplification factor is 36. While some attenuation of vibration occurs for excitation frequencies greater than 530 cps, the transmissibility is 1.3 for the second mode of vibration occurring at 925 cps.

The top surface of the viscoelastic-damped conical structure consists of seven fiberglass sheets between which are constrained thin layers of viscoelastic shear-damping materials. The fundamental resonant frequency of the viscoelastic-damped conical structure is 95 cps, the resonance-amplification factor is 3.6 and vibration attenuation occurs for excitation frequencies greater than 160 cps. For the

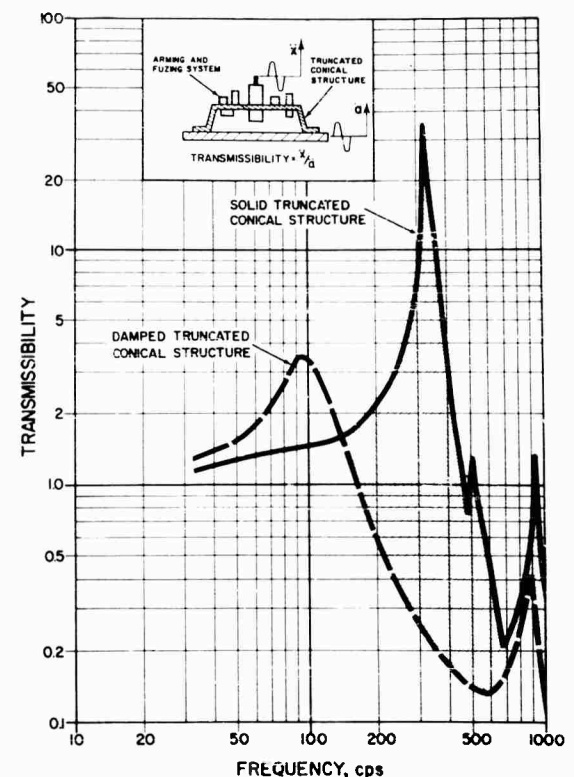


Fig. 25 - Transmissibility curves for a solid truncated conical structure and the viscoelastic-damped design

fundamental mode of vibration, the resonance-amplification factor of the structure is decreased by a factor of 10 by use of the viscoelastic shear-damping concept. Furthermore, because of the reduction of the fundamental resonant frequency and the damping of flexural vibration waves, a high degree of vibration attenuation is provided at high excitation frequencies. Specifically for excitation frequencies greater than 220 cps, less than one-half the amplitude of excitation vibration is transmitted to the arming-and-fuzing electronic components.

Viscoelastic damping techniques are being applied to the design of spacecraft structures to minimize the amplification of vibration imposed by booster vehicles at the resonant frequencies of the spacecraft structures. Successful application of viscoelastic shear-damping structural designs have been made in the fabrication of spacecraft solar panels, electronic support structures, and other critical structural members.

Typical transmissibility curves are presented in Fig. 26 for a 1/2-scale dynamic model of a spacecraft structure in which conventional and viscoelastic-damped solar panels are employed [12]. The spacecraft model tested has an overall height of 69 inches (including the spacecraft/missile adapter section) and a lateral diameter dimension of 30 inches. The two solar panels attached to the spacecraft body are approximately 20 by 48 inches in plan view with a thickness of 0.1 inch at its horizontal center-line tapering down to approximately 1/16 inch at its tips. The solar panel assembly consists of a tapered balsa-wood core to which are

attached two thin aluminum sheets. For the conventional solar panel assembly, the aluminum sheets are bonded to the wood core with an epoxy cement, whereas the damped solar panel is fabricated by bonding the aluminum sheets to the wood core by a viscoelastic shear-damping material.

The transmissibility curves presented in Fig. 26 represent the amplification of vibration from the bottom of the spacecraft/missile adapter to the bottom of the hinge line on the panel transition, for vibration normal to the longitudinal axis of the spacecraft. A number of resonances of the spacecraft structure occur for frequencies less than 50 cps at which the resonance-amplification factors are typically 35 for the conventional structure and 5 for the damped structure. A significant structural resonance occurs at approximately 80 cps at which the resonance-amplification factor is reduced from 30 to 2 by employing the viscoelastic shear-damping mechanism. The reduction in vibration response level provided by the viscoelastic-damped structure design is impressive, particularly in view of the fact that a weight increase of less than 3 percent results in applying the viscoelastic damping technique.

SUMMARY AND CONCLUSIONS

The basic concepts involved in damping structural fabrications by viscoelastic damping materials have been reviewed and experimental evidence has been provided to substantiate that a high degree of vibration control is available if viscoelastic shear-damping mechanisms are properly incorporated in composite structures. Conclusions that may be stated with regard to the vibration response characteristics of viscoelastic-damped structures include:

1. A high value of the structure loss factor can be attained by employing a viscoelastic damping material having a high loss factor and obtaining a near-optimum value of the shear parameter by making appropriate changes in the cross-section geometry and in the thickness and amount of viscoelastic damping material used. A trial-and-error solution is required to maximize damping inasmuch as different damping materials may have to be considered if the optimum thickness of the damping layers are too small or too large from a practical point of view.
2. A high value of the structure geometrical parameter is required to obtain high values of the structure loss factor; however, since increasing the value of the geometrical parameter

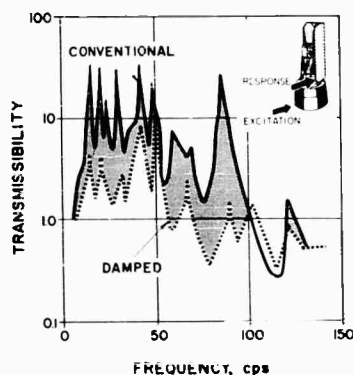


Fig. 26 - Transmissibility curves for 1/2-scale dynamic model of spacecraft structure employing conventional and viscoelastic-damped solar panels

decreases the static stiffness of the structure for a given weight, a compromise between damping and stiffness requirements may be necessary to evolve a satisfactory design.

3. The viscoelastic damping material should be selected so that its transition region encompasses the frequency and temperature ranges of interest in order to obtain high damping for actual operational conditions.

4. The resonant vibration response of practical structural fabrications can be decreased by a factor of 5 to 10 by use of viscoelastic shear-damping techniques, as has been demonstrated in this paper for various types of structures including electronic circuit boards and chasses, arming-and-fuzing system support structures, electronic equipment racks, and spacecraft solar panels.

REFERENCES

1. J. E. Ruzicka, Structural Damping (ASME, New York, 1959).
2. D. Ross, E. E. Ungar, and E. M. Kerwin, Jr., Structural Damping (ASME, New York, 1959), Sec. 3.
3. E. M. Kersin, Jr., J. Acoust. Soc. Am., 31(7):952 (1959).
4. J. E. Ruzicka, SAE Paper No. 100Y (Oct. 1959).
5. B. J. Lazan, SAE Paper No. 100U (Oct. 1959).
6. J. E. Ruzicka, J. Eng. Ind., 83(4):403 (1961).
7. E. E. Ungar, J. Acoust. Soc. Am., 34(8): 1082 (1962).
8. E. E. Ungar, Machine Design, p. 162 (Feb. 1963).
9. J. E. Ruzicka, Electro-Technol., p. 63 (Aug. 1963).
10. E. M. Kerwin, Jr. and D. Ross, Trans. 3rd Int. Cong. on Acoust. (Elsevier Pub. Co., Amsterdam, 1961), p. 410.
11. J. E. Ruzicka, Electro-Technol., p. 75 (Jan. 1964).
12. H. D. Carden and R. W. Herr, "A Study of the Effectiveness of Various Methods of Vibration Reduction on Simplified Scale Models of the Nimbus Spacecraft," NASA TN D-2418 (Aug. 1964).

* * *

MATERIAL DAMPING OF ALUMINUM

BY RESONANCE-DWELL TECHNIQUE

N. Granick and J. E. Stern
Goddard Space Flight Center
Greenbelt, Maryland

Material damping has been considered as stress amplitude dependent in intermediate and high stress levels. In this same stress range, contributions to material damping from frequency dependent anelastic mechanisms have been considered negligible. These conditions are at variance with the findings of this investigation for the material tested. The relation between material damping, stress amplitude and frequency was experimentally examined for aluminum 2024-T4. The test method used was a resonant-dwell technique with "identical" double cantilever reeds. Tests were run in air (760 mm, 70°F) and in vacuum (0.2 mm, 70°F) at stress amplitudes up to 20,000 psi and at frequencies from 15 to 1500 cps. Results showed that damping as measured in air was largely aerodynamic drag and was displacement amplitude and frequency dependent, and damping as measured in vacuum was wholly material damping, independent of stress amplitudes up to 20,000 psi and dependent on frequency. Good correlation with the Zener theory of thermal relaxation was found.

INTRODUCTION

Damping is an energy dissipative process manifested during the mechanical vibration of structural elements and systems. It is of particular interest to the dynamicist and designer whose problems are concerned with the analysis and development of equipment which must function successfully and survive in a mechanically dynamic environment.

The damping of structural systems may be separated into three general types:

1. Joint damping arising from the friction, slippage and slapping between joint interfaces;
2. Air or fluid damping arising from loss or transmission of energy to the surrounding fluids; and
3. Material damping, an internal energy loss, arising from complex internal behavior of the material itself.

To design and predict the behavior of structural systems with greater accuracy, it is necessary to have quantitative damping information. This report is concerned with the

quantitative evaluation of material damping of aluminum. Aluminum was selected for initial investigation because of its extensive use as a structural material for spacecraft. Other materials will be investigated in the near future.

NATURE OF EXPERIMENT

Considerable effort has been made in experimentally determining the material damping properties of metals subject to vibration. Most metals investigated have exhibited a nonlinear dependence of material damping with respect to vibration amplitudes and, in some cases, have also exhibited a dependence on frequency. Crandall [1] investigated the problem of material damping and proposed the following relations:

$$g = \left(\frac{S}{S_0} \right)^n \quad (1)$$

or

$$g = \left(\frac{S}{S_0} \right)^n \frac{\omega \tau}{1 + \omega^2 \tau^2} \quad (2)$$

NOTE: References appear on page 195.

where

g = material damping coefficient,

S = stress amplitude,

ω = vibration frequency (rad),

τ = relaxation time for temperature equalization in a specimen by transverse heat flow, and

S_0, n = material constants.

The frequency dependent term in Eq. (2) was suggested by Zener's [2] relation

$$g = \frac{\alpha^2 ET}{c} \left(\frac{\omega \tau}{1 + \omega^2 \tau^2} \right); \quad (3a)$$

for a flat beam of uniform thickness

$$\tau = \frac{h^2 c}{\pi^2 k}, \quad (3b)$$

where

α = coefficient of linear expansion,

c = specific heat per unit volume,

E = modulus of elasticity,

T = absolute temperature,

h = thickness of cantilever, and

k = thermal conductivity.

From Eqs. (1) and (2), Crandall derived explicit relations for evaluating the specimen damping coefficient of a cantilever beam at its first mode resonance:

$$g_s = R^{\frac{1}{n+1}} \left(\frac{2.71 \sqrt{\rho E}}{S_0} \frac{\alpha}{\omega_1} \right)^{\frac{n}{n+1}} \quad (4)$$

or

$$g_s = R^{\frac{1}{n+1}} \left(\frac{2.71 \sqrt{\rho E}}{S_0} \frac{\alpha}{\omega_1} \right)^{\frac{n}{n+1}} \left(\frac{\omega_1 \tau}{1 + \omega_1^2 \tau^2} \right)^{\frac{1}{n+1}} \quad (5)$$

where

ρ = mass density of beam material,

α = acceleration amplitude of beam root,

ω_1 = first mode resonant frequency,

$R = f$ (material, mode shape), and

g_s = specimen damping coefficient related to g by

$$g_s = gR. \quad (6a)$$

Crandall also showed that

$$g_s = \frac{1}{Q}, \quad (6b)$$

and for a cantilever

$$Q = \frac{\delta_{res}}{1.566 \delta_0}, \quad (6c)$$

where

Q = magnification factor at resonance,

δ_0 = input root displacement at resonance, and

δ_{res} = output tip displacement at resonance.

For a given material, geometry and mode shape R, ρ, E, S_0, n , and τ are constants and Eqs. (4) and (5) reduce to

$$g_s = k \left(\frac{\alpha}{\omega_1} \right)^{\frac{n}{n+1}} \quad (7)$$

and

$$g_s = k \left(\frac{\alpha}{\omega_1} \right)^{\frac{n}{n+1}} \left(\frac{\omega_1 \tau}{1 + \omega_1^2 \tau^2} \right)^{\frac{1}{n+1}} \quad (8a)$$

If the relaxation time τ is large such that $\omega_1^2 \tau^2 \gg 1$, then Eq. (8a) reduces to

$$g_s = k' \left(\frac{\alpha}{\omega_1} \right)^{\frac{n}{n+1}}, \quad (8b)$$

where

$$k' = k \left(\frac{1}{\tau} \right)^{\frac{1}{n+1}} \quad (8c)$$

Equations (6), (7), and (8b) show that:

1. The specimen damping coefficient can be determined by measuring the magnification factor at resonance;

2. The material constant n can be evaluated by measuring the slope of a log-log plot of R_s vs a/ω_1 for Eq. (7), and $g_s \omega_1$ vs a for Eq. (8b); and

3. S_0 can be computed when n has been determined.

A check of Eqs. (7) and (8b) against data taken by Vet [3] showed good correlation of Eq. (7) for steel and brass but failed for aluminum, and good correlation of Eq. (8b) for aluminum but failed for steel and brass. Vet's data included air damping and probably some joint damping. To evaluate more accurately the validity of Crandall's proposed relationships, it was considered necessary to run damping tests which eliminated, minimized, or accounted for these external effects. This was accomplished by testing in air and in a vacuum, and by developing improved test techniques. Details are discussed in a later section of this report.

TEST SPECIMEN

Test Specimen Geometry

The test method selected for this investigation was a steady state excitation of a cantilever beam by an electromagnetic vibrator. Before selecting a beam configuration, consideration was given to two problems affecting the dynamic behavior of the vibrating system: joint damping at the beam-vibrator table interface, and the generation of an undesired rocking mode on the beam-vibrator table system.

An examination of the single reed cantilever, Fig. 1a, shows that a moment reaction M_B^1 at the fastener will always exist and have a value equal to or greater than the root moment M^1 . The moment M_B^1 increases the probability of joint damping. Further, to prevent a rocking mode, it is necessary that $F^1 d^1 = M^1$. To accomplish this, the beam must be positioned by a tedious, time-consuming trial-and-error process until rocking is eliminated.

An examination of the double reed cantilever in Fig. 1b shows that if $F_1 = F_2$, $M_1 = M_2$, and F_1 and F_2 are equidistant from and parallel to the elastic axis, then M_B , the moment reaction at the fastener, vanishes and the probability of joint damping is reduced. Further, the sum of the moments ($F_1 d_1 + F_2 d_2 + M_1 + M_2$) also vanishes and the causes of rock are eliminated. These criteria can be achieved by a double reed cantilever

beam in which the geometry of both reeds are identical and where the center of the base block is located on the geometric center of the vibrator table. For a well-designed table, the geometric center is coincident with the elastic axis, the cg of vibrator table, and the resultant electromagnetic driving force. For these reasons, the double reed cantilever beam was chosen for the test beam configuration.

Adequacy of the test specimen depends on an ability to fabricate carefully each reed of a given specimen to the same geometry in order to have an identical and symmetrical response. In practice, there will always exist a small difference in "identical" reeds due to manufacturing techniques. To overcome this problem, the reeds were manually tuned to the same frequency. This was accomplished by exciting the beam specimen, observing the resonant frequencies of both reeds, then adding additional mass to the tip of the reed exhibiting the higher resonance until the resonant frequencies of both reeds were equal.

The test specimens were designed with first bending mode resonances in the frequency range 15 to 1500 cps. Length-to-width ratios of at least 6:1 were held to minimize the effects of Poisson's ratio. Reed thickness for some specimens was varied to determine the effect of the relaxation time τ . Finally, the root radius was chosen equal to the reed thickness. This choice was based on a compromise which provided a stress concentration factor of only 1.1 with a minor effect on the length and cross-sectional properties of the beam (Table 1).

Specimen Manufacture

A number of restrictions were placed on the methods used to control material homogeneity and finish. For uniformity, all specimens were cut from a single bar stock of 2024-T4 aluminum material. Machining tolerances were held to ± 0.001 inch on reed thickness and to ± 0.005 inch on reed length and root radius.

Machining of the beams was done in successively reduced depths of cut so that final material surfaces would be as free as possible of residual machining stress. For example, the last four cuts were only 0.001, 0.001, 0.0005 and 0.0005 inch thick, respectively. The last operation was a hand polish to an 8 rms surface finish. Specimens were inspected for conformity with these tolerances prior to test.

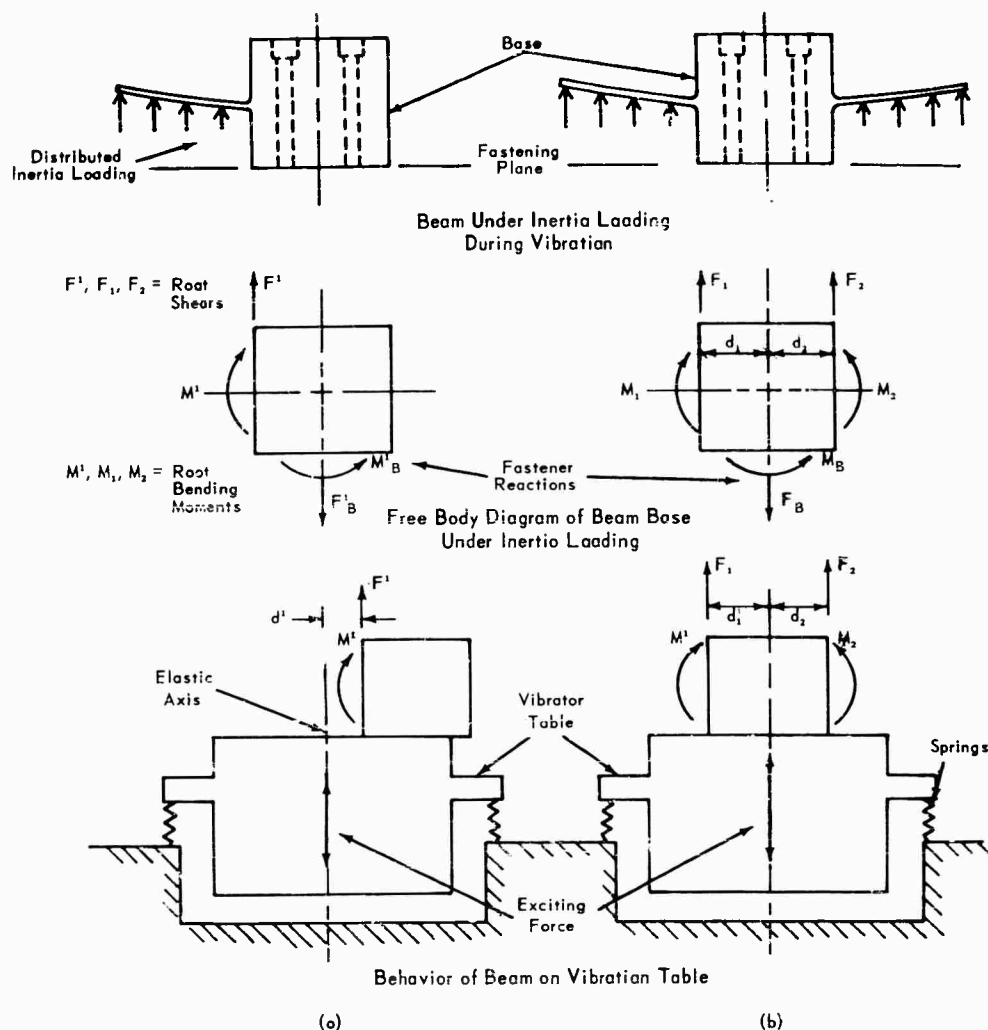


Fig. 1 - Comparison of behavior of (a) single and (b) double reed cantilever beams subject to vibration

ERRORS

Errors Due to External Damping

Material damping is an internal energy loss process. To measure its value accurately, it is necessary to eliminate, reduce, or account for damping contributed from external sources.

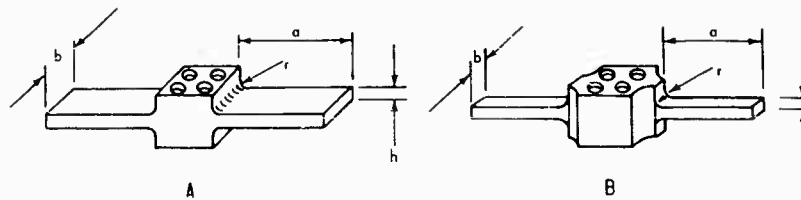
In this investigation, external damping arises from joint damping, eddy current damping and air damping. Joint damping is virtually eliminated by securely clamping the beam specimen to the vibrator table and by eliminating, through design, conditions which foster excessive loads on the joint. Eddy current damping arises from the movement of the beam in the magnetic field of the electrodynamic exciter.

Tests were run on specimens in which the dc field current of the exciter was varied from 10 to 40 amperes. No measurable change in response was observed under these conditions. It was concluded the eddy current damping was negligible in these tests. All subsequent tests were run at an 8-ampere field current. Air damping and energy transfer to the air was eliminated by testing in a vacuum.

Measurement Errors

It was previously shown that the specimen damping coefficient is related to the magnification factor at resonance. Therefore, any errors in producing and measuring the input and output amplitudes must be eliminated.

TABLE 1
Beam Geometry



Beam Type	Thickness h (in.)	Width b (in.)	Length a (in.)	Radius r (in.)	First Mode Frequency, Nominal (cps)
A	0.100	1.000	14.758	0.100	15
A	0.100	1.000	10.436	0.100	30
A	0.100	1.000	6.832	0.100	70
B	0.100	0.500	4.667	0.100	150
B	0.100	0.500	3.300	0.100	300
B	0.100	0.250	2.161	0.100	700
B	0.100	0.250	1.476	0.100	1500
B	0.050	0.250	2.334	0.050	300
A	0.200	1.000	9.334	0.200	75

The technique employed in this investigation requires a translational rigid body response of the beam-vibrator table system in the direction of the exciting force. The appearance of a coupled rocking mode on the system presents two problems in evaluating the relation between the input excitation and the output amplitudes of the reeds, and the amount of beam energy transferred to or dissipated in the vibrator table support system. The use of the tuned double reed cantilever beam virtually eliminated these problems.

Since material damping is small, a high Q may be expected. From Eq. (6c) it can be seen that errors in measuring δ_o and δ_{res} are critical, particularly with respect to δ_o which may be orders of magnitude smaller than δ_{res} . The input displacement δ_o was derived by measuring the input frequency and acceleration with a calibrated high sensitivity, high signal-to-noise ratio, accelerometer-amplifier system. The system sensitivity was 500 mv/g, the system noise level was about 2 mv, and the lowest measured signal during the tests was about 20 mv for an acceleration of about 0.04 g. The accuracy of this measurement technique was about 3 percent of reading. Ripple in the input displacement was eliminated by energizing the vibrator field with direct current from storage batteries rather than by a rectified alternating current supply.

Reed tip displacements were measured by Optron optical displacement followers, a massless noncontacting method of measurement. The Optrons provided an electrical signal proportional to displacement which permitted the simultaneous measurement and comparison of the two reed tip motions on a meter-oscilloscope arrangement. In addition, it was also possible to compare input and output motions. The accuracy of the Optron measurement system was about 1 percent of full scale.

Overall Accuracy of Data

Measurements taken during this investigation were repeatable within 4.5 percent.

TEST TECHNIQUE CRITERIA

Damping and Resonant Frequency Differences

An analog computer study [4] was made to determine the effects on reed motion caused by differences in damping and resonant frequencies between the two reeds of a given test specimen. The results showed:

1. A 1 percent damping difference produced about a 1-1/2 percent amplitude difference and

no significant phase difference between the two reeds;

2. A 0.1 percent resonant frequency difference produced about a 50 percent amplitude difference and about 60-degree phase angle difference between reeds; and

3. For each reed the phase angle between input and output displacements rapidly changed at frequencies very close to the resonant frequency of each reed.

It was concluded from this study that it is critical for each reed to have the same natural frequency if valid data are to be obtained. It also indicated that the phase angle difference between the two reeds can be used as a highly accurate means of tuning the reeds to the same frequency.

Determination of Resonant Frequency

The natural frequencies of the reeds must be experimentally determined before material damping data are obtained. During this determination, it was observed that two significant frequencies appear: a "notch" frequency at which the input (root) amplitude reached a minimum for a fixed input force amplitude, and a "peak" frequency at which the output (tip) amplitude reached a maximum for the same fixed force input amplitude (Fig. 2). The difference between these frequencies was small. It was also observed that large differences in magnification factor existed when the reeds were excited at the "notch" or "peak." This raised the questions, "What are the 'notch' and 'peak' frequencies?" and "At what frequency do we excite the test specimen?"

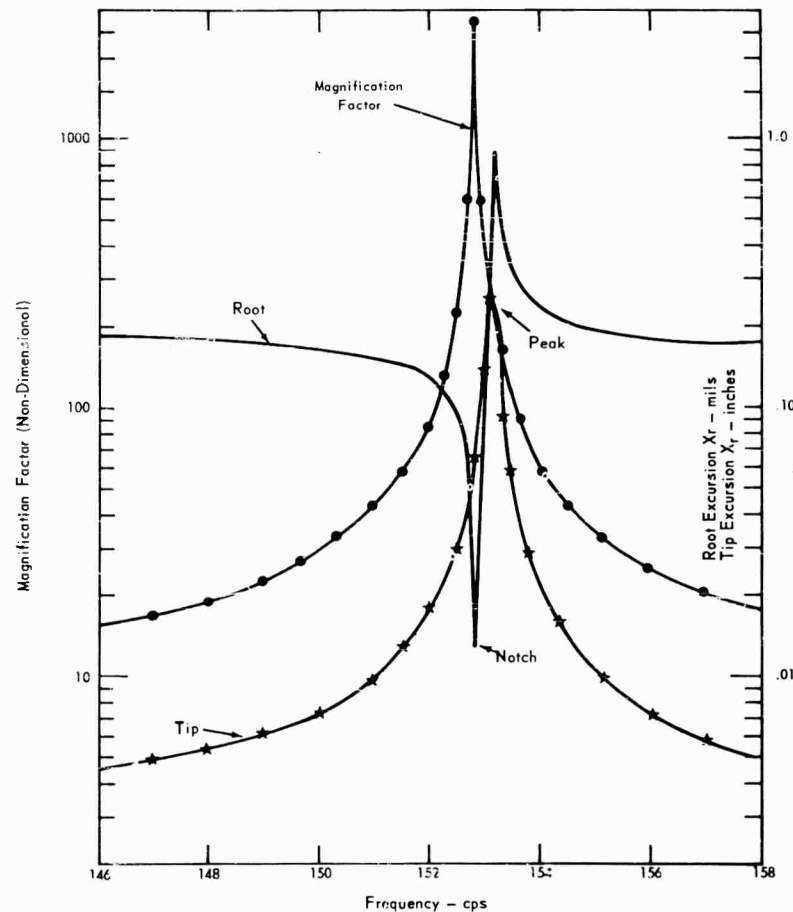


Fig. 2 - Magnification factor plot 150-cps
Beam A-10, 0.10 inch thick

To answer these questions, a simplified analysis was performed. The following assumptions were made:

1. The beam-vibrator table system is a two-degree-of-freedom system with lumped parameters.

2. The system is responsive only in translational modes.

3. Damping is neglected since it is very small and has no effect on resonant frequencies.

A schematic arrangement of the system is shown in Fig. 3. The differential equations of motion for the system are:

$$m_v \ddot{x}_v + (k_v + k_b) x_v - k_b x_b = P_o \sin \omega t \quad (9a)$$

and

$$m_b \ddot{x}_b + k_b (x_b - x_v) = 0. \quad (9b)$$

The solutions to these equations are

$$x_v = \left\{ \frac{1 - \left(\frac{\omega}{\omega_b}\right)^2}{\left[1 - \left(\frac{\omega}{\omega_b}\right)^2\right] \left[1 + \frac{k_b}{k_v} - \frac{\omega^2}{\Omega^2}\right] - \frac{k_b}{k_v}} \right\} \frac{P_o}{k_v} \sin \omega t \quad (10a)$$

and

$$x_b = \left\{ \frac{1}{\left[1 - \left(\frac{\omega}{\omega_b}\right)^2\right] \left[1 + \frac{k_b}{k_v} - \frac{\omega^2}{\Omega^2}\right] - \frac{k_b}{k_v}} \right\} \frac{P_o}{k_v} \sin \omega t, \quad (10b)$$

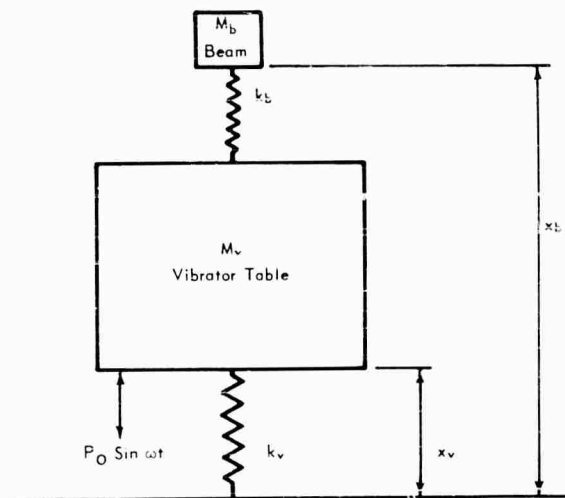


Fig. 3 - Model for analysis of beam-vibrator combination as two-degree-of-freedom system

where

ω = exciting frequency,

$\omega_b = \sqrt{\frac{k_b}{m_b}}$ = natural frequency of the beam,

$\Omega = \sqrt{\frac{k_v}{m_v}}$ = natural frequency of vibrator table assembly,

x_v = displacement of m_v with respect to ground, and

x_b = displacement of m_b with respect to ground.

By setting the denominators of Eqs. (10a) and (10b) equal to zero, the following expression is obtained:

$$\omega^2 = \frac{\omega_b^2}{2} \left\{ \left[1 + \frac{\Omega^2}{\omega_b^2} \left(1 + \frac{k_b}{k_v} \right) \right] \pm \sqrt{\left[1 + \frac{\Omega^2}{\omega_b^2} \left(1 + \frac{k_b}{k_v} \right) \right]^2 - 4 \frac{\Omega^2}{\omega_b^2}} \right\}. \quad (11)$$

Equation (11) identifies two system resonant frequencies, each of which is different from Ω or ω_b . One of these system resonant frequencies is close to the natural frequency ω_b . This is the "peak" frequency.

It was previously shown that Q is related to the specimen damping coefficient by $g_s = 1/Q$. Q is defined as the magnification factor at resonance or the maximum magnification factor. The magnification factor F for the beam is

$$F = \frac{x_b - x_v}{x_v} = \frac{\left(\frac{\omega}{\omega_b}\right)^2}{1 - \left(\frac{\omega}{\omega_b}\right)^2} \quad (12)$$

and

$$Q = F_{\max} = \infty$$

at $\omega = \omega_b$. It can be seen also from Eq. (10a) that when $\omega = \omega_b$ the displacement of the vibrator table x_v equals 0. Hence, ω_b can be identified by the "notch" frequency.

From this it can be concluded that damping data must be observed when the vibrator table motion is a minimum. This occurs at the "notch"

frequency which is the natural frequency of the test specimen.

Determination of Test Stress Levels

Defining the relation between damping and stress amplitudes was one of the major objectives of this investigation. The use of strain gages suggested a simple and effective method for measuring the stresses but was discarded since it might have introduced additional and uncertain damping from the adhesive joint and from the gage backing material. It was decided that root stresses could best be evaluated by measuring the dynamic displacement of a particular point on the cantilever reed, generally the tip, and computing the stresses from the equations of dynamic displacement [5]:

$$\delta_x = \frac{wl^4}{8EI} \left[\frac{1}{2} \left(\cosh 1.875 \frac{x}{l} - \cos 1.875 \frac{x}{l} \right) - 0.368 \left(\sinh 1.875 \frac{x}{l} - \sin 1.875 \frac{x}{l} \right) \right], \quad (13)$$

$$M_r = EI \left(\frac{d^2 \delta_x}{dx^2} \right)_{x=0} = \frac{(1.875)^2}{8} wl^2, \quad (14)$$

and

$$\sigma_r = \frac{M_r(h/2)}{I} = \frac{1.76 hE \delta_x}{l^2 \left[\frac{1}{2} \left(\cosh 1.875 \frac{x}{l} - \cos 1.875 \frac{x}{l} \right) - 0.368 \left(\sinh 1.875 \frac{x}{l} - \sin 1.875 \frac{x}{l} \right) \right]}, \quad (15)$$

where

δ_x = displacement of cantilever at a distance x from the root,

M_r = bending moment at root,

σ_r = stress at cantilever root,

l = reed length, and

h = reed thickness.

To check the stress σ_r as computed by Eq. (15) experimentally, several of the reeds were instrumented with strain gages after the damping tests were run. These were located on the flat portion of the beam near the root radius. The reeds were excited at predetermined amplitudes δ_x , and the measured stresses were

observed. The stresses computed from Eq. (15) were within 5 percent of these measured stresses. This indicated that the technique of indirect stress measurement was satisfactory and reasonably accurate.

FACILITIES AND INSTRUMENTATION

The following are the major items used in the experimental test setup:

1. Unholtz-Dickie Vibration Exciter Model 100, with maximum vector force of 225 pounds and frequency range of 5 to 5000 cps;
2. Unholtz-Dickie Dial-a-Gain Double Integrator Amplifier Model 610 R;
3. Dc power supply for vibration exciter - 4 Rebat aircraft storage batteries Model R-35, 12-volt, 35-ampere-hour capacity;
4. Krohn-Hite Stable Amplitude, Ultra-Low Distortion Oscillator Model 446, with frequency range of 1 cps to 100 kc, amplitude stability of 0.01 percent, harmonic distortion of 0.02 percent, and live frequency modulation of 0.01 percent;
5. Endevco Accelerometer Model 2217;
6. Endevco Power Supply Model 2623;
7. Endevco Input Amplifier Model 2C14B;
8. Optron Displacement Follower Model 701, power supply Model 702, with frequency response flat within 0.01 percent from dc to 3 kc, displacement range of 12 microinches to 2 inches by selection of appropriate lenses, frequency resolution to less than 0.07 percent, and drift of less than 0.01 percent per hour;
9. Dual beam oscilloscope, Tektronic Type 502; and
10. True rms voltmeter, Ballantine Laboratories Model 320, with frequency range of 5 to 5000 kc and voltage range of 100 microvolts to 320 volts rms.

Figure 4 shows the schematic arrangement of the instrumentation.

TEST PROCEDURE

Application of Optical Tracking Targets to Test Specimen

Beam specimens were cleaned with acetone or trichlorethylene to remove all dirt and oil

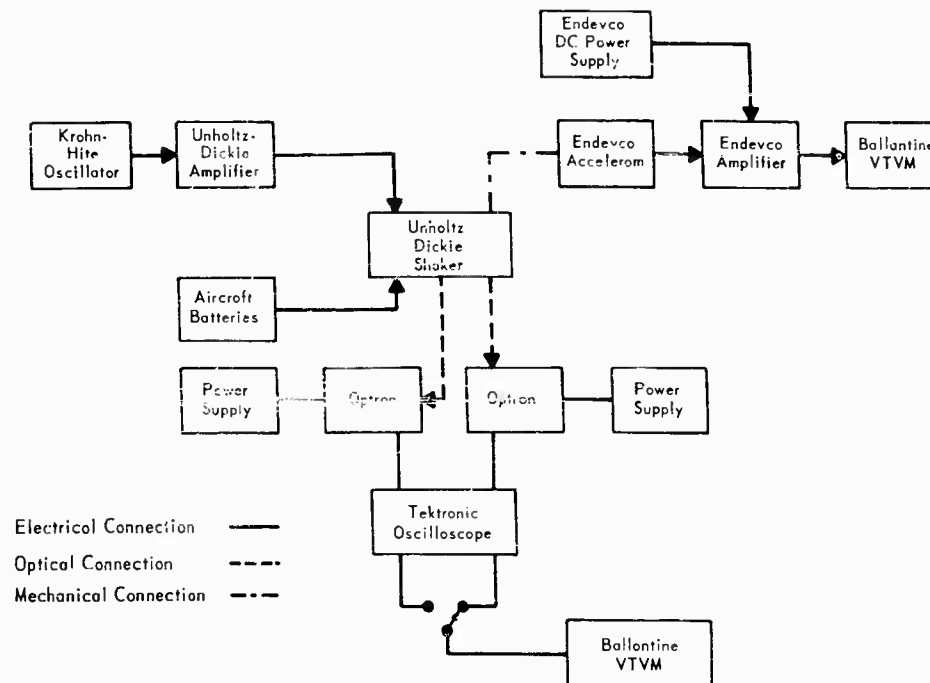


Fig. 4 - Schematic arrangement of instrumentation

film. Adhesive-backed targets were cut to a height equal to the thickness of the reeds and to a width of 1/8 inch. Four targets were applied to the tips of the reeds as shown in Fig. 5. Where the tip amplitudes of the reeds were expected to exceed the range of the Optron Displacement Follower, the targets were moved a known distance in from the tip. The displacement of this point is related to the tip displacement through the bending curve equation. Four symmetrically located targets were used to limit unbalance in the reeds.

Dynamic Beam Balance (Tuning the Reeds)

After the targets were attached, the test specimen was fastened to the vibrator table by four No. 10 cap screws with about 20-inch-pounds torque per screw. Two Optrons were focused or "locked on" the targets, one at each reed. The outputs of the Optrons were fed into a dual beam oscilloscope. The following procedure was then performed:

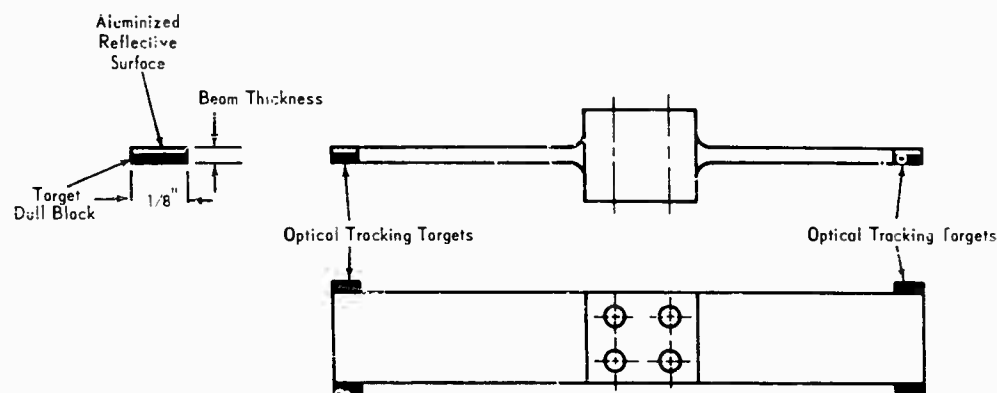


Fig. 5 - Location of optical tracking targets

1. The test specimen was excited with a low-level fixed force amplitude through a frequency range of about 5 percent below and above the calculated natural frequency of the reeds.

2. The Optron output signals were observed on the oscilloscope, noting the frequency at which each reed reached its maximum amplitude and the phase angle between amplitudes as each reed passed through its maximum amplitude (Fig. 6). If the phase angle was zero, the two reeds were tuned to the same natural frequency.

3. Where a phase angle existed, a trial mass was added to the tip of the higher natural frequency reed and Steps 1 and 2 were repeated.

4. If a phase angle still existed after Step 3, then by further trial and error, additional mass was added or some of the previously added mass was removed until the phase angle was zero, indicating that the reeds were tuned to the same natural frequency. The addition or removal of mass was determined by the magnitude and shift in the phase angle, Figs. 6b and 6c.

The added masses consisted of small pieces of plastic electrical tape about 1/16 inch square, symmetrically located on the reed tip to prevent twist under dynamic conditions. The masses were placed at the tip where they are dynamically most effective and where they least affect the specimen damping.

When the reeds were tuned to the same frequency, it was observed, during a frequency sweep, that the displacements were in phase and the peak amplitudes were within 3 percent of each other.

Test Run in Air

1. Predetermined root stress levels were selected at which the tests were to be performed. For the aluminum reeds, the stresses covered the range of 5000 to 20,000 psi in increments of 5000 psi.

2. Reed amplitudes at the target locations were computed from the root stresses.

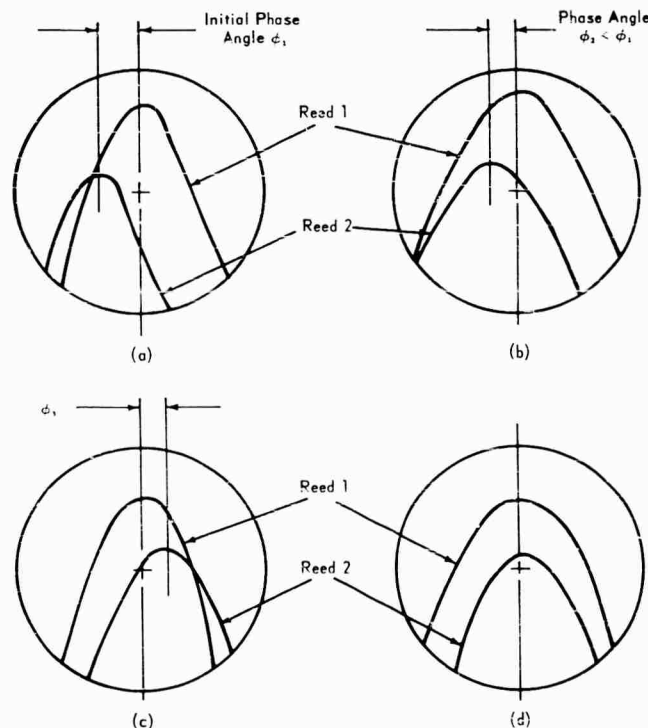


Fig. 6 - Reed tip displacement as seen on dual beam oscilloscope: (a) initial condition, Reed 1 lower natural frequency than Reed 2; (b) after insufficient trial mass has been added; (c) after excessive trial mass has been added; and (d) final condition, reeds tuned to same frequency

3. The accelerometer was attached to the vibration table adjacent to the base block of the tuned test specimen. The Optrons were "locked on" the reed targets. Instrumentation was hooked up as shown in Fig. 4.

4. The "notch" frequency was located by exciting the test specimen with a very low constant force amplitude.

5. The Dial-a-Gain amplifier was adjusted until the predetermined amplitude at the target was obtained.

6. Root acceleration, target displacement, and excitation (notch) frequency were recorded as indicated on the rms voltmeter and oscillator.

7. Steps 5 and 6 were repeated for each predetermined target amplitude.

Test Run in Vacuum

1. A specially designed vacuum chamber was installed over the test specimen and evacuated to 0.2 torr.

2. Steps 4 through 7 were repeated.

RESULTS

Before proceeding with the main part of the investigation, a study was made to determine

whether a stress limit existed beyond which the material damping properties suddenly or significantly changed behavior. A nominal 70-cps resonant cantilever beam was tested in a vacuum through the range of 15,000 to 42,000 psi root stress. The results are shown in Fig. 7, Run 1. Immediately after Run 1, the beam was tested through the range of 8000 to 27,000 psi root stress. These results are shown in Fig. 7, Run 2.

From Run 1, it was observed that damping very slowly increased with stress amplitude between 20,000 and 35,000 psi but drastically changed above 35,000 psi. From Run 2, it was observed that damping remained constant between 8000 and 20,000 psi and noticeably increased with stress amplitude between 20,000 and 27,000 psi. Also, the damping in Run 2 had permanently increased in the lower stress amplitude range after the beam was subjected to the near-yield stresses of Run 1. As a consequence, tests were limited to stress levels up to 20,000 psi to maintain the original material damping characteristics of the beams.

The results of the investigation for aluminum 2024-T4 are shown in Tables 2 and 3 and Figs. 8 through 13. Figures 8 through 10 are plotted in accordance with the log form of Eq. (8b):

$$\log g_s = \log \frac{k'}{\omega_1} + \left(\frac{n}{n+1} \right) \log a.$$

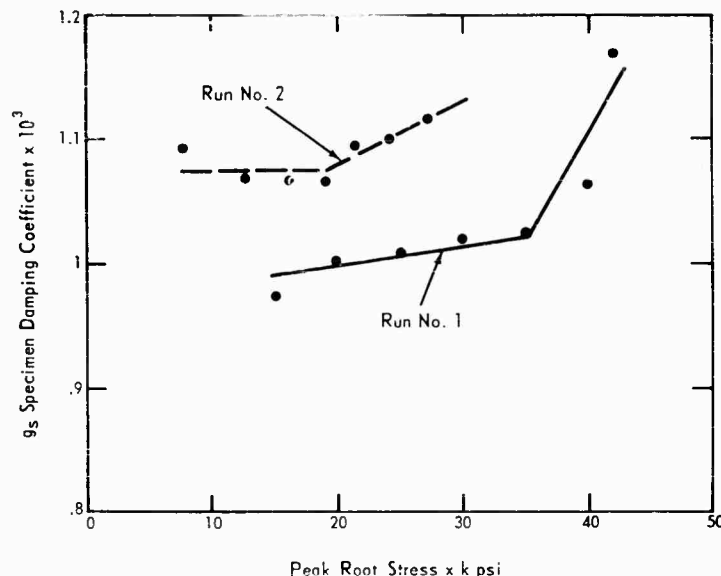


Fig. 7 - High stress on beam (Run 1) permanently changes damping coefficient at lower stress levels (Run 2)

TABLE 2
Damping in Air

Resonant Frequency		Beam Thickness b (in.)	Root Stress (psi)	Root Acceleration (g)	Displacement Double Amplitude		Q	Damping Coefficient ($g \times 10^{-4}$)
Nominal (cps)	Actual (cps)				Root $\sigma \times 10^3$ (in.)	Tip Res (in.)		
15	15.16	0.100	4800	0.056	4.79	1.02	136	73.4
			7200	0.104	8.88	1.54	110	90.6
			9600	0.167	14.3	2.05	91.8	109
			12000	0.234	20.0	2.56	81.6	123
			14400	0.297	25.1	3.07	78.0	128
			16800	0.354	30.1	3.58	75.9	132
			19200	0.448	38.3	4.09	68.2	147
30	30.18	0.100	4700	0.058	1.24	0.505	259	38.6
			7200	0.121	2.61	0.768	187	53.6
			9500	0.189	4.05	1.01	160	62.6
			12000	0.290	6.23	1.28	131	76.1
			14300	0.373	8.02	1.53	122	82.1
			16700	0.475	10.2	1.79	112	89.3
			19200	0.561	12.1	2.05	109	92.1
70	71.50	0.100	4700	0.0495	0.189	0.215	725	13.8
			7100	0.0931	0.356	0.323	578	17.3
			9400	0.157	0.594	0.432	465	21.5
			11900	0.255	0.977	0.543	355	28.2
			14200	0.361	1.38	0.652	302	33.2
			16700	0.471	1.80	0.764	270	37.0
			19000	0.592	2.26	0.873	246	40.7
150	153.2	0.100	4400	0.0472	0.0392	0.0946	1540	6.50
			6600	0.0790	0.0656	0.142	1378	7.26
			8900	0.123	0.102	0.191	1190	8.40
			11100	0.173	0.144	0.237	1052	9.50
			13300	0.237	0.197	0.284	920	10.9
			15800	0.333	0.275	0.337	785	12.8
			18100	0.428	0.356	0.385	690	14.5
300	306.4	0.100	4700	0.0511	0.0106	0.0505	3030	3.30
			7100	0.0890	0.0185	0.0762	2630	3.80
			9500	0.130	0.0263	0.102	2420	4.13
			11900	0.176	0.0367	0.127	2220	4.51
			14300	0.242	0.0503	0.153	1945	5.14
			16700	0.307	0.0639	0.178	1785	5.60
			19100	0.386	0.0803	0.204	1630	6.13
700	715.8	0.100	4800	0.065	0.00248	0.0221	5680	1.76
			7200	0.099	0.00380	0.0331	5550	1.80
			9600	0.145	0.00552	0.0441	5100	1.96
			12000	0.202	0.00770	0.0552	4590	2.18
			14400	0.263	0.0101	0.0661	4180	2.39
			16900	0.341	0.0130	0.0776	3800	2.63
			19000	0.407	0.0156	0.0869	3560	2.81
1500	1571	0.100	4600	0.056	0.000446	0.0098	14050	0.712
			6900	0.090	0.000710	0.0148	13300	0.752
			9300	0.123	0.000975	0.0199	13020	0.768
			11600	0.156	0.00123	0.0248	12900	0.776
			14000	0.196	0.00153	0.0298	12420	0.805
			16300	0.246	0.00195	0.0348	11390	0.878
			18700	0.303	0.00240	0.0399	10620	0.942
70	76.25	0.200	4700	0.0168	0.0565	0.200	2260	4.43
			7000	0.0303	0.102	0.297	1865	5.36
			9300	0.0483	0.162	0.397	1565	6.39
			11600	0.0725	0.241	0.498	1315	7.60
			14000	0.100	0.337	0.599	1135	8.82
			16400	0.132	0.444	0.699	1000	9.99
			18700	0.173	0.581	0.799	880	11.4
300	314.6	0.050	4700	0.158	0.0312	0.0507	1040	9.62
			7100	0.264	0.0521	0.0762	935	10.7
			9500	0.375	0.0739	0.101	878	11.4
			11800	0.506	0.0999	0.126	805	12.4
			14200	0.677	0.134	0.152	725	13.8
			16500	0.863	0.170	0.177	662	15.1
			19000	1.11	0.216	0.203	602	16.6

TABLE 3
Damping in Vacuum

Resonant Frequency		Beam Thickness h (in.)	Root Stress (psi)	Root Acceleration (g)	Displacement Double Amplitude		Q	Damping Coefficient ($g \times 10^3$)
Nominal (cps)	Actual (cps)				Root $\times 10^3$ (in.)	Tip Res (in.)		
15	15.18	0.100	4600	0.0223	1.89	1.01	342	29.2
			7200	0.0345	2.93	1.53	332	30.1
			9600	0.0405	3.43	2.04	379	26.4
			12000	0.0510	4.33	2.55	376	26.6
			14400	0.0632	5.36	3.06	365	27.4
			16800	0.0783	6.65	3.57	342	29.2
			19200	0.0833	7.07	4.08	369	27.1
30	30.30	0.100	4800	0.0307	0.660	0.510	493	20.27
			7200	0.0433	0.924	0.774	535	18.71
			9600	0.0560	1.18	1.02	551	18.13
			12000	0.0729	1.56	1.29	527	18.96
			14400	0.0870	1.85	1.54	532	18.80
			16700	0.101	2.14	1.79	534	18.73
			19300	0.115	2.44	2.06	539	18.55
70	71.60	0.100	4800	0.0340	0.132	0.217	1047	9.55
			7300	0.0520	0.201	0.326	1037	9.64
			9700	0.0690	0.266	0.434	1045	9.57
			12100	0.0860	0.331	0.546	1052	9.50
			14500	0.103	0.395	0.656	1059	9.44
			16900	0.120	0.461	0.766	1060	9.43
			19400	0.135	0.518	0.874	1077	9.28
150	153.2	0.100	4500	0.0370	0.0308	0.096	1990	5.02
			6800	0.0570	0.0474	0.145	1960	5.11
			9000	0.0760	0.0632	0.192	1940	5.15
			11300	0.0930	0.0774	0.240	1980	5.05
			13400	0.114	0.0948	0.287	1935	5.17
			15800	0.132	0.110	0.339	1965	5.09
			18000	0.149	0.124	0.384	1980	5.05
300	306.5	0.100	4700	0.0360	0.0075	0.0497	4240	2.36
			7000	0.0554	0.0115	0.0751	4170	2.40
			9400	0.0742	0.0154	0.0999	4140	2.42
			11700	0.0925	0.0193	0.125	4150	2.41
			14000	0.111	0.0231	0.150	4140	2.42
			16300	0.128	0.0267	0.175	4180	2.39
			18900	0.150	0.0312	0.201	4140	2.42
700	716.2	0.100	4800	0.0420	0.00159	0.0218	8770	1.14
			7100	0.0630	0.00240	0.0326	8720	1.15
			9400	0.0850	0.00323	0.0433	8570	1.17
			11900	0.107	0.00405	0.0545	8640	1.16
			14300	0.126	0.00476	0.0654	8770	1.14
			16700	0.147	0.00558	0.0766	8770	1.14
			19200	0.169	0.00640	0.0880	8770	1.14
1500	1572	0.100	4600	0.038	0.000303	0.0098	20600	0.485
			6900	0.054	0.000423	0.0147	21900	0.456
			9200	0.071	0.000565	0.0197	22200	0.450
			11500	0.088	0.000700	0.0246	22400	0.446
			13800	0.109	0.000839	0.0295	22500	0.445
			16300	0.130	0.00103	0.0348	21600	0.463
70	76.26	0.200	4900	0.0095	0.0326	0.212	4150	2.41
			7200	0.0137	0.0460	0.310	4290	2.33
			9700	0.0186	0.0625	0.413	4250	2.35
			12000	0.0255	0.0856	0.513	3880	2.58
			14400	0.0319	0.107	0.616	3660	2.73
			16500	0.0368	0.124	0.706	3650	2.74
			19200	0.0453	0.152	0.821	3450	2.90
300	314.8	0.050	4500	0.126	0.0248	0.0480	1228	8.15
			6800	0.191	0.0377	0.0733	1238	8.08
			9200	0.257	0.0506	0.0980	1233	8.11
			11300	0.324	0.0639	0.121	1205	8.30
			13800	0.387	0.0763	0.147	1230	8.13
			16000	0.448	0.0884	0.171	1233	8.11
			18400	0.514	0.101	0.197	1240	8.07

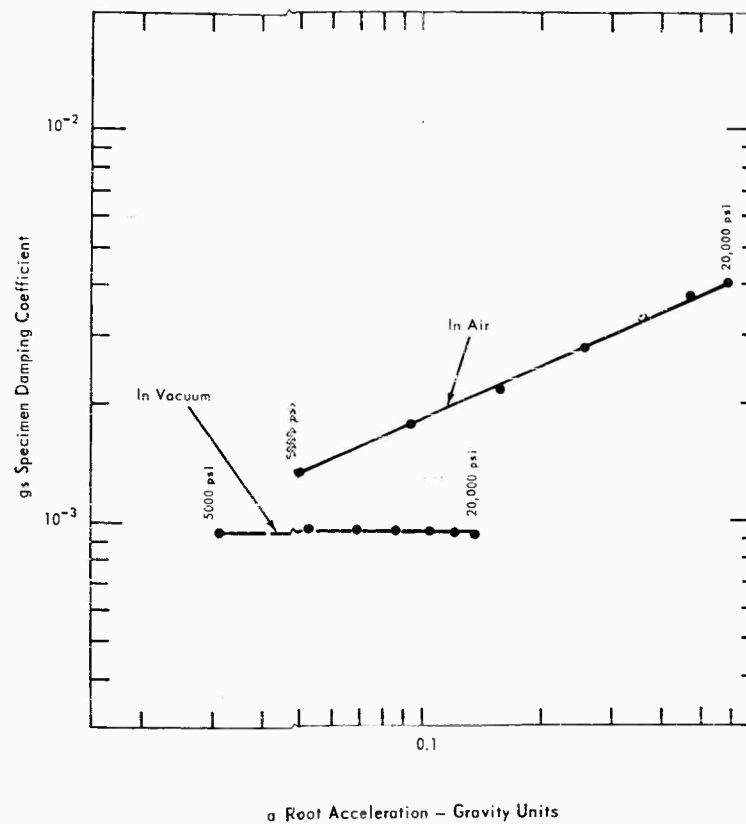


Fig. 8 - Damping in vacuum as in air for nominal 70-cps beam stressed between 5000 and 20,000 psi at root

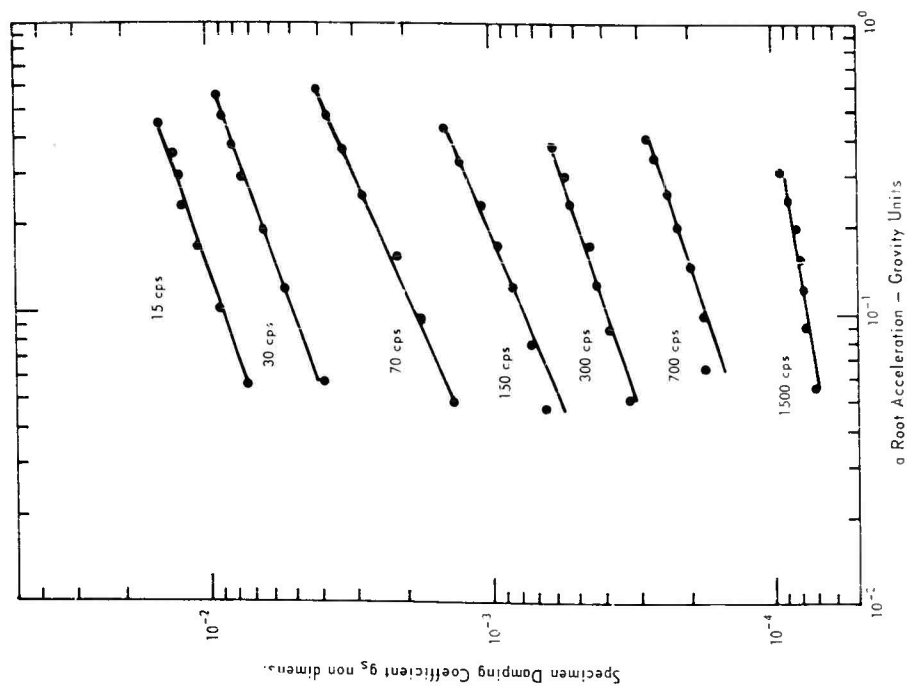


Fig. 9 - Results of damping in air for seven 0.1-inch thick aluminum cantilever beams; resonant frequencies shown

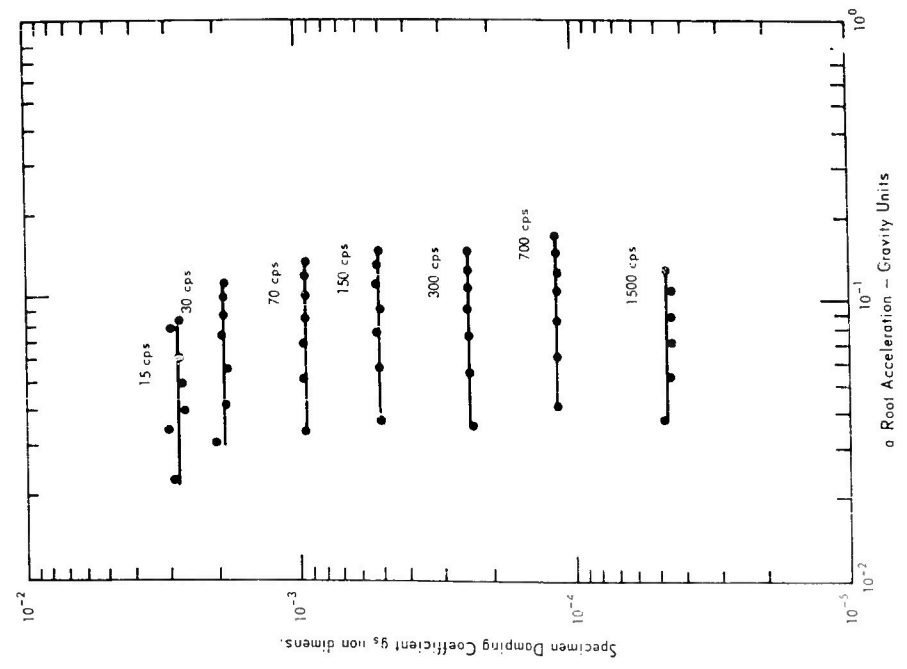


Fig. 10 - Results for seven resonant beams of 0.1-inch thick aluminum tested in vacuum of 0.2 mm Hg

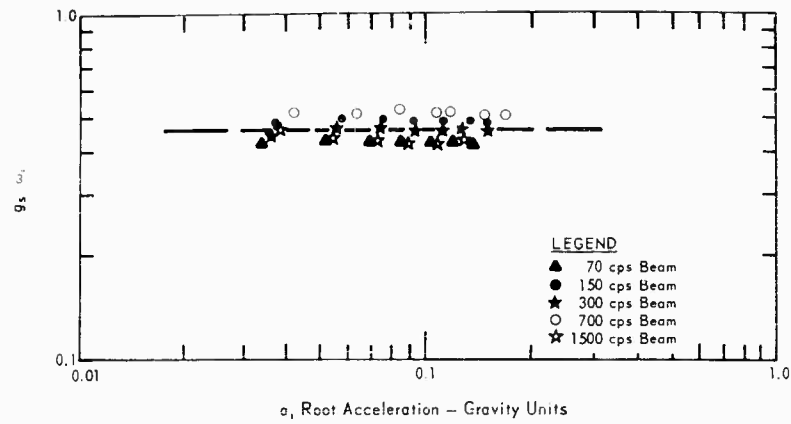


Fig. 11 - Results for five resonant beams of 0.1-inch thick aluminum tested in vacuum of 0.2 torr

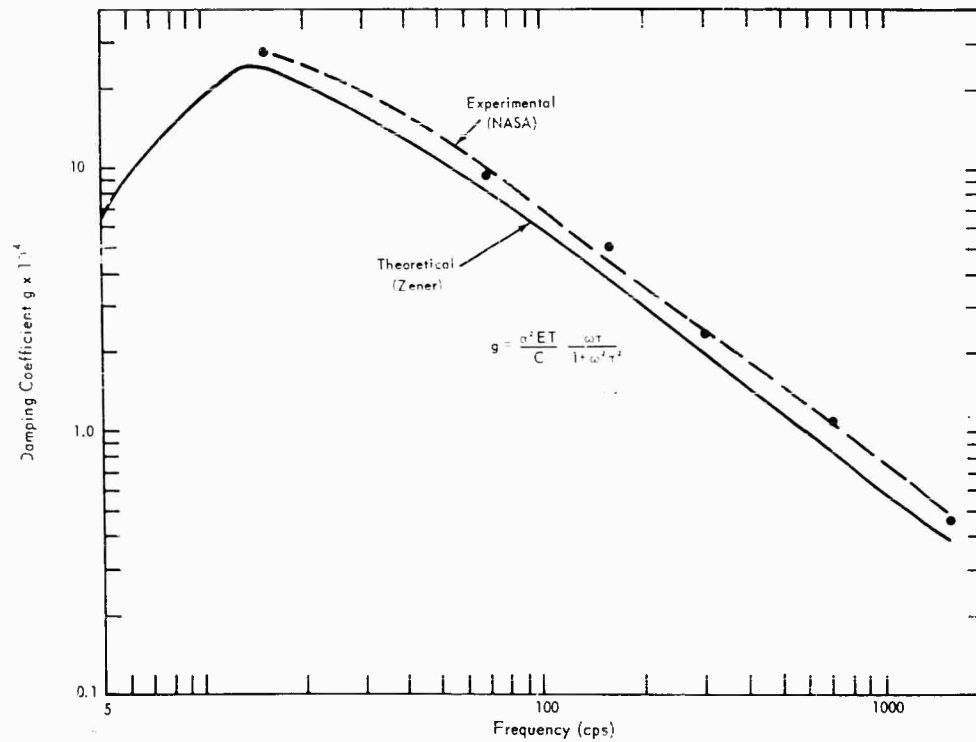


Fig. 12 - Damping calculated by theoretical thermal relaxation equations vs that measured experimentally (for 0.10-inch thick aluminum beams)

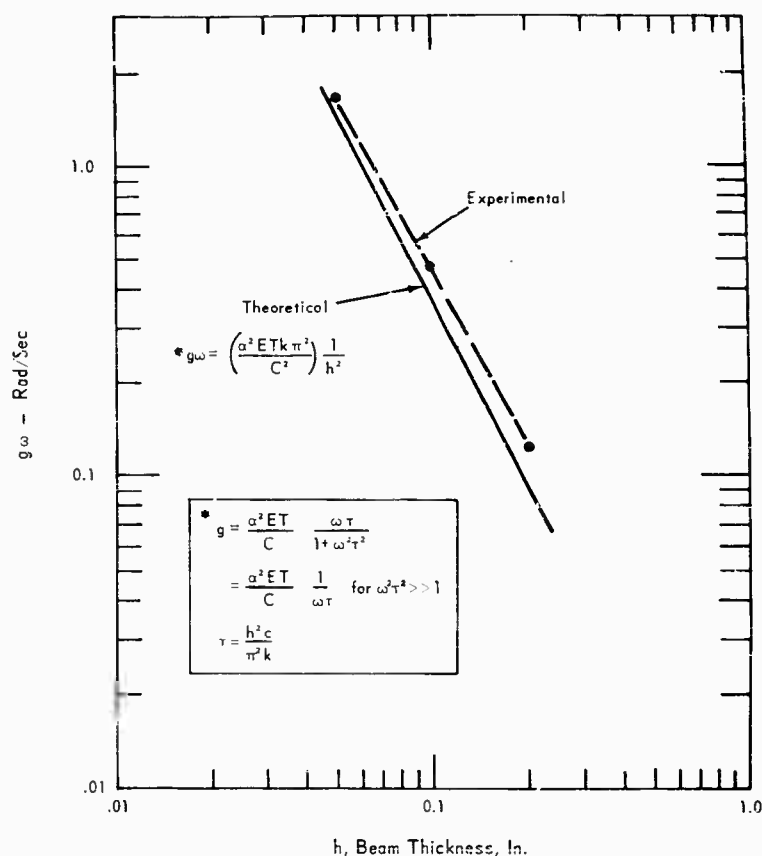


Fig. 13 - $g\omega$ measured on three thicknesses of beams vs theoretical $g\omega$ for beams in same thickness range ($\omega^2\tau^2 \gg 1$)

Figure 11 is plotted in accordance with a modified form of Eq. (8b):

$$\log g_s \omega_1 = \log k' + \left(\frac{n}{n+1} \right) \log \sigma.$$

Figure 8 compares damping for a nominal 70-cps resonant frequency beam as measured in air at ambient pressures and in a vacuum of 0.2 torr and over the same stress amplitude range of 5000 to 20,000 psi. The "in air" plot shows the nonlinear behavior of damping in air where the quantity n has a value of 0.78 as calculated from the slope of the plot. This compares with 0.77 as reported by Crandall [1]. The slope of the "in vacuum" plot is zero, hence the quantity n is zero indicating that the damping in vacuum is independent of stress amplitude. It should be noted here that $g_s = g$ where $n = 0$ [1].

Figure 9 shows the nonlinear behavior of damping in air for the series of beams tested. It shows that damping is frequency and amplitude

dependent. The amplitude dependence appears to be with respect to displacement or velocity and not with respect to stress. This is further revealed on examination of Fig. 10. The nonlinear behavior then may be attributed to air damping.

Figure 10 shows the behavior of damping in vacuum for the same series of beams. The slopes of all the curves are zero, hence n is zero and stress amplitude independence is shown. The damping here is material damping only and its dependence on frequency is clearly evident. Figure 11 further shows the independence of damping on stress amplitude and the constancy of the product $g_s \omega$. Figures 12 and 13 show good correlation with Zener's expression, Eq. (3a).

CONCLUSIONS

1. A unique, simple and accurate technique has been developed for measuring material

damping. Test specimens and test setup are shown in Figs. 14 and 15.

2. Material damping of aluminum 2024-T4 is independent of stress amplitudes up to 20,000 psi and is frequency dependent in the range 15 to 1500 cps.

3. Material damping of aluminum 2024-T4 is independent of stress history at stresses below 20,000 psi.

4. Material damping of aluminum 2024-T4 can be quantitatively evaluated by the Zener relation,

$$g = \frac{1}{2} \frac{E \eta}{E'} \left[\frac{1}{1 + \omega^2 \tau^2} \right]$$

5. Air damping as observed during these tests provides a significant contribution to total damping and may be as much as 10 times greater than material damping.

ACKNOWLEDGMENTS

The authors sincerely appreciate the aid given by Charles Erath and Donald Ochsner with the experimental setup and in obtaining much of the experimental data. Acknowledgment is also made of Herman Gaastra for his assistance with the design of the vacuum covers, John Heine for his work on the analog computer model of the test system, and Margaret Krabill for her contribution in preparing the manuscript for publication.

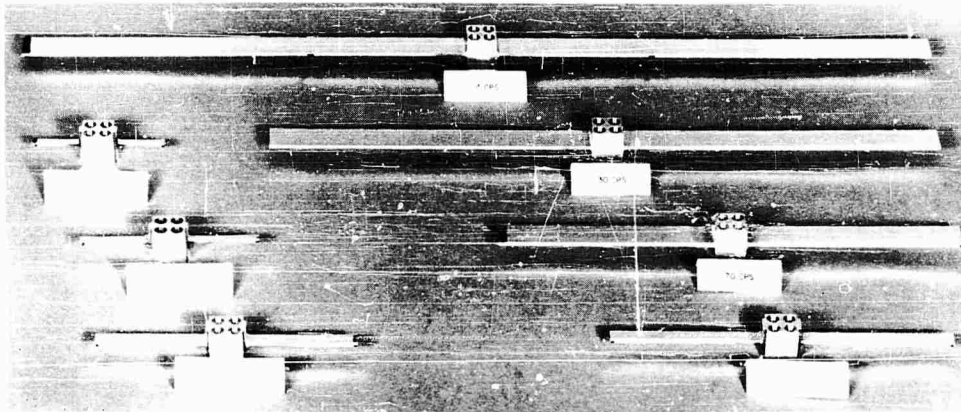
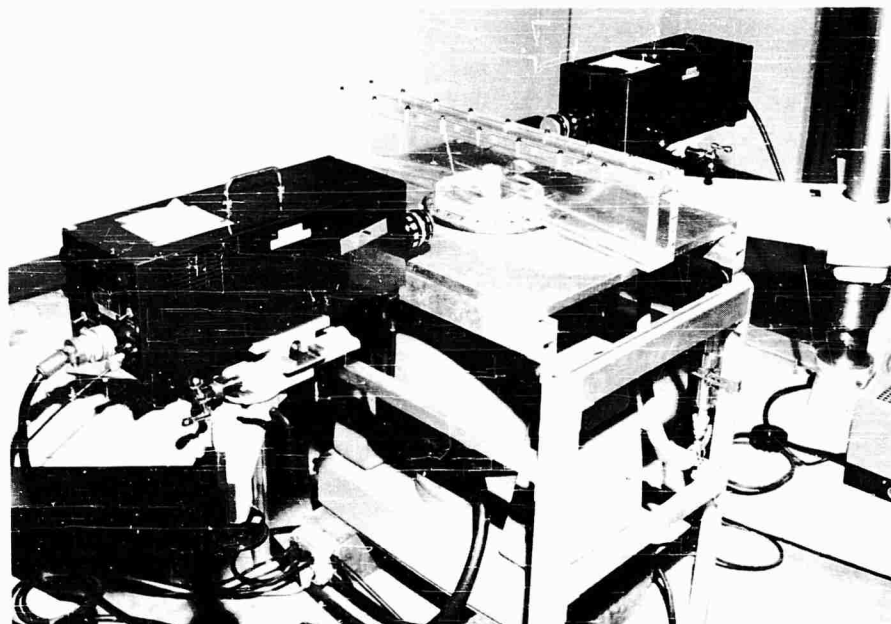


Fig. 14 - Test beams, 0.100 inch thick, showing location of Optron targets and added masses

Fig. 15 - Arrangement for vacuum testing of beams showing Optrons, vacuum chamber, test specimen and vibration exciter



REFERENCES

1. S. H. Crandall, "On Scaling Laws for Material Damping," NASA Tech. Note D-1467 (Dec. 1962).
2. C. M. Zener, Elasticity and Anelasticity of Metals (Univ. of Chicago Press, 1948).
3. M. Vet, "Dwell Sweep Correlation Study," Collins Radio Eng. Report 1582; IES Proc., p. 433 (1963).
4. J. Heine, "Analysis of a Model for the Experimental Determination of Damping," Private Communication.
5. L. S. Jacobsen and R. S. Ayre, Engineering Vibrations (McGraw-Hill Book Co., New York, 1958).

* * *

EFFECT OF PRESSURE ENVIRONMENT ON DAMPING OF VIBRATING STRUCTURES

D. G. Stephens and M. A. Scavullo
NASA Langley Research Center
Langley Station, Hampton, Va.

An investigation was conducted to determine the mechanism of the air damping exhibited by rigid bodies of different shapes oscillating in a pressure environment. Circular and rectangular panels, as well as a sphere and cylinder, were attached to cantilever springs and the free decay of an induced oscillation was measured at pressure levels from atmospheric to 4×10^{-2} torr. Data are presented to show the effect of pressure, vibratory amplitude, shape, and surface area on the air damping of the models. Results indicate that the magnitude of the air damping may greatly exceed the structural damping of the system. The air damping associated with the panels is directly proportional to the pressure and amplitude which is indicative of dissipative loads proportional to the dynamic pressure. Furthermore, the panel damping was found to be independent of shape and a nonlinear function of the surface area. The sphere and cylinder exhibit viscous damping characteristics which are in good agreement with available theory.

INTRODUCTION

The vibratory response of a mechanical system is greatly influenced by the presence of damping. In most situations this damping results from the dissipation of energy in such forms as internal hysteresis, interface or joint friction, and external or air damping. This latter form of damping is highly dependent on the magnitude of the pressure environment and, therefore, deserves particular attention in studying the response of systems designed to operate throughout a wide range of pressure. If, for example, the vibration tests of a space vehicle are conducted under atmospheric pressure conditions, the damping level and, consequently, the response will be somewhat different from those in the actual operating environment which involves reduced pressures. Thus, in interpreting and extrapolating the results of such tests, one must understand and treat the effect of the pressure environment on the results.

The purpose of this paper is to present the results of an examination of the nature and magnitude of the air damping exhibited by rigid two- and three-dimensional shapes oscillating in a variable pressure environment. Circular and

rectangular panels, a sphere and a cylinder were attached to cantilever springs and the free decay of an induced oscillation was studied at pressure levels from atmospheric to 4×10^{-2} torr. Data are presented to show the effect of pressure, vibratory amplitude, shape, and surface area on the air damping of the models.

APPARATUS

The test program and subsequent data reduction were directed toward the isolation and examination of the effects of pressure, amplitude, shape, and area on the air damping of common shapes oscillating in a direction perpendicular to their principal surface. A study of the free decay characteristics was deemed most expedient for examining the effects of these variables independently as well as in combination. The models used in the majority of the tests are shown in Fig. 1. The discs and rectangular panels with surface areas of 15, 30, and 45 square inches, as well as the sphere and cylinder having projected areas of 30 square inches, were subjected to vibration at various pressure levels and amplitudes within a bell jar vacuum system.

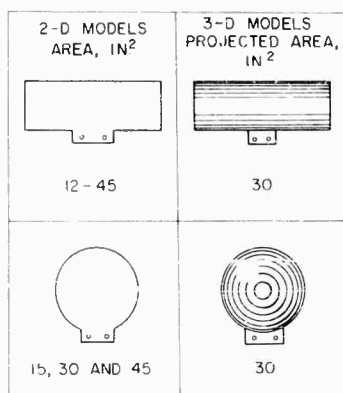


Fig. 1 - Damping models.

The oscillation was provided by the cantilever spring system shown in Fig. 2. The beam, machined from a single piece of stainless steel, had a relatively large foot for mounting to a rigid base plate and a T-section at the tip for attaching the models. In all cases a frequency of 3.8 cps was maintained by adding small tuning masses to the T-section. The excitation was provided by the spring-loaded solenoid. When energized, the slug imparted a static deflection to the beam and upon removal of the current the slug was retracted by the spring. The ensuing oscillation was sensed by a strain gage attached to the root of the beam. The system as shown was enclosed by a bell jar capable of maintaining pressure levels between atmospheric and 4×10^{-2} torr. Additional tests were conducted at atmospheric pressure to better define the dependency of damping on panel area. Nine rectangular panels having surface areas ranging from 12 to 39 square inches were studied using the beam system described above and, in addition, three larger panels having areas of 71.3, 128, and 220 square inches were studied using a larger beam also having a tuned frequency of 3.8 cps.

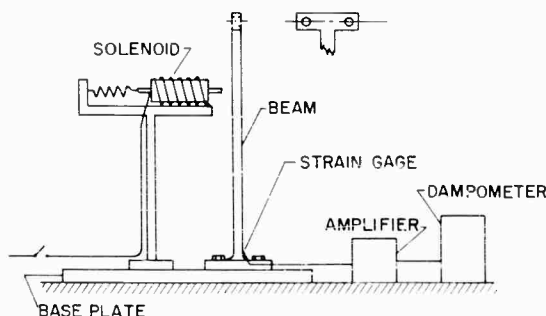


Fig. 2 - Test apparatus and instrumentation

PROCEDURE

The damping characteristics of the beam alone, tuned to 3.8 cps, were studied initially, followed by an examination of the damping of the beam-model system. The procedure was essentially the same in each case. The chamber, when used, was pumped down to the desired pressure level, and for all but the lowest pressure (4×10^{-2} torr), the pump was shut down while the test points were taken. The beam was then deflected, released, and damping of the oscillation was measured at various positions along the envelope. The damping was measured by an electronic dampometer and specified in terms of the logarithmic decrement,

$$\delta = \frac{1}{n} \log \frac{x_0}{x_n} \quad (1)$$

PRESENTATION AND DISCUSSION OF RESULTS

General

For purposes of this investigation, the logarithmic decrement is physically interpreted as the ratio of the energy lost per cycle to twice the total energy [1]:

$$\delta = \frac{\Delta E}{2E} \quad (2)$$

For the system under study, the measured decrements include losses due to the beam (hysteresis, joint friction, air damping, etc.) as well as the air damping of the model or

$$\delta = \frac{\Delta E_a + \Delta E_b}{2E} = \delta_a + \delta_b \quad (3)$$

The air damping attributed to the attached model δ_a is obtained by subtracting the beam damping $\Delta E_b / 2E$, measured in a separate test under identical conditions, from the total measured decrement. These decrements are presented in terms of the variables of interest.

In examining the results, the nature of the resistive or damping forces may be inferred by comparing the measured decrements to those calculated for a single-degree-of-freedom system subjected to known loadings. If, for example, the forces are directly proportional to the velocity (often referred to as viscous) the energy loss per cycle ΔE would equal the work done by the dissipative force, or

NOTE: References appear on page 203.

$$\Delta E = \int_c \dot{x} dx = \int_c c \dot{x} dx, \quad (4)$$

where the velocity is very nearly

$$\dot{x} = x_0 \omega \cos \omega t \quad (5)$$

if the system is lightly damped. Integrating Eq. (4) and dividing the result by twice the maximum energy of the cycle, or

$$2E = M x_0^2 \omega^2 \quad (6)$$

yields a decrement

$$\delta = \frac{\Delta E}{2E} = \frac{\pi c}{M \omega} \quad (7)$$

Thus, in the case of viscous damping, the decrement is independent of the amplitude and inversely proportional to the frequency.

Likewise, a panel subjected to forces proportional to velocity squared will have a decrement of the form

$$\delta = \frac{8}{3} \frac{c x_0}{M} \quad (8)$$

which is a linear function of amplitude and independent of frequency. These two types of damping forces, viscous and velocity squared, are of particular interest because of their common occurrence in steady state aerodynamics.

Beam Damping

The damping associated with the fundamental mode of oscillation of the cantilever beam, tuned to 3.8 cps, is presented in Fig. 3. These data served as a tare for obtaining the air damping from the measured total damping values. The damping factors, in terms of the logarithmic decrement δ , are shown as a function of the pressure for several different tip amplitudes. The tip amplitudes shown are the average tip displacement during the damping measurement. In this case, as well as those to follow, the data points represent an average of five or more measured values. The total damping associated with the beam exhibits a near-linear dependency on pressure in the range between atmospheric pressure and 100 torr. Below 100 torr the damping factors deviate from this linear pressure relationship and approach values at 4×10^{-2} torr which are most probably due to the internal hysteresis and joint friction.

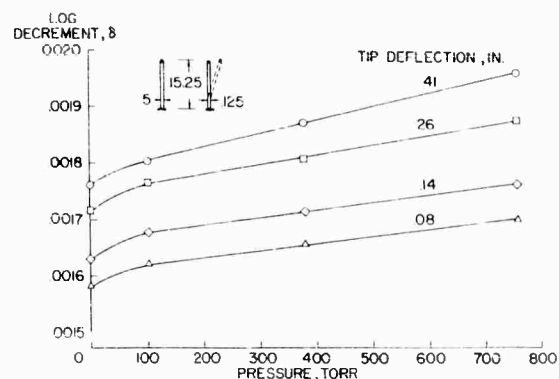


Fig. 3 - Variation of beam damping with pressure

Total Damping of Beam-Model System

A typical sample of the data, as recorded, is shown in Fig. 4 to illustrate the magnitude of the beam damping relative to the total damping. The total damping recorded for the 30-square-inch rectangle mounted on the tip of the beam is presented as a function of pressure and amplitude. The amplitudes refer to the deflection of the center of the panel during the damping measurement and correspond to the beam tip deflections shown in Fig. 3. It is interesting to note the significant increase in the system damping with the addition of the panel. For example, an increase in damping by a factor of approximately five is noted in the high-pressure region. As the pressure is decreased, the values of damping converge to the values measured for the beam alone in the low-pressure region. This indicates that no extraneous damping is introduced into the system with the addition of the panel and, thus, the additional damping may be attributed to the air resistance.

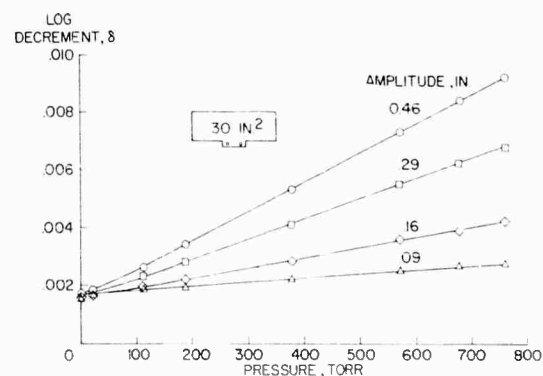


Fig. 4 - Variation of total damping with pressure

Damping of Two-Dimensional Models

Effect of pressure - The dependency of the air damping on the pressure environment is presented in Fig. 5. The air damping, obtained by subtracting the beam damping from the total damping at corresponding pressures and amplitudes, is shown for the 30-square-inch rectangle. The damping factor exhibits a linear dependency on the pressure, and thus density, throughout the range examined. A strong dependency of the damping on the amplitude is also noted, indicating the presence of a nonlinear damping phenomena. Identical trends were noted in the other panels of 15, 30, and 45 square inches and thus these data will be presented in a subsequent section on area and shape.

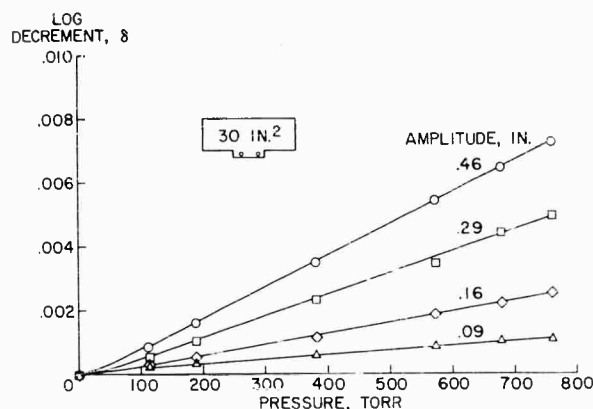


Fig. 5 - Variation of air damping with pressure

Effect of amplitude - The variation of damping with amplitude for the 30-square-inch rectangle is presented in Fig. 6. The trends existing in this case are again representative of the results obtained for the other two-dimensional models. For the range of amplitude examined, the damping is a near-linear function of panel deflection. Because of this linear dependency, the damping is apparently of the velocity-squared type as previously discussed. Thus the resistance force is proportional to the dynamic pressure ρU^2 as would be found in the case of a panel immersed in a steady stream of incompressible fluid. It should be noted that an extension of the faired lines will not intersect the origin. It is probable that in the amplitude range below 0.1 inch, the forces become more viscous in nature and, therefore, the amplitude dependency or slope of the curve is reduced.

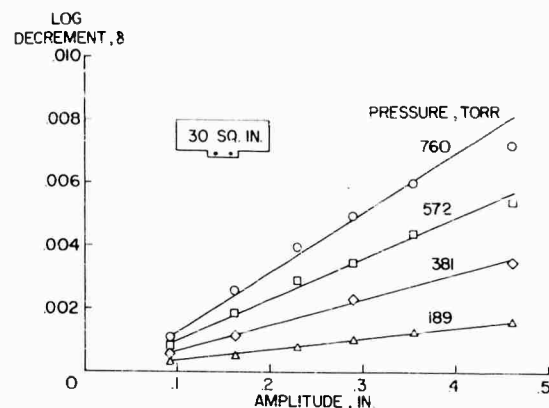
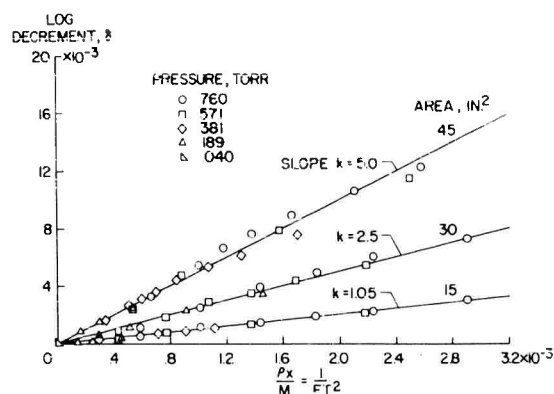


Fig. 6 - Variation of air damping with amplitude

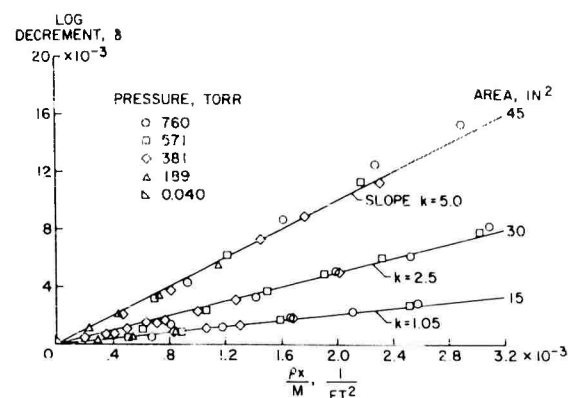
Effect of shape - The effects of panel shape were examined by comparing the damping factors associated with the rectangles and discs of 15, 30, and 45 square inches. In Fig. 7 the decrements, measured over a wide range of pressure and amplitude, are presented as a function of the parameter $\rho x/M$, where ρ is the density of the air within the chamber, x is the amplitude of the panel, and M is the effective mass of the system located at the center of the panel. The symbols indicate the pressure levels at which the measurements were taken. The decrement is a linear function of the parameter $\rho x/M$ which is indicative of velocity-squared damping, Eq. (8). For a particular area, $\delta = k \rho x/M$ where k is the slope of the curve associated with each configuration. In comparing the results of the disc and rectangle, the slopes of the curve k are seen to be independent of shape.

Effect of area - As shown in Fig. 7, the damping increases with panel area but at a much greater rate than one to one. To examine the damping-area relationship in detail, nine rectangular panels having surface areas ranging from 12 to 39 square inches were attached to the beam and studied at atmospheric pressure. In addition, three panels having surface areas of 71.3, 128, and 220 square inches were studied using a larger beam to extend further the range of area. The results of this study are summarized in Fig. 8 where the parameter $\delta M/\rho x (=k)$ is shown for each area. The data of Fig. 7 are indicated by the squared symbols. Results indicate that

$$\delta = 22 \frac{\rho x A^{4/3}}{M}$$



(a) Rectangular plates



(b) Circular plates

Fig. 7 - Variation of air damping with x/M

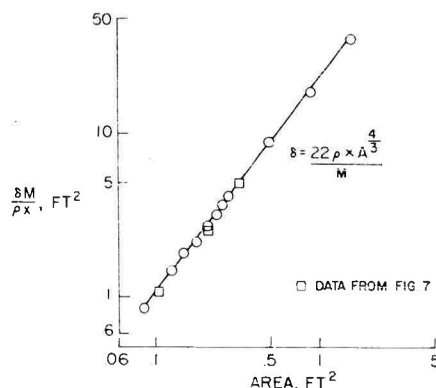


Fig. 8 - Variation of air damping with area for plates

the exponent $4/3$ being determined from the slope of the curve. It appears that within the range of variables covered in these tests, the above relationship can be used for obtaining the variation of air damping with changes in environment.

Limited tests were also conducted within the vacuum system using a beam having a tuned frequency of 21.2 cps and panels with surface areas ranging from 12 to 45 square inches. Results of these tests verify the functional relationship observed in the low-frequency case, i.e.,

$$\delta = \frac{K \rho x A^{4/3}}{M}$$

For amplitudes above 0.1 inch, a constant of proportionality K of 22 appears adequate for

predicting the damping. Below 0.1 inch, the damping ceases to be a linear function of amplitude, as was the case for the low-frequency data, and cannot be adequately represented by the suggested empirical relationship. It may also be noted that the damping values at these low amplitudes are substantially smaller than those associated with the structural damping and it becomes increasingly difficult to ascertain accurately the true contributions of the surrounding air to the overall damping of the system.

Damping of Three-Dimensional Models

Sphere - The problem of sphere performing pendulum oscillations of small amplitude in an incompressible viscous fluid has been examined theoretically by Lamb [2]. The derivation of the resultant force acting on the spherical surface yields a force component which is linearly proportional to and in opposition to the velocity as follows:

$$X = 3\pi\rho a^3 \omega \left(\frac{1}{\beta a} + \frac{1}{\beta^2 a^2} \right) U, \quad (9)$$

where

X = force in opposition to velocity,

ρ = mass density of fluid,

a = radius of sphere,

ω = circular frequency of oscillations,

$\beta = (\omega/2\nu)^{1/2}$,

ν = kinematic viscosity, and

U = velocity.

When substituted into Eq. (7),

$$\delta = \frac{\pi c}{M\omega} = \frac{\pi}{M\omega} \left(\frac{X}{U} \right). \quad (10)$$

The resulting decrement is

$$\delta = \frac{3\pi^2 \rho a^3}{M} \left(\frac{1}{\beta a} + \frac{1}{\beta^2 a^2} \right). \quad (11)$$

The validity of this relationship is shown in Fig. 9 where the damping of the sphere, measured at several amplitudes, is presented as a function of pressure. The data are independent of amplitude, proportional to the square root of the density and are in good agreement with the theoretical curve.

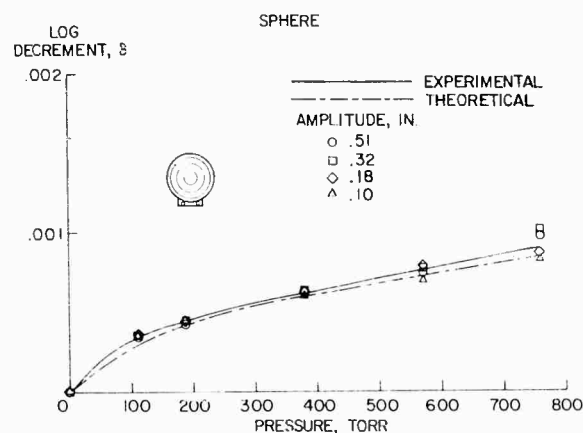


Fig. 9 - Variation of air damping with pressure

Cylinder - A similar theoretical treatment for a cylinder has been presented [3]. The viscous damping force for a cylinder of high length to radius vibrating normal to its length is

$$X = \pi a^2 \rho l \omega \left(\frac{2}{\beta a} + \frac{1}{\beta^2 a^2} \right) U, \quad (12)$$

where a and l are the radius and length of the cylinder, respectively. The resulting decrement for the cylinder is

$$\delta = \frac{\pi^2 a^2 \rho l}{M} \left(\frac{2}{\beta a} + \frac{1}{\beta^2 a^2} \right). \quad (13)$$

The theoretical results are shown in Fig. 10, along with the data measured for the cylinder. In the region of low amplitude, the theory is in

excellent agreement with the experimental results. At higher amplitudes, however, the decrement appears somewhat high, possibly due to end effects or flow separation.

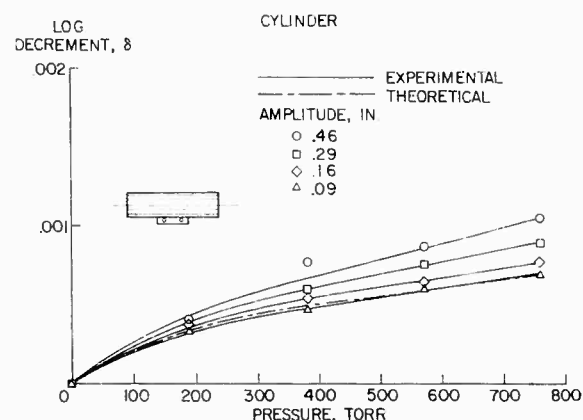


Fig. 10 - Variation of air damping with pressure

CONCLUSIONS

Within the range of variables considered in this investigation the following conclusions are noted:

1. For systems having a relatively large area-to-mass ratio, the magnitude of the air damping may greatly exceed the damping attributed to all other sources. Values of air damping, an order of magnitude greater than the structural damping, were observed during these tests.

2. The damping factors associated with vibrating panels exhibit a near-linear dependency on pressure and vibratory amplitude, which indicates the presence of velocity-squared damping or, more specifically, damping forces proportional to the dynamic pressure.

3. The damping factors associated with panels were found to be independent of shape and proportional to the product of the density, amplitude, and area raised to the 4/3 power, divided by the vibratory mass, i.e.,

$$\delta = \frac{K \rho \omega A^{4/3}}{M}.$$

4. The damping factors associated with the sphere are essentially proportional to the square root of the density, independent of vibratory

amplitude, and in good agreement with available theory based on viscous damping forces.

5. At low amplitude the cylinder exhibits damping factors in excellent agreement with

those predicted by viscous theory. At higher amplitudes the damping exceeds theoretical predictions, possibly due to end effects or flow separation.

REFERENCES

1. William T. Thompson, Mechanical Vibrations, 2nd Ed. (Prentice-Hall, 1953), pp. 55-59.
2. Horace Lamb, Hydrodynamics, 6th Ed. (Dover Publications, 1945), p. 644.
3. G. G. Stokes, Cambridge Philosophical Soc. Trans., 9:8-106 (1851).

* * *

DEVELOPMENT OF HIGHLY DAMPED SUBMARINE MACHINERY FOUNDATION

E. V. Thomas
U.S. Navy Marine Engineering Laboratory

The machinery used in ships generate vibrations which may be amplified due to coincident foundation resonances. Present measures of control are often not adequate. The use of highly damped steel-viscoelastic laminates in a design effectively utilizing the damping is discussed. A shear damped foundation leg is also discussed. Measured attenuation of transmitted vibration by a foundation is presented.

INTRODUCTION

The design of a shipboard machinery foundation sufficiently damped to attenuate machinery vibrations of mounted equipment is rather difficult when the influences of associated dynamic environments entering the design are considered. Three methods are used to reduce vibratory energy transmitted from the machine through isolation mounts and foundation structures to the hull where it is transformed into acoustic energy and radiated into the sea:

1. The foundation design is changed to alter resonant frequencies so that they do not coincide with major forcing frequencies produced by mounted machinery;
2. The foundation design is changed to increase its dynamic stiffness to increase effectiveness of the isolation mounts; and
3. A damping treatment is applied to the foundation to cause losses of resonant vibratory energy by transformation to heat.

A major factor in the design of the machinery mounting system in the submarine environment is its response and resistance to dynamic shock loading, such as that produced by depth charges.

PRESENT APPROACHES TO PROBLEM

A look at the three control methods in a little more detail reveals the problems involved with each method. Resonant frequency control

is a rather cumbersome approach. The time involved, accuracy required in prediction of foundation resonances, and previous knowledge of the machine's vibratory frequency response are all involved. Increasing dynamic stiffness of the foundation to increase the effectiveness of an isolation mount is a good method of controlling the vibratory energy transmitted to the foundation through the mount and of increasing shock resistance. But the method suffers from the disadvantage that it also tends to increase the frequency of the first resonance of the foundation into the range of frequencies more susceptible to detection. Application of a damping treatment to control the magnitude of foundation resonances suffers because of the total weight of damping treatment required to control it to an acceptable value. The combination of increased stiffness and a damping treatment is often used, but it necessitates a much greater damping capacity for resonance control due to the effective spring-dashpot ratio required for sufficient damping.

Originally it was felt that a machinery foundation could be effectively designed with laminated steel-viscoelastic plates having a high inherent damping capacity in place of the conventional welded steel foundation. An experimental study using riveted laminated plates was conducted. Using conventional design techniques with laminates yielded a foundation which had high inherent damping in the plate areas around the isolation mounts, but it was offset by a higher-mass-stiffness ratio in the I-beam sections. The total amount of force transmitted to the hull was about the same as that in the welded steel foundation. This effect is assumed

to be due to shear damping in laminates, a uniplanar action, while machinery foundations are excited in a minimum of three planes. Laminated plates characterized by high damping are inherently weak in the direction of loading where the damping is most effective. This requires laminates to be thicker in cross section than a conventional steel plate used in foundation construction for a

comparable strength. Most machinery foundations use angle, I- or WF-beam, box beam, or pipe configurations in load-carrying members for structural strength. If highly damped laminates are fabricated in any of these shapes, the laminate is prevented from bending in its damping uniplane by the other stiffer members (Fig. 1), with the result that damping is local and ineffective.

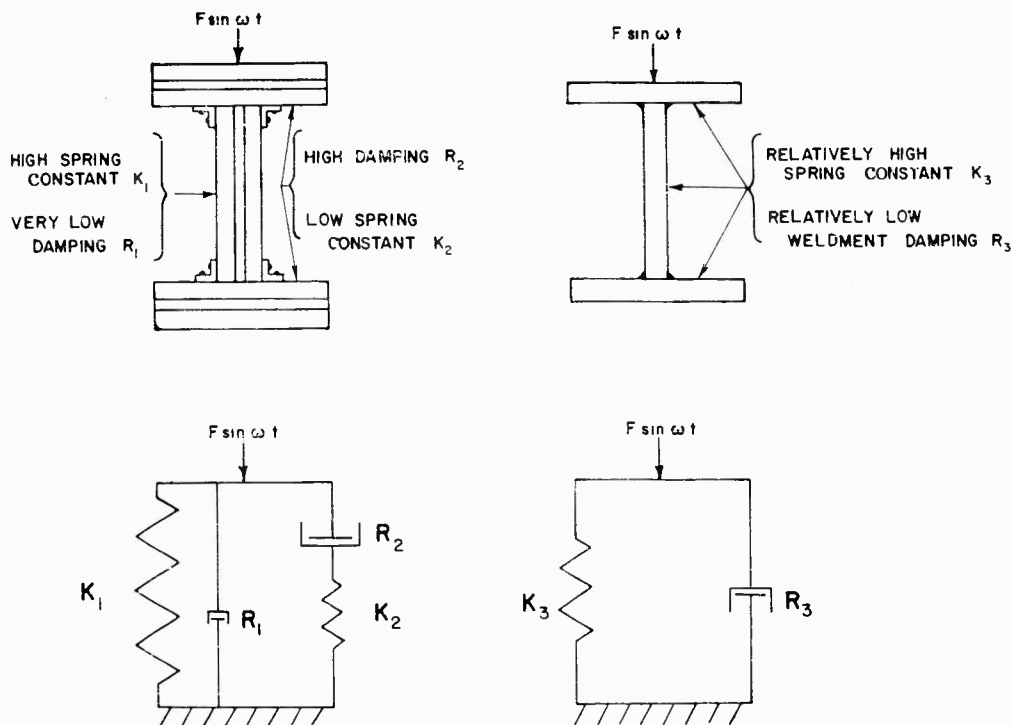


Fig. 1 - Welded steel and laminated I-beam and analog model

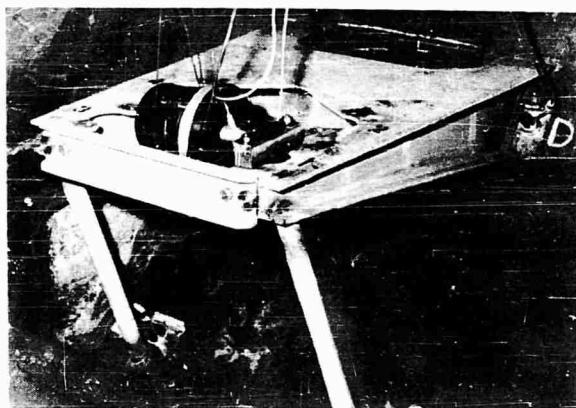


Fig. 2 - Welded steel submarine machinery foundation

PRETWISTED-LAMINATE APPROACH TO FOUNDATION DESIGN

The problem is resolvable for one foundation configuration (Fig. 2) by utilizing a set of pretwisted laminated beams as torsionally loaded members. If the pretwist is in the opposite direction to that of the load, a significant strength can be designed into the foundation. This method of pretwist greatly increases the shock-loading strength of the foundation by causing the shock pulse to be taken primarily as a tensile load on the steel of the laminates. The torsional loading of the laminates also increases the damping in the pretwisted member by increasing the length of the active shear plane in the viscoelastic material.

Studies of a model pretwisted member indicate attenuations of foundation resonances compared to bare steel structures of from 38 db at the first resonant frequency of the models, to 55 db at the third resonance for vertical excitation. With the member under horizontal excitation, attenuations of 43 db at the first resonance and 62 db at the third resonance were measured. These measurements were made on a force-ratio basis using mechanical impedance measuring techniques. The model is pictured in Fig. 3. In addition to the torsionally loaded laminated beams, the damped foundation design incorporates legs constructed as a pipe-within-a-pipe supported by a viscoelastic adhesive. These members act as axial dampers of vibration transmitted from the torsional beams to the hull.

A full-scale machinery foundation has been fabricated and installed on the Marine

system is simplified to a number of two port systems and each transfer impedance

$$Z_T = \frac{F_{\text{drive point}}}{V_{\text{hull}}} \quad (1)$$

is measured as is the hull driving point impedance, and

$$Z_{\text{hull}} = \frac{F_{\text{hull}}}{V_{\text{hull}}} \quad (2)$$

if these hull driving point impedances are divided by the transfer impedances, the quotient becomes a force insertion factor or force ratio due to this vibration path of the foundation:

$$Y = \frac{F_{\text{hull}}}{V_{\text{hull}}} \cdot \frac{V_{\text{hull}}}{F_{\text{drive point}}} = \frac{F_{\text{hull}}}{F_{\text{drive point}}} \quad (3)$$

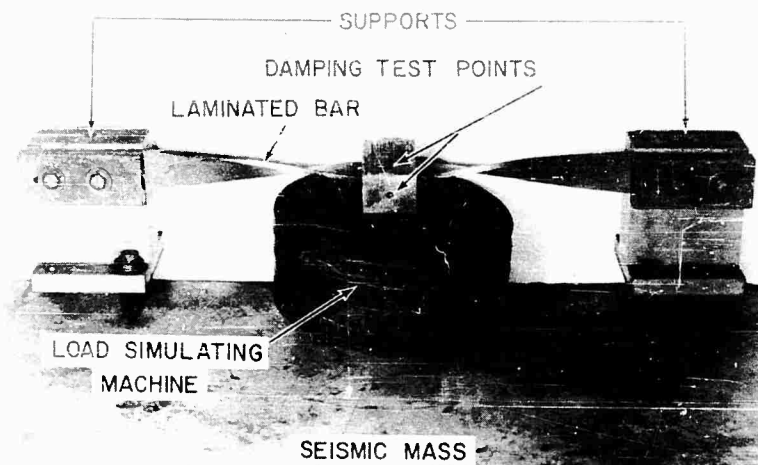


Fig. 3 - Omnidirectional damped foundation model

Engineering Laboratory submarine hull for evaluation. The installed foundation is shown in Fig. 4.

EVALUATION OF FOUNDATION ATTENUATION

Foundation force amplification curves due to resonant frequencies of the foundation were measured by mechanical transfer impedance from each isolation-mount attachment point to each foundation-hull attachment point. The mechanical point impedance of the submarine hull was measured at each point of attachment of the foundation to the submarine hull. If the

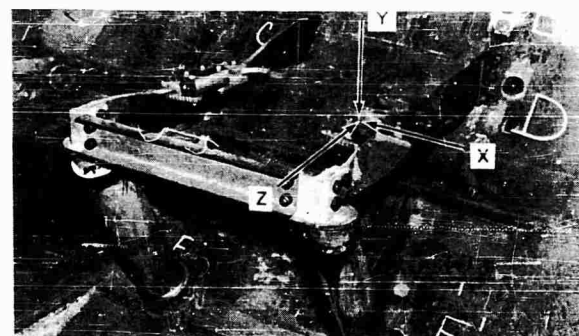


Fig. 4 - Highly damped submarine machinery foundation

If these paths and drive points are then combined by summation, a total foundation insertion or amplification factor can be plotted for each input.

EXPERIMENTAL FOUNDATION ATTENUATION

The overall insertion factor for the X-axis excitation (Fig. 5) shows an average attenuation

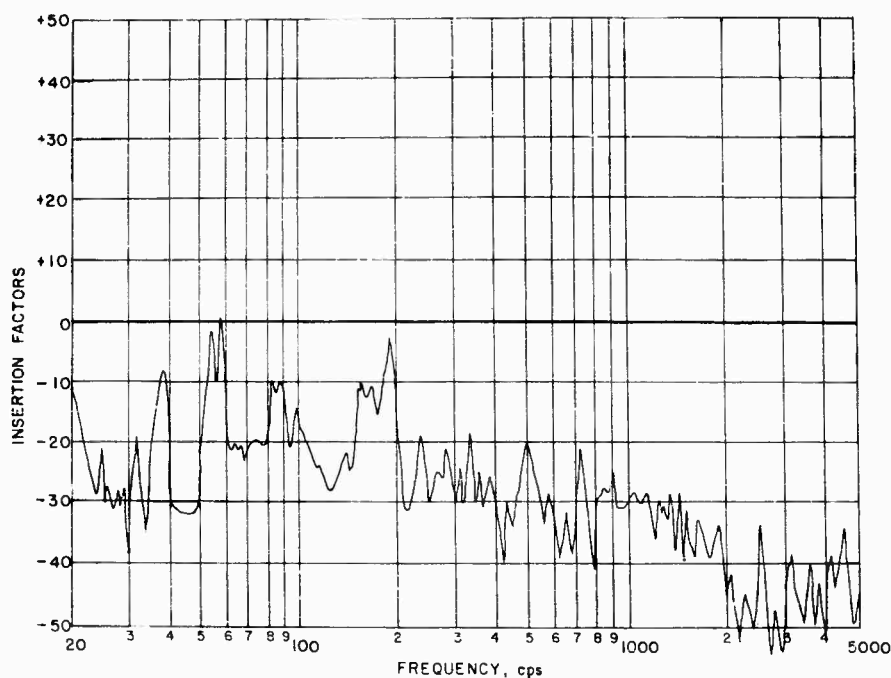


Fig. 5 - x-axis
amplification of
loaded foundation

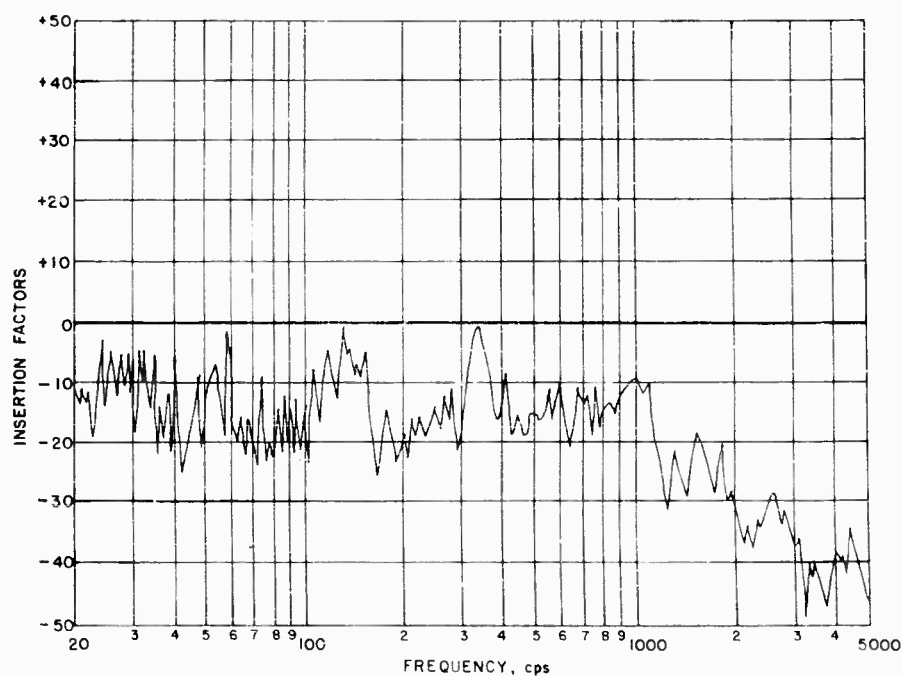


Fig. 6 - Y-axis
amplification of
loaded foundation

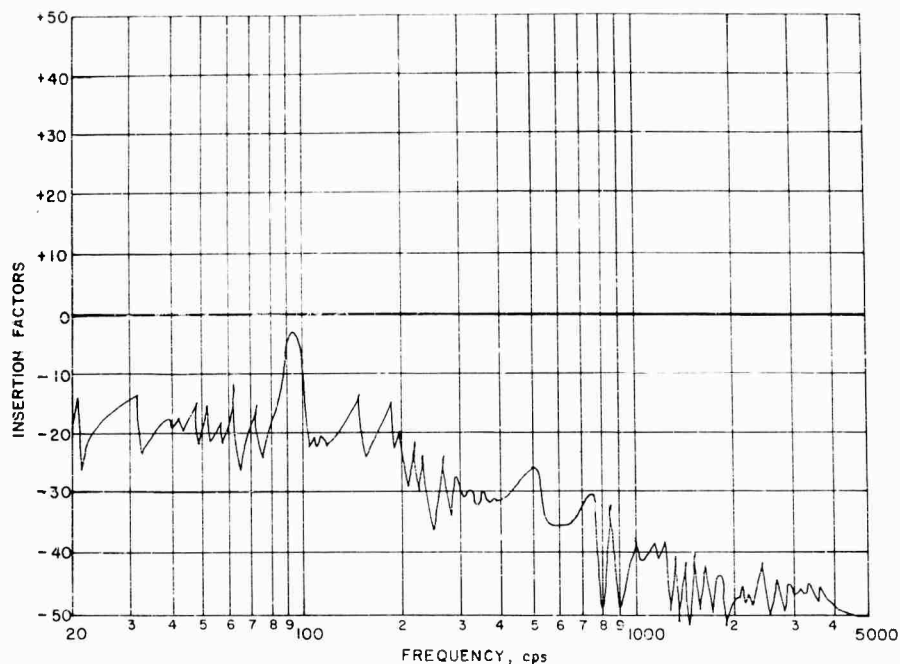


Fig. 7 - Z-axis amplification of loaded foundation

of 20 db up to 200 cps and an increase in attenuation of 6 db per octave to 5000 cps. Specific resonant peaks of 8-db attenuation at 37 cps, -1 db at 58 cps, and 4 db at 190 cps are due to torsional beam resonances of the foundation.

The insertion factor for the Y-axis excitation (Fig. 6) shows an average attenuation of 14 db up to 1000 cps and an increase of 14 db per octave to 5000 cps. Specific resonant peaks of 2 db at 58 cps and 1 db at 140 cps are due to torsional beam resonances of the foundation.

The insertion factor for the Z-axis (Fig. 7) shows an average attenuation of 19 db up to

130 cps and an increase of 6 db per octave to 2000 cps and an average attenuation of 46 db to 5000 cps. A specific resonant peak of 4 db at 93 cps is due to a bending resonance of both torsional beams.

CONCLUSION

The pretwisted-laminate design solves just one of a great number of foundation-design problems involved in silencing machinery. Some insight into the unconventional design techniques required to attenuate machinery vibration is gained.

* * *

DESIGNING STRUCTURES FOR ACOUSTICAL AND VIBRATION ENVIRONMENTS

R. P. Thorn and G. E. Warnaka
Lord Manufacturing Company
Erie, Pennsylvania

Structural resonance is an undesirable condition which exists when a discrete frequency or broadband disturbance excites natural modes of a structure. A resonant condition is characterized by large motions with proportionately high acceleration loads or excessive stress levels resulting in equipment malfunction or fatigue failures. Resonant panels can also radiate acoustical energy which may be harmful to other structures or human beings. Designers of equipment for military applications must consider the response characteristics of plates, beams, and common structural elements since broadband acoustical or structure-borne excitation will be encountered.

Controlled structural response characteristics may be provided by constrained and unconstrained layer damping treatments. Accurate and easy to use design curves are available to assist in the practical application of these materials. Acoustical transmission loss properties and many other attractive characteristics may be obtained from properly designed composite structures. A typical application of these design principles to a sensitive electronic device subjected to acoustical and vibration excitations is discussed.

Composite structures can provide many useful properties and have been successfully applied to many military applications. Response properties including amplitudes, stress levels, and natural frequencies of composite structures can be accurately predicted and applied directly to practical design problems.

Structural resonance is an undesirable condition which exists when a discrete frequency or broadband disturbance excites a natural mode of the structure. Resonant responses can be excited by high-intensity acoustical energy or by mechanical vibration of the structure. A resonant condition is characterized by large motions with proportionately high acceleration loads or excessive stress levels resulting in premature fatigue failure. Equipment mounted on or near resonant structural members may malfunction due to excessive motion or g-loads and may fail due to excessive stress levels. Further, resonant panels may radiate acoustical energy which can be objectionable to equipment, other structures or human beings. Equipment designed for the dynamic environments encountered in military applications must consider the response characteristics of plates, beams, and common structural elements since

broadband acoustical or structure-borne excitation will excite resonant modes in these structural members.

Present design effort is usually based upon the following sequence.

1. Rigidization — The structure is designed so that all resonances are outside the expected range of excitation frequencies, or the various resonant frequencies are separated by a large enough frequency spread so that possible interaction is reduced to acceptable levels.

2. Ruggedization — After tests show that the rigidization has not succeeded, the design is beefed up to eliminate or reduce to acceptable levels structural failures due to fatigue and to limit motions where they are excessive.

3. Isolation or Control of the Environment By Mountings — When tests of the rigidized and ruggedized design fail to produce satisfactory results, isolation is considered to reduce the vibratory levels, particularly in the high-frequency region, and to control the expected shock loads. A typical example of the effective control of system response is shown in Figs. 1 and 2.

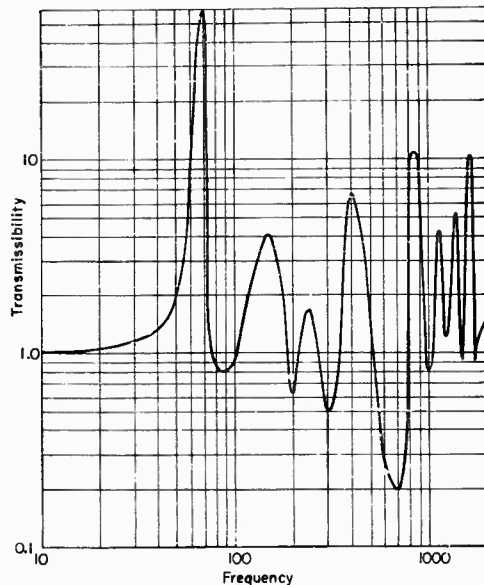


Fig. 1 - System response without isolators or damping

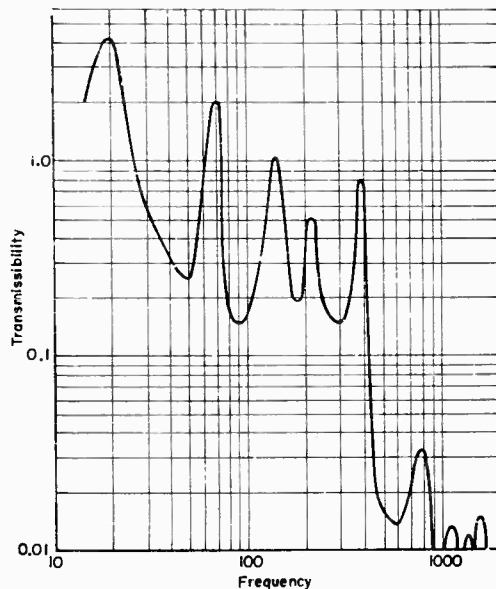


Fig. 2 - System response with isolators but without damping

4. Control of Structural Response — If dynamic performance requirements are exceptionally critical or if isolators cannot be effectively applied, then control of the structural response by energy dissipation methods is the only remaining practical design innovation.

To establish the need for damping in structures, it is necessary to understand how a simple mechanical system responds to a variable frequency mechanical disturbance. Fortunately, even complex structures can usually be reduced to an equivalent single-degree-of-freedom spring-mass system such as shown in Fig. 3. For low-frequency excitations, the motions of the mass slightly exceed the input motion. As the frequency of excitation increases, an infinite response is reached at resonance where the input frequency matches the natural frequency of the spring-mass system. This natural frequency may be calculated directly from the formula

$$f_n = \frac{1}{2\pi} \sqrt{\frac{K_{\text{effective}}}{M_{\text{equivalent}}}} \quad (1)$$

Where $K_{\text{effective}}$ is the effective spring rate acting in the system and $M_{\text{equivalent}}$ is the equivalent mass acting for the mode under consideration, above resonance the response decreases until the mass motion is a very small percentage of the input disturbance. Hence, any mechanical system acts as a low-pass filter and the response is shown in Fig. 4. Even for a simple structure, many natural frequencies exist. Fortunately, a fair approximation of the total system response can be obtained by considering the system as a number of simple single-degree-of-freedom spring-mass combinations. The design of structures exposed to mechanical vibrations or dynamic loads now logically becomes an investigation of the response at the resonance or resonances of the complex structure. At resonance, the system motions will be the greatest; hence, the stress levels and loads will be maximum.

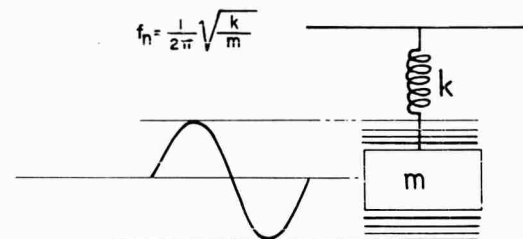


Fig. 3 - Natural frequency is frequency of free vibration in system or structure

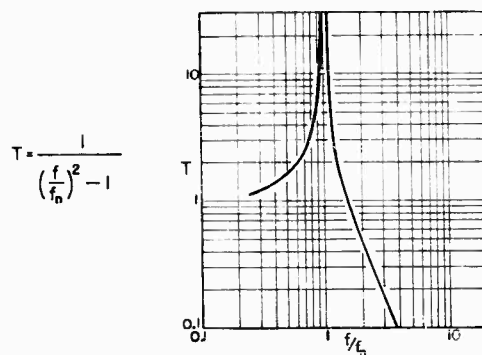


Fig. 4 - Response curve for typical undamped system

At resonance, the mechanical energy being fed into the system is effectively stored by the spring-mass combination. The infinite amplitudes suggested by the response curve do not occur instantaneously but take a finite amount of time to build up. Hence, a small amount of energy can result in a considerable amplitude if it acts for a long period of time. It follows that any interruption of this energy flow would result in a limiting of the amplitude of response. Structural damping is a method for dissipating energy at resonance and may be represented simply by the schematic shown on Fig. 5. The simple system response is now modified as shown in Fig. 6(a) where the amplitude at resonance is limited and is equal to $1/2(C/C_c)$ or $1/\eta$. The complex system response would then be as shown in Fig. 6(b). (C is the damping constant, C_c is the critical damping and η is the loss factor or composite loss factor.)

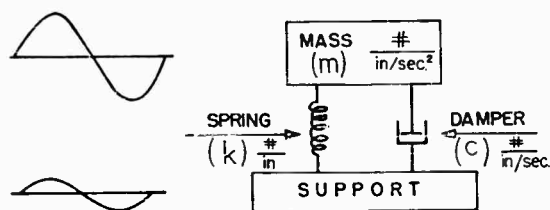
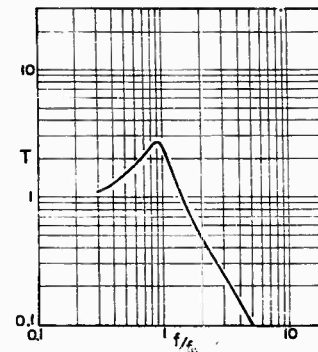


Fig. 5 - Damper controls motion of single-degree-of-freedom system at resonance

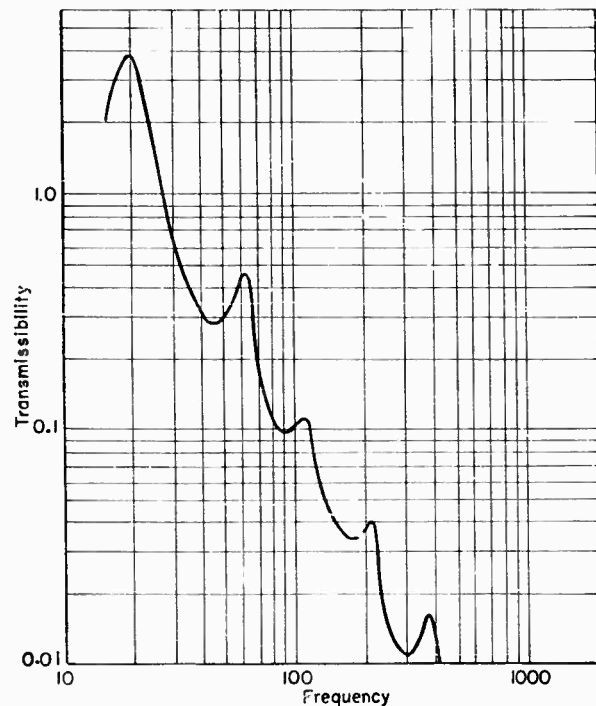
The analogy may be extended directly to plates and beams where the Ritz equation

$$f_n = \frac{\alpha}{2\pi} \sqrt{\frac{K \text{ effective}}{M \text{ equivalent}}} = \frac{\alpha}{2\pi} \sqrt{\frac{EI}{\rho AL^4}} \quad (2)$$

where E is Young's modulus, I is the moment of inertia, and ρ is the mass density, can be used to determine the natural frequency for the various beam and plate modes shown in Figs. 7 and 8. If the natural frequency of a structure can be determined, and the response of that structure predicted at resonance, then a rational approach to the design of controlled response structures can be made.



(a) With damping



(b) With isolators and damping

Fig. 6 - Transmissibility of typical single-degree-of-freedom system

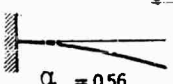
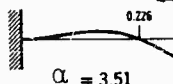
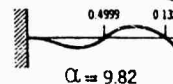
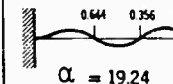
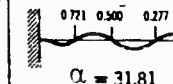
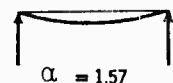
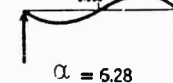
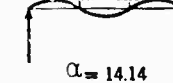
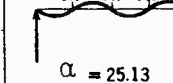
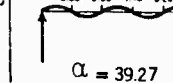
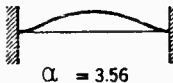
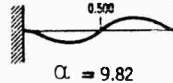
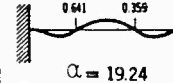
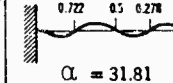
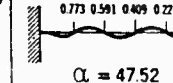
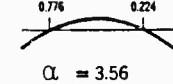
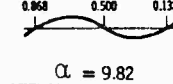
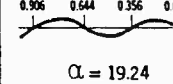
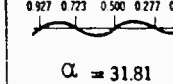
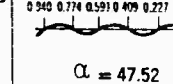
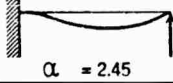
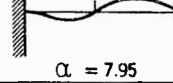
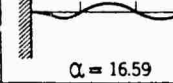
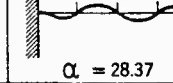
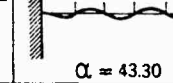
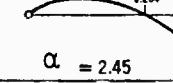
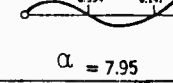
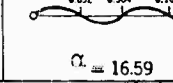
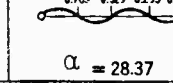
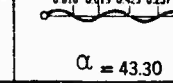
Beam Type	Mode I	Mode II	Mode III	Mode IV	Mode V
Cantilever	 $\alpha = 0.56$	 $\alpha = 3.51$	 $\alpha = 9.82$	 $\alpha = 19.24$	 $\alpha = 31.81$
Simply supported ends	 $\alpha = 1.57$	 $\alpha = 6.28$	 $\alpha = 14.14$	 $\alpha = 25.13$	 $\alpha = 39.27$
Fixed ends	 $\alpha = 3.56$	 $\alpha = 9.82$	 $\alpha = 19.24$	 $\alpha = 31.81$	 $\alpha = 47.52$
Free ends	 $\alpha = 3.56$	 $\alpha = 9.82$	 $\alpha = 19.24$	 $\alpha = 31.81$	 $\alpha = 47.52$
Fixed-hinged	 $\alpha = 2.45$	 $\alpha = 7.95$	 $\alpha = 16.59$	 $\alpha = 28.37$	 $\alpha = 43.30$
Hinged-free	 $\alpha = 2.45$	 $\alpha = 7.95$	 $\alpha = 16.59$	 $\alpha = 28.37$	 $\alpha = 43.30$

Fig. 7 - Mode constants, mode shapes and node locations for uniform section beams with various combinations of support [1]

How can damping be incorporated effectively into structural designs? Two broad categories, constrained and unconstrained layer damping, exist. A constrained layer damping material

consists of a composite laminate made up of a damping or core material sandwiched between skins of structural material in a three- or multi-ply layer. A typical three-ply construction is shown in Fig. 9. The damping action is a direct result of shearing of the viscoelastic core material as the laminate is flexed. The

NOTE: References appear on page 219.






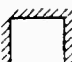
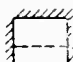
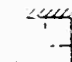








	1ST MODE	2ND MODE	3RD MODE	4TH MODE	5TH MODE	6TH MODE
α	3.494	8.547	21.44	27.46	31.17	
NODAL LINES						
α	35.99	73.41	108.27	131.64	132.25	165.15
NODAL LINES						
α	6.958	21.08	26.80	48.05	63.14	
NODAL LINES						

Fig. 8 - Natural frequencies and nodal line of square plates with various edge conditions [2]

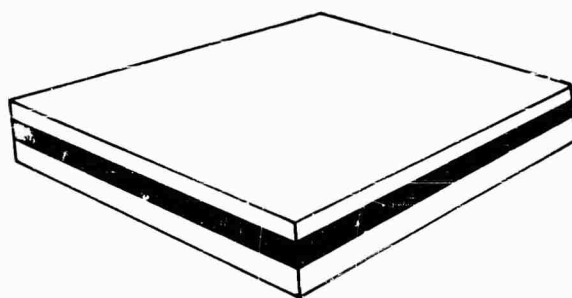


Fig. 9 - Integral damping: damping material applied between laminates of beam or plate

amount of damping obtained is a function of the material properties of both the skin and the damping media, the geometric properties such as size and shape, and other factors such as excitation frequency, strain, and temperature. The complexity of these relationships has been well documented [3,4].

By proper design techniques and choice of damping materials, it is possible to obtain constrained layer damped structures which preserve the structural integrity of the composite yet have predictable response characteristics over a broad frequency range. Prediction of the response characteristics of a simple three-ply laminate may be made directly from Fig. 10. This is a plot of composite loss factor and characteristic mode number α vs frequency parameter. The characteristic mode number describes the mode under consideration and the controlling dimension of the beam or the plate. It is seen from this curve that any three-ply or constrained

layer treatment is frequency sensitive and the laminate must be designed so that maximum damping occurs near the critical resonant modes. Fortunately, the effective band spread of such laminates is in excess of one decade in frequency. Hence, effective damping over a 100 to 1 kc range is easily obtained. By proper choice of the damping material, it is possible to limit structural resonances to 10 to 1 or less and to maintain or increase the dynamic stiffness of the laminate compared to a solid structural material. Design techniques similar to the data shown on these curves are available which will allow for the accurate allowable prediction of composite laminate properties.

An unconstrained or free layer damping treatment consists of a simple two-ply construction as shown on Fig. 11. For this method, a very highly damped material is applied directly to the structure to be controlled. Composite damping is obtained by the alternate extension and compression of the damping layers as the structure is flexed. As with the constrained layer treatment, the effectiveness depends on forcing the damping material to move and dissipate energy. For such a composite laminate, the overall loss factor is equal to

$$\zeta = \zeta_2 e_2 H_2 \frac{3 + 6H_2 + 4H_2^2}{1 + e_2 H_2 (3 + 6H_2 + 4H_2^2)} \quad (3)$$

where ζ_2 is the loss factor constrained layer material, e_2 is Young's modulus constrained layer material, and H_2 is the thickness

ALUMINUM SKINS	Ratio h_2	Skin	Core
1.000	.020	.020	
.625	.032	.020	
.500	.040	.020	

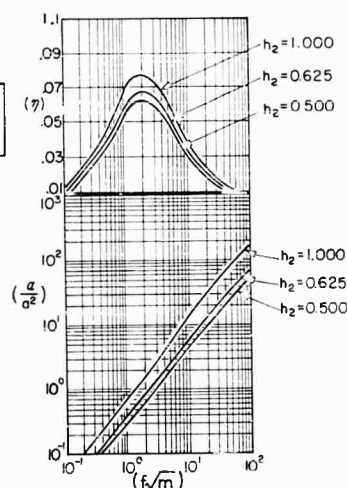


Fig. 10 - Loss factor η and characteristic mode value α/a^2 vs frequency parameter $f\sqrt{m}$

constrained layer material. From this expression, it is apparent that a stiff, highly damped material is essential for an effective damping treatment. A typical effective material would have a Young's dynamic modulus E' of 10^6 and a loss factor ζ_2 in excess of 1. Prediction of the composite loss factor is obtained simply from the following curve which plots loss factor vs relative material thickness (Fig. 12). Unlike the constrained layer treatment, the unconstrained treatment is not basically frequency sensitive and will effectively suppress resonances over a broad range of frequencies as long as the mode results in some motion of the damping material.

This suggests the use of a partial coverage for the control of specific modes. In a circular plate which has many possible mode shapes, the

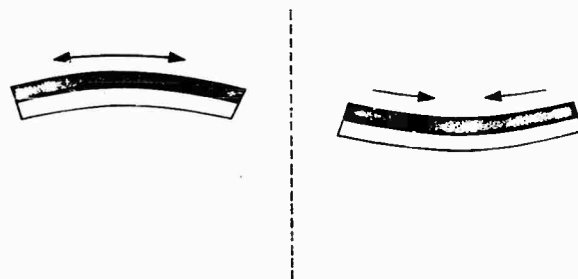


Fig. 11 - Additive damping: damping material applied to surface of beam or plate

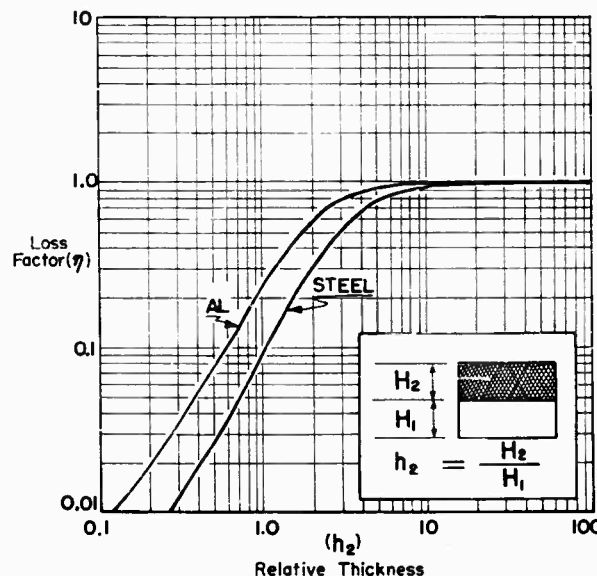


Fig. 12 - Damping compound DC-400-1 results at 80°F and 75 cps

predominant modes are the first two modes, the first mode being the diaphragming of the plate and the second mode having one nodal diameter. These modes suggest a partial treatment as shown on Fig. 13. The result of this treatment is almost as good as the total coverage of the entire plate.

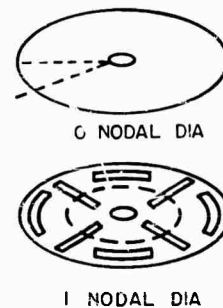


Fig. 13 - Circular plate fixed in center

Fortunately, laminated materials also exhibit attractive acoustical transmission characteristics. By proper design, it is possible to construct a laminate given by the equation

$$C_B = \omega^{1/2} \left(\frac{B}{m} \right)^{1/4} \quad (4)$$

where ω is the excitation frequency, B is the bending stiffness of the composite and m is the mass density per unit area. If this speed of propagation is kept below the speed of sound, then the composite structure will act as an effective acoustical barrier and provide attenuation levels in accordance with a theoretical limp mass given in Fig. 14.

We will consider a typical state-of-the-art electronic device which is to be exposed to the following vibration levels: sinusoidal 3 g peak limited to 0.40-inch double amplitude sweep from 5 to 2000 to 5 cps at 1 octave/min, and random 0.2 g^2 /cps from 100 to 1000 cps with a 12 db/octave rolloff below 100 and above 1000 cps. The device is a cube, two feet on the side, and is resiliently supported on isolators in a center-of-gravity suspension system. It has been established that high acoustical energies are being transferred through the equipment covers and exciting structural resonances which cause component malfunction. In addition, the residual vibration being transmitted through the isolators is also causing excitation of structural resonances and contributing to component malfunction. The design task is to provide a replacement for the present structural covers to provide proper acoustical transmission loss

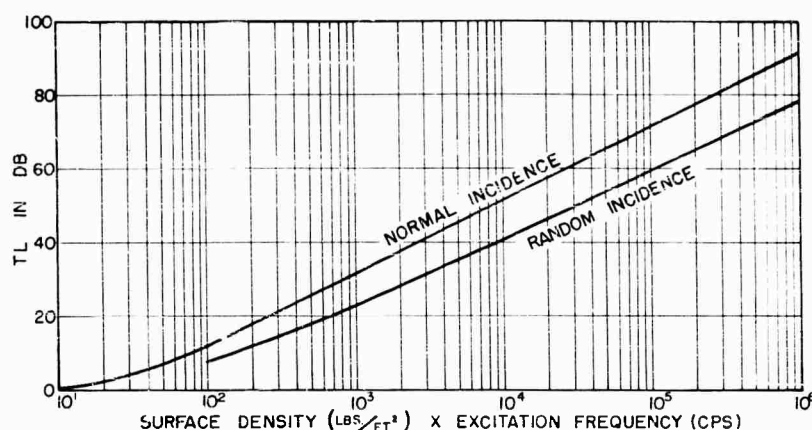


Fig. 14 - Sound transmission loss of limp wall barriers (mass law)

and to introduce sufficient damping to control the potential major structural resonances which may occur.

The cover panels of the device were initially made of 0.020-inch thick magnesium skins. These skins satisfactorily fulfilled the required mechanical function of keeping out foreign matter. However, they were not able to exclude a sufficient amount of the high-intensity noise which was found to be partly responsible for malfunction of the device.

The most apparent method of increasing the attenuation of sound transmitted through the panels is to increase the weight from 0.19 to 1.73 lb/sq ft in accordance with the "random incidence mass law." This classical method of determining the transmission loss of a structure considers the inertial resistance to motion due to the distributed mass of the structure for randomly incident sound waves. Unfortunately, the mass law is based on the assumption that the structure is limp that is, the distributed stiffness is assumed to be negligible. Modern structural design has, for obvious reasons, attempted to maximize stiffness-to-weight ratios. The result has often been that the traditional mass law approach has been found to be inadequate [5]. This difficulty may be readily understood by recalling that distributed systems have a theoretically infinite number of resonances and that at resonance, motions become very large because of the interaction between mass and spring. In short, a structure is not mass controlled at resonance. Therefore, the acoustic transmission loss predicted for a mass-controlled structure cannot be realized.

Typical lightweight structures with normal edge fastening have mechanical Q's between 50 and several hundred. To approach mass law response, the Q should be small. For the panels in question, it was decided to reduce the Q's to five or less by bonding an unconstrained layer of highly damped plastic to the existing panels. The material chosen, after consideration of the temperature environment of the device, was DC-403. Eq. (3) indicated that a 0.035-inch thickness of DC-403 was required to suppress the Q's to five. DC-403 weighs only 95 lb/cu ft so that the total panel weight is still only 0.49 lb/sq ft, not enough to give the required transmission loss. To complete the weight requirement, a 0.07-inch thick layer of DC-100, a soft, high-density polymer, was adhered to the layer of DC-403. The resulting three-layer composite panel provided the required transmission loss as shown in Fig. 15. This panel provided a relatively quick "fix" for the acoustic transmission problem.

A second generation treatment was thought to be desirable. In most instances, the treatment already described would be completely satisfactory, but certain handling problems were anticipated because of the exposed surfaces of relatively soft materials. A three-ply laminated panel with aluminum skins and a core of high-density, moderately damped polymer was designed. Again the panel was carefully designed to give the sound attenuation expected from a limp mass.

It is known that the rigidity of a three-ply laminate varies between two limiting conditions. Under static loading the skins are closely coupled by the core and the flexural rigidity B is given by

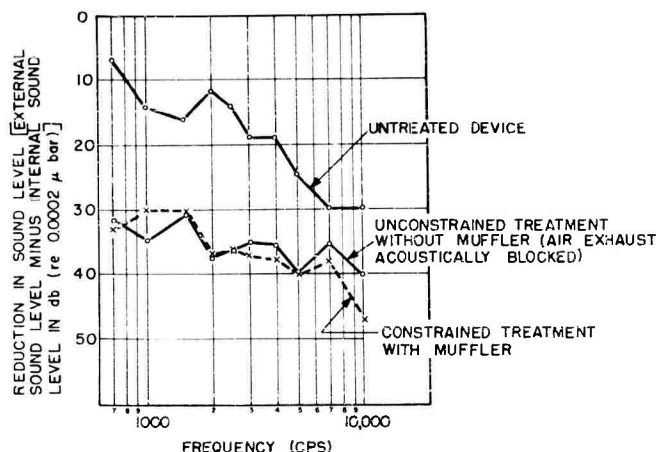


Fig. 15 - Noise reduction of various damping treatments

$$B = E \frac{\frac{1}{2d} (d+t)^2 + \frac{t^3}{12}}{1 - \nu^2} \quad (5)$$

where E is Young's modulus of the skins, d is the core thickness, t is the skin thickness, and ν is Poisson's ratio for the skin material.

At very high frequencies, the skins are decoupled by the compliance of the core material and the flexural rigidity is [4,5]

$$B = 2E \frac{t^3}{12 (1 - \nu^2)} \quad (6)$$

The transition between the two limiting cases occurs at intermediate frequencies when the properties of the elastomer (which couples the skins together) control the laminate response. That is, the compliant properties of the core become evident as the frequency is raised and the skins gradually become decoupled. Thus, a laminated panel has a frequency-dependent stiffness which decreases with frequency. The amount of decrease and the range of transition depend on the limiting values of stiffness and the properties of the core. These characteristics permit the design of laminated panels which have excellent acoustical performance. At low frequencies, a panel may have the high stiffness necessary for mechanical functions. In the important acoustical frequency range, the panel can be designed so that its stiffness decreases with frequency. Consequently, the acoustical attenuation will be in accordance with the mass law.

The total design for reduction of acoustical and vibrational levels was completed by

complementing the panels with a damped acoustical muffler to provide a transition for the cooling exhaust air to the high noise environment and an unconstrained layer damping treatment for the major structural frame which surrounded the equipment (Fig. 16).

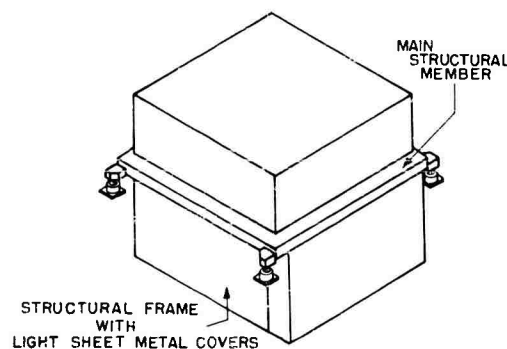


Fig. 16 - Assembled device

The design goal was a 30-db reduction in noise level across the frequency range from 1500 cycles to 10 kc. The results of tests on this design are shown on Fig. 15. Vibration tests were also run and show a considerable improvement in performance across the frequency spectrum (Fig. 17).

The results of these tests clearly indicate the effectiveness of properly designed damping treatments. Constrained layer treatments have been used effectively for the past several years in aircraft and missile substructures where reliability, weight, strength and fatigue life are

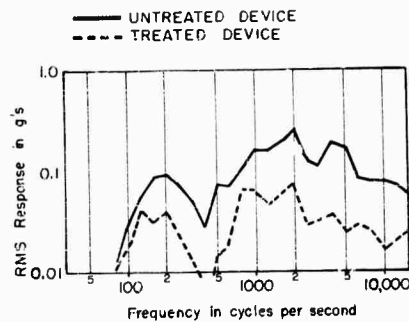


Fig. 17 - Frequency analysis of acceleration of internal circuit board excited acoustically in 62.5 to 125-cps octave band

important factors. Three-ply laminates have been used effectively for panels and shelves for electronic enclosures and mounting bases and multi-ply laminates have been very effective as replacements in new designs for heavy castings,

cooling plates and shelves for both missile and aircraft applications. Most common structural materials can be used in conjunction with a wide range of viscoelastic damping materials for satisfactory dynamic performance. Structural integrity can be maintained with little or no weight penalty and predictable resonant response is possible with properly applied constrained layer treatments.

Unconstrained layer treatments have been used successfully on ship hulls, submarines, aircraft skins, business machine enclosures, enclosures for machinery, and devices in populated areas where controlled structural response and control of noise is important. The ease of application of these materials makes them particularly attractive for large surface treatments. Properly designed damping treatments represent an effective tool for improved structural design. If reliability, performance, weight, or cost are problems, damping materials may offer a quick and effective solution to a structural design problem.

REFERENCES

1. A. H. Church, *Mechanical Vibrations*, 2nd Ed. (John Wiley and Sons, Inc., New York).
2. D. Young, *J. Appl. Mech.*, 17:448 (1950).
3. E. M. Kerwin, "Damping of Flexural Vibrations in Plates by Free and Constrained Visco-Elastic Layers," Bolt, Beranek, and Newman, Inc. Report No. 632 (May 1959).
4. G. Kurtze and B. G. Watters, "New Wall Design for High Transmission Loss or High Damping," *J. Acoust. Soc. Am.*, 31: 739-748 (June 1959).
5. B. G. Watters, "The Transmission Loss of Some Masonry Walls," *J. Acoust. Soc. Am.*, pp. 898-911 (July 1959).

* * *

Section 3 FIXTURE DESIGN

EQUALIZATION AND FIXTURE DESIGN*

R. M. Mains
Advanced Technology Laboratories
General Electric Company
Schenectady, New York

The impedance relationships between the black boxes in a test-article test-fixture-exciter arrangement are developed and used to obtain some rules for test monitoring and fixture design. The problem of equalization is also discussed in terms of impedance relationships. Service vehicle impedance relationships are compared to test arrangement relationships, and some interesting parallels are observed.

GENERAL RELATIONSHIPS

The subject of equalization of a test configuration is one of the most controversial issues in the field of shock and vibration. To discuss what may be proper or improper equalization, let us first examine the impedance relationships involved [1] as illustrated in Fig. 1. For our discussion, we will define the elements at interface 1 as the sensitive or critical elements in the test article whose motions are of concern, and which are not loaded by applied external force. Therefore, $f_1 = 0$ and we wish to relate v_1 to the remaining functions. In impedance terms [2,3] then

$$\begin{bmatrix} f_1 \\ -f_2 \end{bmatrix} = \begin{bmatrix} Z_{112} & Z_{12} \\ Z_{21} & Z_{221} \end{bmatrix} \begin{bmatrix} v_1 \\ v_2 \end{bmatrix} \quad \text{Test Article} \quad (1)$$

$$\begin{bmatrix} f_2 \\ -f_3 \end{bmatrix} = \begin{bmatrix} Z_{223} & Z_{23} \\ Z_{32} & Z_{332} \end{bmatrix} \begin{bmatrix} v_2 \\ v_3 \end{bmatrix} \quad \text{Fixture} \quad (2)$$

$$f_3 = Z_{334} v_3 + rE \quad \text{Exciter} \quad (3)$$

in which

f_i = force vector,

v_i = velocity vector,

Z_{ij} = impedance matrix,

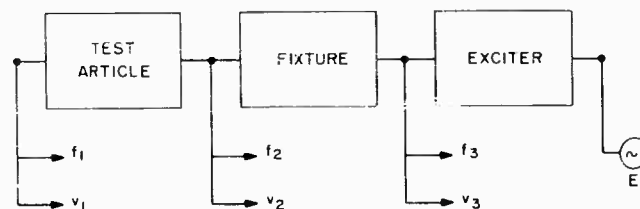


Fig. 1 - Test arrangement

*This paper was not presented at the Symposium.

τ = transfer function, voltage to force [3], and

E = voltage input to exciter system.

If we set $f_1 = 0$, in accordance with the assumption that the critical elements do not have external load applied, then f_2 can be eliminated from Eqs. (1) and (2) to give:

$$\begin{bmatrix} 0 \\ -f_3 \end{bmatrix} = \begin{bmatrix} Z_{113} & Z_{13} \\ Z_{31} & Z_{331} \end{bmatrix} \begin{bmatrix} v_1 \\ v_3 \end{bmatrix}, \quad (4)$$

in which

$$Z_{113} = + Z_{112} - Z_{12} B Z_{21}$$

$$Z_{13} = - Z_{12} B Z_{23}$$

$$Z_{31} = - Z_{32} B Z_{21}$$

$$Z_{331} = + Z_{332} - Z_{32} B Z_{23}$$

$$B = [Z_{221} + Z_{223}]^{-1}$$

Equation (4) can be solved for v_1 in terms of either v_3 or f_3 alone, to give

$$v_1 = -Z_{113}^{-1} Z_{13} v_3 \quad (5)$$

or

$$v_1 = -Z_{113}^{-1} Z_{13} (-Z_{31} Z_{113}^{-1} Z_{13} + Z_{331})^{-1} f_3 \quad (6)$$

Similarly, Eq. (1) can be solved for v_1 in terms of either v_2 or f_2 alone, as

$$v_1 = -Z_{112}^{-1} Z_{12} v_2 \quad (7)$$

or

$$v_1 = -Z_{112}^{-1} Z_{12} (-Z_{21} Z_{112}^{-1} Z_{12} + Z_{221})^{-1} f_2 \quad (8)$$

We can also combine Eq. (3) with Eq. (4) to get

$$(Z_{334} + Z_{331}) v_3 + Z_{31} v_1 = -\tau E \quad (9)$$

The use of Eq. (5) allows us to eliminate v_1 or v_3 and get

$$(Z_{334} + Z_{331} - Z_{31} Z_{113}^{-1} Z_{13}) v_3 = -\tau E \quad (10)$$

or

$$[-(Z_{334} + Z_{331})(Z_{31} Z_{113})^{-1} Z_{31} Z_{113}^{-1} + Z_{31}] v_1 = -\tau E, \quad (11)$$

and Eq. (7) with Eq. (11) gives

$$\begin{aligned} & [(Z_{334} + Z_{331})(Z_{31} Z_{113})^{-1} Z_{31} Z_{113}^{-1} - Z_{31}] \\ & \times Z_{112}^{-1} Z_{12} v_2 = -\tau E. \quad (12) \end{aligned}$$

EQUALIZATION

The foregoing equations provide the information necessary to form some conclusions about proper or improper equalization in the test configuration. We will define equalization for our purposes as the adjustment of τ to linearize v_1 with respect to E . If we develop Eq. (12) directly without the intermediate combinations, it comes out in terms that can be conveniently separated:

$$\begin{aligned} & \left[\underbrace{(Z_{221} - Z_{21} Z_{11}^{-1} Z_{12})}_{\text{Test Article}} + \underbrace{Z_{223} - Z_{23}(Z_{332} + Z_{334})^{-1} Z_{32}}_{\text{Fixture and Exciter}} \right] \\ & \times v_2 = + \underbrace{Z_{23}(Z_{332} + Z_{334})^{-1}}_{\text{Test Force}} \tau E \quad (13) \end{aligned}$$

which can be written as

$$[Z_c + Z_m] v_2 = a E. \quad (14)$$

Similar relations can be derived for v_1 and v_3 through Eq. (5) and (7).

In examining these relationships for general principles, we find from Eqs. (5) through (8) that the specification of either v_2 , v_3 , f_2 , or f_3 uniquely determines v_1 because $f_1 = 0$. Also, pairs of vectors such as v_2 and f_2 or v_3 and f_3 cannot be arbitrarily specified since they are related functions. At the resonant frequencies of the system, forces tend to become large while input velocities tend toward zero. Therefore, a specification of motion input only might easily require a larger force than the exciter could stand, while the specification of a force input could require a responding motion which was impossibly large.

If we assume that a test is going to be monitored by measuring motion at the fixture-component interface v_2 , then four cases for equalization are distinguishable:

1. Linearize v_3 with E when $f_3 = 0$ (no load on exciter)

$$-Z_{334}^{-1} \tau = I \times \text{Constant} \quad (15)$$

which comes directly from Eq. (3).

2. Linearize v_3 with a load on the exciter, fixture or mass, with $f_2 = 0$. Equation (2) gives $v_2 = -Z_{223}^{-1} Z_{23} v_3$ which can be substituted into Eq. (9) to give

$$(-Z_{32} Z_{223}^{-1} Z_{23} + Z_{332} + Z_{334}) v_3 = -\tau E, \quad (16)$$

which yields

$$[+Z_{32} Z_{223}^{-1} Z_{23} - Z_{332} - Z_{334}]^{-1} \tau = I \times \text{Constant}. \quad (17)$$

3. Linearize v_2 with fixture unloaded, $f_2 = 0$. Equation (2) gives $v_3 = -(Z_{32} Z_{223})^{-1} Z_{32} Z_{223} v_2$ which can be substituted into Eq. (9) to give

$$[-Z_{32} + (Z_{332} + Z_{334})(Z_{32} Z_{223})^{-1} Z_{32} Z_{223}] v_2 = \tau E, \quad (18)$$

which yields

$$[-Z_{32} + (Z_{332} + Z_{334})(Z_{32} Z_{223})^{-1} Z_{32} Z_{223}]^{-1} \tau = I \times \text{Constant}. \quad (19)$$

4. Linearize v_2 with fixture loaded and $f_1 = 0$. This uses Eq. (13) to give

$$[-Z_{32} - (Z_{332} + Z_{334})(Z_{32} Z_{223})^{-1} Z_{32} Z_{223} + (Z_{21} Z_{112}^{-1} Z_{12} - Z_{221} - Z_{223})]^{-1} \tau = I \times \text{Constant}. \quad (20)$$

The first case with Eq. (15) is easy, since only the exciter impedance is involved, but it is trivial, since any load on the exciter changes the situation for the other cases. The third case with Eq. (19) is still not enough, because loading the fixture alters the relationships. The fourth case, with Eq. (20), is the proper one for equalizing a test configuration, since in it we have the means for insuring that v_2 is linearly related to E provided that it is physically possible. Equation (20) shows clearly that Z_{334} , the fixture impedances Z_{2-3} , and the test article impedance Z_{1-2} affect the linearization of v_2 with E . From this we must conclude that proper equalization can be done only when everything in the test configuration is in place and exhibiting its proper impedance.

COMPARISON OF TEST AND SERVICE

In Fig. 2 we see the impedance representation of the test article carried on the service structure. The impedance equations are

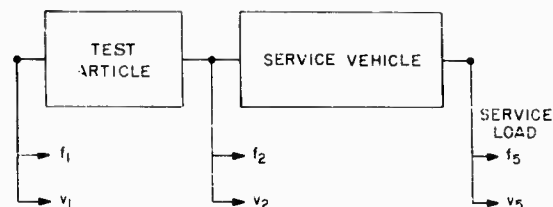


Fig. 2 - Service vehicle

$$\begin{bmatrix} 0 \\ -f_2 \end{bmatrix} = \begin{bmatrix} Z_{112} & Z_{12} \\ Z_{21} & Z_{221} \end{bmatrix} \begin{bmatrix} v_1 \\ v_2 \end{bmatrix}, \quad \begin{bmatrix} f_2 \\ f_5 \end{bmatrix} = \begin{bmatrix} Z_{225} & Z_{25} \\ Z_{52} & Z_{552} \end{bmatrix} \begin{bmatrix} v_2 \\ v_5 \end{bmatrix} \quad (21)$$

and these equations lead directly to

$$\underbrace{\begin{bmatrix} Z_{221} - Z_{21} Z_{112}^{-1} Z_{12} \end{bmatrix}}_{\text{Test Article}} + \underbrace{\begin{bmatrix} Z_{225} - Z_{25} Z_{552}^{-1} Z_{52} \end{bmatrix}}_{\text{Service Structure}} \times v_2 = \underbrace{Z_{25} Z_{552}^{-1} f_5}_{\text{Service Load}}, \quad (22)$$

which can be written as

$$[Z_c + Z_s] v_2 = \rho F, \quad (23)$$

which is now in the same form as Eq. (14). Since Z_c , Z_m and Z_s can be measured or calculated, it follows that service loads can be deduced from measured velocities, and test inputs required to produce specific test article responses can be calculated. In principle, it is then possible to make the v_2 of Eq. (23) identical to the v_2 of Eq. (14), so that test article responses are identical with service load responses.

To scale from one vehicle to another in the same environment, it is better to scale the service load to suit the new vehicle than to assume that component responses are going to be similar or scaled. Scaling the load leaves the designer the freedom of adjusting Z_s to get a favorable response at v_1 , while scaling the v_2 's completely eliminates that possibility.

WHAT A TEST CAN DO

As a result of the discrepancies between what is available to work with and what is theoretically possible, it is appropriate to consider what it is that a test might be expected to do, or not to do. If we consider a test article which has several critical elements, and which is attached at several points to the testing machine or test fixture, then:

1. A test cannot be expected to reproduce exactly the effects of a service environment at every point in the test article.

2. A test can usually be adjusted to produce the same general damage process as a service environment.

3. It may not be possible to adjust a test so as to produce a specific damage process at a particular point.

4. It may be possible to adjust a test so that the general damage process produced by the test is related (on the average) in rate and extent of damage to the service environment.

The first proposition is unarguable because of the nature of measurements and testing; neither process is exact. Where the general damage process is known (e.g., fatigue under sustained vibration) it can usually be reproduced in some way. There are, however, many instances in which we do not know the damage process or how to produce it — we may in fact be measuring the wrong parameters to relate to a damage process. This is particularly true when we get down to specific points where local peculiarities can take precedence over the general damage process.

So only if a particular critical element has a known damage process, related distinctly to a specific environmental parameter, it is possible for a test and an environment to produce the same damage process in that particular element. Wherever we have a multiplicity of critical elements, each with different damage processes; and each damage process related to a different environmental parameter, it is simply not possible to devise a test which will produce the same damage process on each critical element as the service environment does. Even if it were possible to do this, the test usually should not represent some specific measured environment. Rather the test should represent a design environment, adjusted from specific measured environments to reflect what the whole family of articles represented by the test article will experience when they are subjected to the varieties of mission and use for which they are intended. The design environment should then represent a set of conditions such that only some small fraction of the family of articles has a probability of experiencing a more severe environment.

HOW A TEST FIXTURE SHOULD BE DESIGNED

There are at least four distinct purposes to be served by a dynamic test, and as many different kinds of load input:

Test Purpose

Test Load

- | | |
|--|-------------------------|
| 1. Basic data development | 1. Sinusoidal vibration |
| 2. Engineering design development | 2. Swept sinusoidal |
| 3. Prototype qualification or acceptance | 3. Random vibration |
| 4. Quality control or production check | 4. Shock or impact |

For each combination of test purpose and test load, a fixture with a 1:1 transfer function over all frequencies would be quite satisfactory [4]. For restricted frequency ranges (e.g., less than 500 cps) a 1:1 fixture may be approximated if the test article is not too large. For broad frequency ranges (e.g., 0 to 3000 cps) the 1:1 fixture is not practically realizable, except for very small test articles.

A re-examination of Eqs. (7) and (8) recalls that, as long as the motion at the fixture-test article interface is controlled, the fixture impedance does not affect the test article motion. Since this is the case, we can then establish some general rules for fixture design which are based on the practical considerations of test power required, ease of test control, cost of fixture, convenience during test, and the like. For sinusoidal and swept sinusoidal vibration:

1. A test fixture should be designed for minimum weight to conserve test power required.
2. For tests in which a restricted frequency range is to be investigated, there should be no large resonances of the fixture in that range.
3. For tests covering a broad range of frequencies, fixtures with heavy internal damping are desirable, since they come closer to a 1:1 transmissibility than lightly damped fixtures.

For random vibration and shock tests in which it is assumed that equalization for random vibration is done at the fixture-test article interface with at least an impedance simulation of the test article, and that for shock testing the input shock is applied to the test fixture or farther back into the test machine:

4. The test fixture should be designed such that it and the machine to which it attaches present an impedance to the test article which is as near to that which it would see in service as is practically feasible.

5. If Item 4 cannot be accomplished then at least the fixture should be designed such that the first few resonances of the test article as mounted are the same as in the service mounting.

6. If neither Items 4 nor 5 can be achieved, then it is desirable to have the fixture consist of simulations of the next two or three elements in the structural chain which carries the test article.

Item 1 is desirable for economy in testing, which is justification enough in itself. Item 2 is desirable to make control of the test as easy as possible and to minimize force input requirements. Item 3 is supported by the use of laminated structures, wooden fixtures, and cast fixtures, each developed for their relatively high damping qualities. In working toward a fixture with high damping, some rules of thumb worth keeping in mind are:

1. Bolted or riveted joints give more damping than welded joints.

2. Cast metals have higher damping than wrought metals.

3. Laminates can soak up energy in their bonding material, if the cement is a lossy material rather than a stiff, hard one.

The preceding discussion of equalization is important in fixture design for two reasons:

1. It shows that knowledge of the shaker impedance raises the possibility of deliberately aiming for a fixture design which makes easier equalization, as would be the case for $Z_{332} = -Z_{334}$.

2. It shows through Eq. (13) that the test article impedance "feeds back" on the fixture

and affects the value of v_2 . Service environment data which is interpreted without accounting for the interaction effects of component and structure impedance can lead to requirements for v_2 which produce either unrealistic or downright impossible test article responses.

To summarize how a test fixture should be designed, we must refer to Fig. 1 and consider the following situations:

1. When the test is controlled by monitoring and adjusting to get the correct velocity or force input to the test article (control of v_2 or f_2), then fixture impedance does not affect the motion of the test article.

2. When the test is controlled by monitoring and adjusting the velocity and force at the base of the test fixture (control of v_3 and f_3), then the correct velocity or force input to the test article (v_2 or f_2) is achievable through control of v_3 and f_3 despite the fixture impedance. In this case the effects of the fixture impedance are negated by control of two parameters at the fixture base.

3. When the test is controlled by monitoring and adjusting either velocity or force at the base of the test fixture (not both), then fixture impedance affects the test article motion and Eq. (14) applies.

4. When the test is controlled somewhere farther back in the system than the exciter-fixture interface, then only by measurement of the transfer characteristics from that input point to the test article-fixture interface, and adjustment of the input to compensate for these characteristics, it is possible to get the correct test article motions. For this case, the fixture design can be adjusted to minimize the input adjustment.

REFERENCES

1. Colloquium on Mechanical Impedance Methods for Mechanical Vibrations, ASME Pub. (Dec. 1958).
2. S. H. Crandall, "Impedance and Mobility Analysis of Lumped Parameter Systems," ASME Coll. of Mech. Impedance Methods for Mech. Vibrations (Dec. 1958).
3. Karl Unholtz, "The Influence of Electrical and Motional Impedance on the Control and Performance of Some Vibration Machines," Shock and Vibration Instrumentation, ASME, pp. 101-126 (1956).
4. The Design and Use of Vibration Test Jigs and Fixtures, 8 papers, Shock, Vibration, and Associated Environments Bull. No. 27, Part IV (June 1959).

* * *

DEVELOPMENT OF A LAMINATED VIBRATION FIXTURE MATERIAL

R. L. Bergey
Burroughs Corporation
Paoli, Pennsylvania

During the development of a vibration-resistant computer at Burroughs Great Valley Laboratory, it became necessary to construct an 18- by 18-inch angle bracket to orient the 90-pound computer properly during vibration testing. It has been our experience that brackets of this size have considerable internal ringing and amplification when testing from 5 to 2000 cps. To eliminate this, a fixture was made from 1/16-inch sheets of glass-epoxy and aluminum, alternately laminated together. The maximum section thickness was 1 1/16 inches and the amplification factor was not over 1.3. It was completely assembled with epoxy glue. The weight of 80 pounds could be substantially reduced in the future, for the fixture appears considerably overdesigned. The technique appears to be promising for future fixtures.

In designing high-frequency vibration fixtures for items that are too small to permit tubular construction techniques, and, at the same time, too large for construction from solid metal plates, the problem of fixture resonance becomes particularly acute. This problem has been encountered at these laboratories most frequently with test vehicles that are approximately cubic in shape, with the edge dimension varying between 6 and 12 inches and the weight from 25 to 80 pounds. The necessity to vibrate these test vehicles to 2000 cps in three planes, without a slip table, has caused further complications in fixture design.

ORIGIN OF PROBLEM

On the program during which the problem first arose, an attempt was made to formulate a simplified design technique. Various designs of aluminum or aluminum and Masonite (Bene-lux) were tried. The results were made usable, but only by monitoring the input force at critical mounting points, and by introducing prestress into the fixture material. After several attempts with different methods, it became evident that a general design technique or analysis procedure would be difficult to develop, and, further, that an all-purpose material was not available that could be easily applied to many different situations. The conclusion drawn

from experience was that considerable damping must somehow be made an inherent property of the material used for fixturing.

DESIGN BASIS AND FABRICATION

Epoxies and glass-epoxy laminates exhibit considerable capacity for damping; it was thought, therefore, that epoxy-aluminum laminates might be satisfactory. To explore this, several small laminates of aluminum foil glued together with very thin layers of epoxy were made and vibrated to determine resonances and amplification factors. The laminated material was found to resonate at the same frequency as a piece of solid aluminum of similar size, but the amplitude of the displacement was one-third that of the solid aluminum sample. This result seemed to indicate that the search for a material with the appropriate damping characteristics was proceeding along fruitful lines.

When it again became necessary to construct a fixture from high-damping materials, however, time was of the essence. No further investigation had been made of laminated aluminum foil, and the fixture required was too large and the program too poor in risk confidence in a quick solution with an aluminum-foil fixture. There are handling problems in preventing wrinkling with a large amount of foil,

and the foil should receive special surface treatment to assure good bonds to the glue. The solution to this problem, while perhaps not difficult, was felt likely to involve more trial and error than time or money would permit. It was decided, therefore, to use 1/16-inch thick aluminum sheets, as these are readily available, and laminate them alternately with 1/16-inch thick G-11 glass-epoxy sheets. The thicker sheets are easily handled and greatly reduce the number of bondings necessary.

The layers of aluminum and glass-epoxy sheet were bonded together with Permacel sheet epoxy, a glue which cures and bonds upon application of heat and pressure. Working with the Permacel is quite simple, as it is supplied 3 mils thick, on rolls several feet wide, and can be cut with ordinary scissors. Assembly was accomplished by stacking aluminum sheet, glue sheet, glass-epoxy sheet, glue sheet, and so forth, and applying heat and pressure for several hours.

To assure a good bond between aluminum and epoxy, the aluminum sheets were thoroughly cleaned and caustic-etched. This process resulted in a surface not only clean but also somewhat roughened, which further contributed to bond strength.

The combination of materials is not an easy one to machine, for the cutting speed necessary for aluminum is not compatible with that needed for glass-epoxy. The glass fibers in the glass-epoxy sheets are also troublesome during machining. Carbide-tipped mills were used. During a drilling operation on one piece, a drill became hung up, and the resulting wrench caused a lamination joint to fail. The piece was repaired simply by putting the piece back in a press and applying more heat and pressure. No other problem with delamination occurred.

To achieve test vehicle attachment, slugs of aluminum were glued into appropriately positioned holes drilled after the sheets were laminated. All necessary drilling and tapping was then effected with the slugs permanently placed, thus permitting easy drilling and accurate hole location.

Glue was also employed in assembling the laminated pieces together to form the final fixture. To make the final assembly as self-jigging as possible, slots were made in half of the pieces to act as guides and, at the same time, to increase the area of glue application. Bondmaster 666 epoxy cement was used in this operation.

The fixture thus fabricated weighs 80 pounds, and has an amplification factor not greater than 1.3. The material technique appears easily applicable to other fixture needs, where similar problems are encountered. Since internal damping is high, it would appear that sections need not be as thick as those ordinarily used with aluminum. The technique appears at this time to have a promising future in the areas described; however, further experience is necessary to verify this conclusion.

Photographs of the fixture are shown in Fig. 1. (The three blocks in the fixture are counterweights.) It is evident in Fig. 1a that considerable rigidity is achieved from the six main supports, each 13/16 inch thick. The front support plate is 1 3/16 inches thick, and the webs between the six main supports are 9/16 inch thick. The base plate is 1-inch thick aluminum.

Were another such fixture to be fabricated, it would appear that all structures could be somewhat reduced in thickness — the front plate to about 1 inch, the main supports to 9/16 inch, and the webs to about 5/16 inch. These dimensions would reduce the weight of the fixture from 12 to 15 pounds without significant change in performance characteristics.

Several new epoxy glues now available should eliminate the necessity to apply both heat and pressure to the laminates while they are being fabricated. It would appear that no heat is required and only sufficient pressure to assure an even distribution of the glue within the laminate sheets and to control the resultant total thickness, if this dimension is critical.

It is interesting to observe that the front plate was not made as a single piece, but rather as two pieces glued together with a tongue-and-groove joint. This approach was taken simply because the press used could not hold a piece of sufficient size for the front plate; this construction does, however, illustrate the versatility of glued joints.

FURTHER APPLICATIONS

The use of glue to assemble this fixture has some analogy to the welding of aluminum fixtures. Gluing presently appears more versatile, because pieces can be located and securely attached in areas which would be difficult or impossible for a welder to reach, such as the rear supports to the angle plate just described.

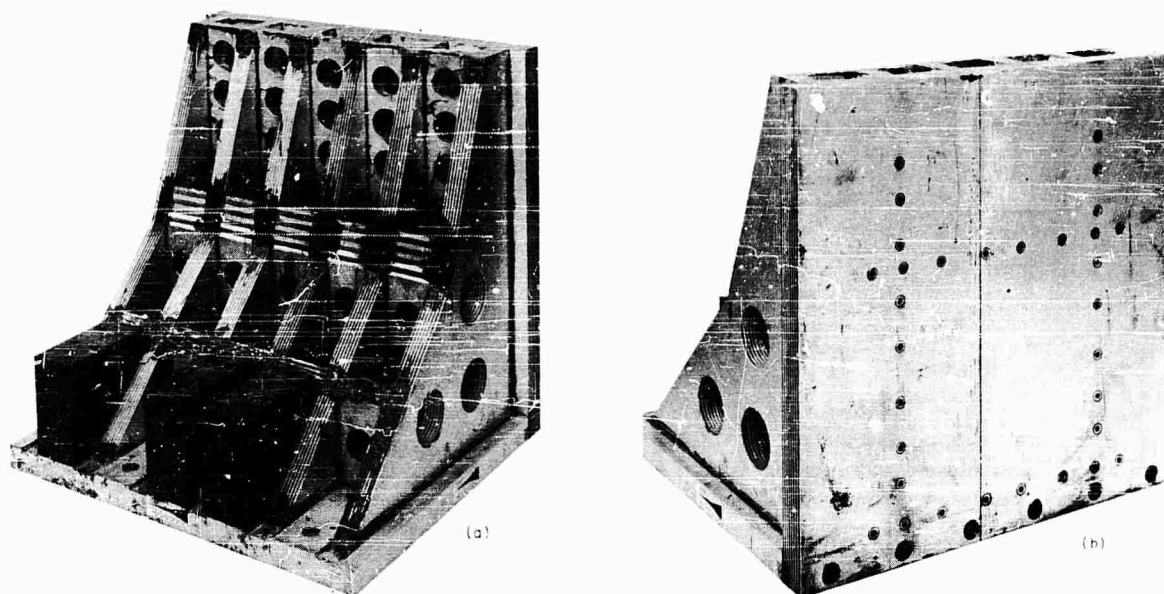


Fig. 1 - Laminated vibration fixture: (a) rear view, and (b) front plate

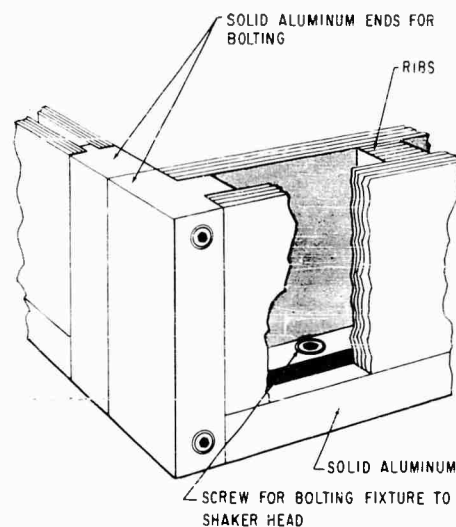


Fig. 2 - Diagram of hollow section with bolted joints

Gluing also makes possible the use of hollow sections, as shown in Fig. 2. Here, the lamination technique is particularly adaptable, because it appears that much thinner sections can be used than with aluminum, and ribs or bosses may be glued in for added rigidity where needed, should resonances appear. A technique for making bolted joints is also shown, along with a method for attaching the fixture to the shaker head or armature. Should rigid joints be preferred, glue can be placed in the joint before bolting, or laminated material used on the ends and then glued. Since the glass-epoxy

material is lighter than aluminum, and since hollow sections appear practical, this technique should produce considerable weight savings over comparable implementations in solid aluminum, and should give improved performance on the vibration table.

ACKNOWLEDGMENT

Credit for selecting glues and gluing techniques is due Mr. Louis J. Dalphone, chief plastics engineer at Great Valley Laboratory.

A REPORT ON THE DESIGN OF INTEGRATED HORIZONTAL AXIS VIBRATION FIXTURES

F. C. Tolleth
Autonetics, A Division of North American Aviation, Inc.
Anaheim, California

The concept of designing a horizontal adaptor and slip plate as an integral unit is not new. Practically all universal slip plates in use today have some means of attachment directly to the exciter head, without having to use a horizontal driver or adaptor. Where a high g-level acceleration is necessary for a large irregular specimen, the common slip plate offers many distinct advantages, such as the elimination of a bolted interface and reduction of fixture length and weight, with a corresponding increase in stiffness and reduced test setup time. The advantages of the integrated concept become apparent by reducing the conventional fixture, slip plate and driver to basic components and using a common sense approach to the design solution. The principles of the design of two fixtures are presented with discussion of the first attempt to apply this method during the design of a very large fixture for high test levels, and a less detailed discussion intended to support the contention that the proper application of the method of integrating the three components into one unit of structure may be applied to fixture design problems which are most severe.

INTRODUCTION

The purpose of this paper is to show that the concept of designing a horizontal adaptor and slip plate as an integral unit has many distinct advantages despite the greater cost and more complex design considerations. In the case where a high g-level acceleration for a large irregular specimen is necessary, the common slip plate can eliminate the bolted interface and reduce the fixture length and weight, with a corresponding increase in stiffness and a reduction in time for test setup.

In many cases this method of combination is overlooked because of its simplicity and because of familiarity by the designer. The inherent value, however, is manifested by reducing the conventional fixture, slip plate and driver to basic components, thus using a common sense approach to the design solution.

This paper does not purport to be the last word on the design of this type of fixture; but, rather, it is intended to point the way to one successful design solution which might be applied by others in the industry with similar problems.

Principles of the design of two fixtures are given: Case I is a discussion of the first attempt to apply this concept during design of a very large fixture for high test levels, and Case II is a discussion designed to support the principles that the proper application of the method of integrating the three components into one unit might be applied to severe problems of fixture design.

BACKGROUND

As far back as 1957, horizontal slip plates, in conjunction with the granite block, have been in use. The advent of these pieces of equipment proved to be of great value to the test engineer when they were compared to the horizontal support systems then in use. Since 1957, many papers have been written on design and use of such equipment. These papers were written to minimize the slip plates' undesirable characteristics. New commercial equipment is now on the market which virtually replaces the slip plate. But perhaps this replacement is premature and a detailed re-examination of the slip plate and its problems is in order.

DESIGN

Reduced to its simplest terms, a vibration fixture is a piece of structure which will ideally transmit vibration from an exciter head to a test specimen, with a frequency response of unity over the frequency bandwidth of the test. The first consideration of the designer, then, is to design a piece of structure with maximum stiffness for a given amount of weight. This implies that the elimination of all joints in the system would be an advantage in terms of weight savings and spring elimination. By reducing this structural system to an equivalent system of masses and springs, one can grasp the design problem and deal with each component of structure in its proper order. Figure 1 is such a reduction of today's standard horizontal test

setup. Figure 2 shows the same basic system, with the joints between the horizontal driver and the slip plate removed. Close examination and comparison of these two figures reveals that the concept found in Fig. 2 has several advantages over the system in Fig. 1.

It is a basic principle that if the most flexible spring is removed from a system of springs in series, as is the case here, the resultant spring stiffness will be greater than the original system. Considering the armature, driver, and slip plate as springs and reducing the parallel systems of bolts of Fig. 1 between the shaker-driver and driver-slip plate to resultant spring rates k_2 and k_4 , respectively, it can be said [1]

NOTE: References appear on page 241.

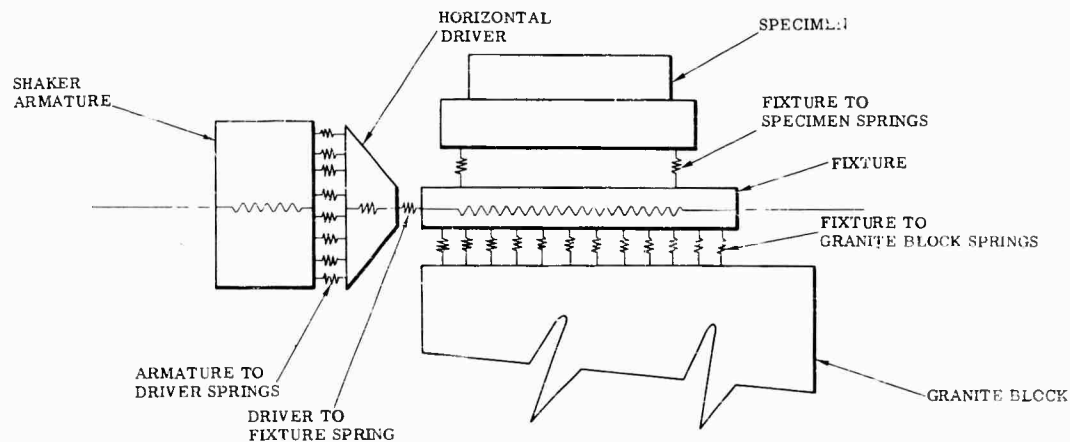


Fig. 1 - Spring and mass diagram of standard test setup

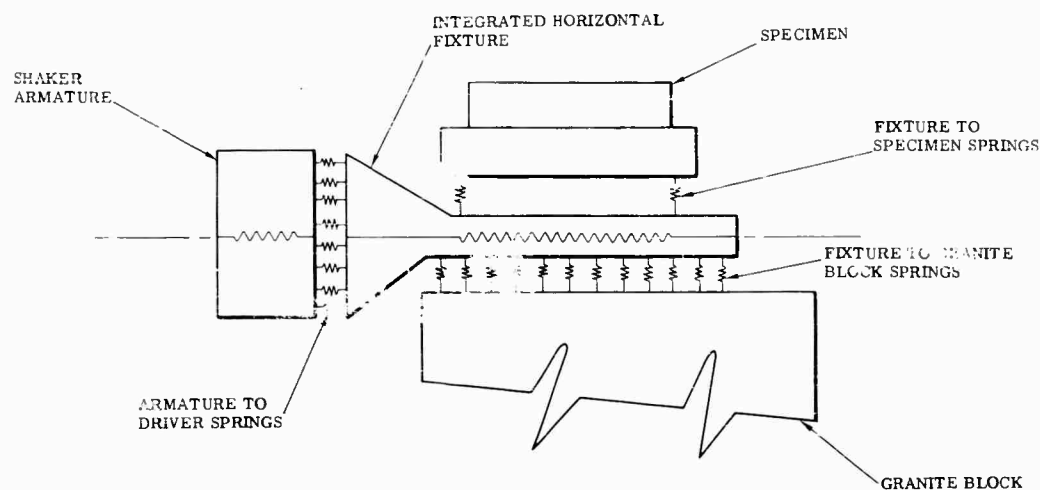


Fig. 2 - Spring and mass diagram of integrated test setup

$$\omega_n = \sqrt{\frac{K_{r1}}{M_1}} \quad (1)$$

where

$$K_{r1} = \frac{(k_{\text{armature}})(k_2)(k_{\text{driver}})(k_4)(k_{\text{slip plate}})}{(k_{\text{armature}}) + (k_2) + (k_{\text{driver}}) + (k_4) + (k_{\text{slip plate}})}$$

The same expression for the system in Fig. 2 may be written as

$$\omega_n = \sqrt{\frac{K_{r2}}{M_2}} \quad (2)$$

where

$$K_{r2} = \frac{(k_{\text{armature}})(k_2)(k_{\text{integrated fixture}})}{(k_{\text{armature}}) + (k_2) + (k_{\text{integrated slip plate}})}$$

It is obvious that K_{r2} is at least equal to K_{r1} because no structure has changed, and K_{r2} may be greater than K_{r1} because the overall length of the fixture is less in Fig. 2. Further, to achieve a high resonant frequency, the moment of inertia for a given area of cross section of the structure must be as large as possible and fixture length a minimum, since resonance is directly proportional to the square root of the cross-sectional area and inversely proportional to the square root of the overall length of the fixture [2,3]. Also, because a conservative estimate for the weight of a joint would be four times the weight of the continuous structure over the span of the joint, the mass M_1 of Eq. (1) would be less than the mass M_2 of

Eq. (2), thus raising the resonant frequency of the system in Fig. 2 above that of Fig. 1.

Figure 3 is a schematic diagram which again depicts a standard horizontal test setup, and shows graphically that it is practically impossible for the designer to design a system so that the centerline of vibration input will pass through the net center of gravity of the test specimen and fixture combination. The net cg of the fixture and specimen lies well above the centerline of drive or vibration input and the overall length of fixture specimen is relatively long.

For this problem, the designer has two alternatives unless he chooses to go to the integrated concept:

1. He can design a thick heavy slip plate and take a weight penalty to minimize over turning moment; or
2. He can design an optimum slip plate and calculate whether the unbalance will be great enough to break the grease seal between the slip plate and granite block for any condition which may be encountered during the test.

Neither of these two alternatives is desirable, since neither really solves the problem of a large unbalancing force.

Figure 4 is a schematic diagram which shows the shaker and specimen with the fixture redesigned to represent the integrated concept. The joint between slip plate and driver has been

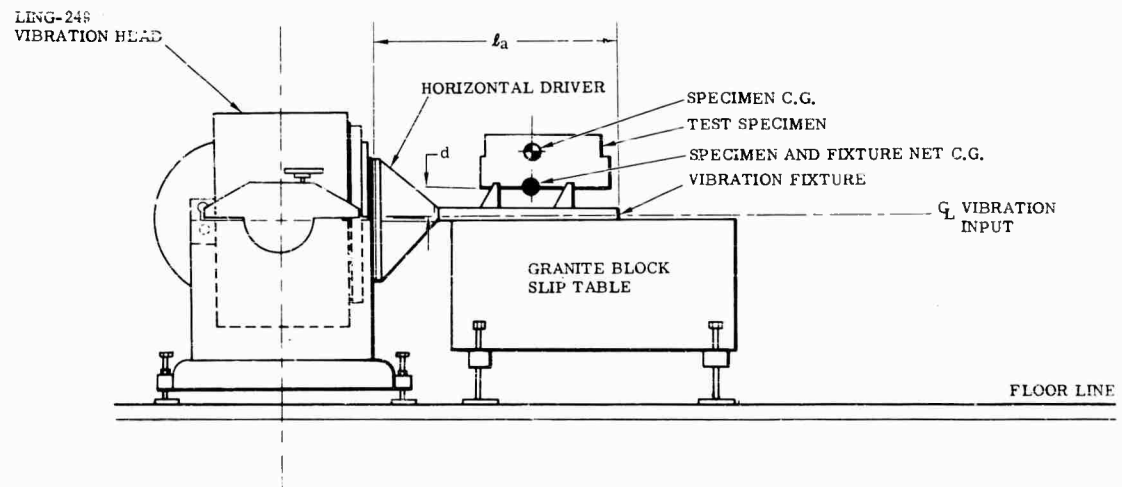


Fig. 3 - Standard horizontal test setup

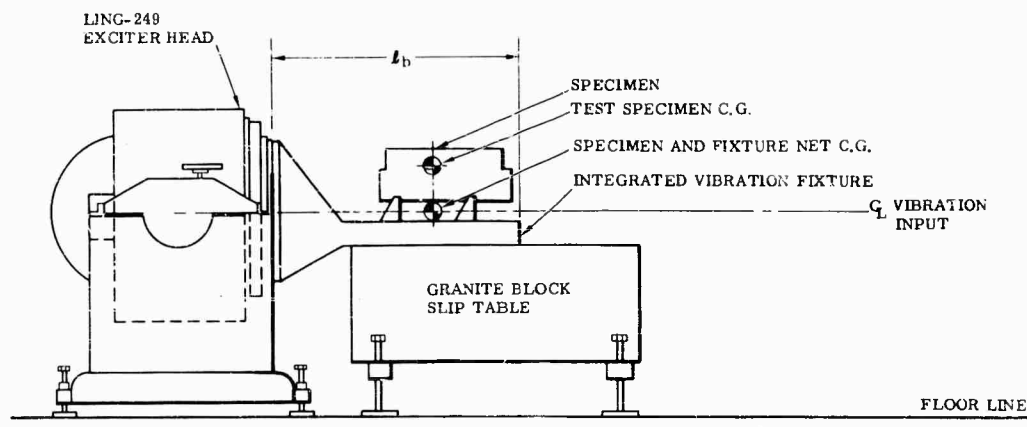


Fig. 4 - Integrated horizontal test setup

removed, thus shortening the fixture and allowing the designer to maintain structural continuity throughout the fixture length. Because the joint between the driver and fixture was eliminated and little or nothing can be done to stiffen the joint between the specimen and fixture, it is necessary to consider only the exciter-fixture interface. Here, all the attachment bolts from the exciter head to the fixture must be used and the length and preloading of these bolts are such that their resonant frequency is at least twice the frequency of the upper limit of the test bandwidth. The slip plate component of the fixture has now been placed well below the horizontal centerline of the shaker to assure the vibration load will be applied directly into cg of the fixture specimen combination, thus eliminating the over turning or angular rotation of the slip plate with respect to the test axis. Length $l_b < l_a$ of Fig. 3 and the net cg of the fixture and specimen now lies on the centerline of the vibration input.

Case I

Figure 5 shows a large cast aluminum fixture designed at Autonetics, which applied the concept of an integral driver-slip plate combination for a specific test specimen and set of test conditions. The test specifications for this design dictated that the package be subjected to a simultaneously applied sine plus random vibration, equivalent to 28 g rms from 5 to 2000 cps along each of three axes of the specimen. The test requirement of 28 g rms, when coupled with the rule of thumb that the weight of the fixture should be at least two to three times the weight of the specimen, limited the choice of the exciter to one which developed at least

28,000 force-pounds, since the specimen weight was approximately 200 pounds.

The vibration system chosen was the Ling-249 and a PP120/150 Ling amplifier which generates 28,000 force-pounds. This meant that the weight of the fixture would have to be revised down to about 350 pounds from the conventional estimate of approximately 500 pounds, since the total moving weight of armature, fixture and specimen exceeded the vibration system capabilities.

The fixture was designed as a heat-treated and stress-relieved aluminum casting. The choice of this method of fabrication was based on several considerations. Experience has shown that generally cast aluminum fixtures perform much better than do welded aluminum fixtures during vibration. Welded fixtures have a tendency to crack adjacent to the welds. This mode of failure is probably due to the fact that large aluminum fixtures are seldom stress relieved and heat treated after welding, usually because additional tooling is required to hold the fixture during these processes. Another major consideration is that the casting process allows the designer to eliminate discontinuities of contour and section, thus reducing the possibilities of local load concentrations which might lead to failures such as weldments exhibit.

The overall length of the fixture from the exciter head is 42 inches and the width, not including outriggers, is 26 inches. The total weight of the fixture is 365 pounds. Fixture material is 356-T6 aluminum alloy, stress relieved and heat treated to T6 condition before machining.

The cost of the fixture shown in Fig. 5 exceeded the cost of more standard fixturing by 30 percent because the extremely large size of the fixture necessitated larger and more expensive machines for the machining processes. However, this particular fixture was very durable and was used to test three later generations of specimens in addition to the test for which it was designed, so net excessive cost for each generation was about 7.5 percent.

Figures 6, 7, and 8 show the actual test setup with the specimen in position and ready for testing.

Case II

Figure 9 shows another integrated horizontal axis vibration fixture. Although the test requirements and conditions were much more difficult from a design aspect than those found in Case I, the application of the integrated concept was again more successful than that of standard fixtures.

Here the test specification levels were equivalent to 60 g rms from 5 to 2000 cps of simultaneously applied sine plus random vibration. The specimen weight for this case was 37 pounds. Using the rule of thumb that the fixture would weigh two to three times the specimen weight, the fixture would weigh 111 pounds.

Because the test was to be run along the horizontal axis, a driver would be needed. The cast aluminum driver on hand weighed 125 pounds. After summing the moving weight, the shaker force output available can be estimated as follows:

$$\frac{28,000 \text{ force-pound}}{400 + 125 + 111 + 37} = 42 \text{ g rms.}$$

or only 63 percent of required g level.

By integrating the horizontal driver and fixture into one unit, the estimated shaker force output available is

$$\frac{28,000 \text{ force-pound}}{400 + 111 + 37} = 51 \text{ g rms.}$$

or 85 percent of the required level. This was just above the lower vibration acceleration tolerance limit.

The cost of this fixture exceeded the cost of the more standard test setup. Because a comparatively inexpensive fixture could be fabricated and used with a driver and slip plate which were on hand, the cost of the integrated cast magnesium fixture was about twice as great as the inexpensive fixture. This cost was justified, since during test the whole system was driven to almost 58 g, which was the test objective.

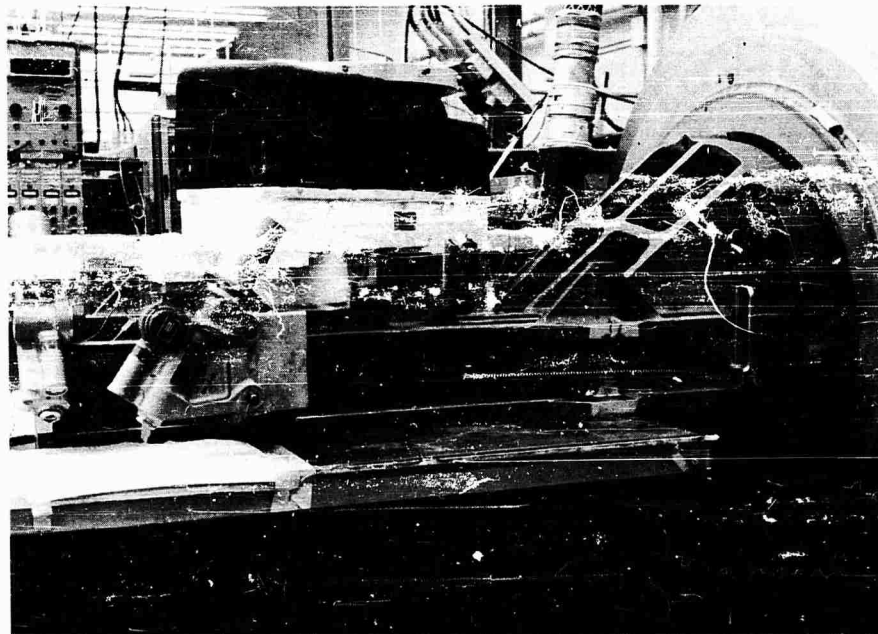
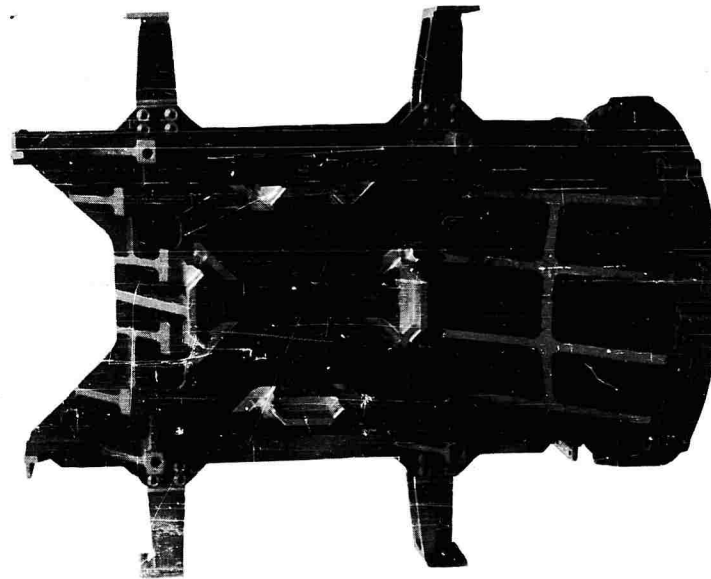
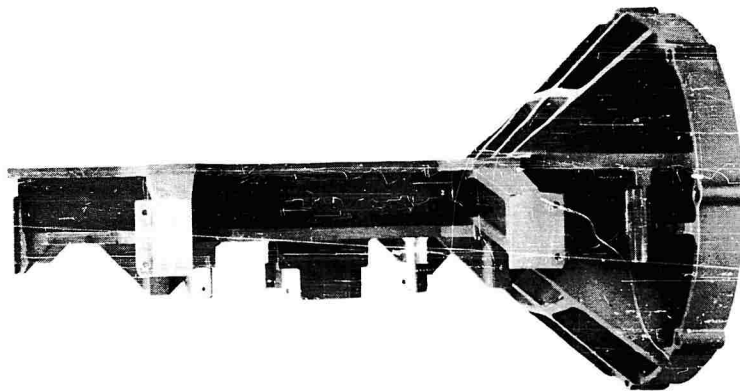


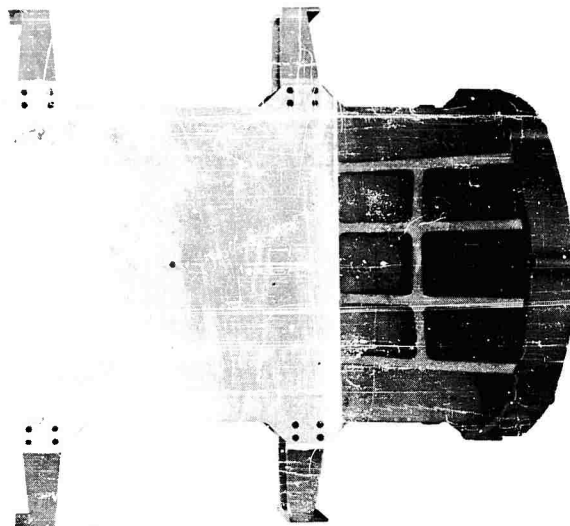
Fig. 6 - Case I integrated fixture test setup (side view)



(a) Top view



(b) Side view



(c) Bottom view

Fig. 5 - Case I integrated fixture

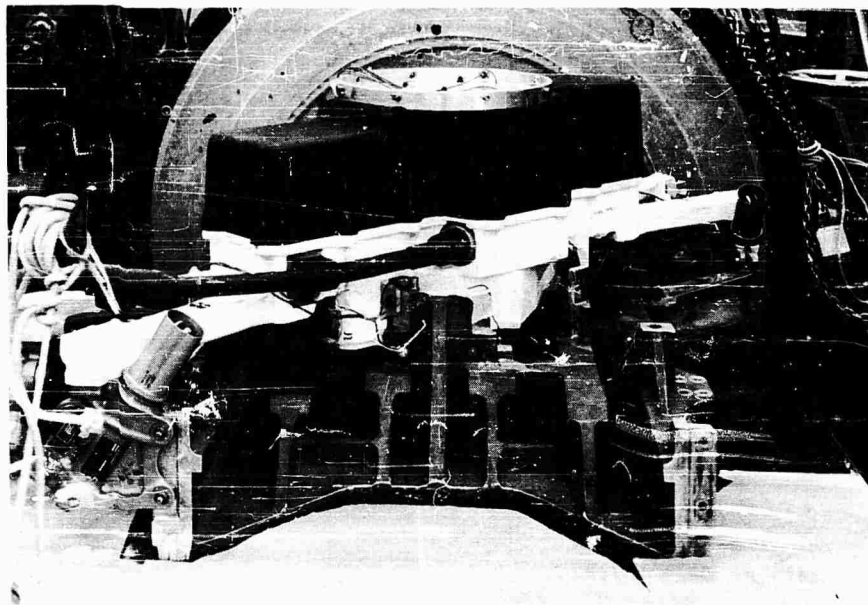


Fig. 7 - Case I integrated fixture test setup (end view)

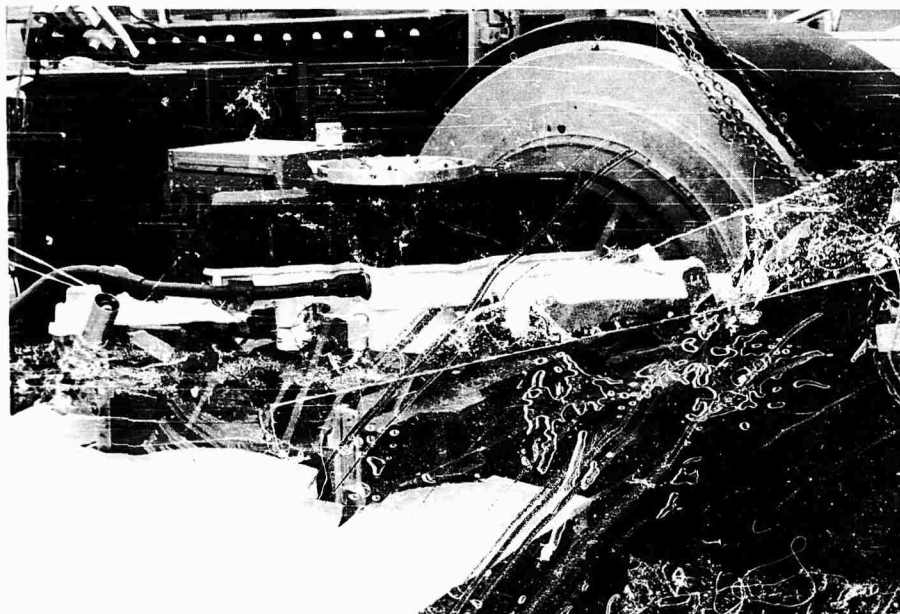
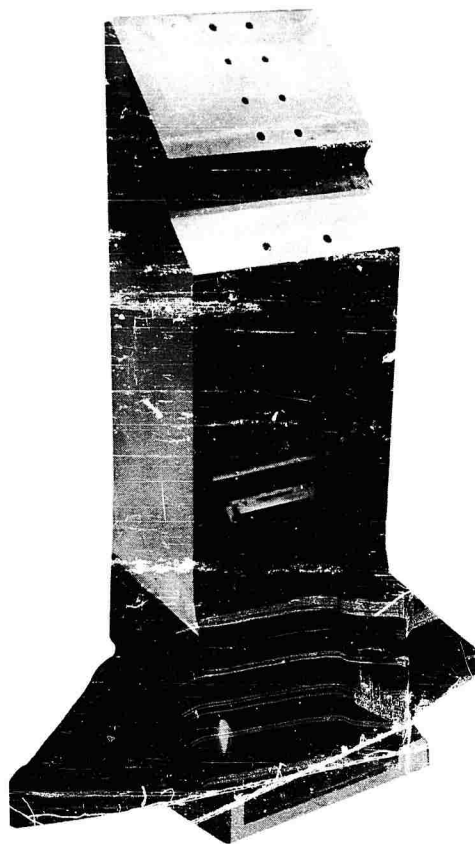
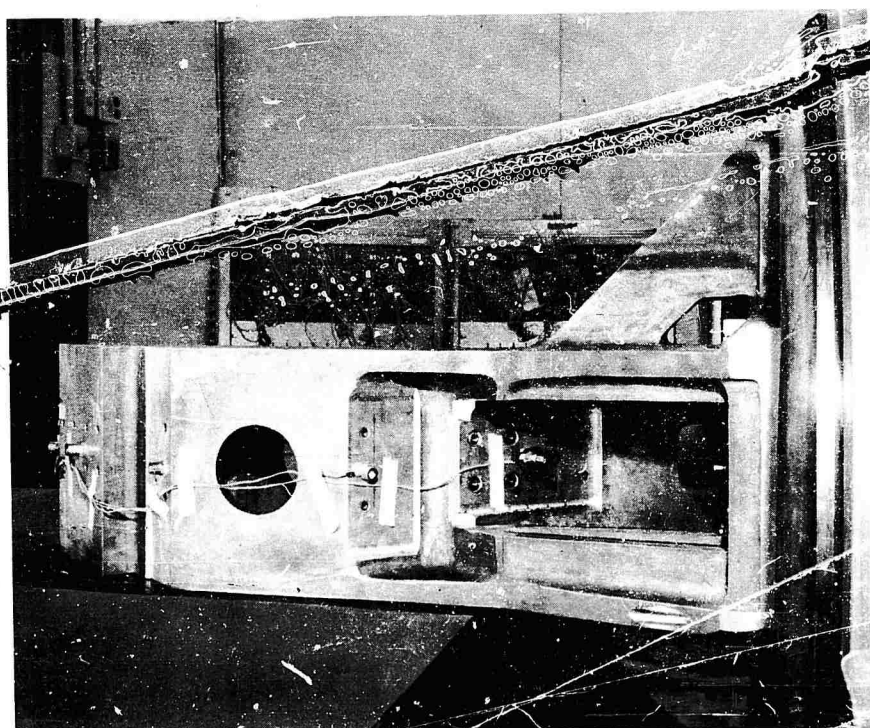


Fig. 8 - Case I integrated fixture test setup (oblique view)

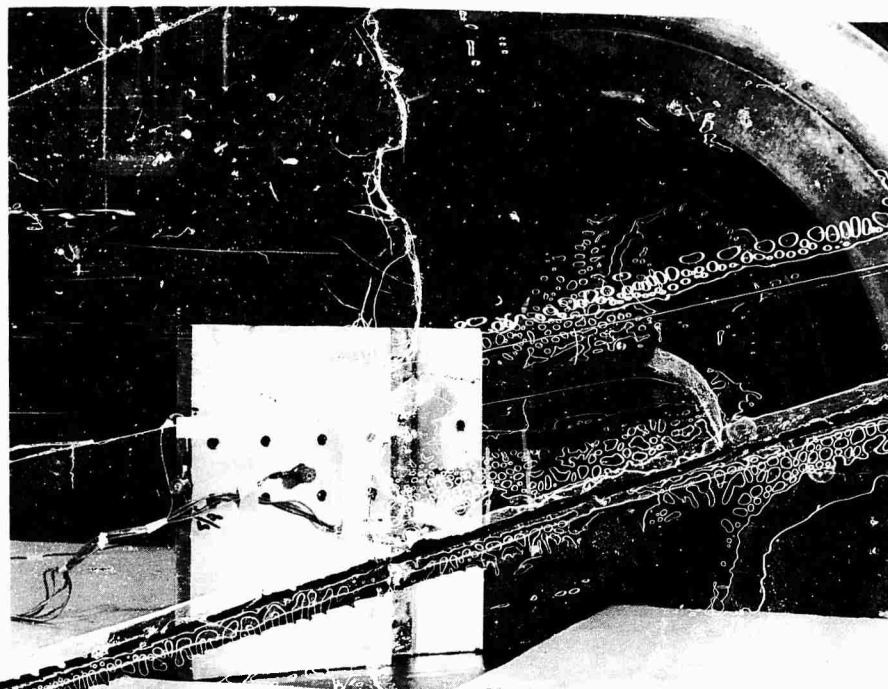


(a) Fixture



(b) Mounted specimen showing specimen mounting pads

Fig. 9 - Case II integrated fixture in mounted position



(c) in test position

Fig. 9 - Case II integrated fixture in mounted position--Continued

Total weight of the fixture shown in Fig. 9 is 105 pounds. The length is 37 inches. Material is AZ63A-T4 magnesium alloy, stress relieved and heat treated before final machining. Figure 10 shows the actual test setup with the specimens mounted and ready for testing.

RESULTS

Data taken from a bare fixture may be as inaccurate as a numerical analysis. The fixture designer must be content with verbal reports of performance and limited data recorded by test engineers. Unfortunately, these fixtures were never thoroughly evaluated as it was necessary to go into the testing phase to meet schedules. Necessarily, all instrumentation available was utilized to record the response of the test specimen during test.

Test engineers reported that overall function of these fixtures was satisfactory. Test setup time was nominal and no problems were encountered in mounting either the specimens or the fixtures.

Resonant frequency for the fixture in Case I, when mounted to the exciter and supporting the specimen, was in the 1500- to 1600-cps range. Although there was a relatively high Q associated

with this resonance, the bandwidth was sufficiently narrow and the resonance caused no problem during equalization.

The completed fixture of Case I weighed 365 pounds, including outriggers and all attachment hardware. Even with this weight, all test levels were met satisfactorily. The fixture was used for the original test program and three additional test programs. By conservative estimate, the fixture has been subjected to at least 6 hours of high-level sine plus random vibration, with no evidence of structural or fatigue failure.

As in Case I, the performance of Case II was satisfactory. The longitudinal resonant frequency of the fixture unloaded but attached to the exciter head was in the 1900- to 2000-cps range, with a Q of approximately 8. Loading the fixture or mounting the specimen caused the resonance to drop approximately 400 cps, and the Q associated with this resonance to rise to about 10.

Vertical and lateral crosstalk was minimum, except at the resonant frequencies in both the loaded and unloaded conditions. The Q associated with the vertical direction of crosstalk at resonance was about 4. In the lateral direction Q was 3.



Fig. 10 - Specimen mounted in actual test setup

There were no problems encountered during the equalization procedure and test engineers reported that fixture response was uniform until resonant frequency was approached.

The final weight of the fixture, including attaching hardware, was 105 pounds. As previously mentioned, with this weight range the system would develop about 52 g. During the test the system was able to develop approximately 58 g which indicates that the fixture performed much better than anticipated.

SUMMARY

The concept of integrated horizontal axis vibration fixtures may be applied in many cases of vibration fixture design. The concept so far has proved advantageous in both the areas of weight savings and increased stiffness. The disadvantages of increased dollar expenditure for manufacturing a special fixture for each test is excessive — but this is returned in terms of fixture performance.

CONCLUSIONS

The critical areas which require special attention during the design procedure are:

1. Vibration input must pass through the net center of gravity of the fixture-specimen combination.
2. The overall length of the fixture must be as short as possible.
3. The slip plate portion of the fixture must have the greatest radius of gyration for its length, consistent with acceptable design practices and fixture allowable weight limits.
4. The exciter-fixture interface bolt system must be designed with a resonant frequency well above the upper limit of the test bandwidth.
5. Distance between shaker face and granite block must be variable and the centerline of vibration input must be adjustable with respect to the surface of the slip table to apply this concept.

REFERENCES

1. C. M. Harris and C. E. Crede, Shock and Vibration Handbook (McGraw-Hill Book Co., New York, 1968).

Standard Environmental Test Method 5, Appendix A." Sandia Corp. Report SC-4452B(M) (1963).

2. N. McDuff and J. R. Cumeri, Vibration Control (McGraw-Hill Book Co., New York, 1958).

* * *

DESIGN OF LARGE VIBRATION FIXTURES FOR SATURN S-IV STAGE DESIGN DEVELOPMENT AND QUALIFICATION PROGRAM

L. G. Smith
Douglas Missiles and Space Systems Division
Huntington Beach, California

The vibration test requirements for development and qualification of Saturn S-IV subsystems necessitated the use of unusually large test specimens. This paper presents examples of the many welded tubular-type vibration test fixtures used by the Douglas Aircraft Company to implement this program. The design philosophy, the successful results obtained with these fixtures, the evolution of improved fixture procedures, and a suggested program for future improvement of vibration test fixture design are discussed.

INTRODUCTION

The development of the Saturn Vehicle S-IV Stage required that unusually large vibration test specimens be tested. The vibration environment of this stage is primarily induced by rocket and boundary layer noise. The test specimens must be designed so the response of the item under test approximates the actual response to the acoustical excitation occurring at the skin, where the specified test levels apply. To achieve this response, it is necessary to include all structural elements contributing to the mechanical impedance between the item and the skin.

It is usually desirable, and often mandatory, to place the test specimen in the same gravitational axis as the vehicle. This consideration usually causes the upper edge of the specimen skin panel to be high above the shaker head in at least one axis. The test fixture must transmit vibration up to 2000 cps to these extreme edges of the specimens. Some of the skin specimen and fixture combinations used have exceeded 96 inches in height and 62 inches in width. The resulting specimens usually are of such a size as to be relatively large for single shaker tests, but too compact for multi-shaker application.

This paper describes the approach to vibration test fixture design used to meet these conditions and requirements.

ORIGINAL S-IV FIXTURE DESIGNS

The first need for a fixture of the type described occurred in the qualification test of the S-IV umbilical assembly. The purpose of this test was to ascertain the ability of the umbilicals and their carrier plate to function and separate during the application of predicted Saturn I launch environments. The test specimen consisted of a portion of the vehicle surrounding the umbilical disconnects, as well as the umbilicals and carrier plate.

Fixture Description

The original fixture design concept was to utilize fully the intrinsic stiffness of axial load-carrying members by using a truss-type design. The truss members consisted of a 1- by 4-inch frame supporting the skin at the top and on two sides, and 4-inch diameter by 1/4-inch tubing connecting the frame to the base. The base was constructed of 1-inch stock. All members were made of 2014 aluminum alloy and welded together. The particular skin specimen involved was 32 inches high by 64 inches wide. It was decided to drive five points on the panel frame from four points on the base.

To join the base to the driven points, only the minimum number of members required to achieve static stability were used. It was

believed that this approach would yield the highest first mode frequency possible. It was also expected that although individual tube and frame members would have resonant frequencies within the test bandwidth, the relatively light weight of these members would minimize the effect of such resonances on the specimen. Rough calculations were made to ascertain that the first mode frequency was reasonably high and that the tubes were not overloaded.

The basic fixture was designed for vertical axis excitation only. For lateral excitation, the base was to be used as a slip plate and drive adapters were to be designed and welded on at the test site. The fixture is shown in Fig. 1.

Changes During Construction

During construction, as the fixture took shape, it became obvious that the 1-inch base was not proportionate to the total size of the test fixture. Reinforcing bars were added to stiffen the base. It also became apparent that the larger vertical member could be partially supported at midspan with a negligible weight increase and this revision was made.

Behavior During Testing

Although the fixture allowed test criteria to be met, difficulty was experienced both in sinusoidal control and in random equalization. Contrary to expectations, fixture member resonances were evidently affecting the specimen. Modification of the test fixture for excitation in the lateral axes required an additional 16 to 24 hours for each axis.

REVISIONS IN DESIGN TECHNIQUE

Having experienced reasonable success in the initial attempt, and due to the size and immediacy of the Saturn IV test program, only those changes to the basic design techniques which were either known to be necessary or which offered a high probability of improvement were considered. Analytical support was minimized and conservative approaches were used.

Material

Later fixtures were made of AZ31-B magnesium. This material was chosen because of

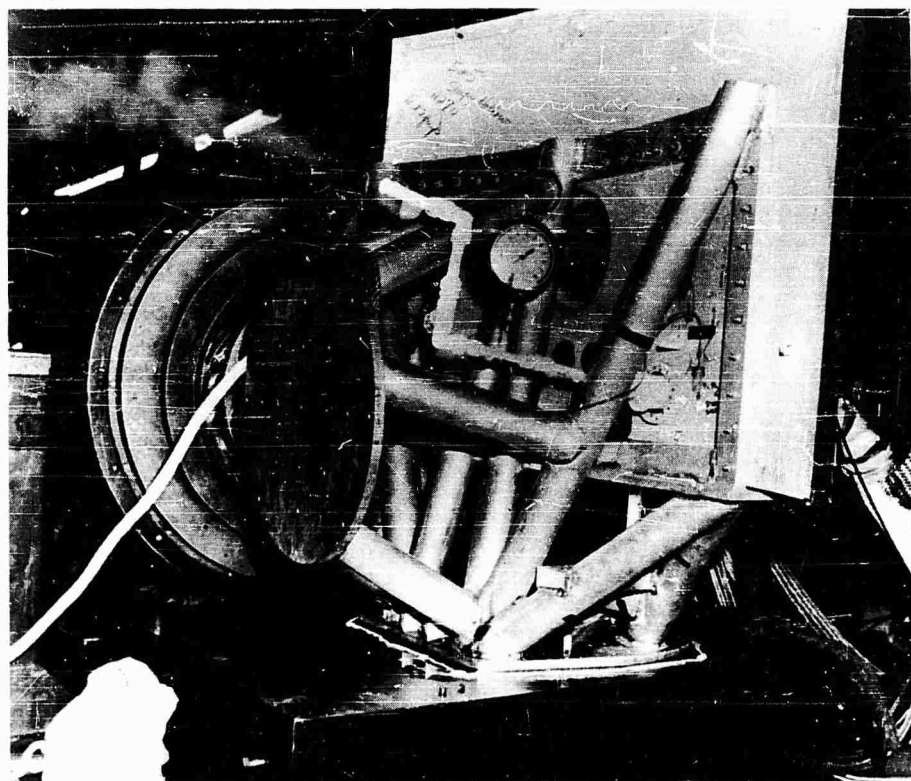


Fig. 1 - First S-IV skin panel mounting vibration fixture

its high specific damping capacity. In addition, it is 37 percent lighter than aluminum and has an equivalent stiffness-to-weight ratio. Although magnesium is more difficult to weld, the damping improvement and weight savings compensated for this.

Skin Panel Attach Frame

To improve the stiffness-to-weight efficiency, frames were made from the same basic tubing as the other truss members and adapted to the skin panels using a minimum amount of 1/4- and 1/2-inch plate. Skin panels were supported on all sides to insure control of the specimen. Figures 2 through 7 show examples of the improved design technique.

Basic Truss

To keep individual tube resonance down to 2300 cps, statically unloaded members were

added to the "minimum" truss in such a manner that single tube spans were 20 inches or less (Figs. 5 through 8). An attempt to use smaller diameter tubing for this purpose was unsuccessful. The 4- by 1/4-inch tubes were retained and performed adequately.

Gusseting was also employed to shorten tube span (Fig. 3) and where bays were too small for tubes (Fig. 9). The length of unsupported edges of the gussets should be minimized.

Base

To avoid base stiffeners, 2-inch bases were adopted as standard.

Foaming

All tubes were filled with polyurethane foam to improve fixture damping characteristics and to control fixture resonances. Polyurethane

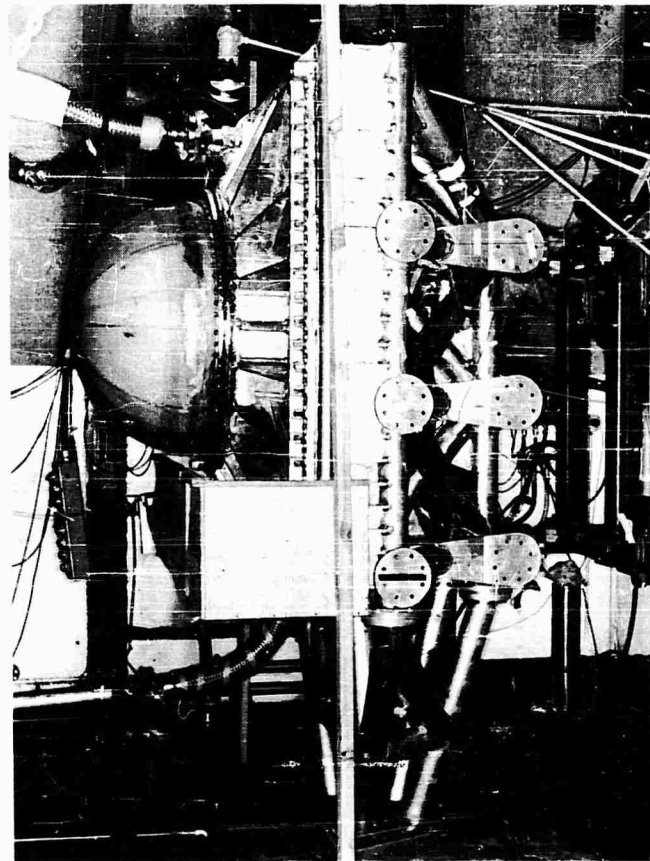


Fig. 2 - Vibration fixture incorporating pressure vessel

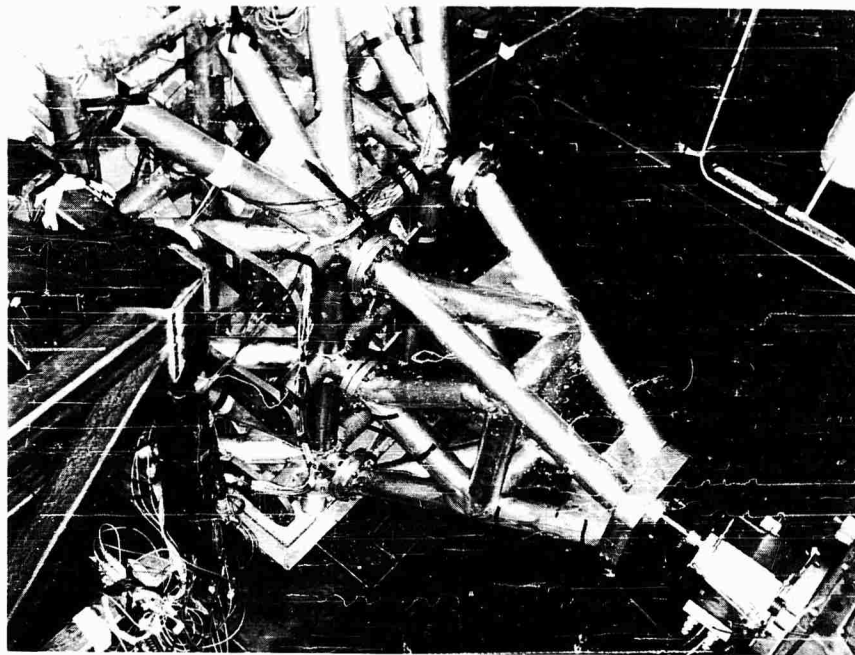


Fig. 3 - View showing lateral vibration adapter

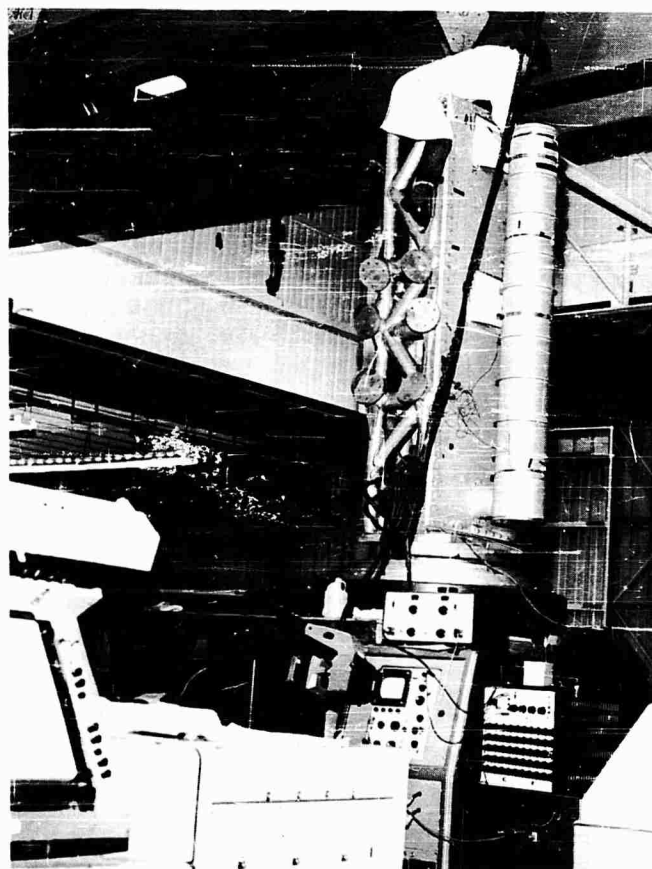


Fig. 4 - Exceptionally long vibration fixture

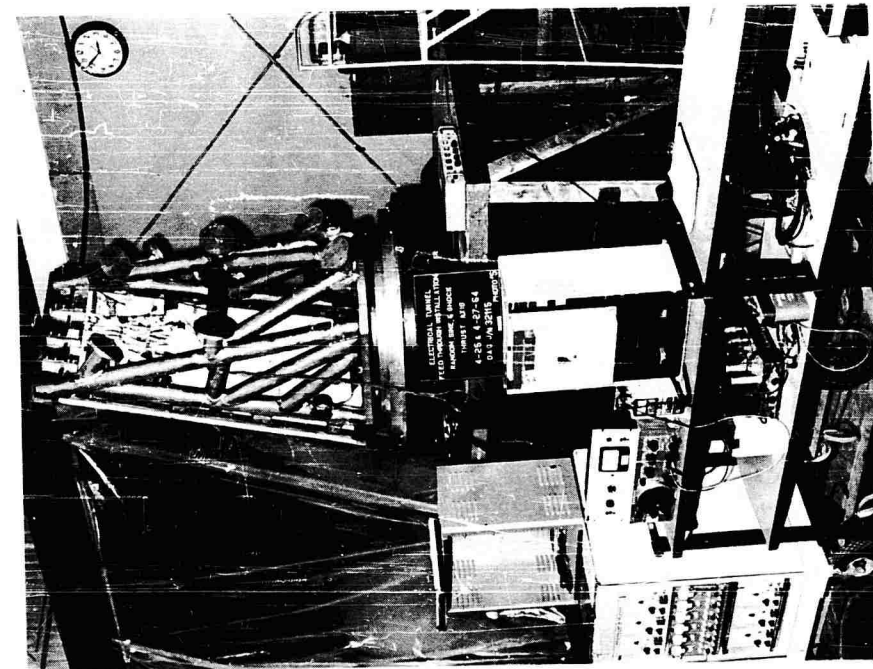


Fig. 5 - View showing provisions
for lateral adapter

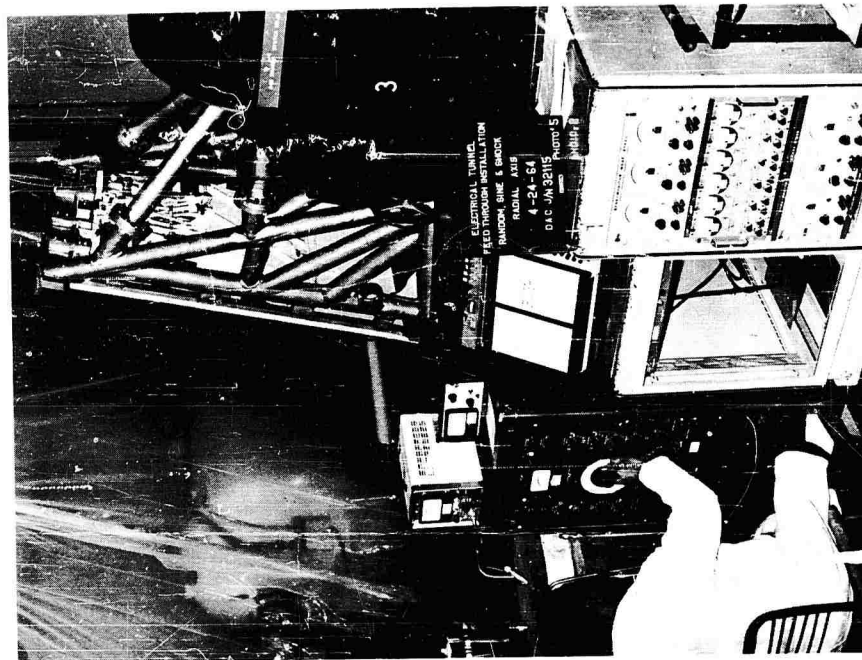


Fig. 6 - Fixture with adapter attached

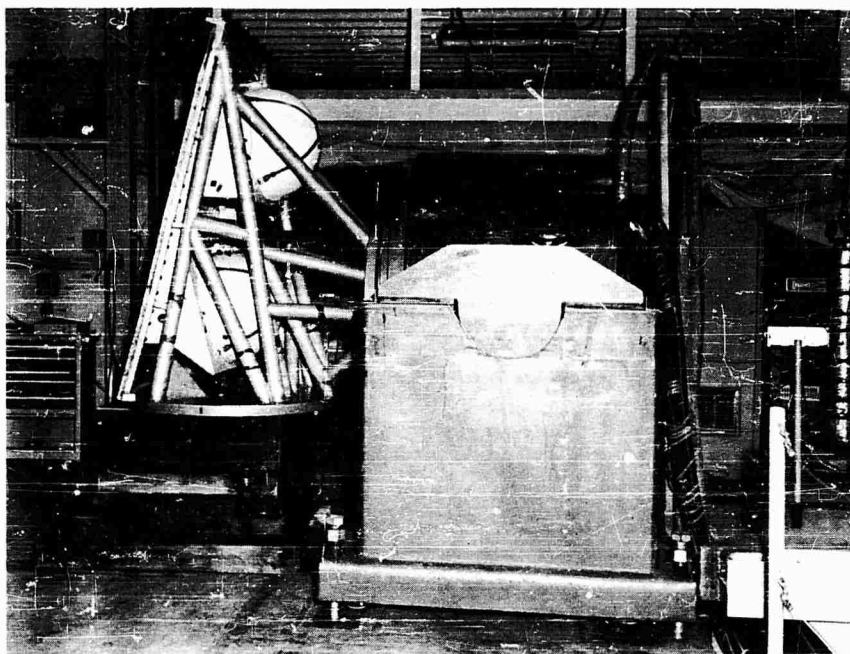


Fig. 7 - Early vibration fixture with welded adapter



Fig. 8 - View of fixture showing desirable truss details

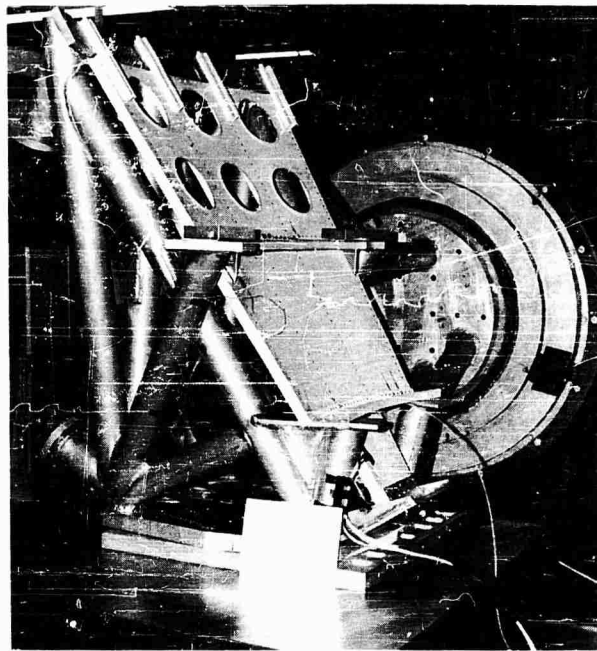


Fig. 9 - Early vibration fixture showing gusseting technique

foam with a negligible 8- to 10-lb/cu ft density was used. Fixtures using the foam-filled tubing was successful. Although the magnitude of the improvement was not determined, all fixture tubing is now filled with this foam.

Lateral Excitation Adapters

As the volume of testing increased, test delays caused by the need to weld lateral adapters became increasingly undesirable. Fixture design personnel were not always available at the test site to determine weld-on adapter requirements, which led to undesirable design details, such as the tubes being driven at midspan (Fig. 7). To alleviate both these situations, bolt-on adapters are now included in the original design of each fixture (Figs. 5 and 6). To avoid low-frequency end loaded cantilever beam mode, the adapter plates on the main specimen fixture are gusseted where the overhang is excessive (Fig. 4).

Fixture Performance

The fixture is shown in Fig. 10. The specimen consisted of a large electronics assembly and its mounting panel attached to the vehicle skin by vibration isolating strips. The control

accelerometer was located on the skin panel adjacent to the isolating strip.

As an indication of the performance of this type of fixture during an actual test, sinusoidal data from the control accelerometer and the shaker head are presented in Fig. 11. These data show that the fixture allows successful test control. The comparison of the curves is indicative of transmissibility of the fixture. No transmissibility plots were made because they are affected by both local fixture resonances and specimen feedback, rather than overall fixture performance. Such plots consequently vary greatly with accelerometer location, especially at the high frequencies.

FUTURE FIXTURE IMPROVEMENT

During the time lapse between the S-IV and S-IVB tests there has been some opportunity to consider further improvement in fixture design. These improvements are aimed at increasing the useful application of the fixtures to a maximum number of tests per fixture, and at stiffening and reducing the weight of the fixtures.

Universal Fixtures

If the test program for a project is examined, it is often possible to find a number of

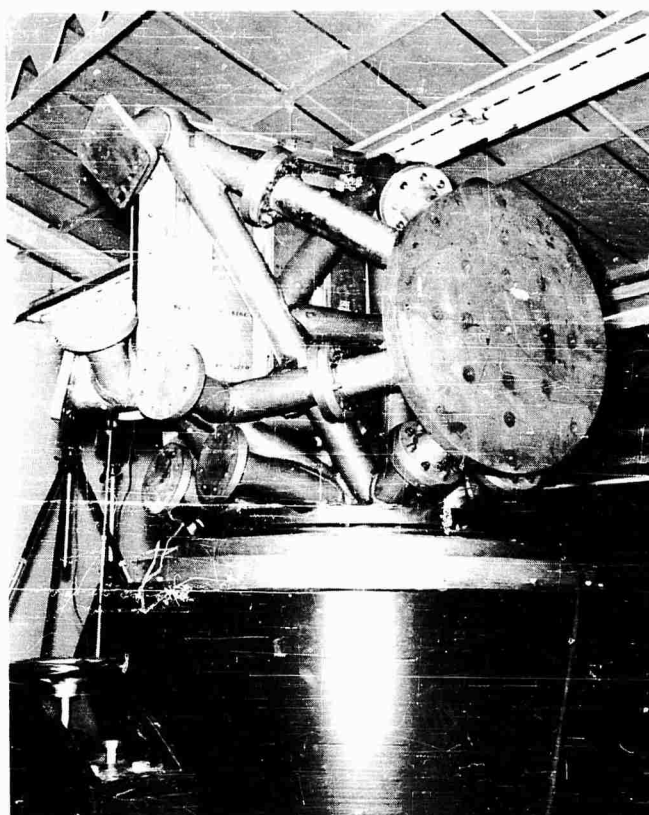


Fig. 10 - Vibration fixture used for gathering
fixture performance data

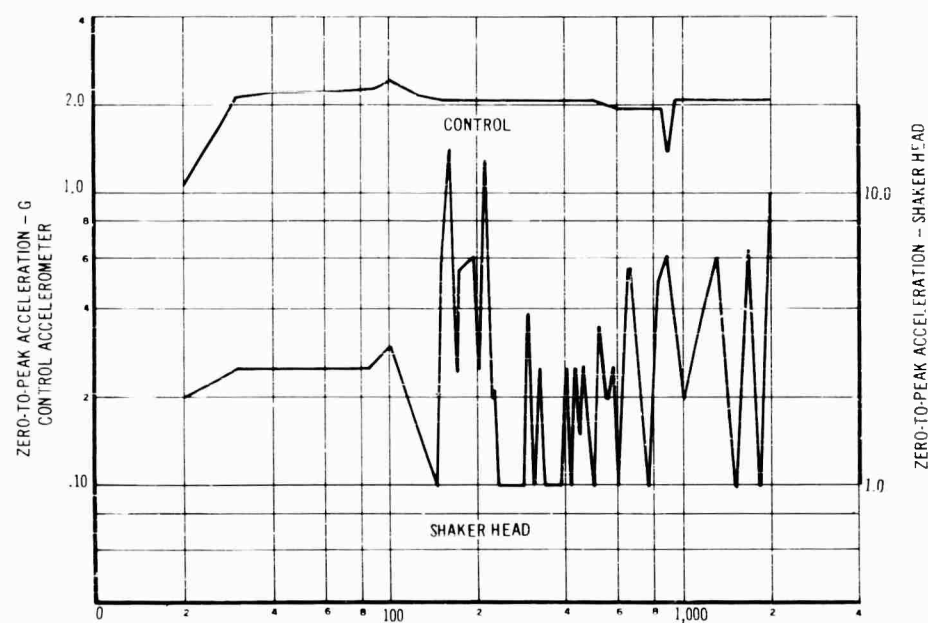


Fig. 11 - Comparison of control accelerometer
response to shaker head input

tests which will require similar size skin panels. A fixture can be designed for the largest size specimen to be tested and the other test specimens can be increased in size so that the same basic fixture can be used for several specimens, other envelope dimensions permitting. This approach has proven feasible for cylindrical portions of the vehicle. In the case of conical sections, the changing skin radius presents a problem. An attempt is being made to incorporate adapters to the skin frames which would overcome this problem.

Base Size

Because of the considerable weight of 2-inch bases (approximately 80 pounds for 30-inch diameter bases) a 1 1/2-inch base is being tried. No attempt will be made to develop built-up bases because of the construction difficulty involved.

Truss Optimization

A method of structural design for minimum weight in vibration test fixture superstructure has been derived. This approach is based on determining the tube cross-section properties required to give the desired ring mode frequency, and the span required to give the desired bending mode frequency. The fixed parameters are the cross-sectional area based on stiffness and strength considerations, whichever is most critical, and member frequency based on test bandwidth.

Strain gage measurements made on existing fixtures have been used to predict load levels for future fixtures. Preliminary results indicate that present stress levels are very low; thus, trusses will probably be designed to the first mode frequency criteria.

It is assumed that the specimen geometry fixes the fixture geometry, so that the truss size and shape is a fixed parameter. For this given size truss, the strength and first mode frequency are both dependent on the cross-sectional area as follows:

$$A = \frac{P_d}{\sigma}, \quad (1)$$

$$A = \frac{\sum_n W_n^2 L_n}{W_{eff} E \delta_{st}}, \quad (2)$$

and

$$f^2 = \frac{9.78}{\delta_{st}}, \quad (3)$$

where

A = cross-section area (sq in.),

σ = fatigue stress (psi) [1],

W_{eff} = effective load (lb),

W_n = static load in truss members due to W_{eff} (lb),

E = elastic modulus (psi),

L_n = overall length of members (in.),

δ_{st} = static deflection of truss (in.),

f = first mode natural frequency (cps), and

P_d = highest dynamic load in truss member due to specimen resonance (lb).

W_{eff} can be applied in any direction to find the natural frequency for vibration in that direction. The effective load of the truss weight is taken as one-third of the total weight, by application of the Rayleigh method [2]. Thus, the total effective load becomes the actual load plus one-third of the truss weight.

Equation (1) expresses the area required to operate at a certain stress level, Eq. (2) utilizes elastic energy considerations to express the area required to achieve a certain static deflection, and Eq. (3) expresses the dependence of natural frequency on static deflection. Combining Eqs. (2) and (3) yields

$$A = \frac{(\sum_n W_n^2 L_n) f^2}{9.78 W_{eff} E} \quad (4)$$

which relates the area directly to the natural frequency. Equations (1) and (4) are both solved to determine the required area, which is the larger of the two solutions.

The first bending and ring mode natural frequency of the individual members is given by

$$\left(\frac{C_b}{10^4}\right)^{10^4} = \frac{f_{n_b} L^2 \sqrt{2}}{K_m R} \quad (5)$$

and

$$\left(\frac{C_r}{10^4}\right)^{10^4} = \frac{f_{n_r} R^2}{K_m t}$$

where

$C_r/10^4$ = ring mode frequency constant (2.51) [3],

NOTE: References appear on page 253.

$C_b/10^4$ = bending frequency constant (71.95) [3],

K_m = material constant (0.965) [3],

f_{nb} = bending natural frequency (cps),

f_{nr} = ring mode natural frequency (cps),

R = tube mean radius (in.),

t = tube thickness (in.), and

L = tube span (in.).

The values given for the constants assume ring modes unrestrained by the ends, rigid ends, and magnesium tubes.

The optimization condition is that $f_{nb} = f_{nr}$. These quantities are redesignated f_n . Equations (5) and (6) are then rearranged and combined with the thin tube approximation, $A = 2\pi Rt$, to yield the optimization expressions,

$$L_{opt} = \sqrt[6]{\frac{\left(\frac{C_r}{10^4}\right) \left(\frac{C_b}{10^4}\right)^3 K_m^4 A \times 10^{16}}{4\pi \sqrt{2} f_n^4}} \quad (7)$$

$$R_{opt} = \frac{f_n L_{opt}^2 \sqrt{2}}{K_m \left(\frac{C_b}{10^4}\right) 10^4} \quad (8)$$

and

$$t = \frac{f_n R_{opt}^2}{K_m \frac{C_r}{10^4} \times 10^4} \quad (9)$$

In these expressions f_n is the desired individual member frequency; f_n should be higher than the maximum test frequency. The "opt" subscript denotes the optimum quantities. Since optimum lengths are not likely to be equal divisions of the basic truss size, the proportions for the next larger and smaller possible lengths are found and compared using the "weight factor" W_f :

$$W_f = (n+1) Rt, \quad (10)$$

where n is the number of divisions of the basic truss resulting from the geometric change associated with keeping the tube spans down to the noted lengths. The size with the lower W_f is the final solution.

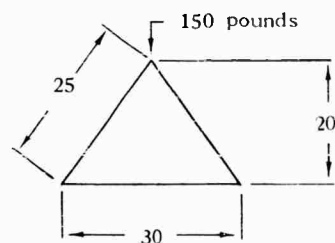
An example of the procedure is given in the appendix.

ACKNOWLEDGMENT

Phases of work presented herein were accomplished by the Douglas Aircraft Missile and Space Systems Division under the Saturn S-IV Contract NAS7-1 sponsored by the George C. Marshall Space Flight Center (MSFC) of the National Aeronautics and Space Administration.

Appendix

The problem is to design a two-dimensional AZ-31B magnesium truss to drive a 150-pound specimen with a resonant transmissibility of 10. The truss-supported specimen must be 20 inches away from a 30-inch diameter shaker head. The test called for a vertical sine sweep of 20 g from 10 to 2000 cps. The truss shall have a first mode of 200 cps and member modes of 2500 cps.



1. Dynamic load = $150 \times 20 \times 10 = 30,000$ pounds.

2. From the geometry,

$$P_d = \frac{30,000}{2} \times \frac{25}{20} = 18,750 \text{ pounds.}$$

3. From Ref. [1], $\sigma = 10,000$ psi (the endurance limit for AZ-31B alloy).

4. From Eq. (1),

$$A = \frac{18,750}{10,000} = 1.875 \text{ sq in.}$$

5. To calculate W_{eff} , a trail tube area of 2 sq in. is chosen. Weight of truss = $2 \times 2 \times 25 \times$

0.0625 = 6.25 pounds. Therefore,

$$W_{eff} = 150 + \frac{6.25}{3} = 152 \text{ pounds.}$$

6. From Eq. (4),

$$A = \frac{\left[\left(\frac{152}{2} \times \frac{25}{20} \right)^2 25 + \left(\frac{152}{2} \times \frac{25}{20} \right)^2 25 \right]}{9.78 \times 152 \times 6 \times 10^6} (200)^2$$

$$= 2.04 \text{ sq in.}$$

Since $2.04 > 1.875$, the desired area is $A = 2.04$ sq in. Since this checks with the assumed area we may proceed. If it did not check, we would return to Step 5, using the solution of Step 6 as the assumed area.

7. From Eq. (7),

$$L_{opt} = \sqrt[6]{\frac{2.51 \times 71.95^3 \times 10^{16} \times 0.965^4 \times 2}{4\pi \sqrt{2} \cdot 2.5^4 \times 10^{12}}} = 16.9 \text{ in.}$$

8. From Eq. (8),

$$R_{opt} = \frac{2.5 \times 10^3 \times 16.9^2 \sqrt{2}}{0.965 \times 71.95 \times 10^4} = 1.455 \text{ in.}$$

9. From Eq. (9),

$$t_{opt} = \frac{2.5 \times 10^3 \times (1.455)^2}{0.965 \times 2.51 \times 10^4} = 0.218 \text{ in.}$$

10. As a check,

$$A = 2\pi R t = 2\pi \times 1.455 \times 0.218 = 2.$$

11. Possible lengths are 12.5 ($n = 2$) or 25 ($n = 1$). For $L = 12.5$,

$$R = 1.455 \times \left(\frac{12.5}{16.9} \right)^2 = 0.795 \text{ in.,}$$

$$t = \frac{A}{2\pi R} = \frac{2}{2\pi \times 0.795} = 0.319 \text{ in.,}$$

$$\text{Diameter} = 2R + t = 1.909 \text{ in.,}$$

and

$$W_f = (2 + 1) \times 0.319 \times 0.795 = 0.759.$$

For $L = 25$

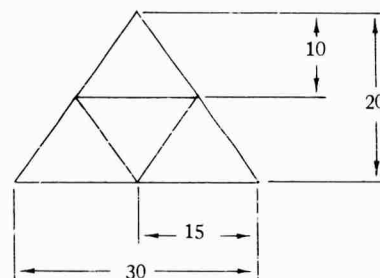
$$R = 1.455 \times \left(\frac{25}{16.9} \right)^2 = 3.18 \text{ in.,}$$

$$t = \left(\frac{3.18}{1.455} \right)^2 \times 0.218 = 1.04 \text{ in.,}$$

and

$$W_f = (1 + 1) \times 1.04 \times 3.18 = 6.61.$$

Since $0.759 < 6.61$, the optimum design is 12.5-inch tube span, 1.909-inch diameter, and 0.319-inch thickness.



REFERENCES

1. Grover, Gordon, and Jackson, "The Fatigue of Metals and Structures," NAVWEPS Report 00-25-534, Chap. 2, App. 3 (
2. MacDuff and Felgar, "Vibration Frequency Charts," Machine Design, Tables 1, 8,
3. S. Timoshenko, Vibration Problems in Engineering (D. Van Nostrand Co., Princeton, N.J., 1955), 2nd Ed., pp. 83-84, Rayleigh Method.

* * *

SHAKER ATTACHMENTS FOR AEROSPACE GROUND EQUIPMENT IN PORTABLE CASES FOR VIBRATION TESTS

Kenneth A. Jenicek
McDonnell Aircraft Corporation
St. Louis, Missouri

The method of securely fastening Aerospace Ground Equipment (AGE) in portable cases to vibration exciters has been the subject of some study at the McDonnell test laboratory, since the specifications are not sufficiently explicit regarding specimen attachments. Three methods of attachment have been utilized by the McDonnell Electrical and Dynamics Laboratory: notched aluminum blocks which fit over the edges of the case (cover removed) and are supported on rigid columns, metal hold-down hooks and turnbuckles which permit consistent repeatability of test conditions, and nylon tie-down straps with wooden radius blocks on the edges of the case. The three methods are discussed in some detail, and it is shown how different tie-down methods can change the apparent resonant frequency of the specimen. Other characteristics of each method are also pointed out.

INTRODUCTION

The method of securely fastening Aerospace Ground Equipment (AGE) which is installed in portable cases to vibration exciters has been the subject of study at the McDonnell General Engineering Division Laboratories. Military specifications (MIL-T-21200C, MIL-E-4970A, and MIL-STD-167), while indicating that the specimen should be "securely" attached to the vibration exciter, are not sufficiently explicit regarding attachment methods (MIL-E-4970A, Paragraph 4.6.8, Procedure VI). Three methods of attaching AGE to exciters have been utilized by the McDonnell Electrical and Dynamics Laboratory:

1. Notched aluminum blocks, which fit over the edges of a case (cover removed) and are supported on rigid columns, are attached to the specimen;
2. Hold-down hooks of formed steel are attached to AGE and then fastened to the shaker with an eye-bolt and turnbuckle; and
3. Nylon tie-down straps are used to secure AGE to the vibration exciter.

The three attachment methods have been utilized with varying degrees of success.

ATTACHMENT METHODS

Notched Blocks and Rigid Columns

The first attachment method involves securing the case with cover removed to the shaker, using notched aluminum blocks and rigid columns. Aluminum blocks are machine notched so as to fit the upper edge of the specimen case. The blocks are secured with long bolts and tubing spacers to the exciter. A typical test setup is shown in Fig. 1. This method is suitable for AGE contained in rigid metal cases which are tested at low test frequency ranges. The sides of the metal case also should be low in height, for as the height of the sides increases, the column length increases. During horizontal excitation this long unsupported rod and mass could experience a resonant condition within the test frequency range. While this method is suitable with rigid metal cases, it is not recommended for use on flexible fiberglass cases or cases having rubber bumper pads, because the specimen separates from the blocks and the subsequent recontact imparts shock pulses to the unit.

Hold-Down Hooks and Turnbuckles

The second attachment method involves the use of hold-down hooks and turnbuckles. This

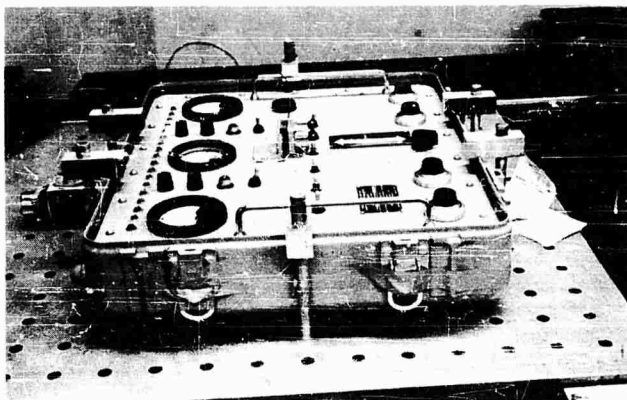


Fig. 1 - Test setup using notched blocks and rigid columns

Fig. 2 - Test setup using hold-down hooks and turnbuckles

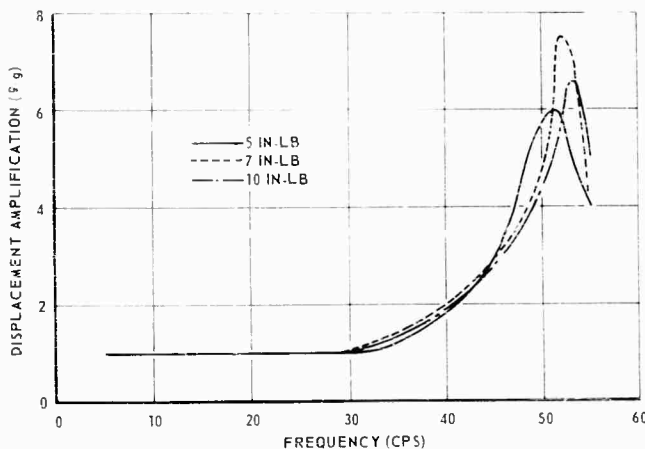
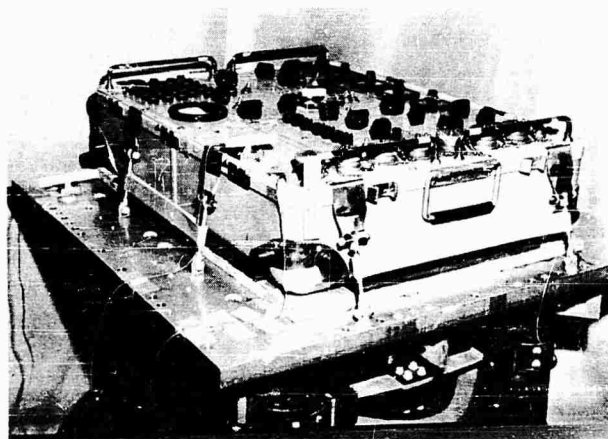


Fig. 3 - Comparison of frequency response of specimen secured by hold-down hooks having different applied torque values

method is most widely utilized because the hooks can be attached to the edges of most case-mounted AGE. This method permits a consistent repetition of the setup because the amount of attachment force is determined by measuring the applied torque value to the turnbuckle. A typical test setup is shown in Fig. 2.

This method works well with fiberglass cases and cases having rubber bumper pads, with one exception: the resonant frequency of these specimens is found to be tunable with variations in the torque value applied to the turnbuckle. The variations in resonant frequency for one specimen with a fiberglass case

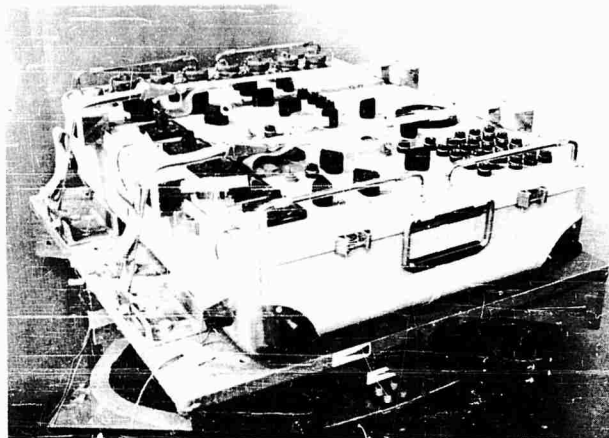


Fig. 4 - Test setup using nylon straps and horizontal restraints on specimen case with cover removed

are shown in Fig. 3. When using this method, the angle subtended between the side of the specimen case and the hook should be a minimum, since excessive horizontal forces can cause structural deformation and specimen failure. This method is also limited to testing conducted at low frequency ranges to avoid resonant responses in the attachment hardware.

Nylon Straps

The third attachment method makes use of nylon straps and rigid block horizontal restraints. Nylon straps are used with AGE, both with the case cover installed and removed. On cases with the cover removed, square-edged wooden radius blocks are used to protect the strap and help distribute the edge loading. Steel channels, mounted around the base of the specimen, are used as horizontal restraints to prevent case slippage during vibration excitation and to secure the nylon straps to the shaker. Typical test setups are shown in Figs. 4 and 5. The strap attachment tension is determined by direct measurement or by use of a scale to determine the force necessary to deflect the strap a known distance.

GENERAL DISCUSSION

The three methods require careful attention to the amount of applied tie-down force while

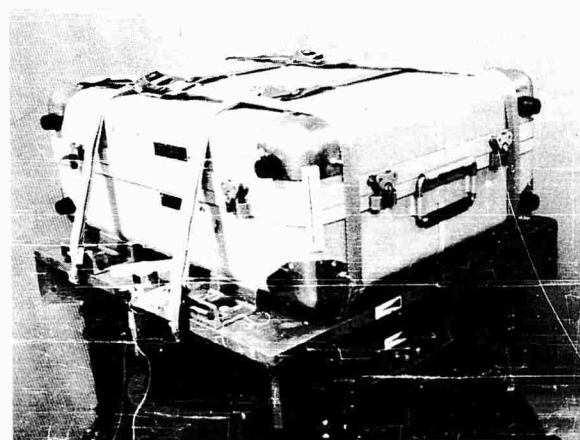


Fig. 5 - Test setup using nylon strap and horizontal restraints on case with cover

securing the specimen to the shaker. Insufficient force can result in slippage, shock pulses and structural damage or failure. Excessive force can structurally deform a specimen, causing premature or unwarranted failure. The notched blocks, hold-down hooks and nylon straps include a limitation in the frequency range upper limit of 100 cps to prevent attachment resonant conditions. However, with these methods virtually any AGE installed in a portable case can be tested and the specification requirement for securely fastening the specimen to the vibration exciter can be satisfied.

* * *

DESIGN CRITERIA FOR VIBRATION FIXTURES

Louis E. Lutz
Honeywell, Aero Division
St. Petersburg, Florida

A practical method for designing vertical and horizontal vibration fixtures is described, and a discussion of the parameters which determine their natural frequencies is included.

INTRODUCTION

Test results are only as good as the test facility. This is especially true in vibration testing. A well-designed vibration fixture is a necessity. The fixture serves two main purposes: it provides a resonant-free interface over a specific frequency range, eliminating undesired angular and linear inputs; and it furnishes a good mechanical interface between the test specimen and vibration machine. By eliminating unwanted inputs, placement of the monitoring pickup for controlled input becomes less critical. Possibility of undertest or overtest is also lessened, since added vibrations are not introduced by the vibration fixture.

This paper discusses fixture design considerations, offers an approach and then evaluates an actual fixture design. The goal is to establish a design for vibration fixtures which considers all aspects and alleviates possible functional problems.

FIXTURE DESIGN CONSIDERATIONS

Structural Rigidity

Perhaps the most important design feature of vibration fixtures that should be considered is structural rigidity. It can be shown that the natural frequency of any configuration is inversely proportional to the square root of its static deflection. Therefore, because it is desirable for the vibration fixture to have a high natural frequency, the fixture should be extremely stiff. In general, vibration fixtures should have a natural frequency higher than that of the test specimen by a factor depending on their mass ratio. For example, where the masses of the fixture and test specimen are approximately equal, the natural frequency of

the fixture should be a minimum of 2 1/2 times the natural frequency of the test specimen.

Weight

In determining the allowable fixture weight, a number of parameters should be taken into consideration:

1. The total weight of the vibration machine driving head (i.e., moving parts), the vibration fixture and the test specimen;
2. The test specimens g level specification;
3. The pound-force limitation of the vibration machine; and
4. Possible attenuation through the vibration fixture after resonance.

Test Specimen Bolting Pattern

In addition to assuring accessibility to the test specimen's mounting hardware, the mounting configuration should simulate as closely as possible that which the specimen will be subjected to during its actual environment.

Bolting Pattern of Vibration Machine

This pattern, of course, would depend on the vibration machine selected or, in some cases, would be the determining factor for the selection. For example, where the choice of two or more vibration machines exists, and each is capable of handling the load, the vibration machine presenting a bolting pattern which reduces fixture "overhang" to a minimum should be selected.

Cabling and Instrumentation Accessibility

Normally, when electrical equipment is undergoing an operating vibration test, interconnections between it and associated testing equipment are required. Therefore, provisions in the design of the vibration fixture should be included to assure cabling and instrumentation accessibility.

Specimen Coolant Accessibility

Provisions should also be included in the fixture design for any coolants required during an operating vibration test. An example of this would be the case where the test specimens cooling air access must be through the fixture itself or where a combination vibration fixture-cold plate design is required.

Electrical Isolation

In many cases, electrical isolation from the vibration machine is required. If so, provisions should be included in the fixture design for such isolation.

Mass Unbalance

To eliminate mass unbalance in both the vertical and horizontal planes, the combined center of gravity of the test specimen and vibration fixture should be in line with the vibration machine center of gravity.

Practical Manufacturing

Ease of manufacturing should be kept in mind at all times when designing a vibration fixture. This would, of course, include the selection of proper tolerances and material.

DESIGN APPROACH

Before beginning any discussion of the technique by which one may approximate the natural frequency of a vibration fixture, one must remember that the natural frequency f_n of a system is merely inversely proportional to the square root of its static deflection; i.e.,

$$f_n = \frac{1}{2\pi} \sqrt{\frac{g}{\delta_{st}}} \quad (1)$$

where f_n is in cycles per second, g is gravitational acceleration in inches per second

squared, and δ_{st} is static deflection in inches.

As the number of degrees of freedom is increased, the complexity of the solution to the natural frequency is increased. Generally, for the each degree of freedom, there will be a natural frequency which will satisfy the system's differential equation. Unfortunately, vibration fixtures are usually of a multiple-degree-of-freedom type and the solution to any differential equation of an order of three or above is enough to discourage any average engineer. It is, therefore, impractical for an engineer to attempt to seek a solution for this type of system. The only practical method for designing vibration fixtures is to reduce the fixture to simple sections that can be dealt with, and solved, by single-degree-of-freedom techniques. The basic technique for determining the natural frequency of a vibration fixture is to divide it into a number of simple shapes that can be dealt with more efficiently than can the total complex structure. The simplest of all shapes, the simply supported beam loaded under its own weight (Fig. 1), should first be considered. The static deflection of this beam is given by

$$\delta_{st} = \frac{5W\ell^3}{384 EI} \quad (2)$$

where

W = total weight (lb),

E = modulus of elasticity (lb/in.²),

I = moment of inertia (in.⁴), and

ℓ = beam length (in.)

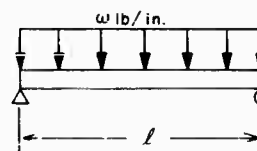


Fig. 1 - Simply supported beam

Substitution of Eq. (2) into Eq. (1) yields

$$f_n = 27.5 \sqrt{\frac{EI}{\rho A \ell^4}} \quad (3)$$

where




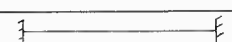
A = area (in.²) = $b \times h$, and

ρ = density (lb/in.³).

Equation (3) indicates that the natural frequency of a simple beam varies directly as $\sqrt{E/\rho}$ (a function of material), directly as $\sqrt{I/A}$ (a function of cross-sectional area), and inversely as l^2 . Also, assuming a rectangular cross section, in which $I = (1/12) bh^3$ and $A = b \times h$, we can see from the relationship $\sqrt{I/A}$ that the natural frequency varies directly as h and independently of b since b adds just as much stiffness as weight. Upon further investigations concerning the $\sqrt{E/\rho}$ function, we find that this parameter for identical geometric shapes is approximately constant for a few of the more common fixture materials (aluminum, steel and magnesium) which leads us to believe that the natural frequencies would be approximately the same.

Similar relationships can be derived for the natural frequency of additional beam configurations loaded under their own weight (Table 1). Since we are attempting to design very stiff vibration fixtures, we should only be interested in the beam configuration's fundamental mode of vibration. Additional modes may be calculated merely by multiplying K by N^2 where $N = 1, 3, 5$, etc.

TABLE 1
Natural Frequency Coefficients for
Beam Configurations Loaded Under
Their Own Weight^a




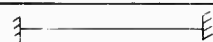
Beam Configuration	K Value
	27.5
	8.9
	42.5
	61.5

^aFrom the relationship,

$$f_n = K \sqrt{\frac{EI}{\rho A l^4}}$$

Evenly distributed loads are rarely the case in fixture design, and in most cases approximations are made by adding the weight of the beam to the load carried and determining the combined deflection as a worst case. The K values for beams with concentrated loads are tabulated in Table 2, along with the percent error in assuming that the total weight is concentrated rather than distributed. In each case, the natural frequency calculated by this method will naturally be lower than the actual frequency by the percent error. It is felt that this error merely acts as a small factor of safety in estimating the actual natural frequency.

TABLE 2
Natural Frequency Coefficients for Beam Configurations Loaded Under Their Own Weight, Assuming a Concentrated Load

Beam Configuration	K ¹ Value	Error (%)
	21.7	19
	5.4	39
	32.0	27
	44.0	28.5

Tables 1 and 2 represent only the simplest of beam configurations and by no means should be the only ones considered. In designing the vibration fixtures for the Dyna-Soar Guidance System, it was necessary to calculate the static deflections of many more complex configurations, including double cantilevered, double simply supported, and simply supported with a cantilever overhang.

EVALUATION OF FIXTURES DESIGNED FOR DYNA-SOAR COUPLER ELECTRONICS UNIT

Vertical Fixtures

The size and weight of the package to be tested are perhaps the greatest determining factors in the design of a vibration fixture. The unit for which this fixture was designed weighs approximately 95 pounds and has a mounting base whose dimensions are approximately 13 1/2 by 20 inches.

Of the number of vibration machines available at Honeywell, the one selected has a capacity of 3500 pounds peak force and a bolting pattern of holes located on 8- and 16-inch diameter circles every 45 degrees.

In selecting a design approach, it was felt that the fixture could be designed more efficiently by assuming a configuration based on the effect of the parameters previously discussed rather than by determining the shape or section modules required from deflection characteristics. Once the basic shape was determined, sections could be modified as required. The final configuration is shown in Fig. 2. The weight of the fixture is 84 pounds and its dimensions are approximately 18 x 21 x 5 1/2 inches. The fixture is manufactured from 1-inch thick aluminum plate and is of a welded-type construction.

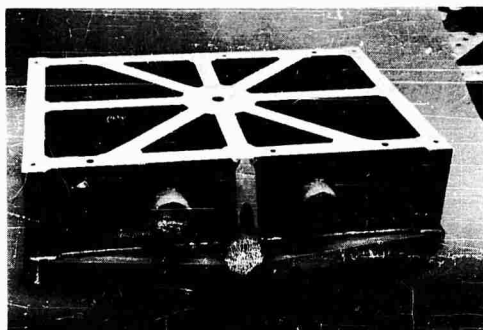


Fig. 2 - Dyna-Soar coupler electronics unit vertical vibration fixture

Once the basic configuration was established, various sections were investigated to determine their natural frequency or deflection characteristics. This is perhaps the most difficult part of this method because various assumptions must be made as to the loading and supporting configurations of the section selected. For instance, sections WR and BJ (Fig. 3) were treated as double simple beams, sections SR and KR were treated as double cantilevers, and section BJ was treated as a simply supported beam, as were various pockets in the bottom plate. Sections LS, SR and KR were treated as a tri-cantilever, and section LSRJK was treated as a complex cantilever. It was fairly evident that the lowest natural frequency of the fixture would occur at the corners, due to the excessive cantilevered over-hang of the fixture with respect to the vibration machine. It was also evident from investigating the stiffness of various sections inside the vibration machine bolting pattern that this section could be treated as if it were fixed or extremely stiff. Actual data taken afterwards have proven both assumptions correct. In addition to the "in-line" natural frequencies, various sections were investigated for additional cross-axis or torsional modes of vibration. Calculations indicated that we could expect a natural frequency of approximately 1500 cps. Actual test results proved that the lowest natural frequency was 1260 cps.

Horizontal Fixtures

As in the case of vertical fixtures, cross-talk motions superimposed on the basic translational vibration input are highly undesirable. One of the major causes of rotational crosstalk is eccentricity between the line of action of the shaker driving force and the test specimen-fixture combined cg. It is, therefore, desirable to have a specimen suspension system such as that of slip-table testing devices which are

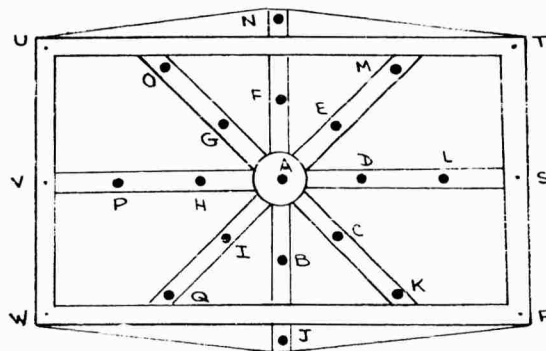


Fig. 3 - Top view of vertical vibration fixture

extremely stiff in the transverse axis to the vibration input. We may first assume that the horizontal fixture approximates a flat plate (Fig. 4) and investigate the overturning and resisting moments. Summing the moments about A, we find that

$$\sum M_A = Wa + M_I + M_D - \frac{W}{g} \ddot{Y}R + \frac{W}{g} \ddot{X}a \quad (4)$$

or

$$R = \frac{g}{W\ddot{Y}} \left[Wa + M_I + M_D + \frac{W}{g} \ddot{X}a \right] \quad (5)$$

where

R = eccentricity between shaker line of force and combined cg,

W = combined weight,

\ddot{Y} = acceleration of combined cg in Y direction,

a = length of beam (i.e., $2a$),

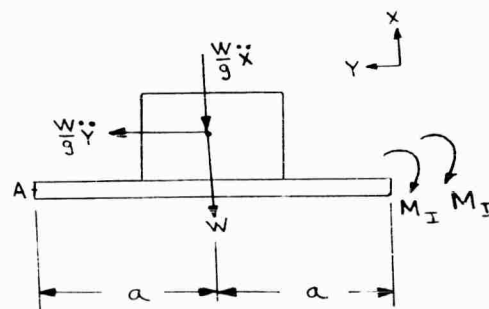


Fig. 4 - Horizontal fixture overturning and resisting moments

M_I = resisting moment caused by inertia of oil,

M_D = resisting moment caused by damping force of oil,

\ddot{X} = acceleration of combined cg in x direction, and

g = gravitational acceleration.

It is extremely difficult to determine the dynamic resisting forces exerted on the plate, but their net effect is one which helps reduce cross-talk inputs into the test specimen.

To evaluate the parameters involved in the design of a horizontal fixture, we will analyze the fixture as if it were an end-loaded longitudinal bar as shown in Fig. 5 [1]. Since the displacement along the bar is a function of both time and distance, we must solve the resulting differential equation by the method of separation of variables.

P = stress (t) \times area (A) or total force on element (lb),

f = unit stress (psi),

A = cross-sectional area ($in.^2$),

E = modulus of elasticity ($lb/in.^2$),

$\frac{\partial \mu}{\partial x}$ = strain ($in./in.$),

$\frac{\rho A dx}{g}$ = mass of element ABCD,

$\frac{\partial^2 \mu}{\partial t^2}$ = acceleration of element ABCD, and

ρ = density of material ($lb/in.^3$).

Summing the forces on the element yields

$$P + \left(\frac{\rho A dx}{g} \right) \frac{\partial^2 \mu}{\partial t^2} - P - dP = 0 \quad (6)$$

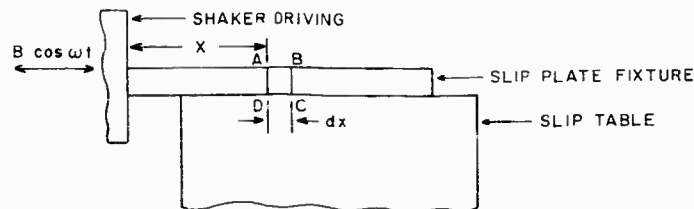


Fig. 5 - Horizontal vibration fixture analysis

The element ABCD as it is displaced dynamically by the input force $B \cos \omega t$ can be analyzed in the following manner:

or

$$dP = \left(\frac{\rho A dx}{g} \right) \frac{\partial^2 \mu}{\partial t^2} \quad (7)$$

But $P = A \times f$ and $f = E(\partial \mu / \partial x)$ and, therefore,

$$P = AE \frac{\partial \mu}{\partial x} \quad (8)$$

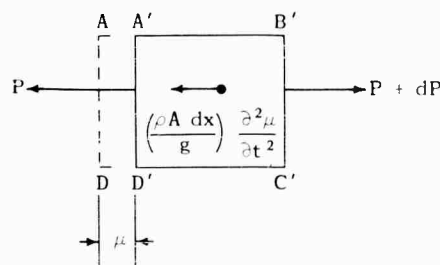
By substitution

$$dP = \frac{\partial P}{\partial x} dx = AE \frac{\partial^2 \mu}{\partial x^2} \quad (9)$$

By equating Eqs. (7) and (9), we find that

$$\frac{\partial^2 \mu}{\partial t^2} = \left(\frac{Eg}{\rho} \right) \frac{\partial^2 \mu}{\partial x^2} \quad (10)$$

By letting $Eg/\rho = a^2$ and substituting, Eq. (10) becomes



where

μ = displacement of cross section AD ($in.$),

NOTE: References appear on page 265.

$$\frac{\partial^2 \mu}{\partial t^2} = -a^2 \frac{\partial^2 \mu}{\partial x^2} \quad (11)$$

Since the displacement μ is a function of both time t and distance along the axis x (i.e., $u(x, t) = X(x) T(t)$), we may consider the solution to be of the form [2]:

$$u(x, t) = X(x) T(t) \\ = \left[C_1 \cos \frac{\omega x}{a} + C_2 \sin \frac{\omega x}{a} \right] B \cos \omega t \quad (12)$$

The problem now is to determine the coefficients C_1 and C_2 from the boundary conditions. When $X = 0$, $u = u_0 = B \cos \omega t$. Substituting this into Eq. (12), we find that $C_1 = 1$. When $X = a$, the stress $E(\partial \mu / \partial x)$ is zero. Since

$$\mu = \left[\cos \frac{\omega x}{a} + C_2 \sin \frac{\omega x}{a} \right] B \cos \omega t$$

$$\frac{\partial \mu}{\partial x} = \left[-\frac{\omega}{a} \sin \frac{\omega x}{a} + \frac{\omega}{a} C_2 \cos \frac{\omega x}{a} \right] B \cos \omega t \quad (13)$$

Substitution of the boundary condition into Eq. (13) yields

$$0 = \left[-\frac{\omega}{a} \sin \frac{\omega a}{a} + \frac{\omega}{a} C_2 \cos \frac{\omega a}{a} \right] B \cos \omega t \quad (14)$$

or

$$C_2 = \tan \frac{\omega a}{a} \quad (15)$$

Therefore, the final solution is of the form

$$u(x) = \left[\cos \frac{\omega x}{a} + \tan \frac{\omega a}{a} \sin \frac{\omega x}{a} \right] B \cos \omega t \quad (16)$$

Since transmissibility of output over input is given by

$$Q = \frac{u_x}{u_0} = \left[\cos \frac{\omega x}{a} + \tan \frac{\omega a}{a} \sin \frac{\omega x}{a} \right] \quad (17)$$

at resonance with no damping, the transmissibility will approach infinity or

$$\tan^{-1} \left(\frac{\omega a}{a} \right) = \frac{\pi N}{2} \quad (18)$$

where $N = 1, 3, 5$, etc. Therefore, at resonance

$$\omega_N = \frac{N \pi a}{2} \text{ rad/sec.} \quad (19)$$

But $a = \sqrt{Eg/\rho}$ and $\omega_N = 2\pi f_N$; therefore, by substitution

$$f_N = \frac{N}{4} \sqrt{\frac{Eg}{\rho}} \text{ cps.} \quad (20)$$

This analysis was made assuming a constant cross section. We can, therefore, see from Eq. (20) that the natural frequency of a slip plate fixture will vary inversely as the length l , directly as $\sqrt{E/\rho}$ which is a function of the fixture material, and independently of the cross-sectional area although the fixture should be as stiff as possible to reduce undesirable crosstalk inputs.

The horizontal fixture designed for the Dyna-Soar coupler electronics unit (Fig. 6) consisted of an aluminum jig plate approximately 20 inches by 26 inches thick and weighed approximately 110 pounds. Its flatness was held to 4 by 10^{-4} inches T.I.R. The calculated first resonant frequency was 1890 cps and actual test results indicated a first resonant frequency of 1600 cps.

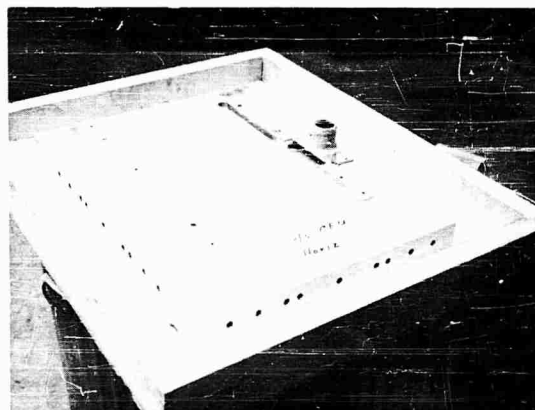


Fig. 6 - Dyna-Soar coupler electronics unit horizontal fixture

SUMMARY

We have found at Honeywell that we can design vibration fixtures and predict with a fair degree of accuracy their natural frequencies by the methods described in this report. It should be noted, however, that this method requires various assumptions to be made as to the loading and supporting characteristics of the fixture sections investigated. This can be extremely difficult for complex structures, but it does give the engineer a fair approximation of the natural frequency which, in most cases, is all that is desired.

REFERENCES

1. C. Anker, G. Kushner, N. Safford, and T. Smith, "An Oil Film Auxiliary Table for the MB-C200 Vibration Exciter," G. E. Tech. Information Ser. R61POD.
2. C. R. Wylie, Advanced Engineering Mathematics (McGraw-Hill Book Co., New York, 1951), pp. 216-218.

BIBLIOGRAPHY

- J. R. Curreri, Fundamentals of Vibrating Structures (The Polytechnic Institute of Brooklyn).
- B. Morrell, Mechanical Vibrations (Ronald Press Co., New York).
- W. T. Thomson, Mechanical Vibrations (Prentice-Hall, Inc., Englewood Cliffs, N.J.).

* * *

DESIGN AND UTILIZATION OF ENVIRONMENTAL TEST FIXTURES*

Wilson S. Gorrell
Martin Company
Baltimore, Maryland 21203

The basic test fixture design parameters applied to a Martin thermal insulation evaluation program are described, with a discussion of fixture weight, size, resonant frequencies, fabrication techniques, cost, specimen operating parameters, electromagnetic shaker force output and center of gravity and specimen effects. These considerations are applied to a fixture that was designed for both static and dynamic loading at ambient temperatures up to 1700°F. The essential purpose of the program was to determine stress-strain relationships, spring constants and dynamic properties of the thermal insulation material.

INTRODUCTION

Throughout the aerospace industry, engineers are confronted with the task of providing reliable, low-cost components that will perform their intended functions when subjected to the mechanical and climatic environments of storage, transportation, and service. Component conformance to the design specification is substantiated through a series of design development, evaluation and qualification test environments. Although components are subjected to both mechanical and climatic environments, the mechanical environments (shock and vibration, in particular) induce the greatest number of structural failures.

A vibration test fixture should provide an inexpensive, lightweight mounting surface that is sufficiently rigid neither to magnify nor to attenuate the test environment. General design guide rules are useful; but due to the large variety in specimen sizes, shapes and weights, each fixture must be evaluated for a particular situation. Specialized test fixtures successfully designed included a cast fixture to permit vibration along three axes not coincident with the major component axes and several "universal" test fixtures eliminating the need for a slide plate. The purpose of this paper is to present the considerations employed in the design of

multiple usage fixtures with specific application to a thermal insulation development program.

Due to electromagnetic shaker limitations, major importance is attached to the fixture's weight and size, which are governed directly by the specimen weight and size. Various methods are available for reducing fixture weight: selection of lightweight materials such as aluminum and magnesium; use of extruded shapes such as I-beams, T's, angles, channels, and tubing; and good engineering design with a minimum safety factor throughout. Generally speaking, a fixture-to-specimen weight ratio of two to one is the best that can be expected.

Resonant frequencies must be considered for fixtures subjected to vibration and shock environments. The resonant frequency of a beam is directly proportional to the square root of the ratio of modulus of elasticity E to weight w :

$$f_n \propto \left(\frac{E}{w}\right)^{1/2} \quad (1)$$

Since the E/w ratios for aluminum, magnesium, and steel are approximately the same, assuming equivalent beam size and end mounting conditions, each of these materials will have essentially the same resonant frequencies:

*This paper was not presented at the Symposium.

$$E_{Al} = 1/3 E_{steel}, w_{Al} = 1/3 w_{steel}, E_{Mg} = 1/5 E_{steel}, w_{Mg} = 1/5 w_{steel}; \text{ therefore,}$$

$$f_{n_{steel}} = f_{n_{Al}} = f_{n_{Mg}} \quad (2)$$

If stiffness and strength are not major requirements, the use of lightweight materials such as aluminum and magnesium is a definite advantage in fixture design.

Present-day vibration specifications generally require a test frequency range of 10 to 2000 cps. The ideal test fixture should be designed to assure that all resonances are outside the operating frequency range of the specimen. Difficulties will arise if a fixture is designed for vibration only in the assumed direction of excitation. Specimen mounting eccentricities, specimen vibration, and shaker-table stiffness irregularities can induce crosstalk in the side planes. Specimen weight and its distribution must, therefore, be considered for fixture stiffness in all three planes. A common fixture fault that contributes to fixture resonances is unsupported overhanging corners of a flat plate. This detrimental effect can in some cases be minimized by removing the unnecessary projections.

Fabrication techniques influence the stiffness of a fixture. A casting, for instance, is more rigid than a weldment; both are superior to bolted constructions. Cross sections of such assemblies are shown in Figs. 1, 2 and 3.

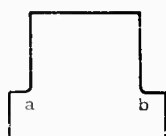


Fig. 1 - Casting

Fig. 2 - Weldment

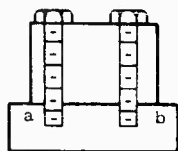
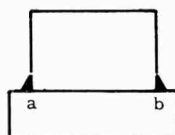


Fig. 3 - Bolted

The one-piece construction of Fig. 1 is completely attached between a-b. Surface a-b in Fig. 2 is not attached since the connection is made only through the welded fillet area. The only connection between the surfaces of Fig. 3 is through friction and tension applied by the bolts. When a bolted construction becomes necessary in soft materials such as aluminum or magnesium, the use of Rosan or Helicoil threaded inserts will aid in applying greater torque to the bolts.

Fixture costs should also be considered. A casting would generally be more expensive than a comparable weldment or bolted construction, but by reducing unnecessary finishes to the casting wood patterns and unnecessary tolerances to the fixture, the cost of a casting could compare favorably with a welded or bolted construction. Expensive materials and nonstandard components should be eliminated where possible.

Fixture design is also influenced by such operating conditions as high temperature, hydraulic pressurization, external wiring, specimen operating space, and normal accessibility provisions. For example, high operating temperatures may require special insulation or cooling techniques. A pressurization system could possibly require the fixture to contain high-pressure liquids. Provisions for accessibility, cabling, and normal specimen operating space may necessitate a larger and more complicated fixture than ordinarily planned.

Finally, the electromagnetic shaker force output and loading techniques must be considered. Each electromagnetic shaker and amplifier system is rated for a maximum force output over a specified frequency range. The maximum available acceleration that can be applied to the specimen and fixture can be determined as follows:

$$\text{acceleration} = \frac{\text{shaker force output (lb)}}{(\text{wt fixture + specimen} + \text{armature + cabling}) \text{ (lb)}} \quad (3)$$

The center of gravity of the fixture and specimen should be designed to eliminate any static eccentric loading to the shaker armature. Although guide rails are provided to restrict the motion of the shaker armature, any offset load condition could cause excessive wear or binding. Cohesive forces exerted between the slide plate and table by the lubricant tend to reduce the bending moment at the shaker armature; however, this force could be exceeded for a large unbalance.

Prior to conducting any vibration program on the specimen, the fixture should be surveyed for critical resonances in the operating test range. This survey should be conducted with a simulated component that duplicates the weight, center of gravity, stiffness and inertia of the specimen. If, in spite of detailed design analysis, further compensation is required to nullify the effects of a fixture resonance within the test frequency range, then the control accelerometer can be judiciously located on the specimen.

THERMAL INSULATION EVALUATION TEST PROGRAM

An evaluation test program was conducted on a material used both for structural support and thermal insulation at high temperatures. The purpose of the test was to determine stress-strain relationships, spring constants, and dynamic properties at various temperatures and then to evaluate the material applicability.

To perform these tests, the fixture had to withstand static loads up to 5000 pounds with temperatures to 1700°F. In addition, the fixture was required to support the material during vibration on a shaker at low-level acceleration inputs (Figs. 4 and 5).

Since the fixture would operate at high temperatures for sustained periods of time,

a method of insulating the fixture had to be developed. Initially, the required temperature of 1200°F was to be supplied by a heating pad arrangement. Since available structurally rigid insulation materials for the fixture lacked the thermal insulation property of the specimen and would have resulted in a bulky and expensive fixture, an internal water-cooled system with a nominal amount of thermal insulation by castable concrete was employed (Fig. 6). The temperature requirement was later increased to 1700°F, a temperature exceeding the output of the original hot pad. The fixture was modified to use a 2 1/2-kw induction heater, which contained its own cooling provision. This system represented improvements in two major areas:

1. The high temperatures could be obtained; and
2. The heater coil circulation system carried a portion of the "waste heat" away from the fixture.

The fixture circulation system presented a secondary problem to the static load and vibration requirements. Since the test fixture was required to support the specimen during static loading, the support should have consisted of a solid plate under the specimen. However, provisions for the cooling system required complete circulation throughout the base plate. The loading head (with springs) was bolted to the

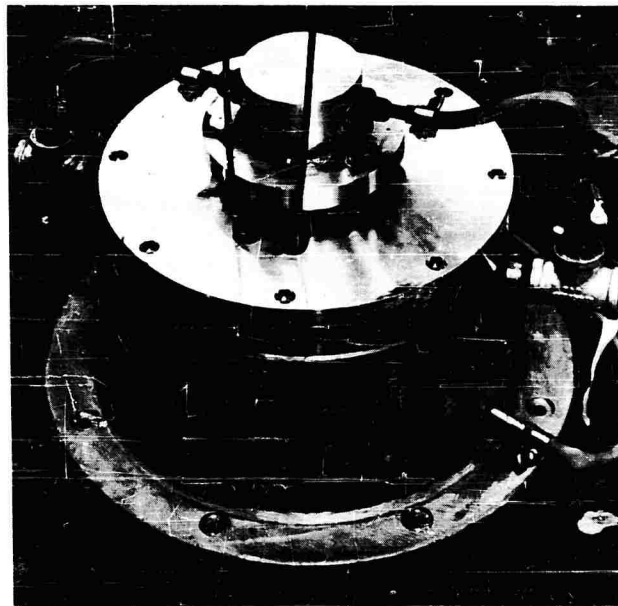


Fig. 4 - Thermal insulation test fixture

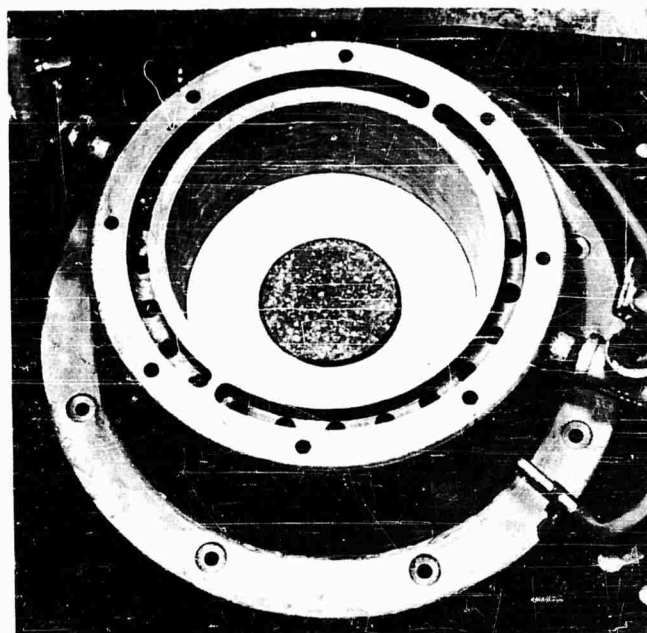


Fig. 5 - Internal view of thermal insulation test fixture

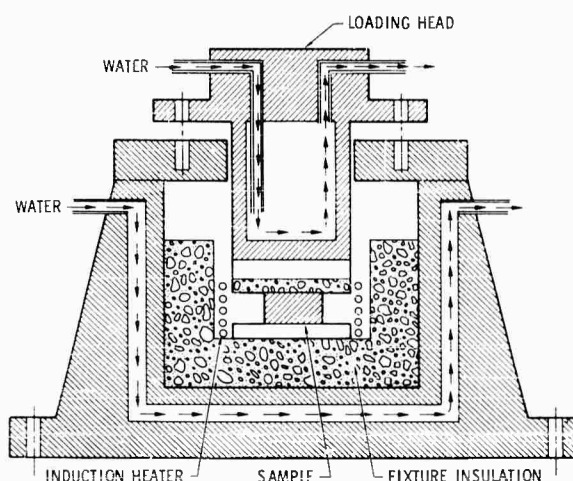


Fig. 6 - Operating diagram of thermal insulation test fixture

top fixture plate to permit prestress loads during vibration.

The fixture base was drilled to match the 16-inch diameter bolthole pattern of a MB C-25 electromagnetic shaker. Due to the inconvenience of removing insulation from the fixture, the center bolthole was not drilled. However, should a base plate resonance have occurred in the test range, provisions were made to

include the center mounting point through the cooling core.

Deflection data were measured between the base plate and the movable loading head. During the static load test, measurements were recorded with the variable force applied by an external hydraulic press. Since deflections were measured relative to the fixture, the temperature of the fixture had to be maintained at a constant level.

The completed fixture was composed of cast and welded aluminum structures. A complete casting with cooling surfaces along the bottom plate of the fixture would have been extremely difficult to fabricate; therefore, the bottom plate was machined separately and welded in position. Vertical holes were drilled in the basic casting for the side cooling core. The movable loading head was also water cooled and consisted of a welded assembly.

An input of 1 g (Accelerometer 1) from 20 to 2000 cps was maintained both with and without preload on the loading head. The fundamental resonant frequency (preload) occurred at 1520 cps with a transmissibility Q of 30 at Accelerometer 3 (Fig. 7). Without the preload, the resonance occurred at 1660 cps ($Q = 20$ at Accelerometer 3). The base plate resonance was 2100 cps ($Q = 30$ at Accelerometer 4). This fixture resonance is higher than that

anticipated for the sample material, thereby assuring sufficient decoupling. With an input load of 5000 pounds to the loading head, the tare deflection of the fixture was 0.024 inch at room temperature and a 0.020 inch at 1000° F.

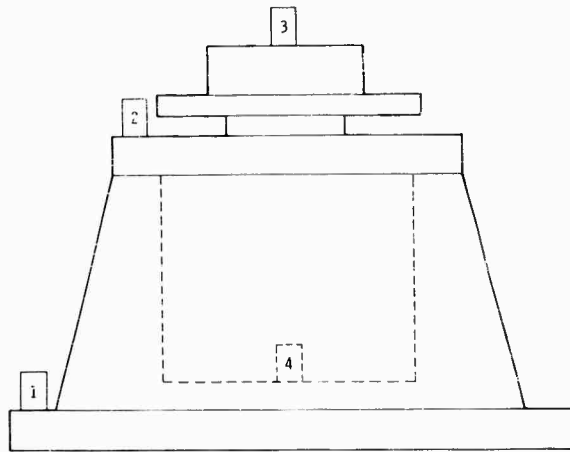


Fig. 7 - Accelerometer location

The original design parameters for a vibration test fixture were considered throughout this analysis. Since a maximum acceleration input of 1 g was to be applied, the fixture weight (112 pounds) was not critical. An MB C-25 shaker with a 3500-pound force output was more than adequate. The fixture assembly was designed symmetrically to eliminate any eccentric loading to the shaker armature. A combination of casting and weldments minimized the manufacturing expenses but maintained the rigidity and high resonant frequency.

With the cooling core, this fixture is capable of operating at even higher temperatures, limited only by the outputs of the induction

heater and the 2400° F limit of the Harbison-Walker castable concrete insulation.

One of the methods proposed for determining the resonant frequency of the thermal insulation material under temperature and preload is illustrated in Fig. 8. It is imperative that the instrumentation be located on the loading head, sufficiently separated from the high temperatures and electrical fields. This setup will be calibrated to determine the resonant frequency of the loading head-spring system.

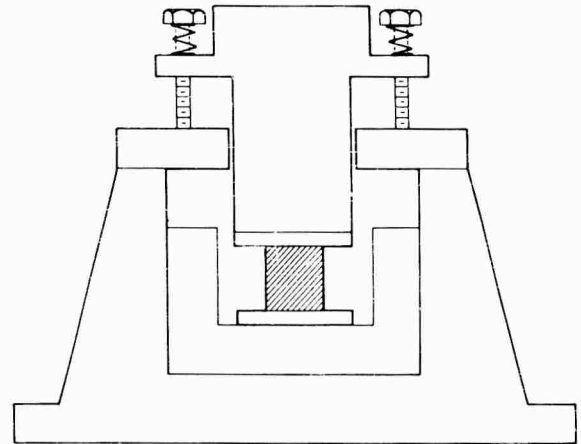


Fig. 8 - Resonant frequency determination of sample

The design of environmental test fixtures requires many considerations. These include fixture weight and size, resonances, fabrication techniques, cost, specimen operating parameters, electromagnetic shaker force output, and center of gravity of fixture and specimen. The design of each test fixture requires special analysis, but the techniques and principles described for the thermal insulation fixture apply.

* * *

DESIGNING TIGHT BOLTED JOINTS FOR VIBRATION ENVIRONMENT

O. John Zamparo
MB Electronics
New Haven, Connecticut

A bolted joint subjected to vibration can decouple, or separate, even though it is satisfactory under static conditions. Ineffective force transfer and loose bolts are often the result of decoupling. The problem can be solved by utilizing large contact areas and short, highly preloaded bolts. All screw locking devices are not helpful; some actually contribute to decoupling. This paper discusses decoupling and presents specific recommendations for bolt selection and tightening.

INTRODUCTION

When two surfaces must be mated to effect force transfer between them, the question of fastening arises. For temporary joints, the usual case for vibration test fixtures, threaded fasteners are the most practical type. The joint thus formed is commonly called a bolted joint even though the "nut" is a threaded hole in one of the structural members.

Under vibration conditions, many factors contribute to the loosening of bolted connections. Decoupling of the mating parts is often the most likely cause of this problem and the least understood. By definition, decoupling is the separation of two masses which are intended to vibrate in unison.

The primary requirement of each fastener is that it remain tight for the desired duration. Loose fasteners can be classified as structurally failed, backed out, or excessively resilient. Structural failure of the vibrating fastener is related to fatigue strength, a subject well documented in the literature and handbooks. Claims are made for many products which eliminate the backing out of screws. The resilience of a joint, however, is often neglected. It is the resilience that determines decoupling which, in turn, affects the structural failure and backing out of screws.

The scope of this paper is a discussion of the factors which affect decoupling, the relationship of decoupling and locking devices,

and recommendations for designing tight bolted joints.

LIST OF SYMBOLS

A	Stressed area (in. ²)
A_b	Stressed area of bolt (in. ²)
A_f	Stressed area of fixture (in. ²)
δ	Deflection or elongation (in.)
δ_b	Bolt deflection (in.)
δ_f	Fixture deflection (in.)
E	Modulus of elasticity (lb/in. ²)
E_b	Bolt modulus of elasticity (lb/in. ²)
E_f	Fixture modulus of elasticity (lb/in. ²)
F	Dynamic force (lb)
f_{max}	Maximum test frequency (cps)
f_r	Resonant frequency (cps)
f_{ra}	Axial resonance (cps)
G	Acceleration level, multiples of g
g	Acceleration due to gravity = 386 in./sec ²

γ	Mass density (lb-sec ² /in. ⁴)
K	Stiffness (lb/in.)
K_a	Assembly stiffness (lb/in.)
K_b	Bolt stiffness (lb/in.)
K_f	Fixture stiffness (lb/in.)
L	Active length (in.)
ΔL_b	Bolt active length change (in.)
ΔL_f	Fixture active length change (in.)
P	Prestress load or preload (lb)
P_{max}	Maximum bolt load (lb)
ΔP	Change in preload (lb)
W	Total weight (lb)
W_f	Fixture weight (lb)
W_s	Specimen weight (lb)
U	Ultimate bolt strength (lb)

AMPLITUDE CONSIDERATIONS

Fixture bolts clamp best when used to counteract forces acting parallel to the bolt axis. By this means, clearance between mating parts is easily eliminated. If bolts are used to counteract forces perpendicular to their axis, the security of the joint is dependent on friction between mating parts, bolt clearance, dowels, or shoulders. The reliability of such joints under action of oscillating forces is questionable.

Inertia-produced decoupling can be analyzed using the simple bolted joint shown in Fig. 1. A bolt of cross-sectional area A_b is used to constrain a section of fixture to the exciter table

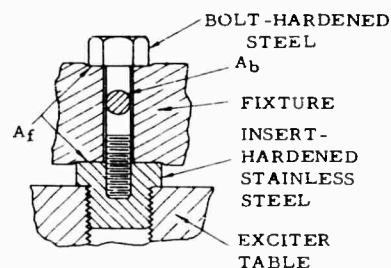


Fig. 1 - Simple bolted joint

insert. When the bolt is tightened, it stretches an amount δ_b and causes a compression δ_f in the fixture. It is assumed here that the stressed area A_f under the bolthead is the same as that at the fixture-insert interface. Further, it is assumed that negligible deflection occurs in the bolthead and insert because of the relatively high stiffness in those areas.

Tensile load P is introduced into the bolt by tightening. The bolt is prestressed in tension and a section of the fixture is prestressed to the same force level in compression. The deflection of each component is inversely proportional to its respective stiffness K , according to the relation $\delta = P/K$, where $K = (EA)/L$, E is the elastic modulus, A is the stressed area, and L is the length of the deformed part.

When vibration occurs, inertia of the specimen-fixture combination exerts an additional fluctuating force F on the joint. This force can be computed from $F = (W_s + W_f)G$, where W_s and W_f are the specimen and fixture weights, respectively, and G is the vibration acceleration level expressed as a multiple of the acceleration due to gravity.

Figure 2 graphically represents these circumstances. The level of preload P is attained as a result of bolt extension δ_b and fixture compression δ_f reaching a condition of equilibrium. Dynamic force F due to acceleration fluctuates about the level of preload. The deflection of the bolt-fixture combination due to the action of dynamic force F is determined by the stiffness of the assembly K_a , which equals $K_b + K_f$. When the deflection of the system reaches the deflection of the least statically

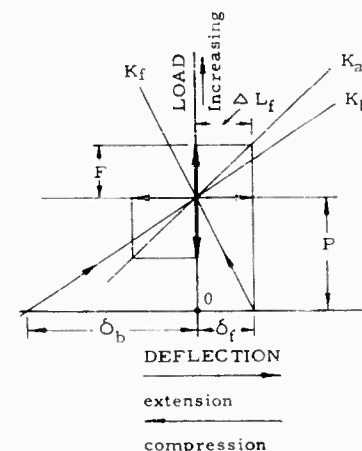


Fig. 2 - Bolted joint load-deflection diagram

deflected component, in this case the fixture, separation occurs.

FREQUENCY CONSIDERATIONS

Figure 3, a schematic of Fig. 1, shows K_b and K_f as springs in parallel. Damping is considered negligible. The resonant frequency of this system is

$$f_r = \frac{1}{2\pi} \sqrt{\frac{K_a g}{W}} \quad (1)$$

where $W = W_f + W_s$, $K_a = K_b + K_f$, and g is the acceleration of gravity. This assumes the worst case, where the table weight is large relative to W .

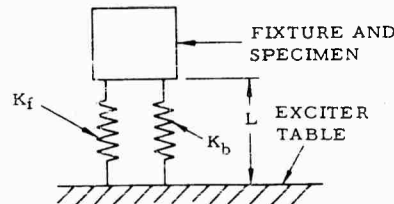


Fig. 3 - Schematic of bolted joint

Since the system readily vibrates at the natural frequency, separation of the joint can occur much more readily at this frequency than at the frequencies much displaced from it. For a given test specimen, fixture, and frequency range, a rigid joint must be designed to avoid decoupling. The stiffness required is proportional to the square of the frequency.

Bolt axial resonance, a more remote mechanism of decoupling, becomes apparent when the bolt itself vibrates in the mode characterized by alternate lengthening and shortening in the axial direction. The frequency at which axial resonance occurs is

$$f_{ra} = \frac{1}{2L} \sqrt{\frac{E}{\gamma}} \quad (2)$$

where L is the free length of the bolt, E is the elastic modulus of the bolt material, and γ is the mass density of the material.

The ratio E/γ is approximately 4×10^{10} in.²/sec² for steel, aluminum, and magnesium. A steel bolt clamping a fixture of those materials will resonate with them if excited at the

proper frequency. The effect produced would be a general softening of the joint without separation of the mating surfaces. The response of the specimen would deviate from that of the exciter. A steel bolt clamping a fixture of beryllium, for which E/γ is approximately 25×10^{10} in.²/sec², would resonate at a lower frequency than the fixture, thereby allowing the mating surfaces to separate at that frequency.

LOCKING DEVICES

Decoupling occurs during vibration when the bolt stretches and allows the fixture to unseat at the fixture-insert interface. For this part of the cycle, inertia forces are acting to separate the fixture from the exciter table. On the portion of the cycle when inertia forces reverse, the bolt loses contact with the fixture and is then free to turn. The resulting loose screw is often considered to be the cause of the problem rather than, more appropriately, the effect. The use of a locking device to prevent screw rotation would not completely solve the problem.

There are situations where decoupling may occur at rare occasions, e.g., the widely spaced high g peaks of random vibration testing or sudden accidental shock loads. In this case, the turning bolt can allow the preload to be permanently lost and cause decoupling at progressively lower force levels. Therefore, there is a place for the bolt locking device.

Locking devices can be classified as mechanical, frictional, and adhesive. Of the mechanical devices, wires and cotterpins are least desirable since they tend to rattle and produce noise on test instrumentation. They can fail if vibrated at their resonant frequency too long. Also in the group are the sundry lockwashers which tend to deface the fixture. The split-ring type, when used with properly tightened screws, flattens and loses much of its effectiveness. These washers and star-type lockwashers often act as springs in series with the fixture flange, thereby softening the joint and inviting decoupling. Short of welding, staking in place is probably the most effective of mechanical locking means, but this can eliminate reuse of the fasteners and fixtures.

Among the friction devices, jamnuts are probably the oldest. Their chief disadvantage is that once loosened, they are no longer effective in retaining the fastener in the joint. In this group, the prevailing-torque screws and nuts which utilize deformed or interference threads and nonmetallic inserts are preferred.

Limitations are temperature effects on the plastic inserts and defaced threads.

Nearly every engineer has at least attempted to disassemble a rusty bolt, the result often being a sheared screw. There are cements available which lock the threads by similar action. One such product can be applied to the assembled and tightened screw, where it wicks into the threads and bonds them in position. Upon removal, screws so treated behave much like prevailing-torque devices.

BOLT DIAMETER DETERMINATION

To obtain a tight, effective bolted joint, the first step is to calculate the maximum unseating force to be experienced from $F = (W_f + W_s) G$, an equation explained previously. Under action of force F , the residual load on the fixture is $P - \Delta P$, where ΔP is a load decrease less than prestress load, a requirement for avoiding decoupling.

The maximum bolt load P_{max} is equal to the residual load in the fixture plus F , or

$$P_{max} = P - \Delta P + F. \quad (3)$$

The change in length of the bolt approximates the change in length of the fixture so that it can be assumed that $\Delta L_f = \Delta L_b$. Therefore,

$$\frac{\Delta P L}{A_f E_f} = \frac{(F - \Delta P) L}{A_b E_b}$$

which reduces to

$$\Delta P = \frac{F}{\frac{A_b E_b}{A_f E_f} + 1}. \quad (4)$$

Published tables of bolts generally list clamping loads as 80 percent of ultimate bolt strength. If the increase in bolt load under dynamic conditions is allowed to be 20 percent of the difference between clamping force P and ultimate bolt strength U , then $P_{max} = 0.20 (U - P) + P$, which reduces to

$$P_{max} = 1.05 P. \quad (5)$$

Combining Eqs. (3), (4) and (5) results in an expression which provides selection of a bolt based on required clamping load or preload,

$$\Gamma = 20F \left(\frac{1}{1 + \frac{A_f E_f}{A_b E_b}} \right). \quad (6)$$

Published clamping loads vary for different SAE bolt grades. This allows the selection of a few diameters for a desired clamping load.

BOLT LENGTH DETERMINATION

To transmit forces effectively across the bolted joint with good response, f_r and f_{ra} should be at least five times the highest anticipated test frequency, f_{max} . For a given bolt diameter, bolt length can be determined from

$$L = \frac{g (E_b A_b + E_f A_f)}{W (10 \pi f_{max})^2}, \quad (7)$$

which is derived from Eq. (1) with appropriate substitutions. The bolt diameter and/or quantity may require an increase to arrive at a reasonable bolt length. By substituting the length into Eq. (2), the possibility of axial resonance can be investigated.

In general, it is best to select a bolt as short as practical to raise f_r and f_{ra} above the test frequency range. However, in addition to physical limitations, bolt length may be dictated by the energy absorption potential required to prevent failure. In cases where a joint is subjected to high accelerations or shock, short highly stressed bolts may fail at the root of a thread because of their inability to deflect and absorb the high impact energy. Use of a larger number of bolts turned to thread root diameter along the free length can prevent failures of this type.

PRELOAD DETERMINATION

To realize the full potential of a high-strength screw, it must be tightened to a high preload level. It is difficult to determine precisely the force in the bolt, especially since friction accounts for a large portion of tightening torque. Handbooks often state an average torque value for both dry and lubricated threads. Variations of 20 to 30 percent between the two values are common.

When uncertain of tightness in a particular application, test samples of identical joints are helpful. Here the torque can be related to load by use of special load-detecting washers of strain gage or calibrated spring type.

If both ends of the sample bolt are accessible, a micrometer can be used to measure bolt elongation and the load computed from $\delta = PL/AE$. To rule out friction variations, bolt

load can be plotted as a function of bolt rotation after the bolt has been tightened "finger-tight." Bolts thus calibrated are ready for the actual assembly, with a high degree of reliability, especially if seasoned with a dash of thread-locking adhesive.

SUMMARY

Decoupling of a bolted joint under vibration conditions contributes to ineffective force

transfer as well as to loose screws. The joint must be stiff to overcome the problem. Satisfactory joint stiffness requires that large areas of contact and short bolts be utilized along with a high degree of bolt preload. Screw locking devices do not necessarily help and they can make conditions worse. This paper has presented an approach to the problem with specific design recommendations for bolt selection and tightening.

* * *

FIXTURE DESIGN

Panel Session

Moderator: Dr. R. M. Mains, General Electric Co.

Panelists: Mr. R. L. Bergey, Burroughs Corp.
Mr. K. A. Jenicek, McDonnell Aircraft Co.
Mr. L. E. Lutz, Honeywell, Inc.
Mr. L. G. Smith, Douglas Aircraft Co.
Mr. F. C. Tolleth, Autonetics
Mr. O. J. Zamparo, MB Electronics

The discussions which took place during the panel session on fixture design make up the following paper. All remarks have been edited for clarity and some have been omitted, usually because they repeated points brought out earlier in the discussion. For the most part the comments appear in the order in which they were made.

Dr. Mains: Mr. Tolleth, what do you do when you get a resonance in the system so that the center of gravity dynamically is not the same as the center of gravity you balanced out so nicely when you set up the fixture?

Mr. Tolleth: It is my opinion that there isn't really a lot you can do about it unless, of course, you have a very simple system; however, in order to minimize the problem of having dynamic unbalance, you want to make sure in the beginning that you are balanced statically. If you don't balance statically, you are accentuating the problem dynamically. For a system of any complexity you will never get rid of dynamic unbalance except, perhaps, by designing some sort of a governor for balancing automatically.

Mr. Cost (White Sands Missile Range): We have had trouble in using T-brackets with welded sections. These welded sections crack, causing high resonance conditions in them and invalidating testing. I noticed there was a lot of welding in the fixtures made by Douglas Aircraft, and the fixture made by Mr. Lutz seemed to be all welded. Wouldn't it have been much simpler to cast the fixture and eliminate all the welded joints, or do we have better welding now?

Mr. Smith: Our fixtures are welded so that we can more readily make any required changes to them. It is easier to change a fixture

that is welded than it is to change one that has been cast. You can't weld all cast materials.

Mr. Lutz: As a point of interest, in most cases you can eliminate cracking adjacent to welds if you will stress relieve and heat treat your weldments before you finally machine them.

Mr. Smith: I'd like to add that the kind of stresses we are talking about are rather low. If you do stress relieve, I don't think you have any problem; at least we don't in our fixtures, and they are pretty big fixtures.

Mr. Jenicek: We have found that making sure our joints are axially loaded takes care of any troubles that we have with cracks.

Mr. Gorton (Pratt & Whitney Aircraft): One gentleman had a very heavy welded fixture that was 4 inches thick made out of 1 inch by 4 inch bar stock and another plate that was 2 inches thick. He said that these were to be attached to some electronic components, I believe. To me, a box full of electronic components is usually quite rubber-like. When you put this in a vehicle somewhere, I presume it is not going to have the 4-inch thick backing plate to keep it from wobbling around. What is the merit of testing it while it is supported by a 4-inch thick backing plate?

Mr. Smith: This is one reason that we have such large skin panels. We try to keep

our associated skin area far enough away from the actual item we are testing so that we philosophically justify the test. You might say we are only looking at an island of our skin panel as the test specimen.

Mr. Gorton: I'm not sure you had the one I'm thinking of. There was a rectangular fixture 4 inches thick and about a foot and a half square.

Mr. Lutz: Our packages are mounted on small bosses so we are not using the fixture itself to stiffen up the package.

Mr. Gorton: As long as there are four or more bosses hooked to this heavy structure, three points determining a plane, you have stiffened the box whether you wanted to or not.

Mr. Lutz: I agree, but this wasn't our responsibility. We're not mounted flush to the fixture itself. We are up on bosses so that the centers are free to deflect between the mounting points.

Mr. Bergey: I was talking to Dr. Mains in this connection earlier today. We had to test a computer which was about the size of the rostrum on a fairly small shaker head and with overhanging mounting points. We wound up with something rather similar to what Mr. Lutz was discussing simply because we wanted to keep all the mounting points going up and down together. There was space underneath for the piece itself to deflect. You need a rather stiff support to make your shaker head appear bigger.

Dr. Mains: That's an interesting philosophic question having to do with the conduct of the test. Should you force the mounting points to stay in a plane when, at some frequency, they want to get out of the plane to accommodate a particular mode? That is a good question and I wish I knew the answer to it.

Mr. Fischer (AiResearch Mfg. Co.): Like many others, we use a lot of magnesium and aluminum in our fixtures. We have found that we have to be careful when bolting down in aluminum. We have used a number of steel washers about 1/8 inch thick with precision-ground, flat surfaces in order to get good transfer. I would like Mr. Zamparo to comment on that.

Mr. Zamparo: If the washer is a hardened washer with flat, parallel surfaces so that it itself does not introduce any spring rate, it will cause the bolt to be longer and therefore will lower the natural frequency a bit. If by virtue

of this washer, however, you pick up a larger area of the fixture, then you are increasing that spring rate and the net result is unpredictable. There is no doubt that a washer is a must when there is a possibility that the bolt head may shear a little of the hole I.D. It must be a fairly heavy washer, however, which has flat parallel surfaces and is very stiff in itself.

Mr. Fischer: We do use a hardened steel which is quite thick. Our fixtures are ground down with a recess point so that the bolt does not have to go through more than 1 inch of material. This keeps our bolts quite short.

Mr. McGinnis (ITT Federal Labs.): Mr. Zamparo, do you use the bolts dry or oiled? Secondly, when you go to the table to get your recommended torque values for a high strength steel bolt which you are going to thread into magnesium, what torque value do you decide upon?

Mr. Zamparo: If you use the bolt elongation technique and bolt rotation, then you bypass torque. A burr on a thread, oil, some epoxy, or anything else in there won't affect the joint too much. My recommendation is to get away from the problem of factors that magnify the torque without actually causing a bolt elongation and freeload. Secondly, you talked about threading into fairly weak materials. Here it would be possible to put an insert into the soft material so that you then have a threaded fastener of a much larger diameter than the bolt diameter. You thereby pick up a lot of the area in the soft material which is the purpose for using inserts in the exciter tables. You would then utilize the strength of the bolt because it is going into a threaded part of a harder material than the soft parent material of the table. Does that answer that question?

Mr. McGinnis: Not completely. Sometimes you are furnished an item that already has a tapped aluminum hole and you don't have the choice of putting an insert in. What kind of black magic do you use to pick the number?

Mr. Zamparo: Well, I can only answer in general terms. Try to use as many bolts as possible as one approach. Another would be, if you can in any way, to drill all the way through the member and don't use the threaded part. Say you have a web and a magnesium structure; drill right through and put a nut on the back. In these weird cases in which there is only a small amount of area to work, helicoils have been used to beef up the structure. If you don't have enough stock, you are just stuck with the situation and you'd have to redesign the whole area to get it to a higher frequency.

Mr. Harvey (USN Underwater Sound Lab.): I think this is the first time I've ever heard six people talk about fixturing and haven't heard that nasty word "impedance." I think sometimes we get so involved with the test that we forget why we run the test. As an example, one of the panelists was talking about strapping down portable gear to assure linear motion. I'm sorry, but I can't quite buy this concept. When a piece of gear is strapped down on a ship or a tank, nobody really cares if the motion is linear. Is the purpose of our test environmental simulation? If it is, we must look back into the fixture where the package is being attached. I quite frankly don't understand why we want this perfect linear motion. Why, on these portable equipment tests, was the gentleman concerned with restraining the motion? He talked about using side rails so the equipment wouldn't kick sideways. This tends to abort the purpose of the specification.

Mr. Jenicek: This is true from strictly a mobility standpoint, but from a vibration standpoint where you are looking for a frequency response, you can't have your specimen sliding on your shaker top.

Mr. Harvey: Is the purpose of your test to simulate the environment or is it an R&D effort to determine the response of some discrete part of your item?

Mr. Jenicek: You are talking about two separate tests. We run R&D tests and we also run environmental tests to simulate actual conditions.

Mr. Harvey: That's the reason you had me confused. You did mention Mil-Std-167, which is purely an environmental specification.

Mr. Jenicek: One of the reasons I mentioned this particular specification was because it was a low frequency test. As I mentioned in my talk, these three attachment methods were strictly for low frequency type testing.

Mr. Brown (Texas Instruments): My question is to Mr. Zamparo from MB. Have you done any work on combined temperature with vibration? When you torque down a specimen or fixture to a vibration carriage and then change the temperature, materials will expand. Would you recommend retorquing or rechecking your torque to prevent decoupling?

Mr. Zamparo: I think the first approach is to see whether there is going to be a problem of differential expansion. Once you've determined that there is a problem, then you want to

know the degree. If you know you are going to tighten something up at room temperature and then have to submit this whole test to a high temperature environment, it's possible to calculate a lower stress for the situation and allow the whole specimen to come up to the test temperature before you apply the vibration. This would limit your bolt stress. It depends upon the situation in that case.

Mr. Gorton (Pratt & Whitney Aircraft): I have another question in the nut and bolt department. Earlier someone was advocating the use of a little steel washer with teflon facing for the measurement of force between the shaker and the specimen. Now it is recommended that the bolts be kept as short as possible. I feel that the shorter the bolt the less likely this washer would be truly measuring the alternating force, because some component of this force would be taken up in changing the tension in the bolt as things deflected. Furthermore, if you put in this kind of washer, what's it going to do to your natural frequency? I would appreciate any comments on that.

I have a comment on the tightening of bolts. I'm not familiar with the details, but I'm reasonably sure that if you look in any aircraft engine overhaul manual you will find detailed instructions on how to tighten bolts repeatedly right up to their yield point. I know they always recommend consistent lubrication. I also think that you are supposed to tighten the bolt up once and back it off, then do your measuring on the second tightening. There are likely to be roughnesses on the threads that interfere either with torque measurement or with your angular measurement on the first attempt. I suspect there may be other little details on bolt tightening which any overhaul manual would cover.

Mr. Zamparo: I am familiar with one type of washer which can be used to measure preload. These washers have a built-in spring which is quite stiff. When you tighten the bolt you keep tightening until you can't get a feeler gauge in between the two serrations of the washer. With respect to the teflon washer, if it is a measuring device of some kind it might give an instantaneous reading, but knowing the cold flow properties of teflon I am sure that you would lose a preload and create a very poor joint.

Dr. Mains: This measuring washer was a different sort of thing from what you are familiar with. As I got the picture, the washer was a solid steel ring coated with a very thin coat of teflon. The purpose of this coating was to provide a smooth surface for pulling the bolt up

with a minimum of friction and to provide a waterproofing device for covering the piezo-electric strain gauges that were around the periphery of the washer. In answer to Mr. Gorton, the washer would affect the natural frequency in the same way that any washer would since it has lengthened the bolt and changed the path of stress. There was also a question of whether the right force is measured. If you have two surfaces with a force between them and the gadget that's between them is measuring that force, how far wrong can you go? You have to satisfy statics there, don't you?

Mr. Gorton: There is a third force coming in through the bolt.

Dr. Mains: From where?

Mr. Gorton: The other end of the bolt.

Dr. Mains: If I cut that bolt in two, there is a force in the bolt and that is the only force in the bolt. Now, that force has to be reacted somewhere and that is on the mating surface that surrounds the bolt.

Mr. Gorton: In Mr. Zamparo's diagram, which is what raised the question, there was a deflection of the bolt and a deflection in compression of the stuff between the two ends of the bolt, part of which is the washer. As you alternate the load both of those deflections are going to change, are they not?

Mr. Zamparo: That is correct.

Mr. Gorton: Well, as the bolt deflection changes does not the tension in the bolt change? If you put a strain gauge on the bolt, you'd measure some alternating load?

Mr. Zamparo: Yes, there will be an accompanying force to the deflection.

Mr. Gorton: The division of this alternating load between the solid stuff and the bolt is somehow related to the relative stiffness between the solid stuff and the bolt. You would have to go through your equations in detail I suspect, but I just had the feeling as I looked at your equation that this washer would not be measuring the total of the alternating force. The bolt would be getting some of it.

Mr. Zamparo: I can see that, if you put the washer under the head of the bolt, it will tend to measure forces when the fixture is trying to go up into the bolt. If you put the washer below you will get the force in the other

direction. But since all the forces are colinear, a free-body diagram would show that there is a force existing in that line and that same force exists anywhere in the line. Otherwise you would not have equilibrium.

Mr. Tustin (Tustin Inst. of Tech.): About 10 years ago, I saw some elongation indicating bolts that I think would be extremely useful in this regard. They could be threaded into a blind hole. At the top there was a little circle in the center and a little close-fitting pin which went through the shank of the bolt and down into the threaded section. As you tightened the bolt and the bolt elongated this pin pulled down a little. The measured depth of this pin below a flush surface would be an indication of bolt elongation. I don't remember the manufacturer. It seems as if this would be an extremely useful thing for bolting down to a shaker table. Does anybody happen to know what that brand was?

Dr. Mains: This was a device that I first ran across in Talbot Laboratory a good long time ago. They used both the fixed pin and also a depth gauge in which the pin was essentially portable from one to the other. These days we use SR-4 gauges, or their equivalent, down inside the shank of the bolt. You drill a hole in the bolt and put an SR-4 gauge in there. Then you pull up the nut until you get the right amount of stress. This is a common device for pre-stressing the bolts in the heads of pressure vessels for nuclear applications.

Mr. Vatz (Brown Engineering Co.): I was involved in a similar problem of bolt evaluation. We just obtained bolts with strain gauges as an integral part. We can very simply tell what the strain is on the bolt.

Dr. Mains: Is the strain gauge on the surface or inside?

Mr. Vatz: The bolts are tapped on the inside and the strain gauge is on the inside in the unthreaded shank of the bolt. We can measure the actual force through the bolt by the strain gauge.

Dr. Mains: These are commercially available?

Mr. Vatz: Yes.

Mr. Moore (Sylvania Electric): I have a question on the laminated fixtures for Mr. Bergey. I wonder if he has any data or maybe a program underway to evaluate how much of the shaker head energy is actually getting to

the specimen through the laminated fixture construction.

Mr. Bergey: I don't. That is rather brief and quick, but I haven't had time to really evaluate this. The vibration design is only part of my job. It was just an idea and I tried it. I was getting the force I wanted at the mounting points, but I don't know whether it really damps or just stops at resonance.

Mr. Beecher (Lear Siegler Inc.): I'm concerned primarily with vibration fixture design for random purposes. The principal object, of course, is to get all of the resonant frequencies of the fixture above the test specification. We all know that this cannot always be done. I have found that even though you have a resonant peak you may not be in too much trouble. However, if you do have a notch in the fixture response within the limits of the test specification, you can be in serious trouble for several reasons. First, you may have harmonic response in which event you can pour energy in at the fundamental trying to eliminate the notch, when all you are actually doing is increasing energy at some frequency far removed from where the notch is. Another thing that can happen is that the energy is going in along the line of the shaker motion but the fixture response is in the transverse direction, so you can pour all kinds of energy into your fixture still without cancelling out your notch. And a third and even more exotic response is when you have two notches in your fixture response. You pour energy in at each of these and all of a sudden you end up with a peak at the sum frequencies. In other words, it is the mechanical equivalent of an electronic mixer. I have found that from my experience that you can live with peaks, but you can't live with notches. I'd like to hear whether other people have found this to be true.

Mr. Smith: I agree with you. We have had very interesting problems with what you're saying about frequencies adding, and so forth. We had one problem that the automatic equalizer couldn't solve. Applying excitation at one frequency was causing response at a different frequency and vice versa. The automatic equalizer was telling one channel to pour in more energy and it turned out that this was being poured into a completely different channel. In other words a random noise was being allowed through one filter and it was coming out at a completely different frequency. So that particular channel told its filter to cut off which did no good at all because it was being fed from over here. All I can say is that each fixture and setup does involve these kind of problems and we take them as they come.

Dr. Mains: This question of having notches and peaks introduced by the fixture in the test system gets to be a real tough problem to get around with respect to the question of how you equalize and why you equalize for a random vibration test. It's tough enough when you have a linear fixture so that when you take a notch out it stays out. But when you have a nonlinear system as so many of them are, especially with heavy damping, you get the subharmonic-superharmonic problem such that you can drive at frequency x and get response at $4x$ or at $1/4$ of x . I don't see how you can even begin to consider equalizing and having it mean anything. As I understand it, the whole purpose of equalization is to get a one-to-one transfer function in between the voltage input and the motion at the specimen. If there is a fixture in between which does not behave as a linear system, I don't see how you can ever accomplish this.

Mr. Lutz: We have sometimes found this to be a problem, too. To get around this we make a dummy of our test specimen before we ever start the test. We use this dummy to check out the fixture, then if the fixture is no good we throw it out and start all over again. We figure out a way to fix it before we use our test specimen, which may cost many thousands of dollars.

Mr. Zamparo: Dummies don't really simulate what the actual test specimen does. We've had some very erroneous results by using them. A discarded part would be a legitimate dummy, but I wouldn't suggest using a manufactured dummy for equalization.

Mr. Lutz: This was our solution. We find it works. We can build dummies that simulate size and cg and they work.

Dr. Mains: It is frequently said that one should equalize with a dead mass in place of the actual test article. If anybody has listened to the discussion of impedance lately, the first question would be how can you ever achieve a dead mass? At some frequency it isn't.

Mr. Mines (Autonetics): We had a similar problem. We have an actuator in a flight control unit which has to be turned on during a vibration test. This was causing quite a problem with our g levels and notches. A big notch happened to occur right at a resonant frequency. We stiffened the thing up by adding mass to the fixture. This was the only thing that changed anything at all.

Dr. Mains: What did you accomplish by doing this?

Mr. Mines: It shifted our resonant frequency slightly, enough to put us inside our specification.

Dr. Mains: Maybe you should have gone to bat to make sure the specification was being properly applied. If that actuator, when it was in the condition that it was going to be during flight, had enough feedback into the system to modify the dynamic behavior then why should you change it? That's what it is supposed to do and if doing that is wrong then you had better redesign, not just dodge around it by adding a mass or something. It's perhaps a case of doing the right thing for the wrong reason. You may have achieved a satisfactory result, but the reason why you got it may have been wrong.

Mr. Plumb (Lockheed Missiles & Space Co.): Dr. Mains suggested that maybe we shouldn't be equalizing. It seems to me that the greatest advantage in the automatic control of vibration, although you may not be getting the same response throughout the system, is that you get a consistent result from one test specimen to the next if you've got a number of packages to test. Perhaps I misunderstood your suggestion that there isn't any advantage to this equalization technique.

Dr. Mains: At the frequencies which the specimen-fixture combination want to have an anti-resonance, you are going to insist on equalizing and forcing some standard level of response at that would-be notch, you are just going to be overdriving the dickens out of that specimen. It may be that you can consistently hit the same place with a hammer and have it break each time, but consistency may be too much of a price to pay. Do you read me?

Mr. Plumb: Yes, I understand what you're saying. I would say that in this particular case we should change the spectrum requirement to include what you are talking about so that we do in fact have a notch at that point in the spectrum. We would still have the consistent result of an automatic which is needed because of the fact that the fixturing in this sort of thing may cause problems that you'll need to equalize out.

Dr. Mains: I would like to mention a case in point. Three or 4 years ago we had a constant force requirement for a vibration test on a piece of gear. At two frequencies in the range the specimen simply wouldn't accept that much force. The only way that we could have gotten that much force into the specimen would have been to buck it up against a mass somewhere so it would hold still long enough for us to push on it. It just got out of the way and

wouldn't accept that much force. The only thing that was reasonable to do was to change the specification requirement. We did.

Mr. Plumb: I agree with you that in the majority of the cases we need to change the specification requirement when we have a problem.

Dr. Mains: Since I don't write specifications I can agree with you.

Mr. Otts (Sandia Corp.): In several of our vibration tests we have found that it is just impossible to fasten onto our test item by bolts or the like. It is a point type application for which you want vibration input at a particular point. We have tried bonding the test item to fixtures. I wondered if any of you gentlemen have tried this bonding technique and, just briefly, what were your results?

Mr. Tolleth: A year or two ago we manufactured a vacuumized, bonded, slip plate and found that we had very good luck with it. It is similar to making a laminated fixture. You can do it and be certain that, if you don't exceed your strength allowables, you will get your load in there.

Mr. Otts: Do you recall what kind of spring constant you had across that bonded joint?

Mr. Tolleth: I don't know if you've ever tried to develop a spring constant for a piece of chewing gum, but it is pretty difficult. You may have a piece of chewing gum and then again you may not. Sometimes we have even used wax. It would depend upon what you were going to use as a glue or adhesive.

Mr. Otts: From all the indications, by controlling the acceleration input at the base of the test item on the fixture, we had a resonance which showed a spring constant of about 10^7 or 10^8 pounds per inch; however, it was a very large test item that weighed a lot. This still threw us down into the 300 to 400-cps range. If you have done this, do you know of a bonding material which is perhaps better or stronger, particularly in shear? Shear seems to be a big problem.

Mr. Bergey: Do you have to get your test item off this thing once it is bonded on?

Mr. Otts: Yes, but that's no problem with what we use. I believe it was an epoxy resin patch kit and there is a material which is a solvent for this. If you allow enough time it will soak in and then, of course, release. We didn't have to use a hammer or anything.

Mr. Bergey: You want something which is strong in shear and I guess you would have to go to some of your epoxies. This Epon 934 is a very good glue but I don't know how to dissolve it. There might be a standard epoxy dissolver that would work.

Mr. Otts: I was talking in terms of not over a 5 square inch contact area on a conical shape for an item that weighed in excess of 1500 pounds.

Mr. Bergey: You're asking for an awful lot. That's pushing the state of the art on glues, I guess. I'm not really familiar with that.

Mr. Lutz: I was going to mention something that I thought might be applicable until I heard the size and contact area. Recently, I read an article describing a repetitive type test where they were taking a fixture off a shaker quite often. They used a vacuum to hold the fixture to the shaker and I understand they got pretty good results.

Mr. Otts: The only trouble there was that we did not have enough contact area. Mr. Smith, what cross talk did you experience at the attachment points between the panel and the fixture? Was your design considered satisfactory?

Mr. Smith: We have gotten very high cross talk in a lot of cases and I'm not sure whether it is due to the fixture or the specimen. Usually, because we have a skin panel with most of the equipment on one side of it, the test item itself generates a lot of cross talk. This is something we just live with. Regardless of the direction of shake, we normally get a one-to-one correspondence along almost any axis that might couple with the drive axis.

Mr. Cost (White Sands Missile Range): Mr. Tolleth is sort of my hero because he is willing to talk about slip tables when others feel they have been talked to death. What sort of lubrication do you use on this thing? I don't see any grooves or anything to transmit oil film across the face. Do you just have a puddle or do you have it force up through the granite block?

Mr. Tolleth: We probably have a very primitive method. The mechanic or the test technician cuts a little piece of sheet metal and paints it on very evenly. It is a heavy grease and, because it is heavy, it has no place to go unless the test is of long duration and it gets hot. So far, with a flat slip plate, we've had no problems with it.

Mr. Cost: Would you accept a suggestion? We've had remarkably good luck at White Sands using a thin sheet of teflon with an oil groove system into which is fed a silicone-type oil. It has very good strength and it eliminates friction down to the point where a 210 square inch plate weighing 33 pounds took a 1/4-pound drag to pull it across the table. It had a very high separation coefficient. I'm just suggesting this since we didn't have anything as massive as yours.

Mr. Tolleth: The problem is that it's difficult enough to sell a fixture like I discussed in the paper to an engineer at that expense. If I went to the expense of using teflon and the like it would probably get way out of hand. I've read about teflon and we will probably try something on it soon. It looked to me like it was a very good idea.

Dr. Mains: It works fine on frying pans. I discovered fried eggs since teflon came along.

Voice: When you have a cylindrically shaped object as long as 100 inches and you have a choice of building one massive large fixture to be used between the payload and a single large shaker, or building two smaller fixtures and using two smaller shakers arranged in tandem from a single amplifier, which method would you choose and why?

Mr. Smith: I would rather use more shakers than to have a very large fixture. However, the kind of tests that we do just don't lend themselves to using a large number of shakers. I associate that with a specimen that is kind of long with the natural drive points not too strongly coupled with each other. You have to look at the individual tests and if you can find an application for a multi-shaker test I would do it.

Mr. Shipley (Wyle Labs.): I have two comments. Mr. Harvey of the Underwater Sound Lab wonders why we worry about cross talk. This brings up the old question of where you start your simulation and where you stop it. We worry about cross talk because our specifications are based on the assumption that we are going to use unidirectional motion. Mr. Cost of White Sands is wondering why we don't use cast fixtures and eliminate concern about weldings. More often than not, whether we like it or not, the dictates of schedule and economics preclude the use of cast fixtures. We've been forced to learn how to use welded aluminum and magnesium fixtures.

Mr. Mutter (Boeing Co.): I want to get back to this question of the notch in the spectrum due to the resonance. Normally, as far as I am concerned, when you are running a test of this nature you usually search your component to see where your resonant frequencies are. When you have a fixture or a specimen of such a size that you have a lot of severe resonances with notches that you can't eliminate, you usually find that the specimen has a fairly low resonant frequency which is probably under 200 cps. This is where most of the damage to the component will occur. If there is a notch up around 12-1500 cps and a component resonance at 100 or 200 cps, I really don't think the notch is so critical that we have to be concerned about reaching the specification level at that frequency. If the component has a low natural frequency and the notch is due to a fixture resonance at a fairly high frequency I think we could normally grant a deviation for that notch. With respect to fixturing in general, we've been having a lot of trouble with vendors doing qualification testing for us who are trying to design a universal fixture for three axis testing. In doing this they come up with a large box instead of a couple of simple angles and thereby get into severe resonance problems so that they can't meet the specification. If they were to build a fixture for each axis instead of one for all three, they would be a lot better off.

Mr. Otts (Sandia Corp.): I just want to make a comment on the use of multiple shakers rather than a single one. We are presently waiting for four small shakers intended for the testing of large items. We're getting quite suspicious of this single point input control business and, in fact, we have proven that because you control at one point you have no guarantee what the input is to some large test item. We are going to try to use a multiple shaker input with at least four shakers so that we will have what we feel is a better definition of the overall input. In fact we hope that we can use separate control at each of these points rather than hooking them in tandem.

Dr. Mains: Are you going to tie your control to some analysis, some preconceived notion of what that control ought to be?

Mr. Otts: Essentially, we are starting a campaign against single point control. We haven't gotten into the exact usage, but we do feel that we will have a better test simulation if we control at multiple points. Once we get the shakers we will do some studies. Perhaps next year we will have some firm results.

Dr. Mains: Multiple excitation testing is old-hat with the aircraft companies. The ground vibration test is something they have been doing for a long time, but such a test must be run in conjunction with a several step analysis. You first analyze and decide what the mode shape is, then locate the shakers in accordance with that mode shape and then see if you can generate it and keep it pure. You never do the first time, so you start moving the shakers around until eventually you are satisfied. If you are getting into the multi-shaker business, you are sure going to have some fun.

Mr. Mutter (Boeing Co.): Some of our vendors are using quite a few shakers simultaneously on qualification tests of long ducts for our Saturn program. We've used as many as four shakers with multiple-bracket attachments to the vehicle. This isn't for the determination of mode shapes, but is a qualification test.

Dr. Mains: Do they go in unison?

Mr. Mutter: Yes, but sometimes they go out of phase.

Dr. Mains: Zero phase lag?

Mr. Mutter: At some frequencies you can't keep them in phase, but when you have four brackets separated by several feet on the aircraft they are not in phase either. For random testing you don't worry about phasing.

Mr. Fischer (AiResearch Mfg. Co.): With respect to dummy weights, we have found that they work very well if there is a great deal of decoupling in your mounting. In other words, if you have a very stiff mount to the fixture from your specimen, you will have problems with dummy weights. The more decoupling you have, the better the dummy weight works out. The dummy weight will only provide good evaluation at the lower frequencies. You can almost evaluate your fixture at the high frequency with no weight and get fairly close.

Mr. Shipley (Wyle Labs.): For multi-shaker testing, how do you control with random excitation? We've tried it a number of ways and are not happy with any of them. I would like to see a device which would measure the excitation in bandwidths much like the automatic control consoles; take an instantaneous average which is not sensitive to phase so that you don't get the phase cancellation, then sum these things up and control from that. I don't think such a device exists.

Dr. Mains: I would think that for random vibration using multiple shakers you would have to control each shaker separately with a separate noise generator and a separate shaping network. Otherwise you would get hopelessly out of control.

Mr. Shipley: We tried it both ways. Controlling each shaker independently with a separate amplifier, we have used a common noise source so that the low frequency is in phase. We ignored the high frequencies which you wouldn't keep in phase anyway. We've had some difficulties both ways and neither seems to be the answer.

Mr. Smith: Dr. Curtis of Hughes has been giving some thought as to whether one needs as many equalizers as there are shakers in a multishaker test. Of course, he hopes the answer is no, because they cost quite a bit of money. In trying to answer the question he looked at it from the standpoint of whether the sum signal can be used as some indication of the average. I'm not going to try to summarize his learned paper, but his conclusion essentially is that with separate generators or uncorrelated signals at each shaker, the sum is not indicative of the average. So, at least from Dr. Curtis's mathematical standpoint, you do need many generators.

Mr. Mutter (Boeing Co.): The vendor I was referring to that has been doing the testing with multishakers for us has been using a common noise source but separate amplifiers for each of their shakers. They equalize each of their shakers separately. Their problem is that the equalization of one shaker affects the other three. It takes quite a while to make the circuit about eight times and get them all fairly well equalized. It would help if they had an automatic equalization system for each shaker, but they only have one automatic system. They use peak notch for the easy three and automatic for the worst one. They want to set up a tape technique by which they use the automatic equalizer to equalize one shaker, tape that as the input, then go on to the next one and so forth. They could reduce their total equalization time. I think this system probably could work although they haven't had time to perfect it because of the schedule in their lab. There might be someone who might have experience and want to comment on a taping technique for equalization.

Mr. Jenicek: At McDonnell we used tape inputs for a couple of years before we got our automatic system and they worked out very well. The only problem for us has been that of making a tape using a dummy specimen. When the actual specimen is used it's not quite the same and the test is no good.

Mr. Smith: We had another interesting experience along that line. I've only worked on one test where we used a tape input and naturally we first tried to equalize our system. This was in the days when we only had 40 manual channels to work with, but we tried to equalize our system before we played the tape through. We were using the engine section of the Thor vehicle, as a matter of fact, and we just couldn't get a decent equalization on the thing. We didn't feel very good about playing the tape through because of that, but we had nothing left to do. We played the tape through the best equalization we could get and, strangely enough, saw that our control accelerometer was doing something very close to what the analysis of the tape indicated was on the tape. It was a very interesting mystery with respect to tape inputs.

Mr. Mutter: Our vendor did use the one-channel equalizer system; they did have to shape the spectrum for all of their shakers. They shaped the spectrum, taped it, and then used that as the input to get the proper shape once they were equalized.

Mr. Beecher (Lear Siegler Inc.): We've had about 5 years experience with tape equalizations. We have only recently acquired an automatic equalizer. We used to equalize two shakers with one equalizer and we used tape equalization for the second system. We found that certain precautions have to be taken or you don't come out correctly. If you have to unbolt your test item and bolt it back on or bolt on a similar test item between tests, you run a considerable risk of losing your equalization. You can partially overcome this by using standard torqueing measurements every time you do it. We found that this cures the worst portions of this problem. Another thing is that there is a long term drift in the equalization characteristics of a given shaker. Because these shakers are mechanical systems there is a certain amount of loosening of the interior bolting of the shaker itself. If, however, you leave the test item bolted and don't do anything to disturb it between tests, tape inputs can be used quite successfully.

* * *

DISTRIBUTION

Aberdeen Proving Ground, Md.		Army Air Defense Center, Ft. Bliss	
Att: Ballistic Research Lab.	1	Att: Technical Library	1
Att: Development & Proof Services	1		
Att: Physical Test Lab.	1	Army Chemical Center, Maryland	
		Att: Library	1
Advisory Group on Electron Tubes, New York		Army Electronics Materiel Agency, Phila.	1
Att: Secretary	1		
Air Defense Command, Ent AFB		Army Electronics Materiel Support Agency,	
Att: Deputy for Civil Engineering	1	Ft. Monmouth	1
Att: ADIRP	1		
Air Force Packaging Evaluation Agency,		Army Electronics R&D Laboratory,	
Brookley AFB		Ft. Monmouth	
Att: MOSPR	1	Att: SELRA/SL-ADT	1
Att: MONE	1	Att: SELRA/SL-PEE	1
		Att: SELRA/SL-PRT	1
Air Proving Ground Center, Eglin AFB		Att: SELRA/SL-G	1
Att: PGTRI, Technical Library	1	Att: SELRA/SL-GTF	1
		Att: Mr. J. J. Oliveri	1
Air Force Headquarters, DC		Army Engineer District, New York	
Att: Operations Analysis Off.,		Att: NANGD	1
Off. Vice Chief of Staff, Library	2		
Att: AFDRD-GW	1	Army Engineer R&D Laboratories, Ft. Belvoir	
Air Force Logistics Command, W-PAFB		Att: Package Development Branch	1
Att: G. P. Civile, MCTEP	1	Att: Mr. A. Carolla	1
		Att: Director of Research	1
Air Force Missile Development Center,		Att: Chief, Spec. Proj. Branch	4
Holloman AFB			
Att: RRRT/Miss R. Porter	1	Army Engineer Waterways Experiment	
Att: MDS/Dr. M. G. Jaenke	1	Station, Vicksburg	
Att: MDSGL-2/Mr. H. J. Dunbar	1	Att: Mr. J. M. Strange	1
Att: MDSGS/Mr. J. H. Gengelbach	1		
Att: MDSTE/Mr. P. N. Sonnenburg	1	Army Erie Ordnance Depot, Ft. Clinton	
Air Force Missile Test Center, Patrick AFB		Att: Chief, Materiel Testing Div.	1
Att: MT LLL-3 (Classified Material)	2		
Att: MU-135, Technical Library		Army Materials Research Agency, Watertown	
(UNCLASSIFIED)	1	Att: Dr. Reinier Becuwkes, Jr.	2
Air Force Office of Scientific Research, DC		Army Materiel Command, DC	
Att: Library	1	Att: AMCRD-RS-CM	1
Air Force Regional Civil Engineer		Army Materiel Command, Redstone Arsenal	
Att: North Atlantic Region,		Att: Technical Library	4
AFRCE-NA-A	1		
Att: South Atlantic Region,		Army Missile Command, Redstone Arsenal	
AFRCE-SA-E	1	Att: AMSMI-RB	1
Air Force Rocket Propulsion Lab., Calif.		Att: AMSMI-RG	1
Att: Mr. A. J. Davies (RPFDE)	1	Att: AMSMI-RL	1
Att: Mr. R. A. Silver	1	Att: AMSMI-RS	1
		Att: AMSMI-RT	1
Air Force Systems Command, Andrews AFB		Att: AMSMI-RTR, Mr. J. M. Taylor	1
Att: Technical Library	2	Att: AMSMI-RSM, Mr. E. J. Wheelahan	1
Air Force Weapons Laboratory, Kirtland AFB		Army Mobility Command, Centerline	
Att: Development Test Division	1	Att: Mr. Otto Renius	1
Att: Dr. W. E. Fisher, WLRS	1		
Att: SWOI 631-276	1	Army, Office Chief of Engineers, DC	
		Att: ENGMC-EM	2
		Army, Office of Quartermaster General, DC	
		Att: Military Planning Division	1

Army, Office Chief of Research & Development, DC		Bureau of Naval Weapons Rep., E. Hartford	2
Att: Scientific & Technical Information Division	1	Bureau of Naval Weapons Rep., Pomonona	1
		Att: Chief Engineer	1
		Att: Metrology Dept. Code 60	1
Army, Office Chief Signal Officer, DC		Bureau of Naval Weapons Rep., Sunnyvale	1
Att: Research & Development Division	1		
Army, Office Chief of Transportation DC		Bureau of Ships, USN, DC	
Att: Director of Transportation Engineering	1	Att: Code 423	20
Army Ordnance Ammunition Command, Joliet		Bureau of Supplies & Accounts, USN, DC	
Att: ORDLY-T	1	Att: Library	1
Att: NNSC/A	1	Bureau of Yards & Docks, USN, DC	
Army Tank-Automotive Center, Warren		Att: Code D-440	1
Att: SMOTA-RRS, Tech. Library	1	Att: Code D-220	1
Att: SMOTA-RCE.3,		Att: Code D-220 (UNCLASSIFIED)	6
Mr. D. J. Hackenbruch	1		
Att: SMOTA-RRC	1	Coast Guard Headquarters, DC	1
Att: Mr. D. W. Rees	1		
Army Transportation Engineering Agency, Ft. Eustis		David Taylor Model Basin, UERD, Portsmouth	
Att: Library	1	Att: Code 281A	1
Att: Mr. L. J. Pursifull	1	Att: Mr. E. W. Palmer	1
Army Transportation Research Command, Ft. Eustis		David Taylor Model Basin, DC	
Att: Dr. R. L. Echols,		Att: Library	3
Physical Sciences Res. Group	1	Att: Mr. Harry Rich	1
		Att: Code 591L, Mr. J. A. Luistro	1
		Att: Contract Res. Administrator	1
Arnold Engineering Development Center, Arnold AFS		Defense Atomic Support Agency, DC	
Att: AEOIM	1	Att: Technical Director	1
		Att: Weapons Development Division	1
		Att: Mr. John G. Lewis	1
Atomic Energy Commission, Oak Ridge		Defense Atomic Support Agency, Livermore	
Att: Office of Technical Information	6	Att: Administrative Officer	1
Atomic Energy Commission, DC		Defense Documentation Center, Va.	20
Att: Library	1	Defense Intelligence Agency, Va.	
Att: Tech. Evaluation Branch (Army Reactors)		Att: DIAAP-1K2	1
Division of Reactor Development	1	District Public Works Office, 14th Naval District	1
Aviation Supply Office, Philadelphia			
Att: Code TEP-1	1	Electronic Systems Division, AFSC, L. G. Hanscom Field	
Ballistic Systems Division, USAF, Norton AFB		Att: Library	1
Att: Technical Data Division	3	Electronics Supply Office, USN, Great Lakes	1
Boston Naval Shipyard, Mass.		Federal Aviation Agency, DC	
Att: Library	1	Att: Emergency Readiness Div., Off. Plans & Requirements	2
Bureau of Medicine & Surgery, USN, DC		Att: Chief, Tech, Processing Br., Library Serv. Div. (UNCLASSIFIED)	1
Att: Research Division	1		
Bureau of Naval Weapons, USN, DC		Forest Products Laboratory, Dept. of Agriculture, Madison	
Att: DLI-3	2	Att: Robert Stern (UNCLASSIFIED)	1
Att: FWAA, C. H. Barr	1		
Att: RREN-5	5	Frankford Arsenal, Philadelphia	
Att: RRMA	1	Att: Library Branch, CC 0270/40	1
Att: RAAE-2	1	Att: Mr. David Askin, CC 1730/230	1
Att: RM-3	2		
Att: RM-2	1		
Att: RSSH	2		
Att: FWAE	1		
Att: RREN-8	1		

Harry Diamond Laboratories, DC		Naval Air Development Center, Johnsville	
Att: Chief, Lab. 700	1	Att: Mr. E. R. Mullen	1
Att: Chief, Branch 850	1	Att: Aeronautical Instrument Lab.	1
Att: Technical Information Officer	2	Att: NADC Library	2
Inspector of Naval Material, San Francisco	1	Naval Air Engineering Center, Philadelphia	
Library of Congress, DC (UNCLASSIFIED)	2	Att: Library	1
Long Beach Naval Shipyard, Calif.		Naval Air Test Center, Patuxent River	
Att: Code 240	1	Att: Electronics Test Div.	1
Los Angeles Air Procurement District, Calif.		Att: VTOL/STOL Branch	1
Att: Quality Control Division	1	Att: Instrumentation Br.,	
Los Angeles Ordnance District, Pasadena		Flight Test Division	1
Att: ORDEV	1	Naval Ammunition Depot, Crane	
Marine Corps Equipment Board, Quantico	1	Att: Code 3540	1
Marine Corps Headquarters, DC		Att: Code 3400	1
Att: Research & Development Section	1	Naval Ammunition Depot, Portsmouth	
Att: Code AO4E	1	Att: Mr. Jerome Smith, Code QALE	1
Maxwell AFB, Air Command & Staff School		Naval Ammunition Depot, Red Bank	
Att: Air University Library	1	Att: Chief Engineer	1
NASA, Ames Research Center, Moffett Field		Naval Ammunition Depot (Oahu)	
Att: Director	1	Att: Weapons Technical Library	1
NASA, Flight Research Center, Edwards		Naval Applied Science Laboratory, Brooklyn	
Att: Library	1	Att: Library	3
NASA, Goddard Space Flight Center, Greenbelt		Naval Attache, Navy No. 100, NY	
Att: Code 320, Mr. J. C. New	1	Att: Logistics Division	1
Att: Code 623.3, Mr. G. Hinshelwood	1	Naval Avionics Facility, Indianapolis	
Att: Code 321.2, Mr. K. M. Carr	1	Att: MAL-Library	1
Att: Code 321.2, Mr. F. Lindner	1	Naval Civil Engineering Lab., Pt. Hueneme	
Att: Dr. Elias Klein	1	Att: Library	2
NASA, Langley Research Center, Hampton		Naval Construction Battalion Center,	
Att: Library	2	Pt. Hueneme	
Att: Mr. S. A. Clevenson	1	Att: Civil Engineer Corps Officers	1
NASA, Lewis Research Center, Cleveland		Naval Medical Field Research Lab.,	
Att: Library	2	Camp Lejeune	1
NASA, Manned Spacecraft Center, Houston		Naval Mine Engineering Facility, Yorktown	
Att: Mr. G. A. Watts	1	Att: Library	1
Att: Technical Library	1	Naval Missile Center, Pt. Mugu	
NASA, Marshall Space Flight Center, Huntsville		Att: Library, N-03022	1
Att: Mr. J. H. Farrow, M-P&VE-ST	1	Att: Env. Div., N314	2
Att: Mr. R. M. Hunt, M-P&VE-S	1	Naval Operations, Office of Chief, DC	
Att: AMSMI-RBLD	1	Att: Op 31	1
NASA, Scientific & Technical Info. Facility,		Att: Op 34	1
Bethesda		Att: Op 75	1
Att: NASA Representative	1	Att: Op 07T6, Mr. T. Soo-Hoo	1
National Bureau of Standards, DC		Att: Op 725	1
Att: Mr. B. L. Wilson	1	Naval Ordnance Laboratory, Corona	
Att: Mr. S. Edelman, Mech. Div.	1	Att: Code 234, Technical Library	1
National Security Agency, DC		Att: Code 56, Sys. Eval. Division	1
Att: Engineering	1	Naval Ordnance Laboratory, Silver Spring	
		Att: Technical Director	1
		Att: Library	3
		Att: Environmental Simulation Div.	6
		Att: Mr. George Stathopoulos	1

Naval Ordnance Test Station, China Lake		Navy Underwater Sound Laboratory, New London	
Att: Technical Library	1	Att: Technical Director	1
Att: Code 3023	1	Att: Mr. J. G. Powell,	
Att: Code 3073	1	Engrg. & Eval. Div.	1
Att: Code 4062	2		
Att: Code 4066	1		
Att: Code 5516	1	Navy Underwater Sound Reference Lab., Orlando	
		Att: Mr. J. M. Taylor, Code 120	1
Naval Ordnance Test Station, Pasadena			
Att: P8087	3	Norfolk Naval Shipyard, Portsmouth	
Att: P8092	1	Att: Design Superintendent	1
Att: P8073	1		
Att: P80962	1		
		Norton AFB, Off. of Inspector General	
Naval Postgraduate School, Monterey		Att: AFIMS-2-A	1
Att: Library	1		
		Office Director of Defense R&E, DC	
Naval Propellant Plant, Indian Head		Att: Technical Library	3
Att: Library	1	Att: Mr. Melvin Bell	1
		Att: Mr. W. M. Carlson	1
Naval Radiological Defense Lab., San Francisco			
Att: Library	3	Office of Naval Material, DC	1
Naval Research Laboratory, DC		Office of Naval Research, DC	
Att: Code 6250	1	Att: Code 439	6
Att: Code 6260	1	Att: Code 104	1
Att: Code 6201	1		
Att: Code 4021	2	Office of Naval Research Branch Office, Boston	1
Att: Code 2027	2		
		Office of Naval Research Branch Office, Pasadena	1
Naval Security Engineering Facility, DC			
Att: R&D Branch	1	Office of Naval Research Branch Office, San Francisco	1
Naval Supply R&D Facility, Bayonne		Ogden Air Materiel Area, Hill AFB	
Att: Library	1	Att: Service Engineering Dept., OONEOO	1
Naval Torpedo Station, Keyport		Oklahoma City Air Materiel Area, Tinker AFB	
Att: QEL, Technical Library	1	Att: Engineering Division	1
Naval Training Device Center, Pt. Washington		Pearl Harbor Naval Shipyard, FPO	
Att: Library Branch	1	Att: Code 264	1
Att: Code 4211	1		
Naval Underwater Ordnance Station, Newport		Philadelphia Naval Shipyard, Pa.	
Att: Technical Documents Library	1	Att: Ship Design Section	1
		Att: Naval Boiler & Turbine Lab.	1
Naval Underwater Weapons Systems Engrg. Center, Newport	1		
Att: Library		Picatinny Arsenal, Dover	
		Att: Library SMUPA-VA6	1
Naval Weapons Evaluation Facility, Albuquerque	1	Att: SMUPA-VP7, R. G. Leonardi	1
Att: Library, Code 42		Att: SMUPA-T, R. J. Klem	1
		Att: SMUPA-D, E. Newstead	1
Naval Weapons Laboratory, Dahlgren	1	Att: SMUPA-VP3, A. H. Landrock	1
Att: Technical Library			
		Portsmouth Naval Shipyard, NH	
Navy Electronics Laboratory, San Diego	1	Att: Code 246	1
Att: Library		Att: Mr. E. C. Taylor	1
		Att: Mr. J. E. Smith	1
Navy Marine Engineering Laboratory, Annapolis	1		
Att: Library		Puget Sound Naval Shipyard, Bremerton	
		Att: Code 275	1
Navy Mine Defense Laboratory, Panama City	1	Att: Material Laboratories	1
Att: Library		Att: Code 242, Mr. K. G. Johnson	1
		Att: Code 281	1
Navy ROTC and Administrative Unit, Cambridge	1		